1127-21
1521

JOURNAL OF
COLLOID SCIENCE

Editor-in-Chief
Victor K. La Mer, Columbia University, New York

Advisory Board

C. O. Beckmann
K. F. Bonhoeffer (deceased)
J. A. Christiansen
P. J. W. Debye
John T. Edsall
I. Fankuchen
John D. Ferry
Wilfried Heller
John G. Kirkwood
E. C. Lingafelter
L. G. Longsworth
S. G. Mason
J. Th. G. Overbeek
R. Ruyssen
William Seifriz
Leo Shedlovsky
Theodore Shedlovsky
Robert Simha
R. H. Smellie
Jacinto Steinhardt
The Svedberg
Hugh S. Taylor
Arne Tiselius
Robert D. Vold
Bernard Vonnegut
Ralph W. G. Wyckoff
Bruno H. Zimm

VOLUME 12

1957

ACADEMIC PRESS INC.—PUBLISHERS
NEW YORK, N. Y.

JOURNAL OF COLLOID SCIENCE **12**, 1–9 (1957)

EFFECT OF A POLYANION ON THE RHEOLOGY OF A KAOLINITE SUSPENSION

Norman Street

Geology Department, University of Melbourne, Australia

Received October 30, 1956

ABSTRACT

Following the addition of a polyanion, rheological and zeta-potential measurements were made on a kaolinite suspension. The increase in yield stress of a hydrogen clay suspension at low concentration of polyanion is interpreted as being due to interparticle linkage by the polyanion. The decrease in yield stress of a sodium clay suspension at all concentrations of the polyanion is regarded as being due to neutralization of the positive edge charges by polyanion adsorption.

INTRODUCTION

Although flocs of clay particles may be stabilized by polyanions, nevertheless these same polyanions may under different conditions result in the formation of a stabilized deflocculated suspension, and it is possible to relate the rheological behavior of a kaolinite suspension to zeta-potential measurements (1). It is possible to describe the flocculation in terms of rheological behavior.

Rheological Measurements

It is customary to describe the rheology of kaolinite suspensions in terms of yield stress and plastic viscosity, the yield stress being a measure of the "residual flocculation" (2) and the plastic viscosity presumably being a measure of the shape and volume concentration of the flow units.

Even if a true statically measurable yield stress cannot be determined, it is usually possible to describe the flow behavior in terms of the dynamically measured yield. For dilute suspensions of kaolinite particles it is possible that the flow curve is continuous to zero rate of shear, and that the behavior of suspensions at increasing rates of shear can be described in terms of η_0 and η_∞ (1, 3). Thus increased yield stress *may* be caused by the breaking of links between particles during shear, as has been shown experimentally (4), *or* it may be caused by increased stretching and orientation of chainlike floccules (5). In either case the yield stress, i.e., the intercept on the stress axis of the extension of the straight portion of the curve produced by a plot of rate of shear against shearing stress, is a useful parameter to describe interparticulate forces.

Zeta-Potentials

The measurement of zeta-potentials of kaolinite particles has been discussed by Street and Buchanan (6), who have shown that, at the particle size and ionic concentrations used in this work, it is possible to calculate zeta from measured electrophoretic mobilities without appreciable error. It has also been shown (7) that the surface conductance correction would be negligible.

The zeta-potentials given here for both the hydrogen and the sodium clays at zero polyanion concentration are calculated from mobilities and corrected for the relaxation effect by the method of Stigter and Mysels (8). The values given for either hydrogen or sodium clay plus polyanion are calculated from electrophoretic mobilities by the Helmholtz-Smoluchowski equation.

This is justified on the following grounds. The value of a for these particles is 0.15×10^{-4} cm. (9), and it has been shown (6) that κa is of the order of 10 even with slight excess of sodium hydroxide past the equivalence point; thus the relaxation effect would tend to give an acceleration to the electrophoretic mobility such as to approach the H-S equation even for 1:1 electrolytes (5). Also, the presence of a polyanion in solution will further increase the acceleration such that the H-S equation will be obeyed at even lower κa, the effect of multivalent anions on the velocity of negatively charged particles being to produce an acceleration at lower value of κa, the higher the anion valency. It is also likely that the actual value of κ will be much greater than that calculated from the known ionic concentration as the result of two effects, (*1*) the polyanion will change the ionic strength to some value intermediate between that calculated as if it behaved as a multivalent small ion of equal charge, and that calculated as if its charges behaved independently of each other (10), and (*2*) as stated by Cutler and Cook (11) "The concentration of negatively charged clay particles produced in water suspensions by dissociation of cations controls the ionic strength of the suspension even in salt solutions up to 0.01 molar."

EXPERIMENTAL

Preparation of Suspension

The kaolinite used was obtained from Egerton, Victoria, Australia (12), and an analysis of the untreated material is given in Table I.

X-ray diffraction data and an electron micrograph, both carried out by the Commonwealth Scientific and Industrial Research Organization, Melbourne, indicate that this material contains no other clay mineral.

After deflocculation with sodium carbonate it was separated by repeated settling into a relatively narrow range of particle sizes. The fraction used in this study was filtered on a large Büchner funnel and treated with 1%

TABLE I

Analysis of Egerton Kaolinite

Al_2O_3	39.27
SiO_2	45.41
Fe_2O_3	0.49
TiO_2	0.35
CaO	0.37
MgO	Trace
K_2O	0.35
Na_2O	0.33
H_2O	13.68
	100.25

(clay basis) of 30% hydrogen peroxide for removal of organic matter (13). After one week of this treatment the clay was again dispersed (with sodium hydroxide) and washed by centrifugation until electrolyte free. It was then converted to the hydrogen form by repeated leaching with 0.05 *N* hydrochloric acid, and washed with doubly distilled water (second distillation from alkaline permanganate) until the filtrate conductivity was of the order of 0.5×10^{-5} mho.

A stock suspension of high specific gravity hydrogen clay was stored in Jena-glass flasks. This fraction had a surface area, determined by the B.E.T. method (N_2 at liquid air temperature), of 176,000 cm.^{2} per gram.

Sodium kaolinite was formed by the addition of the exchange capacity, i.e., 6 meq./100 gm. (6), of sodium hydroxide to the hydrogen clay suspension followed by extensive washing to a filtrate conductivity of the order of 0.5×10^{-5} mho.

A stock solution of the polyanion was prepared and addition of aliquots of it to obtain the correct concentration, plus water to give a suspension specific gravity of 1.03, were made to the high S.G. kaolinite suspension. These suspension samples were stored in Pyrex stoppered flasks for 24 hours, with intermittent shaking, before measurements of viscosity and zeta-potential were made.

Rheological Measurements

All rheological measurements were carried out on 1.03 S.G. suspensions in a concentric cylinder viscometer so constructed that the speed of the outer cylinder (cup) was continuously variable and the torque on the inner suspended cylinder (bob) could be measured (1, 9). The dimensions of the cup and bob were:

Diameter of bob = 39.6 mm.
Diameter of cup = 43.8 mm.
Height of bob = 44.7 mm.
Height of cup = 82.2 mm.

This instrument had been calibrated (9) so that absolute values of the rheological constants could be measured on it. The cup and bob were immersed in a bath through which water was circulated from a thermostat; measurements were conducted at 25°C.

From a plot of torque against rotational speed (at least six points) the plastic viscosity of a slurry could be calculated from the slope of the graph, and the yield stress from the intercept on the torque axis.

Zeta-Potential Measurements

The micro-electrophoresis cell used was all-Pyrex and of cylindrical cross section (radius = 1.08 mm.); dark field illumination was used. The cell was carefully calibrated for apparent cell length and location of correct stationary level, due notice being taken of the optical corrections necessary in focusing (6, 9).

After viscosity determination each sample was centrifuged and a volume of the original suspension sufficient to give a volume concentration of 0.01 % added to the filtrate. The electrophoretic mobility was determined on these diluted suspensions, and the motion of at least 10 particles in each direction past a calibrated eyepiece scale was timed with a stop-watch. The magnification used was 70× and the scale divisions were 7.6 microns.

Polyanion

The polyanion used was obtained from Monsanto Chemicals (Aust.) Ltd., Braybrook, Victoria, and was described as the sodium salt of a partially hydrolyzed acrylonitrile. A stock solution of it was made up for addition to the clay suspensions.

Conductivity

Conductivity measurements were carried out at 25°C. using a normal Wheatstone bridge net and an oscillator providing 1000 cycles per second.

RESULTS

An indication of the amount of polyanion adsorbed may be gained from the surface conductivity of the clay particles when present in solutions of the polyanion. The surface conductivity (λ_s) of these particles was calculated from a determination of the conductivity of the suspension (K) and its filtrate (K_1); then, as shown elsewhere (7)

$$\lambda_s = (FK - K_1)\frac{\phi}{S_w}$$

where ϕ = volume fraction of liquid, S_w = surface area of solid per milliliter of suspension, and F = a factor dependent on the volume concentration and geometry of the suspended particles.

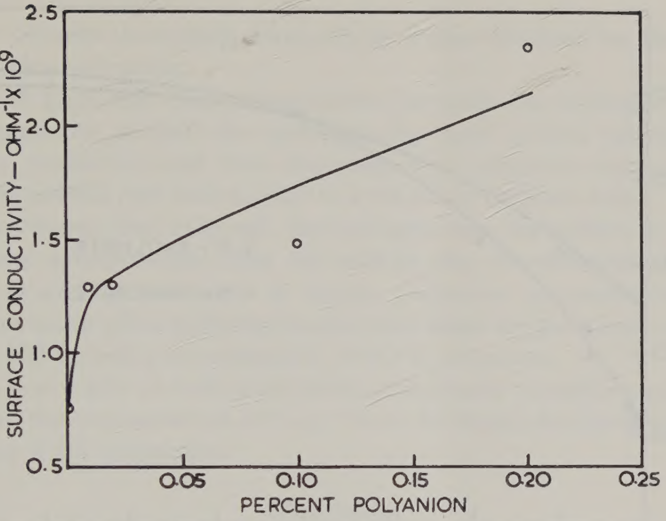

Fig. 1. Surface conductance of a kaolinite suspension with added polyanion (% per weight of clay).

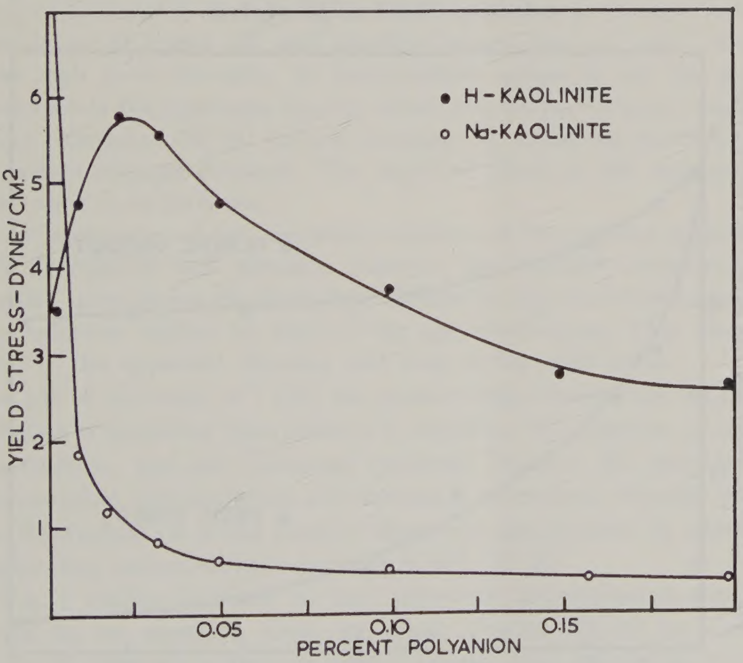

FIGURE 2

Fig. 2. Yield stress of hydrogen and sodium kaolinite suspensions with added polyanion (% per weight of clay).

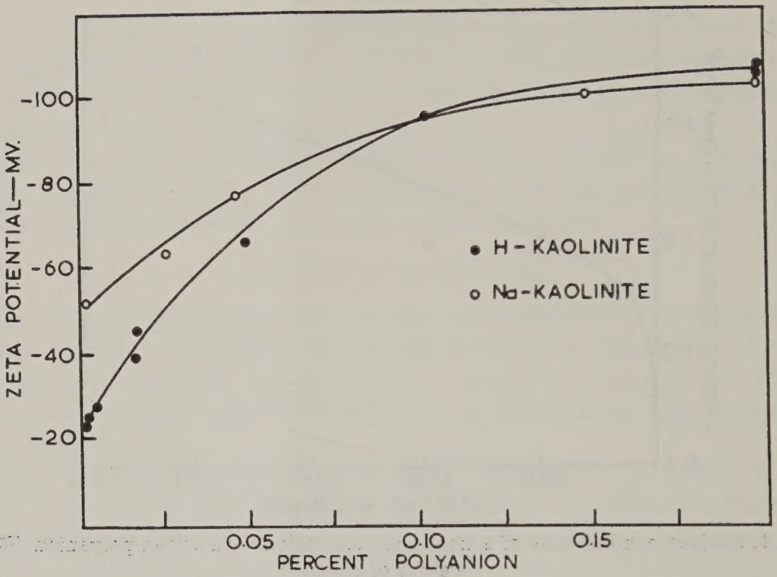

FIG. 3. Zeta-potential of hydrogen and sodium kaolinite particles with added polyanion (% per weight of clay).

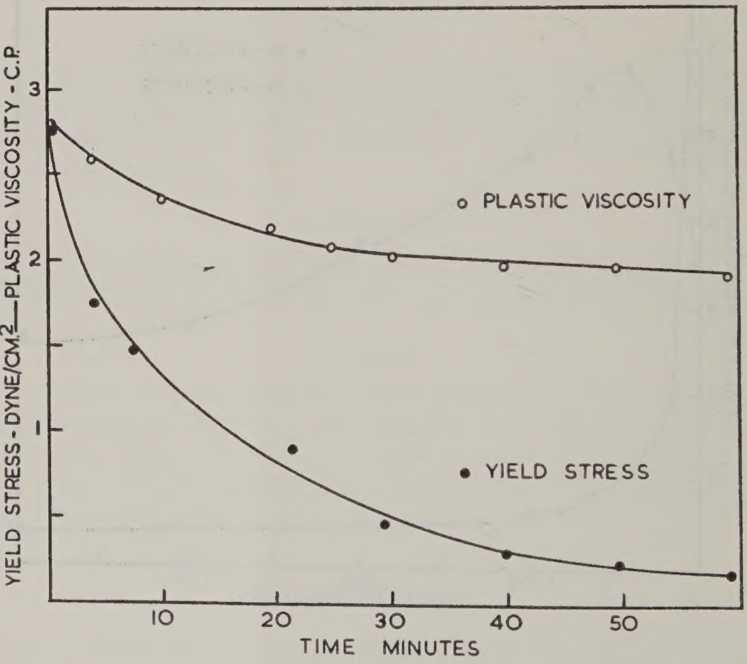

FIGURE 4

FIG. 4. Yield stress and plastic viscosity of hydrogen kaolinite suspensions plus 0.2% polyanion *against* time of shear at 472 sec.$^{-1}$.

Figure 1 shows the surface conductivity values obtained for the sodium kaolinite plus polyanion.

Figure 2 gives the yield stress results for both the hydrogen and the sodium kaolinite; whereas the hydrogen clay yield at first increases, goes through a maximum, and then decreases to a relatively constant value, that of the sodium clay falls rapidly to a relatively constant value.

Figure 3 shows that although the hydrogen clay starts from an initially much lower zeta-potential than the sodium clay, nevertheless they both reach approximate constancy at higher polyanion concentration. Tests carried out using silica particles showed that these too gave zeta-potentials of about 100 mv. at a concentration of 0.2% polyanion.

Figure 4 is a plot of both yield stress and plastic viscosity against time of shear in the viscometer at 472 sec.$^{-1}$ for a hydrogen kaolinite suspension containing 0.2% polyanion.

DISCUSSION

The rheological behavior of hydrogen kaolinite suspensions can be adequately described (1) in terms of edge to face (bipolar) flocculation at low pH due to association of negative face and positive edge charges; complete deflocculation at higher pH; and lamellar (face-to-face, or "salt") flocculation at high ionic strength. At intermediate values of pH the gradual replacement of the hydrogen ions by alkali ions during titration causes the negative charges of the 001 faces to increase (6), whilst the positive charge of the edges remains constant. The observed effect on the zeta-potential in this range is an increase.

As a consequence of the continued existence of the positive edges, edge-to-face flocculation still persists; however, the repulsion between neighboring 001 faces causes the floccule to assume an extended-chain configuration a behavior similar to that of the polyelectrolytes. This causes an increase in the apparent viscosity and thus of the yield stress.

At a pH of the order of 7 (14) the positive edge charges are neutralized and change in character from positive to negative, the cessation of edge-to-face attraction, and the increased repulsion between the particles now causes complete deflocculation and decreased anomalous viscosity or yield stress. Neutralization of the positive charges is also possible by adsorption of multivalent anions without increase in pH (15, 6).

In Fig. 2 sodium kaolinite at zero polyanion concentration shows the behavior to be expected from an alkali clay at pH <7 i.e. a sodium kaolinite at this pH is flocculated by edge-to-face attraction (14) but possesses an extended-chain configuration and it requires either an increase in pH, or adsorption of a multivalent anion, to neutralize the positive edge charges and cause deflocculation. Thus increasing polyanion concentration, and presumably therefore increasing adsorption of the polyanion, effectively decreases the yield stress as shown in Fig. 2. The zeta-potential shows an increase as the positive charges are neutralized (Fig. 3).

Hydrogen kaolinite at zero polyanion concentration with its low zeta-potential (Fig. 3) will be agglomerated by both bipolar and lamellar flocculation, and consequently will exhibit an intermediate yield value. As shown in Fig. 2 increasing concentration of polyanion causes at first an increase and then a decrease in yield stress of the hydrogen clay; at the same time the zeta-potential increases to a value equal to that exhibited by the sodium clay.

It is possible to explain these observed facts as follows. The polyanion is adsorbed on the exposed positive edges and neutralizes them; this causes the increase in negative zeta-potential. However, in this early stage the 001 faces retain their low negative charge, and thus lamellar flocculation remains, although the bipolar flocculation is weakened owing to the reduction of the positive edge charge. Also following Ruehrwein and Ward (16) one can conceive that in this early stage the long polyanion chains bridge the clay particles at their points of contact and, by increasing the energy necessary to separate them, increase the anomalous viscosity or yield stress. The sodium clay because it is present in the suspension in extended-chain configuration does not present the same opportunity for interparticle bridging as does the hydrogen clay which is present in the suspension as floccules associated closely face to face and edge to face.

It is interesting to note that Riseman and Harper (17) have shown that the yield stress of carbon black suspensions may increase owing to structure reinforcement caused by the binding of carbon particles by adsorbed polymer.

Increasing the polyanion concentration increases its adsorption on the clay particles, this adsorption being in part at least on the 001 faces; this generally increased negative charge causes some deflocculation and decrease of the yield stress. This increase of the face charge will not cause the floccules to form an extended chain in this case since the positive edges have already been neutralized and edge-to-face attraction no longer exists.

The curves in Fig. 4 show the results of shearing, a hydrogen clay suspension, containing 0.2% of the polyanion at the maximum rate of shear available on the viscometer used, for extended periods. The yield value and plastic viscosity values were calculated from downcurves run at intervals throughout this shearing. An infinity reading taken after 15 minutes shearing in a vitamiser showed zero yield stress.

These curves indicate that an originally flocculated clay gradually becomes deflocculated (giving decreased yield stress) as it is progressively sheared. This suggests that as links between the particles are broken the freshly exposed faces can immediately adsorb polyanion and acquire a negative charge which prevents reagglomeration of the now smaller particles.

The plastic viscosity reflects this behavior to a more limited extent. It decreases steadily to a low value; this is probably due to a reduction in the volume concentration of the suspended particles brought about by the release of trapped water on deflocculation.

REFERENCES

1. STREET, N., *Australian J. Chem.* **9,** No. 4 (1956).
2. DE WAELE, A., AND LEWIS, G. L., *Kolloid-Z.* **133,** 86 (1953).
3. STREET, N., *J. Oil & Colour Chemists' Assoc.* **39,** 391 (1956).
4. HARVEY, E. N., *J. Colloid Sci.* **8,** 543 (1953).
5. KRUYT, H. R., "Colloid Science." Elsevier, Amsterdam, 1949.
6. STREET, N., AND BUCHANAN, A. S., *Australian J. Chem.* **9,** No. 4 (1956).
7. STREET, N., *Australian J. Chem.* **9,** 333 (1956).
8. STIGTER, D., AND MYSELS, K. J., *J. Phys. Chem.* **59,** 45 (1955).
9. STREET, N., Thesis, University of Melbourne, 1956.
10. ABRAMSON, H. A., MOYER, L. S., AND GORIN, M. H., "Electrophoresis of Proteins." Reinhold, New York, 1942.
11. CUTLER, I. B., AND COOK, M. A., *J. Am. Ceram. Soc.* **36,** 165 (1953).
12. BAIN, A. D. N., AND SPENCER-JONES, D., *Mining and Geol. J.* (*Victoria*) **5,** 30 (1953).
13. JOHNSON, A. L., AND NORTON, F. H., *J. Am. Ceram. Soc.* **24,** 189 (1941).
14. SCHOFIELD, R. K., AND SAMSON, H. R., *Discussions Faraday Soc.* **18,** 135 (1954).
15. VAN WAZER, J. R., AND BESMERTNUCK, E., *J. Phys. & Colloid Chem.* **54,** 80 (1950).
16. RUEHRWEIN, R. A., AND WARD, D. W., *Soil. Sci.* **73,** 485 (1952).
17. RISEMAN, J., AND HARPER, R. C., *J. Colloid Sci.* **9,** 438 (1954).

JOURNAL OF COLLOID SCIENCE **12**, 10–18 (1957)

THE SURFACE PLASTICITY OF A HOMOLOGOUS SERIES OF SODIUM SOAP SOLUTIONS[1]

Emil J. Burcik and Robert C. Newman

The Pennsylvania State University, College of Mineral Industries, University Park, Pennsylvania

Received February 6, 1956

INTRODUCTION

Soap solutions under proper conditions form plastic surfaces even though the viscosity of the bulk liquid is essentially that of pure water. These surfaces have a finite yield value and their viscosity is a function of the rate of shear. This surface plasticity may manifest itself in many ways. Surface plastic foams drain more slowly than those which are nonplastic and maintain a "creamy" appearance for a longer time. Another manifestation is that a bubble floating on a plastic solution surface does not move freely when disturbed. A more quantitative measurement of surface plasticity can be made by the oscillating disk method. If a disk is allowed to oscillate in the plastic surface, a plot of the logarithm of the amplitude versus the number of swings will not yield a straight line but instead exhibits a distinct curvature. This is a consequence of the fact that the apparent viscosity increases as the rate of shear decreases.

It has been found that plastic solution surfaces are temperature-sensitive, and there is a sharp transition from a plastic surface to a nonplastic surface as the temperature is increased. Recent work (3) by one of us with sodium myristate solutions showed that the temperature for the transition from a plastic to a nonplastic surface is a function of concentration. Furthermore, it was suggested that the plasticity is due to the presence of acid soap, since plastic surfaces became nonplastic when the pH was increased. The purpose of this research was to measure the transition temperature as a function of concentration for sodium laurate, sodium myristate, sodium palmitate, and sodium stearate. The effect of pH on surface plasticity was more fully investigated and experiments were conducted to ascertain the effect of various additives on surface plasticity.

---

[1] This investigation is a joint undertaking of The Pennsylvania State University Mineral Industries Experiment Station and the Office of Naval Research.

EXPERIMENTAL

Materials

The sodium laurate, sodium myristate, and sodium palmitate were prepared from the corresponding methyl ester (obtained from Distillation Products Industries, Rochester 3, New York) which was hydrogenated and repeatedly fractionally distilled through a 4-foot packed column at 20 mm. Hg pressure. The middle fraction was saponified with analytical reagent NaOH and the acid reformed by boiling with hydrochloric acid. The acid was recrystallized several times from acetone, dissolved in alcohol, and then neutralized with a carbonate-free solution of the NaOH to the phenolphthalein end point. The sodium stearate was prepared from Eastman White Label methyl stearate in the same manner, except that the distillations were conducted in a 2-foot column. The potassium laurate was made from the purified lauric acid by neutralizing with a carbonate-free solution of analytical reagent KOH. The melting points of the purified methyl esters and acids are shown in Table I.

The pH of the soap solutions are given in Table II and compared with those obtained by other investigators.

These results indicate that the samples employed in this research were reasonably pure. This is important since, as will be shown later, the surface plasticity of soap solutions is markedly influenced by the presence of impurities and pH.

TABLE I

Melting Points of Fatty Acids and Their Methyl Esters

	Methyl ester m.p., °*C.*	Literature (6)	Acid m.p. °*C.*	Literature (6)
Laurate	4.6– 4.9	5°C.	43.4–43.8	43.5°C.
Myristate	19.0–19.5	19°C.	53.3–54.0	54.4°C.
Palmitate	—	29°C.	61.0–61.9	62.9°C.
Stearate	37.2–37.8	38°C.	68.0–68.4	69.6°C.

TABLE II

pH of Soap Solutions

Material	Normality	Temperature, °*C.*	pH	Literature
Sodium laurate	0.01	25	8.1	8.2 (4) at 20°C. 7.9 (9)
Potassium laurate	0.01	25	8.2	8.1 (9)
Sodium myristate	0.001	25	8.08	8.1 (9)
Sodium palmitate	0.0001	50	7.7	7.7 (9)
Sodium stearate	0.0001	50	7.6	7.5 (9)

Apparatus

The oscillating disk method (10) was used to determine surface plasticity. Essentially, this apparatus consisted of a disk which oscillated on the surface of the liquid being tested. A stem was attached to the disk and weights were added to the top as shown in Fig. 1. The weight disk was marked on its circumference in arbitrary units so that the angle of rotation could be observed with the aid of a cathetometer telescope. The oscillating disk was hollowed out underneath as shown in Fig. 1, so that the viscous forces damping the oscillations were minimized. A small hole was drilled up through the disk and another into the stem to allow pressure equalization under the disk. The stem was long enough to allow the disk to oscillate on the surface of the liquid being tested while the weight disk was outside of the surrounding bath. The weight and wire combination was chosen to give a period about 6 seconds.

The disk was supported on a No. 30 Nichrome wire about 30 inches long which was threaded through a horizontally mounted du Noüy tensiometer head. This head allowed the disk to be set into oscillation without any lateral motions. The tensiometer head was fastened to a vertical slide

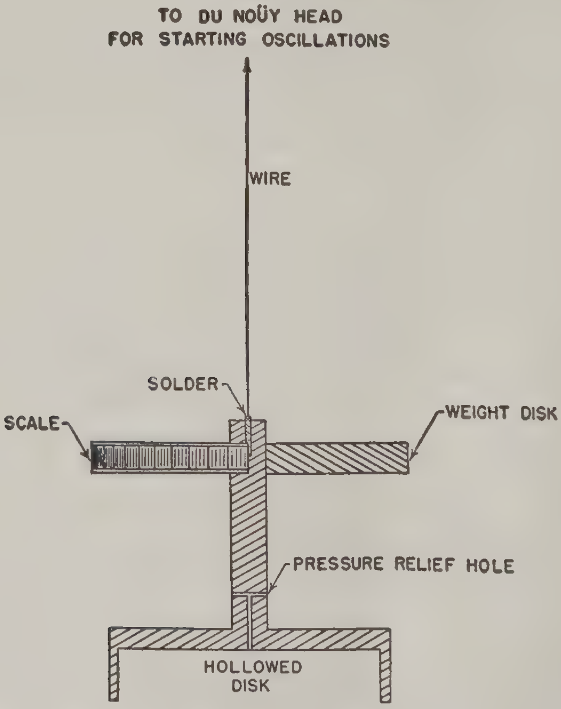

FIG. 1. Oscillating disk. The disk was oscillated with the bottom cylindrical edge just touching the liquid surface.

which was raised and lowered by a screw adjustment device clamped to a ring stand. This allowed the head to be raised and lowered about 1 inch for final adjustment at the liquid surface.

The solutions to be tested were placed in a 20 × 100 mm. Petri culture dish supported in an insulated water bath. The bath was a copper cylinder 6 inches in diameter and 2½ inches deep. It was supplied with an inlet and an outlet tube for the circulation of water at the proper temperature. A snugly fitting Lucite cover was made for the bath. A hole was drilled in the center for the disk stem and the cover was split so that the disk could be readily removed. The bath was continually flushed with a slow stream of carbon dioxide free air. The temperature was maintained by withdrawing the water in the bath into a large constant-temperature reservoir and returning the water to the bath. The temperature was measured with a precision thermometer.

RESULTS

The transition temperature as a function of the concentration for the sodium salts of lauric, myristic, palmitic, and stearic acids are shown in Fig. 2. These curves for the soaps other than sodium laurate show a very rapid rise to a maximum and then a rather slow drop to a transition

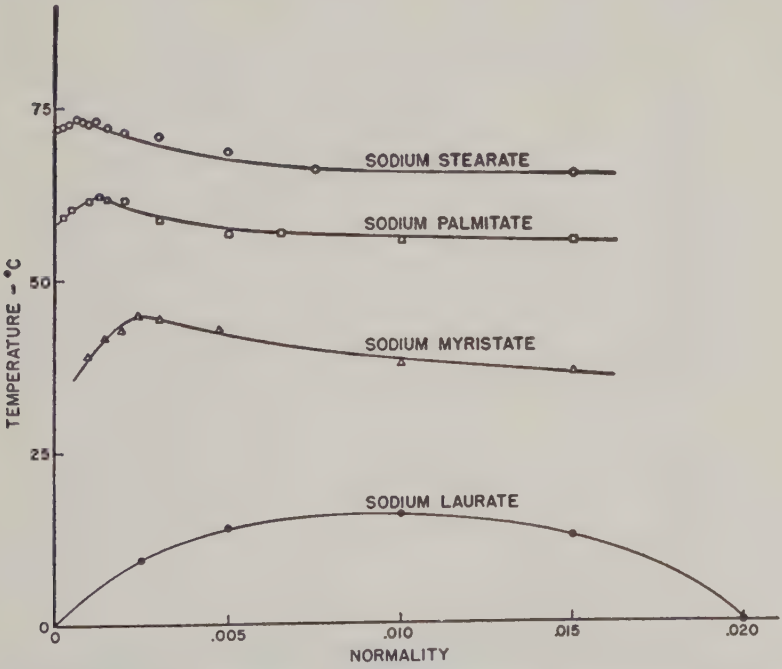

Fig. 2. Transition temperatures in °C. as a function of concentration for various sodium soaps.

temperature which remains nearly constant as the concentration is further increased. In the case of the stearate this temperature is about 65°C., in the case of the palmitate, 55°C., while that for the myristate is below 35°C. The peak in the curve becomes sharper for the higher molecular weight homologues and becomes less pronounced for the lower ones.

The transition temperatures of 0.01 *N* sodium laurate were obtained as a function of the pH and the results are plotted in Fig. 3. These results show that suppression of hydrolysis brought about by an increase in pH decreases the transition temperature. These results suggest that the plasticity may be attributed to hydrolysis products. This conclusion is supported by results previously obtained with sodium myristate (3) which showed that a plastic surface could be converted to a nonplastic one by the addition of sodium hydroxide.

The transition temperature versus concentration curve for sodium

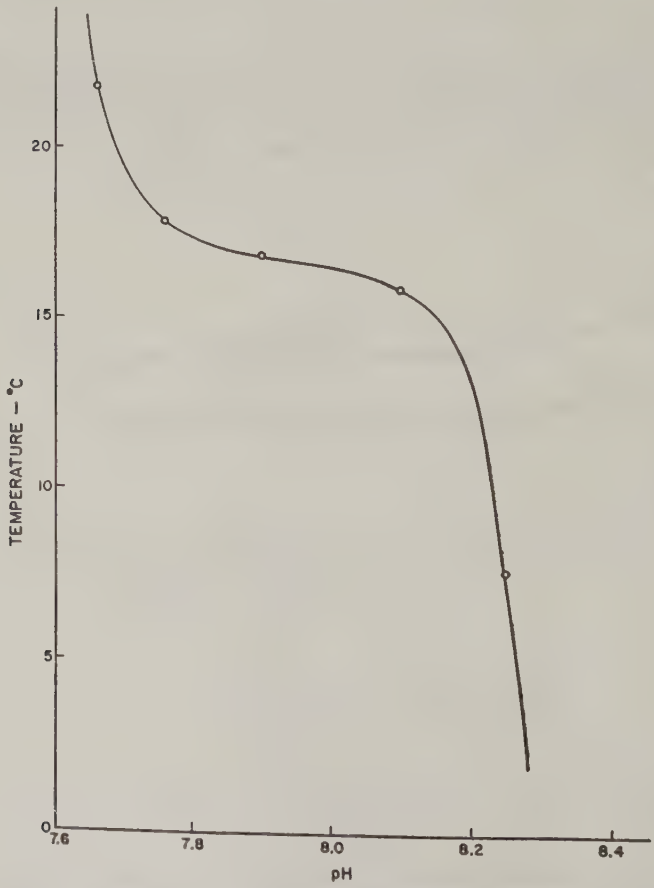

Fig. 3. Transition temperature of 0.01 *N* sodium laurate solution as a function of pH.

myristate determined previously (3) is compared with the present results in Fig. 4. These results were obtained with two different samples of sodium myristate and the earlier results were obtained with an oscillating disk rather than a cylinder. The present sample had a pH of 8.08 for a 0.001 *N* solution while the sample previously used had a pH of 8.0. The concentration which yields the maximum transition temperature agrees between the two sets of data, although the present work indicates somewhat lower values for the transition temperatures. This difference may well be due to the slightly higher pH of the sample prepared for this research.

Other investigators (1) have reported that a 0.01 *N* solution of potassium laurate prepared from commercial lauric acid was surface plastic. The fact that sodium laurate was reported to be nonplastic at 20°C. by one of us (2) led them to suggest that the oscillating disk method was not sensitive enough to determine surface plasticities of this order of magnitude. Oscillating disk experiments conducted in this laboratory with a 0.01 *N* solution of potassium laurate (pH = 8.2) indicated that the solution was not

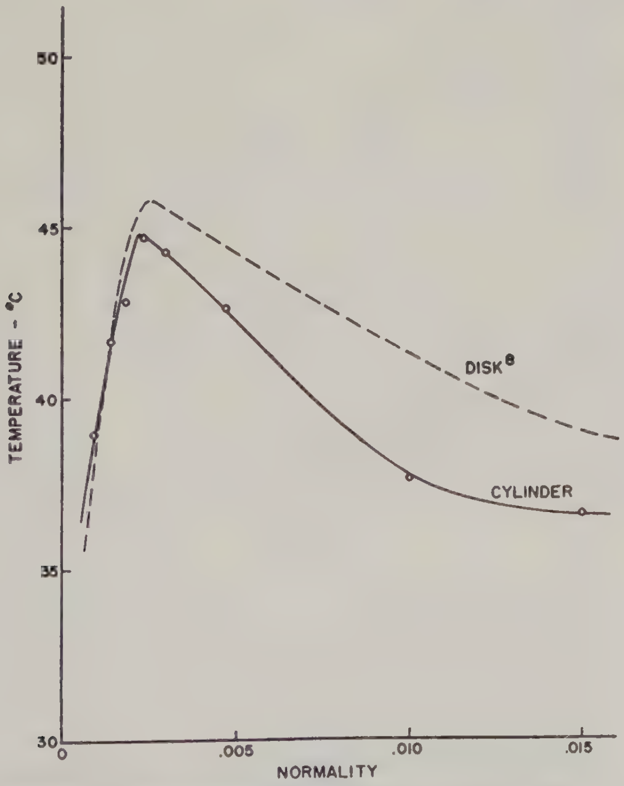

Fig. 4. Comparison of present results for sodium myristate with those obtained previously.

plastic at 0°C. However, when sodium laurate containing 1% sodium palmitate as an impurity was employed to prepare a 0.01 *N* solution, a marked surface plasticity was observed at room temperature. As shown in Fig. 5 the transition temperature for this impure solution was 32.2°C. These results show the very marked effect that a relatively small amount of an impurity can have on the surface plasticity of sodium laurate solutions and indicate that the transition temperatures reported in this investigation should be interpreted as being maximums. They also suggest that the surface plasticity of potassium laurate solutions observed by other investigators was due to the presence of higher molecular weight soaps.

Since soap solutions react with carbon dioxide in the atmosphere to form acid soap, they become plastic on standing in air which has not been treated to remove carbon dioxide. To show this effect, a 0.01 *N* sodium laurate solution was allowed to stand open to the air for 80 minutes. The results shown in Fig. 6 indicate that this solution developed a marked surface plasticity.

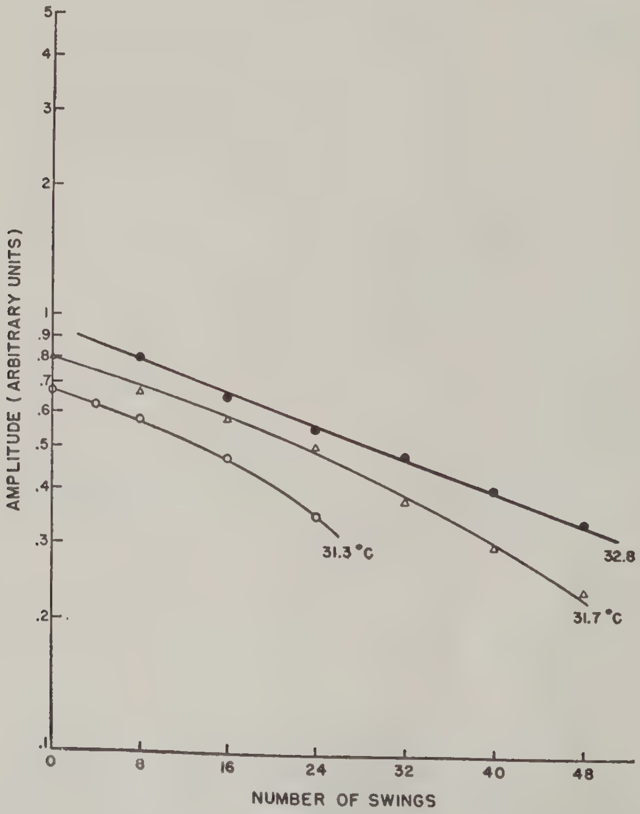

Fig. 5. Surface plasticity of 0.01 *N* sodium laurate containing 1.0% sodium palmitate as an impurity.

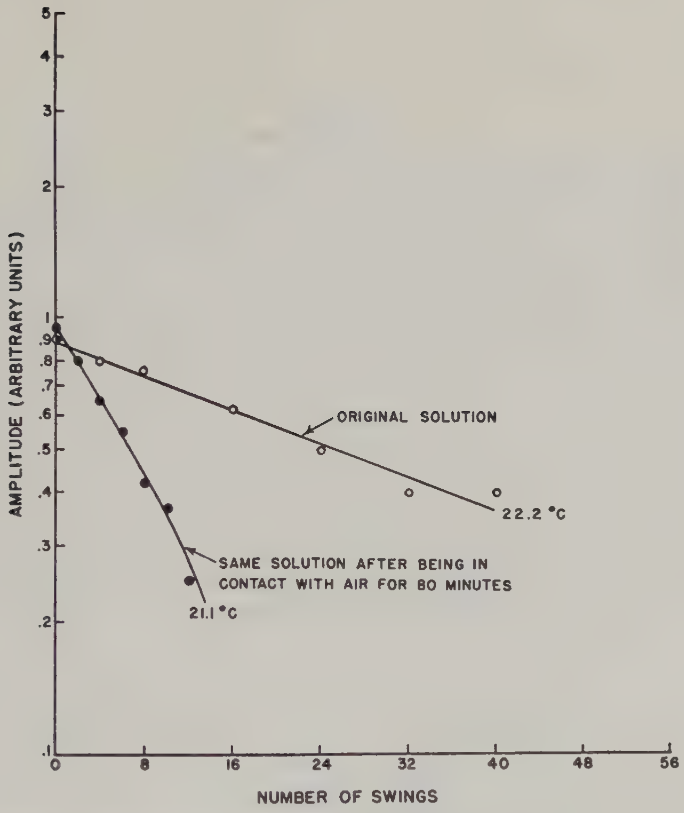

FIG. 6. Surface plasticity of 0.01 *N* sodium laurate in contact with air containing carbon dioxide.

TABLE III

Critical Micelle Concentrations

	Maximum temperature, °*C*.	Normal conc. at maximum temp.	CMC at this temp.	Observer
Sodium laurate	16.0	0.01	0.026	8
Sodium myristate	44.7	0.0025	0.0074	7
Sodium palmitate	62.0	0.00125	0.0027–34	5
Sodium stearate	73.4	0.00050	0.0015–17	This laboratory

TABLE IV

Summary

Change in System	Effect on system properties
1. Increase in temperature	Transition from plastic to nonplastic at transition temperature.
2. Increase in concentration	Transition temperature rises rapidly to a maximum, then decreases.
3. Increase in pH	Transition temperature is lowered and plasticity may even disappear.
4. Addition of higher homologues	Transition temperature is raised.
5. Addition of CO_2 by standing in air	Transition temperature is raised.

Discussion

It was found that the maximum in the transition temperature versus concentration curve occurred at concentrations which were always well below the so-called critical micelle concentration for this temperature. The concentrations at these maxima and the CMC's reported by various investigators are shown in Table III.

No reliable data for sodium stearate were readily available so an approximate value of the CMC was determined by the pinacyanole dye method at 73°C.

The results obtained in this research are summarized in Table IV.

These results show that under the proper conditions of concentration, pH, and temperature the hydrolysis products of the sodium soaps of lauric, myristic, palmitic, and stearic acids form plastic surfaces, although the bulk liquid has a viscosity essentially that of pure water. Because the plastic surfaces may be eliminated by raising the pH it is probable that the hydrolysis products are responsible for this behavior.

References

1. Brown, A. G., Thuman, W. C., and McBain, J. W., *J. Colloid Sci.* **8,** 491 (1953).
2. Burcik, E. J., *J. Colloid Sci.* **5,** 421 (1950).
3. Burcik, E. J., Sears, J. R., and Tillotson, A., *J. Colloid Sci.* **9,** 281 (1954).
4. Ekwall, P., and Lindblad, *Kolloid-Z.* **94,** 42 (1941).
5. Ekwall, P., *Kolloid-Z.* **101,** 135 (1942).
6. Hilditch, T. P., "The Chemical Constitution of Natural Gas," 2nd ed., p. 391. Chapman and Hall, London, 1947.
7. Klevins, H. B., *J. Colloid Sci.* **2,** 301 (1947).
8. Klevins, H. B., *J. Am. Oil Chemists' Soc.* **30,** 74, (1953).
9. McBain, J. W., Laurent, P., and John, L. M., *J. Am. Oil Chemists' Soc.* **25,** 77 (1948).
10. Wilson, R. E., and Ries, E. D., *Colloid Symposium Monograph* **1,** 145 (1923).

JOURNAL OF COLLOID SCIENCE **12**, 19–24 (1957)

STUDIES ON MECHANOCHEMICAL SYSTEMS. PART I

Sadhan Basu and Phanibhusan Roy Chaudhury

Department of Chemistry, University College of Science & Technology, 92 Upper Circular Road, Calcutta-9, India

Received May 21, 1956

INTRODUCTION

It has been shown by Kuhn (1) and Katchalsky (2) that the microscopic expansion and contraction of a linear polyelectrolyte could be reproduced on a macroscopic scale on cross-linked compounds. The expansion-contraction of such systems has been termed a "mechanochemical" property, since in these cases the chemical energy is converted directly into mechanical energy and the process remarkably simulates muscular contraction.

The underlying mechanism of such mechanochemical behavior rests on the fact that because of mutual repulsion between similarly charged groups a coiled up molecule unfolds and expands. The extent of expansion depends on the intensity of repulsive force, i.e., on the charge density as well as the distance separating the charged groups along the chain. It may be argued that interchain cross linkings in Kuhn and Katchalsky's polymer had no other function but to make the system insoluble in water and were in no way responsible for the expansion-contraction of the system. It follows therefore that a chain molecule, if it be insoluble in water and if it contains dissociable groups along the chain, will manifest a mechanochemical property.

With this end in view the mechanochemical behavior of a sample of polymethyl acrylate of average degree of polymerization of 16,310 hydrolyzed to the extent of 33 % has been studied; the results are reported in the present communication. It may be mentioned that the technique utilized in the present case has also been used by other workers in the study of physical changes in insoluble molecular aggregates (3).

EXPERIMENTAL

Preparation of Polymer Sample

The polymethyl acrylate was prepared by polymerizing methyl acrylate with benzoylperoxide at 80°C. The polymer was dissolved in benzene and precipitated with alcohol. The average degree of polymerization as determined viscometrically at 30°C. (−0.1) was 16,310. The polymer was dissolved in acetone and alkali necessary to half hydrolyze the product was added and the system shaken in a mechanical shaker at room temperature (29°C.). After about 1½ hours a thick gelatinous precipitate appeared, when the whole was poured into water with rapid stirring. The alkali was neutralized with hydrochloric acid when the polymer was obtained in a granular form. It was dialyzed free of electrolyte and dried. The polymer was completely insoluble in normal alkali; its equivalent weight was determined by adding 0.2 *N* alkali and back titrating the excess alkali both directly and electrometrically. The equivalent weight thus determined was 268.4, indicating an extent of hydrolysis of about 33%. The dried partially hydrolyzed polymer was dissolved (or dispersed) in acetone containing 20% water and poured on a clean mercury surface to allow the solvent

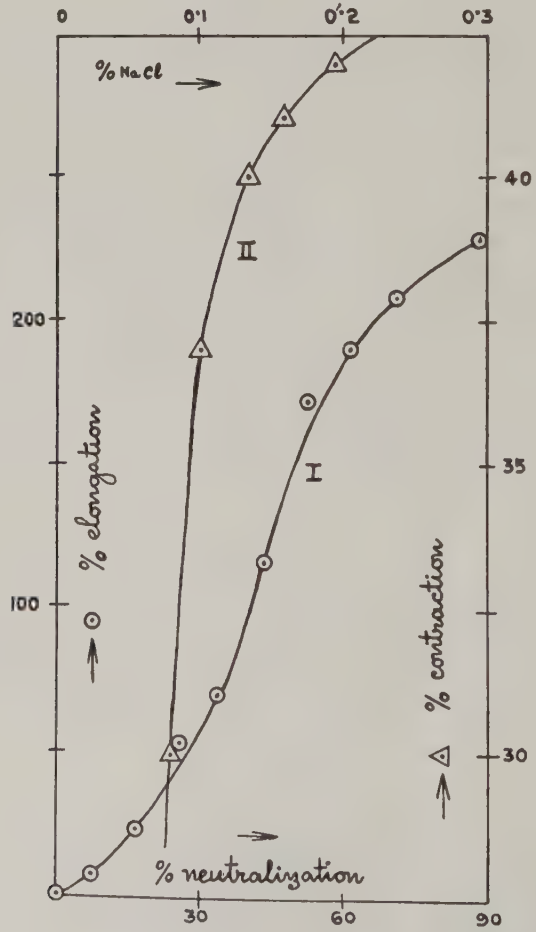

Fig. 1. Expansion-contraction of polyacrylic acid film.

to evaporate. The film thus obtained was heated on a water bath to get a dry and continuous film of polymer.

Expansion with Extent of Neutralization

A thin strip of polymer film (2 cm. × 1 cm. × 0.1 cm.) was suspended in water and allowed to swell for about 2 hours. A small weight (about 0.05 g.) was attached to the end of the film to keep it stretched under water. Over a period of more than 8 hours the attached weight did not cause any elongation of the film. The length of the film was measured by means of a cathetometer to ±0.01 cm. The calculated amount of alkali necessary to neutralize the polymer to different extent was added to the water and the length of the film measured after the attainment of equilibrium. Practically the whole of the alkali was taken up by the film in about 2 to 3 hours at the early stage and in about half an hour in the latter stage. The film underwent more than 200% elongation on complete neutralization. The operation is illustrated graphically in Curve I, Fig. 1. When the neutralized film was placed in 0.1 *N* hydrochloric acid it underwent violent contraction and on washing free of electrolytes the original length was regained, showing thereby that the expansion-contraction was completely reversible.

Expansion-Contraction in Presence of Neutral Electrolyte

When completely neutralized polymer film was dipped in water and the sodium chloride concentration was increased in water, the film gradually contracted as shown in Curve II, Fig. 1. The curve could be retraced by gradually lowering the concentration of sodium chloride by dilution.

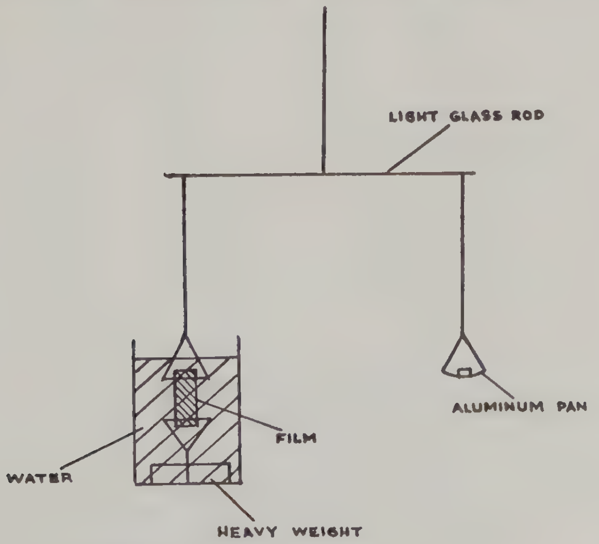

FIG. 2. Experimental setup for studying contractile work cycle.

A Mechanochemical Carnot Engine

A direct consequence of the existence of mechanochemical property is the possibility of constructing a mechanochemical Carnot engine. In order to follow the cycle the following experimental setup was used which is shown schematically in Fig. 2. A thin strip of film (2 × 1 × 0.1 cm.) was made out of the sodium salt of the partially hydrolyzed polymer. The film was dipped in water, the lower end being fixed to a heavy weight resting at the bottom of the container of water. The upper end was attached by means of a fine thread to one arm of a balance made out of a light and thin glass rod. From the other arm of the balance was suspended a light pan of aluminum on which weights could be placed. The whole system was kept inside a glass case in order to eliminate any disturbance due to air blast. The system was so adjusted as to keep the film under water in a stretched condition and the beam of the balance in a horizontal position. The position of the beam and the length of the film was read on a cathetometer scale.

In the first operation increasing amounts of weight was placed on the pan in steps and the expansion of the film measured in each step. Maximum weight placed on the pan was 2 gm., attained in steps of 0.5 gm. Keeping this weight constant a strong solution of sodium chloride was added to the water in steps up to a value of 0.026% of salt concentration. The contrac-

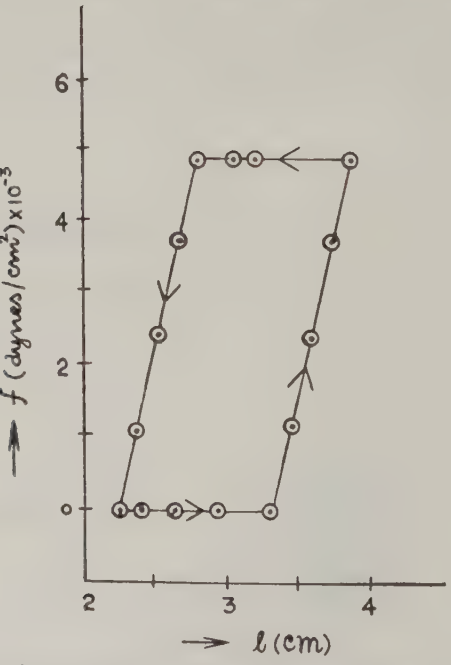

FIG. 3. Mechanochemical Carnot cycle.

tion of the film was measured at each salt concentration. Then keeping the sodium chloride concentration constant the weights were removed from the pan in steps, whereupon the film underwent further contraction. In the final operation water was added to the container in steps lowering the salt concentration below 0.006%, when the film expanded again. The whole operation is represented graphically in Fig. 3. The work done in the complete cycle as calculated from the area of the closed curve was found to be about 5268 ergs.

Discussion

The expansion which the film underwent with the extent of neutralization is similar to that observed by Kuhn (1) and Katchalsky (2) in cross-linked polymers. This can be easily explained by the expansion-contraction of a polyelectrolyte molecule as suggested by Fuoss (4) in order to explain the peculiar viscosity behavior of polyelectrolyte solutions. As the COOH groups are neutralized the polymer is left with a number of COO^- groups distributed along the chain. The mutual electrostatic repulsion between these groups counteracts the Coutschouc type of contraction of neutral polymers and causes the chain to unfold and expand (Curve I, Fig. 1). As the ionic strength of the medium is increased by the addition of neutral electrolyte some of the oppositely charged ions are drawn back into the polymer coil, thereby neutralizing the charge on the chain partially, with the consequent contraction of the chain (Curve II, Fig. 1).

Figure 3 shows that the polymer film can be made to perform contractile mechanical work by reversible ionization of the charged groups. It is therefore a mechanochemical engine which transforms chemical ionization energy into mechanical work in an isothermal process. In this respect the film resembles the mechanochemical behavior of muscle, which also transforms chemical energy into mechanical energy in an almost isothermal cycle. The Young's modulus of the film was 0.27×10^5 dynes/cm.^{2} (under water), comparable to rubber (0.2 to 8×10^5) and muscle (10^5). Although the transformation in the present case was fully reversible, only a small amount of chemical energy could be converted into work owing to the limited extensibility of the molecule. It should be clearly stated at this stage that the present work does not establish in any way that the muscular contraction arises from a similar cause.

It has been suggested that the expansion-contraction of a polyelectrolyte gel may be a swelling-deswelling phenomenon due to the Donnan osmotic effect (5). In order to test this point a swollen film was placed in a strong sugar solution of osmotic pressure at least ten times higher than that of the total ions present inside the gel. The film did not undergo any contraction whatsoever. Thus we may conclude that at least in the present case the osmotic effect is negligible.

SUMMARY

A film of partially hydrolyzed (about 33%) polymethyl acrylate (of av. D.P. 16,310) has been found to undergo reversible mechanochemical expansion-contraction with the extent of neutralization and in salt solutions. An amount of work equivalent to 5268 ergs has been performed using the contractile mechanism isothermally. Donnan osmotic contribution to the swelling of the gel has been found to be negligible in the present case.

REFERENCES

1. KUHN, W., *Experientia* **8**, 318 (1949); KUHN, W., AND HARGITAY, B., *Z. Elektrochem.* **55**, 90 (1951).
2. KATCHALSKY, A., *Experientia* **8**, 319 (1949).
3. ENGELHARD, V. A., *Advances in Enzymol.* **6**, 147 (1946); HAYASHI, T., *J. Gen. Physiol.* **36**, 139 (1952).
4. FUOSS, R., AND STRAUSS, U. P., *J. Polymer Sci.* **3**, 246 (1948).
5. KATCHALSKY, A., *J. Polymer Sci.* **12**, 159 (1954).

JOURNAL OF COLLOID SCIENCE **12**, 25-39 (1957)

EXPERIMENTAL INVESTIGATIONS ON THE LIGHT SCATTERING OF COLLOIDAL SPHERES

II. SOURCES OF ERROR IN TURBIDITY MEASUREMENTS[1]

Wilfried Heller and Richard M. Tabibian[2]

Chemistry Department, Wayne State University, Detroit, Michigan

Received May 23, 1956

INTRODUCTION

Particle size determinations by means of turbidity measurements are attractive for several reasons: (*a*) Absolute diameters, D, or particle weights M, are obtained directly (no apparatus constant or calibrating substance is necessary). (*b*) The limiting specific turbidity, $(\tau/c)_0$, is a monotonic function of D over a wide range of colloidal particle sizes, if visible light is used (1). (*c*) The practically useful range extends, in general, from D-values as low as about 50 mμ up to more than 1μ[3]. (*d*) The accuracy of D-values is comparable to electron microscopic values (2). (*e*) Turbidity measurements are experimentally comparatively simple. Particularly because of the last-named feature, turbidity measurements are being used at a rapidly increasing rate without its being generally realized that a number of precautions are necessary, in addition to those well-known for spectrophotometric work, in order to obtain truly significant data. The most important ones will be discussed in this paper.

I. INTERFERENCE OF LATERALLY SCATTERED LIGHT

Laterally scattered light may leave the scattering (absorption) cell and may, by diffuse reflection from the inner walls of the cell housing—even though they are blackened—reach the phototube unless this is avoided by proper apparatus construction or shielding (see, e.g., the schematic pencil of diffuse reflected light, L_d, in Fig. 4). This will result in an apparent

---

[1] This work was supported by the U.S. Office of Naval Research.

[2] Present Address: Jackson Laboratory, E. I. duPont de Nemours and Co., Wilmington, Delaware.

[3] Diameters smaller than 50 millimicrons require the use of very long absorption cells (W. Heller and H. B. Klevens, *Phys. Rev.* **67**, 61 (1945)) or the experimental use of rather high concentrations (S. H. Maron and R. L. Lou, *J. Polymer Sci.* **14**, 29 (1954)). The former are somewhat impractical. In the latter case, extrapolations to zero concentration do not necessarily yield correct $(\tau/c)_0$-values.

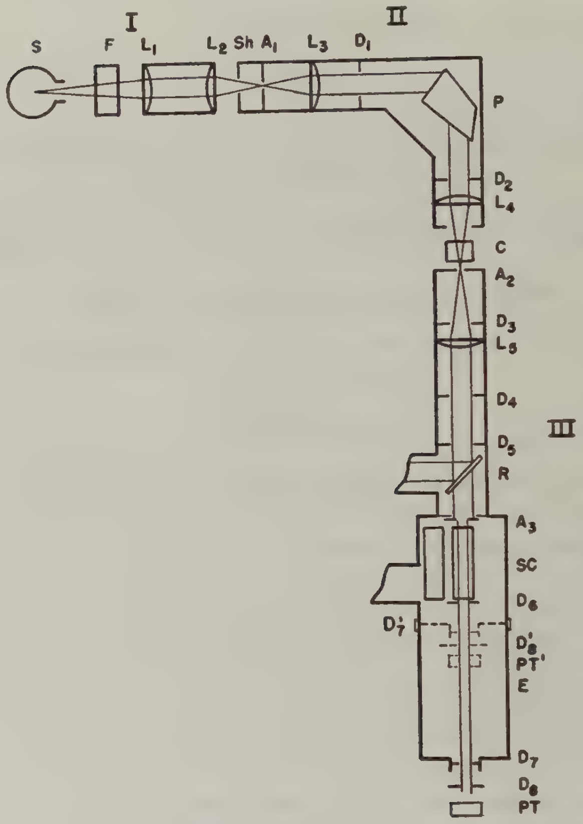

Fig. 1. Apparatus.

turbidity smaller than the true one. This situation is very often found with commercial equipment. It can be created with the apparatus used for the turbidity measurements shown in Fig. 1 and described in the preceding paper (2) by omitting diaphragms D'_7 and D'_8. Photography can make the subjectively very weak effect objectively evident. To that effect a photographic plate was placed at the position PT', normally occupied by the phototube, using an aperture of 4.9 cm. A 10-cm. scattering cell containing only double distilled water gave the picture of the primary light beam shown in Fig. 2*a* (no stray light). Figure 2*b* was obtained[4] after replacing the water by a dilute latex. The scattered stray light is very pronounced. Photo 2*c* was obtained on painting the walls of the cell, containing the latex, black except for the exit and entrance windows (no stray light). In all measurements of turbidity it is, therefore, advisable—and with some apparatus

---

[4] The exposure time was drastically increased from 2*a* to 2*b* in order approximately to equalize the total flux of the primary beam incident on the photographic plate.

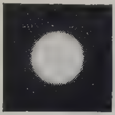

FIG. 2*a*.

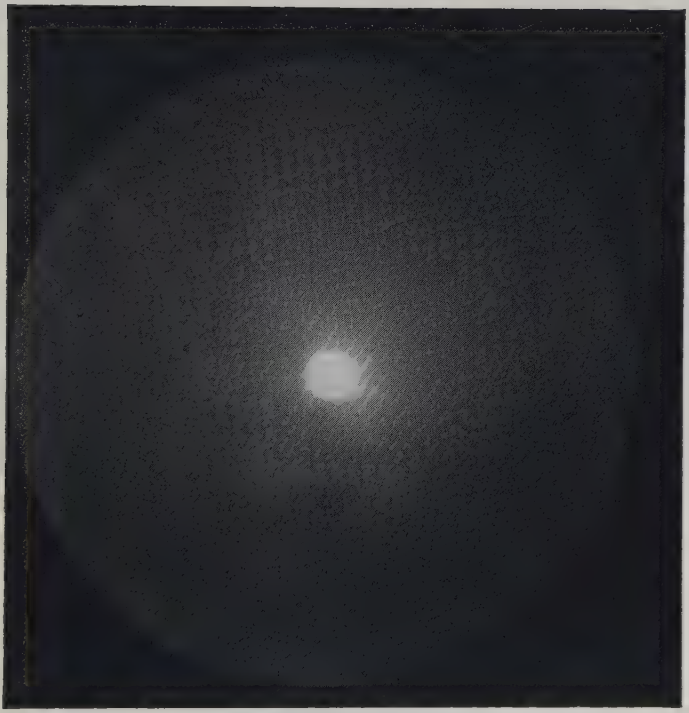

FIG. 2*b*.

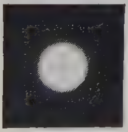

FIG. 2*c*.

FIG. 2. Photographs illustrating stray light and its elimination.

- *a*. Primary beam after passing through water in unblackened cell.
- *b*. Primary beam after passing through scattering solution in unblackened cell. Note background of stray light.
- *c*. Primary beam after passing through scattering solution in blackened cell without exit diaphragm D_6.

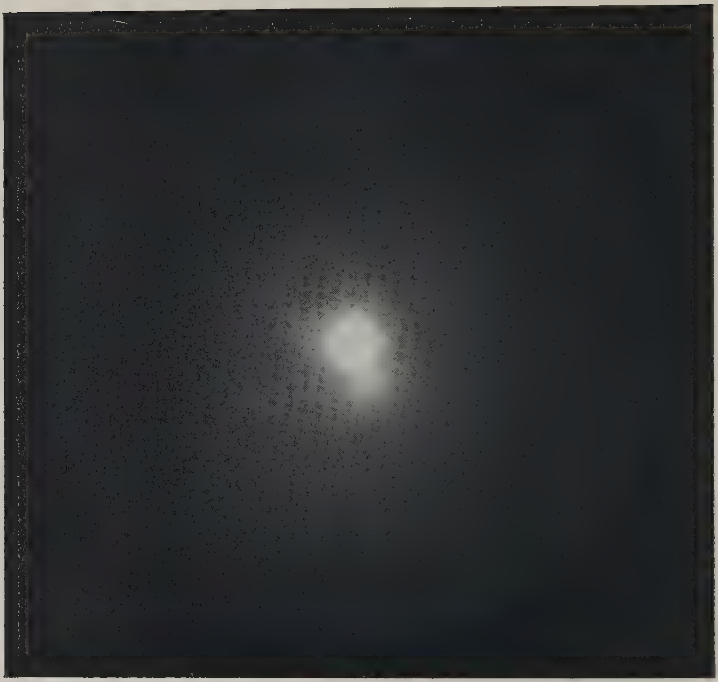

Fig. 3*a*.

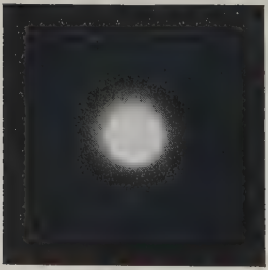

Fig. 3*b*.

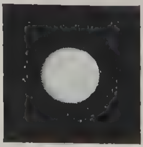

Fig. 3*c*.

Fig. 3. Photographs illustrating the Corona effect and its elimination.

a. Same conditions as in Fig. 2*c* except that exposure time was increased sixfold.

b. Primary beam after passing through scattering solution in blackened cell with exit diaphragm D_6 being inserted.

c. Primary beam after passing through scattering solution in blackened cell with both exit diaphragm D_6 and diaphragm D_7 being inserted.

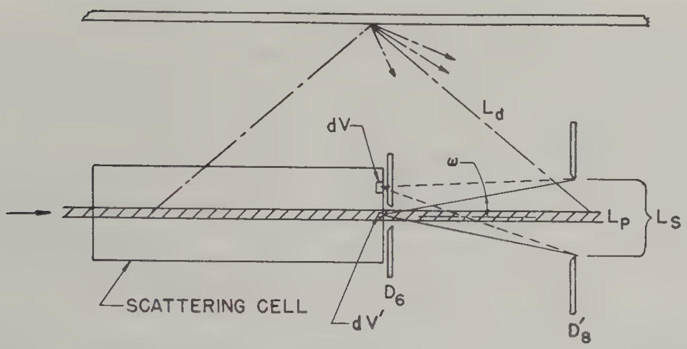

FIG. 4. Sources of error in turbidity measurements. L_d scattered stray light, L_p primary beam, L_s primary and secondary scattered light, D_6 and D'_8 diaphragms.

absolutely necessary—to work with cells whose lateral walls have been blackened.

The intensity of the stray light, although it is very small compared to that of the primary beam, is strong enough to falsify the concentration dependence of the turbidity.

II. THE "CORONA EFFECT"

The light received by the aperture D'_8, preceding the phototube, consists, in the absence of D_6, of three components. By far the major portion of the light flux is accounted for by the primary beam, L_p (Fig. 4). Superimposed upon and adjacent to it is scattered radiation, L_s. The latter consists of both primary scattered light, i.e., light scattered directly from the primary beam in the central irradiated part of the cell, and secondary scattered light originating within those portions of the cell not traversed by the primary beam. Both types of scattered light will falsify the turbidity data obtained unless proper precautions are taken to sufficiently reduce or eliminate their contribution to the total light flux measured. We shall first discuss the nature of the effect produced by the secondary scattered light and a method for eliminating it.

Two dashed lines in Fig. 4 represent the projection of the cone of secondary scattered light reaching the aperture D'_8 from a selected volume element dV extending by the distance dx into the cell. Secondary scattering from the differential volume $\pi R^2\, dx$ (R is the radius of the cell) will, therefore be finite across the entire face of the cell window, although its intensity will decrease exponentially (disregarding relatively minor periodic intensity variations due to interference) towards the periphery because of the turbidity losses in the primary scattered light. The next differential liquid layer will produce an effect of similar magnitude. For, whereas the secondary scattered light from a given layer decreases exponentially with the distance x, giving to x the value of 0 at the exit window, its original intensity increases exponentially with x. The contribution of inner layers to the flux of secondary scattered light through the exit window is, therefore, by no means small. The magnitude of the entire effect becomes apparent on looking at the cell towards the primary beam. A corona around the primary beam is observed. It is demonstrated in Fig. 3*a*, which was taken under the same conditions as Fig. 2*c* except that the exposure time was increased sixfold to make the effect very distinct. The corona can easily be excluded, as shown by Fig. 3*b*, by placing at the exit end of the cell a diaphragm, D_6 (Figs. 1 and 4), with an opening only slightly larger than the diameter of the beam. This photo was obtained under precisely the same exposure time and development procedure as photo 3*a*.

The luminosity of the corona obviously approaches zero at infinite dilution. Like the laterally scattered stray light (section I) it falsifies the concentration dependence of the turbidity and, thus, also the concentration dependence of τ/c.

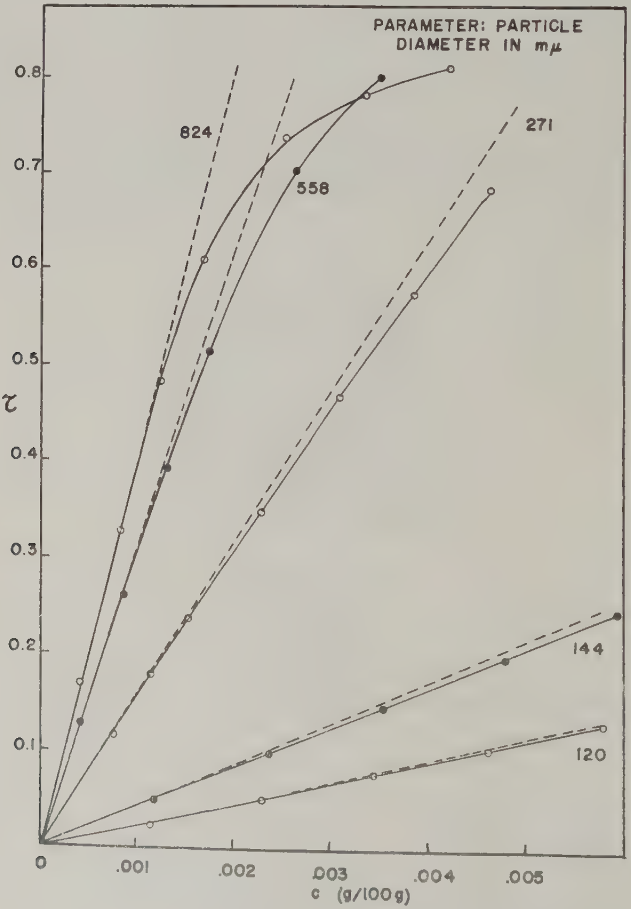

FIG. 5. Concentration dependence of turbidity.

III. EFFECT OF A COMBINATION OF BOTH SOURCES OF ERROR

On placing the phototube at *PT* in the absence of D_6, D_7, and D_8 and using an unblackened 10 cm. cell, a combination of the effects discussed in sections I and II is operative. They are reduced but still appreciable on inserting D_8 (aperture = 1 cm.). The result for the latter case is illustrated by the full curves in Fig. 5. The dashed lines refer to the data obtained under otherwise identical conditions except that the scattering cell was blackened and D_6 inserted. It is apparent that the value of the specific turbidity obtained directly from $\tau(c)$-plots under the former conditions is too small. For particle diameters in excess of 0.5 μ an additional complication arises because of the early departure of the τ vs. c curve from a straight line which makes the evaluation of $(\tau/c)_0$-values difficult.

IV. EFFECT OF THE SOLID ANGLE

Primary scattered light originating in the central cell section traversed by the primary beam also interferes with turbidity measurements. A central volume element dV' located near the exit end of the cell in Fig. 4 will emit a cone of scattered light defined by a solid angle, ω_0, reduced in the drawing to the two-dimensional angle 2ω, where ω is one-half of the vertex angle of the planar projection of the cone.[5] This angle and, with it, the amount of scattered light entering the photocell is determined by both the distance from the scattering volume element to D'_8 and the aperture of D'_8. Since the scattered light contains contributions of all the elements in the cylindrical volume illuminated by the primary beam, the integral effect is by no means negligible. This is evident from a comparison of photos 3*b* and 3*c*. The former was taken with D_6 in place. The latter was obtained on inserting an additional diaphragm D'_7 (not shown in Fig. 4; see Figs. 1 and 6) which reduced the aperture of the photocell to slightly less than the diameter of the primary beam (2 mm. at the exit end of the cell). The halo of scattered light visible in Fig. 3*b* is thus eliminated and the residual contribution of light scattered from dV' is reduced to that of a light cone whose base is defined by the circumference of the primary beam.[6]

The effect of the solid angle can be evaluated theoretically by integrating the contributions of all the volume elements which are in the path of the primary beam along the entire length of the cell, the limits of integration being furnished by the corresponding solid angles.[7] This possibility will be considered briefly at the end of this section. An alternate possibility of eliminating the effect consists of making a series of measurements with systematically varied solid angles and extrapolating the specific turbidities thus obtained to zero solid angle. This is the method selected here.

---

[5] ω and ω_0 are connected by the relation $\omega_0 = 2\pi\ (1 - \cos \omega)$.

[6] Since this residual contribution increases approximately with the square of the diameter of the primary beam, it is clear (see also section V) that it may cause serious errors if the cross section of the primary beam is much larger than in our apparatus.

[7] The solid angle considered here disregards the occurrence of refraction for the scattered beam leaving the cell. This has to be taken into account in eliminating the effect of the solid angle by theoretical corrections. This refraction is immaterial for the experimental elimination discussed below.

It is not possible to define a given experimental condition by a unique solid angle since both layer thickness and cross section of the primary beam are finite. An arbitrary standard must therefore be selected. The $(\tau/c)_0$-value extrapolated to $\omega_0 = 0$ is, of course, independent of the standard, but the slope of the $(\tau/c)_0$ vs. (ω_0) curve—which is also of interest—is meaningful only if the standard selected does not differ too much from the mean angle. Considering first the differential layer, $\pi r^2 dx$, at the exit window of the cell —r being the radius of the primary beam and x the length of the scattering cell (Fig. 6)—the angle 2ω and the corresponding actual solid angle ω_0 (steradians) were chosen as being most suitable. This angle defines strictly the contribution of dV', considered in Fig. 4, but in a very good approximation also that of all other elements in the differential layer since $2\omega \cong 2\omega'$. The solid angle decreases with increasing x ($x = 0$ at the exit window) so that the angle ω_0 is somewhat larger than the effective mean angle $\bar{\omega}_0$. Two alternate angles which might be considered (Fig. 6) exaggerate (angle α) or partially neglect (angle β) the contributions of the peripheral volume elements. The angle β, in addition, would be misleading because it approaches zero as the dimensions of the primary beam and D_8 become equal even though there is still a finite solid angle.

In order to study the quantitative effect of the solid angle upon the turbidity, the former was varied either by changing the distance between the scattering cell and the phototube from 2.3 to 29.0 cm. and/or inserting the additional diaphragm, D_7, already mentioned, thus changing the aperture of the phototube from 1.04 cm. $(D_8)(D'_8)$ to 0.4 cm. The layer thickness (10 cm.) and the aperture of D_6 were kept constant. The range

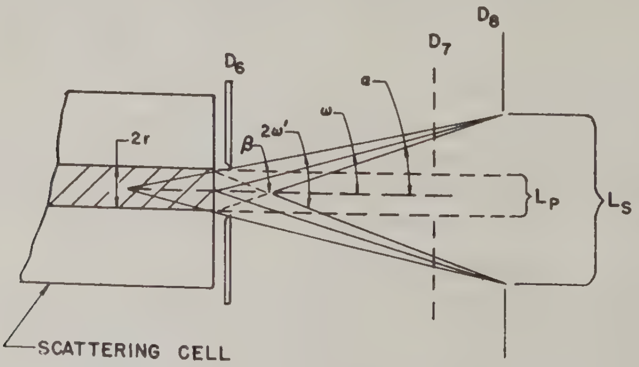

FIG. 6. Schematic definitions of the cone of scattered light.

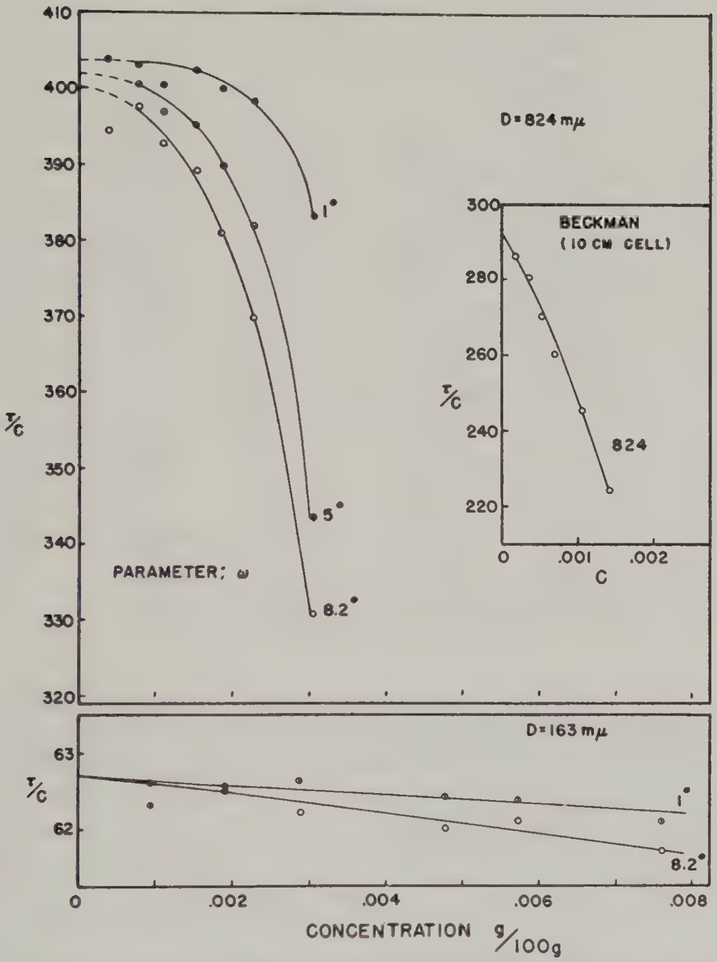

FIG. 7. Concentration dependence of the specific turbidity. Parameter: ω.

of ω-values covered in this manner is 8.2° to 0.4° ($\omega_0 = 64.5 \times 10^{-3}$ to 0.2×10^{-3} steradians).[8]

Figure 7 shows the variation of the specific turbidity with concentration for both a small and a large particle size latex. Numerical data for two intermediate particle sizes are given in Table I. The angle, ω, is the parameter in these experiments in which the effects discussed in sections I and II have been excluded. The data show that extrapolation to zero concentration is not sufficient to obtain both secure and correct $(\tau/c)_0$ data unless

---

[8] It will be seen from the following data that a reduction of the angle below the standard value adopted ($\omega = 1.0°$) is not necessary.

TABLE I

Variation of Specific Turbidity with ω and c

Sample 44B; D = 620 mμ; λ_0 = 5461A; c: g./100 g.

$c \times 10^3$	ω: 0°	0.4°	1.0°	5.0°	8.2°
0	(326.5)[a]	(326.5)	(326.5)	(323.5)	(321.0)
0.3685	(318.5)	318.6	318.3	319.7	319.9
0.7370	(325.0)	324.7	325.1	324.4	321.4
1.105	(326.5)	326.4	326.1	323.0	321.0
1.474	(327.0)	326.6	327.7	324.8	320.2
1.842	(325.5)	325.4	325.6	320.2	317.2
2.211	(325.5)	325.2	325.1	318.5	315.1
2.948	(322.5)	321.8	320.9	312.4	304.4
3.685	(315)	—	311.3	294.2	280.6
Sample 44A; D = 492 mμ					
0	(272)	(272.0)	(272.0)	(269.2)	(267.5)
0.6134	(273.5)	273.2	273.5	267.9	265.0
1.227	(272.5)	272.4	271.9	269.7	268.1
1.840	(270.5)	269.6	270.0	267.9	266.8
2.454	(271)	270.7	271.4	269.3	266.6
3.067	(273)	272.9	272.4	268.7	264.6
3.680	(271)	271.1	272.0	265.7	260.5

[a] Values in parentheses represent extrapolated values.

either particle size or solid angle is small enough. Additional extrapolation to $\omega_0 = 0$ may, therefore, be indicated. If the particle diameter is not less than 0.5 to 0.6 μ, it is of advantage to combine both types of extrapolation, by plotting (τ/c) as a function of both c and ω_0, as shown, for one example, in Fig. 8. Simplified plots, limited to $c = 0$, are given in Fig. 9 for five samples of systematically varied D. An interesting and practically helpful result is the fact that the limiting specific turbidity, $(\tau/c)_0$, varies linearly with the solid angle, ω_0, within the range of angles investigated.[9] This facilitates safe extrapolations to $(\tau/c)_0$ at $\omega_0 = 0$ from measurements at only a few solid angles. The linearity indicates that the small section of the radiation envelope pertinent to the angles investigated can be approximated to a section of the surface of a sphere, as one would expect it at small ω_{00}-values. It is quite certain that this linearity cannot be expected to hold for ω-values much larger than those considered here.

Figure 9 shows that the effect of the solid angle upon $(\tau/c)_0$ is negligible for diameters less than 200 mμ (for λ_0 = 5461 A. and a relative refractive index $m = 1.20$) if $\omega \leqslant 8.2°$. For larger particles, the error may increase to 2% (cf. parenthetic values in Table I). The effect of the solid angle in-

---

[9] This is the reason why it is not necessary here to use, instead of ω_0, the solid angle corrected for refraction[7], ω_{00}. At finite concentration, (τ/c) does not vary linearly with ω_0.

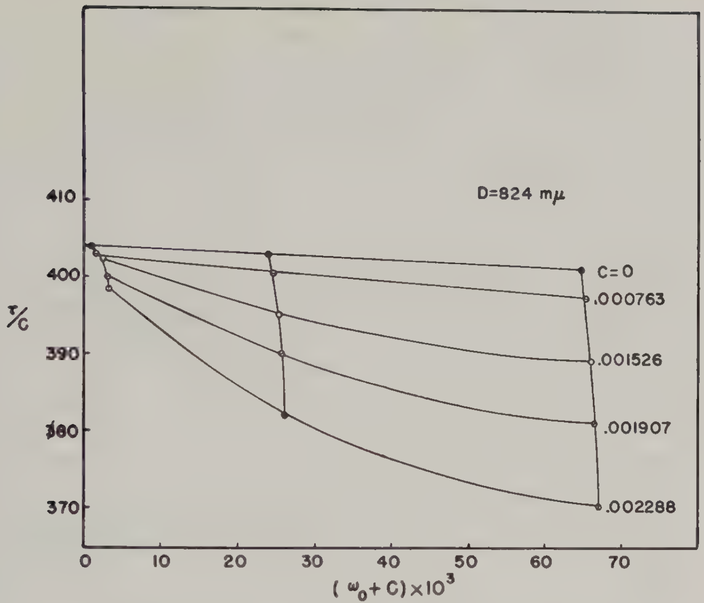

FIG. 8. Variation of specific turbidity with solid angle and concentration.

creases rapidly with concentration, more so the larger the particle size. For $D = 620$ mμ and $c = 0.002948$ g./100 g., (τ/c) decreases by 5.4% as ω is varied from 0.4° to 8.2°. Unless ω is sufficiently small, simple extrapolation of τ/c to $c = 0$, at constant solid angle, will therefore not only yield inaccurate τ/c values with such large particles but the extrapolation to these inaccurate values will be very difficult and insecure, as already seen from Fig. 7.

Figure 9 and Table I show, furthermore, that at an ω-value of 1° the systematic error involved in $(\tau/c)_0$ is hardly larger than the nonsystematic error involved in $(\tau/c)_0$ measurements. It is, therefore, safe to dispense with $(\tau/c)_0$ vs. ω_0 extrapolations upon carrying all measurements out at this angle. It is for this reason that an angle ω of 1° was used as a standard for all measurements reported in a preceding publication (2). It is quite clear, however, that the "safe" solid angle will depend to some extent upon the particular apparatus used.

Table II summarizes in columns 2 and 3 the error in $(\tau/c)_0$ on using the ω-angles 5° and 8.2° at systematically varied particle sizes. It compares this error with the theoretical error (3) calculated for $m = 1.20$ by means of the procedure outlined earlier in this section. Although theoretical data are not available at present for larger diameters, it can be seen that the observed and expected effects of the solid angle agree within the limits of experimental error even without corrections for refraction.

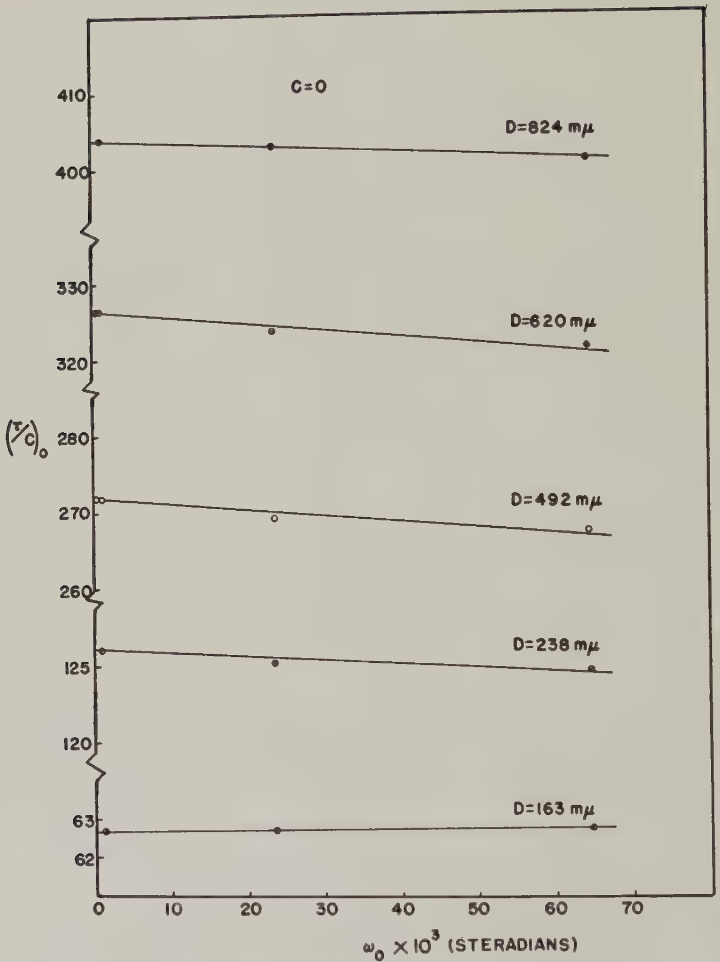

FIG. 9. Variation of the limiting specific turbidity with the solid angle, ω_0.

TABLE II

Per cent Error in $(\tau/c)_0$ *for* $\omega = 5.0°$ *and* 8.2°

D (mμ)	Exptl.		Calc.	
	5.0°	8.2°	5.0°	8.2°
163	0	0	0.2	0.5
238	1.0	1.5	0.4	1.0
492	2.8	4.5	—	—
620	3.0	5.5	—	—
824	1.5	3.5	—	—

V. TURBIDITY MEASUREMENTS WITH THE BECKMAN SPECTROPHOTOMETER

In order to demonstrate and evaluate the effect of laterally scattered stray light, of the corona at the exit window of the scattering cell, and of the solid angle of the scattered beam the operating conditions with our apparatus had to be made purposely unfavorable. The extent to which this could be done was limited. With some of the commercially available apparatus, the normal operating conditions are more unfavorable than the extreme conditions established above. In addition, other unfavorable features may be found such as appreciable width and pronounced divergence of the primary beam. It was therefore desirable to supplement the preceding studies by a few exploratory experiments with a suitable commercial apparatus. To that effect, a series of experiments were carried out with a Beckman spectrophotometer model DU. This instrument, whose satisfactory performance for routine absorption measurements is recognized, has been and is being used frequently for turbidity measurements also, and it is, by virtue of its basically sound construction, potentially more suitable for them than some apparatus specifically built for light-scattering work. The selection of the Beckman instrument for the following experiments was governed exclusively by the fact that it was easily accessible to us. A thorough critical test of other commercial instruments used or constructed for light-scattering work would be desirable but is not intended by the authors.

The Beckman spectrophotometer was used at 5461 A. with either conventional 1-cm. cells of square cross section or blackened 10-cm. cylindrical cells. A slit width of 0.045 mm. was used in the former case and 0.08 mm. in the latter. The divergence of the primary beam in the Beckman is defined by an angle ω_p of approximately 2° and the angle, ω, of the scattered beam is approximately 35° and 30° for 1 cm. and 10 cm. cells, respectively.[10]

Figure 10 shows the variation of the apparent specific turbidity $(\tau/c)_a$ with concentration for various particle diameters using the standard 1-cm. cells without excluding stray light and corona. The slope of the $(\tau/c)_a$ vs. C curve increases with decreasing concentration, more so the larger the particle size. This makes a secure extrapolation of $(\tau/c)_a$-values to zero concentration more difficult, the larger the particles. On using the blackened 10-cm. cell with an exit diaphragm slightly larger than the primary beam (0.3 cm.^{2}) (elimination of stray light and corona) the slope changes in exactly the opposite direction (insert to Fig. 7). It is noteworthy that in the latter, more favorable, case the apparent specific turbidity still changes 17.4% over a concentration range from 0 to 0.00114. Under the standard conditions used in this laboratory with our light-scattering apparatus ($\omega = 1°$) the change over the same concentration range was 0.9% (Fig. 7).

Far more serious than the difficulties of extrapolating (τ/c)-data to $c = 0$ is the fact that these extrapolated values are incorrect. This is shown by Fig. 11, which gives the per cent deviation of the extrapolated Beckman $(\tau/c)_a$-data relative to the true data (2) as a function of particle diameter.

[10] Since the aperture of the photocell is rectangular in the Beckman instrument, no unique definition of ω is possible. The ω-values indicated represent the mean between two values.

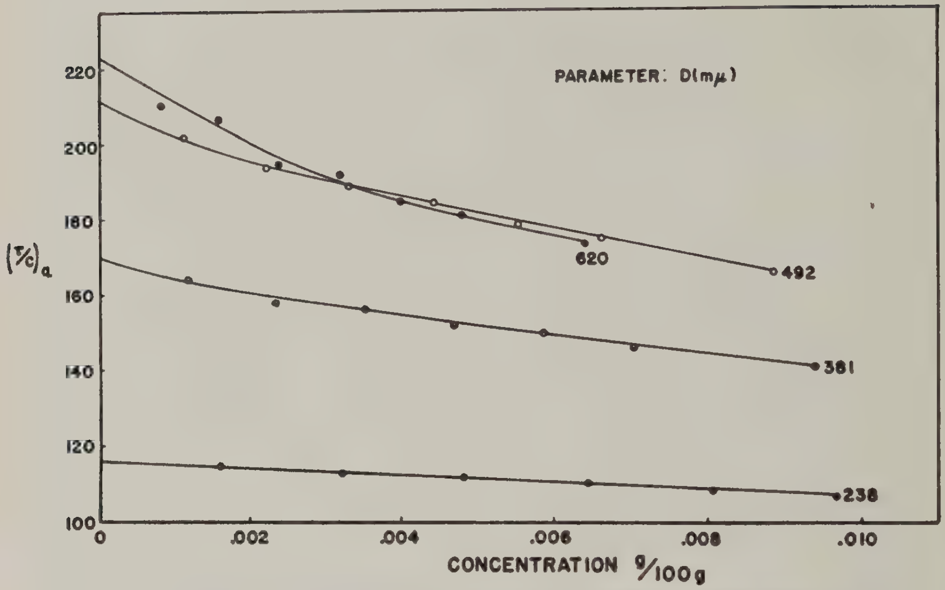

FIG. 10. Concentration dependence of the apparent specific turbidity obtained with a Beckman spectrophotometer.

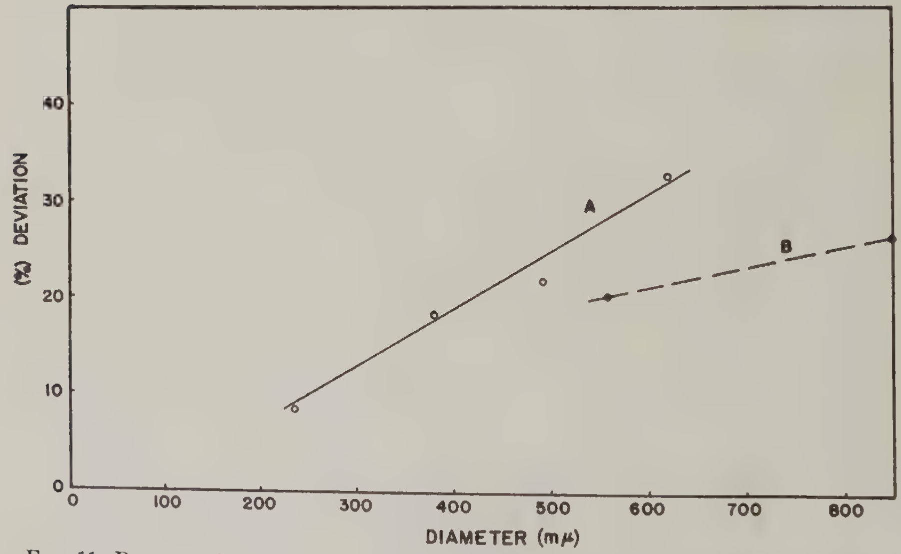

FIG. 11. Per cent deviation of $(\tau/c)_a$ from $(\tau/c)_0$ as a function of particle size. *A*, 1-cm. unblackened cell; *B*, 10-cm. blackened cell.

It is apparent that the data obtained and, implicitly, the particle diameters derived therefrom, have no quantitative significance except for particle diameters <150–200 mμ no matter whether the 1-cm. cell is used, as is, or the 10-cm. cell is used after blackening and attachment of the exit window diaphragm. The bearing of the results in Fig. 11 upon the evaluation of light-scattering and particle size data recorded in the literature and obtained with an unmodified Beckman is obvious.

The use of the 10-cm. cell with the specified precautions eliminates all the discussed sources of error except those connected with the rather large solid angle of the scattered beam and with the large width and divergence of the primary beam. Extrapolation, on the basis of the straight-line relationship illustrated in Fig. 9, would tend to indicate that the major source of error among the three possible ones mentioned is the large solid angle of the scattered beam. Since extrapolation to such large angles is not safe and the ω-values are not well defined[16]; a definite conclusion is, however, not possible.

Obviously, the Beckman spectrophotometer and, similarly, other commercial instruments suffering from deficiencies can be modified to allow their use for measurements yielding data of only moderate deviations from the true $(\tau/c)_0$ value. The investigation described in this paper should provide the key to such modifications, of which part pertain to the modifications of absorption cells to make them suitable for scattering work and part to modifications of the optical features of the apparatus proper. With regard to the latter, attention may be drawn to a partial remedy introduced by Sliepcevich (4).

SUMMARY

The most important sources of error in turbidity measurements are discussed and their quantitative effect is studied by suitable experiments. Particular attention is paid to the effect of scattered straylight, of the "corona" at the exit of the scattering cell, and of the solid angle of scattered light reaching the photocell. Relatively simple precautions are described by means of which the two former effects can be eliminated, and a relatively simple procedure is proposed which allows one to obtain turbidity values pertinent to zero solid angle. It is shown that errors as large as 30% may result if instruments which are perfectly suitable for ordinary absorption measurements are used for turbidity measurements without proper modifications and precautions.

REFERENCES

1. HELLER, W., AND PANGONIS, W. J., *J. Chem. Phys.*, in press.
2. TABIBIAN, R., HELLER, W., AND EPEL, J. N., *J. Colloid Sci.* **11,** 195 (1956).
3. PANGONIS, W. J., AND HELLER, W., *Phys. Rev.* **90,** 345 (1953).
4. GUMPRECHT, R., AND SLIEPCEVICH, C., *J. Phys. Chem.* **57,** 90 (1953).

JOURNAL OF COLLOID SCIENCE **12,** 40–52 (1957)

THE DIFFUSION OF SODIUM AND IODIDE IONS AND OF UREA IN CLAY PASTES[1]

A. H. Bloksma[2]

Laboratory of Agricultural Chemistry, Agricultural University,
Wageningen, Netherlands

Received February 20, 1956; revised July 30, 1956

Abstract

By means of layer analysis and the use of radioactive isotopes the author measured the rates of self-diffusion of sodium and iodide ions in clay-water pastes. In the same pastes the diffusion rates of sodium iodide and of urea were measured. The clays used were montmorillonite and kaolinite having sodium ions as adsorbed ions.

By comparison of the diffusion rate of iodide ions with that of urea it could be made plausible that the retardation of the iodide ions in these pastes is due to steric hindrance; the mobilities of the iodide ions, as calculated from these data, were approximately 0.4 to 0.5 times as large as the mobilities in aqueous solutions. Assuming that the dissolved sodium ions in the pastes are retarded in the same degree as the iodide ions one obtains for the mobility of the adsorbed sodium ions in the montmorillonite pastes 0.37 and in the kaolinite pastes 0.28 of their mobility in aqueous solutions. On the basis of these experiments the retardation of the adsorbed ions cannot be divided into a part caused by the geometry of their diffusion path and a part caused by forces exerted upon them by the wall charges.

Introduction

Recently Overbeek has pointed out that for a correct interpretation of the Donnan-e.m.f. knowledge of the mobilities of all particles in the system is necessary (1). The mobilities of ions in solution are rather well known. The mobilities of the colloid particles can easily be determined by electrophoresis. The present study is an attempt to obtain data about the mobilities of ions adsorbed on the clay minerals montmorillonite and kaolinite; it forms part of an experimental test of Overbeek's treatment of the Donnan-e.m.f. with suspensions of these minerals (2).

Mobilities of ions may be derived from diffusion rates and from electric conductances; Spiegler and Coryell (3) demonstrated for some colloidal systems the agreement between the electric and diffusion measurements.

---

[1] This paper is based on a portion of a thesis, entitled "Het suspensie-effect," submitted to the University of Amsterdam, March, 1955. Details can be found in Chapter 3 of this thesis (in Dutch).

[2] Present address: Cereals Dept. of the Centr. Inst. for Nutrition Research T.N.O., Wageningen, Netherlands.

From the conductometric titrations of silver iodide sols (4), the electric conductances and transport numbers in these sols (5), diffusion rates in different ion exchangers (3, 6, 7), rates of ion exchange (8), and the electric resistance of ion exchangers in the form of plugs or membranes (3, 9, 10) t is concluded that adsorbed ions have a lower mobility than the same ions n the dissolved state. The quantitative results of these investigations, however, cannot be applied to the colloids used in the present study as a consequence of differences in geometry and in ion-exchanging properties. Therefore new experiments were needed for quantitative data about the mobilities of ions adsorbed on the clay minerals mentioned.

Because of their simplicity diffusion measurements were preferred to measurements of the electric conductance. The measurement of self-diffusion with radioactive isotopes allows the determination of single ion mobilities. Diffusion measurements in suspensions are made difficult by the complications of sedimentation, convection currents, and mechanical vibrations; to minimize these the measurements have been made in clay pastes. Sodium iodide has been chosen as salt since it is a uni-univalent electrolyte like potassium chloride which is generally used in salt bridges and since sodium and iodine have easily obtainable radioactive isotopes. Experiments were also carried out with urea in order to test the applied theory.

THEORY

Let the mobility w_i of an ion i be defined as the velocity of the ion in its environment under the influence of an external force of 1 dyne. Then in sufficiently dilute solutions the relation between the mobility, the self-diffusion coefficient D_i, and the equivalent conductance λ_i of the ion is (11):

$$D_i = kTw_i = \frac{\lambda_i RT}{|z_i| F^2} \qquad [1]$$

k is Boltzmann's constant, R the gas constant per mole, T the absolute emperature, F the Faraday, and z_i the valency of the ion).

In porous materials diffusion is affected by adsorption and by the geometry of the diffusion path.

It is supposed that allowance can be made for the geometry of the diffusion path by adding a labyrinth factor[3] h to the second term of Eq. [1]:

$$D_i = kTw_i h. \qquad [2]$$

f the diffusion coefficient is defined by Eq. [5] h is not proportional to the atio of the volume of the pores to the total volume (pore fraction S) (14);

---

[3] The term labyrinth factor has been proposed by K. E. Ziemens (12). The formaion resistivity factor used by petroleum production engineers corresponds with /Sh (13).

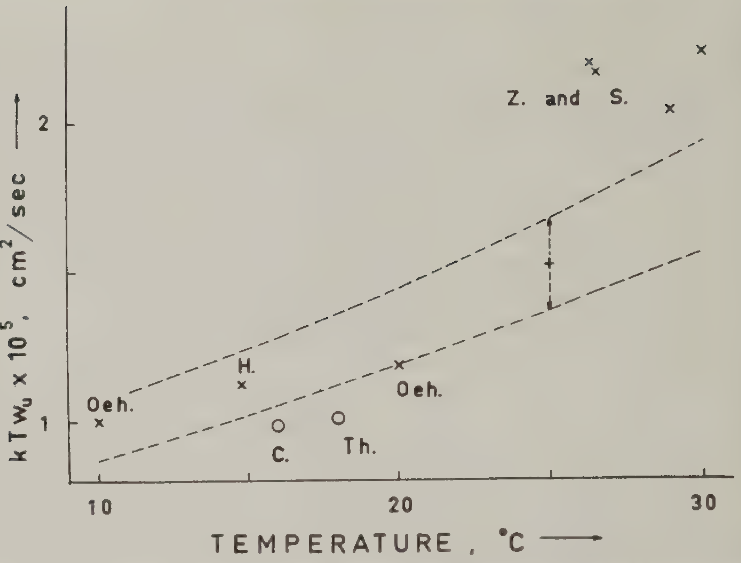

Fig. 1. The diffusion rate of urea in water (20, 21). × = 0.2 M; O = other con centrations (C.: unknown; Th.: 0.04 M); + = used by the present author. The dashe lines correspond with an activation energy of 5 kg.-cal. per mole.

the labyrinth factor may be considered as the mean value of the square c the cosine of the angle between the channels through which the diffusio occurs and the direction of overall diffusion (*cf.* 6, 15). De Vries has calculated the labyrinth factor h for unarranged assemblies of oblate spheroid and has shown how it is dependent on the eccentricity of the particles an on the pore fraction S (16)[4].

Equation [2] is supposed to be valid for the diffusion of urea (D_u an w_u) and the self-diffusion of iodide ions (D_- and w_-) in clay pastes in so fa as these molecules and ions are not adsorbed. Under these conditions th same labyrinth factor h may be expected to describe both types of diffusio

In the case of ion adsorption the following argument may be set up i order to allow for the influence of adsorption on the diffusion rate. The cla pastes with which the experiments have been carried out contained sodiu ions adsorbed on the clay mineral (say s per cm.^{3} of paste) and sodium io belonging to the sodium iodide in solution (say n per cm.^{3}). The mobilit of the ions in solution is w_+. The mobility of the adsorbed ions is not know moreover their labyrinth factor is expected to be different from h. Tl present experiments do not allow a division of the retardation of tl adsorbed ions into a part caused by the geometry of the diffusion path ar part caused by forces exerted upon them by the electric charges of the olloid particles. Therefore a factor g is assigned to them which is treated s a labyrinth factor. It is supposed, however, to describe the joint effects f both retarding causes. A determination of the factor g is sufficient for ne object proposed; a division into two factors corresponding to the two fects mentioned above is not necessary (see below). Since ion exchange a fast process compared with diffusion one may consider all sodium ions uring a fraction of time $s/(n + s)$ as having the properties of adsorbed ns and consequently an apparent labyrinth factor g; during the re- ainder of time they may be considered to have a labyrinth factor h equal o that of the iodide ions. Then the coefficient of self-diffusion of the odium ions is given by:

---

[4] It should be realized that in the graphs of De Vries the product Sh of the po fraction and the labyrinth factor is plotted against the pore fraction itself.

$$D_+ = kTw_+(nh + sg)/(n + s). \qquad [3]$$

When calculating the diffusion rate of the salt sodium iodide $D_\pm$ one has o take into account a possible liquid junction potential that accelerates ne slower and retards the quicker ions resulting in a net zero transport of ectricity. Assuming ideal behavior of the iodide ions and taking $n + \gamma s$ r the activity of the sodium ions[5], one obtains:

$$D_\pm = kT \cdot \frac{2(nh + sg)w_+ w_-}{(nh + sg)w_+ + nhw_-} \cdot \frac{2n + \gamma s}{2n + 2\gamma s} \cdot h. \qquad [4]$$[6]

In real solutions allowance should be made for the change of the activity oefficient with the concentration (11) and in the case of ions for relaxation henomena (18) and electrophoresis (11). The magnitude of these effects estimated to be maximally a few per cent in the solutions used. Therefore, ey may be neglected in respect of the experimental error.

The most reliable values for the mobilities of the ions in solution are lculated from the equivalent conductances by means of Eq. [1]. Using miting values one obtains from the data in the literature (19): $kTw_- =$ 05 and $kTw_+ = 1.33 \times 10^{-5}$ cm.²/sec. at 25°C.

Urea concentrations in the pores of the pastes have been about 0.2 M. iffusion velocities of urea taken from the literature (20, 21) and inter- olated or extrapolated to this concentration as far as possible are given in ig. 1. The results of Zuber and Süllmann (Z. and S., ref. 21) are considered o be less reliable because these investigators used an impure sample and und an exceptional concentration dependence. Moreover their figures together with the data obtained by other investigators at lower temperatures lead to an improbably high value for the activation energy, viz., 9 kg.-cal. per mole; the upper limit for diffusion in aqueous solutions is about 5 kg.-cal. per mole (22). In Fig. 1 the diffusion velocity at 25°C. used by the present author is indicated: $kTw_u = 1.51 \times 10^{-5}$ cm.^{2}/sec. ± 10%

---

[5] This assumption corresponds to a mean activity coefficient of the salt equal to $\sqrt{1 + \gamma s/n}$; γ is comparable with the "fraction active" as used by Marshall (17).

[6] Having finished this study the author became acquainted with a more extensive eoretical treatment of the diffusion of electrolytes through ion exchanging media Mackie and Meares (15). Equation [4] can be proved to be a special case of their uation (3.9).

Measurements of D_u and D_- in the clay pastes provide two ways of estimating the labyrinth factor h by means of Eq. [2]. This factor h, D_+, and n/s being known, Eq. [3] permits calculating g. From these quantities and $D_\pm$ one can estimate γ by means of Eq. [4].

EXPERIMENTAL PART

Apparatus. Diffusion constants were determined by layer analysis. The construction of the apparatus was based on that of Cohen and Bruins (23) it is composed of a pile of horizontal, circular disks of 8.5 cm. radius mad from a phenolformaldehyde resin. The disks can be turned separatel around a common vertical steel axis through their centers. They are presse one against another by means of a spring. In all disks at a distance of 6. cm. from the axis a number of vertical cylindrical holes are drilled; the are placed on a circumference at distances of 20° or alternately 20° and 40 (Fig. 2).

The apparatus can be used either with two disks of 1.5 cm. thickness o with four disks of 1.0 cm. thickness between an upper and a lower disk tha are the same in both cases. Figs. 3 and 4 illustrate the way the experiment are carried out. In stage 1 the holes are filled with two pastes a_1 and a_2 these pastes are made identical except as to the concentration of the diffus

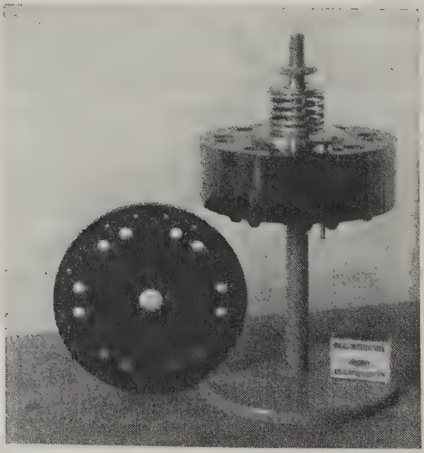

FIG. 2. Assembled diffusion apparatus and a single disk with holes at distanc of alternately 20 and 40°.

ing component. When the disks are turned to stage 2 the two pastes come into contact one with another and the diffusion process starts; moreover the excess of paste a_2 is separated from the desired volume of this paste. The disks are immediately turned to stage 3. Now the room in which the diffusion occurs is isolated completely; moreover the excess of both pastes can be removed from the apparatus. After a chosen time the disks are turned to stage 4; the diffusion is terminated. Paste a_1 (in the case of two disks) or halves of both pastes (in the case of four disks) are taken out for analysis; in stage 5 the remaining pastes are taken out for analysis.

The apparatus permits six experiments of this type to be performed at the same time.

Materials

The pastes were prepared of a montmorillonite from Osage (Wyoming) and a kaolinite from Drybranch (Georgia). Their identity was confirmed by x-ray diffraction, differential thermal analysis, and electron micrographs. Particles larger than 50 microns were removed before use. The remainder of the montmorillonite contained 90% by weight of particles smaller than 1 micron; for the kaolinite this was 52%. They were purified by oxidation with hydrogen peroxide, by washing with 0.05 N hydrochloric acid and subsequently with distilled water, and by electrodialysis. Then the suspensions were adjusted to a pH of between 6.5 and 7.0 by means of 790 ± 20 (montmorillonite) or 55 ± 4 (kaolinite) microequivalents sodium hydroxide per gram mineral. The appropriate amounts of sodium iodide and urea (see below) were added. By evaporation of the water a paste of the desired mineral content was obtained. The different pastes needed for one experiment were made up to the same weight of mineral per gram of total paste. The pastes were carefully made homogeneous.

Methods

In most experiments the mean value of the quotient n/s in the combined pastes was chosen equal to 1/2. For the determination of $D_{\pm}$ one paste with $n/s = 1$ was joined to one paste without sodium iodide ($n/s = 0$). For the determination of D_{-} and D_{+} two chemically identical pastes were used; in one of them part of the sodium or iodide ions was replaced by radioactive ions (Na^{22} or I^{131}). For the determination of D_u both pastes were provided with sodium iodide according to $n/s = 1/2$; besides one of them contained 2 millimoles urea per gram montmorillonite or 0.2 millimole per gram kaolinite.

All experiments were carried out at 25° ± 1°C.

The mineral content of the pastes had to be chosen in order to obtain the proper consistency. Pastes which are too stiff cannot be put into the holes

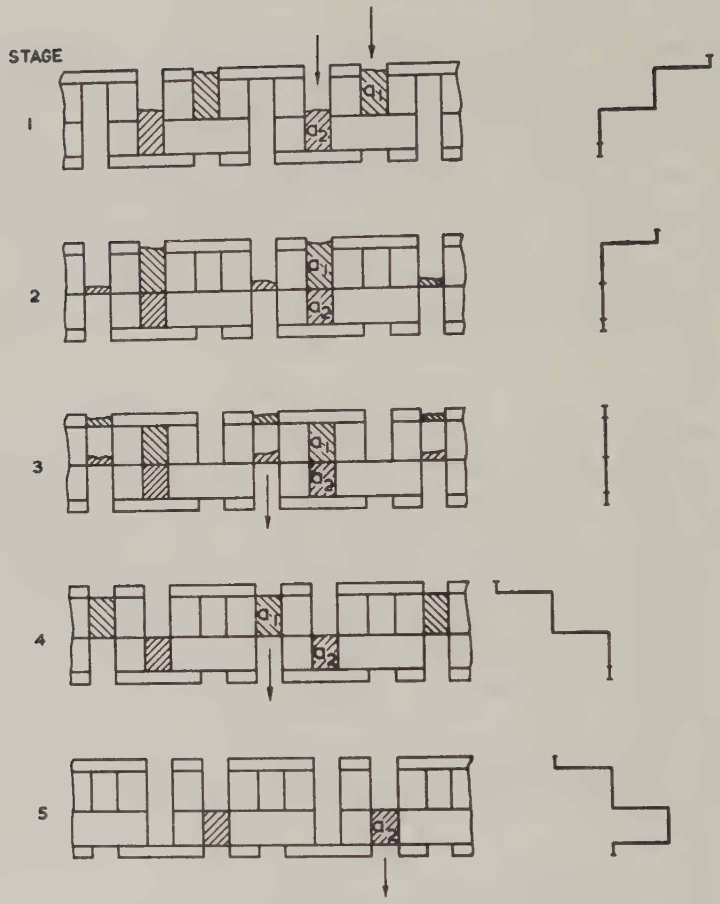

FIG. 3.

FIGS. 3 & 4. Schematic section of the diffusion apparatus along the vertical cylinde through the holes. Fig. 3: using two disks; Fig. 4: using four disks, in both case plus the upper and the lower one. The figures on the right-hand side of the section indicate the way in which the disks are turned; they are formed by some vertica lines, one on the cylindrical surface of each disk, and placed in such positions as t form a straight line together in stage 3. Arrows indicate the filling of the apparatu (stage 1), and the removal of excess material (stage 3) and of the samples to be ana lyzed (stages 4 and 5).

without including air bubbles. In pastes with too low a mineral conten settling of the mineral during the diffusion was a disturbing factor. Th mineral content of the pastes could not therefore be varied arbitrarily.

The use of thinner disks seems advantageous. It is true that then chem cal analyses would have to be abandoned except in the cases of very hig values of n/s. On the other hand, the filling of the apparatus will be easi and the diffusion times may be chosen shorter.

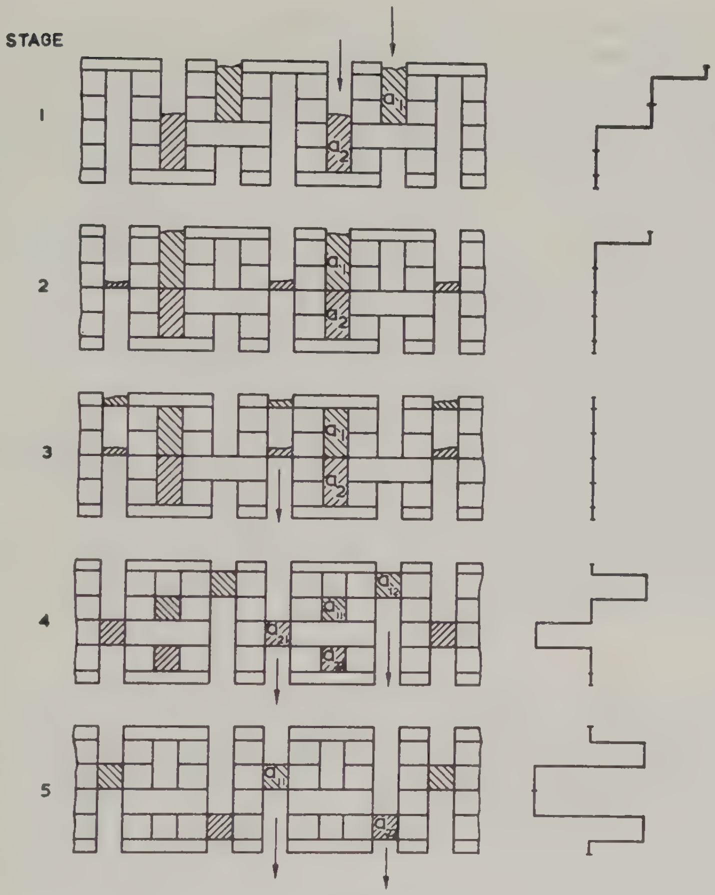

FIG. 4.

For analysis the pastes were shaken with sufficient neutral salt solution to cause flocculation and complete ion exchange. After sedimentation the supernatant liquid was analyzed. Iodide was titrated potentiometrically with silver nitrate. Sodium was determined by means of a flame photometer and urea according to Kjeldahl. The radioactivity was determined by evaporation of the supernatant liquid and measuring the specific activity of the solid by means of a bell-jar type Geiger-Mueller-counter.

Evaluation of the Diffusion Coefficient from the Analytical Results

If the diffusion coefficient is not dependent on the concentration c, diffusion can be described by the equation

$$\frac{\partial c}{\partial t} = D \frac{\partial^2 c}{\partial x^2} \qquad [5]$$

and the appropriate boundary conditions. The concentration c in Eq. [5] is the amount of diffusing substance per unit volume paste.

Solutions of [5] with the boundary conditions of restricted diffusion are to be found in textbooks (24). Integration and numerical evaluation of a rapidly converging series furnished tables of the amount of diffusing substance in each of the holes after diffusion has proceeded for a time t as dependent on the dimensionless quantity Dt/l^2 in which l denotes half of the total thickness of the two or four disks. A part of these tables could also be calculated from Stefan's tables (25); comparison of some figures proved the identity of the results of both methods.

By the aid of these tables and graphical interpolation values for Dt/l^2 are to be obtained from the analytical results. The length l and the time t being known, D may be calculated.

An analysis of the influence of the analytical errors on the accuracy of the diffusion constant determined led to the conclusion that their influence was slightest when Dt/l^2 had a value between 0.35 and 0.45. Many other sources of error, however, steadily increase with increasing diffusion time. Therefore, in most experiments the diffusion time was chosen to be shorter than corresponding to the above value.

RESULTS AND DISCUSSION

Table I gives the experimental results. The mineral contents of the pastes and the quotients n/s in the headings have been obtained by analysis of the starting materials; the values mentioned are the means of a series of determinations on slightly different pastes used in successive experiments. The pore space S was calculated from the mineral content assuming a density of 2.65 g./cm.^{3} for both minerals (26). Columns 3, 6, and 9 contain the experimental diffusion velocities obtained in the number of single experiments indicated in columns 4, 7, and 10.

From the experimental diffusion velocities the factors h, g, and γ are calculated as indicated in the last paragraph of "Theory." The set of values that fits best into the combined experimental results is given in Table II. Afterwards the diffusion velocities in columns 2, 5, and 8 of Table I have been obtained by substituting the factors from Table II into Eqs. [2] to [4].

The results of the experiments carried out with four disks permit a test of the assumption that the diffusion coefficients are independent of the concentration. No evidence of a concentration dependence of any of the coefficients was found, although Eq. [4] predicts the diffusion coefficient of sodium iodide $D_{\pm}$ to be dependent on n/s in a rather complicated way. The test, however, is rather insensitive to this type of concentration dependence.

The agreement between the calculated and the experimental values in Table I may be improved by certain refinements of the theory as, e.g., taking into account relaxation phenomena and electrophoresis in the diffusion of the ions and sodium iodide.

TABLE I

Results of the Diffusion Measurements
Diffusion Coefficients Are Given in 10^{-5} cm^2./sec.

Mineral	Montmorillonite			Montmorillonite			Kaolinite		
Mean NaI conc.	$n/s = 1.00$			$n/s = 0.49$			$n/s = 0.53$		
Mineral cont. (% by weight)	4.0			6.2			56		
Pore fraction	$S = 0.985$			$S = 0.976$			$S = 0.68$		
Diffusing substance 1	D calc. 2	D exptl. 3	No. expts. 4	D calc. 5	D exptl. 6	No. expts. 7	D calc. 8	D exptl. 9	No. expts. 10
urea Eq. [2]	—	—	—	0.74	0.75 ±0.13	3	0.62[a]	0.56 ±0.05	5
I^--ions Eq. [2]	—	—	—	1.00	0.97 ±0.12	2	0.84	0.83 ±0.10	2
Na^+-ions Eq. [3]	0.58	0.51 ±0.09	3	0.55	0.56 ±0.04	8	0.43	0.41 ±0.02	9
Sodium iodide Eq. [4]	0.98	0.95 ±0.09	3	1.06	1.08 ±0.06	8	1.01	1.11 ±0.09	26

[a] 0.55 after correction for adsorption (see text).

TABLE II

Constants To Be Substituted into Eqs. [2] to [4] for an Adequate Description of the Experimental Results

	Montmorillonite	Kaolinite	Uncertainty (%)
h	0.49	0.41	5–10
g	0.37	0.28	5–10
γ	0.2	0.0	100

Probably the diffusion of urea in the kaolinite pastes is retarded by adsorption. The author made a crude determination and found an adsorption of 5 micromoles per gram mineral from a 0.05 M solution for both minerals in accordance with Conrad's results with a fine sandy loam (27). Assuming a linear adsorption isotherm and a mobility equal to zero for the adsorbed urea molecules one calculates a retardation of the diffusion by 11 % in the kaolinite pastes but by only 0.5 % in the montmorillonite pastes (cf. 14); application of this correction improves the agreement markedly. So it seems probable that the retardation of the iodide ions is a proper measure for the labyrinth factor for all dissolved ions and molecules owing to the particular geometry of their diffusion path as prescribed by the impenetrability of the mineral particles.

A comparison of the values of the pore fraction S and the labyrinth factor h obtained and the graphs of De Vries (16) permits an estimation of the eccentricity of the oblate spheroids that may serve as a model for the mineral particles in the pastes; the axial ratios are greater than 100 for montmorillonite and a little smaller than 10 for kaolinite. These results confirm the platelike shape of the particles. Grim records dimensions of clay minerals obtained by electron micrographs with shadow-casting (28). From these dimensions one estimates for the ratio of the diameter and the thickness of the plates 10 to 100 for montmorillonite and 2 to 6 for kaolinite. The electron micrographs of the kaolinite actually used, however, yielded values between 10 and 20 for the better developed crystals. It should be realized that application of the graphs of De Vries may furnish too low values for the axial ratio since he neglects the parallel orientation of the platelike particles to be expected in a paste.

The mobility of the adsorbed sodium ions in the montmorillonite pastes used is a fraction $g = 0.37$ of that in aqueous solutions provided that the solved sodium ions are retarded to the same extent as the iodide ions in the pastes; for the kaolinite pastes the factor g equals 0.28. It is emphasized that the apparent labyrinth factor g describes the geometry of the diffusion path of the adsorbed ions as well as the effect of the forces exerted upon them by the electrical charges of the colloid particles.

For the object proposed, knowledge of the mobilities of adsorbed ions in suspensions is needed. If a paste is diluted into a suspension the labyrinth factor h for the particles in solution approaches the limiting value 1. If, however, in the suspension the motion of the adsorbed ions is restricted to the same surfaces of the colloidal particles as it is in the paste the factor g for the adsorbed ions may be expected to remain constant upon dilution independent of the shape of these surfaces. As a consequence of the frequent transitions between the solved and the adsorbed states the above conclusion holds irrespective whether the surfaces touch one another or not. Therefore, the values of g determined by diffusion experiments in pastes may be applied to dilute suspensions too. In suspensions a complication arises if the colloidal particles show a directed motion as in the case of electrophoresis. In a following paper (2) in which the results of the present diffusion experiments will be applied to the comprehension of the Donnan-e.m.f. allowance will be made for this effect.

The value for γ reported in Table II is in agreement with Marshall's results (17) in the case of montmorillonite but not in the case of kaolinite. Marshall, however, calculated his fractions active from e.m.f.-measurements in salt-free suspensions instead of in salt-containing pastes.

An extension of the measurements reported here with other ions adsorbed is desirable. The results of Spiegler and Coryell (3) and of Heymann and O'Donnell (9) suggest that g is lower for polyvalent ions and for the ions from the subseries of the periodic table; probably a relation exists between the displacing power of the ions in exchange reactions and their retardation in the adsorbed state. Especially data about the mobility of adsorbed calcium ions are wanted (2). Experiments with ratios n/s varying between 0 and 1/2 may provide a test of the theory used.

ACKNOWLEDGMENTS

The author is indebted to Miss C. v. d. Scheer for making the electron micrographs, to Dr. J. Ch. L. Favejee for the x-ray analyses, and to Mr. R. Arnold Bik for the differential thermal analyses. Dr. A. Nijenhuis helped with mathematical problems. Mrs. H. C. M. Schneider-Pieters and Mr. J. G. J. Kok carried out many of the experiments.

REFERENCES

1. OVERBEEK, J. TH. G., *J. Colloid Sci.* **8,** 593 (1953).
2. BLOKSMA, A. H., *J. Colloid Sci.*, in press.
3. SPIEGLER, K. S., AND CORYELL, C. D., *J. Phys. Chem.* **57,** 687 (1953).
4. OVERBEEK, J. TH. G., "Electrokinetic phenomena," in H. R. Kruyt, ed., "Colloid Science," Vol. 1, p. 239 et seq. Elsevier, Amsterdam, 1952. BRUIJN, H. DE, AND OVERBEEK, J. TH. G., *Kolloid-Z.* **84,** 186 (1938). OS, G. A. J. VAN," Ionenuitwisseling en geleidingsvermogen van het zilverjodidesol," Thesis, p. 14. Utrecht, 1943.
5. TATTJE, P. H. E., "Beweeglijkheden van ionen in het AgJ-sol," Thesis. Utrecht, 1942.
6. SCHLOEGL, R., *Z. Elektrochem.* **57,** 195 (1953).
7. BOYD, G. E., AND SOLDANO, B. A., *J. Am. Chem. Soc.* **75,** 6091 (1953). SOLDANO, B. A., AND BOYD, G. E., *J. Am. Chem. Soc.* **75,** 6099 (1953). BOYD, G. E., SOLDANO, B. A., AND BONNER, O. D., *J. Phys. Chem.* **58,** 456 (1954). HUSTED, R. F., AND LOW, P. F., *Soil Sci.* **77,** 343 (1954).
8. BOYD, G. E., ADAMSON, A. W., AND MYERS, L. S., JR., *J. Am. Chem. Soc.* **69,** 2836 (1947).
9. HEYMANN, E., AND O'DONNELL, I. J., *J. Colloid Sci.* **4,** 405 (1949).
10. SHAROV, V. S., *Doklady Akad. Nauk S.S.S.R.* **60,** 829 (1948); *Chem. Abstr.* **42,** 8573e (1948). MANECKE, G., AND BONHOEFFER, K.-F., *Z. Elektrochem.* **55,** 475 (1951). MANECKE, G., *Z. physik. Chem.* **201,** 193 (1952). JUDA, W., ROSENBERG, N. W., MARINSKY, J. A., AND KASPER, A. A., *J. Am. Chem. Soc.* **74,** 3736 (1952). CLARKE, J. T., MARINSKY, J. A., JUDA, W., ROSENBERG, N. W., AND ALEXANDER. S., *J. Phys. Chem.* **56,** 100 (1952).
11. HARNED, H. S., AND OWEN, B. B., "The Physical Chemistry of Electrolytic Solutions," 2nd ed., Ch. 4. Reinhold, New York, 1950. GOSTING, L. J., AND HARNED, H. S., *J. Am. Chem. Soc.* **73,** 159 (1951).
12. ZIEMENS, K. E., "Handb. d. Katalyse," Bd 4, p. 257, 1943; cited by WICKE, E., AND BROETZ, W., *Chem.-Ing.-Tech.* **21,** 219 (1949).
13. ARCHIE, G. E., *Trans. Am. Inst. Mining Met. Engrs., Petroleum Development and Technol., Petroleum Div.* **146,** 54 (1942). WYLLIE, M. R. J., AND GREGORY, A. R., *Trans. Am. Inst. Mining Met. Engrs., Petroleum Development and Technol., Petroleum Branch* **198,** 103 (1953).
14. HENRY, P. S. H., *Proc. Roy. Soc. (London)* **A171,** 215 (1939).
15. MACKIE, J. S., AND MEARES, P., *Proc. Roy. Soc. (London)* **A232,** 498 (1955).
16. VRIES, D. A. DE, *Trans. 4th Intern. Congr. Soil Sci. Amsterdam* **2,** 41 (1950); "Het warmtegeleidingsvermogen van grond," Thesis. Leiden, 1952; *Mededel. Landbouwhogeschool Wageningen* **52,** 1 (1952).
17. MARSHALL, C. E., AND KRINBILL, C. A., *J. Phys. Chem.* **46,** 1077 (1942). MARSHALL, C. E., *Soil Sci.* **65,** 57 (1948); *Trans. 4th Intern. Congr. Soil Sci. Amsterdam* **1,** 71 (1950); "The Colloid Chemistry of the Silicate Minerals," p. 115. Academic Press, New York, 1949.
18. ONSAGER, L., *Ann. N. Y. Acad. Sci.* **46,** 241 (1945). GOSTING, L. J., AND HARNED, H. S., *J. Am. Chem. Soc.* **73,** 159 (1951).

19. Harned, H. S., and Owen, B. B., "The Physical Chemistry of Electrolytic Solutions," 2nd ed., p. 172. Reinhold, New York, 1950. Kortuem, G., and Bockris, J. O'M., "Textbook of Electrochemistry," p. 701. Elsevier, Amsterdam, 1951.
20. Thovert, J., *Compt. rend.* **135**, 579 (1902). Heimbrodt, Fr., *Ann. Physik* [4] **13**, 1028 (1904). Oeholm, L. W., *Medd. Vetenskapsakad. Nobelinst.* **2**, No. 23 (1912). Calvet, E., *Compt. rend.* **221**, 403 (1945).
21. Suellmann, H., *Protoplasma* **13**, 546 (1931). Zuber, R., *Z. Physik* **79**, 291 (1932).
22. Glasstone, S., Laidler, K. J., and Eyring, H., "The Theory of Rate Processes," p. 522 et seq. McGraw-Hill, New York, 1941.
23. Cohen, E., and Bruins, H. R., *Z. physik. Chem.* **103**, 349 (1923); *ibid.* **113**, 157 (1924); cf. also Wang, J. H., and Kennedy, J. W., *J. Am. Chem. Soc.* **72**, 2080 (1950).
24. Frank, Ph., and Mises, R. von, "Die Differential- und Integralgleichungen der Physik," 2. Aufl., II (physikalischer) Teil, p. 578, eq. (28). Vieweg & Sohn, Braunschweig, 1935. Carslaw, H. S., and Jaeger, J. C., "Conduction of Heat in Solids," p. 85, eq. (6). Clarendon Press, Oxford, 1947.
25. Stefan, J., *Sitz.ber. Akad. Wiss. Wien, Math.-naturw. Kl.*, Abt. II, **79**, 161 (1879); cf. also Jost, W., "Diffusion in Solids, Liquids, Gases," p. 63 et seq. Academic Press, New York, 1952.
26. Grim, R. E., "Clay Mineralogy," p. 312 et seq. McGraw-Hill, New York, 1953.
27. Conrad, J. P., *Soil Sci.* **49**, 253 (1940).
28. Grim, R. E., "Clay Mineralogy," p. 108 et seq. McGraw-Hill, New York, 1953.

JOURNAL OF COLLOID SCIENCE **12**, 53–67 (1957)

DYNAMIC MECHANICAL PROPERTIES OF POLYETHYL METHACRYLATE[1]

John D. Ferry, William C. Child, Jr.,[2] Robert Zand, Donald M. Stern, Malcolm L. Williams,[3] and Robert F. Landel[4]

Department of Chemistry, University of Wisconsin, Madison, Wisconsin

Received July 30, 1956

INTRODUCTION

A series of methacrylate polymers, synthesized, fractionated, and characterized at the Samuel Feltman Ammunition Laboratories, Picatinny Arsenal, has been made available for measurements of dynamic mechanical properties in this Laboratory, encompassing in each case the transition from rubberlike to glasslike consistency. These studies extend our earlier work on polyisobutylene (1), polystyrene (2), polyvinyl acetate (3), and polymethyl acrylate (4). The cooperative program with the Arsenal will provide an opportunity for correlation of properties in dilute solution, studied by Mr. J. D. Matlack and his associates (5, 6), with mechanical properties of the undiluted polymers.

The presence of long side chains introduces some phenomena not perceived in the vinyl polymers previously studied here (1–4). Specific mechanical loss mechanisms attributed to side-chain motions have been detected near or below the glass transition temperature (T_g) by Hoff (7) in many polymethacrylates. The possibility of such motions coupling with motions of the main chain backbone above T_g has been discussed qualitatively by Koppelmann (8) in terms of the *Platzwechsel* concept of Müller (9). We have found it possible to separate, at least approximately, the loss contributions of backbone and side chain motions and to evaluate the retardation spectra and their temperature dependence for both. The analysis is facilitated by dielectric dispersion data obtained by Strella at Picatinny Arsenal (10).

The present paper reports data on two fractions of polyethyl methacrylate. The properties of this polymer in dilute solution have been investigated by Chinai and Samuels (6).

---

[1] Part XXV of a series on Mechanical Properties of Substances of High Molecular Weight.

[2] Now at Carleton College, Northfield, Minnesota.

[3] Now at The Chemstrand Corporation, Decatur, Alabama.

[4] Now at the Jet Propulsion Laboratory, Pasadena, California.

MATERIALS AND METHOD

The synthesis and fractionation of the polymer have been described (6). The two fractions used in this study, FF-1 and FF-2, had weight-average molecular weights of 1.73×10^6 and 0.164×10^6, respectively. They had been dried from frozen benzene solution, and were further dried *in vacuo* for several days before molding.

Measurements of the complex shear compliance ($J^* = J' - iJ''$) were made with the Fitzgerald Apparatus manufactured by Atlantic Research Corporation, Alexandria, Virginia, which is similar to the double transducer of Fitzgerald and Ferry (11). Three pairs of disc-shaped samples of each fraction were employed, molded at 250°F. and 10,000 lb./sq. in. The samples were quite clear and light brown in color. They were introduced into the apparatus while supported by specially designed inserts, warmed by a blast of hot air until they softened, and then compressed slightly between the sample slabs of the floating mass and the driving tube flats, to provide good contact with both surfaces.

The sample coefficients ($A_1/h_1 + A_2/h_2$, where A and h are the respective face areas and thicknesses) were calculated at room temperature from the masses of the samples, the density, ρ (estimated as 1.122 g./cc. at 25°C.), and the values of h measured *in situ* after compression. At other temperatures, sample coefficients were calculated assuming no change in thickness with a volume expansion specified by values of α (the thermal expansion coefficient) of 2×10^{-4} deg.$^{-1}$ below T_g and 6×10^{-4} above T_g. The value of T_g was taken as 62°C., as determined for a similar sample by Mandelkern and Quinn (12). (These authors have also reported T_g for a sample of polyethyl methacrylate from their own laboratory as 65°C., together with a value of ρ at 25°C. of 1.125, in reasonable agreement with the above.) Detailed descriptions of the samples follow.

Fraction FF-1. Samples 58, approximate dimensions $^{11}\!/\!_{16}$ in. diam. by $^{3}\!/\!_{32}$ in. thickness, were compressed in the apparatus about 7% and the sample coefficient was 24.18 cm. at 130°C. Measurements were made at approximately 5° intervals from 110° to 135°C., with subsequent check runs at 110° which agreed satisfactorily with the initial results. (The exact temperatures are given in the legend of Fig. 1.)

Samples 61, approximate dimensions $^{11}\!/\!_{16}$ in. by $^{1}\!/\!_{32}$ in., were compressed about 8%, and the nominal sample coefficient was 52.10 cm. at 130°. Measurements were made at approximately 5° intervals from 130° to 155° with subsequent check runs at 135° and 130° which agreed with those on the upward temperature sequence. The values of J' and J'' at overlapping temperatures were larger than those of Samples 58 by about 8%, but the ratios J''/J', which are independent of the sample coefficient, were in good agreement; the difference in J' and J'' was attributed to an error in the sample coefficient of Samples 61 (difficult to measure because

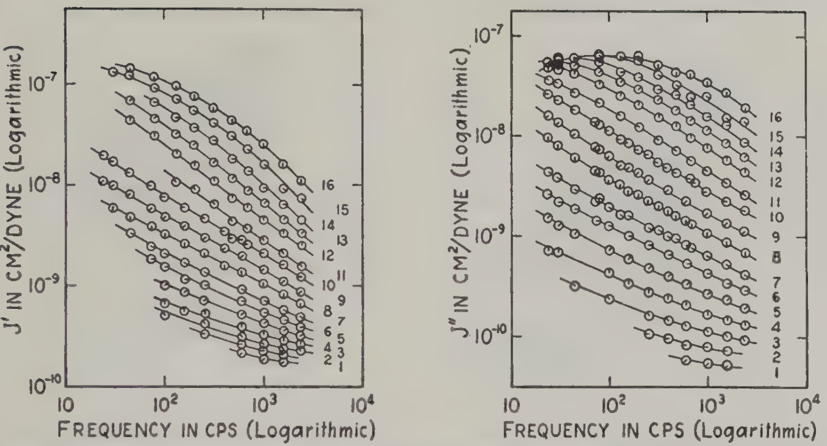

FIG. 1. Variation of the real part of the dynamic shear compliance, J' (left) and the imaginary part, J'' (right) with frequency for polyethyl methacrylate FF-1 at 16 temperatures; numbers correspond to the temperature sequence 79.7, 85.2, 89.8, 95.0, 99.9, 104.7, 108.7, 114.6, 119.4, 124.7, 129.2, 135.5, 139.9, 144.4, 149.8, and 155.0°C.

of their extreme thinness), and the data for the latter were corrected by an empirical factor of 0.92.

Samples 77, approximate dimensions 3/16 in. by 5/16 in., were compressed about 5 %, and the sample coefficient was 3.76 cm. at 125°C. Measurements were made at approximately 5° intervals from 110° to 125°, followed by a downward sequence at approximately 5° intervals from 105° to 80°, and then a satisfactory check run at 110°. The values of J' and J'' at overlapping temperatures agreed well with those of Samples 58, and no empirical correction was required.

Fraction FF-2. Samples 63, 11/16 in. by 3/32 in., were compressed about 5 %, and the sample coefficient was 23.57 at 130°C. Measurements were made at approximately 5° intervals from 110° to 140°, followed by a satisfactory check run at 110°. (The exact temperatures are given in the legend of Fig. 2.)

Samples 71, 11/16 in. by 1/32 in., were compressed about 8 %, and the nominal sample coefficient was 53.9 at 130°C. Measurements were made at approximately 5° intervals from 130° to 155°, followed by a satisfactory check run at 130°. Values of J' and J'' at overlapping temperatures agreed fairly well with those of Samples 63, but better agreement was obtained by applying an empirical correction factor of 1.04.

Samples 76, 3/16 in. by 5/16 in., were compressed about 8 %, and the nominal sample coefficient was 3.265 at 125°C. Measurements were made at approximately 5° intervals from 110° to 120°, followed by 100°, 105°, and a downward sequence from 95° to 75°, a satisfactory check run at 110°,

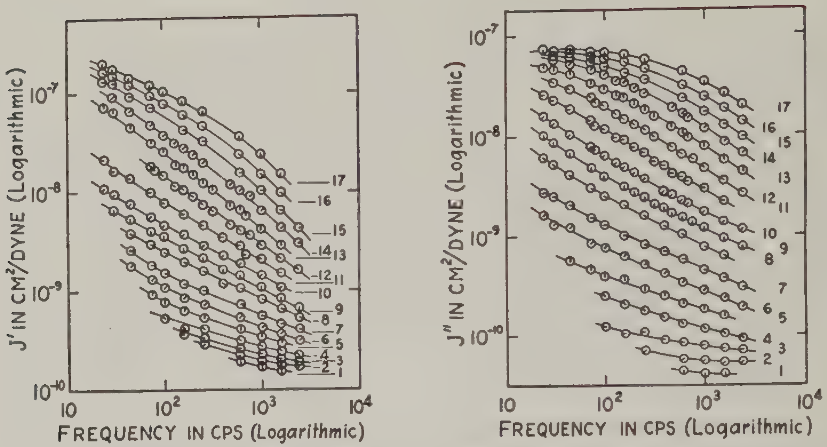

FIG. 2. Variation of the real part of the dynamic shear compliance, J' (left) and the imaginary part, J'' (right) with frequency for polyethyl methacrylate FF-2 at 17 temperatures; numbers correspond to the temperature sequence 74.6, 79.8, 84.6, 89.8, 94.8, 99.9, 104.7, 110.8, 114.9, 118.8, 124.4, 130.1, 135.4, 140.2, 145.1, 150.0, and 155.1°C.

and finally 125°. Values of J' and J'' at overlapping temperatures were about 7 % higher than those of Samples 63—a difference readily attributable to bulging of the thicker samples, as explained in previous communications (11). The data for Samples 76 were accordingly corrected by an empirical factor of 0.93.

RESULTS

The original data for J' and J'', measured at 17 temperatures from 75° to 155°C., and at numerous frequencies between 24 and 2400 cycles/sec. at each temperature, are shown for the two fractions in Figs. 1 and 2. Where data on different samples were taken at the same frequencies and temperatures, the values have been averaged.

The values for the two fractions at corresponding temperatures are practically identical, except that J'' is slightly higher for Fraction FF-2 at the highest temperatures and lowest frequencies. The expectation is thus fulfilled that mechanical properties in the transition region between rubberlike and glasslike consistency will be independent of molecular weight so long as the latter is fairly high; in this case the agreement is within experimental error, except at the extreme rubberlike end, though the molecular weights differ by a factor of over tenfold.

For reduction to a standard temperature, chosen as 100°C., J'_p and J''_p were calculated by the usual formulas (13), using the thermal expansion coefficients given above. The value of J_∞, the limiting high frequency compliance, was chosen as 10^{-10} dyne/cm.², but its choice was not critical because the temperature range where J' is small lies close to the reference temperature.

Although logarithmic plots of J''_p at different temperatures from 90° to 155°C. could be superposed quite well by the usual arbitrary shift factors a_T, and plots of J'_p could be superposed from 140° to 155° by identical shifts, outside these temperature ranges the method of reduced variables proved to be inapplicable. This failure, the first which has appeared among the numerous amorphous polymer systems studied in this Laboratory, was attributed to the presence of a secondary relaxation mechanism as detected in polymethyl methacrylate by several investigators (14–18) and by Hoff in other methacrylate polymers (7). The temperature dependence of the relaxation times associated with the secondary mechanism (involving side chain motions, and symbolized by β following Hoff) is different from that for the primary mechanism (involving chain backbone motions, and symbolized by α). The method of reduced variables applies only in ranges of temperature and frequency where the compliance contributions of the secondary mechanism are comparatively negligible.

Where the latter condition was fulfilled—above 90°C. for J'' and above 140° for J'—the empirical a_T values followed closely an equation of the WLF form (19):

$$\log a_T = -c_1^0(T - T_0)/(c_2^0 + T - T_0). \qquad [1]$$

Here for convenience the reference temperature is chosen as $T_0 = 373$°K. instead of the adjustable T_s which corresponds to certain approximately universal values of c_1 and c_2. With the value of $T_g = 335$°K., and formulas previously given (19), the values of c_1' and c_2' appropriate to T_g as reference temperature may be calculated, and from these the parameters f_g and α_f which represent the fractional free volume at T_g and its expansion coefficient relative to the total volume (20). All these values are given in Table I. The fact that f_g and α_f are close to the figures for other polymers in which reduced variables are applicable throughout the transition zone—the approximate "universal" values being 0.025 and 4.8×10^{-4} deg.$^{-1}$, respectively—supports the conclusion that Eq. [1] correctly describes the

TABLE I

Parameters for Temperature Dependence of α Mechanism

		Fraction FF-1	Fraction FF-2
Reference $T_0 = 373$°K.:	c_1^0	11.92	11.18
	c_2^0, deg.	108.8	103.5
Reference $T_g = 335$°K.:	c_1'	18.3	17.6
	c_2', deg.	70.8	65.5
	f_g	0.024	0.025
	α_f, deg.$^{-1}$	3.4×10^{-4}	3.7×10^{-4}

temperature dependence of chain backbone motions. It will therefore be used to calculate a_T values for the α mechanism over the entire temperature range, in the analysis which follows.

ANALYSIS OF α AND β MECHANISMS

Relative Weighting of the Two Mechanisms

Both α and β mechanisms involve groups of processes, of course, with distributions of retardation and relaxation times. It is assumed that the overall retardation spectrum L is the sum of L_α and L_β. From the well-known relations between L and the complex compliance (21)

$$J' = \int_{-\infty}^{\infty} L/(1 + \omega^2\tau^2)\, d \ln \tau \qquad [2]$$

and

$$J'' = \int_{-\infty}^{\infty} \omega\tau L/(1 + \omega^2\tau^2)\, d \ln \tau + 1/\omega\eta \qquad [3]$$

it follows that $J' = J'_\alpha + J'_\beta$ and $J'' = J''_\alpha + J''_\beta$. From various sources of information on polymethyl methacrylate (14–18), it is evident that with decreasing temperature L_α moves to long times more rapidly than L_β, and the same may be presumed true for polyethyl methacrylate. Thus at low temperatures the two mechanisms become separated with the dispersion region of the α mechanism being associated with such very long times that they are actually out of the range of our frequency scale, and our measurements reflect primarily the β mechanism. At high temperatures, on the other hand, the two mechanisms overlap; but at high temperatures and long times (low frequencies), J'_α and J''_α are so large that J'_β and J''_β make negligible contributions, and our measurements reflect primarily the α mechanism.

Where the two mechanisms overlap, the effect of the β mechanism would be much more apparent in the relaxation spectrum Φ than the retardation spectrum L. This may be seen from the relation of Gross (21)

$$\Phi(\tau) = \frac{G_\infty^2 L}{\left[1 - \frac{\tau G_\infty}{\eta} + \tau \int_0^{\infty} \frac{G_\infty L(u)\, du}{u(\tau - u)}\right]^2 + \pi^2 G_\infty^2 L^2}, \qquad [4]$$

where G_∞ is the limiting high-frequency rigidity modulus and η is the steady flow viscosity. In the region of interest, $\tau G_\infty/\eta \ll 1$, and the above may be approximated, if L is a fairly broad spectrum, by

$$\Phi(\tau) = \frac{L(\tau)}{\left[J_\infty + \int_{-\infty}^{\ln \tau} L\, d \ln u\right]^2 \pi^2 L^2(\tau)}, \qquad [5]$$

where $J_\infty = 1/G_\infty$. It is clear from Eq. [5] that Φ at a point τ on the time scale depends not only on L at that point but also on the integral under

L from that point out to shorter times—where the effect of the β mechanism will be most prominent. Accordingly, if we wish to minimize the effect of the β mechanism, we should analyze L (or compliance) rather than Φ (or rigidity); moreover, of the two components of compliance, we should choose J'' because Eqs. [2] and [3] show that it is weighted more at long times than is J', whereas J' by contrast is weighted at short times where the β anomaly appears. This explains why the method of reduced variables, with a_T given by Eq. [1], is applicable to the J'' data over a much wider temperature range than to the J' data.

In the detailed analysis, only one fraction is treated because the properties of the two are so nearly identical. For this, FF-2 was chosen because the data for it are slightly more extensive.

First Approximation to the α Mechanism

Insofar as the reduced compliance data superpose, they may be taken as representing the α mechanism at 100°C.; the composite curves, not shown here, provide J' over a range of $\log \omega a_T$ (where ω is the circular frequency) from -1.7 to 0, roughly, and J'' from -1.7 to 3. But there is no way of extrapolating these curves to higher frequencies. As an expedient, therefore, it was assumed that their shapes at high frequencies would be approximately the same as those for polyisobutylene. The latter was chosen because it also has disubstituted carbon atoms (a feature which is apparently important in determining the shape of the dispersion (20)) and its dispersion is accurately known (1). It has the disadvantage that its loss tangent as a function of frequency is somewhat asymmetrical and probably atypical. However, the distortion introduced by this feature is believed to be slight.

In comparing different polymers, all contributions to J^* should be proportional to M_0/ρ (where M_0 is the monomer molecular weight and ρ the density), an inverse measure of the number of monomer units per unit volume. The ratio of M_0/ρ for polyethyl methacrylate to that for polyisobutylene is 1.71, and composite curves for J' and J'' for polyisobutylene were accordingly multiplied by this factor. It was then found that such curves (logarithmic) for polyisobutylene at 25°C. did indeed coincide with the low-frequency composite curves of J' and J'' for polyethyl methacrylate at 100° when empirically shifted 4.23 decades on the logarithmic frequency scale. Accordingly, the shifted polyisobutylene curves were taken to represent J'_α and J''_α for polyethyl methacrylate in first approximation.

First Approximation to the β Mechanism

The above values of J'_α and J''_α were subtracted from J' and J'' at each temperature at corresponding values of reduced frequency to give J'_β and J''_β. At high reduced frequency, the subtracted corrections were small, so the uncertainty as to whether the modified polyisobutylene values are correct is not serious here. A plot of J'_β against J''_β in the complex plane gave a Cole circular arc (22) with maximum and minimum values of J'_β as 0.9×10^{-9} cm.^{2}/dyne and zero, respectively, and maximum J''_β as 0.13×10^{-9} cm.^{2}/dyne; the Cole parameter α was 0.648. The minimum value of J'_β is zero because J_∞ is defined as part of J'_α. The maximum value is not unreasonable compared with dynamic measurements by Schmieder and Wolf (15) on various polymers at roughly constant frequency, where the shear modulus G' shows a secondary plateau of the order of 10^9 to $10^{9.5}$ dynes/cm.^{2} in certain temperature ranges in addition to a higher plateau at lower temperatures. A similar plateau is seen in the measurements of Maxwell (18) on polymethyl methacrylate. The fit of the data to a Cole plot lends some confidence to the analytical procedure. There were, however, few reliable points on the right half of the arc, and the estimated maximum J'_β may be somewhat too high.

Logarithmic plots of J'_β and J''_β against ωa_T did not of course superpose, since the a_T factors appropriate for the α mechanism cannot serve also for the β mechanism. They could, however, be superposed by empirical horizontal shifts representing $\log a_{T\beta} - \log a_T$, where $a_{T\beta}$ is the reduction

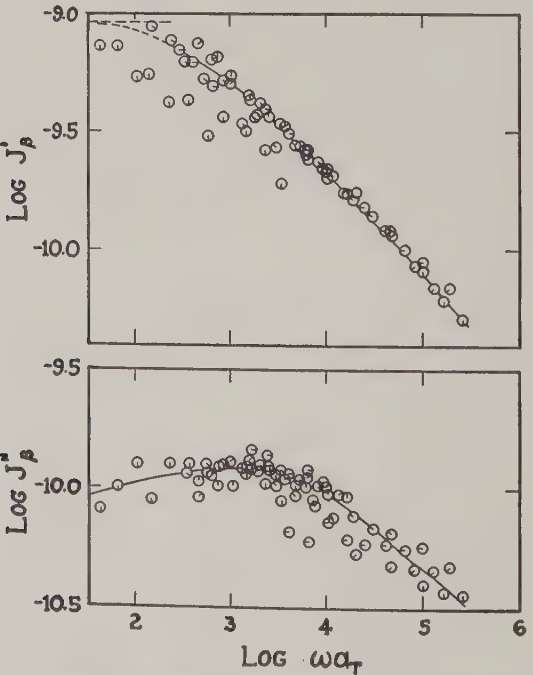

Fig. 3. Real and imaginary parts of the complex compliance of the β mechanism for fraction FF-2 reduced to 100°C. (on the basis of a constant apparent activation energy of 31 kcal.) and plotted logarithmically against reduced frequency. Pip down at right 74.6°C.; successive 45° rotations clockwise correspond to increasing temperatures at approximately 5° intervals (exact temperatures given under Fig. 2).

factor for the β mechanism. From such shifts, accompanied by values of log a_T derived from Eq. [1], log $a_{T\beta}$ was calculated. From 75° to 105°, log $a_{T\beta}$ was a linear function of the reciprocal absolute temperature with a slope corresponding to an apparent energy of activation of 31 kcal. Above 105°C., the data were somewhat scattered because the J_β components represent small differences between J and J_α.

Strella and Zand (10) have studied the dielectric dispersion of the same two fractions of polyethyl methacrylate over the temperature range from −74° to 133°C. Comparison with Hoff's data on polymethyl methacrylate (17) indicates that the principal dispersion in their data represents the β mechanism. Although at lower temperatures the dispersion changes markedly in shape with temperature, preventing the direct application of reduced variables, from 107° to 133° (Fraction FF-1) the shape is fairly constant; reduction factors b_T (11) obtained in this range and referred to 100° fall on the same logarithmic plot against $1/T$ as the above described $a_{T\beta}$ factors, lending confidence to the value of 31 kcal. for the apparent activation energy of this mechanism. From the latter, values of $a_{T\beta}$ were calculated at temperatures above 105° so that all the mechanical data for the β process could be plotted with reduced variables.

Figure 3 shows J'_β and J''_β reduced to 100°C. in this manner. The super-

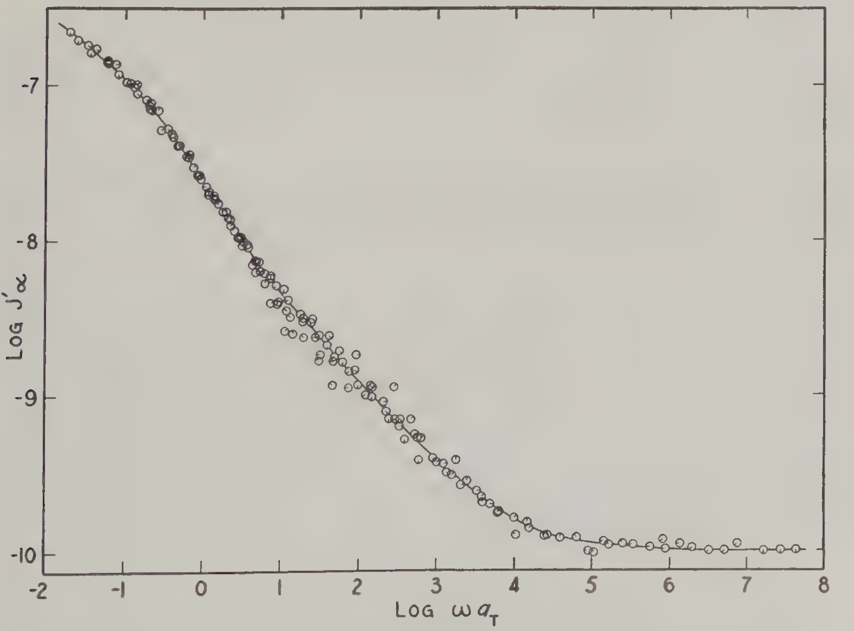

FIG. 4. Real part of the complex compliance of the α mechanism for Fraction FF-2 reduced to 100°C. (on the basis of the WLF equation with the coefficients given in Table I) and plotted logarithmically against reduced frequency. Temperature key same as in Fig. 3.

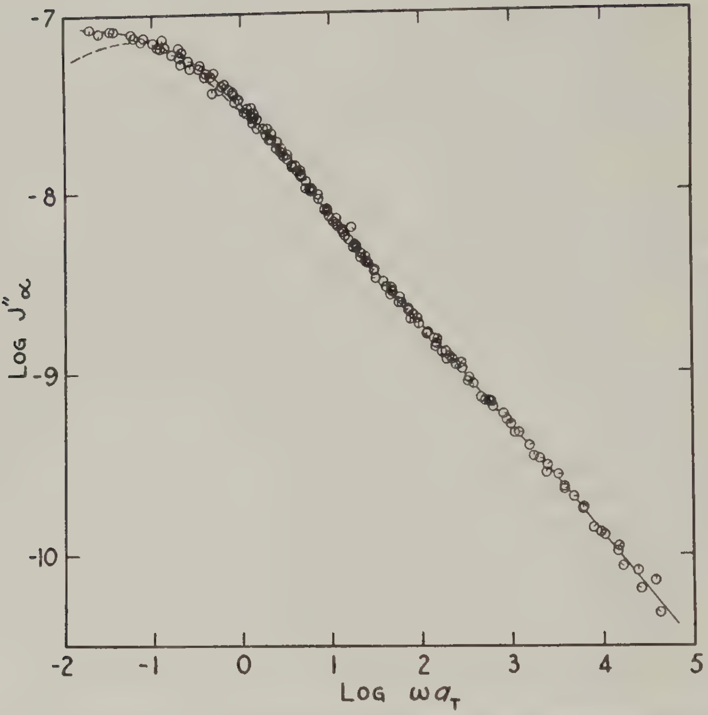

Fig. 5. Imaginary part of the complex compliance of the α mechanism for Fraction FF-2 reduced and plotted as in Fig. 4. The dashed line gives the reduced imaginary compliance for Fraction FF-1.

position is fairly good (except for J''_β at the lowest temperatures), and shows the general features of a moderately broad dispersion.

Second Approximation to the α Mechanism

Smoothed values of J'_β and J''_β were finally taken from Fig. 3 and subtracted from J' and J'' at corresponding values of ωa_T to obtain revised values of J'_α and J''_α. The latter are plotted logarithmically against ωa_T in Figs. 4 and 5. The superposition is extremely good except near the middle of the J' plot, giving further confidence in our rather indirect procedure of analysis. The validity of this separation of mechanisms is also borne out by a similar analysis for poly-*n*-butyl methacrylate (23) which does not require introducing the dispersion of polyisobutylene.

Distribution Functions

The retardation spectra or distribution functions, L, have been calculated for the two mechanisms from the data of Figs. 3–5 by the second approximation formulas of Williams and Ferry (24), and are given in Table

TABLE II

Relaxation and Retardation Distribution Functions Reduced to 100°C.

Log τ_p (sec.)	Log L_p ($cm.^2/dyne$)		Log Φ_p ($dyne/cm.^2$)	
	From J'	From J''	From G'	From G''
		α Mechanism		
−5.0	−11.15	−11.01	9.23	9.10
−4.5	−10.91	−10.61	9.40	9.27
−4.0	−10.42	−10.31	9.27	9.30
−3.5	−10.11	−10.00	9.03	9.04
−3.0	−9.84	−9.69	8.70	8.78
−2.5	−9.55	−9.41	8.36	8.51
−2.0	−9.26	−9.14	8.09	8.19
−1.5	−8.94	−8.88	7.83	7.89
−1.0	−8.63	−8.63	7.50	7.55
−0.5	−8.25	−8.23	7.14	7.12
0	−7.85	−7.86	6.82	6.77
0.5	−7.51	−7.52	6.49	6.42
1.0	−7.28	−7.36	6.29	6.15
1.5	−7.14	−7.24	6.05	5.84
		β Mechanism		
−5.5	−10.69	−10.74	9.71	9.65
−5.0	−10.47	−10.57	9.51	9.40
−4.5	−10.29	−10.42	9.32	9.18
−4.0	−9.98	−10.23	9.08	8.90
−3.5	−9.90	−10.10	8.86	8.51
−3.0	−9.82	−10.08	8.68	8.25
−2.5	−9.79	−10.13	8.45	8.07
−2.0	−9.93	−10.15	8.17	7.83

II. The agreement between calculations from real and imaginary components is quite good except for the long time end of the β mechanism, where the values from J'_β are probably not too reliable. The distribution function from the β mechanism has also been calculated analytically by the formula of Cole and Cole (22), using the parameters determined from the circular arc plot, and it agrees fairly well with the graphical calculation, as shown in Fig. 6. The overall retardation spectrum, the sum of the two individual mechanisms at 100°C., is also reproduced in Fig. 6.

The relaxation spectra or distribution functions, Φ, have also been calculated from corresponding plots of the complex shear modulus and are given in Table II. Again, the agreement between calculations from real and imaginary components is quite good except for the values from G'_β at long times. The relaxation spectra are plotted in Fig. 7.

It may be remarked that the overall function L at any other temperature than 100° may be obtained by an appropriate shift of the α and β curves in Fig. 6 relative to each other followed by addition of the individual L values (not their logarithms as plotted). At lower temperatures, the β

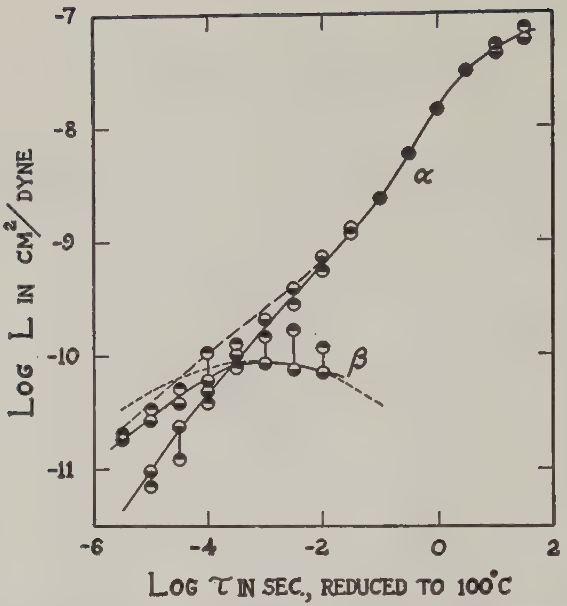

Fig. 6. Retardation distribution functions of the two mechanisms reduced to 100°C. Points top black, from J'; bottom black, from J''. The dashed line gives the total retardation distribution function at 100°C.; dotted line, the β distribution calculated from the Cole arc plot.

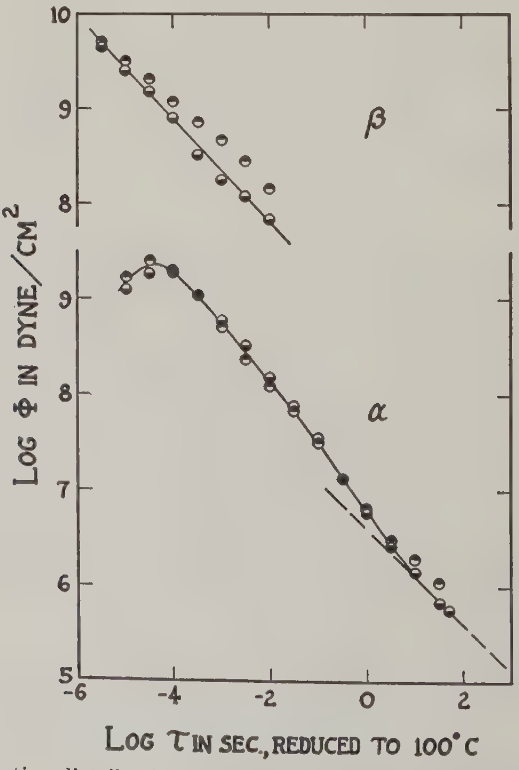

Fig. 7. Relaxation distribution functions of the two mechanisms at 100°C. Points top black, from G'; bottom black, from G''. The dashed line is drawn with the theoretical slope of $-1/2$.

curve will lie further exposed to the left; at higher temperatures, it will lie relatively to the right and become increasingly submerged by the α curve. The overall function Φ cannot, however, be obtained by any such simple procedure.

DISCUSSION

Temperature Dependence

The temperature dependence of relaxation times in the α mechanism is described by the parameters in Table I. The values for the two fractions are close together, and it is doubtful whether there is a significant dependence on molecular weight in this range.

The temperature dependence of relaxation times in the β mechanism does not follow the WLF equation, but can be described within experimental error by a constant apparent activation energy of 31 kcal. This is comparable with estimates for the activation energy of the β mechanism in polymethyl methacrylate (14–17); in particular, Iwayanagi and Hideshima (14) obtained 29 kcal.

It is of interest that the apparent activation energy of the α process, calculated from the WLF equation (19), is 69 kcal. at 100°C., but would fall to 31 kcal. at 189°C. (127° above T_g). At this scarcely practical temperature, the α and β mechanisms would shift with temperature at the same rate and would not be separable. Moreover, the β mechanism would lie so far to the left on the frequency scale that J'_α would always exceed J'_β by several powers of ten, and the latter would scarcely be distinguishable in any case. This is probably the situation in most amorphous polymers even a short distance above their glass transition temperatures; our measurements, extending usually down to within 25° of T_g, have never before revealed β anomalies, even though others' measurements near or below the glass transition have shown secondary loss mechanisms in some of the polymers we have studied. It is implied, then, that in polyethyl methacrylate the side chain motions are more rapid relative to the backbone motions than in the other polymers with shorter side chains.

Time and Frequency Dependence

The retardation and relaxation spectra associated with the α mechanism are normal and similar in shape to those of other polymers; the shape of the function Φ resembles that for other disubstituted carbon chains (20) rather than the more sharply curved spectra which appear to be characteristic of monosubstituted chains.

A tangent drawn to the Φ curve with the theoretical slope (25, 26) of $-1/2$, as indicated in Fig. 7, provides the usual calculation of the monomeric friction coefficient. Taking for a, the root-mean-square end-to-end distance per monomer unit, the value of 5.9 A. derived from light-scattering measurements in a Θ solvent (6), we obtain $\log \zeta_0$ (in dyne sec./cm. at 100°C.) $= -0.21$. Reduction to T_g, using the data of Table I, gives

$\log \zeta_0 = 6.22$ at 335°K. This is of the same order of magnitude as the friction coefficients of polymethyl acrylate and polyvinyl acetate at their respective glass transition temperatures (20), indicating similar mobilities of the chain backbones when compared in this manner—despite the steric hindrance in polyethyl methacrylate which is evident in molecular models.

The retardation and relaxation spectra associated with the β mechanism are probably not too reliable in view of the method of calculation, but are clearly rather broad in shape. The only other polymer for which the retardation spectrum of the β mechanism can be adduced from published data appears to be polymethyl methacrylate; the data of Iwayanagi and associates (27) and of Lethersich (28) lead to a much broader spectrum still. On the other hand, that for poly-*n*-butyl methacrylate is considerably sharper. A quantitative comparison will be made in a later communication.

Influence of Molecular Weight

In Fig. 5, where the points are derived from data for Fraction FF-2, a dashed line is also drawn to show the slight divergence of J'' for Fraction FF-1 at low reduced frequencies. The difference would also be reflected in the spectrum L at long times. It is probably associated with differences in the disposition of the entanglements (29) which are responsible for the plateau in the relaxation spectrum and the first maximum in the retardation spectrum (26). It may, however, reflect the $1/\omega\eta$ term in Eq. [3]; measurements of steady flow viscosity are not yet available to test this possibility.

ACKNOWLEDGMENTS

This work was supported by Picatinny Arsenal, Ordnance Corps, Department of the Army. We are especially grateful to Prof. Edwin R. Fitzgerald, Pennsylvania State University, for supervising installation of the Fitzgerald Apparatus, and to Messrs. Russell Riley and Robert Schmelzer for making certain modifications in the floating mass, thermostat, and other features. We are indebted to Mrs. Garrett Droppers for making most of the calculations, to Mr. D. J. Plazek for assistance with the apparatus, and to Messrs. Stephen Strella and Robert Zand for the opportunity of examining their dielectric data in advance of publication.

SUMMARY

The real (J') and imaginary (J'') components of the complex compliance have been measured between 24 and 2400 cycles/sec. in the temperature range from 75° to 155°C. for two fractions of polyethyl methacrylate of weight-average molecular weights 1.73×10^6 and 0.164×10^6. The data were practically identical for the two fractions except that J'' was slightly higher at the highest temperatures and lowest frequencies for the lower fraction. The method of reduced variables did not give superposed curves for J' and J'' over the entire temperature range. However, the data could be analyzed in terms of two additive mechanisms; for the α mechanism J' and J'' superposed with reduction factors a_T whose temperature de

pendence followed an equation of the WLF form, and for the β mechanism they also superposed with reduction factors $a_{T\beta}$ whose temperature dependence corresponded to a constant activation energy of 31 kcal. The coefficients of the WLF equation, reduced to the glass transition temperature, were similar in magnitude to those observed in other polymers. Relaxation and retardation spectra have been calculated for both mechanisms. Those for the α mechanism, attributed to the usual chain backbone motions, resemble in form those for other disubstituted vinyl chains; the friction coefficient per monomer unit in backbone motion has been calculated from the extended Rouse theory. The spectra for the β mechanism, attributed to side chain motions, are relatively broad. The relative locations of the two mechanisms on the time scale change rapidly with temperature.

References

1. Fitzgerald, E. R., Grandine, L. D., and Ferry, J. D., *J. Appl. Phys.* **24,** 650 (1953).
2. Grandine, L. D., Jr., and Ferry, J. D., *J. Appl. Phys.* **24,** 679 (1953).
3. Williams, M. L., and Ferry, J. D., *J. Colloid Sci.* **9,** 479 (1954).
4. Williams, M. L., and Ferry, J. D., *J. Colloid Sci.* **10,** 474 (1955).
5. Chinai, S. N., Matlack, J. D., Resnick, A. L., and Samuels, R. J., *J. Polymer Sci.* **17,** 391 (1955).
6. Chinai, S. N., and Samuels, R. J., *J. Polymer Sci.* **19,** 463 (1956).
7. Hoff, E. A. W., Robinson, D. W., and Willbourn, A. H., *J. Polymer Sci.* **18,** 161 (1955).
8. Koppelmann, J., *Kolloid-Z.* **144,** 12 (1955).
9. Müller, F. H., *Proc. 2nd Intern. Congr. Rheology, London,* p. 38 (1954).
10. Strella, S., and Zand, R., Private communication.
11. Fitzgerald, E. R., and Ferry, J. D., *J. Colloid Sci.* **8,** 1 (1953).
12. Mandelkern, L., and Quinn, F. A., Jr., Private communication.
13. Ferry, J. D., and Fitzgerald, E. R., *J. Colloid Sci.* **8,** 223 (1953).
14. Iwayanagi, S., and Hideshima, T., *J. Phys. Soc. Japan* **8,** 365, 368 (1953).
15. Schmieder, K., and Wolf, K., *Kolloid-Z.* **134,** 149 (1953).
16. Heyboer, J., Dekking, P., and Staverman, A. J., *Proc. 2nd Intern. Congr. Rheology, London,* p. 123 (1954).
17. Deutsch, K., Hoff, E. A. W., and Reddish, W., *J. Polymer Sci.* **13,** 565 (1954).
18. Maxwell, B., *J. Polymer Sci.* **20,** 551 (1956).
19. Williams, M. L., Landel, R. F., and Ferry, J. D., *J. Am. Chem. Soc.* **77,** 3701 (1955).
20. Ferry, J. D., and Landel, R. F., *Kolloid-Z.* **148,** 1 (1956).
21. Gross, B., "Mathematical Structure of the Theories of Viscoelasticity." Hermann & Cie., Paris, 1953.
22. Cole, K. S., and Cole, R. H., *J. Chem. Phys.* **9,** 341 (1941).
23. Child, W. C., Jr., and Ferry, J. D., *J. Colloid Sci.*, submitted.
24. Williams, M. L., and Ferry, J. D., *J. Polymer Sci.* **11,** 169 (1953).
25. Rouse, P. E., Jr., *J. Chem. Phys.* **21,** 1272 (1953).
26. Ferry, J. D., Landel, R. F., and Williams, M. L., *J. Appl. Phys.* **26,** 359 (1955).
27. Sato, K., Nakane, H., Hideshima, T., and Iwayanagi, S., *J. Phys. Soc. Japan* **9,** 413 (1954).
28. Lethersich, W., *Brit. J. Appl. Phys.* **1,** 294 (1950).
29. Bueche, F., *J. Chem. Phys.* **20,** 1979 (1952).

JOURNAL OF COLLOID SCIENCE **12,** 68–79 (1957)

HOMOGENEOUS FLUID FLOW THROUGH CONSOLIDATED POROUS MEDIA[1]

Robert T. Johansen and H. N. Dunning

Surface Chemistry Laboratory, Petroleum Experiment Station, Bureau of Mines, U. S
Department of the Interior, Bartlesville, Oklahoma

Received February 6, 1956

INTRODUCTION

Better understanding of the fundamental laws governing fluid flov through petroleum-reservoir rock is a key to engineering developments capable of improving the efficiency of petroleum production methods. Th flow of fluids in a natural petroleum reservoir usually involves a multi phase system of gases and liquids flowing through heterogeneous porou materials. However, the understanding of a simple, homogeneous systen is a prerequisite to the understanding of the more complicated system found in petroleum reservoirs.

Many investigators have studied the single phase flow of pure liquid through unconsolidated sand beds (1–4, 14), and some have studied flov through consolidated media (5–10). As a result of these investigations several anomalies have been reported from time to time in the literature but most of these have been explained by later workers. However, an in crease in permeability to an electrolyte solution accompanying an in creasing concentration of the electrolyte and an increase in permeabilit when the surface of the porous medium is made nonwetting to the flow ing liquid (7, 15), still are controversial subjects. Templeton (11) recentl has shown that the flow of fluids in capillaries 4 μ in diameter may b described adequately by Poiseuille's law. An explanation of the elec trolyte-concentration and wettability effects would determine the ap plicability of Poiseuille's law to the flow of homogeneous fluids throug inert, consolidated, porous media as well.

The effects of wettability and electrolyte concentration on single phase flow through porous media were investigated. Wettability wa controlled by using coatings on the surfaces of the porous media an surface-active substances in the liquids. The effects of wettability on flui distribution in pores that have only a single opening and in unique intersecting-capillary systems have been observed. Correlations of the permeability data with microscopic observations of these systems indicate that differences in wettability may affect fluid distribution, which in turn affects permeability if complete liquid saturation of the porous medium is not achieved.

---

[1] Presented before the Division of Colloid Chemistry at the 128th National Meetin of the American Chemical Society in Minneapolis, Minnesota, September 11–16, 195

EXPERIMENTAL

Materials

The alundum (aluminum oxide) used for the flow studies was obtained from the Norton Co., Worcester, Massachusetts, in rods having permeabilities of approximately 200 and 1000 millidarcys.

The samples used for study were cut from these rods with diamond-edged tools and cleaned by boiling them in mixtures of nitric and sulfuric acids; the acid salts were removed by prolonged flushing with boiling and distilled water. Alternate heating and cooling of the cleaning solutions caused them to be flushed through the pores of the alundum. Final removal of any remaining organic material was accomplished by heating the alundum samples to a red heat.

The liquids used in the flow study were water, acetone, and isooctane. The water was distilled originally from alkaline potassium permanganate ($KMnO_4$) and then redistilled and cooled immediately before it was introduced into the apparatus to eliminate dissolved air that might form bubbles in the porous medium. Water was found to be usable for a maximum of 5 days without restricting flow apparently by the growth of microorganisms not removed by filtration (2).

The acetone was ACS reagent grade obtained from Fisher Scientific Co. Studies of its surface properties indicated that it contained no surface-active impurities. Therefore, it was used without further purification. The "isooctane" (2,2,4-trimethylpentane) was the purest grade obtainable from the Rohm & Haas Co. Before being used, it was passed through Davison silica gel (28- to 200-mesh) and distilled over sodium in an atmosphere of helium. Physical constants for the isooctane were compared with National Bureau of Standards values in an earlier report (2).

Apparatus

Figure 1 is a diagram of the permeability apparatus, which was of the pressure-decline type (2). The apparatus is designed to eliminate contact of the flowing fluid with stopcock grease and to minimize contact with air before its permeation through the alundum plugs. The overflow tube and the pressure manometer are of the same diameter to compensate for surface-tension effects.

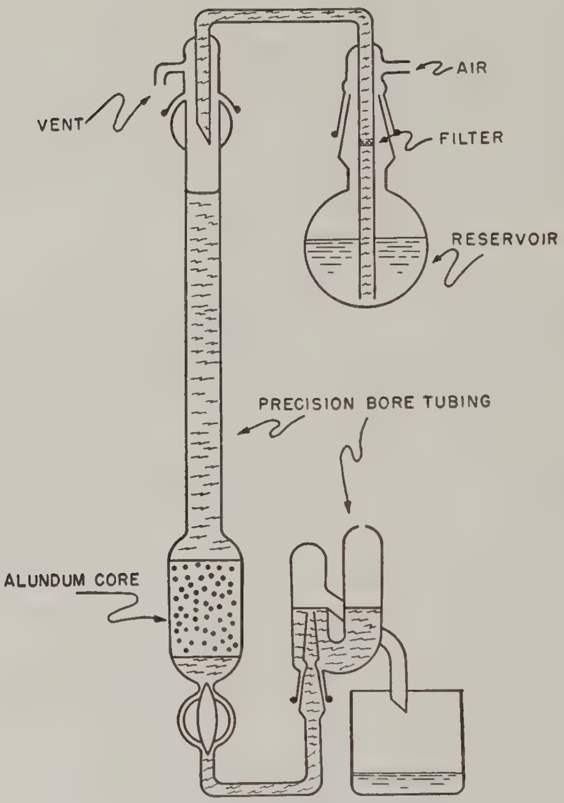

Fig. 1. Pressure-decline permeability apparatus.

Porous Alundum Media

The alundum samples were sealed in Pyrex tubing by placing each precleaned test sample in a closely fitting glass tube equipped with a means for evacuating the tubing and sample and, at the same time, allowing rotation of the assembly. The glass was heated evenly with an oxygen-gas torch to red heat and forced against the sample by atmospheric pressure during evacuation of the tube. Continued heating caused the glass to fuse to the surface of the sample, forming a liquid-tight bond between the glass tube and the porous medium. Extreme care was required to avoid folding of the glass over the ends of the porous plug during heating and evacuation. The assembly was annealed carefully and sealed to the rest of the apparatus (Fig. 1).

X-ray diffraction studies showed that the alundum was substantially pure corundum. Heating to 550°C. (red heat) caused no detectable changes in crystalline structure of the alundum, and prolonged heating at 1000°C. resulted only in slightly greater crystalline perfection. Therefore, the

TABLE I

Properties of Alundum Samples

Manufacturer's specifications		Experimental data				
Sample no.	Permeability (*md.*)	Permeability (*md.*)	Porosity (calc.) (%)	Length (*cm.*)	Diameter (*cm.*)	Weight (*gm.*)
TA-7921	1000	960	28.2	4.045	2.540	58.6973
TA-7916	200	196	26.5	3.525	1.886	28.9615

sealing process at 550°C. would not be expected to alter the structure of the alundum. However, such drastic treatment may fracture the porous body or cause molten glass to enter the outer pores.

The permeabilities of the sealed samples to air were determined at a mean pressure of about 1 atm. These measurements were used to test the sealing method and were not intended to correlate with liquid permeability values. Therefore, the Klinkenberg (8) effect, which is small for flow through highly permeable media, was neglected. Comparison of the manufacturer's specifications, average permeability measurements made with air, and properties of the test samples are shown in Table I.

The permeability of each test sample to air was measured at intervals throughout the investigations and did not change beyond the limits of experimental error even when the surfaces were coated with Silane.

Capillary Systems

Special "blind-pore systems" used in this study were prepared by blowing a "bubble" on the side of a conventional capillary tube. The openings from the capillary to the blind pores were considerably larger than the capillary proper. The capillary was immersed in a liquid having the same refractive index as the glass to eliminate optical interferences with photography.

Intersecting-capillary systems used in this study were prepared by grinding minute grooves, intersecting at right angles, on a piece of plate glass. These grooves were polished, and a second piece of plate glass was fused to the first in an annealing oven. The resulting capillary systems are unique in that the capillaries have practically no distortion at their intersections.

The depths of the capillaries about equaled their widths. Photomicrographs of the capillaries are shown in Fig. 4. As seen in this figure, the diameters of the horizontal and vertical capillaries were 0.033 and 0.040 cm., respectively. The outer ends of the horizontal capillary were sealed to trap the air contained in it.

Experimental Methods

It is evident that Calhoun and Yuster (5) realized the importance and difficulty of achieving 100% liquid saturation of the porous bodies from the precautions taken in preparing samples for flow tests. In a study in this laboratory, one of the 200-md. alundum samples continued to evolve small amounts of gas after it had been evacuated for 600 hours at room temperature and 0.03 mm. Hg. This is another indication of the difficulty of evacuating porous materials. The average pore diameter in a 200-md. porous medium often is of the order of 10 μ. At 25°C. the average mean free path of air molecules is 5090 μ at 1 mm. and 6.69 μ at 760 mm. of Hg (12).

In the early stages of the study, the liquids were used in cycles in which each liquid was displaced by the next one to be used. For example, permeability values of core TA-7921 to isooctane, acetone, water, acetone, and isooctane were determined successively. These results showed that the plug properties were unchanged by contact with the liquids. However, later studies showed that more reproducible results were obtained when the plug was cleaned and dried between determinations. Although this method was more tedious, it was adopted because of the increased precision.

The following procedure for saturating permeable test plugs with liquid was developed and adopted as the most satisfactory. The plugs and tubing were evacuated for several hours, and then a small amount of liquid was allowed to enter the system slowly and to vaporize. This vapor was flushed through the plug for another period of several hours. Finally, the liquid was allowed to enter the bottom of the tube and be imbibed by the porous sample. The gases that were displaced from the porous bodies by the liquid were pumped away. After the pores and attached tubing were filled completely, several pore volumes of the liquid were allowed to flow through the test sample to dissolve trapped gases that might remain. The removal of gases from the porous medium during a flow test would be manifested by an increase in permeability in the succeeding test.

An attempt was made to increase the saturation of the alundum plug by flushing the plug and tubing with a soluble gas before and during the evacuation process used above. This procedure resulted in a very small but apparently significant increase in permeability.

Large changes in permeability, such as those caused by the development of new channels or plugging of the existing flow channels, would be indicated by a change in the slope of the plot of time versus the logarithm of the height of the falling meniscus. The slopes of the plots were constant within less than 0.5%, indicating that the permeability of the porous plug remained constant during each test, as well as from test to test. Figure 2 shows the plot of a typical permeability determination with isooctane.

The method of measurement is similar to the viscosimeter measure-

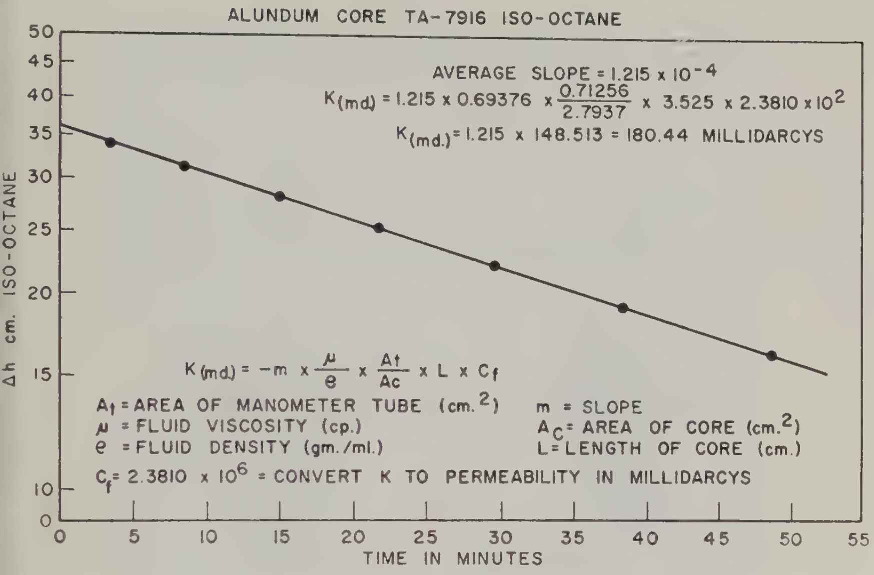

FIG. 2. Typical permeability determination.

ments made by Calhoun and Yuster (5), in that the only variables measured were time and height, which are capable of being measured with precision and accuracy.

RESULTS

Table II summarizes the results of 146 permeability determinations on the two test alundum samples with isooctane, acetone, and water with water-wet (clean) or oil-wet (Silane-treated) surfaces.

The permeabilities of the clean alundum plugs to water are slightly lower than those measured with isooctane and acetone as the flowing fluids. Conversely, the permeability of the Silane-treated plug to water is nearly the same as the permeability to acetone; both liquids indicate a higher permeability than isooctane. The small differences between values determined with isooctane and acetone in the clean plugs or between water and acetone in the Silane-coated plug are not statistically significant. The differences between values determined with water and isooctane or acetone in the clean plugs or between isooctane and water or acetone in the Silane-coated plug have an average probability of 95% of being valid.

The overall decrease in permeability caused by the Silane treatment of the alundum probably results from a small amount of plugging by the Silane, not detectable by the less precise air-permeability measurements.

Effects of surface tension on permeability values were determined by

TABLE II

Summary of Permeability Measurements (Millidarcys)

Liquid	Sample TA-7921 Clean	Sample TA-7921 Silane	Sample TA-7916 Clean
Isooctane	975	920	180
Acetone	971	940	178
Water	963	945	172
Number of determinations	32	70	44
Avg. standard deviation (each liquid)	3	5	2
Maximum deviation, %	1.2	2.7	4.6

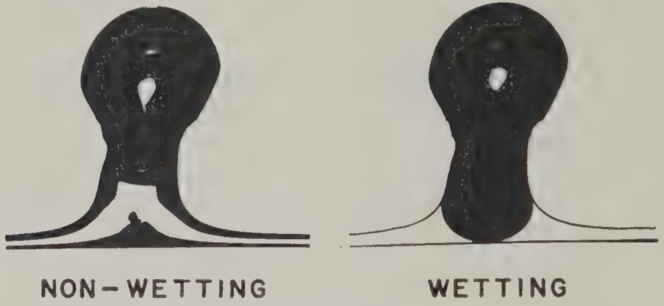

FIG. 3. Fluid distribution in blind-pore type capillaries.

using solutions of Alro Amine-O[2], an oil soluble detergent, in isooctane and Triton X-100[3], a water-oil–soluble nonionic detergent, in water as the permeating fluids. Permeability values determined with plug TA-7921 (clean) and 0.15 wt. % solutions of these detergents did not differ statistically from values determined with the pure solvents.

Solutions of KCl in water were used to study the effect of electrolyte concentration on the permeability of plug TA-7916 (clean). The average permeability values determined with water, 0.01 *N* KCl, and 1.0 *N* KCl were 172.0, 172.4, and 172.5 md., respectively. The average standard deviation of these determinations was 2 md.

One kind of capillary encountered in consolidated media is the "ink-bottle or blind pore." Figure 3 is a photomicrograph showing the behavior of a wetting and nonwetting liquid in such a capillary. The wetting liquid again bypasses the opening and allows the trapped gases, shown in black, to obstruct the capillary, thereby reducing the size of the channels. A nonwetting liquid partly fills the side capillary opening to the vug before the liquid advances beyond the opening, thus leaving a completely filled, unobstructed channel for fluid flow during the permeability measurements.[4]

[2] Trademark of the Alrose Chemical Co., Providence, Rhode Island.

[3] Trademark of Rohm & Haas Co., Philadelphia, Pennsylvania.

[4] The distribution of fluids in pore doublets has been the subject of considerable recent discussion: Moore, T. F., and Slobod, R. L., *Producers Monthly*, Vol. 20, No.

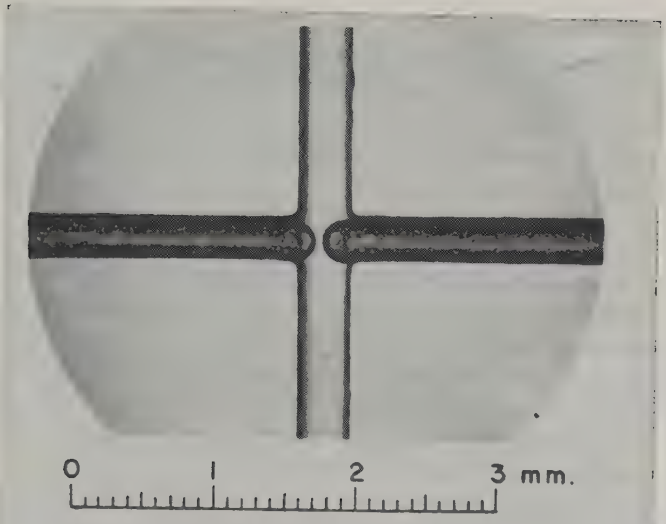

WATER — CLEAN CAPILLARY

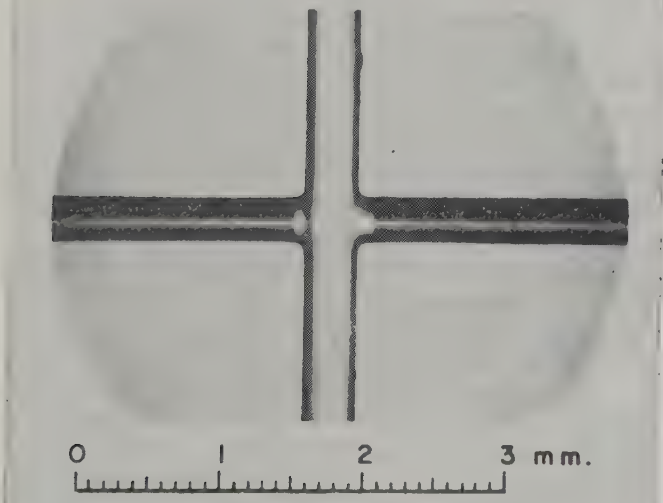

WATER — SILANE CAPILLARY

FIG. 4. Fluid distribution in wetting and nonwetting intersecting capillaries.

Figure 4 is a photomicrograph illustrating the fluid distribution in wetting and nonwetting systems composed of unique intersecting capillaries

---

10, pp. 20–30 (1956); Rose, W., and Witherspoon, P. A., *Producers Monthly*, Vol. 21, No. 2, pp. 32–38 (1956). However, it appears that under certain boundary conditions, gas may be trapped in the larger of a pair of interconnected capillaries. Such a doublet represents another type of capillary network that may account for the differences in permeability observed with wetting and nonwetting liquids.

described previously. Water was used as the liquid in both systems so that the surface tension would be the same in both systems. The wetting system was prepared by carefully cleaning the capillaries; the nonwetting system was prepared by Silane treatment. Again, it is observed that the column of wetting liquid is restricted while the capillary filled with nonwetting fluid allows unrestricted flow.

Discussion

The experimental results indicate that, for most practical purposes, such as the interpretations of petroleum-reservoir behavior from core-laboratory measurements, permeability values determined with inert cores in the laboratory are independent of the liquid used. This agrees with API Code No. 27 (13) on permeability measurement, and also with extensive early work (5, 6, 8), but is in contradiction to recent scattered reports of marked effects of wettability on permeability (7, 15).

The small differences in permeabilities of the alundum samples used in this study to liquids of different surface properties, however, have theoretical interest.

Grunberg and Nissan (9) reported a dependence of permeability on the surface tensions of the permeating fluids and a large increase in permeability as electrolyte concentration was increased. The experimental results with detergent solutions described above show that surface tension does not affect permeability. This agrees with the work of Calhoun and Yuster (5, 6). The results with KCl solutions corroborate the measurements of Calhoun and Yuster (5) and indicate that the earlier results, with plugs of comparable permeability (9), are invalid.

Small differences in the permeabilities of plugs to water and benzene were reported by Calhoun and Yuster (5). The results summarized above (Table II) are similar. It appears unlikely that these differences are caused by electrokinetic phenomena (16). A possible explanation of these small differences in permeability to various liquids may be deduced from considerations of the capillary systems described (Figs. 3 and 4).

All the liquids used would be expected to spread spontaneously over a clean mineral surface (or to rise in a capillary), such as that present in the clean alundum media, although the attendant decreases in free surface energy would vary considerably. Capillary pressures are directly proportional to the surface tensions of the liquids used, if the contact angles are the same. As acetone and isooctane have nearly equal surface tensions (20 to 25 dynes/cm.), any differences due to capillary-pressure effects should be negligible when these two liquids are used in clean alundum. It was observed that values of permeability determined with acetone and isooctane in clean alundum were statistically the same. Because of much higher surface tension of water (72 dynes/cm.), capillary pressures with water in the same alundum samples would be greater, and effects due to wettability would be correspondingly magnified. The data support this conclusion if permeabilities are decreased by capillary-pressure effects in wetting systems.

The maintenance of completely water-wet surfaces in a porous alundum medium is difficult. The detergent solution helped to assure complete wetting of alundum, even though the surfaces may have tended to become slightly hydrophobic. This increased wetting tendency of the detergent solutions may have masked the effect of lowered surface tension.

Isooctane would be expected to spread spontaneously over a surface treated with Silane, but such a surface is almost entirely nonwetting to water. Acetone has a finite contact angle with a Silane-treated surface. Calculations combining the results of measurements of capillary rise and surface-tension measurements with the pendent-drop instrument show that the contact angle between acetone and a glass surface covered with Silane is 25°. Therefore, the capillary properties of acetone do not parallel those of isooctane in a Silane-treated system. Because of this intermediate contact angle, acetone would be expected to displace air from the alundum samples rather efficiently. The differences in permeability values determined with the three liquids and a Silane-treated medium are in harmony with the preceding conclusion that capillary-pressure effects result in decreased permeability to wetting fluids. The experimental results indicate that the permeabilities of inert materials are lowered when an efficient wetting fluid is used. This does not necessarily mean that permeability per se is influenced by wettability but may reflect the influence on permeability of other variables that are affected by wettability. Degree of liquid saturation and fluid distribution in the core are two of the most obvious of such variables. Many scientists report extreme difficulty in obtaining complete liquid saturation of cores, and it is likely that such a condition is seldom, if ever, actually attained.

In laboratory work oil-field cores usually are filled with liquids by techniques allowing capillary, rather than viscous, forces to control fluid distribution during saturation of the cores. Liquid permeability determinations commonly are made with pressures and flow rates so low that capillary forces again determine fluid distribution if even small amounts of gas remain in the cores. This applies particularly to precise permeability studies using inert media. Viscous forces may predominate over capillary forces at high pressures and high flow rates. However, if high enough pressures and rates of flow could be attained, the flowing fluids, whether wetting or nonwetting, in effect would be represented by the case of the nonwetting fluids at low pressures. Therefore, the effects of wettability presumably would be eliminated.

SUMMARY

The permeabilities of clean and Silane-treated alundum plugs to liquids vary slightly with the capillary properties of the liquids. These effects are negligible for practical purposes.

Solutions of surface-active agents in isooctane and water did not cause a significant change from the permeability values determined with the pure solvents.

Studies of fluid distribution in blind-pore and intersecting-capillary systems indicate that incomplete liquid saturation probably is the cause of the small differences observed in permeability. These studies indicate that fluid distribution, and therefore fluid saturation, is affected by wettability. The saturation in turn affects the permeability, resulting in an apparent relationship between permeability and wettability. Such effects would not explain the differences in observed permeabilities of porous media to electrolyte solutions from those with water. However, the addition of KCl to water was found to have no effect on permeability values in the present investigation. Although extreme care was taken to obtain complete liquid saturation, this condition may not have been achieved. As a result of these considerations, it seems logical to attribute the differences in permeability to incomplete and variable saturation of the test samples.

ACKNOWLEDGMENTS

The authors are indebted to Drs. C. C. Templeton and S. T. Yuster for constructive discussions and criticisms of the manuscript.

REFERENCES

1. Dodd, C. G., Davis, J. W., and Pidgeon, Frances D., "Measurements of specific surface areas of nonporous powder by a pressure-decline liquid-permeability method," *J. Phys. & Colloid Chem.* **55**, No. 5 (1951).
2. Johansen, R. T., Lorenz, P. B., Dodd, C. G., Pidgeon, Frances D., and Davis, J. W., "The permeation of water and iso-octane through plugs of microscopic particles of crushed quartz," *J. Phys. Chem.* **57**, 40 (1953).
3. Carman, P. C., "Fluid flow through granular beds," *Trans. Inst. Chem. Engrs. (London)* **15**, 150 (1937).
4. Sullivan, R. R., and Hertel, K. L., *Advances in Colloid Sci.* **1** (1942).
5. Calhoun, J. C., Jr., and Yuster, S. T., "A study of the flow of homogeneous fluids through ideal porous media," Drilling and Production Practice 1946, pp. 335–355, American Petroleum Institute, New York, 1947.
6. Yuster, S. T., "Homogeneous permeability determination," Drilling and Production Practice 1946, pp. 356–363, American Petroleum Institute, New York, 1947.
7. Henniker, J. C., "Retardation of flow in narrow capillaries," *J. Colloid Sci.* **7**, No. 4, 443 (1952).
8. Klinkenberg, L. J., "The permeability of porous media to liquids and gases," Drilling and Production Practice 1941, pp. 200–213, American Petroleum Institute, New York, 1942.

9. Grunberg, L., and Nissan, A. H., "The permeability of porous solids to gases and liquids," *J. Inst. Petroleum* **29,** 193 (1943).

10. Witherspoon, P. A., "The flow of fluids through sandstones," *Illinois State Geol. Survey Circ.* No. **194** (1955).

11. Templeton, C. C., "A study of displacements in microscopic capillaries," *Trans. Am. Inst. Mining Met. Engrs.* **201,** 162 (1954).

12. Dushman, S., "Scientific Foundations of Vacuum Technique," 882 pp. Wiley, New York, 1949.

13. American Petroleum Institute, Code No. 27, "Standard Procedure for Determining Permeability of Porous Media," 2nd ed., April, 1942.

14. Johnson, T. W., and Taliaferro, D. B., "Flow of air and natural gas through porous media," *U. S. Bur. Mines Tech. Paper* No. **592** (1938).

15. Deryagin, B. V., and Krylov, N. A., "Conference on viscosity of liquids and colloidal solutions," *Akad. Nauk S.S.S.R., Otdel. Tekh. Nauk, Inst. Mashinovedeniya, Soveshchanie Vyazkosti Zhidkost. i kolloid. Rastvorov* **2,** 52 (1944); *Chem. Abstr.* **40,** 3314 (1946).

16. Lorenz, P. B., "Electrokinetic relations in the quartz-acetone system," *J. Phys. Chem.* **57,** 430 (1953).

JOURNAL OF COLLOID SCIENCE **12**, 80–98 (1957)

STUDIES UPON FLUORESCENT INSULIN CONJUGATES[1]

R. F. Steiner and Archie McAlister

Naval Medical Research Institute, National Naval Medical Center, Bethesda, Maryland

Received February 17, 1956

INTRODUCTION

The fluorescence polarization method for obtaining relaxation times of dissolved macromolecules, developed primarily by Singleterry and by Weber (1–4), while suffering from the usual drawbacks of the dynamic methods of studying large molecules, possesses several advantages shared by no other method. The great sensitivity of the available techniques for measuring polarization permits measurements to be extended to concentrations as low as 10^{-3} g./l. The method is also free from any nonspecific effects of charge or ionic strength, enabling measurements to be made upon globular proteins in electrolyte-free water over a range of pH.

The principal drawbacks of the method are its inability to yield a molecular weight directly, without the introduction of assumptions as to shape and hydration, and the possibility, which sometimes arises, of complications owing to internal degrees of rotational freedom. To these there has been added, until now, the practical one that the excited lifetimes of the fluorescent residues most suitable for protein studies had not been measured directly and had to be inferred indirectly by using relaxation times computed from dielectric dispersion methods. As the interpretation of the latter is now somewhat in doubt, it appears to be important for successful application of the method that excited lifetime measurements be made directly upon fluorescent protein conjugates.

The present paper has two main objectives. The first of these is to determine the excited lifetimes of 1-dimethylaminonaphthalene-5-sulfonic acid residues coupled to insulin for a variety of conditions. In this manner the suitability of this residue for obtaining relaxation times may be ascertained, and in addition the validity of relaxation times heretofore computed, using an assumed value for the excited lifetime, may be confirmed. Also it is of interest to observe to what extent coupling to the protein serves to protect the residue from collisional quenching.

---

[1] The opinions or assertions contained herein are the private ones of the writers and are not to be construed as official or as reflecting the view of the Navy Department or the naval service at large.

The second objective is to use combined measurements of polarization and excited lifetime to extend studies on the molecular state of insulin into regions inaccessible to other techniques. The possibility of working at extreme dilutions provides an opportunity of eliminating effects due to molecular association and makes it possible to obtain information as to the effect of various agents upon the limiting molecular state of insulin.

The fluorescence method is particularly advantageous for the study of insulin, inasmuch as the tendency of this protein to associate makes it difficult to obtain information as to the properties of the monomer at the range of concentrations accessible to the usual methods. Furthermore, the method is also well suited to the study of insulin under more drastic conditions, as in the presence of urea and organic solvents.

THEORETICAL

The degree of polarization of fluorescent radiation emitted by a small oscillator attached to a large particle in solution has been considered by Perrin and by Weber (2–6). In order to reach a useful solution it has proved necessary to replace the actual large molecule by an equivalent ellipsoid of revolution and in addition to make the following two assumptions.

a. The solvent medium may be considered as a continuum, the effective viscosity for molecular rotation being equal to the bulk viscosity. This assumption breaks down, as might be expected, when the bulk viscosity reflects the contribution of a macromolecular component comparable in size with the particle in question. However, its validity is highly probable when the particle to which the fluorescent residue is attached is of a much larger order of size than the solvent molecules. Direct evidence for its validity comes from the agreement in the values of limiting polarization, P_0, found by extrapolation of data in water and from direct measurement in concentrated sucrose or glycerol (4).

b. At least one of the following holds:

1. The axes of absorption and emission are coincident.

2. The macromolecule is spherical.

3. The axes of emission and absorption are randomly oriented with respect to the mechanical axes of the macromolecule.

The first two of these obviously hold only in special cases. The third, however, is very likely to be the case for protein conjugates, where the fluorescent residue may be attached at any one of a large number of possible sites.

Weber has derived the following general expression for the polarization of fluorescent radiation, employing assumptions (*a*) and (*b*). For unpolarized incident light:

$$R = (1/P + 1/3)/(1/P_0 + 1/3)$$

$$= \frac{\left(1 + \frac{3}{n_1}\frac{\tau_0}{\rho_0}\right)\left(1 + \left[\frac{4}{n_2} - \frac{1}{n_1}\right]\frac{\tau_0}{\rho_0}\right)}{1 + \left(\frac{2}{n_2} + \frac{1}{n_1}\right)\frac{\tau_0}{\rho_0} - \frac{6}{5}\left(\frac{1}{n_2} - \frac{1}{n_1}\right)^2 \frac{\tau_0^2}{\rho_0^2} \Big/ \left(1 + \left[\frac{2}{n_1} + \frac{1}{n_2}\right]\frac{\tau_0}{\rho_0}\right)}, \qquad [1]$$

where P = polarization
$= I_V - I_H/I_V + I_H$.
I_V, I_H = vertical and horizontal components of fluorescent radiation.
P_0 = limiting value of polarization at very high viscosities.
τ_0 = excited lifetime.
ρ_0 = relaxation time of equivalent sphere of same volume as ellipsoid.
n_1, n_2 = ratios of relaxation times about axes of ellipsoid of revolution to relaxation time of sphere.

For a spherical shape $n_1 = n_2 = 1$ and [1] reduces to [2]:

$$R = 1 + \frac{3\tau_0}{\rho_0} = 1 + \frac{\tau_0 R'T}{\eta V}. \qquad [2]$$

As $\rho_0 = 3\eta V/R'T$, where V = molar volume and η = solvent viscosity' the initial slope of R as a function of T/η predicted by [1] is given by [3]:

$$\frac{S_i}{S_0} = \frac{\rho_0}{\rho_h} = \frac{1}{3}\left(\frac{1}{n_1} + \frac{2}{n_2}\right) \qquad [3]$$

where S_i, S_0 = the initial slopes for ellipsoidal and spherical macromolecules and

$$\frac{1}{\rho_h} = 1/3\left(\frac{1}{\rho_1} + \frac{2}{\rho_2}\right).$$

Thus ρ_h is a harmonic mean of the relaxation times about the principal axes of the equivalent ellipsoid.

In practice the usual procedure for obtaining ρ_h for standard conditions (20° C. in water) is to plot $1/P + 1/3$ as a function of T/η. Thus $\rho_h^{20°}$ is related to the initial linear slope by the Eq. [4]:

$$\rho_h^{20°} = 3\left(\frac{1}{P_0} + \frac{1}{3}\right)\tau_0\left(\frac{\eta}{T}\right)^{20°} \Big/ S_i. \qquad [4]$$

The range of T/η at which appreciable deviation from linearity in $1/P$ begins depends upon the values of V/ρ_0 and n_1/n_2. If $\tau_0 \cong 10^{-8}$ and $V = 10^4$, as in the present instance, curvature may be detected at temperatures <50° in water if the axial ratio is greater than 5.

Finally some attention should be paid to the significance of ρ_h, as computed by the above means; ρ_h refers to the average *rotational* kinetic unit to which the fluorescent residue is attached and is not necessarily identical with the translational kinetic unit. Thus for a protein molecule consisting of subunits free to rotate about a given axis ρ_h will reflect the shortened relaxation time about that axis.

Experimental

a. Excited Lifetime Measurement

The apparatus employed for measuring excited lifetimes was essentially a copy of that developed by Ravilious, Farrar, and Liebson (7). Inasmuch as the details of the latter instrument have been published, only a cursory description will be made here. A schematic diagram of the present apparatus is given in Fig. 1.

The principal components of the apparatus were the light source, the modulating unit, the detecting unit, the delay unit, and the receiver. The various components, apart from the delay box and the receiver, were mounted rigidly upon an optical bench enclosed by a metal lined box.

The light source consisted of an AH-4 mercury arc, mounted in a brass housing. To avoid 60 cycle modulation of intensity, the lamp was run from a 210-volt d.-c. source, utilizing a bank of 6-volt storage batteries. A Tesla coil was used to strike the arc. A variable slit of 0.2–0.5 mm. aperture limited the beam, which then passed through a collimating lens. The parallel beam passed through an X-cut quartz crystal with both ends ground and polished

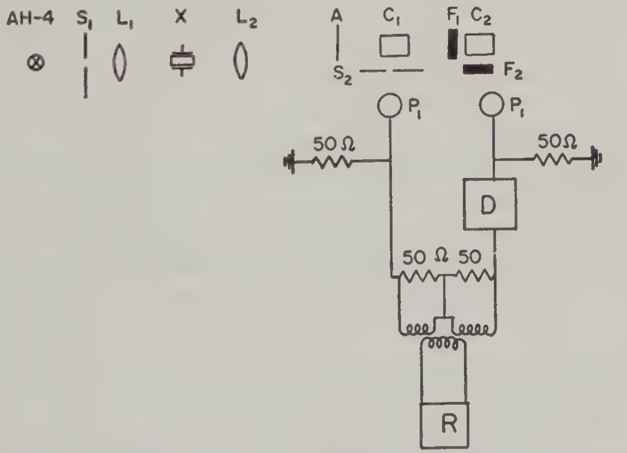

Fig. 1. Schematic diagram of excited lifetime apparatus. The meaning of the symbols is as follows: S_1: variable slit; S_2: variable aperture; L_1, L_2: lenses; X: quartz crystal; A: stop; C_1, C_2: square cells; F_1, F_2: filters; P_1, P_2: 6217 photomultiplier tubes; D: delay box; R: receiver.

to optically flat surfaces and was then focused to a line image by a second lens of 60 cm. focal length.

Modulation of the light intensity at 9.5 mc was accomplished by using the quartz crystal as a supersonic shutter. It was driven by an ARC-5 transmitter at 4.75 mc. Electrical contact was made by coating the sides of the crystal with a silver-containing lacquer.

The line image produced by the second lens was focused upon a stop consisting of a vertical line of graphite upon a quartz plate. This served partially to eliminate the zeroeth order line which correspond to unmodulated light.

When driven, the quartz crystal acted effectively as a diffraction grating. The higher order spectra, corresponding to modulated intensity, appeared as a very marked blurring and widening of the initially sharp line image.

The modulated beam then passed through two square cells in series, each adjacent to a photomultiplier tube. The first of these always contained an aqueous ludox suspension. The modulated light scattered from this suspension was sampled by the first phototube, before which a variable aperture was placed. The second cell contained either ludox, for reference readings, or the fluorescent sample. In the latter case a pair of complementary filters, a Corning 5970 for the incident beam and a Corning 3387 for the fluoresced beam, served to isolate the fluorescent radiation and eliminate scattered and reflected light.

Both detecting units were 6217 photomultiplier tubes, which viewed the square cells at an angle of 90° to the incident beam. The power supplies were two banks of dry cell batteries arranged in parallel in order to equalize the stage voltage for the two phototubes at all times.

The output of the second cell passed through a delay box consisting of a series of lengths of accurately calibrated cable which could be inserted in the circuit either individually or in series combination by means of a set of relay-activated switches. Finally the outputs of the two phototubes were combined in an inductive coupling unit and the combined output fed into a RBC receiver tuned to the frequency of modulation.

The outputs of both photomultipliers were terminated by resistors equal to the characteristic impedance of the associated transmission lines. The transmission lines were also terminated at the receiver in their characteristic impedance.

In making a measurement, the amplitudes of the individual signals from the two photocells were adjusted to equality as closely as possible by means of the variable aperture in front of the first phototube. Then, with ludox in the second cell, both phototubes were activated simultaneously and the length of delay line was varied until a null or minimum signal was observed by means of the S-meter of the receiver, corresponding to a 180° phase difference between the two signals. The second cell was then replaced by another containing the fluorescent sample. The individual amplitudes were readjusted to equality and the length of delay line was then altered until the new null was attained. Because of the finite excited lifetime of the fluorescent sample, less delay line had to be inserted to reach the null.

Because of the very high frequencies used, shielding was a major problem. Coaxial cable was used for all signal transmission lines and each section of the apparatus was enclosed in a grounded metal box.

The delay time introduced by a given length of transmission line was given by

$$t = \frac{l}{c/K^{1/2}}$$

where t = delay time.
c = velocity of light.
K = dielectric constant of the polyethylene insulation of the coaxial cable;
= 2.27.
l = length of delay line.

The difference between the lengths of delay line required for the reference ludox null and the fluorescent null was related to the excited lifetime by the equation:

$$\tau_0 = \frac{1}{\omega} \tan \omega t$$

where τ_0 = excited lifetime.
$\omega = 2\pi f$.
f = frequency of modulation;
$= 9.54 \times 10^6$.

b. Materials

Fluorescent conjugates of insulin were prepared as follows. 1-Dimethylaminonaphthalene-5-sulfonic acid (kindly supplied by Dr. G. Weber) was converted to the sulfonyl chloride by grinding with PCl_5. To 0.3 g. of crystalline zinc insulin dissolved in 50 ml. of 0.1 M $NaHCO_3$ at pH 8.2 was added slowly, with stirring, 1 ml. of acetone solution containing about 5 mg. of sulfonyl chloride. The reaction was carried out at 3° C. for 24 hours. The solution was then freed from uncoupled sulfonic acid by overnight dialysis versus redistilled water, followed by electrodialysis. The preparation was then redissolved at pH 3 and reprecipitated at pH 6 an average of three times.

The amount of coupled residue per 10^4 weight was determined from the extinction coefficient at 330 mμ, using a value for the extinction coefficient of 4.3×10^6. The values for the various preparations studied here are given in Table I.

TABLE I

Preparation	Number of residues per 12,000 units
I-C-2	0.19
I-C-3	0.20
I-C-4	0.17
I-C-5	0.12
I-C-6	0.18
I-C-7	0.051
I-C-8	0.25
I-C-9	0.14
I-C-12	0.49

The degree of labeling was rather slight. Preparation I-C-12, the most heavily labeled, had, on the average, only one residue per two 12,000 units. The other preparations were coupled to from ½ to ¹⁄₁₀ this extent.

Crystalline zinc insulin was furnished by the Eli Lilly Company.

The following criteria were adopted to insure that all the naphthalene derivative present was chemically coupled and that no free dye was present.

a. Each preparation was reprecipitated until the supernatant displayed no detectable fluorescence and the polarization of fluorescence under a standard set of conditions (H_2O, pH 2.5, 0.1 g./l.) did not change further.

b. The paper electrophoresis pattern of each preparation revealed that the fluorescent component migrated at the same rate as the protein.

Measurements of the polarization of fluorescent radiation at an angle of 90° to the incident beam were made with an adaptation of a Brice-Speiser light-scattering photometer, as has been described in an earlier publication.

RESULTS

a. Excited Lifetimes

Table II and Fig. 2 summarize all the excited lifetime data. When available, other literature values are given for comparison. The values of τ_0 for fluorescein and for rhodamine B are in agreement with those of Ravilious *et al.* (7), but are a little higher than those obtained by earlier workers (8).

The value of τ_0 for coupled insulin in water is seen to be almost independent of pH and ionic strength. The average value, about 1.28×10^{-8}, is remarkably close to that surmised by Weber. It is of particular interest that the value of τ_0 does not fall at pH's acid to 3.0, although the intensity of fluorescence falls off markedly in this range. This confirms the hypothesis of Weber that the acid quenching of the sulfonamido conjugate is noncollisional in nature (4).

The addition of ethanol, however, causes a very marked fall in excited lifetime, particularly at acid pH. It thus appears that the quenching by

TABLE II

Values of Excited Lifetimes

Fluorescent dye or conjugate	Medium	pH	$\tau_0 \times 10^8$	Other values of	Reference
Fluorescein[a]	Ethanol		$0.65 \pm .05$	0.5	8
	95% glycerol		$0.69 \pm .05$	0.63, 0.5	7, 8
Rhodamine[a] B	95% glycerol		$0.48 \pm .05$	0.44	7
I-C-12[b]	H_2O	2.1	$1.23 \pm .10$		
	H_2O	2.2	$1.26 \pm .10$		
	H_2O	2.9	$1.34 \pm .10$		
	H_2O	3.0	$1.38 \pm .10$		
	H_2O	4.2	$1.28 \pm .10$		
	H_2O	7.8	$1.36 \pm .10$		
	H_2O	7.9	$1.32 \pm .10$		
	H_2O	9.8	$1.20 \pm .10$		
	H_2O	10.7	$1.23 \pm .10$		
	H_2O	11.1	$1.24 \pm .10$		
	0.17 *M* NaCl	7.8	$1.37 \pm .10$		
	28% C_2H_5OH	1.9	$0.65 \pm .06$		
	28% C_2H_5OH	2.1	$0.61 \pm .06$		
	28% C_2H_5OH	2.2	$0.54 \pm .06$		
	28% C_2H_5OH	2.8	$0.51 \pm .06$		
	28% C_2H_5OH	7.4	$0.81 \pm .08$		
	28% C_2H_5OH	9.8	$0.85 \pm .08$		
	28% C_2H_5OH	9.9	$0.81 \pm .08$		
	28% C_2H_5OH	10.7	$0.73 \pm .08$		
	6 *M* urea	3.1	$1.13 \pm .10$		
	6 *M* urea	3.1	$1.10 \pm .10$		
	6 *M* urea	5.8	$0.98 \pm .10$		
	6 *M* urea	7.0	$1.00 \pm .10$		
	6 *M* urea	9.15	$1.00 \pm .10$		
	97% CH_3COOH		$0.96 \pm .10$		
	91% CH_3COOH		$0.96 \pm .10$		

[a] The concentration ranged from 0.01 to 0.02 mg./ml., which is well below the limit of self-quenching (8). The values cited are averaged without regard to concentration.

[b] The concentration of protein ranged from 10.0 to 1.0 mg./ml. No concentration dependence of τ_0 was observed.

ethanol is at least partly collisional in nature. Urea and glacial acetic acid likewise produce a fall in excited lifetime, although to a somewhat smaller extent.

Some mention should also be made of the accuracy of the excited lifetime results. As the frequency of modulation was known to better than 0.5 %, there was no appreciable uncertainty in the value of ω. The calibrated lengths of transmission line were known to within about 1 % and the value for the dielectric constant of the polyethylene insulation to within about

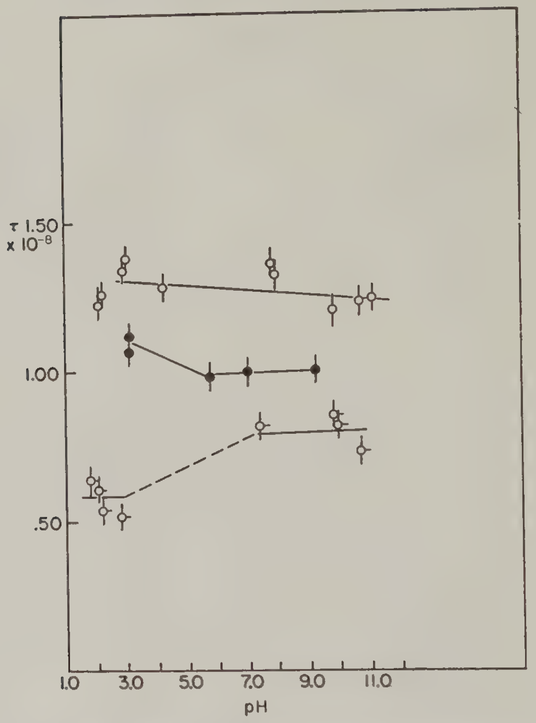

Fig. 2. Values of excited lifetime as a function of pH for I-C-12 in aqueous solution: ⊙ = H_2O; ● = 6 *M* urea; ȯ: = 28% C_2H_5OH.

1%. Hence any systematic errors should contribute to the uncertainty only to the extent of about 2%. There remain certain random errors resulting from the difficulty in locating the null precisely, as well as from occasional erratic fluctuations in phase. These limited reproducibility to about ±8% for a lifetime of 1.0×10^{-8}. As a result of the various uncertainties, the values of τ cited are probably accurate to within about ±10%.

b. Polarization Data

First of all it was necessary to ascertain the extent to which conjugation modifies the physical properties of insulin in aqueous solution and in particular to what extent its tendency to association was altered. Table III gives the sedimentation constants of a solution of I-C-12, the most heavily conjugated derivative, with a solution of native insulin under the same conditions. As can be seen, the sedimentation constants were identical within the limits of precision of the method. The appearance of the sedimentation patterns was identical. Table III also gives the relaxation times for a coupled insulin derivative and a mixture of native and conjugated

TABLE III

Comparison of Properties of Labeled and Native Insulin

Preparation	Concentration	Medium	pH	$S^{20} \times 10^{13}$	$\rho_h^{20} \times 10^8$
I-C-12	5.5	0.15 *M* NaCl	2.2	2.00	
Native insulin	5.5	0.15 *M* NaCl	2.2	2.05	
I-C-6	1.5	0.10 *M* KCl	3.15		7.9
I-C-6 plus native insulin in ratio 1:10	1.5	0.10 *M* KCl	3.15		8.0

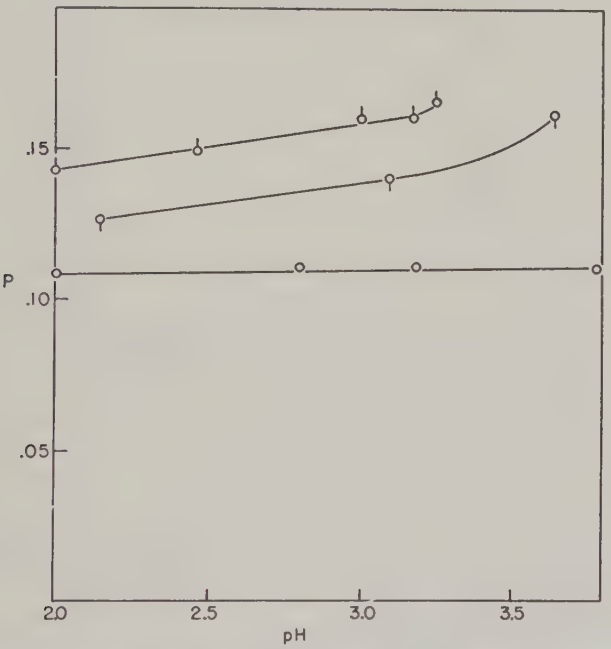

FIG. 3. Polarization as a function of pH for I-C-5 at several concentrations and ionic strengths. The temperature is 15.8° C. $\dot{\odot}$ = 0.73 g./l., 0.16 *M* KCl; $\underset{\cdot}{\odot}$ = 0.16 g./l., 0.16 *M* KCl; $\odot$ = 0.16 g./l., H_2O.

insulin in the ratio 10:1 of the same total concentration, under conditions where association is considerable. It can be seen that the relaxation times are the same. These results appear to indicate that the gross physical properties of insulin are not markedly altered by substitution to the extent employed here.

As insulin becomes insoluble between pH's 4 and 7, measurements had to be confined to the pH regions acid and alkaline to this range. The effect of pH in the acid region is given by Fig. 3. At a given concentration and ionic strength the polarization decreases markedly with decreasing pH in the region of saturation of the hydrogen ion titration curve. The decrease

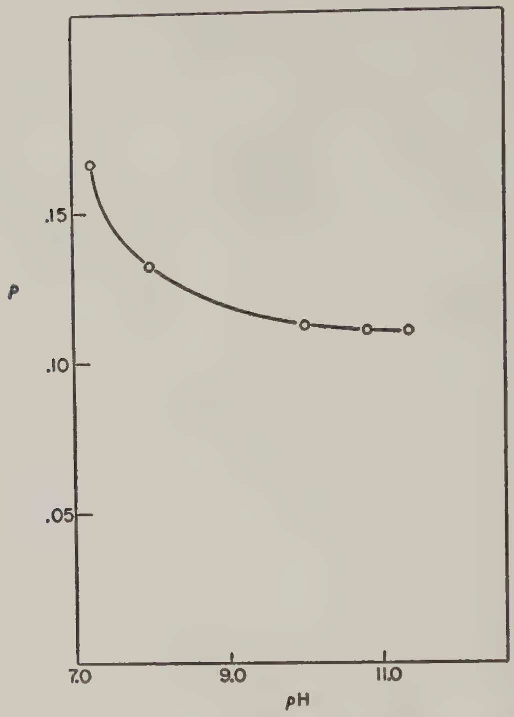

FIG. 4. Polarization as a function of pH in the alkaline region for I-C-6. The temperature is 13.9° C. The concentration is 1.49 g./l.

in polarization corresponds to a decrease in relaxation time, inasmuch as the excited lifetime does not change. Figure 4 shows the corresponding effect in the alkaline region. The polarization falls off rapidly with increasing pH, approaching a limit at pH 11.

Figures 5 and 6 show the effect of added electrolyte at an acid and an alkaline pH. In both cases the polarization rises rapidly with increasing ionic strength. Figure 6 gives $1/P$ as a function of T/η for two ionic strengths. The slope is markedly less for the higher ionic strength while the limiting value of P, P_0, is the same. Thus it is qualitatively evident that an increase in ionic strength at a given concentration results in an increased mean relaxation time. As Fig. 6 shows, the curves of $1/P + \frac{1}{3}$ as a function of T/η were linear within experimental error up to the highest temperatures studied (~48° C.).

The effect of pH and electrolyte upon $\rho_h^{20^\circ}$ for aqueous solutions of insulin is qualitatively entirely consistent with the results of studies by other methods upon the effect of these variables upon the state of association. In all probability the effect of pH and electrolyte upon the relaxation time reflects primarily changes in the state of association of the monomer.

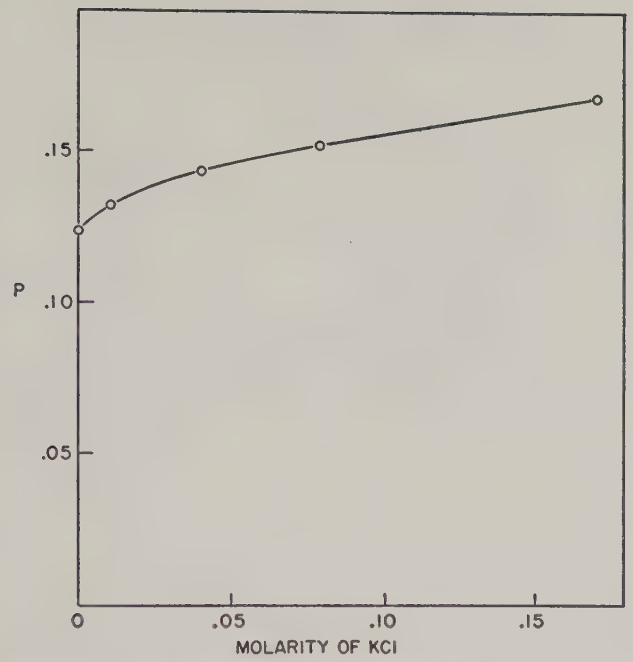

FIG. 5. Polarization as a function of ionic strength for I-C-5 at pH 3.59. The temperature is 13.1° C. The concentration is 0.66 g./l.

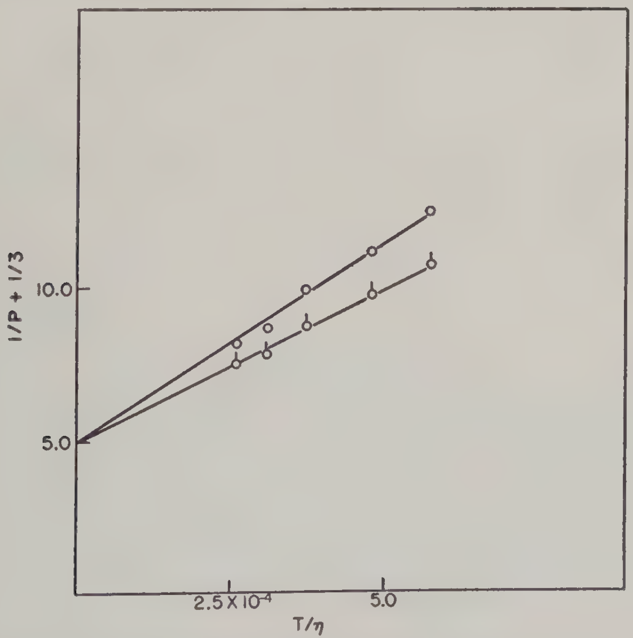

FIG. 6. $1/P + 1/3$ as a function of T/η for two ionic strengths at pH 8.97. The protein concentration is 1.34 g./l. The sample is I-C-7. $\odot$ = 0.05 M $NaHCO_3$ $\dot{\odot}$; = 0.05 M $NaHCO_3$ plus 0.5 M NaCl.

TABLE IV

Variation of P_0

pH	Medium	P_0	λ
2.5	H_2O	0.234	20.4°
2.2	H_2O	0.234	20.4
1.9	H_2O	0.234	20.4
2.95	6.1 *M* urea, 0.1 *M* KCl	0.234	20.4
2.3	28% C_2H_5OH	0.234	20.4
10.7	H_2O	0.193	30.1
10.9	5.3 *M* urea, 0.08 *M* $CO_3^=$	0.177	30.3
10.9	28% C_2H_5OH, 0.12 *M* $CO_3^=$	0.167	30.4

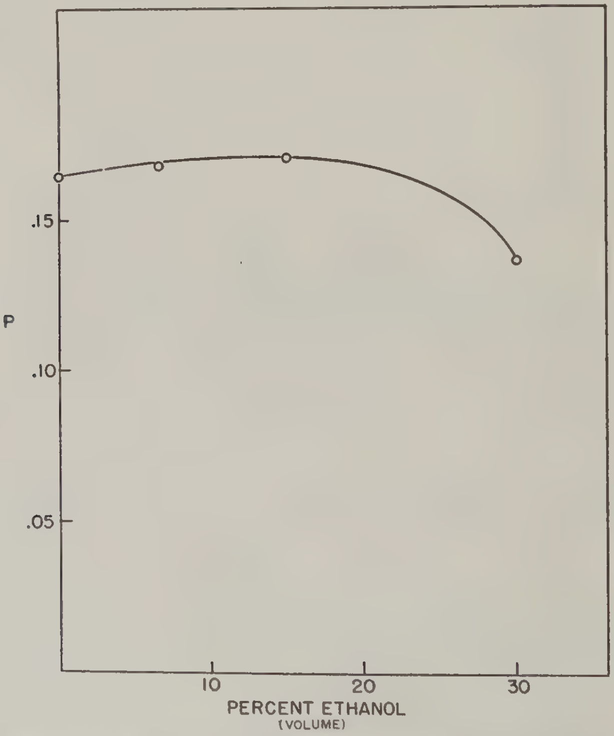

FIG. 7. Polarization of I-C-6 as a function of per cent ethanol at pH 3.15 in 0.1 *M* KCl. The temperature is 14.4° C. The protein concentration is 1.5 g./l.

Table IV gives P_0 for various conditions. The values at pH's acid to the insolubility zone are remarkably constant and close to the value obtained in glycerol. At alkaline pH's a marked fall in P_0 occurs. Table IV includes values of λ, the average angle between the axes of absorption and emission, according to the equation of Jablonski (8):

$$P_0 = \frac{3\cos^2\lambda - 1}{7 - \cos^2\lambda}.$$

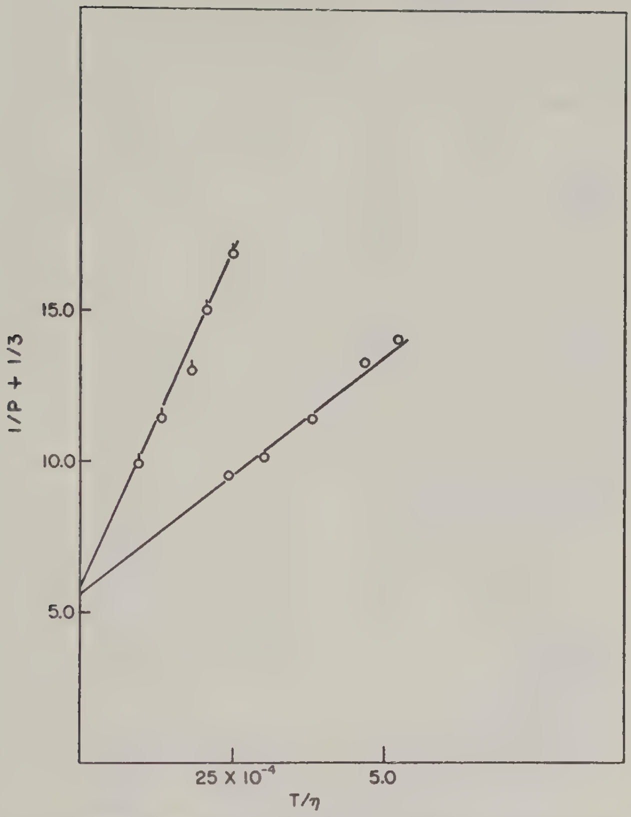

FIG. 8. $1/P + 1/3$ as a function of T/η for I-C-7 at pH 10.5 in 0.12 *M* carbonate in C_2H_5OH. The protein concentration is 0.325 g./l. ⊙ = buffer alone; $\dot{\odot}$ = 28% C_2H_5OH.

Inasmuch as it is unlikely that any pronounced change in the mechanism of fluorescence occurs with pH, it appears probable that the increase in λ reflects an increased mobility of the side chain to which the fluorescent residue is attached.

The effect of ethanol at a given concentration and ionic strength at an acid pH is shown by Figs. 7 and 8. The stepwise addition of ethanol causes first a slight increase and then a marked decrease in polarization, as Fig. 7 shows. The initial increase is attributable to the combined effects of decreasing excited lifetime and increasing viscosity. At higher ethanol concentrations these effects appear to be offset by decreasing relaxation time so that a net decrease in polarization results. Figure 8 compares $1/P + 1/3$ as a function of T/η in 28% ethanol and in buffer alone. The addition of ethanol thus markedly lowers the mean relaxation time at both acid and alkaline pH's.

Figure 9 shows $1/P + 1/3$ as a function of T/η in the presence and absence

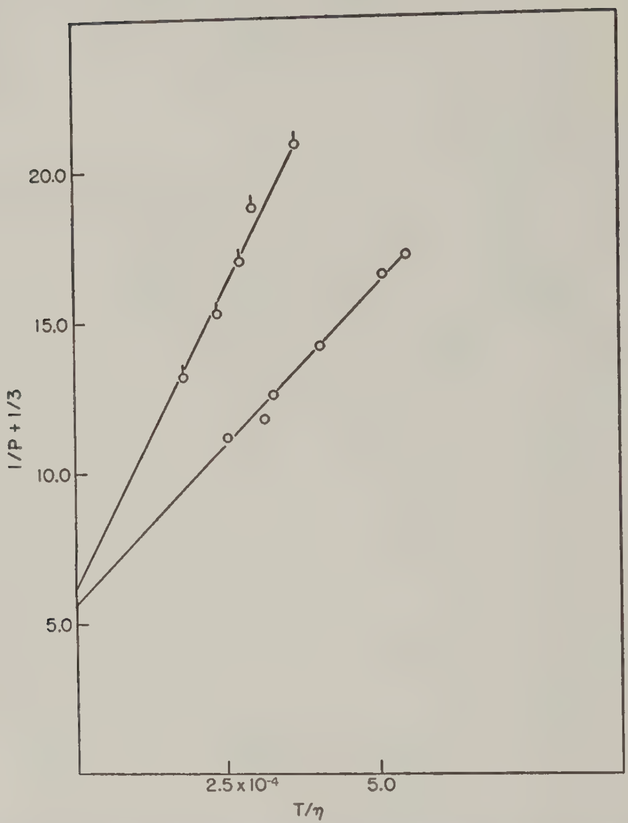

FIG. 9. $1/P + 1/3$ as a function of T/η for I-C-9 at pH 10.9 in 0.08 *M* carbonate in the presence and absence of 5.3 *M* urea. The protein concentration is 0.33 g./l. ⊙ = buffer alone; $\dot{\odot}$ = 5.3 *M* urea.

of 6 *M* urea at an alkaline pH. It can be seen that the effect of concentrated urea is to pronouncedly decrease the relaxation time, inasmuch as it has already been noted that the excited lifetime decreases in concentrated urea.

c. *Computation of Relaxation Times*

The polarization data cited above can be combined with the excited lifetime data to yield a harmonic mean of the characteristic relaxation times of the protein molecules, approximated by ellipsoids of revolution, as was discussed in the theoretical section.

The computation of the relaxation time in a pure solvent is unambiguous. However, its computation in mixed solvents involves the assumption that the effective "microscopic" viscosity is identical with the bulk viscosity. This is difficult to prove directly. The best evidence for its validity in the

TABLE V

Summary of Polarization Data

Preparation	Concentration (g./l.)	pH	Medium	$\rho_h^{20°} \times 10^8$
I-C-2	0.66	2.17	H_2O	3.84
	0.50			3.77
	0.31			3.40
	0.17			3.15
I-C-3	0.395	2.5	H_2O	3.67
	0.14			3.49
I-C-12	0.91	2.5	H_2O	3.63
	0.31			3.32
	0.10			3.43
	0.02			3.32
I-C-2	0.65	2.2	0.2 *M* KCl	4.30
	0.22			3.70
I-C-5	0.60		91% CH_3COOH	1.35
I-C-12	0.167		91% CH_3COOH	1.52
	0.075			1.52
I-C-8	0.027	2.6	28% C_2H_5OH	1.29
I-C-12	0.167	2.3	28% C_2H_5OH	1.20
	0.055			1.20
I-C-5	0.66	2.95	6.1 *M* urea, 1 *M* KCl	1.95
	0.22			1.95
I-C-5	0.66	7.3	5.6 *M* urea, 0.1 *M* KCl, 0.03 *M* phosphate	1.34
	0.22			1.34
I-C-3	0.141	11.8	H_2O	2.81
I-C-8	0.281	10.0	H_2O	3.31
I-C-12	0.565	10.7	H_2O	3.09
	0.115			2.95
	0.030			2.84
I-C-7	0.325	10.5	28% C_2H_5OH, 0.12 *M* $CO_3^=$	1.14
I-C-7	0.325	10.5	0.12 *M* $CO_3^=$	4.17
I-C-8	0.32	10.9	28% C_2H_5OH, 0.12 *M* $CO_3^=$	1.18
	0.085			1.08
	0.060			1.04
	0.017			1.08
I-C-5	0.66	9.9	5.8 *M* urea, 0.04 *M* $CO_3^=$ 0.1 *M* KCl	1.52
I-C-9	0.325	10.9	5.3 *M* urea, 0.08 *M* $CO_3^=$	1.54
	0.185			1.54

present instance is the agreement of the limiting values of polarization, P_0, obtained by measurement in glycerol and by extrapolation.

Table V summarizes the relaxation times obtained for a variety of conditions. Fig. 10 shows the concentration dependence of relaxation time for low concentrations (<1 g./l.) for a variety of conditions. Table VI gives

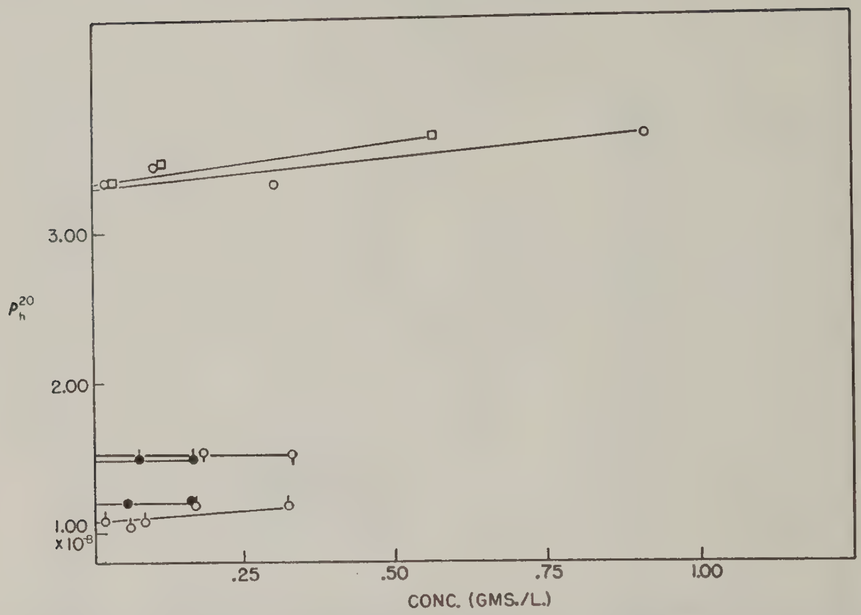

FIG. 10. Concentration dependence of ρ_h^{20} for various conditions. ⊡ = I-C-12 in H_2O, pH 10.7; ⊙ = I-C-12 in H_2O, pH 2.5; ♀ = I-C-9 in 5.3 *M* urea plus 0.08 *M* $CO_3^=$, pH 10.9; ● = I-C-12 in 91% CH_3COOH; ● = I-C-12 in 28% C_2H_5OH, pH 2.3; ♁ = I-C-8 in 28% C_2H_5OH plus 0.12 *M* $CO_3^=$, pH 10.9.

TABLE VI

Apparent Limiting Values of Relaxation Times

Preparation	pH	Medium	$\rho_h^{20°}/\tau_{c\to 0}$	$\rho_h^{20°}{}_{c\to 0} \times 10^8$
I-C-2	2.17	H_2O	2.26	2.90
I-C-12	2.5	H_2O	2.48	3.22
I-C-5		91% CH_3COOH	1.37	1.32
I-C-12		91% CH_3COOH	1.58	1.52
I-C-8	2.6	28% C_2H_5OH	2.22	1.29
I-C-12	2.3	28% C_2H_5OH	2.06	1.20
I-C-5	2.95	6.1 *M* urea, 0.1 *M* KCl	1.82	1.95
I-C-5	7.3	5.6 *M* urea, 0.1 *M* KCl, 0.03 *M* phosphate	1.35	1.34
I-C-2	2.2	0.2 *M* KCl	2.58	3.30
I-C-3	11.8	H_2O	2.25	2.81
I-C-8	11.0	H_2O	2.65	3.31
I-C-12	10.7	H_2O	2.25	2.81
I-C-7	10.5	28% C_2H_5OH, 0.12 *M* $CO_3^=$	1.42	1.14
I-C-8	10.9	28% C_2H_5OH, 0.12 *M* $CO_3^=$	1.35	1.08
I-C-5	9.9	5.8 *M* urea, 0.1 *M* KCl 0.04 *M* $CO_3^=$	1.53	1.52
I-C-9	10.9	5.3 *M* urea, 0.08 *M* $CO_3^=$	1.55	1.54

the apparent limiting relaxation times at zero concentration for a range of conditions. From Tables V and VI it can be seen that no important systematic variation in limiting relaxation time with the extent of conjugation occurs.

DISCUSSION

We shall first discuss the implications of the excited lifetime measurements. The values of τ_0 in water agree remarkably well with the estimates of Weber (4). Thus, assuming that similar values hold for other protein conjugates, it appears that the relaxation times computed by Weber (4) and by Tsao (9) are essentially correct. In turn, inasmuch as the relaxation times computed by Weber (4) for serum albumin and egg albumin agree with those obtained by Oncley with the dielectric dispersion method (10), this result serves to confirm the validity of the latter.

It is also of interest that ethanol can quench the fluorescence of the conjugated residue by a collisional mechanism. This would appear to indicate that ethanol, despite its unfavorable solvent characteristics, can penetrate the inner hydration shell of the protein.

In considering the results presented earlier it must again be emphasized that the data presented in Tables IV and V give the harmonic mean of the characteristic relaxation times of the effective *rotational* kinetic unit. This will be equivalent to the translational kinetic unit only if no internal degrees of rotational freedom are present.

The principal conclusion of the present paper is that high concentrations of urea, ethanol, or acetic acid serve to produce a "rotational dissociation" of the limiting rotational kinetic unit to a unit of relaxation time ½ to ⅓ that of the limiting unit in water which appears to be the same for both acid and alkaline pH's. The change is much too large to arise solely from a change in the degree of solvation and must reflect either an actual dissociation into units of smaller molecular weight or else an internal change in configuration in which new degrees of rotational freedom are gained. It is of course quite possible that both may occur.

The effect of urea is most logically explained on the basis of its well-known capacity to break hydrogen bonds. The effects of ethanol and glacial acetic acid appear to be explicable in terms of lowered dielectric constant, which maximizes electrostatic repulsion.

Inasmuch as detailed independent information on the shape of the limiting subunit under these conditions is not as yet available owing to the inaccessibility of the very low concentration range to the conventional methods, it is not feasible to convert the limiting relaxation time to reliable molecular weights. It might, however, be observed that the ratio of the limiting relaxation times in water and in the organic solvents is roughly that to be expected if dissociation to half molecules occurred in the latter case, as a 12,000 to 6000 dissociation.

SUMMARY

Measurements of excited lifetime and of degree of polarization have been made upon fluorescent conjugates of insulin with 1-dimethylaminonaphthalene-5-sulfonic acid. These results indicate that several organic agents serve to produce a limiting rotational kinetic unit of lower relaxation time than that found in water.

REFERENCES

1. SINGLETERRY, C., AND WEINBERGER, L. A., *J. Am. Chem. Soc.* **73,** 4574 (1951).
2. WEBER, G., *Biochem. J.* **47,** 114 (1950).
3. WEBER, G., *Biochem. J.* **51,** 145 (1952).
4. WEBER, G., *Biochem. J.* **51,** 155 (1952).
5. PERRIN, F., *J. phys.* **7,** 390 (1926).
6. PERRIN, F., *Ann. phys.* **X, 12,** 169 (1929).
7. RAVILIOUS, C., FARRAR, R., AND LIEBSON, S., *J. Opt. Soc. Amer.* **14,** 238 (1954).
8. PRINGSHEIM, P., "Fluorescence and Phosphorescence." Interscience, New York, 1949.
9. TSAO, T. C., *Biochim. et Biophys. Acta* **11,** 227 (1953).
10. ONCLEY, J. L., *Chem. Revs.* **30,** 433 (1942).

JOURNAL OF COLLOID SCIENCE 12, 99–107 (1957)

APPLICATION OF REE-EYRING GENERALIZED FLOW THEORY TO SUSPENSIONS OF SPHERICAL PARTICLES. II. FLOW IN LOW SHEAR REGION

Samuel H. Maron and Arthur W. Sisko

Physical Chemistry Laboratory, Department of Chemistry and Chemical Engineering, Case Institute of Technology, Cleveland, Ohio

Received May 4, 1956

Introduction

In the first paper of this series Maron and Pierce (1) described the successful application of the Ree-Eyring generalized theory of flow (2, 3) to a suspension of spherical particles. The data employed were those of Maron and Fok (4) on the flow of X-667 synthetic rubber latex at concentrations from 0 to 0.60 volume fraction, v; temperatures of 20°–50°C.; and shear stresses from 50 to 800 dynes/cm.^{2}. In this intermediate shear stress region the flow behavior could be expressed in terms of two flow units, namely, a Newtonian solvent, and a latex flow unit which, depending on concentration, was Newtonian or non-Newtonian.

Recently Maron and Belner (5) studied at 30°C. the flow behavior of a different sample of X-667 latex at shear stresses lower than those used by Maron and Fok. They found that below a volume fraction of 0.25 the latex was Newtonian. However, at volume fractions above 0.25 and below 0.54 the latex was non-Newtonian, but became Newtonian as the shear stress reached a low value which was different for each concentration. Finally, above $v = 0.54$ the latex remained non-Newtonian over the entire shear stress region covered.

Since the measurements of Maron and Belner correspond to lower rates of shear than those involved in Maron and Pierce's test of the Ree-Eyring theory, it was felt that an application of the theory to the low shear region would be highly desirable. Further, this region is of particular interest, since the Ree-Eyring theory predicts approach to Newtonian flow as the rate of shear approaches zero. The present paper describes the analysis of Maron and Belner's data in terms of the Ree-Eyring theory, and summarizes the results obtained.

Theoretical Considerations

The Ree-Eyring theory considers a non-Newtonian system to be composed of flow units of different relaxation times, and gives for the viscosity

η, defined as F/G, F being the shear stress and G the rate of shear, the expression

$$\eta = \sum_{n=1}^{n} \frac{x_n \beta_n}{\alpha_n} \frac{\sinh^{-1} \beta_n G}{\beta_n G} = \sum_{n=1}^{n} \frac{x_n \beta_n}{\alpha_n} \theta_n \qquad [1]$$

where

$$\theta_n = \frac{\sinh^{-1} \beta_n G}{\beta_n G}. \qquad [2]$$

In the above equations β_n is the relaxation time of the n'th flow unit, while x_n and α_n are theoretical flow parameters. All three of these quantities depend on concentration, and at least two of them, β_n and α_n, are also temperature-dependent. For the latex system under consideration, we may assume the medium, water, to be Newtonian at all rates of shear. Equation [1] takes then the form

$$\eta = \frac{x_1 \beta_1}{\alpha_1} + \frac{x_2 \beta_2}{\alpha_2} \theta_2 + \frac{x_3 \beta_3}{\alpha_3} \theta_3 + \cdots \qquad [3]$$

$$= a + b_2 \theta_2 + b_3 \theta_3 + \cdots \qquad [3a]$$

where a is the contribution made to the viscosity by the solvent, and $b_2, b_3 \cdots$ are the coefficients of the θ's for the various latex particle flow units. At constant temperature and concentration these coefficients should be constant, and hence under the specified conditions Eq. [3] should represent the variation of viscosity with rate of shear.

The quantity θ_n, as defined by Eq. [2], has the following properties. When $\beta_n G \rightarrow 0$, $\theta_n \rightarrow 1$, and the contribution to the viscosity made by a given flow unit at a given concentration becomes b_n. When all the θ's $\rightarrow 1$, Eq. [3a] reduces to

$$\eta = a + b_2 + b_3 + \cdots, \qquad [4$$

the viscosity becomes independent of rate of shear, and the flow is Newtonian. Again, when $\beta_n G \rightarrow \infty$, $\theta_n \rightarrow 0$. Hence, when all the θ's approach zero the viscosity reduces to $\eta = a$, the flow is again Newtonian, but η i now equal only to the solvent flow contribution.

DEPENDENCE OF VISCOSITY ON RATE OF SHEAR

Maron and Pierce (1) found that the flow of X-667 latex in the region of 50–800 dynes/cm.^{2} could be represented in terms of two flow units, Newtonian water unit and a non-Newtonian latex particle unit. In th present instance two flow units were sufficient to represent the data c Maron and Belner only between $v = 0.293$ and $v = 0.430$. Above th latter concentration a second non-Newtonian latex flow unit had to b introduced in order to represent the variation of η with G. In other words

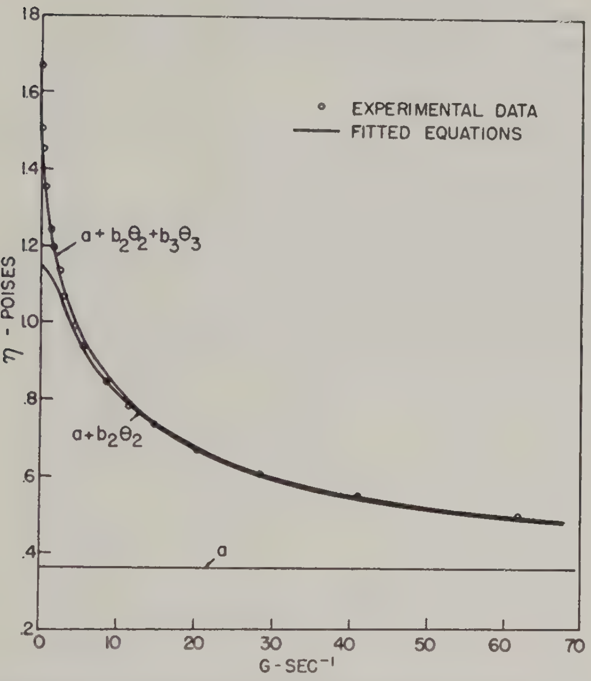

FIG. 1. Contribution of flow units to viscosity of X-667 Latex at $v = 0.564$.

ive parameters were required to reproduce the curves, namely, a, b_2, b_3, β_2, and β_3.

The procedure employed to find these parameters was as follows. At ach value of v a plot was first prepared of η vs. G, and extrapolated to $G =$). Since at $G = 0$ both θ_2 and θ_3 go to unity, the extrapolated value of η, $\eta_{G=0}$, becomes according to Eq. [4]

$$\eta_{G=0} = a + b_2 + b_3. \qquad [5]$$

Next values of β_2 were selected, and plots prepared of η vs. θ_2. With the ppropriate values of β_2 such plots were linear at the higher values of G ut showed curvature at low G's. Consequently, straight lines drawn hrough the linear portions gave b_2 as the slope and a as the intercept. Vith a and b_2 known, b_3 was obtained through Eq. [5]. Finally, θ_3 was ound at each value of G through the relation

$$\theta_3 = \frac{\eta - (a + b_2\theta_2)}{b_3} \qquad [6]$$

rom these θ_3's and the corresponding G's, β_3 was evaluated and averaged. Vhenever necessary slight adjustments were made in the constants thus btained in order to yield the best fit with the experimental curves.

Figure 1 shows the contributions made by the three flow units to the

TABLE I

Fitted and Calculated Flow Parameters

v	$a \times 10^2$		$b_2 \times 10^2$		$\beta_2 \times 10^2$		$b_3 \times 10^2$		β_3	
	Fitted	Calc.	Fitted	Calc.	Fitted	Calc.	Fitted	Calc.	Fitted	Calc.
0.293	2.30	2.39	0.48	0.26	1.00	0.58	—	0.01	—	1.00
0.341	3.28	3.16	0.60	0.55	1.20	0.88	—	0.04	—	1.34
0.387	4.35	4.32	1.11	1.15	1.50	1.43	—	0.11	—	1.86
0.430	5.93	6.10	2.55	2.46	2.25	2.41	—	0.33	—	2.67
0.468	8.70	8.76	4.57	5.21	4.00	4.23	1.0	1.02	4.0	3.94
0.511	14.6	14.6	14.5	14.3	9.75	9.32	5.0	4.88	7.0	6.86
0.546	25.0	25.0	41.3	40.4	22.5	21.7	25.0	25.3	12.0	12.6
0.564	36.4	35.3	78.0	78.6	35.0	37.6	74.0	73.5	18.9	18.8

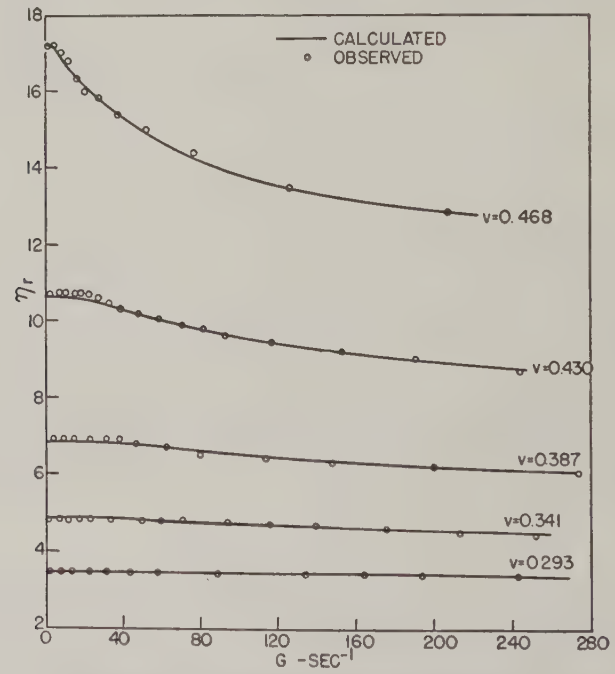

FIG. 2. Comparison of observed and calculated relative viscosities.

total viscosity of the latex at v = 0.564, the highest concentration used by Maron and Belner. It will be observed that above about G = 15 sec.$^{-}$ practically the entire viscosity is due to the first two flow units. Only below G = 15 sec.$^{-1}$ does the third flow unit begin to contribute, and the contribution becomes the more significant the lower is the value of G The effect of the third flow unit is less pronounced at lower concentrations and becomes, within experimental error, insignificant below v = 0.468.

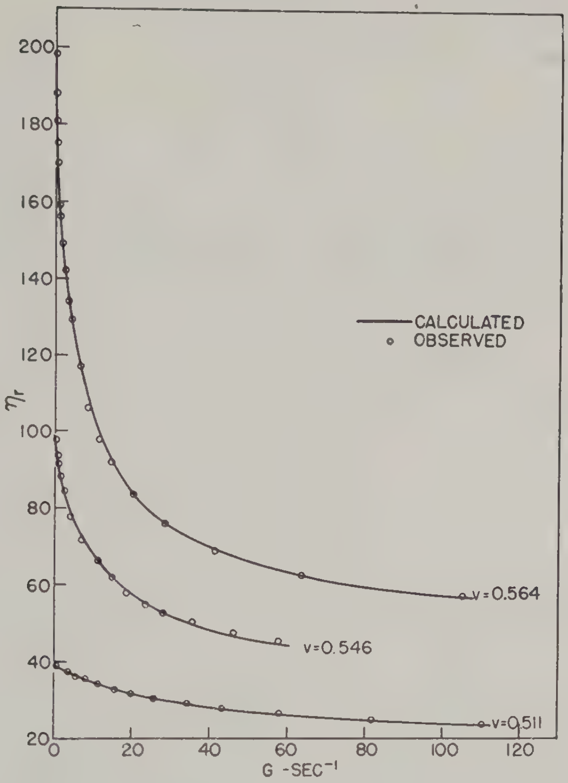

FIG. 3. Comparison of observed and calculated relative viscosities.

The values of the flow parameters deduced at the various concentrations are summarized in Table I under the headings designated as "fitted." These parameters reproduce the observed data satisfactorily, as may be seen from Figs. 2 and 3. In these figures, the points are experimental data; the solid lines are the curves calculated from the parameters given in Table I.

DEPENDENCE OF PARAMETERS ON CONCENTRATION

It was found possible to express the fitted parameters as a function of volume fraction by means of the following equations:

$$a = \frac{K_a}{(1 - \epsilon_a v)^2}. \tag{7}$$

$$b_2 = \frac{K_{b_2}(\epsilon_{b_2} v)^2}{(1 - \epsilon_{b_2} v)^3}. \tag{8}$$

$$\beta_2 = \frac{K_{\beta_2}}{(1 - \epsilon_{\beta_2} v)^3}. \tag{9}$$

$$b_3 = \frac{K_{b_3}(\epsilon_{b_3} v)^2}{(1 - \epsilon_{b_3} v)^5}. \qquad [10]$$

$$\beta_3 = \frac{K_{\beta_3}}{(1 - \epsilon_{\beta_3} v)^2}. \qquad [11]$$

The values of the various K's and ϵ's in these equations are summarized in Table II. The parameters calculated at various volume fractions by means of these equations are given in Table I under the heading "calc.", and their agreement with the "fitted" values is quite good.

TABLE II

Values of Constants in Eq. [7]–[11]

Parameter	K	ϵ
a	7.37×10^{-3}	1.517
b_2	2.05×10^{-3}	1.55
β_2	9.68×10^{-4}	1.53
b_3	3.03×10^{-5}	1.55
β_3	0.297	1.55

Equations [7] and [8] are identical in form to those found by Maron and Pierce (1) for a and b_2. However, the expression for β_2 is different, since the expression employed before would not reproduce β_2 as a function of v in the present instance. Further, it may be seen from these relations that $b_2 = b_3 = 0$ when $v = 0$, while at the latter limit $a = K_a$, $\beta_2 = K_{\beta_2}$, and $\beta_3 = K_{\beta_3}$. Since at $v = 0$ the parameter a represents the viscosity of the pure solvent, K_a should equal 7.98×10^{-3} at 30°C. As may be seen from Table II, the value of K_a actually found is 7.37×10^{-3}. This difference of 7.6% between the two quantities must be considered reasonable in view of the large extrapolation, and the fitting manipulations involved.

VISCOSITIES IN THE NEWTONIAN REGION

As was pointed out above, Maron and Belner (5) found the latex to be Newtonian at concentrations below $v = 0.25$. This means that at all values of v below 0.25 $\theta_2 = \theta_3 = 1$, and hence the viscosity should be given by Eq. [4]. For three flow units this equation becomes

$$\eta = a + b_2 + b_3 \qquad [12]$$

or

$$\eta_r = \frac{\eta}{\eta_0} = \frac{a + b_2 + b_3}{\eta_0} \qquad [13]$$

Employing Eqs. [7], [8], and [10], a, b_2, and b_3 were evaluated at the various volume fractions for which Newtonian viscosities were measured, and then η_r calculated. In Table III is given a comparison of the calculated and observed η_r's. The agreement between the two is good, especially when it is

TABLE III

Comparison of Calculated and Observed Relative Viscosities in Newtonian Region

v	$\eta_{r_{\text{obs.}}}$	$\eta_{r_{\text{calc.}}}$
0.0504	1.16	1.09
0.0979	1.36	1.28
0.149	1.63	1.57
0.198	2.00	1.96
0.246	2.49	2.51

remembered that the equations for the parameters are being extrapolated from the non-Newtonian region above $v = 0.25$ into the Newtonian region below this concentration.

LIMITING CONDITIONS OF FLOW

If Eqs. [7], [8], and [10] be substituted for a, b_2, and b_3 in Eq. [13], and also $\eta_0 = K_a$, then we obtain

$$\eta_r = \frac{1}{(1 - \epsilon_a v)^2} + \frac{K_{b_2}(\epsilon_b v)^2}{K_a(1 - \epsilon_b v)^3} + \frac{K_{b_3}(\epsilon_b v)^2}{K_a(1 - \epsilon_b v)^5}. \qquad [14]$$

On performing the indicated divisions, Eq. [14] becomes

$$\eta_{sp} = \eta_r - 1 = 2\epsilon_a v + [3\epsilon_a^2 + (B + C)\epsilon_b^2]v^2 + [4\epsilon_a^3 + (3B + 5C)\epsilon_b^3]v^3 + \cdots, \qquad [15]$$

where $B = K_{b_2}/K_a$ and $C = K_{b_3}/K_a$. In this equation v is the volume fraction of the latex particles only, and not of these plus the adsorbed soap which they carry, namely, v_t. The relation between v_t and v has been shown by Maron, Madow, and Krieger (6) to be $v_t = \gamma v$, where γ depends on the volume-to-surface average diameter of the latex particles and the length of the adsorbed soap molecule. For the latex involved here $\gamma = 1.136$. Substituting $v = v_t/\gamma$ into Eq. [15] we get

$$\frac{\eta_{sp}}{v_t} = \frac{2\epsilon_a}{\gamma} + \left[\frac{3\epsilon_a^2 + (B + C)\epsilon_b^2}{\gamma^2}\right] v_t + \left[\frac{4\epsilon_a^3 + (3B + 5C)\epsilon_b^3}{\gamma^3}\right] v_t^2 + \cdots \qquad [16]$$

From Eq. [16] it follows that as $v_t \rightarrow 0$,

$$\left(\frac{\eta_{sp}}{v_t}\right)_{v_t \rightarrow 0} = \frac{2\epsilon_a}{\gamma} = \frac{2(1.517)}{1.136} = 2.67.$$

This limiting value of η_{sp}/v_t is in good accord with that found by Maron and Pierce (1), namely, 2.60, and the expected Einstein value of 2.50 for suspensions of rigid spheres. Further, Eq. [16] predicts for the second and third coefficients 5.85 and 11.7. The values found by Maron and Pierce (1) were 5.80 and 11.8.

When $\epsilon v = 1$, Eqs. [7], [8], and [10] predict that a, b_2, and b_3 will become infinite, and hence the viscosity will also go to infinity. The volume fraction of polymer at which this will occur will be $v = 1/\epsilon$, and the total volume fraction of polymer plus adsorbed soap $v_t = 1.136/\epsilon$. On substitution of the ϵ's from Table II we obtain values of v_t ranging from 0.73 t 0.75. These are again in good agreement with those found by Maron and Pierce, and with the volume fraction expected for close packing of spheres namely, 0.74.

DISCUSSION AND CONCLUSIONS

The results presented above indicate that the Ree-Eyring theory can b used effectively to represent flow data on suspensions of spherical particle at low shear rates as well as at higher ones. However, whereas it was pos sible to represent the data of Maron and Fok at intermediate rates o shear by means of only one non-Newtonian flow unit, the latex particle two latex flow units of different relaxation times were required to represen the low shear data of Maron and Belner. The nature of this second late flow unit cannot now be defined. The only explanation which suggests itsel at present is based on the fact that latices are generally mixtures of particle which may range in size over rather wide limits. Under such condition the flow of the system at low shear rates may depend not only on the relaxa tion response of the smaller particles, which will have a smaller β, bu also on those of the larger particles, whose β will be larger. At higher rate of shear the effect of the latter will become progressively less importan and hence the system will become dependent on only one latex flow uni as was found by Maron and Pierce. Whether this surmise is valid can b tested by studying the flow behavior of a system of spherical particles c uniform size, where only a single latex flow unit would be expected to b operative at all rates of shear.

A second point of interest is the fact that the expression for β_2 foun here, Eq. [9], is different from that found by Maron and Pierce for th quantity. In the latter instance the denominator of K_{β_2} was $(1 - \epsilon_{\beta_2} v$ whereas here the cube of this expression was required. No reason can b advanced at present for this difference.

Finally, the applications of the Ree-Eyring theory, given in this and th preceding paper, raise the question as to the number of flow units whic may be required to represent the flow behavior of systems of the ty under discussion all the way from very low to very high rates of shea This problem is at present under investigation.

ACKNOWLEDGMENT

The work described herein was performed as part of the synthetic rubber resear project sponsored by the National Science Foundation.

SUMMARY

The generalized flow theory of Ree and Eyring has been applied to the data of Maron and Belner (5) on the flow behavior of X-667 latex at low rates of shear in both the Newtonian and non-Newtonian regions. Whereas in the intermediate shear regions, Maron and Pierce (1) were able to represent the results in terms of two flow units, three such units were required at the low rates of shear. These were a Newtonian water unit, and two latex flow units of different relaxation times. As a result, the dependence of viscosity on rate of shear, at any given concentration in the non-Newtonian range, required five parameters for satisfactory representation of the experimental data.

Equations have also been deduced for the dependence of the parameters on concentration, and these were used to predict the Newtonian viscosities measured by Maron and Belner below $v = 0.25$. Good agreement was found between the observed and calculated viscosities. Further, on extrapolation to $v = 0$, η_{sp}/v_t was found to be 2.67 as against the expected Einstein 2.50 for suspensions of spheres, while extrapolation to infinite viscosity gave a volume fraction in very good accord with that expected for rhombohedral close packing of spheres.

REFERENCES

1. Maron, S. H., and Pierce, P. E., *J. Colloid Sci.* **11,** 80 (1956).
2. Ree, T., and Eyring, H., *J. Appl. Phys.* **26,** 793 (1955).
3. Ree, T., and Eyring, H., *J. Appl. Phys.* **26,** 800 (1955).
4. Maron, S. H., and Fok, S. M., *J. Colloid Sci.* **10,** 482 (1955).
5. Maron, S. H., and Belner, R. J., *J. Colloid Sci.* **10,** 523 (1955).
6. Maron, S. H., Madow, B. P., and Krieger, I. M., *J. Colloid Sci.* **6,** 584 (1951).

JOURNAL OF COLLOID SCIENCE **12**: 108–130 (1957)

THE FORMATION AND PROPERTIES OF ALUMINUM PECTINATES[1]

M. A. Joslyn and Guido de Luca

Department of Food Technology, University of California, Berkeley, California

Received April 16, 1956

ABSTRACT

The extent of precipitation of pectinic acids by aluminum chloride, aluminu sulfate, and potassium alum as affected by pH, concentration of aluminum salt, an concentration of pectinic acids was determined and optimum conditions for the formation of aluminum pectinate were evaluated. Changes in viscosity, turbidity, and pH during precipitation were related to changes in properties of the aluminum pect nate recovered, and it was concluded that ion exchange rather than mutual colloida precipitation was involved in formation of aluminum pectinates.

INTRODUCTION

Pectinic and pectic acids have long been known to form insoluble salt with cations, particularly the heavy metal polyvalent cations, and in th early investigations these salts were used for the characterization of pecti substances (1). In recent years, other methods have largely supplanted thi objective, and with the exception of the use of thorium nitrate to distinguish between pectin and certain gums (2) investigations in this fiel in the United States have been limited largely to the study of film properti of pectinate salts (3). Deuel and his collaborators, however, have mac important contributions to the chemistry of coagulation of sodiu pectinates by various electrolytes (4–11). The precipitation of pectins fro dilute acid extracts of citrus wastes by aluminum sulfate and ammonia wa introduced by Jameson *et al.* in 1924 (8), but aside from brief reference to this in technological literature (1, 13–19) few if any basic investigatio of this have been reported.

Aluminum chloride in place of aluminum sulfate was proposed by Bak and Goodwin (15) and has now largely replaced the former in the industr (19). Sodium carbonate (19, 20) and calcium carbonate (21) have bee suggested in place of ammonia. The concentration of pectic substances the extract usually is about 0.5 %, but the order of addition and concentr tion of aluminum salt and alkali varies. In the original process the amou f ammonia required was added first, taking precautions to avoid local kalinization by vigorously agitating the pectin solution, and then the equired amount of 25% aluminum sulfate was added (12, 13). The pH alue at which the precipitation is carried out varies from 4.0 to 4.2 (1, 13), .0 to 4.5 (15, 21), 3.8 to 4.2 (19). In the usual German modification 1% uminum sulfate is added to the pectin solution and the pH then adjusted 4.0 with ammonia (17). The quantity of reagents required was deter- ined empirically on a test sample (1, 17, 19, 20); the conditions that sult in the formation of a precipitate (curd) of the desirable properties in ghest yield (19, 20) or in minimum viscosity of the solution in which he aluminum pectinate is suspended (15) are taken as correct. Cole and olton (20) suggest, for precipitating the pectins from extracts containing 5% pectin and having a titratable acidity equivalent to 0.015 N, the ldition of 12 ml. of aluminum chloride solution (150 g. per liter) and 24 l. of a 15% soda ash solution per liter of pectin solution. They caution, wever, that the ratio of aluminum chloride to soda ash will vary with the idity of pectin extract, the concentration of pectin present, the method ed in preparing the extract, and other factors. To facilitate precipitation d separation of pectinates a small amount of copper sulfate was used at st with aluminum sulfate (1), but because of the difficulty of removing residual copper from the precipitated pectinate this was abandoned ter.

---

[1] Taken in part from Ph.D. Thesis of G. de Luca in Agricultural Chemistry, Un versity of California, Berkeley, June 1954.

Wilson (11) explained this precipitation as the mutual colloidal floccula- n of the negatively charged pectin miscelles by positively charged alumi- m hydroxide. Joseph and Havighorst (19) in describing precipitation th aluminum chloride and sodium carbonate suggest that the aluminum lt first hydrolyzes and remains in solution in the pectin solution until e pH reaches about 3.5, when colloidal aluminum hydroxide forms and precipitates with pectin. Baker and Goodwin (14), however, in proposing e use of aluminum chloride neutralized with ammonia to pH 3.55 to ecipitate pectin at pH 4.0 to 4.5, postulated cationic precipitation, since e formation of aluminum hydroxide had to be avoided during formation aluminum pectinate if good recoveries were to be obtained.

The degree of esterification and molecular weight were shown by Deuel *al.* (4–11) to affect the coagulability of sodium pectinates by cations. At v degrees of esterification (0–10%), they are readily coagulable by mono- lent ions, but as the degree of esterification increases above 10% this no ger occurs. Above 40–50% esterification, divalent ions (Ca^{++}, Mg^{++}, $^{+++}$) no longer coagulate, and above 90% neither Cu^{++} nor Al^{+++} will agulate pectinates. In the range of 0–90%, the concentration of $AlCl_3$ uired for coagulation rapidly increases with increase in esterification. rease in molecular weight, as determined by increase in intrinsic vis- sity, results in increase in tendency to coagulate. Deuel and his collaborators (9–11) ascribe the coagulation of negatively charged pectinic acids to simple flocculation by cations on the basis that for this coagulation the usual ion series of Schulze-Hardy and Hofmeister are valid, and that the milliequivalents of chloride salt required to coagulate 1 g. of polygalacturonic acid decrease markedly with increase in charge on cation, varying from 280 meq. for NaCl to 3 meq. for $CaCl_2$ and 0.3 meq. for $AlCl_3$. The decreasing coagulability on esterification of free carboxyl groups by methanol or esterification of secondary hydroxyl groups by acetic acid is explained on the basis of changes in electrical charge on the macromolecule or hindrance to mutual approach of the chain molecules. They do not indicate the pH region in which the coagulation was observed and do not give quantitative data on the recovery of pectinic acid, the metal content of the pectinate precipitate obtained, or the appearance of pectinates formed.

Industrial experience has indicated that the recovery of pectinic acids from even partially purified extracts by precipitation with aluminum salts is rarely complete. Losses as high as 50% of the total uronides present may occur, but it is not known whether these are due to poor control of precipitating conditions or to differences in characteristics of the pectic substances present. The precipitation usually is carried out on extracts containing lower concentrations of pectins (0.1–0.5%) than when alcohol or acetone is used as precipitant but the pectin recovered is less contaminated with nonuronide matter. Thus when the pectinic acids present in two aliquots o orange peel extract were precipitated with ethanol (added to final concentration of 60%) and with aluminum chloride followed by washing with alcoholic HCl to remove aluminum salt, the alcohol precipitate containe 76% of anhydrouronic acid on an ash-free dry weight basis while the pecti from aluminum pectinate tested 86.50%.

The conditions affecting the precipitation of pectinic acids by aluminum salts (type and concentration of aluminum salt, nature and concentratio of pectinic acid, pH, temperature of precipitation; order of addition o alkali, pectin, and aluminum salt) were investigated to define optimum conditions for recovery of pectin and to obtain aluminum pectinates o low ash content. Changes in pH, viscosity, and turbidity which occur du ing the precipitation of the aluminum pectinate were observed in compar son with similar changes occurring when other cations (calcium and iron were added. From these and other observations the mechanism of th precipitation process was deduced. The results of these observations a presented in this paper.

Experimental Methods

Chemicals. The aluminum salts and other chemicals used were of th C.P. or Analytical Reagent grade and were used without further pu fication.

Pectin Preparations. Freshly prepared extracts of orange and lemon peel nd various pectin and pectinic acid preparations were used. Their prepara-ion is described in the pertinent experimental data sections.

pH. The pH of the various solutions and mixtures was determined at room emperature by an industrial model line operated Beckman glass electrode neter carefully and frequently adjusted with standard buffers of pH and 9.

Turbidity. Changes in light scattering during precipitation were measured a photoelectric tyndallometer constructed on the basis of a circuit sug-ested by Professor C. T. O'Konski using a 3-amp. light source, 34-mm. ocal length achromatic lens focusing the beam of light on a phototube with null point amplifying circuit. The galvanometer deflection was balanced otentiometrically and the potential reading was used as measure of the 0° scattered light. This was adjusted to zero with distilled water and its nternal constancy was checked with a turbidity standard prepared by uspending fine talc particles in methyl methacrylate resin.

Determinations and Characterization of Pectins and Pectinic Acids. The otal pectin content present initially and that remaining after precipitation as determined by the calcium pectate method (1). Since the residual luminum salts present in the liquid from which the precipitated aluminum ectinate was removed interfered, the aluminum and other cations present ere first separated by use of cation resin in the H-form by percolating an liquot of test solution which would yield approximately 25 mg. of calcium ectate. The recovery of pectin present was determined also from the ronide content of the alcohol precipitate of the pectin extract before recipitation with aluminum salts and from the uronide content of the luminum pectinate. Both the alcohol precipitate and the aluminum ectinate were dried under vacuum at 70°C. before determination of total ronide. The anhydrogalacturonic acid content was determined by the ydrochloric acid distillation procedure (22) and the colorimetric carbazole ethod (23, 24). The calcium pectate method and the hydrochloric acid istillation method gave results that agreed closely for the aluminum pec-nate precipitate. The pectin content of the filtrate obtained after separa-on of the aluminum pectinate, however, was lower by the hydrochloric id distillation than by the calcium pectate method. This was due to the ell-known incomplete recovery of residual pectins from dilute solutions alcohol precipitation before acid distillation. When the colorimetric rbazole method was used, however, the results obtained agreed closely ith the hydrochloric acid distillation and titration method (24). The ethoxyl content was determined by the saponification method (24) as ell as colorimetrically after oxidation to formaldehyde. The acetyl con-nt was determined by the saponification method (24). The relative scosity was measured with an Ostwald capillary viscosity pipet at 25°C. d the intrinsic viscosity calculated from measurements at three concentrations (0.05, 0.10 and 0.15 g. per 100 ml.) in presence of sodium chloride added to reduce the electroviscous effect (24).

RESULTS

Changes Occurring during Neutralization of Aluminum Salts

The mechanism of the precipitation of pectins by solutions of aluminum salts at various pH values is partly dependent upon the species present in solution, which are known to be complex and to depend on type of salts and methods used in preparing the solutions (25). In experiments with pectin solutions it was observed that aluminum chloride was much more efficient than aluminum sulfate or alum as precipitating agent. Experiments were conducted to determine how aluminum chloride differs from the other two salts, when alkalis are added.

Electrometric titrations of aluminum chloride, aluminum sulfate, and potassium alum by sodium and potassium hydroxide, ammonia, and sodium carbonate were made in the pH range 3–7. Changes in pH, appearance, and turbidity were determined during titrations of 10-ml. portions of aluminum salt solution, 0.1 M in Al^{+++} (containing 0.27 g. of aluminum ion per 100 ml. of solution) with 1 N solutions of the various alkalis.

Effect of Rate and Method of Addition of Alkali. The alkali solutions were added dropwise as well as 1 ml. at a time. The solution in a 400-ml. beake was vigorously stirred continuously during titration and the stirrer was stopped only while the pH value was measured. The rate and the amoun of alkali added, however, had little or no effect either on the course o change in pH during titration or on the percentage of neutralization a which the precipitate starts to form. The influence of the velocity of reaction on the titration curve was studied by Kohlschütter and Hautelma (26) with similar results.

Effect of Concentration of the Aluminum Salt. The effect of the concentration of aluminum salt on the course of pH changes during the titration an the point at which a precipitate formed was investigated. Aluminum sulfa solutions, both 1 M and 0.1 M in Al^{+++}, were used, and a permanent precipitate resulted when the same percentage of anions were substituted b hydroxyl groups. The same results were obtained when 0.1 M and 0.01 M solutions of aluminum chloride were used.

Chernov (27) studied the precipitation at lower aluminum sulfate concentration. His data, at the total aluminum sulfate concentration in whic the pectin precipitation takes place (0.03 M), show a decrease in solubili of the hydroxysulfate. However, his data are not directly comparable ours, since he varied the aluminum concentration and maintained a constant percentage of neutralization of the aluminum sulfate.

Titration Curves of Aluminum Chloride, Aluminum Sulfate, and Alu Neutralized by Different Alkalis. The changes in pH during the titrati

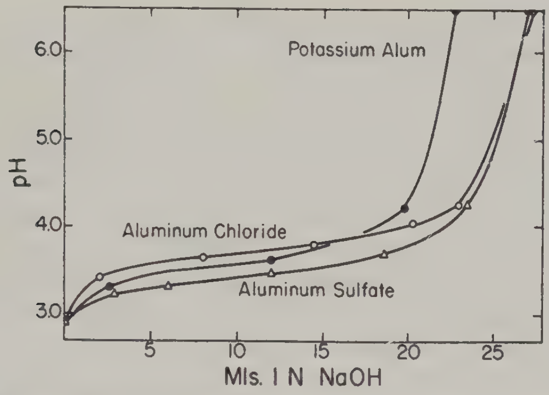

FIG. 1. Changes in pH during titration of potassium alum, aluminum sulfate, and aluminum chloride 0.1 M as Al^{+++} with 1 N NaOH.

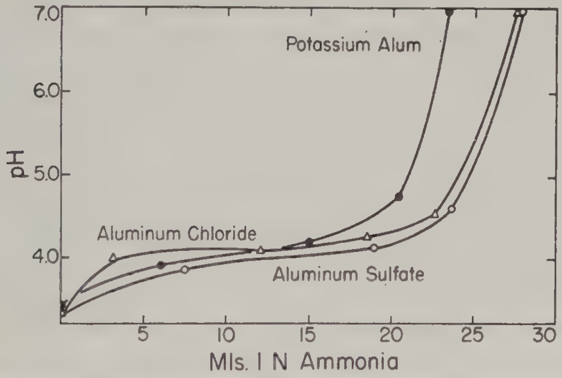

IG. 2. Changes in pH during titration of potassium alum, aluminum chloride, and aluminum sulfate 0.1 M in Al^{+++} with 1 N ammonia.

f 100-ml. aliquots of aluminum chloride, aluminum sulfate, and potassium lum 0.1 M in Al^{+++} with sodium and potassium hydroxide, ammonia, and odium carbonate were measured. The alkalis were added 1 ml. at a time nd the pH measured after 4 minutes, as suggested by Kolschütter and autelman (26). Typical of the data obtained are the pH values, plotted gainst the milliliters of normal alkalis added, shown in Figs. 1 and 2. he titration curves for the three aluminum salts behaved similarly and ere characterized by three phases. In the first zone the basic salts always emained in solution and the pH increased rapidly. In the second zone, hich was very broad and corresponded to about 65–70% of the total mount of alkali required, precipitation of a solid phase of basic salt ocurred, during which the pH value decreased very slowly. According to hernov (27) aluminum sulfate in this phase, which extends to pH 5.0, quantitatively precipitated. In the third zone a rapid rise of pH occurs, and a pH of 7.0 is reached when less than 1 equiv. of alkali is added. In each titration the theoretical equivalent of alkali should be 30 mls., but this was observed only in the case of aluminum chloride, aluminum sulfate, and alum when titrated with sodium carbonate. In the other cases, less than this amount of alkali was required. This is due probably to the adsorption or occlusion of ionic aluminum in the micellar aluminum hydroxide. Tewari and Ghosh (28) obtained similar results when aluminum chloride was neutralized with ammonia. They concluded that the more concentrated the aluminum salt was, the less alkali is required. In our experiments, this adsorption effect was greater with alum solutions than with aluminum chloride or sulfate, since the former required less alkali to reach neutrality. In all cases the pH of the alum solution increased more rapidly at lower levels of alkali added than was true of aluminum chloride and sulfate, which were almost identical.

Effect of Type of Alkali Used. The different alkalis used, with the exception of sodium carbonate, gave similar titration curves. Only with sodium carbonate was the stoichiometrical amount of alkali obtained.

pH Range in Which the Basic Aluminum Salts Begin to Precipitate. To determine the pH range at which the basic salts begin to precipitate, two series of observations were made. In the first, to a series of volumetric cylinders containing 50 ml. of aluminum salt solutions, 0.1 *M* in Al^{+++}, progressive amounts of different alkalis were added. After 24 hours the solutions were examined visually for formation of a precipitate and their pH was measured. Typical of the results obtained is that for aluminum chloride adjusted to various pH values with ammonia, shown in Fig. 3. It was

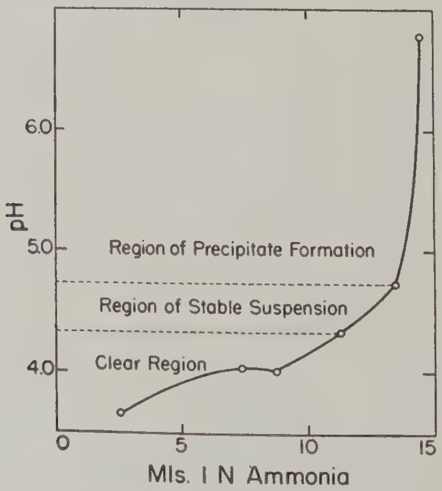

FIG. 3. Appearance of aluminum chloride solution adjusted to various pH value by addition of 1 *N* ammonia (24 hours after standing).

observed (Table I) that the aluminum chloride remains in solution at a higher pH value, that is, at a higher degree of basicity than does aluminum sulfate or alum. At a pH value of about 4.5, that is, when 78% of the chloride is substituted by hydroxyl groups, the aluminum chloride solutions were still clear. The aluminum sulfate starts to precipitate at a lower pH value (about 3.9–4.0) with each alkali, when only 27% of the sulfate anions are substituted by the hydroxyl groups of the alkalis used. Alum solutions, when titrated with different alkalis, precipitate at a pH value between 3.0 and 4.1 and a percentage of substitution of about 34–35%.

Joffe and McLean (29) reported that a 0.0075 N aluminum sulfate solution starts to precipitate at pH 3.9, and at pH 4.7 precipitation is complete. According to the same authors, aluminum chloride solutions start to precipitate at pH 4.5 and are completely precipitated at pH 5.4. In spite of the fact that they used very dilute solutions, 0.0075 N, the results obtained are very close to those found above with 0.1 N solutions. Another difference between aluminum chloride and the other two salts is that the aluminum chloride remains in the colloidal state over a wide range of pH while the other two salts precipitate directly in solid form. This phenomenon was observed by Chernov (27). According to him, on titration of aluminum chloride solutions with alkali, aluminum hydroxychloride of the composition, Al_2O_3HCl, is formed. Thomas (25, 30–32), Weiser (33), and others, however, have shown that solutions prepared from aluminum salts contain variable amounts of anions depending on the salt used and method of preparation and aging but that even the clear solution from $AlCl_3$ contains appreciable quantities of chloride. Aqueous solutions of compounds of aluminum and simple anions are now known to contain highly solvated, polymerized cations as a result of hydrolysis, polymerization, and formation of complexes in solution (25).

In this series of experiments, again the stoichiometrical amount of sodium carbonate was required to neutralize the aluminum salts.

In the above experiments the pH regions in which the solutions remained clear, became cloudy, or formed a precipitate were estimated by visual inspection. To obtain more quantitative data the pH zone in which the precipitate is formed was investigated by determining the turbidity intensity by means of a light-scattering apparatus. Measurements were taken after 15 minutes and after 24 hours, to investigate the influence of the time of reaction. In the same experiments, in order to find out if the precipitate formed was charged or not, the light-scattering intensity was measured before and after centrifugation (2500 r.p.m.). Each measurement was run with 300 ml. of 0.1 N aluminum salt to which 1 N alkali was added. Typical of the data obtained is that for aluminum chloride shown in Fig. 4 in detail, and comparative data are summarized in Table II.

The data obtained indicate that solutions of aluminum sulfate and alum

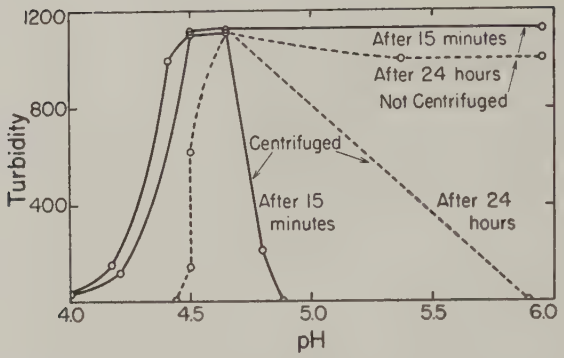

FIG. 4. Turbidity of 0.1 M aluminum chloride adjusted to various pH's by 1 N ammonia, 15 minutes and 24 hours after adjustment of pH, before and after centrifuging.

TABLE I

pH Range at Which Changes in Appearance of Aluminum Salt Solutions Occurred

Aluminum salt 0.1 M in Al^{+++}	Alkali added 1.0 N	pH range limits: Clear region	Region of stable suspension	Region of precipitation
Aluminum chloride	Ammonia	<4.3	4.3–4.65	>4.65
	Sodium carbonate	<4.2	4.2–4.6	>4.6
	Sodium hydroxide	<4.5	4.5–5.4	>5.4
	Potassium hydroxide	<4.5	4.5–5.0	>5.0
Aluminum sulfate	Ammonia	<3.95	3.95–4.0	>4.0
	Sodium carbonate	<3.95	3.95–4.05	>4.05
	Sodium hydroxide	<3.9	3.9–4.05	>4.05
	Potassium hydroxide	<3.9	3.9–4.0	>4.0
Potassium alum	Ammonia	<4.0	—	>4.0
	Sodium carbonate	<4.0	4.0–4.05	>4.05
	Sodium hydroxide	<3.95	—	>3.95
	Potassium hydroxide	<4.05	—	>4.05

TABLE II

Degree of Neutralization and pH at Which Precipitate Formed

Aluminum salt	Alkali	Per cent of replacement of anions by OH^-	pH
Aluminum chloride	Ammonia	76.0	4.50
	Sodium carbonate	66.0	4.26
	Sodium hydroxide	72.0	4.32
Aluminum sulfate	Ammonia	27.8	3.92
	Sodium carbonate	38.6	4.0
	Sodium hydroxide	27.8	4.0
Potassium alum	Ammonia	27.8	4.12
	Sodium carbonate	33.0	4.03
	Sodium hydroxide	27.8	4.01

increase in turbidity with the time, i.e., after the alkali is added the turbidity, and hence the quantity of precipitate, increases. With aluminum chloride, however, with increasing time the precipitate of basic salt is peptized. The data presented in Figs. 3 and 4 and Tables I and II indicate also that aluminum chloride remains in clear solution at a higher pH value than does aluminum sulfate or alum, and that after aluminum chloride starts to precipitate, it remains in suspension over a wider pH range than do the other salts.

Recovery of Pectins as Aluminum Pectinates

In the industry the conditions of precipitation are selected so as to obtain the maximum yield of fibrous, readily separable aluminum pectinate ("curd") from which pectins of high jelly grade can be prepared by treatment with dilute hydrochloric acid-alcohol solution. In investigations on recovery of pectins from purified orange peel extracts (34), it was found that aluminum pectinate of the desirable properties would form when 30 ml. of aluminum chloride or aluminum sulfate, 1 *M* in Al^{+++}, adjusted to the pH of 3.6–4.2 with ammonia or sodium carbonate, were added to 1 l. of an extract containing 0.5% alcohol precipitable material (having a polygalacturonide content equivalent to 0.36% anhydrogalacturonic acid) adjusted to this range of pH. With potassium alum under similar conditions, aluminum pectinate did not form but precipitation occurred when the alum was added first and then alkali was added. Even under these conditions the recovery of pectin was low; only 25–40% of the pectin present was precipitable. With aluminum chloride, the recovery of pectin present was greater than with aluminum sulfate and was at a maximum at pH 3.8, where over 95% of the pectin present was recovered when ammonia was used to neutralize the pectin and aluminum chloride solution and over 90% when sodium carbonate was used. Aluminum chloride precipitated pectin in the pH range 3.4–4.3. With aluminum sulfate precipitation occurred in a narrower range, 3.7–4.2, and the optimum pH was 3.96 for ammonia and 4.1 for the sodium carbonate-neutralized solutions. The ash contents of the aluminum pectinates obtained varied from 8% to 25%, but were lower with aluminum chloride than with aluminum sulfate and increased as the pH of precipitation increased in the range 3.4–4.2. In the pH range 3.6–4.2, the aluminum pectinate forms first as a fibrous curd which rises to the top of the solution and is easily separated and pressed. When this is separated and the pH increased, one or more additional precipitates form but these are pulverulent and settle to the bottom.

The nature of the differences between these pectinates was investigated by comparing the properties of pectinates obtained from orange peel extracts and solutions of commercial citrus pectin (citrus pectin NF). The pectins in the orange peel extract were precipitated with aluminum chloride and aluminum sulfate at pH 3.9 and the first crop of pectinate, a fibrous curd rising to the top, was separated, the pH of the mother liquid was adjusted to 5, and the second crop, a light precipitate which settled to the bottom, was separated. Both crops of pectinates were purified by washing first with alcohol containing 5% hydrochloric acid, then with neutral ethanol. The residue was redissolved in water, passed through a cation-exchange column, and again precipitated with alcohol. The composition of the pectinate and the pectinic acid obtained from it is shown in Table III. Similar results for a 0.5% solution of commercial citrus pectin (Exchange Pectin NF) are shown in Table IV. Here the pH was adjusted to

TABLE III

Analyses of Aluminum Pectinates Isolated from Orange Peel Extracts

	Fractions separated	
	1	2
	Aluminum Chloride as Precipitant	
Total pectin recovered, %	55.50	80.60
Ash in pectinate, %	8.30	12.37
Methoxyl content, %	8.52 (8.59)[a]	8.68 (9.35)
Galacturonic acid content, %	68.6 (69.6)	66 (71.4)
Esterification, %	70 (70.5)	74.7 (80.8)
Intrinsic viscosity	2.90	2.55
	Aluminum Sulfate as Precipitant	
Total pectin recovered, %	33.6	61.1
Ash in pectinate, %	9.51	16.12
Methoxyl content, %	9.60	10.70
Galacturonic acid content, %	74.28	71.89
Esterification, %	70.80	75.85

[a] Second run.

TABLE IV

Analyses of Aluminum Pectinates Isolated from Commercial Citrus Pectin Solutions

	Fraction separated			
	1	2	3	4
	Aluminum Chloride as Precipitant			
Ash in pectinate, %	8.95	33.11		
Methoxyl content, %	8.83	10.25		
Galacturonic acid content, %	80.52	80.96		
Esterification, %	63.30	71.75		
Intrinsic viscosity	1.85	1.65		
	Aluminum Sulfate as Precipitant			
Total pectin recovered, %	65.75	22.60	10.33	—
Ash in pectinate, %	6.23	4.40	30.05	66.35
Galacturonic acid content, %	91.34 (89.70)[a]	90.46 (87.35)	90.20	—
Methoxyl content, %	9.43 (10.0)	10.58 (11.51)	12.80	—
Esterification, %	60.11 (67.47)	67.01 (75.00)	77.70	—
Intrinsic viscosity	2.15	2.30	1.55	—

[a] Second run.

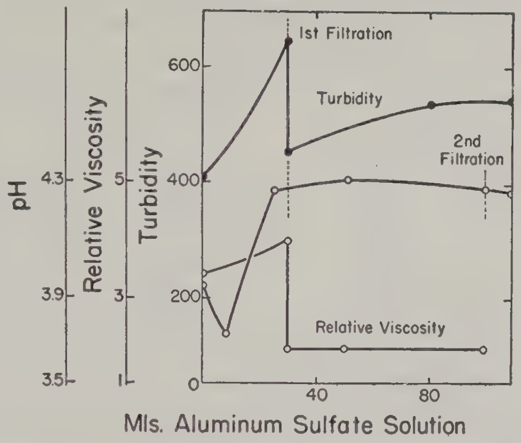

FIG. 5. Changes occurring during addition of aluminum sulfate (0.33M in Al^{+++}) to orange peel extract containing 0.36% pectin.

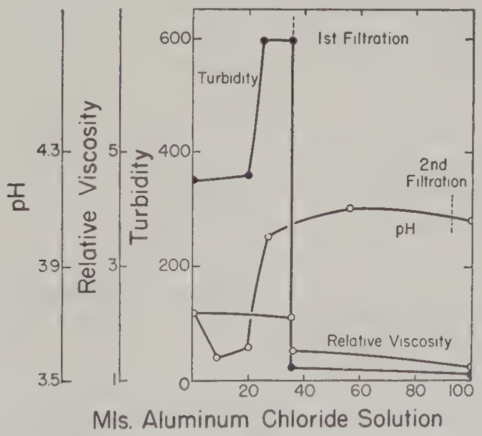

FIG. 6. Changes occurring during addition of 0.33 M aluminum chloride to orange peel extract containing 0.36% pectin.

3.8 and increasing amounts of aluminum salt were added to obtain different crops. With this only two crops were obtained with aluminum chloride but four were obtained with aluminum sulfate. The changes occurring in pH, turbidity, and relative viscosity during these precipitations are shown in Figs. 5 and 6 for orange peel extracts; and the pH changes in the precipitation of commercial pectin solution by aluminum sulfate in Fig. 7.

The data shown in Table III indicate that the ash content of pectinates obtained at optimal pH for formation of the fibrous curd was lower and the degree of esterification and molecular size of the pectinic acids obtained was higher than for the second crop. This effect was even more pronounced with commercial pectin. Even with aluminum chloride the second crop had

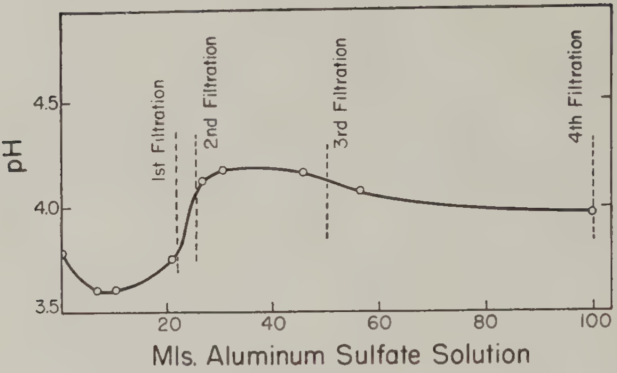

FIG. 7. Changes in pH occurring during addition of aluminum sulfate (0.33 *M* in Al^{+++}) at pH 3.8 to a 0.5% pectin at pH 3.8.

a considerably higher ash content as well as a higher degree of esterification and lower molecular weight. With aluminum sulfate the first two crops were obtained under conditions in which the basic aluminum salt did not precipitate but the third crop, much higherin ash content, apparently precipitated at pH values high enough to form basic aluminum sulfate which coprecipitated with aluminum pectinate and the fourth crop apparently was aluminum hydroxide with adsorbed sulfate, since its ash content was higher than the theoretical for pure aluminum hydroxide.

Since these data indicated that the extent of esterification, which is a measure of the number of free carboxyl groups in the polygalacturonide chain available for reaction with aluminum cations, has an important effect on ease of precipitation and type of aluminum pectinate formed this was investigated in more detail.

For this purpose, samples of pectin were prepared in which the percentage of esterification of the carboxyl groups varied between 33 % and 98 %. Samples A, B, C, D, E were prepared from the same commercial pectin (Exchange Citrus Pectin). Sample F was prepared from orange peel. Sample G with its carboxyl groups 98 % esterified was prepared by Dr. Pippen at the Western Utilization Research Branch by the diazomethane method of Vollmert (35). All the samples were purified by dissolving the pectin in water, precipitating the solution by alcohol, redissolving it again in water and precipitating a second time in alcohol and acetone, after passing the solution through a cation-exchange column. Samples A, B, C, D were demethoxylated with sodium hydroxide at the proper pH and time of contact, according to the method suggested by McCready *et al.* (36). Sample E was the original Exchange Pectin, which was purified by the same procedure. Sample F was obtained from orange peels by precipitating the extract in alcohol and acetone and purifying as above.

All samples were dissolved in distilled water and precipitated at pH 4.

TABLE V

Effect of Degree of Esterification on Recovery as Aluminum Pectinate

Pectin	Esterification, %	Pectin recovery, %	
		Aluminum chloride	Aluminum sulfate
A	33.30	99.90	99.13
B	35.00	99.95	99.39
C	43.95	99.95	99.80
D	52.55	99.95	99.93
E	66.81	98.85	95.94
F	76.30	89.35	55.30
G	98.95	0.00	0.00

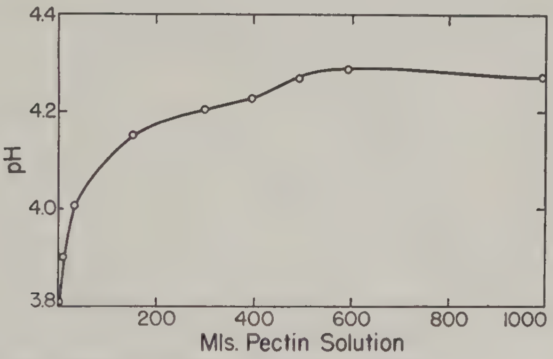

FIG. 8. Changes in pH occurring during addition of 0.5% pectin at pH 3.9 to a 0.33 *M* aluminum chloride at pH 3.8.

with aluminum chloride and aluminum sulfate. The recovery of pectin obtained is shown in Table V.

The data in Table V show that samples with a degree of esterification in the range of 33.30–52.55% are almost quantitatively precipitated. When the degree of esterification is increased, the recovery of pectin decreases. The almost completely methoxylated sample did not form a precipitate. It is interesting to note that Sample E, which was a commercial pectin which had been previously obtained as aluminum pectinate, was almost quantitatively recovered by either aluminum sulfate or chloride, whereas F, not previously precipitated as aluminum pectinate, was more highly esterified than E and gave lower recovery.

pH Changes during Formation of Aluminum Pectinate

It was observed repeatedly that the addition of solutions of aluminum salts adjusted to a particular pH value close to optimal for formation of aluminum pectinate to a pectin solution at the same pH value, resulted at first in decrease in pH value to a minimum and was then followed by a rise in pH as the pectinate formed. This change occurred whether the aluminum salt was added to a pectin solution at once or gradually, as shown in Fig. 7. When the order of addition was reversed, Fig. 8, the pH rose rapidly from

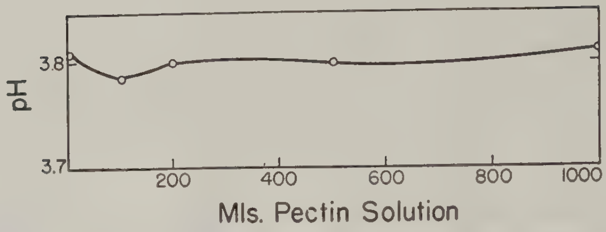

FIG. 9. Changes in pH occurring during addition of 0.5% pectin at pH 3.8 to aluminum sulfate solution (0.33 *M* in Al^{+++}) at pH 3.82.

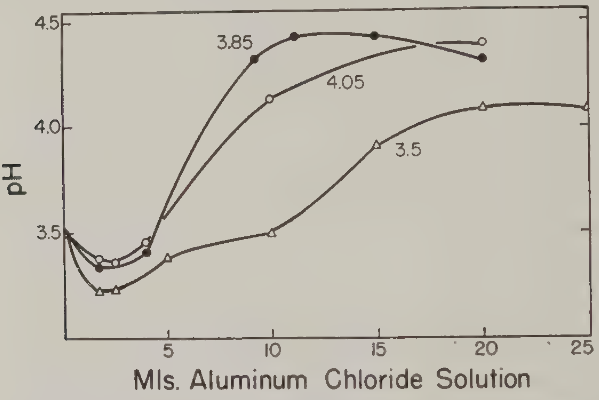

FIG. 10. Changes in pH occurring during addition of various amounts of 0.33 *M* aluminum chloride at pH levels of 3.5 to 4.05 to 0.5% purified commerical pectin adjusted to pH 3.5.

3.8 to 4.2 and then remained essentially constant. During the initial drop in pH value, the relative viscosity of the solution increased rapidly until precipitation occurred; the turbidity also increased rapidly but reached a maximum when the "curd" formed, which continued to rise after the pH minimum had been attained and the pH rose again. Maximum yield of curd occurred when the pH of the solution again reached its initial value. Aluminum sulfate gave results similar to aluminum chloride when increasing amounts were added to pectin solutions, but in the reverse case the pH did not rise as did that with aluminum chloride (Fig. 9).

The effect of initial pH of aluminum chloride solution on pH changes occurring during the addition to a 0.5 % pectin solution is shown in Fig. 10. The data plotted indicate that in the pH range 3.5–4.05, the lower the pH of the aluminum chloride solution, the greater is the degree of initial decrease in pH but the volume of aluminum chloride added to reach the minimum is the same.

When the concentration of pectin present was varied and the aluminum chloride concentration (0.33 *M*) and pH were kept constant (3.8), the data plotted in Fig. 11 showed that the higher the concentration of pectin present

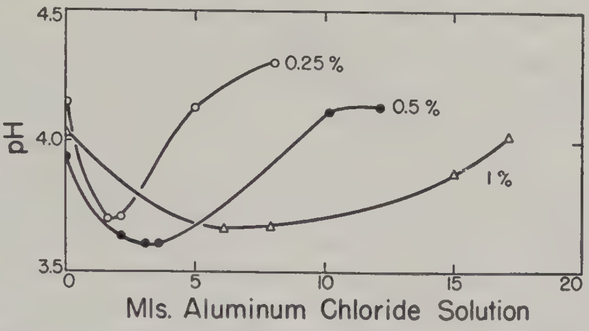

FIG. 11. Effect of concentration of pectin on pH changes in purified commercial pectin solutions following addition of 0.33 *M* aluminum chloride.

the more aluminum salt solution was required to reach the point of minimal pH. Thus a 0.25 % pectin solution needed only 1.5 ml. of aluminum chloride solution, the 0.5 % pectin solution required 3 ml., and the 1.0 % pectin solution required 6 ml.

These observations indicate that the lower the pH value of the aluminum chloride solution, the greater is the hydrogen ion exchange with aluminum ions. The greater the concentration of pectin present, the more hydrogen ions from the carbonyl groups of pectin are exchanged for the aluminum ions and the greater the decrease in pH.

The changes in pH during the addition of aluminum salts to pectin solution may be due either to absorption or desorption of hydrogen ions or hydroxyl ions at the surface of precipitates, similar to those reported for precipitation of barium sulfate which we have confirmed (37), or to simple ion-exchange reactions between the hydrogen ions of the free carboxyl groups of pectin with cations. When to 1 l. of distilled water, aluminum chloride solution at pH 3.8 was added gradually, the pH of the water at first rapidly increased from 3.8 to 4.6 owing to hydrolysis in dilute solution and then decreased to about 4.3 and remained at this pH. Similar changes probably occur in presence of pectin, the initial decrease in pH being due to release of hydrogen ions by pectin until most of the precipitable pectin forms the aluminum pectinate curd when excess aluminum salt hydrolyzes and pH increases.

pH Changes during Precipitation of Pectins by Other Cations

In addition to the investigations described above, changes in pH during precipitation of commercial citrus pectin (purified by precipitation with ethanol, passage through cation-exchange resin, and reprecipitation and vacuum drying) by cupric chloride and ferric chloride were determined. The addition of a 0.33 *N* cupric chloride solution at pH 2.5 to a 0.5 % pectin solution at pH 4.0 resulted in rapid decrease in pH and formation of a gelatinous precipitate. After the addition of only 15 ml. of cupric chloride solution to 1 l. of pectin solution, the pH dropped to 3.1 and the precipitate of copper pectinate was so gelatinous that it was impossible to stir the mixture. When the pectin solution was added gradually to 100 ml. of 0.33 *N* cupric chloride solution the pH dropped rapidly to 2.3 and remained at this point until 200 ml. of the pectin solution were added and then gradually rose until pH 2.32 was reached at 800 ml. and 2.37 after addition of 1 l. On addition of 0.33 *N* calcium chloride solution at pH 8.5 to 1 l. of pectin solution at pH 3.83, the pH at first remained constant and then dropped rapidly to 3.6 after 30 ml. of solution were added, and then decreased more gradually to pH 3.3 at 100 ml. of solution. In the converse case, addition of pectin solution to 100 ml. of calcium chloride solution resulted in rapid decrease in pH from 8.5 to 3.8 after addition of but 80 ml. of pectin solution, and then the pH remained essentially constant up to addition of the remainder of 1 l. No precipitation of calcium pectinate occurred, however, since pectinic acids more than 50% esterified do not form calcium pectinates (6). The addition of 0.33 *N* ferric chloride solution at a pH 0.9 to pectin solution at pH 3.85 resulted in an initial rapid drop in pH value to 3.6 after addition of but 8 ml. of solution; the pH remained constant during the subsequent addition of 7 ml., then rapidly dropped to pH 3.0 after 30 ml. had been added, and decreased more gradually to 2.5 after addition of 100 ml. On addition of 0.5% pectin solution at pH 2.82 to 100 ml. of 0.33 *N* ferric chloride solution at pH 0.9, the pH at first rose rapidly to 1.5, remained constant, and then more slowly increased to 2.0 when the remainder of the 1 l. of pectin solution had been added. A voluminous precipitation of ferric pectinate occurred during the addition of the first 25 ml. of ferric chloride solution, and this precipitation was complete when the pH had dropped to 3.1. During the precipitation the relative viscosity at first remained constant and then rapidly increased, but the turbidity of the solution increased continuously to a maximum. In the case of the calcium chloride addition, the turbidity gradually increased throughout the entire range of addition of calcium solution and the relative viscosity gradually decreased, probably influenced by changes in pH.

The decrease in pH of pectin solutions on addition of calcium, even without precipitation of a pectinate, was observed also by Hinton (16). Hinton reported that when a pectin solution was mixed with a calcium chloride solution, allowed to stand for an hour, and then precipitated with 60% acetone, the precipitated pectin after washing with acetone increased in calcium content from 0.05% to 1.51%, although its chloride content remained constant. The increase in calcium content was accompanied by a decrease in acidity of the pectin equivalent to the calcium absorbed. This phenomenon is typical of ion exchange in which the hydrogen ions of pectinic acid are replaced by calcium cations.

Aluminum Pectinate as Ion Exchanger

Since the above data are consistent with the theory that the formation of aluminum pectinate involves ion exchange, the ion-exchange properties of the aluminum pectinate were determined by treatment with sodium chloride and ion-exchange resins.

A sample of aluminum pectinate, prepared in the laboratory by precipitating Exchange commercial pectin with aluminum chloride, was washed thoroughly with boiling distilled water until no chloride was found in the wash water. The pectinate, purified by this method, was dried under vacuum at 70°C. Two samples of this pectinate of 4 g. each, were mixed for 10 minutes with 250 ml. of 0.5 *N* and 2 *N* sodium chloride. After filtration and washing, the aluminum was determined in the liquid fraction. As shown below, the aluminum ion was displaced by the sodium:

	0.5 *N* NaCl	2 *N* NaCl
Al_2O_3 in solution, grams	0.0205	0.0461
% exchange	0.622	1.39

Two samples of the same pectinate, 5 g. each, were kept suspended for 24 hours with the same amount of cation-exchange resins in the H form and in the Na form in slight agitation. The aluminum was determined in the resin. After 24 hours the pectinates were completely in the soluble form.

	% exchange	pH change
H-resin	94.42	From 4.60 to 2.8
Na-resin	80.60	From 4.60 to 6.20

In the case of resin in H form, the pH drops, because hydrogen ions are released from the resin in exchange for aluminum ions, which remain bound in the resin. In the case of resin in Na form, in the exchange, sodium ions are released and the pH value rises. These results demonstrate that pectin as well as pectinates has a certain exchange capacity.

Effect of Basicity of Aluminum Cations on Appearance of Aluminum Pectinates

The ionic species present in aqueous solutions are now known to be highly complex owing to solvation, hydrolysis, polymerization, and complex formation (25–27, 30–33, 38–44). It is possible, however, to characterize the basic cations on the basis of their content of hydroxyl groups per Al^{+++}, and this has been done by several investigators (27, 41–43). If the formation of aluminum pectinates involves covalent bond formation between the carboxylate ions and aluminum cations with the liberation of H^+ from the pectin micelle and Cl^- or SO_4^{--} ions from the aluminum salts, the pectinates should contain the hydroxides of the basic aluminum salts. The basicity of the aluminum cation complex was determined by Feigl and Krauss (44) by taking advantage of the ability of aluminum to form neutral oxalate complex, but their volumetric iodometric method for the determination of changes in H^+-ion concentrations was not found by Chernov (27) to be as quantitative as the method based on formation of neutral fluoride complexes first observed by Craig (45). This depends on the following reaction:

$$Al_2(OH)_5^+ + 12\ F^- \rightarrow 2\ AlF_6^{---} + 5\ OH^-$$

To favor this reaction to the right, excess hydrochloric acid as well as sodium fluoride is added and the hydrochloric acid remaining is titrated with standard alkali.

Aluminum pectinates were analyzed for the presence of combined hydroxyl groups. The pectinates were precipitated from a purified pectin solution at a low pH value, 3.8, with aluminum sulfate. The pectinate floated to the top of the beaker in the characteristic fibrous form which, because of its spongy structure, was easily filtered and pressed. The mother liquor, after the elimination of the precipitate, was brought to pH 5 with ammonia. A precipitate was formed again, this time not in a fibrous form, but as a light precipitate, which could be isolated by centrifugation. Each precipitate was divided into two aliquots, one of which was washed with distilled water, the other with 96% ethyl alcohol. All samples were washed thoroughly, until sulfate was not detected in the wash liquid. The samples were analyzed for aluminum and hydroxyl groups, and the results are given below, expressed as the ratio between equivalents of hydroxyl groups and aluminum:

	Water washing	Alcohol washing
Precipitation at low pH (3.8)	1.30	1.25
Precipitation at high pH (5.0)	2.23	2.30

The results show that in aluminum pectinates precipitated at low pH the ratio of OH:Al is over one, whereas at higher pH it is more than two.

The difference in physical structure and in the ratio OH:Al suggested the possibility that at low pH the aluminum functions as a bridge between two different pectin molecules. In other words, the aluminum ion is shared by two adjacent chains in this form of precipitate. The bridge between two pectin molecules has to be between two carboxyl groups of the polyuronic acids. The more cross-linkages through carboxyl groups, the greater will be the fibrous appearance of the precipitate.

The pectin which is not bound by the aluminum bridges remains in solution and precipitates as a light precipitate when the pH of the mixture is increased further. Cross-linkages between pectin molecules are possible only at a lower pH, when the basic aluminum ion is still in the bivalent form.

At a lower pH, the bivalent aluminum complex ion will easily form a bridge between the two pectin chains and hydrochloric acid will be liberated, decreasing the pH value.

$$2\ \text{Pectin} - COO^-H^+ + Al(OH)^{++}\ Cl^-Cl^- \text{——} \text{Pectin} - COO^-Al(OH)^{++-}OOC$$
$$- \text{Pectin} + 2\ H^+ + 2\ Cl^-$$

This would explain the fact that at a lower pH the ratio OH:Al is almost one. Since the mono- and bivalent aluminum cations are in equilibrium at the pH of precipitation, we always will have a certain amount of aluminum ions in the monovalent form and for this reason the ratio is always higher than one.

At higher pH values the monovalent basic aluminum ions cannot form a bridge, and therefore the salt formation or colloidal precipitation probably occurs.

Pectinates precipitated at different pH values with aluminum chloride and aluminum sulfate were prepared, washed with boiling distilled water until the wash water was free from sulfates and chlorides, and analyzed for ash and residual chloride or sulfate. The results obtained are given below:

			SO_4^-	
		Ash % in pectinate	In pectinate	In ash
Aluminum sulfate precipitation	pH 3.8	8.26	0.44	2.48
	pH 4.0	18.05	None	None
			Cl^-	
			In pectinate	In ash
Aluminum chloride precipitation	pH 3.7	9.15	None	None
	pH 4.2	18.70	None	None

Thomas and his collaborators (30–32) assumed that sols of aluminum are polymeric systems with the metal atom bound by "diol" (dihydroxy) bridges in which there was less than 1 equiv. of anion (other than hydroxide or oxide) per equivalent of Al^{+++}. Pokras (25) explained the increase in pH of aluminum hydroxide sols on addition of various salts observed by Thomas on the assumption that the hydrated aluminum ion is an acid in the Brönsted sense and that the hydroxides in the conjugated base are bound firmly in the complex. The increase in pH of the aluminum hydroxide sol on addition of SO_4^{--}, for example, is explained by displacement of coordinated hydroxide. In the case of aluminum pectinate formation, hydroxide displacement does not occur, at least in the initial stages of "curd" formation (but may occur later), and this can not explain the marked differences in hydroxyl:Al ratios in the different penctinates obtained. Thomas reported that the proportion of sulfate to aluminum in ignited hydrated oxides precipitated in presence of sulfate markedly decreased with decrease in pH, but this would not account for the differences in ash content and anion content of pectinates. The presence of sulfate in aluminum precipitates was observed also by Miller (40). He obtained precipitates at various pH values with 0.005 mole of aluminum per liter (using potassium alum and sodium hydroxide and aluminum chloride and sodium hydroxide).

After washing, no chloride was found in the precipitate, while the sulfate was always present in high amount in the precipitations made at low pH values. As a result of this work, he concluded that the negative ions were held in solid solution in the floc micelle. Hopkins (46) confirmed Miller's observations and noted that for dilute alum solutions the precipitate could be washed free from $SO_4^=$ ions, providing the molar ratio of OH to Al was greater than three.

It is interesting to observe that aluminum pectinates, thoroughly washed with boiling distilled water, when suspended in water give an acid reaction to the suspension. Thus when 100 g. of aluminum pectinate with 91% of moisture were suspended in 100 ml. of distilled water, the pH of the suspension was 4.4. This may be due to the existence of free unbound dissociated carboxyl groups.

Discussion

Aluminum chloride remains in solution over a wider pH range and at higher degree of neutralization than aluminum sulfate or potassium alum owing to its ability to form basic cations of lower molecular weight. Because of this ability it is able to form pectinates free of anions; this is not true of the sulfates. This soluble basic cation complex can precipitate pectinic acids by forming covalent bonds shared between two or more colinear copolymer polyuronides which thus form a fibrous macromolecule containing aluminum and displaceable hydroxyl groups, at pH of 3.8. At higher pH values such cross-linkages apparently do not form and salt formation or coprecipitation occurs. For the formation of fibrous aluminum pectinates free carbonyl groups must be present on the polyuronide micelle, and the more of these that are available, the more readily and more completely can the pectinate form. The fibrous aluminum pectinate formation can be accounted for on this basis but not on simple mutual colloidal precipitation.

Summary and Conclusions

1. The behavior of aluminum chloride, aluminum sulfate, and potassium alum when titrated with different alkalis such as sodium hydroxide, potassium hydroxide, ammonia, and sodium carbonate, was studied in relation to the pH changes and the pH range within which further addition of alkali causes a precipitate.

2. The effect of these salts on the precipitation and recovery of pectin and the changes occurring during the precipitation was studied.

3. It was found that aluminum chloride remains in a soluble form, i.e., in ionic form, at a higher degree of neutralization than the aluminum sulfate and the alum. Therefore, at the same pH value, basic aluminum chlorides are still in a clear solution, whereas the other two salts are almost quantitatively precipitated. Aluminum chloride was found to be much more efficient than the other two salts as precipitating agent for pectin.

4. The best recovery of pectin was achieved when both the aluminum chloride and the pectin extract were brought separately to a pH value of 3.9–4.0.

5. The recovery of pectin by aluminum salt precipitation is never complete. Under the best conditions, 6–10% remains in solution. Differences in degree of polymerization, degree of esterification, and distribution of methyl ester groups on the polyuronide chain influence the extent of recovery of pectins by aluminum precipitation.

6. Free carboxyl groups of pectinic acids have a predominate role in the precipitation and recovery of pectin. The higher is the degree of esterification, the more difficult is it to precipitate pectin by aluminum salts. Pectins completely methylated did not precipitate at all with aluminum chloride at its optimum pH value.

7. In the precipitation of pectin by aluminum salts apparently ion exchange rather than mutual colloidal precipitation is involved.

REFERENCES

1. KERTESZ, Z. I., "The Pectic Substances," pp. 258–259, 454–6. Interscience, New York, 1951.
2. BRYANT, E. F., *Ind. Eng. Chem., Anal. Ed.* **13,** 103 (1941).
3. SCHULTZ, T. H., OWENS, H. S., AND MACLAY, W. D., *J. Colloid Sci.* **3,** 53 (1948).
4. DEUEL, H., *Mitt. Lebensm. Hyg.* **34,** 41 (1943).
5. ANYAS-WEISZ, L., AND DEUEL, H., *Helv. Chim. Acta* **33,** 559 (1950).
6. DEUEL, H., HUBER, G., AND ANYAS-WEISZ, L., *Helv. Chim. Acta* **33,** 563 (1950).
7. DEUEL, H., AND SOLMS, J., *Kolloid-Z.* **124,** 65 (1951).
8. SOLMS, J., AND DEUEL, H., *Helv. Chim. Acta* **34,** 2242 (1951).
9. DEUEL, H., SOLMS, J., AND ALTERMATT, H., *Vierteljahrsschr. naturforsch. Ges. Zürich* **98,** 49 (1953).
10. DEUEL, H., SOLMS, J., AND DENZLER, A., *Mitt. Lebensm. Hyg.* **45,** 73 (1954).
11. DEUEL, H., AND SOLMS, J., *Advances in Chem. Ser. No.* **11,** 62 (1954).
12. JAMESON, E., WILSON, C. P., AND TAYLOR, F. M., U. S. Patent No. 1,497,884, June 17, 1924.
13. WILSON, C. P., *Ind. Eng. Chem.* **17,** 1065 (1925).
14. BAKER, G. L., AND GOODWIN, M. W., *Delaware Agr. Expt. Sta. Bull.* **216,** (1939).
15. BAKER, G. L., AND GOODWIN, M. W., *Delaware Agr. Expt. Sta. Bull.* **234** (1941).
16. HINTON, C. L., *Dept. Sci. and Ind. Research (Brit.) Food Invest. Special Rept.* No. **48** (1939). (Reprinted by Chemical Pub. Co., New York, 1939).
17. HOTTENROTH, B., *Chem. Ing. Tech.* **21,** 142 (1949).
18. HOTTENROTH, B., "Die Pektine und ihre Verwendung." Munich, 1951.
19. JOSEPH, G. H., AND HAVIGHORST, C. R., *Food Eng.* **11,** 87 (1952).
20. COLE, G. M., AND HOLTON, H. H., U. S. Patent No. 2,300,651, Nov. 3, 1942.
21. LEO, H. T., AND TAYLOR, C. C., U. S. Patent No. 2,392,854, Jan. 15, 1946.
22. MCCREADY, R. M., SWENSON, H. A., AND MACLAY, W. D., *Ind. Eng. Chem., Anal. Ed.* **18,** 290 (1946).
23. MCCOMB, E. A., AND MCCREADY, R. M., *Anal. Chem.* **24,** 1630 (1952).
24. OWENS, H. S. *et al.*, "Methods Used at Western Regional Research Laboratory for Extraction and Analysis of Pectic Materials." *U. S. Dept. Agr., Bur. Agr. and Ind. Chem. Mimeographed Circ. Ser.* AIC **340** (1952).
25. POKRAS, L., *J. Chem. Educ.* **33,** 152, 223, 282 (1956).
26. KOHLSCHÜTTER, W. D., AND HAUTELMAN, P., *Z. anorg. Chem. u. allgem. Chem.* **248,** 319 (1941).
27. CHERNOV, V. A., "On Nature of Soil Acidity," U.S.S.R. Academy of Science, Lenigrad, 1947. (Translation available in U.C. Dept. of Soils, Berkeley.)

28. Tewari, S. W., and Ghosh, S., *Kolloid-Z.* **124,** 69 (1951).
29. Joffe, J. S., and McLean, H. C., *Soil Sci.* **26,** 318 (1924); *Proc. 1st Intern. Congr. Soil Sci.*, p. 230 (1927).
30. Thomas, A. W., "Colloid Chemistry." McGraw-Hill, New York, 1934.
31. Thomas, A. W., and Whitehead, T. H., *J. Phys. Chem.* **35,** 27 (1931).
32. Thomas, A. W., and Tai, A. P., *J. Am. Chem. Soc.* **54,** 841 (1932).
33. Weiser, H. B., and Milligan, W. O., *Chem. Revs.* **25,** 1 (1939).
34. De Luca, G., and Joslyn, M. A., *Food Technol.*, in press, 1956.
35. Vollmert, B., *Makromol. Chem.* **5,** 101 (1950).
36. McCready, R. M., Owens, H. S., and Maclay, W. D., *Food Inds.* **16,** 794 (1944).
37. Coley, E. R., and Stoffer, R. L., *Science* **118,** 749 (1953).
38. Weiser, H. B., "Inorganic Colloid Chemistry," Vol. 2. Wiley, New York, 1935.
39. Weiser, H. B., "A Textbook of Colloid Chemistry." Wiley, New York, 1949.
40. Miller, L. B., *Public Health Repts.* (*U.S.*), **39,** 1502 (1924).
41. Treadwell, W. D., and Lien, O. T., *Helv. Chim. Acta* **14,** 473 (1931).
42. Treadwell, W. D., and Zürcher, M., *Helv. Chim. Acta* **15,** 980 (1932).
43. Denk, G., and Bauer, L., *Z. anorg. u. allgem. Chem.* **267,** 89 (1951).
44. Feigl, F., and Krauss, G., *Ber.* **58B,** 398 (1925).
45. Craig, M., *J. Soc. Chem. Ind.* (*London*) **1911,** 30.
46. Hopkins, E. S., "Water Purification Control." Williams & Wilkins, Baltimore, 1948.

JOURNAL OF COLLOID SCIENCE **12,** 131–134 (1957)

IRREVERSIBLE THERMODYNAMICS BY THE PRINCIPLES OF J. N. BRØNSTED AND ITS APPLICATION TO ELASTIC SOLUTIONS

LETTER TO THE EDITORS

In his last book Brønsted (1) extended his "Energetic theory" to include a group of irreversible phenomena. He introduced for that purpose the concepts of transport complexes and transport-complex potentials, but did not give detailed information on the proper application of these concepts. Later attempts by Holtan (2) to complete the system have not been successful (3).

In the present note we will summarize a new interpretation of Brønsted's transport-complexes which permits the derivation of Onsager's reciprocal relations (4). All systems, therefore, to which these apply, fall within our theory. As a general feature, the treatment along Brønsted's lines offers the advantage of giving mechanistic pictures of considerable didactic value when other theories give a formal and purely phenomenological treatment.

Brønsted pointed to the fact that the energetic quantities (K_1, K_2, $K_3 \cdots$) such as entropy, volume, chemical mass, are not transported independently of each other. When particles move they carry entropy, charge, volume, etc., as well as chemical mass and possibly also other chemical particles. These quantities are said to form a Transport-Complex (TC), and each kind of potential (P_i) for which there is an amount of the conjugate quantity (K_i) in the TC will influence the flow of the whole TC in proportion to its content of K_i. For each physically possible TC we can define a conjugate TC-potential P^{TC}, by the equation (1):

$$dP^{TC} = \Sigma_i K_i^{TC} dP_i = S^{TC} dT - V^{TC} dP + N_1^{TC} d\mu_1 + \cdots . \qquad [1]$$

Brønsted did not, however, indicate clearly how to determine the K_i's, but it appears that he meant them to be the ordinary partial molar quantities of the particles. This may be right sometimes, but as a general definition it is ruled out by the existence of a thermoelectric force between identical single crystals in different orientation. The answer is that although the electrons are alike in the two leads, those which actually carry the current may well be selected in different ways according to the orientation of the current in the anisotropic crystal.

In order to make sense, therefore, the entropy and the other quantities to be inserted in [1] must relate to the actually transported particles. The question of assigning a definite entropy value to these is the same which is met in the transition-state theory of chemical reactions. For the soundness in doing so both statistical and thermodynamic arguments can be given which are similar to those by which pseudo-components were introduced in the treatment of phase transitions (5).

For systems in internal equilibrium a Gibbs-Duhem equation will hold for all TC's and for all physically possible changes in the potentials; hence according to [1] in all systems in internal equilibrium:

$$dP^{TC} = 0. \qquad [2]$$

States of nonequilibrium or incomplete equilibrium can be established either by restrictions on the transportability of one or more of the components (semipermeable membranes, osmotic cells) or by the maintenance of a steady current of some energetic quantity.

The general theorem on which to build the treatment is now, that the current J^{TC} of any TC depends on the potential gradients through—and only through—the gradient in the conjugate TC-potential. In a rather wide class of cases the relation is linear.

$$J^{TC} = J(\text{grad } P^{TC}) = -\lambda \text{ grad } P^{TC}. \qquad [3\ a, b]$$

The conductivity coefficient, λ, of any mobile TC is different from zero, except across membranes which are impermeable to TC, and with the same exception we have the general relation:

$$J^{TC} = 0, \text{ if } P^{TC} = \text{constant}, \quad \text{or:} \quad dP^{TC} = 0. \qquad [4]$$

Comparison with [2] shows the analogy between states in equilibrium and states in which a TC is static. This works out to be an expression of the famous principle of Thomson (Lord Kelvin), but without the ambiguity as to which processes may be singled out as quasi-reversible.

Onsager's relations are derived by substitution into the phenomenological equation:

$$J_i = \Sigma_k L_{ik} X_k\ . \qquad [5]$$

The generalized forces X_k are:

$$X_k = -\text{grad } P_k \qquad [6]$$

and the currents J_i are made up of contributions from those TC's which contain the i'th quantity (the TC's are numbered by the index l):

$$J_i = \Sigma^l J^{TC,l}\ K_i^{TC,l}\ . \qquad [7$$

Applying [3*b*] to each TC, we obtain for the coefficients in [5]:

$$L_{ik} = \Sigma^l \lambda^l K_i^{TC,l} K_k^{TC,l} = L_{ki}\ . \qquad [8$$

Each TC is dragged by the k'th gradient with a force proportional to its content of the k'th quantity, K_k, and its contribution to the i'th current is proportional to its content of the i'th quantity, K_i. Passing to the symmetrical coefficient we find the same two quantities only with their roles inverted.

The detailed discussion of the basic assumptions and of the general application of this new method will be the object of a monograph under preparation. Among its virtues are the uniformity in the treatment of membrane equilibria and steady-state systems and the possibility of treating systems with nonlinear elements to which Onsager's relations do not apply. In the latter group we find, for example, rectifiers (p-n Junctions), polarographic cells, and non-Newtonian flow. Because of its novelty we will add a short account of the analysis of the elastic recoil (6) and of the flow-potential effects (7) in polyelectrolyte solutions. In the flourishing theories of non-Newtonian flow the recoil is generally neglected and the electrical effects have been left undiscovered until very recently.

In a recoil experiment (6), when the column of polymer solution is virtually at rest in a displaced position, it withstands a pressure difference and must be in a state of nonequilibrium. Very long relaxation times are involved in the attainment of equilibrium in the network of polymer molecules, but water must be in equilibrium. The state can be described as an osmotic equilibrium in which the polymer acts as it own membrane, and we can apply Gibbs-Duhem's equation to any segment along the column, the coordinate being x, $0 \leq x \leq l$, index P designating polymer and index o water:

$$-Vdp + N_P d\mu_P + N_o d\mu_o = 0 \tag{9}$$

$$\partial p/\partial x = \Delta p/l;\ \partial\mu_o/\partial x = 0\ . \tag{10}$$

$$N_P \partial\mu_P/\partial x = V\partial p/\partial x = V\Delta p/l\ . \tag{11}$$

When the polymer is a polyelectrolyte it dissociates, e.g., in ν cations K^+ to each polyanion $A^{-\nu}$, and we can introduce electrochemical potentials into [9]. Assuming K^+ to be in equilibrium throughout the solution just as the water, we find an electrical potential gradient which we identify with the "flow potential":

$$-Vdp + N_A d\bar{\mu}_A + \nu N_A d\bar{\mu}_K + N_o d\mu_o = 0\ . \tag{12}$$

$$\partial\bar{\mu}_K/\partial x = 0 = \partial\mu_o/\partial x;\ d\bar{\mu}_A = d\mu_A - \nu N_A F d\psi\ . \tag{13}$$

$$N_A \partial\mu_A/\partial x - \nu N_A F \partial\psi/\partial x = V\partial p/\partial x = V\Delta p/l\ . \tag{14}$$

The flow potential is the Donnan potential of the osmotic distribution and except at fairly high salt concentrations the electric term will dominate on the left-hand side of [14].

Within the elastic range (6) where recoil is almost complete a column of polyelectrolyte will therefore act as a transducer and give electric response to mechanical impetus with small dissipation of energy. A possible significance of this effect in the sensory functions of the inner ear has been proposed (7, 8).

When at higher pressure gradients the solutions flow at a reasonable rate, we can no longer use this static treatment but must insert in an equation like [3*a*] the nonlinear law according to which the polymer network yields to an increasing shearing force, but there will still be an osmotic distribution and a flow-potential phenomenon, possibly masked by a streaming potential.

Streaming potentials are characterized (*1*) by having their origin in the shearing motion in the double layer on the walls and (*2*) by depending on shearing *rate* and being zero at zero velocity. They can be treated by Onsager's equations and have the electroosmosis as their reciprocal effect. Electroosmosis in polyelectrolyte solutions depends on the aquotization of the ionic species and the effect may even have the opposite sign of that which would be expected from a misapplication of Onsager's equations.

Experiments with polyelectrolyte solutions have been made and await completion and publication.

REFERENCES

1. BRØNSTED, J. N., "Principles and Problems in Energetics," Interscience, New York, 1955; cf. J. KOEFOED, IUPAP Symposium on Thermodynamics, p. 107, Brussels, 1948.
2. HOLTAN, H., *J. Chem. Phys.* **19,** 519 (1951).
3. MAZUR, P., *J. Chem. Phys.* **19,** 1431 (1951).
4. ONSAGER, L., *Phys. Rev.* **37,** 405 (1931); *ibid.* **38,** 2265 (1931).
5. KOEFOED, J., *Acta Chem. Scand.* **2,** 53 (1948).
6. JENSEN, C. E., and KOEFOED, J., *J. Colloid Sci.* **9,** 460 (1954).
7. JENSEN, C. E., KOEFOED, J., and VILSTRUP, T., *Nature* **174,** 1101 (1954); *Ann. Otol., Rhinol. & Laryngol.* **64,** 406 (1955).
8. KOEFOED, J., Symposium on Information Theory, London, 1955.

Universitetets Fysisk-Kemiske Institut, Copenhagen JØRGEN KOEFOED
Received December 13, 1956

AN EXPERIMENTAL TEST OF OVERBEEK'S TREATMENT OF THE SUSPENSION EFFECT[1]

A. H. Bloksma[2]

Laboratory of Agricultural Chemistry, Agricultural University, Wageningen, Netherlands

Received February 20, 1956; revised July 30, 1956

ABSTRACT

The author has not been able to reproduce the capillary effects described by Loosjes (6). It is concluded that the effects observed by Loosjes were due to an insufficient electric insulation.

Suspension effects (Donnan-e.m.f.'s) were measured with clay suspensions. A simplification of Overbeek's (5) results permits calculating the suspension effects from the measured ionic concentrations and the mobility of adsorbed ions as determined by diffusion (7). The measured effects are significantly smaller than those calculated. Two possible causes for this discrepancy are mentioned.

INTRODUCTION

Two papers published by Jenny, Coleman *et al.* in 1950 (1) revived interest in the nature of the so-called suspension effect or Donnan-e.m.f. (2–4). The issue was clarified largely by a theoretical treatment by Overbeek (5). Assuming a number of simplifying circumstances Overbeek derives the following equation for the Donnan-e.m.f. in the case of a suspension of a negatively charged colloid in equilibrium with a potassium chloride solution:

$$E = -\frac{RT}{F} \cdot \frac{u + v + (1 - 2y)r}{u - v + r} \cdot \ln\left(1 + \frac{u - v + r}{2} \cdot \frac{c_P}{c_0}\right) \qquad (\mathrm{O}.27)^3$$

in which E is the Donnan-e.m.f., c_P the colloid concentration, and c_0 the concentration of the dialyzate, both in equivalents per unit volume, R is the gas constant per mole, T the absolute temperature, and F the Faraday. The parameter y describes the concentration of the ions in the suspension; it is supposed that the concentrations c_K and c_{Cl} in a suspension in equilibrium with a potassium chloride solution of concentration c are given by

---

[1] This paper is based on a portion of a thesis, entitled Het Suspensie-effect, submitted to the University of Amsterdam, March 1955. Details can be found in this thesis (in Dutch).

[2] Present address: Cereals Dept. of the Centr. Inst. for Nutrition Research T.N.O., Wageningen, Netherlands.

[3] Equations cited from Overbeek's paper (5) are indicated in this paper by their number in the former one preceded by the letter O.

$$\begin{aligned} c_K &= c + xc_P \\ c_{Cl} &= c - yc_P \end{aligned} \qquad (O.17)$$

for all values of c between c_0 and the concentration of the potassium chloride in the salt bridges; because electroneutrality holds

$$x + y = 1.$$

Further it is supposed that the contributions of the potassium ions, the chloride ions, and the colloidal particles to the electrical conductivity of the suspension are, respectively (*cf.* equations (O.19) and (O.24)):

$$\lambda_0(c + uc_P)$$

$$\lambda_0(c - vc_P)$$

and

$$\lambda_0 rc_P\,.$$

Here λ_0 is the equivalent conductance of both potassium and chloride ions in solutions.

The capillary effect was studied by Loosjes (6) as a model for the suspension effect. It is the change in the e.m.f. of a cell when a liquid junction between a concentrated potassium chloride solution and a dilute solution is allowed to enter from a wide tube into a capillary one. Overbeek derives the following equation for it, assuming that the dilute solution also consists of potassium chloride:

$$E_{\text{cap.}} = -\frac{RT}{F} \cdot 2t \cdot \frac{2\sigma}{\rho\lambda c_0}, \qquad (O.12)$$

in which t is the transference number of the chloride ions in potassium chloride solutions, σ the specific surface conductance along the glass wall, supposed to be carried completely by potassium ions, ρ is the radius of the capillary tube, λ the equivalent conductance of potassium chloride, and c_0 the concentration of the dilute solution.

When Overbeek's paper was published the present author was engaged in an experimental study of the suspension effect. The experiments could easily be brought into line with Overbeek's treatment. Results are reported in this paper and the preceding one (7). Determinations of the surface conductance in glass capillaries permitted a check of equation (O.12). An estimation of the mobility of cations adsorbed on clay minerals by means of diffusion experiments (7) provided a basis for the check of equation (O.27) for the suspension effect.

CAPILLARY EFFECT

The electrical resistance of Corning 015 glass capillaries filled with 10^{-4} M solutions of potassium chloride or hydrochloric acid was measured by a method similar to that of Jones and Wood (8). From this resistance, the specific conductance of the solutions, and the geometry of the capillary, the surface conductance can be calculated. It proved to be of the order of 1×10^{-8} mho. Substitution of this value into equation (O.12) yields a capillary effect of only 2 mv. in capillaries of 0.026 cm. diameter.[4] In accordance with this result the author could not observe any measurable capillary effect provided the electrical insulation was sufficient. The apparent capillary effects reported by Loosjes (6) are believed to be a consequence of electric leakage currents through the wall of the capillary. This hypothesis permits a nearly quantitative description of Loosjes' experimental results and explains some other phenomena observed by Loosjes for which he gave no explanation. Moreover the present author demonstrated a connection between the apparent capillary effects and the potential difference between the two solutions on either side of the glass wall in accordance with his hypothesis of leakage currents.

SUSPENSION EFFECT

Theory

Equation (O.27) will be used as a starting point for some further simplifications. In order to measure sufficiently large suspension effects large values of the ratio c_P/c_0 are required. Therefore the assumption $c_P/c_0 \ll 1$, which enabled Overbeek to simplify equation (O.27) to a great extent, cannot be introduced into this treatment.

The quantity y can be evaluated by analysis. It is supposed that v equals y:

$$1 - x = y = v. \tag{1}$$

The ratio u can be related to x, r, and the apparent labyrinth factor g from the preceding paper (7). The definition of mobility implies that the environment exerts a frictional force $-v_i/w_i$ upon a particle i with mobility w_i that moves with a velocity v_i in respect to its environment. Suppose that the presence of resting colloidal particles reduces the mobility to gw_i; then these particles exert directly or indirectly an additional frictional force $-v_i(1 - g)/gw_i$, the total frictional force obviously being

---

[4] The surface conductance of 2×10^{-7} mho mentioned by Overbeek was estimated by Loosjes using equations different from equation (O. 12); application of equation (O. 12) to Loosjes' experimental results yields surface conductances of $2\text{–}12 \times 10^{-7}$ mho.

$-v_i/gw_i$. If the colloidal particles have a velocity v_P themselves the frictional force exerted by them equals

$$\frac{v_P - v_i}{w_i} \cdot \frac{1-g}{g}.$$

Suppose in an electric field $\bar{F}$ the velocities of the adsorbed potassium ions and of the (negative) colloidal particles are v_K and v_P, respectively. In the steady state the forces upon these potassium ions balance each other:

$$\epsilon\bar{F} + \frac{v_P - v_K}{w_K} \cdot \frac{1-g}{g} - \frac{v_K}{w_K} = 0 \qquad [2]$$

(ϵ is the electric charge of the potassium ion, w_K the mobility of the potassium ions in solution). By definition r equals $-v_P/\epsilon\bar{F}w_K$. Substitution of this into Eq. [2] yields:

$$u/x = \frac{v_K}{\epsilon\bar{F}w_K} = g - r\{1 - g\}. \qquad [3]$$

The denominator of the second term equals the velocity of the potassium ions in solution. Therefore and because of the definition of u the second term equals u/x.

Until now the solvent through which the adsorbed ions are moving is supposed to be at rest. Probably it is carried along more or less by the colloidal particles. Suppose it has a mean velocity θv_P $(0 < \theta < 1)$; then in the last term of the left-hand side of Eq. [2] $-v_K$ has to be replaced by $\theta v_P - v_K$. The result is then instead of [3]:

$$u/x = \frac{v_K}{\epsilon\bar{F}w_K} = g - r\{1 - (1-\theta)g\}. \qquad [4]$$

Substitution of [1] and [4] into equation (O.27) yields:

$$E = -\frac{RT}{F} \cdot \frac{A+B}{A-B} \cdot \ln\left\{1 + \frac{A-B}{2} \cdot \frac{c_P}{c_0}\right\}, \qquad [5]$$

in which

$$\begin{aligned} A &= gx\{1 + (1-\theta)r\}; \\ B &= (1-x)(1-r). \end{aligned} \qquad [6]$$

Because of the known values of g, x, and r (see below) it is to be expected that both A and B are positive and that in the systems studied B is much smaller than A. Then one may write:

$$E = -\frac{RT}{F} \cdot \ln\left\{1 + \frac{A}{2} \cdot \frac{c_P}{c_0}\right\}. \qquad [7]$$

The ratio r may be estimated from the electrophoretic mobility of the colloid particles. For the clay minerals used and in dilute solutions this is about 3×10^{-4} cm.^{2}/v.sec (9) corresponding to an equivalent conductance of 30 mho.cm.^{2}/val or $r = 0.4$. In the transition layer between the suspension and the salt bridge the electrolyte concentration is very high locally; there the electrophoretic mobility will be much smaller. So the mean value of r that has to be substituted into Eq. [6] will be between 0 and 0.4.

The values of E, c_P, c_0, and x can be determined experimentally. The quantity g is known from diffusion experiments to be equal to 0.37 and 0.28 (±10%) in the case of sodium ions adsorbed on montmorillonite and kaolinite, respectively (7). It is supposed that the same values apply to adsorbed potassium ions. The ratio r lies between 0 and 0.4; so the factor $\{1 + (1 - \theta)r\}$ lies between 1.0 and 1.4 and is estimated to be 1.15 ± 0.15. By substitution of these values and the value of x determined by analysis into Eq. [6] one can calculate A. Then Eq. [7] yields a value of E that is to be compared with the experimental value.

Although Overbeek's derivation is made for a colloidal suspension in equilibrium with a dilute potassium chloride solution the present author also applied Eq. [7] to systems containing some hydrochloric acid as well as potassium chloride. It is believed that this extension does not change the general character of the conclusions.

Experimental Part

Materials. The colloids used are the same clay minerals as described in the preceding paper (7). They were purified in the same way; however, electrodialysis was not necessary. The acid suspensions were neutralized partially with potassium hydroxide.

Methods. Two cellophane tubes each containing 200 ml. suspension were placed in a glass tube with 150 ml. of a 0.001 M solution. The two suspensions contained different quantities of the same mineral; at the beginning of the experiment the two suspensions contained the same amount of adsorbed potassium ions per gram mineral. The solution was composed of potassium chloride and hydrochloric acid in a proportion that was expected to correspond with the equilibrium solution of the suspensions. The solution and the suspensions were equilibrated for 100 hours in an end-over-end shaker.

After equilibration three e.m.f.-measurements were made in each of the suspensions and dialyzates, viz., between a glass (hydrogen) electrode (Philips GM4241), a silver/silver chloride electrode prepared according to Brown (10), and a calomel electrode (Cambridge). The calomel electrode was connected to the system to be studied by a siphon containing an agar-agar gel soaked in a solution containing 7/4 M potassium nitrate and 1/4 M sodium nitrate; this salt mixture is believed to behave electrically like potassium chloride without contaminating the system studied with chlorine ions (11). The e.m.f.-measurements are thought reliable to 1 mv. They are reported below as *pa*-values that are defined as follows (φ is the electrical potential of an electrode with respect to the solution in millivolts):

$$\begin{aligned} \varphi^{\mathrm{glass}} - \varphi^{\mathrm{AgCl}} &= P - Q - 59.14 \times 2 \times pa\mathrm{HCl} \\ \varphi^{\mathrm{glass}} - \varphi^{\mathrm{cal.}} &= P - 59.14 \times pa\mathrm{H} \qquad [8]^{5} \\ \varphi^{\mathrm{AgCl}} - \varphi^{\mathrm{cal.}} &= Q + 59.14 \times pa\mathrm{Cl} \end{aligned}$$

The constants P and Q were determined by the arbitrary assumption that in a 1.00×10^{-3} M hydrochloric acid solution $pa\mathrm{H} = pa\mathrm{Cl}$ holds; then in that solution at 25°C. $pa\mathrm{H} = pa\mathrm{Cl} = pa\mathrm{HCl} = 3.015$ holds (13).

No direct measurements of the Donnan-e.m.f. were made. However, if the equilibrium between the suspension and the dialyzate has been established, the Donnan-e.m.f. E is identical with the suspension effect:

$$E/59.14 = pa\mathrm{H}^{\mathrm{susp.}} - pa\mathrm{H}^{\mathrm{dial.}} = -pa\mathrm{Cl}^{\mathrm{susp.}} + pa\mathrm{Cl}^{\mathrm{dial.}} \qquad [9]$$

A check of the equilibrium is furnished by the condition $pa\mathrm{HCl}^{\mathrm{susp.}} = pa\mathrm{HCl}^{\mathrm{dial.}}$; column 7 of Table I shows that only slight deviations from the equilibrium occurred. The differences between the columns 10 and 11 are caused by these deviations in cooperation with errors in the electric measurements.

To aliquots of the suspensions were added tenfold volumes of water containing an amount of barium nitrate that was at least ten times the equivalent of the base exchange capacity of the mineral. After sedimentation the supernatant liquid was analyzed. Hydrogen and chlorine were titrated potentiometrically with sodium hydroxide and silver nitrate, respectively. Potassium was determined by means of a flame photometer. The dialyzates were analyzed directly. The mineral content was determined by evaporation of the water and drying at 105°C.; it is converted into equivalents per liter by means of the exchange capacities of the minerals (790 and 55 microequivalents per gram montmorillonite and kaolinite, respectively).

Results and Discussion

The results have been summarized in Table I.

From the analytical results it is concluded that x has a value between 0.95 and 1. The negative charge of the mineral particles is neutralized almost completely by an excess of cations and not by negative adsorption

---

[5] The value of 59.14 mv. for $2.30 \times RT/F$ is applicable because all e.m.f.-measurements have been made at 25°C. (12).

TABLE I

Analyses of the Suspensions and Dialyzates, and a Comparison of the Measured and Calculated Suspension Effects

$\Delta paX = paX^{\text{susp.}} - paX^{\text{dial.}}$

Tube and mineral	Analyses (*milliequivalents per liter*)					Measurements of e.m.f.			Suspension effect			
									Measured		Calculated	
1	c_P 2	c_K 3	c_H 4	c_{Cl} 5	Σc* 6	paHCl 7	paH 8	paCl 9	$-\Delta pa$H 10	ΔpaCl 11	I† 12	II† 13
A	0	1.1	<0.003	1.0	+0.1	4.41	5.79	3.05	—	—	—	—
montm.	3.9	3.3	0.9	1.0	−0.7	4.37	5.62	3.12	0.17	0.07	0.26	0.23
	10.7	7.7	1.3	1.0	−2.7	4.36	5.37	3.32	0.42	0.27	0.52	0.43
B	0	1.3	0.05	1.6	−0.2	3.75	4.62	2.88	—	—	—	—
montm.	4.3	3.8	1.6	1.4	−0.3	3.72	4.51	2.95	0.11	0.07	0.21	0.20
	10.7	5.3	3.1	1.3	−3.6	3.71	4.37	3.09	0.25	0.21	0.40	0.31
C	0	1.0	0.03	1.1	−0.1	4.19	5.40	3.00	—	—	—	—
kaol.	4.2	4.1	0.5	0.9	−0.5	4.16	5.25	3.09	0.15	0.09	0.21	0.19
	11.0	9.2	1.2	1.0	−1.6	4.13	5.04	3.26	0.36	0.26	0.42	0.38
D	0	0.9	0.01	1.0	−0.1	3.81	4.62	3.00	—	—	—	—
kaol.	3.6	3.2	0.5	1.0	−0.9	3.81	4.54	3.10	0.08	0.10	0.20	0.16

* $\Sigma c = c_K + c_H - c_P - c_{Cl}$.

† Column 12 was obtained by substitution of the values of column 2 into Eq. [7]; for the calculation of column 13 c_P has been replaced by $c_K + c_H - c_{Cl}$.

of anions. This result is to be expected in suspensions of particles with rather strong negative wall potentials and diffuse electrical double layers that do not interpenetrate (14).

Column 6 shows that either the analyses in the suspensions are not completely reliable or the exchange capacities used are too high.

The suspension effects calculated (columns 12 and 13) have been obtained by substitution of $x = 1.00$ and the values of g and $\{1 + (1 - \theta)r\}$ mentioned above into Eqs. [6], [7], and [9]. Because of the uncertainties in each of these quantities the possible error in the calculated suspension effects is about 0.04 unit for the dilute and about 0.08 unit for the concentrated suspensions.

The differences between the measured and the calculated suspension effects are considered to be real. Two possible causes for these differences exist.

In the first place the values of g originated from diffusion experiments with sodium ions. In the preceding paper a connection was suggested between the displacing power of the ions in exchange reactions and the value of g (7); potassium ions being more strongly adsorbed (15) it might be expected that for the potassium ions used in the present experiments the real values of g are smaller than the values used.

In the second place in the transition layer between the salt bridge and the suspension the electrolyte concentrations are higher than in the suspension itself. With increasing electrolyte concentrations and under the condition of constant charge the wall potentials decrease and, therefore, x decreases from 1 to the minimum value $\frac{1}{2}$ (14). The value of x to be substituted into Eq. [6] may be much smaller than that determined by analysis of the bulk of the suspension.

The results of the present experiments do not give a conclusive proof of the correctness of Overbeek's approach. Nevertheless the agreement between the theory and the experiments is sufficient to suggest that his approach is useful and that its experimental verification and attempts to reduce the number of approximations in its working out should be the objects of further investigations.

The relationship between the ionic concentrations and the Donnan-e.m.f. or suspension effect may be summarized qualitatively as follows. The Donnan-e.m.f. is much smaller than corresponds with the ratio of the concentrations of the counter ions in the suspension and in the dialyzate; it is a little greater than corresponds with the ratio of the concentrations of the ions carrying an electric charge of the same sign as the colloidal particles. The same relationship has been found with sols of congo red (16), tin-IV-oxide (17), edestin (18), gum arabic (14), and montmorillonite suspensions (19).

Remarkably Peech, Olsen, and Bolt (3) and Raupach (20) independently measured positive Donnan-e.m.f.'s with suspensions of clay minerals carrying bivalent ions adsorbed; nevertheless the electrokinetic potentials were negative. Marshall's (4) criticism of the explanation by Peech *et al.* seems to be correct. Suppose application of Eq. [5] to a system containing potassium as well as calcium ions is permitted. Then a positive suspension effect is possible if B is negative, its absolute value being higher than A. This may occur if the electrophoretic mobility of the colloidal particles is very high ($r > 1$), the adsorbed ions have a strongly reduced mobility (g small), x is small, and θ is high; the first two conditions seem to be incompatible. For a solution of this problem the determination of g for divalent ions seems desirable.

In further experiments more dilute dialyzates in order to excite larger suspension effects will be advantageous. Then some of the analyses will have to be carried out by means of radioactivity.

ACKNOWLEDGMENT

The author is indebted to Mrs. H. C. M. Schneider-Pieters for her help with the experiments.

REFERENCES

1. Jenny, H., Nielsen, T. R., Coleman, N. T., and Williams, D. E., *Science* **112,** 164 (1950). Coleman, N. T., Williams, D. E., Nielsen, T. R., and Jenny, H., *Soil Sci. Soc. Amer. Proc.* **15,** 106, 111, 114 (1950).
2. Babcock, K. L., and Overstreet, R., *Science* **117,** 686 (1953). Eriksson, E., *Kgl. Lantbruks-Högskol. Ann.* **17,** 92 (1950); *Science* **113,** 418 (1951). Low, P. F., *Soil Sci.* **77,** 29 (1954). Marshall, C. E., *Soil Sci. Soc. Amer. Proc.* **15,** 110 (1950); *Science* **113,** 43 (1951); *ibid.* **115,** 361 (1952). Mysels, K. J., *Science* **114,** 424 (1951); *ibid.* **118,** 603 (1953). Peech, M., and McDevit, W. F., *Soil Sci. Soc. Amer. Proc.* **15,** 112 (1950). Sollner, K., *J. Colloid Sci.* **8,** 179 (1953).
3. Peech, M., Olsen, R. A., and Bolt, G. H., *Soil Sci. Soc. Amer. Proc.* **17,** 214, 220 (1953).
4. Marshall, C. E., *Soil Sci. Soc. Amer. Proc.* **17,** 218, 221 (1953).
5. Overbeek, J. Th. G., *J. Colloid Sci.* **8,** 593 (1953).
6. Loosjes, R., "pH-metingen in suspensies," Thesis, Utrecht 1942; *Chem. Weekblad* **46,** 902 (1950). For a brief account in English see: Overbeek, J. Th. G., "Electrochemistry of the double layer," in H. R. Kruyt, ed., "Colloid Science," Vol. 1, p. 185 et seq. Elsevier, Amsterdam, 1952, and Peech, M., Olsen, R. A., and Bolt, G. H., *Soil Sci. Soc. Amer. Proc.* **17,** 214, (1953).
7. Bloksma, A. H., *J. Colloid Sci.,* **12,** 40 (1957).
8. Jones, G., and Wood, L. A., *J. Chem. Phys.* **13,** 106 (1945).
9. Marshall, C. E., "The Colloid Chemistry of the Silicate Minerals," p. 148. Academic Press, New York, 1949.
10. Brown, A. S., *J. Am. Chem. Soc.* **56,** 646 (1934).
11. Laar, J. A. W. van "Het ladingsnulpunt van zilverjodide," Thesis, Utrecht, 1952.
12. Manov, G. G., Bates, R. G., Hamer, W. J., and Acree, S. F., *J. Am. Chem. Soc.* **65,** 1765 (1943).
13. Harned, H. S., and Owen, B. B., "The Physical Chemistry of Electrolytic Solutions," 2nd ed., p. 547. Reinhold, New York, 1950. Kortuem, G., and Bockris, J. O'M., "Textbook of Electrochemistry," p. 672. Elsevier, Amsterdam, 1951.
14. Klaarenbeek, F. W., Over Donnan-evenwichten bij solen van arabische gom, Thesis, Utrecht, 1946. Overbeek, J. Th. G., "Electrochemistry of the double layer," in H. R. Kruyt, ed., "Colloid Science," Vol. 1, p. 192 et seq. Elsevier, Amsterdam, 1952.
15. Marshall, C. E., "The Colloid Chemistry of the Silicate Minerals," p. 122. Academic Press, New York, 1949.
16. Azuma, R., and Kameyama, N., *Phil. Mag.* [6] **50,** 1264 (1925).
17. Ghosh, B. N., *J. Chem. Soc.* **1929,** 2290.
18. Adair, G. S., *Proc. Roy. Soc. (London)* **A120,** 573 (1928), Table I.
19. Whitney, R. S., and Peech, M., *Soil Sci. Soc. Amer. Proc.* **16,** 117 (1952).
20. Raupach, M., *Australian J. Agr. Research* **5,** 716 (1954).

JOURNAL OF COLLOID SCIENCE **12,** 144–160 (1957)

THE THEORY OF THE ELECTRIC CHARGE DISTRIBUTION OF MONODISPERSED LIGHTLY CHARGED AEROSOLS OF SPHERICAL PARTICLES COAGULATING IN A BIPOLAR IONIZED ATMOSPHERE[1]

George Luchak[2]

Defence Research Board of Canada, Suffield Experimental Station, Ralston, Alberta, Canada

Received March 27, 1956

ABSTRACT

Equations describing the changes with time of the electric charge distribution of coagulating aerosols are solved for lightly charged systems. The solutions are compared with experimental data from the literature on the electric charge distribution of initially uncharged ammonium chloride aerosols and good agreement is obtained. The theory is used to describe qualitatively the change in electric charge distribution of silica dusts previously studied experimentally by Gillespie.

INTRODUCTION

Aerosols created by chemical means, air blasts, or electrical arcs are usually charged. The mechanism of the charging process has been discussed by many authors but will not be considered in this paper. The subsequent change in electrification during the aging of an aerosol may be due to coagulation of its particles, their collision with ions normally present in the atmosphere, or photoelectric ejection of electrons due to ionizing radiations. The effects of such mechanisms on the charge distribution in aerosols has not been well explored. Patterson (17) has considered the effects of coagulation and ion capture on the ratio of charged to uncharged particles in certain cases; Arendt and Kallman (1) have worked out the charging of aerosols exposed to an atmosphere of ions all of which were of the same polarity; Lissowskii (11) has discussed the electrical charge distribution of rarefied aerosols in an equilibrium state due to ion capture; and Kunkel (9) has studied the discharging of highly charged dust particles suspended in air and has given experimentally determined electrical charge distributions of ammonium chloride aerosols which were originally uncharged. More recently, Gillespie (4, 5) has made experimental determinations of the electrical charge distributions in vycor dusts as a function of time (see also Gunn (6, 7)).

---

[1] This paper constitutes Suffield Technical Paper 66.

[2] Now with Special Defense Projects Department, General Electric Company, Philadelphia, Pennsylvania.

In this paper we shall consider the variation with time of the electrical charge distribution of lightly charged coagulating aerosols. We shall be concerned only with initially symmetrically charged, monodispersed systems of spherical particles which are kept so well mixed as to be spatially homogeneous and of particle size greater than 2×10^{-5} cm.

NOTATION

The following symbols are used throughout the paper:

$N_1(q, v, t)dq\,dv$ is the number of aerosol particles per cubic centimeter at time t whose volumes lie between $(v - \frac{1}{2}\,dv)$ and $(v + \frac{1}{2}\,dv)$ and which have a charge between $(q - \frac{1}{2}\,dq)$ and $(q + \frac{1}{2}\,dq)$ electronic units.

$$N(q, t)\,dq = \int_0^{\infty} N_1(q, v, t)\,dv\cdot dq.$$

$$\bar{N}(t) = \int_{-\infty}^{+\infty} N(q, t)\,dq.$$

$$\bar{N}_0 = \bar{N}(0).$$

The probability is $k(q, p, v, u)\,dt$ that a particle of electronic charge between $(q - \frac{1}{2}\,dq)$ and $q + \frac{1}{2}\,dq)$ and volume between $(v - \frac{1}{2}\,dv)$ and $(v + \frac{1}{2}\,dv)$ will coagulate with a particle of electronic charge between $(p - \frac{1}{2}\,dp)$ and $(p + \frac{1}{2}\,dp)$ and volume between $(u - \frac{1}{2}\,du)$ and $(u + \frac{1}{2}\,du)$ during time dt; the constant k is taken to represent $k(q, p, v, u)$ independently of q, p, v, u. $\beta(q, v)\,dt$ is the probability of a particle of charge between $(q - \frac{1}{2}\,dq)$ and $(q + \frac{1}{2}\,dq)$ and volume between $(v - \frac{1}{2}\,dv)$ and $(v + \frac{1}{2}\,dv)$ being lost to the aerosol by sedimentation or by collision with the aerosol chamber walls during time dt; the constant β is taken to represent $\beta(q, v)$ irrespective of q and v.

$\phi_1(q, v, n)\,dt$ is the probability that a particle of charge between $(q - \frac{1}{2}\,dq)$ and $(q + \frac{1}{2}\,dq)$ electronic units and volume between $(v - \frac{1}{2}\,dv)$ and $(v + \frac{1}{2}\,dv)$ picks up an atmospheric ion of the same polarity in time dt.

$\phi_2(q, v, n)\,dt$ is the probability that a particle of charge between $(q - \frac{1}{2}\,dq)$ and $(q + \frac{1}{2}\,dq)$ electronic units and volume between $(v - \frac{1}{2}\,dv)$ and $(v + \frac{1}{2}\,dv)$ picks up an atmospheric ion of the opposite polarity in time dt.

$n_+(t)$ is the number of positive ions per cubic centimeter of the aerosol at time t.

$n_-(t)$ is the number of negative ions per cubic centimeter of the aerosol atmosphere at time t.

γ is the number of ion pairs produced per second per cubic centimeter of the aerosol atmosphere.

α is the recombination coefficient expressing the probability of a positive ion recombining with a negative ion in unit time in an atmosphere of unit positive and negative ion density.

D_+, D_- are the diffusion coefficients of positive and negative ions, respectively, in the aerosol atmosphere.

X_+, X_- are the mobilities of positive and negative ions, respectively, in the aerosol atmosphere.

a is the radius of the spherical aerosol particles.

$r = X_+e/D_+a = X_-e/D_-a$, where e is the electronic charge in e.s.u.

$\bar{N}(S, t) = \int_{-\infty}^{+\infty} \exp(2\pi iqs) N(q, t)\, dq$, the Fourier transform of $N(q, t)$.

$\tau(t) = \int_0^t 4\pi a D_+ n_+\, dt = \int_0^t 4\pi a D_- n_-\, dt$. It will be established later that for all practical purposes we may take $D_+n_+ = D_-n_- = Dn$.

$\lambda(t) = \exp(-r\tau)$.

THE FUNDAMENTAL EQUATIONS

The following are the general equations describing the process of aging of an aerosol:

$$\begin{aligned}\frac{\partial N_1(q, v, t)}{\partial t} &= \frac{1}{2}\int_0^v du \int_{-\infty}^{+\infty} k(q-p, p, v-u, u) N_1(q-p, v-u, t) N_1(p, u, t)\, dp \\ &\quad - N_1(q, v, t)\int_0^\infty du \int_{-\infty}^{+\infty} k(q, p, v, u) N_1(p, u, t)\, dp - \beta(q, v) N_1(q, v, t) \\ &\quad + [\phi_1(q-1, v) N_1(q-1, v, t) + \phi_2(q+1, v) N_1(q+1, v, t) \\ &\quad - \{\phi_1(q, v) + \phi_2(q, v)\} N_1(q, v, t)],\end{aligned} \tag{1'}$$

$$\begin{aligned}\frac{\partial n_+}{\partial t} = \gamma - \alpha n_+ n_- - \int_0^\infty du \Big[&\int_0^\infty \phi_1(q, u) N_1(q, u, t)\, dq \\ &+ \int_0^\infty \phi_2(q, u) N_1(-q, u, t)\, dq \Big]\end{aligned} \tag{2'}$$

and

$$\begin{aligned}\frac{\partial n_-}{\partial t} = \gamma - \alpha n_+ n_- - \int_0^\infty du \Big[&\int_0^{+\infty} \phi_2(q, u) N_1(q, u, t)\, dq \\ &+ \int_0^\infty \phi_1(q, u) N_1(-q, u, t)\, dq \Big]\end{aligned} \tag{3'}$$

where all the integrals are to be interpreted in the Stieltjes sense. Equations [1′], [2′], and [3′] are generalizations of equations given in part by Tunitskii (15), Kunkel (9), and probably others. Their derivation is obvious from the definitions of the symbols.

If we restrict ourselves to systems which remain reasonably monodisperse, take $k(q, p, v, u) \equiv k$ and $\beta(q, v) \equiv \beta$ to be constants throughout and integrate both sides of Eq. [1′] with respect to v from 0 to ∞, we obtain the following equations:

$$\begin{aligned}\frac{\partial N(q,t)}{\partial t} = \frac{k}{2}\int_{-\infty}^{+\infty} N(q-p,t)N(p,t)\,dp - kN(q,t)\tilde{N}(t) - \beta N(q,t) \\ + [\phi_1(q-1)N(q-1,t) + \phi_2(q+1)N(q+1,t) \\ - \{\phi_1(q) + \phi_2(q)\}N(q,t)],\end{aligned} \qquad [1]$$

$$\frac{\partial n_+}{\partial t} = \gamma - \alpha n_+ n_- - \left[\int_0^\infty \phi_1(q)N(q,t)\,dq + \int_0^\infty \phi_2(q)N(-q,t)\,dq\right], \qquad [2]$$

and

$$\frac{\partial n_-}{\partial t} = \gamma - \alpha n_+ n_- - \left[\int_0^\infty \phi_2(q)N(q,t)\,dq + \int_0^\infty \phi_1(q)N(-q,t)\,dq\right]. \qquad [3]$$

In order to solve Eqs. [1] to [3], it is necessary to obtain analytical expressions for $\phi_1(q)$ and $\phi_2(q)$ by solving the appropriate equations of diffusion. The assumptions under which the equations are solved are those used by Von Smoluchowskii (14), who considered a particle of an aerosol as a perfect absorber in the field of the other aerosol particles and calculated, by diffusion theory, the rate at which it pulled up its neighbors, due consideration being taken of the average particle concentration at that time in the aerosol. To a high degree of approximation, this was taken as the accretion rate due to a concentration gradient at the particle equal to the quasi-stationary state concentration gradient when the concentration at infinity is taken to be the average concentration in the aerosol at that time. Von Smoluchowskii's model is valid if the adaptation to the quasi-stationary concentration gradient at the particle can keep step with the changing particle concentration. Following the model just described, the aerosol is considered to consist of perfect spheres of radius a suspended in a bipolar ion atmosphere. Since the aerosol particles are large compared to the ions, the particles are considered as stationary in space with respect to the ions while the latter are considered to move about in Brownian motion under the influence of the Coulomb forces between them and the aerosol particles. If it is assumed that the ion concentration is so small compared to the aerosol concentration that interactions between ions can be neglected, the diffusion equations give

$$\phi_1(q, n) = 4\pi aDnrq/[1 - \exp(-rq)], \qquad [4']$$

$$\phi_2(q, n) = -4\pi aDnrq/[1 - \exp(rq)], \qquad [5']$$

where $r = Xe\ Da$, and n, X, and D can carry the subscripts + or −. In this paper we shall consider only those cases for which the first two terms of the Taylor expansions of Eqs. [4′] and [5′] are sufficient. Thus, in all that follows

$$\phi_1(q, n) = 4\pi aDn\left(1 - \frac{r}{2}q\right), \qquad [4]$$

and

$$\phi_2(q, n) = -4\pi aDn\left(1 + \frac{r}{2}q\right). \qquad [5]$$

THE GENERAL SOLUTION OF THE FUNDAMENTAL EQUATIONS

Subject to the limitations of Eqs. [4] and [5], Eq. [2] and [3] can now be written

$$\frac{\partial n_+}{\partial t} = \gamma - \alpha n_+ n_- - 4\pi aD_+ n_+ \int_{-\infty}^{+\infty}\left(1 - \frac{r}{2}q\right)N(q, t)\,dq, \qquad [2'']$$

and

$$\frac{\partial n_-}{\partial t} = \gamma - \alpha n_+ n_- - 4\pi aD_- n_- \int_{-\infty}^{+\infty}\left(1 + \frac{r}{2}q\right)N(q, t)\,dq. \qquad [3'']$$

For most aerosols considered in practice,[3] an ion quasi-equilibrium is reached so quickly that the initial charge distribution of the aerosol is not appreciably changed during the time required to attain the state. In these cases we can write

$$4\pi aD_+ n_+ = \frac{\gamma}{\int_{-\infty}^{+\infty}\left(1 - \frac{r}{2}q\right)N(q, t)\,dq},$$

and

$$4\pi aD_- n_- = \frac{\gamma}{\int_{-\infty}^{+\infty}\left(1 + \frac{r}{2}q\right)N(q, t)\,dq}.$$

---

[3] For example, if $a = 2 \times 10^{-5}$ cm., $N(0) = 10^5$/cm.^{3}, and $\gamma = 12$/cm.^{3}/sec., quasi-equilibrium is obtained in less than 30 sec., in which time at most 3500 ions are captured by aerosol particles. These can have no appreciable effect on the initial charge distribution.

Now if the initial distribution $N(q, 0)$ is symmetrical, and t is measured from the time quasi-equilibrium is attained,

$$4\pi a D_+ n_+(0) = 4\pi a D_- n_-(0) = \frac{\gamma}{N(0)}$$

and Eq. [1] gives

$$\left(\frac{\partial N(q, t)}{\partial t}\right)_0 = \left(\frac{\partial N(-q, t)}{\partial t}\right)_0$$

so that $N(q, \partial t)$ is symmetrical and, in general, by repeating the process it is clear that $N(q, t)$ is symmetrical. Thus

$$4\pi a D_+ n_+(t) = 4\pi a D_- n_-(t) = \frac{\gamma}{N(t)}, \qquad [2, 3]$$

and Eq. [1′] becomes

$$\frac{\partial N(q, t)}{\partial t} = \frac{k}{2}\int_{-\infty}^{+\infty} N(q - p, t)N(p, t)\, dp - kN(q, t)\bar{N}(t) - \beta N(q, t)$$
$$+ \frac{\gamma}{\bar{N}(t)}\left[\left\{1 - \frac{r}{2}(q - 1)\right\} N(q - 1, t)\right. \qquad [1]$$
$$\left. + \left\{1 + \frac{r}{2}(q + 1)\right\} N(q + 1, t) - 2N(q, t)\right]$$

Equation [1] is solved by taking its Fourier transform. Writing

$$\bar{N}(s, t) = \int_{-\infty}^{+\infty} \exp(2\pi i\, sq) N(q, t)\, dq,$$

$$z = \exp(2\pi i\, s),$$

and

$$\chi(z, t) = [\bar{N}(z, t)]^{-1},$$

we get

$$\frac{\partial \chi}{\partial t} - \frac{\gamma}{2\bar{N}(t)} r(1 - z^2)\frac{\partial \chi}{\partial z} + \left[\frac{\gamma}{\bar{N}(t)}\frac{(z - 1)^2}{z} - (k\bar{N}(t) + \beta)\right]\chi \qquad [6]$$
$$+ \frac{k}{2} = 0$$

To solve Eq. [6] we restrict ourselves, first of all, to the surface

$$t = t(b),$$

and

$$z = z(b) \qquad [7]$$

so that

$$\chi = \chi(b),$$

where b is a running parameter. On the surface given by Eq. [7]

$$\frac{d\chi}{db} = \frac{\partial \chi}{\partial t}\frac{dt}{db} + \frac{\partial \chi}{\partial z}\frac{dz}{db}, \tag{8}$$

an equation which must be identical with Eq. [6], so that we must have

$$\frac{dt}{db} = 1, \tag{9}$$

$$\frac{dz}{db} = -\frac{\gamma r}{2\tilde{N}(t)}(1 - z^2), \tag{10}$$

and

$$\frac{d\chi}{db} = \left[k\tilde{N}(t) + \beta - \frac{\gamma}{\tilde{N}(t)}\frac{(z-1)^2}{z}\right]\chi - \frac{k}{2}. \tag{11}$$

Equations [9] and [10] have the solution

$$\lambda(t)\frac{(1 - z)}{(1 + z)} = \alpha, \tag{12}$$

where

$$\lambda(t) = \exp(-r\tau), \tag{13}$$

$$\tau = \int_0^t 4\pi a\ Dndt = \gamma \int_0^t \frac{dt}{\tilde{N}(t)}, \tag{14}$$

and α is an undetermined parameter. Equation [12] can be solved for z in terms of α and $\lambda(t)$, so that Eq. [11] can be written in the form

$$\frac{d\chi}{dt} = f(\alpha, t)\chi - \frac{k}{2}, \tag{15}$$

where

$$f(\alpha, t) = \left[(k\tilde{N}(t) + \beta) - \frac{\gamma}{\tilde{N}(t)}\frac{4\alpha^2}{\lambda^2(t) - \alpha^2}\right]. \tag{16}$$

Equation [15] has the solution

$$\chi = \exp\left[\int_0^t f(\alpha, t)\, dt\right]\left[\frac{1}{g(\alpha)} - \frac{k}{2}\int_0^t \exp\left\{-\int_0^t f(\alpha, t)\, dt\right\} dt\right], \tag{17}$$

and thus

$$\tilde{N}(\alpha,t) = \frac{g(\alpha)\exp\left\{-\int_0^t f(\alpha,t)\,dt\right\}}{1-\frac{k}{2}g(\alpha)\int_0^t \exp\left\{-\int_0^t f(\alpha,t)\,dt\right\}dt}, \qquad [18]$$

where $g(\alpha)$ is an arbitrary function of α and $\tilde{N}(\alpha, t)$ is the value of $\tilde{N}(z, t)$ corresponding to the solution of Eq. [1] on the surface represented by Eq. [7].

To evaluate $\int_0^t f(\alpha, t)\,dt$, we use the fact that

$$\frac{d\tilde{N}(t)}{dt} = -\frac{k}{2}\tilde{N}^2(t) - \beta\tilde{N}(t), \qquad [19]$$

which is the form of Eq. [6] when $z = 1$ (cf. Gillespie and Langstroth (3)); it is to be noted that we write $k/2$ for the coagulation "constant" whereas k itself is used in the afore-mentioned paper), and obtain the result

$$\int_0^t f(\alpha,t)\,dt = \ln\left[\left(\frac{1-\alpha^2/\lambda^2(t)}{1-\alpha^2}\right)^{2/r}\left(\frac{\partial\tilde{N}(t)}{\partial t}\right)_0 \Big/ \left(\frac{\partial\tilde{N}(t)}{\partial t}\right)\right]. \qquad [20]$$

Thus

$$\tilde{N}(\alpha,t) = \frac{\left(\frac{1-\alpha^2}{1-\alpha^2/\lambda^2(t)}\right)^{2/r} g(\alpha)\left(\frac{\partial\tilde{N}(t)}{\partial t}\right)\Big/\left(\frac{\partial\tilde{N}(t)}{\partial t}\right)_0}{1-\frac{k}{2}g(\alpha)\int_0^t\left(\frac{1-\alpha^2}{1-\alpha^2/\lambda^2(u)}\right)^{2/r} \cdot\left[\left(\frac{\partial\tilde{N}(u)}{\partial u}\right)\Big/\left(\frac{\partial\tilde{N}(u)}{\partial u}\right)_0\right]du.} \qquad [21]$$

To obtain the solution independent of the surface given by Eq. [7], put

$$\alpha = \lambda(t)\left(\frac{1-z}{1+z}\right) = -i\lambda(t)\tan\pi s, \qquad [22]$$

and

$$(1-\alpha^2)^{2/r}g(\alpha) = h(i\alpha)$$

and get

$$\tilde{N}(s,t) = \frac{h(\lambda(t)\tan\pi s)\left[\left(\frac{\partial\tilde{N}(t)}{\partial t}\right)\Big/\left(\frac{\partial\tilde{N}(t)}{\partial t}\right)_0\right]}{(1+\tan^2\pi s)^{2/r} - \frac{k}{2}h(\lambda(t)\tan\pi s) \cdot\int_0^t\left[\frac{1+\tan^2\pi s}{1+\frac{\lambda^2(t)}{\lambda^2(u)}\tan^2\pi s}\right]^{2/r}\left[\left(\frac{\partial\tilde{N}(u)}{\partial u}\right)\Big/\left(\frac{\partial\tilde{N}(u)}{\partial u}\right)_0\right]du,} \qquad [23]$$

where $h(x)$ is an arbitrary function of x. When the initial conditions are satisfied we get

$$\bar{N}(s,t) = \frac{\left[\left(\dfrac{\partial \tilde{N}(t)}{\partial t}\right) \Big/ \left(\dfrac{\partial \tilde{N}(t)}{\partial t}\right)_0\right]\left[\dfrac{1 + \lambda^2(t)\tan^2 \pi s}{1 + \tan^2 \pi s}\right] \bar{N}\left\{\dfrac{1}{\pi}\tan^{-1}(\lambda(t)\tan \pi s), 0\right\}}{1 - \dfrac{k}{2}\bar{N}\left\{\dfrac{1}{\pi}\tan^{-1}(\lambda(t)\tan \pi s), 0\right\} \cdot \displaystyle\int_0^t \left[\dfrac{1 + \tan^2 \pi s}{1 + \dfrac{\lambda^2(t)}{\lambda^2(u)}\tan^2 \pi s}\right]\left[\left(\dfrac{\partial \tilde{N}(u)}{\partial u}\right) \Big/ \left(\dfrac{\partial \tilde{N}(u)}{\partial u}\right)_0\right] du} \qquad [24]$$

Equation [24] can be written in the form

$$\bar{N}(s, t) = a_0 + 2 \textstyle\sum_{n=1}^{\infty} a_n \cos 2\pi ns, \qquad [25]$$

where

$$a_n = \frac{1}{2\pi}\int_{-\pi}^{+\pi} \bar{N}\left(\frac{\phi}{2\pi}, t\right) \cos n\phi \, d\phi, \qquad [26]$$

and the solution of Eq. [1] takes the form

$$N(q, t) = a_0 + \sum a_n[\delta(q + n) + \delta(q - n)], \qquad [27]$$

a result which is obtained by inverting Eq. [25], where $\delta(q)$ is the Dirac delta function defined by the equations

$$\delta(q) = 0, \; q \neq 0$$

and

$$\int_{-\infty}^{+\infty} \delta(q)\, dq = 1.$$

THE PARTICLE CHARGE DISTRIBUTION IN A NONCOAGULATING AEROSOL

In this section we shall consider a dilute aerosol for which coagulation has little effect on the changes in charge distribution.

a. First of all, for simplicity, consider the case for which $(r/2)q \ll 1$ for most particles of the aerosol. Then Eq. [1] can be written

$$\frac{\partial N(q, t)}{\partial \tau} = N(q - 1, \tau) + N(q + 1, \tau) - 2N(q, \tau). \qquad [28]$$

As before, we take the Fourier transform of Eq. [28] and get, finally,

$$\bar{N}(s, t) = \bar{N}(s, 0) \exp\{2(\cos 2\pi s - 1)\tau\}. \qquad [29]$$

A known expansion, however, gives

$$\exp\{2\tau \cos 2\pi s\} = I_0(2\tau) + 2 \textstyle\sum_{n=1}^{\infty} \cos 2\pi\, ns\, I_n(2\tau),$$

(cf. Whittaker and Watson (16)), where $I_n(2\tau) = J_n(i2\tau)$ is the Bessel function of the first kind of imaginary argument.

Inverting Eq. [29] we get

$$\begin{aligned} N(q, t) &= N(q, 0)\, I_0(2\tau)e^{-2\tau} \\ &\quad + \textstyle\sum_{n=1}^{\infty} [N(q + n, 0) + N(q - n, 0)]\, I_n(2\tau)e^{-2\tau}, \end{aligned} \qquad [30]$$

which is the solution of the problem. If the aerosol is initially uncharged

$$N(q, 0) = \tilde{N}_0\delta(q),$$

and

$$\begin{aligned} \frac{N(q, t)}{N_0} &= I_0(2\tau)e^{-2\tau}\, \delta(q) \\ &\quad + \textstyle\sum_{n=1}^{\infty} [\delta(q + n) + \delta(q - n)]\, I_n(2\tau)e^{-2\tau}. \end{aligned} \qquad [31]$$

b. For more highly charged aerosols, we may put $k = 0$ in Eq. [24] and get

$$\tilde{N}(s, t) = \left[\frac{1 + \lambda^2(t) \tan^2 \pi s}{1 + \tan^2 \pi s}\right]^{2/r} \tilde{N}\left\{\frac{1}{\pi} \tan^{-1}(\lambda(t) \tan \pi s), 0\right\}. \qquad [32]$$

As in subsection (*a*), we consider the case for which $N(q, 0) = \tilde{N}_0\delta(q)$ and get

$$\begin{aligned} a_n &= \frac{\tilde{N}_0}{2\pi} \int_{-\pi}^{+\pi} \left[\frac{1 + \lambda^2(t) \tan^2 \phi/2}{1 + \tan^2 \phi/2}\right]^{2/r} \cos n\phi\, d\phi, \\ &= \frac{\tilde{N}_0}{\pi}\left[\frac{1 + \lambda^2(t)}{2}\right]^{2/r} \int_{-\pi}^{+\pi} \left[1 + \frac{1 - \lambda^2(t)}{1 + \lambda^2(t)} \cos \phi\right]^{2/r} \cos n\phi\, d\phi\, . \end{aligned} \qquad [33]$$

It is well known, however, that

$$P_{2/r}^{n}(x) = \frac{\Pi(n + 2/r)}{2\pi} \int_{-\pi}^{+\pi} [x + (x^2 - 1)^{1/2} \cos \phi]^{2/r} \cos n\phi\, d\phi$$

(Whittaker and Watson (16)), where $P_{2/r}^{n}(x)$ is the associated Legendre function $|\arg x| < \pi/2$ and

$$\pi(n + 2/r) = (1 + 2/r)(2 + 2/r) \cdots (n + 2/r).$$

Thus

$$a_n = \frac{\tilde{N}_0\, \lambda^{2/r}(t)}{\Pi(n + 2/r)}\, P_{2/r}^{n}\left[\frac{1 + \lambda^2(t)}{2\lambda(t)}\right], \qquad [34]$$

and finally

$$\frac{N(q, t)}{\tilde{N}_0} = \lambda^{2/r}(t)\ P^n_{2/r}\left[\frac{1 + \lambda^2(t)}{2\lambda(t)}\right]\delta(q)$$

$$+ \textstyle\sum_{n=1}^{\infty} \frac{\lambda^{2/r}(t)}{\Pi(n + 2/r)}\, P^n_{2/r}\left[\frac{1 + \lambda^2(t)}{2\lambda(t)}\right]\{\delta(q + n) + \delta(q - n)\}, \qquad [35]$$

which is the solution to the problem.

To show that Eq. [35] approaches the form of Eq. [31] it is only necessary to note that

$$\lim_{r\to 0} \frac{1}{\Pi(n + 2/r)}\, P^n_{2/r}\left(\frac{1 + \lambda^2(t)}{2\lambda(t)}\right) = \lim_{r\to 0} \frac{P^n_{2/r}\ (\cosh\ r\tau)}{\Pi(n + 2/r)} = I_n\ (2\tau),$$

a result which is obtained by a slight alteration of an example in Whittaker and Watson (16).

It is worth deriving a simple expression for the equilibrium charge distribution in an aerosol. This can be found by letting $t \to \infty$ in Eq. [34]. In this case

$$\frac{a_n}{\tilde{N}_0}\, \frac{1}{2\pi} \int_{-\pi}^{+\pi} \cos^{4/r}(\phi/2)\, \cos n\phi\ d\phi. \qquad [36]$$

If $(4/r)$ is an integer, however, we get (MacRoberts (12), p. 287)

$$\frac{a_n}{\tilde{N}_0} = \frac{\Gamma(1 + 4/r)}{\Gamma\left(1 + \frac{2}{r} + n\right)\Gamma\left(1 + \frac{2}{r} - n\right)}\, \frac{1}{2^{4/r}}$$

or, by Stirling's approximation,

$$\frac{a_n}{\tilde{N}_0} = \sqrt{\frac{r}{2\pi}}\, \exp -\left(\frac{r}{2}\, n^2\right). \qquad [37]$$

Equation [37] was first obtained by Lissowskii (11).

THE PARTICLE CHARGE DISTRIBUTION IN AN AEROSOL IN WHICH THE EFFECTS OF ION CAPTURE ARE IGNORED

In this case it is only necessary to let $\gamma \to 0$ in Eq. [24]. Then

$$\bar{N}(s, t) = \frac{\left[\left(\frac{\partial N(t)}{\partial t}\right) \Big/ \left(\frac{\partial N(t)}{\partial t}\right)_0\right] \bar{N}(s, 0)}{1 - \frac{k}{2}\left[\frac{\bar{N}(t) - \bar{N}(0)}{\left(\frac{\partial \bar{N}(t)}{\partial t}\right)_0}\right] \bar{N}(s, 0)}.$$

If, for simplicity, we consider an aerosol for which $\beta = 0$, we get

$$\frac{a_n}{\tilde{N}(t)} = \frac{1}{2\pi} \int_{-\pi}^{+\pi} \frac{\dfrac{\tilde{N}(\phi/2\pi, 0)}{\tilde{N}_0} \cos n\phi \, d\phi}{1 - \dfrac{k}{2} \tilde{N}_0 t \left[\dfrac{\tilde{N}(\phi/2\pi, 0)}{\tilde{N}_0} - 1 \right]}. \tag{39}$$

If

$$\frac{N(q, 0)}{\tilde{N}_0} = \alpha_0 \delta(q) + 2 \sum \alpha_n \left[\frac{\delta(q + n) + \delta(q - n)}{2} \right], \tag{40}$$

$$\tilde{N}(\phi/2\pi, 0) = \alpha_0 + 2 \sum \alpha_n \cos n\phi. \tag{41}$$

Consider the special case $\alpha_n = 0$ for $n > 2$ and evaluate $a_n/\tilde{N}(t)$ to the first order in t. In this case we get

$$\left.\begin{aligned}
\frac{a_0}{\tilde{N}(t)} &= \alpha_0 \left[1 - \frac{k}{2} \tilde{N}_0 t \left\{ 1 - \alpha_0 - 2 \frac{(\alpha_1^2 + \alpha_1^2)}{\alpha_0} \right\} \right], \\
\frac{a_1}{\tilde{N}(t)} &= \alpha_1 \left[1 - \frac{k}{2} \tilde{N}_0 t \, \{ 1 - 2(\alpha_0 + \alpha_2) \} \right], \\
\frac{a_2}{\tilde{N}(t)} &= \alpha_2 \left[1 - \frac{k}{2} \tilde{N}_0 t \left\{ 1 - \frac{\alpha_1^2 + 2\alpha_0 \alpha_2}{\alpha_2} \right\} \right], \\
\frac{a_3}{\tilde{N}(t)} &= 2\alpha_1 \alpha_2 \frac{k}{2} \tilde{N}_0 t, \\
&\text{and} \\
\frac{a_4}{\tilde{N}(t)} &= \alpha_2^2 \frac{k}{2} \tilde{N}_0 t.
\end{aligned}\right\} \tag{42}$$

Equations [42] can be useful for determining the effect of coagulation on the electrical charge distribution if the initial distribution is dense about the origin.

Tunitskii (15) made calculations of the electrical charge distribution of aerosols when the effect of the electrical charge of the particles on the coagulation rate is taken into account to the first order in q and concluded that, for symmetrical distributions, the mean absolute magnitude of the charge on the particles decreases with time and does not depend on the parameter characterizing the first-order effect; i.e., the result of the calculation to the first order is identical with the corresponding result to the zeroth order and is independent of the original charge distribution. Equations [42], however, indicate that the initial electrical charge distribution determines the subsequent behavior of the mean value of the absolute charge. If, for example, we take

$$\alpha_0 = 1/3, \qquad \alpha_1 = 2/9, \qquad \alpha_2 = 1/9,$$

the mean value of the absolute charge is

$$\bar{q} = \frac{8}{9}\left[1 + \frac{4}{9}\frac{k}{2}\tilde{N}_0 t\right],$$

a function which, to the first order, increases with time.

COMPARISON OF THE THEORY WITH EXPERIMENT

The amount of data from experiments suitably designed to elucidate the fundamental mechanisms theoretically considered in this paper is small. Lissowskii (11) has shown that Eq. [37] describes the electrical charge distribution in mineral oil aerosols when equilibrium has been attained. Recently Kunkel (9) has determined experimentally the charge distribution in an ammonium chloride aerosol which was initially uncharged. Since Kunkel gave no indication of the initial particle number density, the particle size, or the rate of creation of atmospheric ions in his aerosol chamber, data obtained by Gillespie and Langstroth (3) were taken to be representative for Kunkel's aerosol at 3 hours, γ was taken to be equal to 12 ion pairs per cm.^{3} per sec., a value intermediate to the value $\gamma = 10$ theoretically determined by Hess (8) and the value $\gamma = 15$ on average experimental value between 11 A.M. and 5 P.M. reported in the Compendium of Meteorology (1954) for Washington, D. C., in 1935. In the case of the Kunkel aerosol, coagulation has little or no effect on the particle charge distribution since, when the aerosol is dense in the initial stages of the aging, it is uncharged; on the other hand, when the aerosol has become more highly charged it has thinned to such an extent that ion capture is much more important than is coagulation in changing the charge distribution. Calculations, therefore, were made from Eqs. [31] and [35]. As can be seen from Fig. 1, there is excellent agreement between theory and experiment.

Gillespie (4, 5) has made measurements of the time variation of the electrical charge distribution in an aerosol formed by blowing up silica dust with a blast of air at 10 lb./in.^{2}. Although the dust is too highly electrified to provide a suitable test of the formulas developed in this paper, nevertheless a qualitative description of the effect of the aging of the aerosol on its electrical charge distribution can be given here. It is, first of all, useful to consider the dimensionless number σ_0 for a rough assessment of the relative importance of coagulation and ion capture in changing the proportion of neutral particles, where

$$\sigma_0(t) = \frac{k}{2}\frac{\tilde{N}^2(t)P_c}{2\gamma}\left[\frac{1 - 2\left(\frac{P_1P_{-1} + P_2P_{-2} + \cdots}{P_0P_c}\right)}{1 - \left(\frac{P_1 + P_{-1}}{2P_0}\right)}\right], \qquad [43]$$

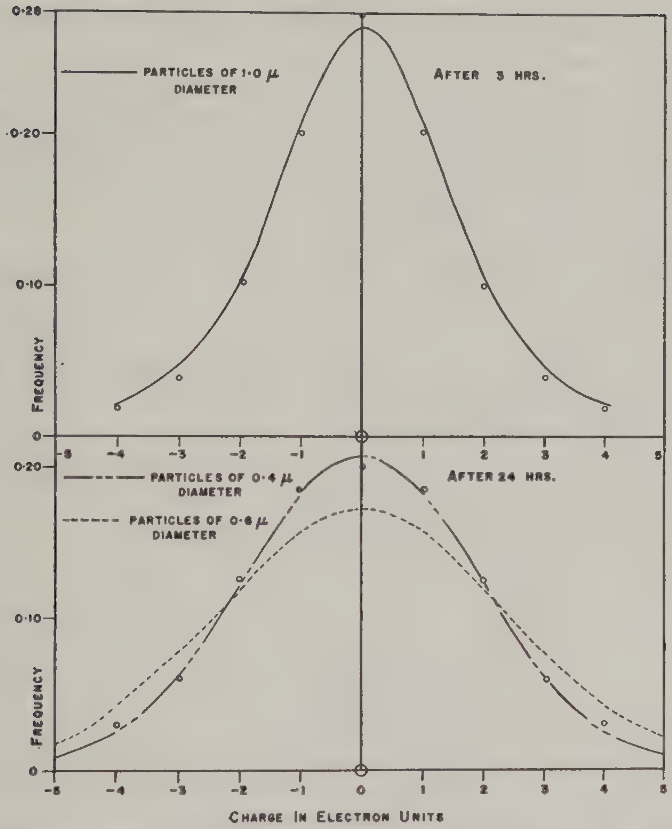

FIG. 1. Comparison of theoretical curves plotted from Eqs. [31] and [35] of this paper and experimentally determined charge distributions of ammonium chloride aerosols studied by Kunkel (10). In spite of the fact that ammonium chloride particles are in no sense spherical, the agreement between theory and experiment is excellent.

and P_0 is the proportion of neutral particles, P_n the proportion of particles having n charges, and P_c the proportion of charged particles at time t. For Gillespie's aerosol we get

$$\sigma_0(5) = 0.41, \qquad \sigma_0(30) = 0.62, \qquad \sigma_0(60) = 0.68, \qquad \sigma_0(120) = 0.12.$$

Thus coagulation and ion capture are both important initially but, after 2 hours, coagulation becomes relatively unimportant and the process of ion capture determines the changes in the proportion of neutral particles as a function of time. It is also worth noting the equilibrium distribution to which the electric charge distribution will tend when the aerosol has aged sufficiently. For a particle diameter of 1.5 μ the percentage of neutral particles at electrical equilibrium is 11 %, a result obtained from Eq. [37].

For 1-μ particles the figure rises to 13% and for 0.75-μ particles it becomes 16%.

Taking the distribution given by Gillespie (4) for the 10 lb./in.^{2} blast silica aerosol at 5 min. as symmetrical by averaging corresponding positive and negative sides of the distribution it is required to predict the distribution at 60 min. Since Porton Technical Paper 289 is rather inaccessible, an extract of Gillespie's data on the 10 lb./in.^{2} aerosol is given in Appendix 1.

In order to integrate Eq. [26] in this case it is, first of all, necessary to evaluate

$$\int_0^t \left[\frac{1+\tan^2\pi s}{1+\dfrac{\lambda^2(t)}{\lambda^2(u)}\tan^2\pi s}\right]^{2/r}\left[\left(\frac{\partial\tilde N(u)}{\partial u}\right)\Big/\left(\frac{\partial\tilde N(u)}{\partial u}\right)_0\right]du, \qquad [44]$$

an integral which appears in Eq. [24]. In the integrand of [44]

$$\left[\left(\frac{\partial\tilde N(u)}{\partial u}\right)\Big/\left(\frac{\partial\tilde N(u)}{\partial u}\right)_0\right] \geq 0 \text{ for } 0 \leq u \leq t;$$

also

$$\left[\frac{1+\tan^2\pi s}{1+\dfrac{\lambda^2(t)}{\lambda^2(u)}\tan^2\pi s}\right]^{2/r}$$

is continuous for all u and all real s. Thus we can apply the mean value theorem and get

$$\bar N(s,t) = \frac{\left[\left(\dfrac{\partial\tilde N(t)}{\partial t}\right)\Big/\left(\dfrac{\partial\tilde N(t)}{\partial t}\right)_0\right]\cdot\left[\dfrac{1+\lambda^2(t)\tan^2\pi s}{1+\tan^2\pi s}\right]^{2/r}\bar N\left\{\dfrac{1}{\pi}\tan^{-1}(\lambda(t)\tan\pi s),0\right\}}{1-\dfrac{k}{2}\bar N\left\{\dfrac{1}{\pi}\tan^{-1}(\lambda(t)\tan\pi s),0\right\}\cdot\left[\dfrac{1+\tan^2\pi s}{1+\dfrac{\lambda^2(t)}{\lambda^2(t_1)}\tan^2\pi s}\right]^{2/r}\left[\dfrac{\tilde N(t)-\tilde N(0)}{\left(\dfrac{\partial\tilde N(t)}{\partial t}\right)_0}\right]}, \qquad (45)$$

where $0 \leq t_1(s) \leq t$. In most cases $\lambda^2(t)$ is a slowly varying function, and it will be sufficiently accurate to put $t_1 = t/2$.

For $a = 7.5 \times 10^{-5}$ cm., $\tilde N(5) = 8.7 \times 10^4$/cm.^{3}, $\tilde N(60) = 3.5 \times 10^4$ $t = 60$ min., $\gamma = 12$ ion pairs/cm.^{3}/sec., $\beta = 4 \times 10^{-3}$/min., and $k/2 =$ 20×10^{-8}cm.^{3}/min., the average value of the coagulation "constant" fo the first hour of the aerosol studied by Gillespie (4), we get $\lambda^2(t) = 0.8$

and $\lambda^2(t/2) = 0.92$. The evaluation of Eq. [26] was done graphically with the following results:

Theory	*Experiment*
$a_0 = 0.100$	$a_0 = 0.074$
$a_1 = 0.078$	$a_1 = 0.065$ (average)
$a_2 = 0.070$	$a_2 = 0.057$ (average)
$a_3 = 0.057$	$a_3 = 0.052$ (average)

At 120 min., the calculations indicated that the number of neutrals had decreased to 8.3%, which is to be compared with 10% obtained experimentally.

If the diameter of the aerosol particles is taken to be 0.75 μ, the percentage of neutrals at 60 min. turns out to be 8.3%, which is in somewhat better agreement with experiment. In this case, at 120 min. a calculation gives the percentage of neutrals to be 8.9, which is to be compared with the figure of 10% obtained experimentally.

Taking the electrical charge distribution at 120 min. from Gillespie's (4) paper, we obtain from a calculation of the distribution 1 hour later the percentage of neutrals to be 9.2, which is to be compared with 14% obtained experimentally. Thus, in the latter case, the agreement with experiment is not good. The inadequacy of the theory to explain the 180-min. distribution, given the 120-min. distribution, is probably due to the neglect of the electric charges of the high proportion of particles with more than five electronic charges. The competition for ions, in this case, would be in favor of the highly charged particles and thus one would expect equilibrium (16% neutrals for particles of diameter 0.75 μ) to be attained more quickly than our formulas would predict.

DISCUSSION

It is evident, from the considerations of this paper, that the results of an experimental investigation of aerosol electrification cannot be adequately explained in terms of theory unless the investigation is made sufficiently broad to include a consideration of not only particle charge distributions but also size distributions and ion production rate during the aging of the aerosol. As yet, unfortunately, such experimental data do not exist.

ACKNOWLEDGMENT

I should like to thank Mr. W. J. Francissen of Suffield Experimental Station for translating a paper by Lissowskii (11) from the Russian.

REFERENCES

1. ARENDT, P., AND KALLMAN, H., *Z. Physik* **35**, 421 (1926).
2. COURANT, R., AND HILBERT, D., "Mathematische Physik," Vol. 1 (1931) and Vol. 2 (1937). Springer, Berlin, 1931, 1937.

3. Gillespie, T., and Langstroth, G. O., *Can. J. Chem.* **30,** 1003 (1952).
4. Gillespie, T., *Porton Technical Paper* **289** (1952).
5. Gillespie, T. *Proc. Roy. Soc. (London)* **216,** 569 (1953).
6. Gunn, R., *J. Meteorol.* **11,** 339 (1954).
7. Gunn, R., *J. Colloid Sci.* **10,** 107 (1955).
8. Hess, V. F., "The Electrical Conductivity of the Atmosphere and its Causes," translated by L. W. Codd. Constable, London, 1928.
9. Kunkel, W. B., *J. Appl. Phys.* **21,** 820 (1950).
10. Kunkel, W. B., *J. Appl. Phys.* **21,** 833 (1950).
11. Lissowskii, P., *J. Phys. Chem. U.S.S.R.* **14,** 521 (1940); *Acta Physiochim. U.S.S.R.* **13,** 157 (1940).
12. MacRoberts, T. M., "Functions of a Complex Variable." Macmillan, New York, 1947.
13. Sachsse, H., *Ann. Physik* **14,** 396 (1932).
14. Von Smoluchowskii, M. V., *Z. physik. Chem.* **92,** 129 (1918).
15. Tunitskii, N., *J. Phys. Chem. U.S.S.R.* **13,** 1141 (1939).
16. Whittaker, E. T., and Watson, G. N., "Modern Analysis," Cambridge, 1940.
17. Whytlaw-Gray, R. W., and Patterson, H. S., "Smoke: A Study of Aerial Disperse Systems." Arnold, London, 1932.

APPENDIX[a]

The Determined Charge Distribution at Various Times for a Typical Silica Dust Aerosol Produced with the 10 lb/in² Air Blast (Actual Data Have Been Condensed)
% of total particles having charge q electron units

q	5 min.		30 min.		60 min.		120 min.		180 min.	
0	37.2		14.9		7.4		10.0		14.3	
	pos.	*neg.*	*pos.*	*neg.*	*pos.*	*neg.*	*pos.*	*neg.*	*pos.*	*neg.*
1	4.8	6.0	9.1	6.5	6.1	7.0	7.9	7.0	10.3	11.0
2	3.9	4.0	4.8	4.7	5.0	6.4	6.3	5.5	6.3	9.1
3	3.3	3.5	2.9	4.0	5.3	5.0	4.9	5.1	5.2	7.4
4	3.4	2.2	2.5	4.0	4.5	4.6	4.0	3.8	3.9	5.2
5	2.4	1.9	2.4	4.0	3.0	4.0	3.6	3.2	2.0	4.0
6	2.8	1.7	2.0	3.6	2.9	3.6	3.0	3.1	1.8	2.9
7–9	5.6	3.3	4.2	8.3	5.5	8.0	5.5	6.4	4.2	5.0
10–15	5.0	3.1	5.6	6.7	3.9	9.0	4.4	7.0	2.8	2.3
16–21	1.4	1.5	2.8	2.5	2.6	2.5	2.7	3.3	1.3	0.4
22–30	1.0	0.9	1.8	1.4	1.8	1.1	1.8	0.7	0.2	0.2
31–40	0.5	0.2	0.4	0.6	0.2	0.5	0.4	0.4	0.2	—
41–60	0.14	0.12	0.08	0.15	0.1	0.02	0.02	0.03	—	—
61–80	0.03	0.05	0.08	0.04	0.02	—	—	—	—	—
81–100	0.03	0.02	—	—	—	—	—	—	—	—

[a] This appendix contains data from Porton Technical Paper 289 (1952).

JOURNAL OF COLLOID SCIENCE 12, 161–172 (1957)

ON THE FILTRATION OF AEROSOLS BY FILTER MODELS OF VARIOUS POROSITIES[1, 2]

Isaiah Gallily[3]

Tel-Aviv, Israel

Received July 15, 1956

ABSTRACT

In order to study the filtration of aerosols under defined conditions of flow and geometry of fibers, a new filter was built. This filter consisted of an array of grids set perpendicularly within a metallic pipe. Each grid was composed of equally spaced similar metallic wires.

To achieve parabolic laminar flows, the Reynolds numbers were kept below the critical value of 2000 and the whole array was preceded by a "calming device." The filtration of homogeneous, electrically neutral aerosols of dioctyl phthalate by this filter has been studied at various velocities of flow, radii of particles, and inter-wire distances.

It was found that the inertial mechanism of filtration was effective even at ψ values lower than the critical ψ's given in the theories. When comparing the collection efficiencies of a wire in filters of varying inter-wire distances, a clear maximum could be discerned.

It is believed that this unexpected phenomenon is caused by the nonadherence of some of the impacting particles to the wires—a possibility which has been taken into consideration only lately by Gillespie and Rideal.

INTRODUCTION

The calculation of the collection efficiency of a single fiber within a filter constitutes one of the most important and difficult problems in the theory of filtration of aerosols.

Much research has been devoted to the deposition of particles on the simplest type of fibrous mat, the infinitely long cylindrical wire perpendicular to the initial direction of flow (1–4), but very little has been done on the problem of filtration by a whole assembly of fibers (4–6).

As the path of an aerosol through the tortuous pores of the commercial mat is extremely complicated, the theories had to be restricted to imaginary

---

[1] This work has been carried out under the auspices of the Scientific Department, Israeli Ministry of Defence.

[2] Extracted from a thesis submitted to the Hebrew University, Jerusalem, in partial fulfillment of the requirements for the degree of Ph.D.

[3] Present Address: Department of Chemistry, Columbia University, New York 27, New York.

models with a high degree of orderliness and to simple types of flow. These theories neglect any effects arising from electrostatic forces, but differ in the field of flow they assume within the filters and in the importance they attribute to the various mechanisms of deposition. Likewise, it has been assumed that under the practical conditions of filtration all the aerosol particles which impinge on the fibers adhere to them, though recently this has been questioned by several workers (7, 8).

The filters dealt with in the theories are composed of a multitude of parallel cylinders perpendicular to the initial direction of flow. The collection efficiency (η) of a cylinder within such an assembly is obviously different from that of the single one because of the effect of the neighboring cylinders on the field of flow around it.

Langmuir assumes (5) that this effect can be expressed in the constant of Lamb's equation for viscous flow around the single cylinder (9) and calculates the value of the latter from the pressure drop through the filter.

Davies (4), using the equations of Kovasznay (10) for viscous flow behind an infinite grid of parallel wires, estimates the interference effect and proposes the general equation for the collection efficiency of a cylinder within the filter:

$$\eta = (0.16 + 10.9\alpha - 17\alpha^2)[R + (0.50 + 0.80R)(\psi + D) - 0.1052R(\psi + D)^2] \quad [1]$$

where α is the packing density of the filter, ψ is the inertial parameter, R is the interception parameter, and D is the diffusion parameter.

Chen (6) measured the relation between η and the packing density of the filter and arrived at the simple equation:

$$\eta = \eta_0 (1 + K\alpha) \quad [2]$$

for $0.01 \leq \alpha \leq 0.09$, where η_0 is the efficiency of a geometrically similar single cylinder and K is a constant.

The experiments carried out with commercial fiber mats (6, 11, 12) have not always confirmed the theoretical conclusions, nor have their results been unambiguous regarding the existence of "a most penetrating size o particles" and the role of the inertial mechanism in filtration. As it was likely that these divergences were due to the difference between the theoretical imaginary filters and the real fiber mats, it appeared worth while to construct a geometrically defined filter model with which the various parameters of filtration could be investigated. This model had to be made entirely from metal so that it could be earthed and freed from electrostatic charges which usually play a role in commercial mats (13, 14).

FILTER

The filter, which has been briefly described before (15), consisted of long cylindrical pipe into which were put, in planes perpendicular to its axis, 76 grids of parallel metallic wires. The wires were wound by a special technique (using the wormlike motion of a lathe) on metallic frames and these were inserted between fixed frames in specially prepared grooves (Fig. 1 of ref. 15). In order to have a simple and well-defined type of flow through this filter, laminar viscous motion having the Poiseulle profile of velocities was chosen. This was achieved by using a pipe with a circular bore, keeping the Reynolds numbers of the flow well below the critical value of 2000, and inserting a "calming device" before the filter. The device consisted of a long narrow tube, a diverging cone of 6°, and a cylindrical pipe of a length determined according to the equation of Schiller (16) for the unfavorable condition of Reynolds number equal to 660.

Of the many problems study of which this filter permits, it seemed most interesting to inquire into the relation between the collection efficiency of the fiber and one of the "proximity parameters" such as the inter-wire, or the inter-grid, distance. To simplify things, the distance between the grids was chosen so that the flow after each one of them would almost regain its initial parabolic pattern halfway before the next grid.

According to Kovasznay (10), the steady viscous flow behind an infinite grid of parallel wires is given by:

$$1 + U = 1 - e^{\lambda x} \cos 2\pi y \tag{3}$$

and

$$V = -\frac{\lambda}{2\pi} e^{\lambda x} \sin 2\pi y \tag{4}$$

where $(1 + U)$ and V are the local velocities in the x and y direction, respectively, expressed in units of the initial velocity U_0, x and y are expressed in units of the inter-wire distance (d_i), and λ is defined by $\lambda_{1,2} = \frac{Re}{2} \pm \sqrt{\frac{Re^2}{4} + 4\pi^2}\left(Re = \frac{U_0 d_i}{\nu}\right)$.

These equations, which are accurate only for the limiting case of an nfinite grid with wires of negligible diameter, represent a good approxination for the immediate neighborhood of the geometric axis, where the low can be assumed to be quite homogeneous; i.e., a unidirectional flow with constant velocity over the field.

In the present series of experiments, the inner diameter of the pipe was 5.00 cm., the grids were made of Kanthal-D a (Swedish Nichrome type) wire of 0.0050 cm. diameter and spaced apart at an inter-grid distance of 0.550 cm., which is reasonable according to Eqs. [3–4] even under the most unfavorable conditions of flow.

The inter-wire distances were 0.0132, 0.0198, and 0.0270 cm. in three sets of grids (with a standard deviation of approximately 4%). The total length of the filter was 44.75 cm. In selecting this length, it was borne in mind that though the use of a long filter enhances the accuracy of the measurements, the loss of particles by sedimentation and diffusion is also increased under these conditions.

Assuming a homogeneous spatial distribution of particles in every cross-section of the filter, the penetration through the grids (defined as the ratio between the effluent and influent concentration of the aerosol, n/n_0) may be expressed by:

$$\frac{n}{n_0} = (1 - \Delta x)^{n_1} = \left(1 - \eta \frac{d_f}{d_i}\right)^{n_1}, \qquad [5]$$

where Δx is the fraction filtered by a single grid, d_f is the diameter of the wires, d_i is the inter-wire distance, and n_1 is the number of grids. Equation [5] is derived in Appendix A.

Calculating the collection efficiency of the fiber (η) from Eq. [1], it appeared that with 76 grids the penetration could be measured accurately. Likewise, it was shown that in this case the errors introduced by the loss to the walls were negligible in comparison with the experimental accuracy achieved.

APPARATUS

The experiments were carried out by passing through the filter electrically neutral submicron aerosols of various radii and at several velocitie of flow, and measuring the pentration by a light-scattering method. In order to achieve this it was necessary to have particles of a very narrow size distribution and to keep their radii and concentration constant fo long periods of time. Moreover, the particles had to be stable with regar to coagulation and evaporation during their passage through the filter.

To fulfill the latter condition, aerosols of dioctyl phthalate, which consis of liquid spherical droplets of very low vapor pressure ($\sim 10^{-7}$ mm. H at room temperature) were used.

The apparatus constructed consists of a LaMer-Sinclair homogeneou aerosol generator (17), the model filter, and a "right-angle penetrometer..

The generator described previously (15), produces usually aerosols of very narrow size distribution ($\sigma/\bar{r} \sim 0.1$, where σ is the standard deviatio and $\bar{r}$ is the mean radius of the particles). The mean radii of the aeroso used in the present experiments (measured in a convection-free ultramicroscope cell with a standard error of the mean of 0.007μ and by the "owl (18)) were 0.5–0.8 micron and their concentration could be varied, b dilution, between 10^4 and 10^5 particles/cm.^{3}.

The aerosol, after issuing from the electrostatic precipitator where th charged particles were removed, was mixed with air in a T-shaped tu in which some protuberances generated a moderate turbulence, and pa of it was sucked into a secondary line. By this last arrangement it has be

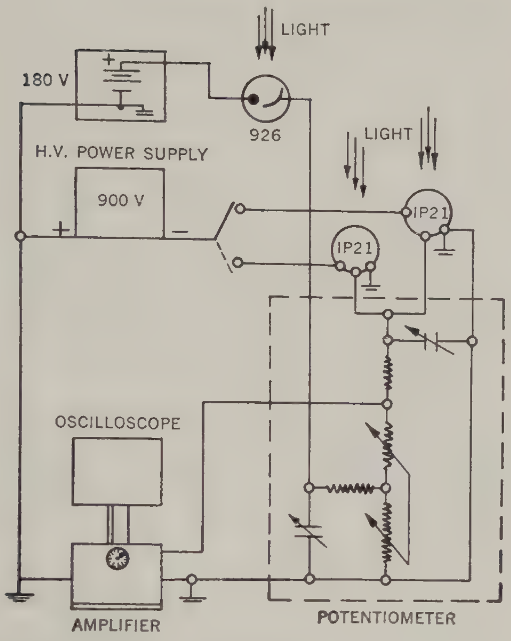

Fig. 1. Block diagram of the electronic parts of the penetrometer.

ossible to lead into the filter aerosols of constant radius and concentration, ut at various volume rates of flow.

The right-angle penetrometer has been described before (15). The main ptical system was made so as to have two almost symmetrical arms con-isting of a 100-watt AH-4 mercury light source, doublets of plano-convex enses, and first-surface coated mirrors. Likewise, a second photomultiplier IP21), fed separately from the high-voltage D.C. power supply, was ncluded in the electronic parts of the instrument (Fig. 1).

In order to measure the light scattered only from the axial zone of the ipe, where the flow may be assumed to be homogeneous, the field of view f the photomultipliers was cut down to a small central region (of $1.48.10^{-2}$ m.^{3}) by appropriate stops that were introduced into the auxiliary optical ystem. Owing to this restriction, it was also assured that the size distribu-ion of the aerosols within the central region would not change by sedi-entation during the passage through the filter. Similarly it was shown hat the effect of diffusion there, as estimated by Einstein's equation: $^{2} = 2D_{BM}$, could be practically neglected.

Procedure

As the places of measurement before and after the filter were not strictly lentical with regard to volume and the intensity of incident light, and as

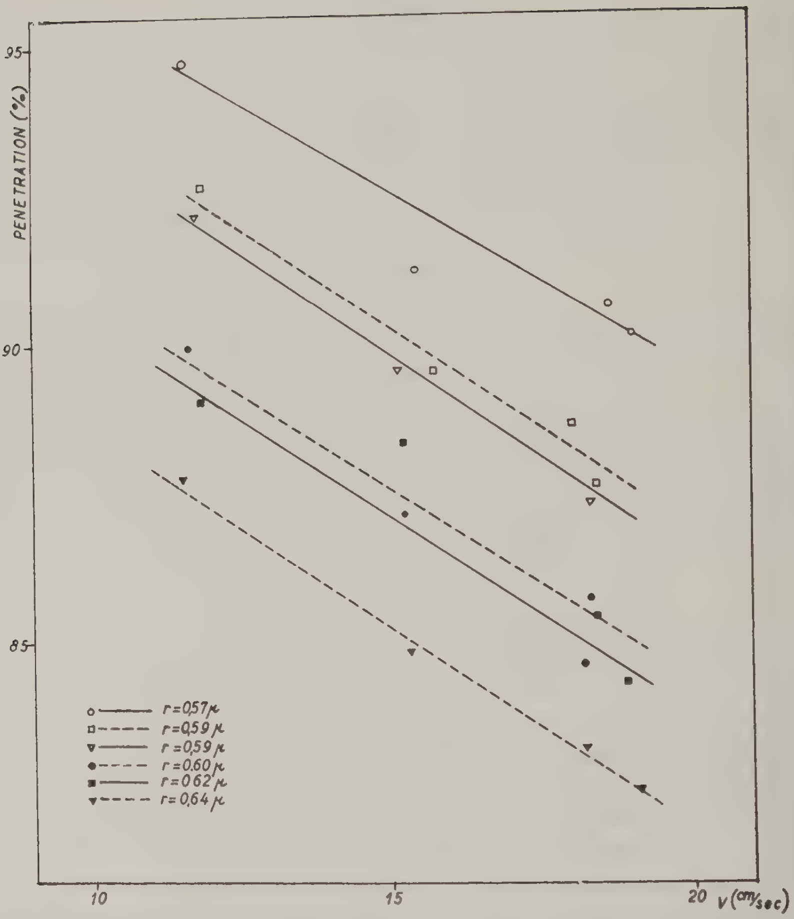

Fig. 2. Penetration vs. average linear velocities. Diameter of wire—0.0050 cm.; inter-wire distance—0.0132 cm.; inter-grid distance—0.550 cm.

the two photomultipliers had different sensitivities, it was necessary to determine the ratio of their responses to a signal from the same aerosol. Consequently, after obtaining a suitable aerosol, the grids were set aside so as to leave a free bore within the pipe, the aerosol was passed through the latter at several velocities of flow, and the ratio of the signals received by the photomultipliers was noted. This ratio constituted the correction factor by which the readings of the penetration were multiplied afterwards

After replacing the grids, the radius of the generated particles was checked by the ultramicroscope and the "owl," and adjusted by changin the temperature of the source of the nuclei. The aerosol was then passe into the filter at various rates of flow and the penetration was determine

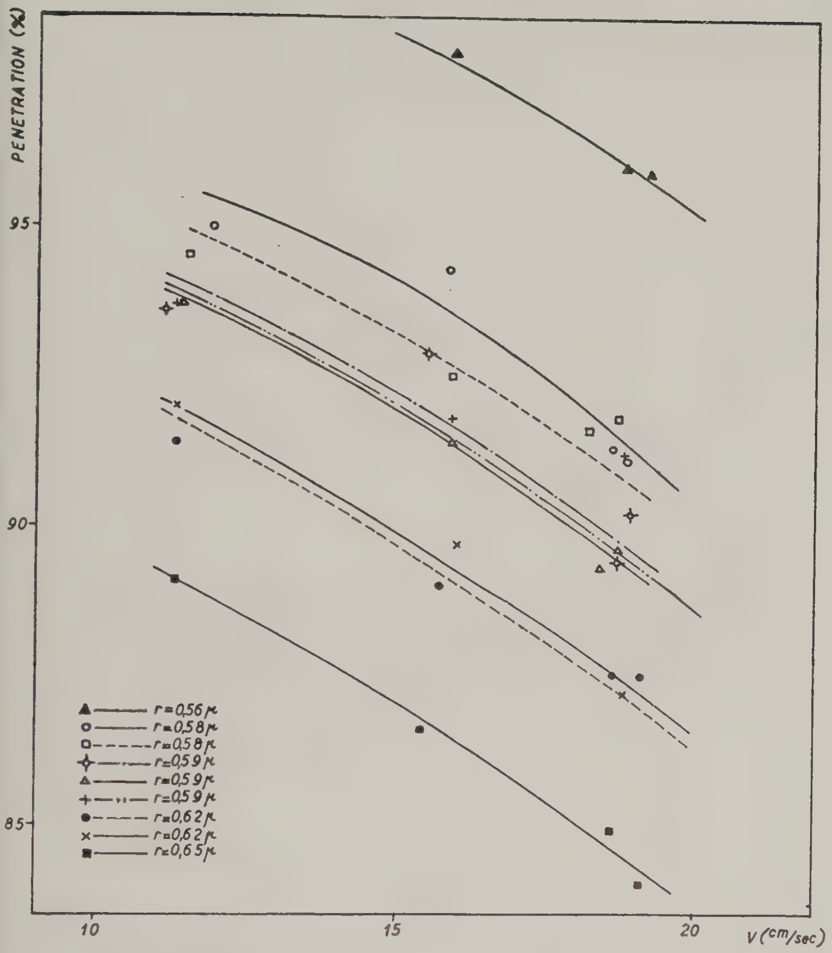

FIG. 3. Penetration vs. average linear velocities. Diameter of wire—0.0050 cm.; inter-wire distance—0.0198 cm.; inter-grid distance—0.550 cm.

several times for each velocity by the "right-angle penetrometer." At the end of each experiment, the radius of the particles was checked again.

EXPERIMENTAL RESULTS

The parabolic profile of velocities at the end of the "calming pipe" was checked with the aid of a hot-wire anemometer to which a very fine probe was fitted. (The ratio between the cross sections of the probe and the bore was 0.0025.)

This probe, immersed 9.4 cm. into the pipe, could be moved by a special carriage along a preferred diameter of the bore.

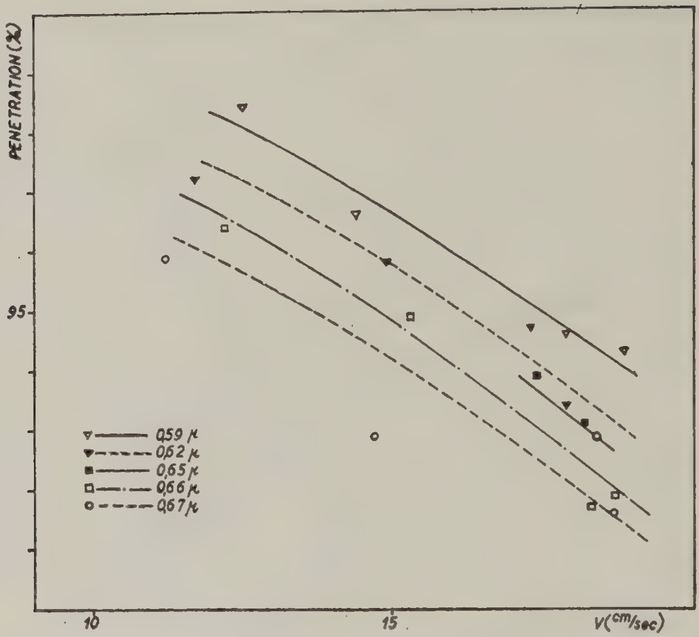

FIG. 4. Penetration vs. average linear velocities. Diameter of wire—0.0050 cm.; inter-wire distance—0.0270 cm.; inter-grid distance—0.550 cm.

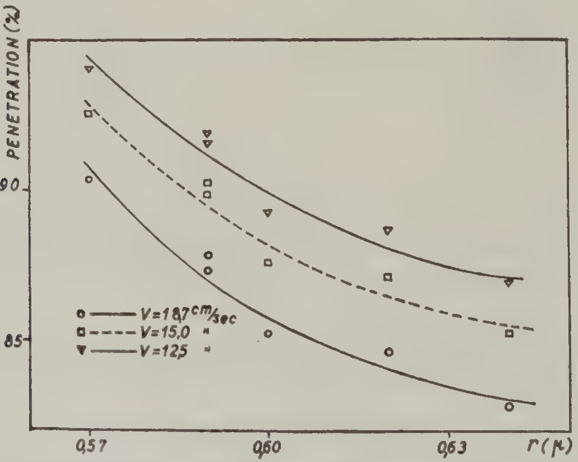

FIG. 5. Penetration vs. radius of aerosol. Diameter of wire—0.0050 cm.; inter-wire distance—0.0132 cm.; inter-grid distance—0.550 cm.

Since the velocity of flow was found to be a linear function of the square of the radial distance from the axis of the pipe, it was concluded that the parabolic profile was really achieved.

In Figs. 2, 3, and 4 the measurements of penetration through the grids

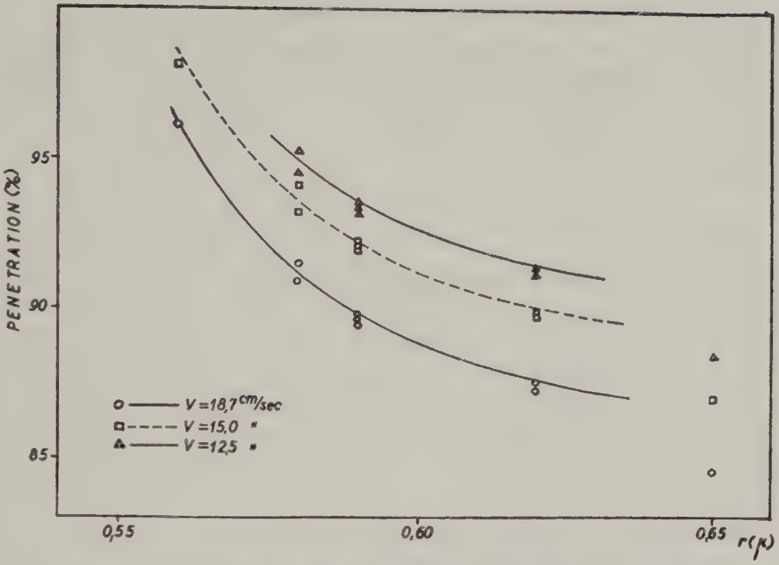

Fig. 6. Penetration vs. radius of aerosol. Diameter of wire—0.0050 cm., inter-wire distance—0.0198 cm., inter-grid distance—0.550 cm.

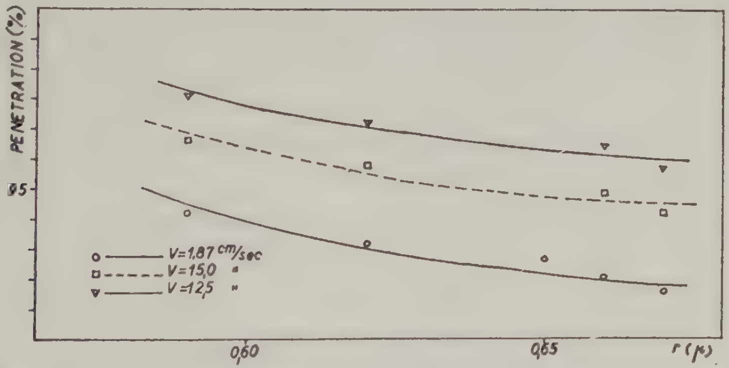

Fig. 7. Penetration vs. radius of aerosol. Diameter of wire—0.0050 cm., inter-wire distance—0.0270 cm.; inter-grid distance—0.550 cm.

of 0.0132, 0.0198 and 0.0270 cm. inter-wire distance are summarized as a function of the average linear velocity. From these measurements, the curves of Figs. 5, 6, and 7 are obtained by interpolation.

Discussion

From Figs. 2–4 it can be inferred that, under the given experimental conditions, the diffusional mechanism of deposition is definitely not effective, and also that interception probably does not play any appreciable part. The impingement of particles on fibers by Brownian motion would increase monotonously with the diffusion parameter $D_{BM}/U_0 d_f$ (where D_{BM} is the diffusion coefficient of the particles), which is not so in the present experiments. Likewise, had interception been predominating, the dependence of the penetration on the velocity of flow, as expressed for this mechanism by Langmuir's equation (5):

$$\eta = \frac{1}{2(2{,}002 - \ln N_{Re})} \left[2(1 + R) \ln (1 + R) - (1 + R) + \frac{1}{1 + R} \right] \qquad [6]$$

(where N_{Re} is the Reynolds number based on the diameter of the wire) would have been much less pronounced. It appears, therefore, that the main mechanism effective in these experiments is the inertial impaction.

The importance of this mechanism in the filtration of aerosols has been discussed before (11, 12). According to some theories, no inertial impaction exists below a certain critical value of ψ (0.0625 according to Langmuir and 0.09 according to Albrecht), although recent experiments have shown these values to be too high.

As the present filter model makes it possible to define the inertial parameter ψ more exactly than could be done before, its values were calculated for the various aerosol radii and velocities of flow. The minimum values (0.019–0.022, in the various grids) were found to be significantly smaller than the critical values of Langmuir or Albrecht.

When the collection efficiencies of a single wire (η) were calculated according to Eq. [5] for each case and plotted, for pairs of constant average linear velocity and $\bar{r}$, as a function of the inter-wire distance, an unexpected maximum of η, which proved to be statistically significant according to "Student's Test", was revealed (Fig. 8).

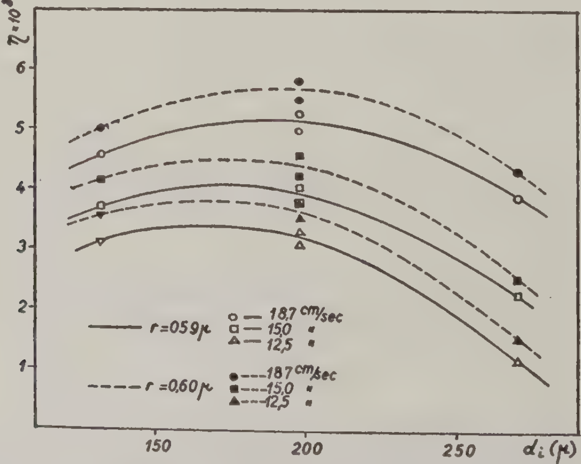

FIG. 8. Single wire collection efficiency vs. inter-wire distance. Diameter of wire—0.0050 cm.; inter-grid distance—0.550 cm.

Actually, as the radius of the aerosol and its average velocity are maintained constant and the inter-wire distance decreases, the velocity with which the particles approach the fibers increases. Therefore, in view of the preponderance of the inertial mechanism, the collection efficiency η should also increase. To check this phenomenon, a fourth set of grids (of d_i = 0.0198 cm.) was made and studied. The same maximum was found with this set of grids.

For the time being, the only available explanation for this maximum seems to be the hypothesis of Gillespie and Rideal (8) that not all the impinging particles adhere to the obstacle.

It may be assumed that as the inter-wire distance decreases and the velocity of the approaching particles, at constant radius and rate of flow, increases, a point is reached at which the bouncing and the peeling off the wire overcompensate the process of impingement. Likewise, the shift of the maximum (see Fig. 8) at greater radii and velocities of flow to larger inter-wire distances may be qualitatively understood from this hypothesis.

As the processes following the impaction of particles on solid obstacles are obscure and as data concerning the adhesional forces between aerosols and solid walls are lacking, no quantitative explanation is offered.

A comparison of the collection efficiencies (η) calculated from the experiments with those predicted by Eq. [1] reveals a marked divergence (Fig. 9). However, it should be noted that such a comparison is somewhat misleading, as the theory does not take into account at all the possibility of bouncing.

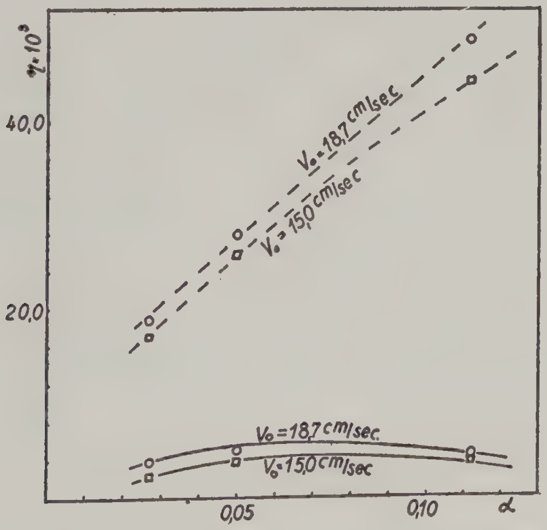

FIG. 9. A comparison between the experimental and the theoretical (according to Eq. [1]) curve of η vs. α. ——— experimental curve. - - - - - theoretical curve.

ACKNOWLEDGMENT

The author expresses his thanks to Professor A. Katchalsky and to Mr. G. Volinez for their helpful advice and criticism during this work.

Appendix

After passing the first grid the concentration of the aerosol will be $n = n_0 (1 - \Delta x)$ and after n_1 grids it will be $n = n_0 (1 - \Delta x)^{n_1}$.

$$\Delta x = \frac{[\text{filtering cross section of grid}]}{[\text{cross section of grid}]} = \frac{\eta \cdot L_i \cdot d_f}{\pi R_1^2}$$

where L_i is the total length of the wires in a grid and R_1 is the radius of the cross section of the grid.

The average length of the wires in a grid is $\pi R_1/2$. The total number of wires in a grid is $2R_1/d_i$.

Thus

$$\Delta x = \frac{\eta(\pi R_1/2 \cdot 2R_1/d_i)\, d_f}{\pi R_1^2} = \eta \frac{d_f}{d_i}.$$

REFERENCES

1. ALBRECHT, F., *Physik. Z.* **32,** 48 (1931).
2. SELL, W., *Forsch. Gebiete Ingenieurw.* **2,** *Forschungsheft* No. 347 (Aug. 1931).
3. LANGMUIR, I., AND BLODGETT, K. B., Report No. RL-2245, General Electric Research Laboratory, 1944–45.
4. DAVIES, C. N., *Inst. Mech. Engrs. (London) Proc.* (b) **1B,** 185 (1952).
5. LANGMUIR, I., O.S.R.D. Report No. 865 (1942).
6. CHEN, C. Y., *Chem. Revs.* **55,** 595 (1955).
7. GILLESPIE, T., *J. Colloid Sci.* **10,** 266 (1955).
8. GILLESPIE, T., AND RIDEAL, E., *J. Colloid Sci.* **10,** 281 (1955).
9. LAMB, H., "Hydrodynamics," p. 616. Dover Publications, New York, 1932.
10. KOVASZNAY, L. I. G., *Proc. Cambridge Phil. Soc.* **44,** 58 (1948).
11. LAMER, V. K., *et al.*, Final Report NYO-512, Contract AT(30-1)-651, Columbia University, New York, 1951.
12. RAMSKILL, E. A., AND ANDERSON, W. L., *J. Colloid Sci.* **6,** 416 (1951).
13. GOYER, G. G., GRUEN, R., AND LAMER, V. K., *J. Phys. Chem.* **58,** 137 (1954).
14. GILLESPIE, T., *J. Colloid Sci.* **10,** 299 (1955).
15. GALLILY, I., *J. Colloid Sci.* **10,** 558 (1955).
16. GOLDSTEIN, S., "Modern Developments in Fluid Dynamics," p. 299. Oxford University Press, 1950.
17. SINCLAIR, D., AND LAMER, V. K., *Chem. Revs.* **44,** 245 (1949).
18. "Handbook on Aerosols," p. 106. A.E.C., Washington, D. C., 1950.

JOURNAL OF COLLOID SCIENCE **12**, 173–180 (1957)

DENSITY OF POLYSTYRENE AND POLYVINYLTOLUENE LATEX PARTICLES[1]

Thomas L. Pugh and Wilfried Heller

Chemistry Department, Wayne State University, Detroit, Michigan

Received October 22, 1956

I. Introduction

The accurate determination of particle diameters from light scattering requires the use of the Mie theory (1) if the refractive index of the spheres differs appreciably from that of the surrounding medium. This means that this theory should be used for a relative refractive index in excess of about 1.05. On applying the Mie theory, it is necessary to know the refractive index of the light-scattering spheres very accurately. It can be shown easily (2) that four and, if possible, five significant figures should be obtained. In the absence of reassuring evidence to the contrary, it is therefore somewhat risky to assign to the dispersed polymer spheres—which contain adsorbed stabilizer—the refractive index of the corresponding bulk material. The refractive index of the suspended particles should therefore be calculated from the refractive index of the entire system by using a suitable mixture rule. To that effect it is necessary to know the volume concentration of the particles with an accuracy equivalent to that desired for the refractive index. The volume concentration must, in addition, be known for the evaluation of scattering data from the Mie theory. This concentration, therefore, enters twice in the calculation of particle sizes from light scattering (3). Sufficiently accurate determination of the volume concentration requires that the density of the colloidal particles be known to four or, if possible, five significant figures. In view of this requirement, it is, here again, a priori risky to assume for the dispersed particles the same density as that obtained rather easily from macroscopic specimens. Apart from conceivable intrinsic differences in density, surface-adsorbed stabilizers may differ appreciably in density from the ultramicroscopic material itself.

Density measurements were, therefore, carried out on monodisperse polystyrene and polyvinyltoluene latices (4) of systematically varied particle size in connection with simultaneous light-scattering and refractive index experiments.[2] Systematic density measurements on these systems were also of interest in themselves in order to answer the question as to whether or not the density of colloidal polymer particles may change measurably with particle size.

---

[1] This work was supported by the U. S. Office of Naval Research.

II. Theoretical Considerations

The latices investigated contained, besides water and dispersed polymer spheres, a small amount of truly dissolved stabilizer whose concentration was, a priori, unknown. The systems were, therefore, three-component systems to which an equation previously given (5) could not be applied. The basic equation to be considered is:

$$\phi_{123} = 1/\rho_{123} = c_1\phi_1 + c_2\phi_2 + c_3\phi_3 \tag{1}$$

where c_1, c_2, and c_3 are the weight fraction of water, latex particles, and stabilizer, respectively; ϕ_1, ϕ_2, and ϕ_3 are the respective specific volumes, and ϕ_{123} and the density ρ_{123} apply to the total system.

Equation [1] presupposes volume additivity. It was, a priori, certain that this would apply to the polymer particles (6). It was also proved for the dissolved stabilizer by special experiments with latex serum.[3] Since $c_1 + c_2 + c_3 = 1$:

$$\phi_{123} = c_1\phi_1 + \frac{(1 - c_1)\,\phi_2}{1 + K} + \frac{(1 - c_1)\,K\phi_3}{1 + K}, \tag{1a}$$

where $K = c_3/c_2$. Rearranging, one obtains

$$\phi_2 = 1/\rho_2 = \frac{(1 + K)(\phi_{123} - c_1\phi_1)}{1 - c_1} - \phi_3 K. \tag{2}$$

This is the equation to be used in the following work. Of the quantities given, both K and c_1 are determined gravimetrically. Both the values of ϕ_{123} and ϕ_3 are obtained by a differential pycnometric technique. The former is obtained by a measurement of the density difference, $\Delta\rho$, of the latex relative to that of pure water, i.e.,

$$\Delta\rho = \rho_{123} - \rho_1 = \frac{1}{\phi_{123}} - \frac{1}{\phi_1} \tag{3}$$

The value of ϕ_3 is obtained by a measurement of ρ_{13} of the latex serum (the

---

[2] These latices were generously supplied by Dr. J. W. Vanderhoff of the Dow Chemical Co. of Midland, Michigan.

[3] Even if this had not been the case, the use of Eq. [1] would still have been permissible since the contribution of the solute to the overall density, ρ_{123}, is small enough to make the effect of a deviation from additivity negligible for the value of ρ_2.

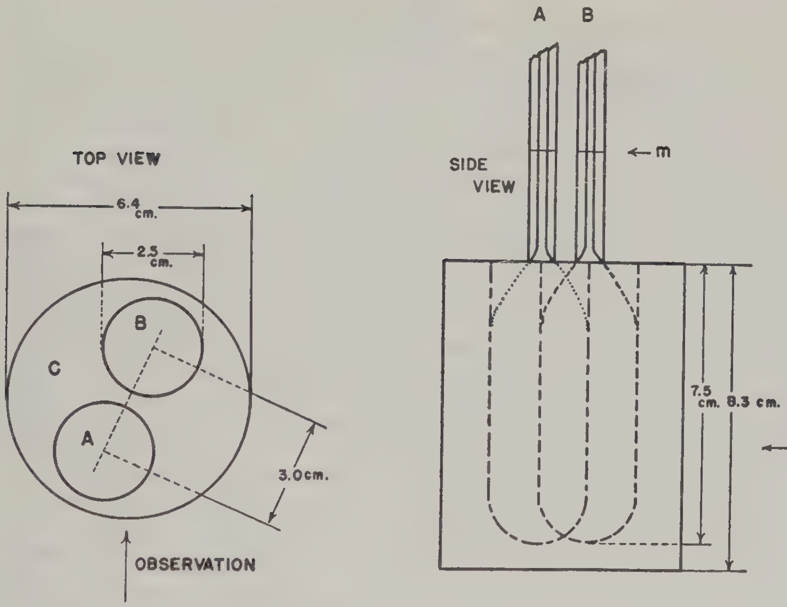

FIG. 1. Pycnometers and holder in the differential technique used.

latex freed from all polymer particles by centrifuging)[4] relative to ρ_1 of water and subsequent substitution of the ϕ_{13} obtained into

$$\phi_3 = 1/\rho_3 = \frac{\phi_{13} - c_1'\phi_1}{c_3'} = \frac{\phi_{13} - \phi_1}{c_3'} + \phi_1 . \qquad [4]$$

The primed quantities in Eq. [4] are numerically different from the corresponding unprimed quantities pertinent to the latex.

III. THE DIFFERENTIAL PYCNOMETRIC METHOD

Since the density of polystyrene was, a priori, known not to differ by much more than 0.05 from that of water, it was clear that—on choosing pycnometry—a differential technique had to be used in order to obtain four or five significant figures for ρ_2.[5] The device used for the differential measurements is illustrated in Fig. 1.

---

[4] In some instances the latex had to be frozen in order to effect efficient settling out during the centrifugation following thawing.

[5] This can be proved easily: Assuming the use of a single pycnometer of 20 ml. capacity, a latex concentration between 25 and 50%, and a knowledge of the latex weight to seven figures, it can be shown that ρ_2 will be obtained to five significant figures provided ρ_{12} (the density of a simple, two-component latex) is known to six significant figures. It is therefore necessary that all the errors of measurement inherent in the determination of the latter quantity be relegated to the sixth decimal in order to prevent their affecting, by cumulative effect, the number of significant

The glass-stoppered pycnometers, A and B, had a volume of 19.2174_8 and 19.6053_2 (cm.^{3}) respectively at 24.84° C., excluding the volume above the calibration marks m shown. The weight of a pycnometer filled with water or latex, was approximately 42 g. and the pycnometer weight alone was about ½ of this. Each of the two pycnometer volumes had been determined by calibration with pure water (7). Each pycnometer was filled at about 25° C. until the meniscus was about midway in the capillary, one with pure water and the other with the latex (or with latex serum). The two pycnometers were then placed into a brass block C and immersed with it into a thermostated bath held at 24.840° C. ± 0.003° C. The temperature and its constancy were frequently checked with a Beckmann thermometer installed immediately adjacent to the brass block. The actual fluctuationsn and differences in the pycnometers were less than 0.001° C. owing to the high heat capacity of the metal block and the high heat conductance within it. After thermal equilibrium was reached in the pycnometers (constant height of the meniscus requiring about one-half hour of waiting), the height of the two menisci relative to the respective calibration marks was measured by sharply focusing a traveling microscope simultaneously on the two capillaries using to that effect a sufficiently long optical path. From these data, the volume of the liquid contained in either pycnometer was calculated by means of calibration curves.[6] The weights of the pycnometers, both empty and full, were obtained with a semimicro balance observing the necessary precautions and applying the conventional buoyancy corrections[7] dependent on temperature, humidity, and barometric pressure.

The primary calculations for latex or serum relative to water were made with Eq. [5].

$$\Delta\rho = \frac{(W_{123} - W_1) - (P_{123} - P_1) - \rho_1(V_{123} - V_1) + D_{\text{air}}(V'_{123} - V_1')}{V_{123}}, \quad [5]$$

where W is the weight of the respective full pycnometer, P is the weight of the respective empty pycnometer, V is the volume of the respective sample in the thermostat, V' is its volume at the balance temperature,[8] and D_{air} is the density of air. The value of $\Delta\rho$ thus obtained was substituted into Eq. [3], in the case of latex, or into a corresponding equation for the serum. From the data ϕ_3 was calculated, by using Eq. [4], and then ϕ_2 using Eq. [2].

---

figures desired. The errors in buoyancy corrections would have to be held below 0.1%, if the value of ρ_{12} is to be uncertain only in the sixth decimal. Such precise buoyancy corrections are most difficult with a simple pycnometer. Temperature differences of 0.01° also would reduce the number of significant figures below that required. Use of the differential technique eliminates most of the critical buoyancy corrections, and it is also not as exacting regarding temperature control as is simple pycnometry.

[6] Each of these capillaries had been calibrated in the conventional manner by shifting a small, exactly known volume of mercury, stepwise, along its length and by measuring each time the length of the mercury column using a traveling microscope. The respective diameters varied by not more than 0.0014 cm., over their entire length of 8 cm., the average diameters being 0.1264 and 0.1314 cm., respectively.

[7] These corrections apply in the differential technique only to volume differences (see Eq. [5]). All of these excepting the pycnometer contents were found to cancel out with our pycnometers.

[8] Owing to the small contribution of $D_{\text{air}}(V'_{123} - V_1')$ and the fact that the constant bath temperature differed only slightly from room temperature, it was possible to assume that $V'_{123} - V_1' = V_{123} - V_1$.

TABLE I

Reproducibility of ρ_2-Values

Diameter (mμ)	Sample No.	ρ_2
280	1	1.0588
	2	1.0585
300	1	1.0550
	2	1.0546

It is of some interest to define the number of significant figures which can in principle be obtained with the differential technique as used here. The weights needed in Eq. [5] were determined with a semi-micro balance to five decimals. The buoyancy correction for the volume differences was of the order of 0.0005, affecting the fifth figure of $\Delta\rho$ in Eq. [5]. The measurement of the displacement in the capillary was reproducible to within 10 microns resulting in an error in volume measurement not in excess of 10^{-5} cc.[9] The effect of temperature differences in the two pycnometers was, by comparison, entirely negligible with the technique used. Each of the quantities entering into Eq. [5] was therefore known to at least the fifth decimal. The number of significant figures obtained for $\Delta\rho$ depends on both the concentration of the latex and the volume of the sample. The concentrations (20 to 40 weight %) were large enough to give to the numerator a value in excess of 0.1. Since the volume of the pycnometers, as stated, was two orders of magnitude larger, the $\Delta\rho$-values obtained were precise to the seventh decimal. Since ρ_1 is known to six decimals, the data obtained subsequently with Eq. [3] are still precise to the seventh decimal and accurate in the sixth decimal. The precision and accuracy of ϕ_2 which one finally obtains from Eq. [2] depends decisively on the precision and accuracy of c_2. Neglecting for the purpose of this discussion the contribution of c_3, it follows from Eq. [2*a*]

$$\rho_2 = \frac{c_2\,\rho_1\rho_{123}}{\rho_1 - c_1\rho_{123}} \qquad [2a]$$

that an accuracy to within six decimals can be obtained for ρ_2, if c_2 is known to seven figures. The only practical requirement therefore is that a sufficient amount of latex (between 15 and 30 g. of concentrated latex) is evaporated and the dry weight is determined on a semi-micro balance. This illustrates the very high precision and accuracy with which ρ_2 can be obtained in a two-component system. Neither could have been obtained in the present case since not enough latex was available to get for c_2 more than six figures on using a semi-micro balance. The accuracy of ρ_2 would then have been limited to five decimals, if the latex system could have been treated as a two-component system. The fact that it was a three-component system, with $c_3 < 0.01\ c_2$, and the resulting uncertainty in the value of ρ_3(ρ_3 and c_3 were on the average 3.1 and 0.0025, respectively) made it questionable whether the fifth decimal of ρ_2 would be truly meaningful, even on reducing a comparatively large volume of latex or serum to dryness without risking minute losses sufficient to affect the sixth figure of either c_2 or c_3'. The two complications stated made it pointless to use a semi-micro balance for determining c_2. The data reported below were therefore obtained using an analytical balance with a sensitivity slightly better than 0.1 mg. The value of K (Eq. [1*a*])[10], however, was determined with a semi-micro balance in order to obtain the minimum of three significant figures necessary to expect five significant for ρ_2.[11] The data of ρ_2, should therefore, theoretically, be reproducible to the fourth decimal. The actual reproducibility of ρ_2 given in Table I, for two samples, is defined by an uncertainty of ±0.0002.

---

[9] The absolute volume of the pycnometers was known only to the fourth decimal. This affects the seventh decimal in $\Delta\rho$.

[10] The determination of K was accomplished by centrifuging the polymer out of a latex sample and pipetting off the supernatant liquid. After adding double distilled water to the residue, shaking and centrifuging again, the supernatant liquid was removed and combined with the first sample. Another portion of distilled water was

IV. Results and Discussion

Tables IIa and IIb give the data obtained with polystyrene and polyvinyltoluene latices, respectively. The last column contains the density of the polymer spheres, ρ_2. Except for one bracketted doubtful case[12] these data are identical within three figures, meaning that changes in density are less than 1%, within the particle size range defined. The fourth figure of the data, however, varies. These variations are in excess of the experimental uncertainty (Table I) and are systematic for polystyrene spheres <0.5 micron. Their density seems to increase with decreasing particle size. In view of the high density of the water-soluble component (or components), given in column five, it is inviting to assume that this change in ρ_2 is due to the adsorption of stabilizer which of course would affect the value of ρ_2 more, the smaller the particle size.[13] The average value for the density of polystyrene, 1.0569 ± 0.0019, would have to be revised slightly downward to 1.0559 or even slightly lower if the results obtained with the smallest particles were, in fact, affected by surface adsorption. The absence of a systematic variation of ρ_2 with the particle diameter in the case of polyvinyltoluene does not conflict with the findings for polystyrene, since the proportion of meta to para vinyltoluene used in the polymerization is not certain to have been the same throughout. Since the density of the pure meta polyvinyltoluene differs by nearly 1% from that of pure para vinyltoluene (4), possible variations on this account are apt to be in excess of those connected with the change in size.

It is of interest to compare the average polystyrene value with the data obtained by other authors (Table III). All data agree to three figures. However, the fourth figure shows wide variations. The most precise alternate data appear to be those obtained by Schachman and Cheng (8), which

---

added and the process repeated. The centrifuged residue and the serum were dried under a partial vacuum at 80° and weighed, using the semi-micro balance. The ratio of these two weights is K.

[11] As a matter of fact, the refractive index of the particles could be determined only to $\pm 2 \times 10^{-3}$ so that more than five figures would be of little use in the present investigation.

[12] The data for one polyvinyltoluene sample (diameter: 935 mμ) are questionable. This latex was partially coagulated before the beginning of the experiment so that c_2 after filtration was too small to guarantee precise ρ_2 data. In addition and in consequence of this filtering, this sample contained a relatively large amount of the water-soluble materials (c_3) further reducing the reliability of ρ_2.

[13] Since a variation in density with molecular weight for polystyrene is limited to molecular weights of 30,000 or less—far exceeded in our case—this alternate variable can be excluded. Another possibility, however, may be a minute porosity of the polymer spheres if this should increase with particle size.

TABLE II

Densities of Polystyrene and Polyvinyltoluene Latices (ρ_{123}), Polymer Particles (ρ_2), and Stabilizers (ρ_3), at Various Polymer Particle Sizes

Particle diameter (mμ)	c_1 (g./g.)	K	ρ_{123}	ρ_3	ρ_2
		a. Polystyrene			
240	0.59535	0.007842	1.02318	2.62	1.0593
280	0.55769	0.005121	1.02480	3.07	1.0587
300	0.61442	0.005339	1.02016	4.74	1.0546
540	0.67425	0.006960	1.01685	2.78	1.0559
950	0.75856	0.00683	1.01143	2.24	1.0556
				Avg.	1.0569 ± .0019
		b. Polyvinyltoluene			
47	0.74054	0.009894	1.00989	4.91	1.0243
381	0.54691	0.008348	1.01323	3.28	1.0276
590	0.68535	0.00555	1.00692	2.569	1.0255
(935	0.96598	0.1984	1.00108	2.052	1.0386)
				Avg.	1.0258 ± .0012

TABLE III

Comparison of Density Data on Polystyrene Particles

ρ_2	Source	Year
1.052	Williams and Backus (dried sample)	1949
1.050	Kennedy and Morton (dried sample)	1952
1.055 ± .001	Kahler and Lloyd (latex and ultracentrifuge)	1951
1.054	Sharp and Beard (latex and ultracentrifuge)	1950
1.0520 ± .0002	Schachman and Cheng (latex and ultracentrifuge)	1955
1.057 ± .002	This paper (latex and differential pycnometer)	

appeared in print after the present work had been completed. They differ from our average value by 0.5%. This difference is not surprising, since the latter, ultracentrifugal data were most likely obtained on samples by several orders of magnitude more dilute than ours (the concentration was not indicated by those authors). This, in conjunction with the mixing of the dilute latex with heavy water, is bound to have reduced the surface adsorption of the very dense stabilizer very considerably. Consequently the ρ_2-values of Schachman and Cheng are necessarily smaller than ours and cannot be considered as representative of the density of polystyrene in the original latex. A comparatively minor additional reason for the difference in the data may be the uncertainty in the temperature of the samples in the centrifuge.[14]

The only literature data available for polyvinyltoluene are bulk values for the pure para and pure meta polymer, 1.022 and 1.030, respectively (4). These values were determined on dried samples of the polymer. It is our understanding that the samples investigated consisted of about 65% meta and 35% para polyvinyltoluene. From this ratio one would expect a ρ_2 of 1.027. This value agrees satisfactorily with the average ρ_2-value given in Table II.

---

[14] The respective publication does not indicate whether and by how much the experimental temperature in the ultracentrifuge differed from the 25° C. used for the calculations.

The average values for the two polymers, as given in Table II, were used for calculating the refractive index of the polymer particles from interferometric measurements and a suitable mixture rule (see subsequent paper). This index was needed for the evaluation of particle size from light scattering (3). Since, as described in a subsequent paper, the refractive index data had to be determined on comparatively very dilute dispersions (less surface adsorption of stabilizer), all of the indices derived by means of the density values given here are bound to contain a very small systematic error which, however, is smaller than the overall nonsystematic error inherent in those refractive index data (2). Entirely negligible, at least for these strongly scattering systems, is the additional effect of this systematic error upon the volume concentrations needed for the evaluation of specific light-scattering quantities.

Summary

The accurate determination of particle diameters from light scattering by means of functions derived from the Mie theory requires that the density of the particles be known very accurately since it enters the evaluation of both refractometric and scattering data. For this reason the densities of a series of monodisperse polystyrene and polyvinyltoluene latices were determined by using differential pycnometry introducing a few new features into this technique. It is shown that the technique, as used, should be capable of giving, with suitable systems, seven significant figures for the particle density. Such a high accuracy could not be aimed for in the three-component system used nor was it needed, the actual uncertainty occurring in the fifth figure. The data, apart from satisfying the purpose stated, showed that the density varies only a little with the particle diameter within the colloidal range.

References

1. Mie, G., *Ann. Physik* **25,** 377 (1908).
2. Heller, W., and Pugh, T., to be published shortly.
3. Tabibian, R., Heller, W., and Epel, J. N., *J. Colloid Sci.* **11,** 195 (1956).
4. Bulk densities for these polymers are available in the literature. Boundy, R. H., and Boyer, R. F., "Styrene," p. 1239. Reinhold, New York, 1952.
5. Heller, W., and Thompson, A. C., *J. Colloid Sci.* **6,** 58 (1951).
6. Kahler, H., and Lloyd, B. J., Jr., *Science* **114,** 34 (1951).
7. Weissberger, A., "Physical Methods of Organic Chemistry," Vol. 1, p. 256. Interscience, New York, 1949.
8. Cheng, P., and Schachman, H., *J. Polymer Sci.* **16,** 19 (1955).

JOURNAL OF COLLOID SCIENCE **12**, 181–194 (1957)

ORIENTATION FIELD EFFECT OF POLYELECTROLYTES IN SOLUTION

Manfred Eigen and Gerhard Schwarz

Max-Planck-Institut für physikalische Chemie, Göttingen, Germany

Received April 3, 1956

Abstract

The conductance of a solution of potassium polyphosphate becomes anisotropic if an alternating electric field is applied. An increase of conductivity is found parallel to the direction of the field and a decrease perpendicular to it. Relaxation effects occur after applying and removing the field. This phenomenon can be explained in the following way: The polyion has the shape of a rod or a long rotational ellipsoid and is surrounded by a relatively dense ionic atmosphere. A part of this atmosphere is associated with the polyion owing to the strong Coulombic attraction. After applying an electric field this part of the ionic atmosphere is shifted with respect to the polyion, thereby inducing a dipole moment without leading to dissociation. The field tends to direct the axis of the polarized particle parallel to the field. Taking into account an anisotropy of mobility of the polyions this orientation will cause an anisotropy of conductance. A theory of this effect results in equations which are in agreement with the experiments described in this article.

I. Introduction

Many polyvalent ions, e.g., high polymer chains with ionizable monomers, have in solution approximately the shape of rods or long rotational ellipsoids. The chains are not statistically coiled like uncharged fibers but exceedingly stretched out because of the electrical charges regularly distributed over them (1). The polyion is surrounded by a dense atmosphere of counter ions which are primarily held in the immediate neighborhood of the surface of the polyion by Coulombic forces due to its large electrical charge (2). The inner part of this "atmosphere" moving with the polyion and partially shielding its charge may be described by the formal introduction of a degree of dissociation α, where $(1 - \alpha)c$ and αc give the concentrations of the bound and freely movable counter ions, respectively (c = total counter ion concentration). This is a rather rough manner of description, but it is adequate for our purposes here; a more detailed treatment of the ionic atmosphere would result only in some improvement in quantitative respects. The inner counter ions are still rather mobile on the surface of the polyion, because within this layer they do not have to overcome the large electrical attraction of the polyion. This mobility along the long axis of the particle may be made detectable by using an electric field to induce a dipole. Measurements of the dissociation field effect and its relaxation support the assumption of easy shifting of the inner ionic atmosphere and show that such movement can take place within a very short time, apparently less than 10^{-5} sec. (3, 4). Therefore one should expect that alternating fields with frequencies up to at least 10 kc./sec. should still give complete polarization.

Simultaneously with the induction of a dipole the electric field produces an angular momentum at the dipole tending to direct it parallel to the field. This orientation causes an experimentally detectable effect, demonstrating the polarizability of the polyion: viz., an anisotropy of conductance of polyions in the electric field.

Some decades ago D. Edwards (5) and R. Gans (6) were able to show by hydrodynamic methods that the translatoric mobility of rotational ellipsoids in a viscous fluid should depend on the direction of the acting force. The mobility parallel to the axis of rotation $w_{||}$ is according to these authors different from the mobility perpendicular to it ($w_{\perp}$), approaching $2w_{\perp}$ for very long ellipsoids. In general, due to this anisotropy of mobility the velocity vector $\mathbf{v}$ does not have the same direction as the vector of acting force $\mathbf{f}$. Thus $\mathbf{v}$ is equal to $\mathbf{W}\cdot\mathbf{f}$, where $\mathbf{W}$ is a tensor depending on $w_{||}$, $w_{\perp}$, and the direction of the axis of the particle. These results may be applied to all polyions which fulfill the conditions stated above and which therefore should show an anisotropy of electrical conductance. In the extreme case of complete orientation we have two limiting conductivity values, one corresponding to $w_{||}$ and one to $w_{\perp}$.

An anisotropy of electrical conductance in solutions of polyelectrolytes has already been found by several authors (7–9) using flow gradients. Heckmann (7) and Schindewolf (8) were able to explain this effect with the arguments described above. The polarization and orientation in alternating electric fields have been observed recently by the authors (4). A detailed theory of these effects will be presented elsewhere (10). In the present paper we shall concern ourselves with the experimental results in the light of this theory.

II. Theoretical Basis

As far as it is possible to treat a polyion as a rotational ellipsoid with freely movable charges on the surface the polarizability in the direction of the long axis may be written according to Maxwell (11) as

$$\alpha_{||} = \frac{\epsilon_s}{24 \ln(2p)} \cdot l^3 \qquad [1]$$

where l = length of the particle, p = ratio of length to diameter, ϵ_s = dielectric constant of the solvent.

The dependence of $\alpha_{||}$ on the third power of l is also given by all other rodlike models. Because of this dependence on l^3, very long polyions result in extremely large values for $\alpha_{||}$ (in this case the polarizability perpendicular to the axis of the particle can be neglected). The above Eq. [1] is only a rather rough approximation corresponding to a maximal value of $\alpha_{||}$; the experiments with polyions should give considerably smaller values, since the assumption of freely movable charges (like electrons in metals) is not completely met. In addition a considerable error is introduced by the uncertainty in the particle length due to incomplete stretching ($\alpha_{||} \sim l^3$).

The electric field acting upon the dipole introduces an angular momentum which is proportional to the square of the field density and therefore independent of its sign.[1] Thus in an alternating field the angular momentum always acts in the same direction, tending to orient the ions into the direction of the field (as long as the half period of the field allows a sufficient polarization of the particle). If the field density is not too large, complete orientation is prevented by the thermal movements of the molecules (rotational diffusion). In any case, after applying the field the directional distribution of the polyion axes is no longer regular, leading to anisotropy of conductance.

The orientation distribution of the axes of the particles is given by a distribution function ψ. From this function the conductivity is obtained by integration, taking into account the anisotropy of mobility. ψ must satisfy the equation of continuity $\dot{\psi} + \operatorname{div} \mathrm{j} = 0$ (j denotes the flux of axes caused by the electric field plus the flux of rotational diffusion).

The theory gives for the relative change in conductivity:

$$\frac{\kappa(\theta, t) - \kappa_0}{\kappa_0} = \tfrac{1}{2}(3 \cos^2 \theta - 1) \cdot \frac{\kappa_{||}(t) - \kappa_0}{\kappa_0} \qquad [2]$$

θ = angle between field and direction of measuring, $\kappa(\theta, t)$ = specific conductivity corresponding to θ at the time t $\kappa_{||}(t)$ = specific conductivity parallel to the field and

$$\kappa_0 = \alpha c(\Lambda_c + \alpha\Lambda_0) \qquad [3]$$

specific conductivity in absence of electric field, independent of direction. Here α = degree of dissociation, c = equivalent concentration of the monomer, Λ_c and Λ_0 = equivalent conductivities of counter ion and polyion corresponding to complete dissociation.

An increase in conductivity always appears in the direction of the field $\left(\frac{\kappa_{||}(t) - \kappa_0}{\kappa_0} > 0\right)$. Perpendicular to it the following equation holds (see Eq. [2]):

$$\frac{\kappa_{\perp}(t) - \kappa_0}{\kappa_0} = -\frac{1}{2}\frac{\kappa_{||}(t) - \kappa_0}{\kappa_0} \qquad [2a]$$

---

[1] Dipole moment $\mathbf{p} = \alpha_{||}(\mathbf{rE})\mathbf{r}$; angular momentum $\mathbf{M} = \mathbf{p} \times \mathbf{E} = \alpha_{||}(\mathbf{rE})(\mathbf{r} \times \mathbf{E})$; $\mathbf{r}$ = directional vector of the axis.

This means that this relative change is negative, equal to one-half of the increase of conductivity parallel to the field. In the stationary state, where $\lim\limits_{t\to\infty} \kappa_{\|}(t) = \kappa_{\|}$, we have

$$\frac{\kappa_{\|} - \kappa_0}{\kappa_0} = \Phi(\gamma) \cdot \frac{\bar{\kappa} - \kappa_0}{\kappa_0} \tag{4}$$

with

$$\gamma = \frac{1}{2}\frac{\alpha_{\|} E^2}{kT}, \quad \Phi(\gamma) = \frac{3}{2}\left\{\frac{\int_0^1 x^2 e^{\gamma x^2}\, dx}{\int_0^1 e^{\gamma x^2}\, dx} - \frac{1}{3}\right\} \tag{5, 6}$$

and

$$\lim_{E\to\infty} \frac{\kappa_{\|} - \kappa_0}{\kappa_0} = \frac{\bar{\kappa} - \kappa_0}{\kappa_0} = \frac{2}{3}\,\frac{w_{\|} - w_{\perp}}{w_0 + \frac{w_c}{\alpha\nu}}. \tag{7}$$

E = effective amount of the electric field density, w_c = mobility of the counter ion, ν = total valency of the polyion.

For the time dependence of the conductivity change after applying higher field densities one obtains

$$\frac{\kappa_{\|}(t) - \kappa_0}{\kappa_0} = f\,(4\gamma D_r t).\,\frac{\kappa_{\|} - \kappa_0}{\kappa_0} \tag{8}$$

with

$$f(x) = \frac{1}{1 - e^{-x}}\left\{1 + \frac{1}{2}e^{-x} - \frac{3}{2}\,\frac{\operatorname{arctg}\sqrt{e^x - 1}}{\sqrt{e^x - 1}}\right\} \tag{8a}$$

and D_r = rotational diffusion coefficient of the polyion. For $x \leq 2$ the function [8a] can be approximated well by

$$f(x) = \frac{x}{5}. \tag{8b}$$

The relaxation time of the orientation process at higher field densities (with the definition $f(4\gamma D_r \tau_E) = 1 - e^{-1}$) is

$$\tau_E = 1.68 \times \frac{kT}{\alpha_{\|} D_r} \times E^{-2}. \tag{8c}$$

This means that the time necessary to obtain the stationary state is inversely proportional to the square of the electric field density. At small field densities the rotational diffusion determines the time of relaxation. The dependence of conductivity on t

$$\frac{\kappa_{\|}(t) - \kappa_0}{\kappa_0} = (1 - e^{-6D_r t})\,\frac{\kappa_{\|} - \kappa_0}{\kappa_0} \qquad \text{with } \tau = \frac{1}{6D_r} \tag{9, 9a}$$

is then purely exponential and independent of E. After switching off the field (at $t = 0$), the rotational diffusion always leads to reestablishment of the original conductivity. Here the following equation is valid:

$$\frac{\kappa_{||}(t) - \kappa_0}{\kappa_0} = e^{-6D_rt} \frac{\kappa_{||}(0) - \kappa_0}{\kappa_0} \tag{10}$$

where for the time of relaxation:

$$\tau_0 = \frac{1}{6D_r} \, . \tag{10a}$$

III. Experimental Methods

In order to test these theoretical results a number of experiments were performed with an appropiate polyelectrolyte. Dilute aqueous solutions of a potassium polyphosphate $(KPO_3)_x$ were chosen as suitable for this purpose. This compound had already been used and described by U. Schindewolf (8, 12). In our case the number of monomer units x was about 10^4, so that the length of the stretched polyion was approximately $l \approx 4 \cdot 10^{-4}$ cm. In highly dilute solutions just the normal CO_2 content of the water used as solvent is already sufficient to cause a detectable hydrolysis of the phosphate and thereby a decomposition of the chain. Therefore CO_2-free water was used. The conductance was determined with a normal Wheatstone bridge using a vacuum tube voltmeter as bridge instrument, and a 1000-cycle frequency generator as voltage source. As the final voltage was about 3 volts, the corresponding field density was always too small to cause any measurable orientation. Immediately after switching off the orienting field the time change of conductance was measured by the deflection of the bridge instrument. The latter was calibrated before and after each measurement against an adjustable standard resistance (ohmic resistance coupled in parallel with a capacity). The conductance at the moment of switching off the orienting field was determined by extrapolation. At the time the experiments were carried out the special circuit did not permit a conductance measurement in the presence of the orienting field. In order to prevent electrode polarization an alternating field of 50 cycles (and sometimes also 1000) was used as orienting field. During the application of the orienting field disturbances due to Joule heat effects appeared, which could be eliminated in the following manner. The temperature coefficient of conductivity of the polyphosphate (2.27%/°C.) was not very different from those of simple electrolytes (LiCl: 2.26%/°C.; NaCl: 2.21%/°C.). Each measurement was therefore repeated with LiCl (or NaCl) solutions of the same conductivity under the same conditions. Thus the two solutions (i.e., polyphosphate and LiCl) behave identically except for the orientation effect, avoiding all disturbing effects. Greater difficulties appeared when the measurement was tried perpendicularly to the orienting field,

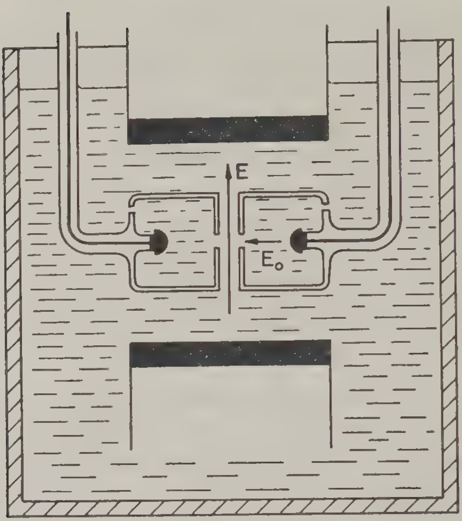

FIG. 1. Screened electrodes for measuring perpendicular to the orienting field The resistance between the two measuring electrodes is determined almost completely by the conductance through the solution between the small holes.

since normal measuring electrodes distort the orienting field so strongly that well-defined relationships are no longer given. In order to avoid this distortion a special set-up was constructed. The electrodes were screened by Plexiglas tubes as shown in Fig. 1.

All measurements were conducted at field densities between 100 and 1100 volts/cm. (alternating fields). In addition experiments were also performed at very high field densities. For this purpose an apparatus for production of high tension impulses was used, which recently has been described (13). The above-mentioned experiments were carried out with impulses of field densities up to 100 kv./cm.; also the dissociation field effect of the $(KPO_3)_x$ solution and its relaxation were measured (for procedure, see (13)).

IV. EXPERIMENTAL RESULTS AND DISCUSSION

1. *Conductance Parallel to Field in Stationary State*

All measurements of the conductivity parallel to the orienting field were carried out with two preparations of $(KPO_3)_x$ solution, designated below as I and II. The concentration was in each case about 10^{-3} equivalent KPO_3 per liter. Figure 2 shows the experimental results for the change of conductivity parallel to the orienting field as a function of electric field density. The curve corresponds to values calculated from Eq. [4] using the parameters

$$\alpha_{||} = 1.2 \times 10^{-13} \text{ cm.}^3, \qquad \frac{\bar{\kappa} - \kappa_0}{\kappa_0} = 18.2\,\% \qquad \text{for solution I.}$$

$$\alpha_{||} = 1.8 \times 10^{-13}\ \text{cm.}^3, \qquad \frac{\bar{\kappa} - \kappa_0}{\kappa_0} = 17.3\,\% \qquad \text{for solution II.}$$

The agreement between theory and experiment is very good. The above parameters do not agree exactly with one another. The discrepancy in $\frac{\bar{\kappa} - \kappa_0}{\kappa_0}$ may be due primarily to experimental errors. On the other hand, the different values for the polarizability $\alpha_{||}$ are in all probability to be traced back to differences in production and storage of the solutions; even slight hydrolysis causes noticeable changes in $\alpha_{||}$ because of its dependence on l^3.

Values for $\frac{\bar{\kappa} - \kappa_0}{\kappa_0}$ and $\alpha_{||}$ can be estimated with $l = 4 \times 10^{-4}$ cm., $\nu = 10^4$ (see III), and $p = 10^4$ (it is not necessary to have an exact value for p, since it will appear only logarithmically). It is assumed that the polyion may be treated as a rotational ellipsoid. Using the equations derived by R. Gans (6) one obtains $w_{||} = 3.78 \times 10^5$ cm. sec.$^{-1}$/dyne, $w_{\perp} = 2.10 \times 10^5$ cm. sec.$^{-1}$/dyne, and $w_0 = 2.66 \times 10^5$ cm. sec.$^{-1}$/dyne. The mobility of the potassium ion amounts to $w_c = 4.45 \times 10^8$ cm. sec.$^{-1}$/dyne. The equivalent conductivities Λ_0 and Λ_c in Eq. [3] are then $\Lambda_0 = 0.412$ ohm^{-1} cm.$^{-1}$ equiv.$^{-1}$ liter, $\Lambda_c = 0.065$ ohm^{-1} cm.$^{-1}$ equiv.$^{-1}$ liter. With the measured value of $\kappa_0 = 2.85 \times 10^{-5}$ ohm^{-1} cm.$^{-1}$ the degree of dissociation α

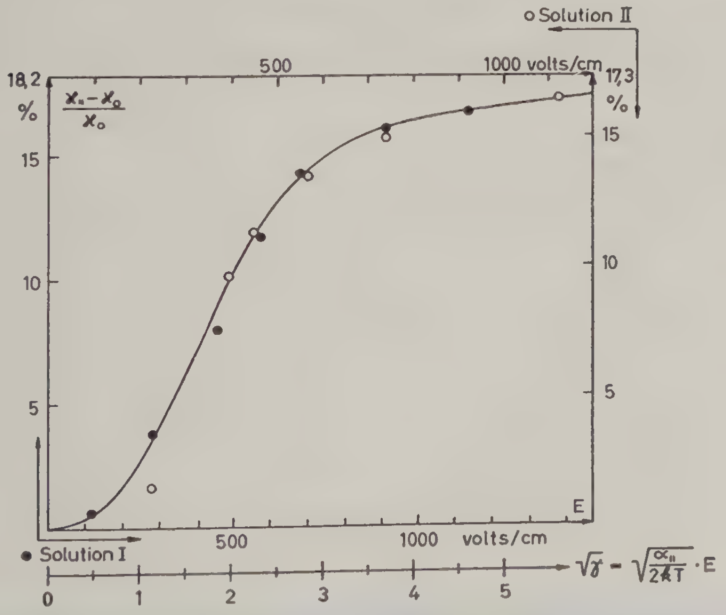

FIG. 2. Relative change of conductivity in stationary state parallel to the orienting field: theoretical curve (full line) and experimental values for solution I (●) and solution II (○).

may be estimated from Eq. [3] to $\alpha = 19.5\%$. Malmgren (14) found by analytical measurements degrees of dissociation between 15% and 20%, Schindewolf (12) by potentiometric measurements approximately 25%.

Using the above values of $w_{||}$, etc., one obtains according to Eq. [7]

$$\frac{\bar{\kappa} - \kappa_0}{\kappa_0} = 22.8\,\%$$

as compared to the experimental value of about 18%. This result is satisfactory if one takes into consideration the fact that the calculation was intended to be only an approximation.

A *maximal* value of $\alpha_{||}$ (for a rotational ellipsoid with the dimensions of the polyion) may be computed with Eq. [1] to

$$\bar{\alpha}_{||} = 2.2 \times 10^{-11} \text{ cm.}^3.$$

As is to be expected, the result lies far above the measured polarizability. One of the reasons for this could be that the experimental value of $\alpha_{||}$ corresponds to a particle length of 0.85×10^{-4} cm. instead of the value 4×10^{-4} cm. calculated with the assumption of complete stretching. The discrepancy between the estimated value of $\alpha_{||}$ and the experimental value could therefore be traced back to an incomplete stretching and a slight hydrolysis.

2. Relaxation Effects

Figure 3 shows the experimental values for $\frac{\kappa_{||}(t) - \kappa_0}{\kappa_0}$ as a function of

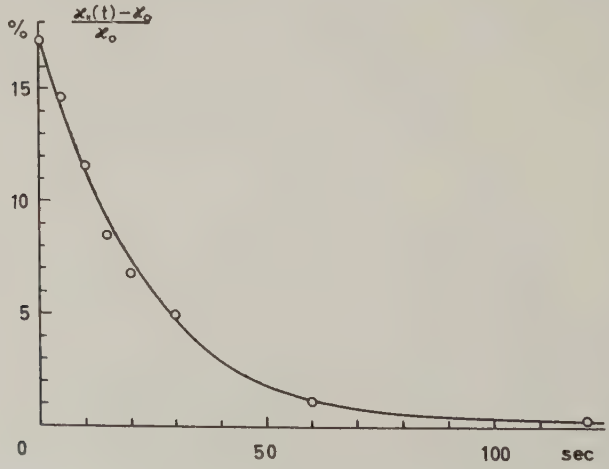

FIG. 3. Relative change of conductivity after removing the orienting field (solution II).

time immediately after removing the orienting field (solution II). The curve corresponds to the exponential function (see Eq. [10])

$$17.2 \exp\left(-\frac{t}{22 \text{ sec.}}\right).$$

From the time of relaxation

$$\tau_0 = \frac{1}{6D_r} = 22 \text{ sec.}$$

one can calculate the rotational diffusion coefficient

$$D_r = 7.6 \times 10^{-3} \text{ sec.}^{-1}.$$

(This procedure is a simple method of determining the rotational diffusion coefficient of polyelectrolytes.) The rotational diffusion coefficient D_r^0 for a noncharged rotational ellipsoid in highly dilute solutions is given by R. Gans (6):

$$D_r^0 = \frac{3kT}{2\pi\eta_0 l^3} \cdot (2 \ln(2p) - 1)$$

(η_0 = viscosity of the solvent). For a particle of the dimensions given above one obtains $D_r^0 = 5.8 \times 10^{-1}$ sec.$^{-1}$. The measured value of D_r is considerably smaller than D_r^0. According to a theory of Joly (15) this is to be expected at the concentration used because of the strong (mainly Coulombic) interactions between the highly charged polyions.

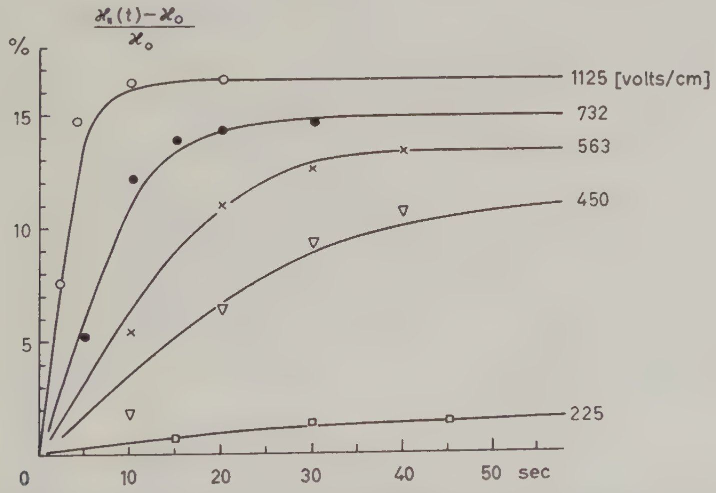

FIG. 4. Relative change of conductivity after applying the orienting field: theoretical curves (full lines) and experimental results for a number of field densities (solution II).

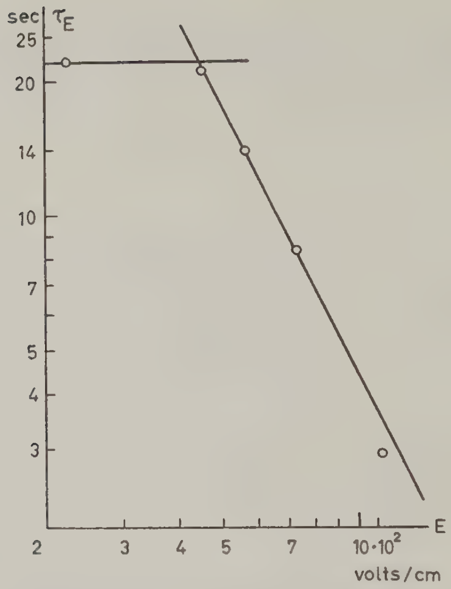

FIG. 5. Time of relaxation after applying the orienting field: limiting straight lines and experimental values.

The dependence of the conductivity on time after applying the field has been measured for a number of field densities. The experimental values are shown in Fig. 4 (solution II). For the higher field densities the curves were calculated according to Eq. [8] (derived for larger values of γ) using the above values of $\alpha_{||}$ and D_r. At the lowest field density (225 volts/cm.) the exponential function $(1 - e^{-t/22\text{ sec.}}) \frac{\kappa_{||} - \kappa_0}{\kappa_0}$ was used, since at smaller field densities Eq. [9] should be applied. According to the theory the time of relaxation τ_E is equal to $\frac{1}{6D_r} = 22$ sec. in the limiting case of small field densities and $4.5 \times 10^6 E^{-2}$ sec. (where E is in volts/cm.) in that of higher field densities. In the log-log diagram of Fig. 5 the theoretical functions have been drawn as limiting straight lines; the times of relaxation computed from the experimental values agree well with the theory within the limits of experimental error. It is possible to calculate the polarizability from the time of relaxation only (Eq. [8c]) yielding the same result as in paragraph 1 (Fig. 2).

3. Conductance Perpendicular to Field

In these experiments a concentration of 3.5×10^{-3} N was chosen in order to obtain resistances smaller than 10^5 ohms. The total change of conductivity (including Joule heat effect) after removing the field was plotted against time. Figure 6 shows one of these curves. Measurements

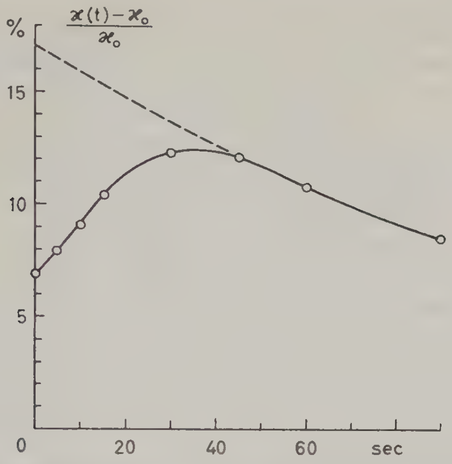

FIG. 6. Full line: total relative change of conductivity (orientation and heat effect) measured perpendicular to the orienting field (after removing the field); dashed line: heat effect only (extrapolated).

with LiCl solutions resulted normally in slowly decreasing curves, as is to be expected by a slow dissipation of the Joule heat (approximately a straight line in logarithmic coordinates). In Fig. 6 the corresponding curve is represented by a dashed line. The peculiar shape of the experimental curve for polyphosphate is explainable only by a decrease in conductance which superimposes the Joule heat effect but decays considerably faster. This decrease may be evaluated from the difference between the measured curve and the extrapolated curve for pure cooling. The experimental results for two different orienting voltages and durations of application are given in Table I.

The relaxation time is as before about 22 sec. (Fig. 6). With the aid of the theory one may use the 380-volt measurements to calculate the values quoted in Table I, under the assumption that the field density is proportional to the applied voltage. (It is difficult to calculate the field density from the applied voltage because of the complicated cell geometry.) The theoretical decrease of conductivity at complete orientation is -9.2%,

TABLE I

Voltage (*volts*)	Duration (*sec.*)	Change in conductivity (%)	
		Measured	Calculated
220	5	−3.9	−3.1
220	15	−6.9	−6.9
220	∞		−8.0
380	5	−7.7	
380	15	−8.7	
380	∞		−8.8
∞	>0		−9.2

corresponding to an increase of conductivity of 18.4% parallel to the field, in good agreement with the measurements (see paragraph IV, 1).

4. High Field Measurements

The above-described measurements parallel to the field were repeated using high field densities (up to 100 kv./cm.) and impulse durations of 1 to 5 × 10^{-6} sec. (strongly damped harmonic oscillations). After the decay of a high field impulse an increase of conductivity due to orientation was observed only when the orienting field density reached 100 kv./cm. and the impulse duration a value of the order of 5 × 10^{-6} sec. In the determination of the heat effect one has to take into account the appreciable dissociation field effect of the polyelectrolyte. The experiment shows a conductivity increase of 0.14% due to the orientation effect (solution II). This amount lies definitely outside the error in these experiments. The theory (Eqs. [8] and [8*b*]) gives:

$$\frac{\kappa_{||}(t) - \kappa_0}{\kappa_0} = 0.13\%.$$

It is also possible to calculate from the experiment the time of relaxation. One obtains $\tau_E = 4.1 \times 10^{-4}$ sec., compared to the theoretical value $\tau_E = 4.3 \times 10^{-4}$ sec. ($\tau_E \sim E^{-2}$). Thus the measurements at high field densities are also in good agreement with the theory.

Furthermore the dissociation field effect and its relaxation were investigated at 20°C. using a solution of about 1.3 × 10^{-3} equivalents/liter $(KPO_3)_x$. The high tension impulses had the shape of a nearly aperiodically damped oscillation; therefore $E = Ae^{-kt}e^{i\omega t}$. With these impulses the slope $\frac{\partial\kappa}{\partial E}$ was determined in the linear part of the function $\kappa \equiv \kappa(E)$ (at $\omega = 3.6$ Mc./sec. the function was only approximately linear). As average slope we found

$$\frac{1}{\kappa_0}\frac{\partial\kappa}{\partial E} = \begin{array}{lll} 1.48 \times 10^{-2}\ \text{cm./kv.} & \text{at} \quad \omega = & 0.44\ \text{Mc./sec.} \\ 0.91 \times 10^{-2} & & 1.45 \\ 0.47 \times 10^{-2} & & 3.60 \end{array}$$

Figure 7 shows the ratio of $\frac{\partial\kappa}{\partial E}$ at the frequency ω to that at $\omega = 0$ as a function of log $\omega\tau_D$, where τ_D is the relaxation time of the dissociation field effect. This representation is advantageous for showing dispersion effects and leads directly to the time of relaxation according to the theory cited above (14). One obtains here

$$\tau_D = 2 \times 10^{-6}\ \text{sec.}$$

Similar results have been found by Bailey, Patterson, and Fuoss (3). From this result we may conclude that it is possible to shift the counter ions along the surface of the polyion within a very short time.

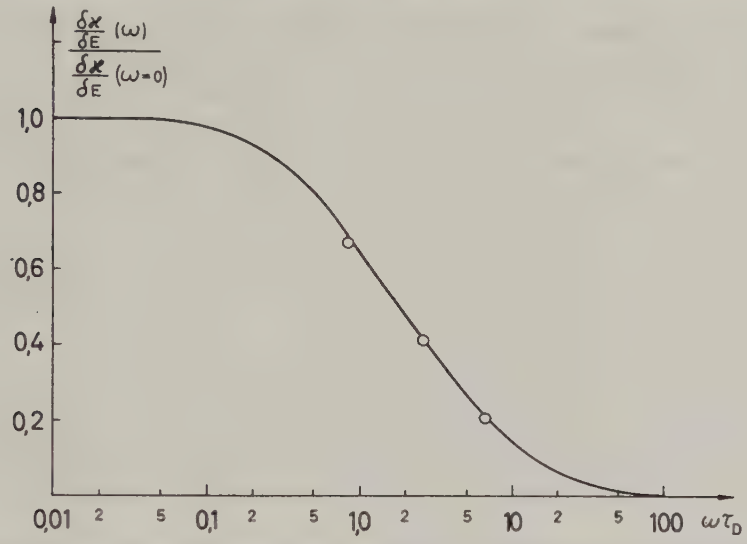

FIG. 7. Relaxation of dissociation field effect: theoretical curve (full line) and experimental values.

V. SUMMARY

In the previous sections we have described measurements on a polyphosphate, which represents a special kind of polyelectrolyte. The polyvalent ions are particles which may be treated to a first approximation as rods, fibers, or long rotational ellipsoids. Our experiments lead to the following conclusions:

1. The mobility of the polyions must be larger in the direction of the axis than in the direction perpendicular to the axis. Quite generally the mobility depends on the angle between the axis of the particle and the direction of the force. This is the only plausible explanation for the experimental fact that by orientation of the axes into a definite direction a decrease of conductance appears perpendicular to this direction which is only half as large as the increase in conductivity parallel to this direction.

2. In an electric field the polyion is polarized in the direction of its axis. This means that an electric dipole moment proportional to the field density is induced. Therefore in the field an orientation occurs which is a function of the square of field density. This orientation is independent of the sign of the field density, and appears also in alternating fields, even when the period is small compared to the time required for orientation. The only requirement is that the frequency is not so high that polarization of the polyion is prevented. The polarizability of the polyion probably is due to a shifting of the inner ionic atmosphere with respect to the polyion. At greater particle length the polarizability assumes values of orders of magnitude greater than the sum of the polarizabilities of a number of normal molecules corresponding to the number of monomers in the polyion (this is to say that 10^4 normal molecules bound in a linear macromolecule would have a total polarizability of about $10^{-24} \times 10^4$ cm.^{3} = 10^{-20} cm.^{3}, as compared to 10^{-13} cm.^{3} measured here ($\alpha_{||} \sim l^3$)). This is shown for example in the fact that saturation effects already appear at about 1000 volts/cm. The corresponding dipole moment at this field density amounts to 6.10^5 Debye, whereas normal polar molecules have dipole moments of the order of 1 Debye.

3. A theory of the field effect of anisotropy of conductance established on the arguments of the two previous paragraphs, only summarized in this article, results in equations substantiated by the experiments in the stationary and time-dependent cases.

4. The parameters occurring in these equations result in absolute values for the degree of dissociation, the maximum increase of conductivity, the polarizability, and the rotational diffusion coefficient which are of the orders of magnitude to be expected from the structure of the polyvalent ions.

Finally it may be pointed out that the observed effects are of magnitude considerably greater than any possible experimental error. Special care was taken to avoid spurious results due to temperature or electrode effects.

Further experiments with other electrolytes at various concentrations, frequencies, and field densities are planned for more detailed investigation of the phenomenon discussed in this article. Until now the anisotropy of conductance has been considered exclusively. In addition, analogous effects should appear in the dielectric constants of such polyelectrolyte solutions.

Acknowledgment

We are greatly indebted to Professor Dr. K. F. Bonhoeffer for his kind interest and encouragement in this work.

References

1. Kuhn, W., Künzle, O., and Katchalsky, A., *Helv. Chim. Acta* **31,** 1994 (1948).
2. Alfrey, T., Berg, P. W., and Morawetz, H., *J. Polymer Sci.* **7,** 543 (1951).
3. Bailey, F. E., Patterson, A., and Fuoss, R. M., *J. Am. Chem. Soc.* **74,** 1845 (1952).
4. Eigen, M., and Schwarz, G., *Z. physik. Chem.* [N. F.] **4** (5/6) 380 (1955).
5. Edwards, D., *Quart. J. Math.* **26,** 70 (1893).
6. Gans, R., *Ann. Physik* **86** [4. Folge], 652 (1928).
7. Heckmann, K., *Naturwiss.* **40,** 478 (1953); *Kolloid-Z.* **136,** 67 (1954).
8. Schindewolf, U., *Naturwiss.* **40,** 435 (1953); *Z. physik. Chem.* [N. F.] **1,** 129 (1954); *Z. Elektrochem.* **58,** 697 (1954).
9. Jacobson, B., *Rev. Sci. Instr.* **24,** 949 (1953).
10. Schwarz, G., *Z. Physik* **145,** 563 (1956).
11. Maxwell, C., "Treatise on Electricity and Magnetism," 1873.
12. Schindewolf, U., and Bonhoeffer, K. F., *Z. Elektrochem.* **57,** 3, 216 (1953).
13. Eigen, M., and Schoen, J., *Z. Elektrochem.* **59,** 483 (1955).
14. Malmgren, H., *Acta Chem. Scand.* **6,** 1 (1952).
15. Joly, M., *Kolloid-Z.* **126,** 77 (1951).

JOURNAL OF COLLOID SCIENCE **12**, 195-203 (1957)

EXTRUSION OF SOFT SOLIDS THROUGH A TUBE[1]

Wayne S. Brown and Ivan B. Cutler[2]

University of Utah, Salt Lake City, Utah

Received April 5, 1956

ABSTRACT

The flow, without plug action, of soft solids through a cylindrical tube is analyzed using the Eyring plasticity equation. Experiments were conducted with lead and wax flowing at various rates at several temperatures. A satisfactory correlation is obtained with the theoretical expression and the experimental data.

INTRODUCTION

The extrusion of metals, plastics, and ceramic materials is largely an art, and only experience and empirical relationships have aided engineers in design work. Extrusion has become such an important forming operation that a mathematical correlation between pressure, rate of flow, and temperature is highly desirable. The application of fundamental relationships to a complicated process such as extrusion naturally results in complicated expressions relating rate of flow to temperature and pressure. It is hoped that further research will bring these relationships closer to engineering application.

Reports of experimental research in extrusion processes are extensive, but little information on the flow of soft solids through a tube without plug flow is available for analysis. Pearson (1) obtained empirical relationships to correlate his results on the extrusion of metals. Sachs (2) has presented equations for the energy expended in extrusion. Ward (3) has applied the plasticity relationship developed by Nadai to the extrusion of lead. Hill (4) developed theoretical expressions for the flow in a sharp-edged die which were checked experimentally by Purchase and Tupper (5) with fair agreement.

If flow through a die with a finite length of cylindrical throat is considered, the flow process may be divided into two parts. The first part concerns flow from the extrusion cylinder into the die opening. The second part consists of flow without plug action through the length of the die.

---

[1] Financial assistance for this research originated with the Office of Naval Research Contract No. N7 ONR 45101 and University Research Fund.

[2] The authors are Assistant Professors of Mechanical and Ceramic Engineering, respectively.

Eyring and Tobolsky (6) derived an expression for plastic flow of material through a tube of uniform cross section based on fundamental properties of the materials. The purpose of this investigation has been to isolate the second part of the flow process and to utilize relationships derived from fundamental considerations to correlate the experimental results.

Experimental Procedure

Two materials with distinctly different physical properties were selected for this study. The metal lead was selected because of its plastic character. American Smelting and Refining Company granulated test lead with a purity of 99.9949% was used. The other material was a paraffin wax with a melting point of 48°C. obtained from a local supplier. The viscosity of the wax was sharply temperature dependent. This advantage was partially offset by the necessity of precisely controlling the temperature to prevent fluctuations in flow rate.

A. Lead

The apparatus used for the tests on lead is shown in Fig. 1. The indirect extrusion method was used. This method eliminates motion between the lead and the wall of the cylinder and therefore eliminates the friction which results from such motion in the direct extrusion method. The temperature was controlled by a thermocouple placed in the extrusion cylinder which was connected to a potentiometer controller, which in turn controlled the current to the Nichrome heating element. The load was applied with a hydraulically operated materials testing machine. Rate of flow was obtained by measuring the travel of the testing machine head with a dial indicator for a given time.

The granulated test lead was packed into the cylinder, covered with powdered graphite to prevent oxidation, and melted by heating the cyl-

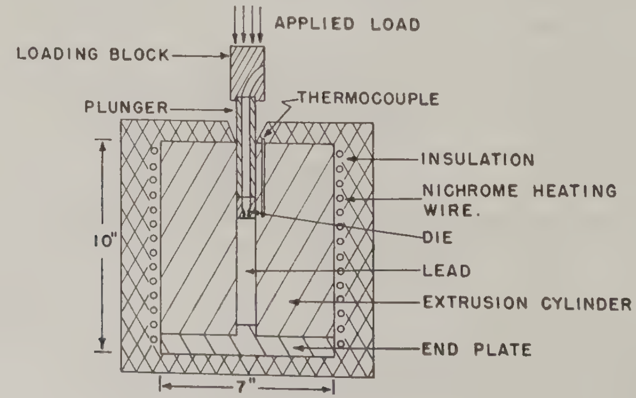

Fig. 1. Lead extrusion apparatus.

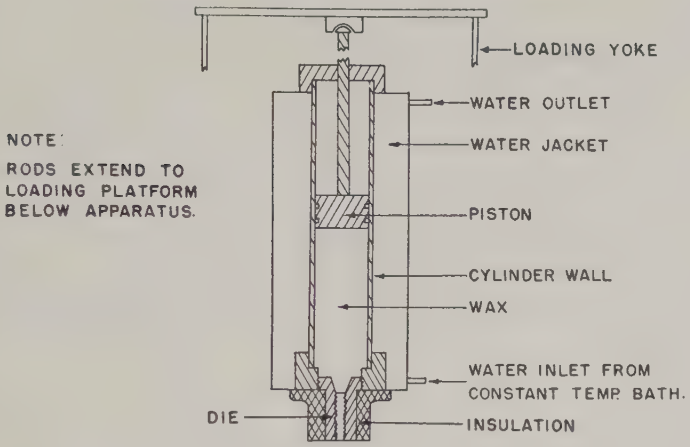
LOADING YOKE
WATER OUTLET
NOTE:
RODS EXTEND TO LOADING PLATFORM BELOW APPARATUS.
WATER JACKET
PISTON
CYLINDER WALL
WAX
WATER INLET FROM CONSTANT TEMP. BATH.
DIE
INSULATION

FIG. 2. Wax extrusion apparatus.

inder. The lead was allowed to cool and the top surface scraped clean before inserting the die.

Two dies were used in the tests to isolate the flow in the tube. The flow length in one die was 1.27 cm. and the other die had a sharp edge or effectively zero length. The diameter of both dies was 1.31 cm. The long die was threaded to insure zero velocity at the wall (i.e., to prevent plug flow).

The pressure required to force the lead through a cylinder 1.27 cm. long was obtained by plotting curves of flow rate vs. pressure for each die and subtracting the pressures for a given flow rate. Figure 3 shows typical flow rate curves for the two dies. It is apparent from Fig. 3 that the pressure required to force the lead from the extrusion cylinder through a sharp-edged die is greater than the pressure required to force the lead through the length of the die.

B. Wax

The wax was placed in a modified commercial hydraulic cylinder 6 cm. in diameter and 50 cm. long mounted as shown in Fig. 2. The load was applied by stacking weights on a loading platform below the cylinder. The loading platform was connected by a yoke to the piston rod. This arrangement insured a vertical load. Three different dies were used in the tests, with diameter 0.993 cm. and lengths of 10.17 cm., 7.62 cm., and 1.27 cm. The inside of each die was threaded to insure zero velocity at the wall. Water from a constant-temperature bath circulated through the water jacket on the cylinder to maintain the desired temperature.

During the testing the weight was applied and the wax was extruded through the die. The flow rate was obtained by weighing the wax extruded

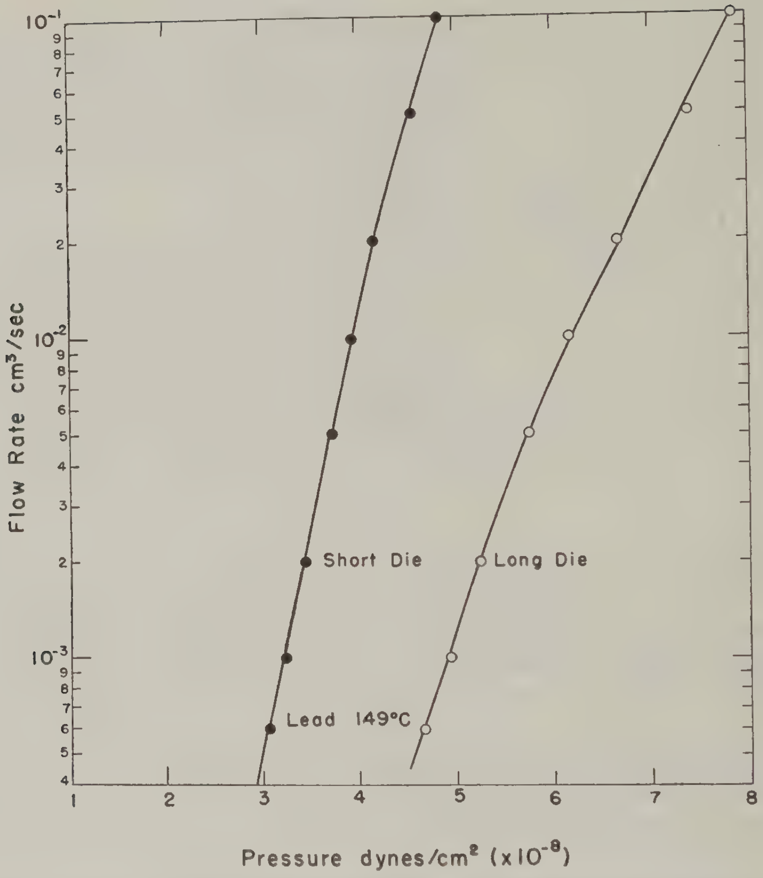

FIG. 3. Flow rate vs. pressure required to force lead from the cylinder through the die.

in a given time. Experiments showed that the flow rate did not vary significantly with the position of the piston, indicating that the friction between the wax and the cylinder wall was negligible compared with the force necessary to cause the wax to flow through the die.

The upper flow rate was governed by localized heating effects at the die due to internal friction in the wax. Since the viscosity of the wax varies markedly with temperature, an increase of only a few degrees caused unusually high flow rates. The loads were not increased above the point where this effect caused noticeable fluctuation in the flow rate.

The pressure required to force the wax through a length of the cylindrical throat was obtained by subtraction as in the case of lead.

EXPERIMENTAL RESULTS

Typical results of the tests are shown in Fig. 3. Since the flow rate has exponential dependence on temperature and pressure small fluctuations in either of these quantities were strongly reflected in the flow rate. Attempts to reproduce the data generally resulted in pressure variations within 4% for a given rate of flow for the lead and within 10% for the wax.

It was possible to closely control applied loads in either system, and the reported values are estimated as correct within 2%.

Temperature variation was estimated as being within 2% over the length of the cylinder in the lead apparatus and within 1% with the wax apparatus. It was not possible to measure localized temperature fluctuations at the die entrance in either apparatus. At high flow rates the temperature varied enough owing to friction to cause unusually high flow rates. These data were not considered in the correlation.

THEORETICAL CORRELATION

The equation for plastic flow may be derived as follows:

Consider flow from an enlarged cylinder through a cylindrical tube of length L and diameter $2R$. The entrance effect will not be considered. Then a force balance on a small cylindrical element of the flowing material with diameter $2r$ and length L results in

$$P\pi r^2 = f 2\pi r L, \tag{1}$$

where P is the pressure differential over the length of the die and f is the average unit shearing stress along the length of the cylindrical element. From the Eyring plasticity relations[3] the shearing velocity gradient is:

$$\frac{du}{dr} = 2\frac{\lambda}{\lambda_1}\frac{kt}{h}e^{-\Delta F\ddagger/RT}\sinh\frac{f}{2f_0 g} \tag{2}$$

(See Table II in the appendix for the meaning of all symbols.) Equation [2] may be written in a more convenient form by letting

$$\alpha = \frac{1}{2f_0 g}, \quad \text{and} \quad K = 2\frac{\lambda}{\lambda_1}\frac{kt}{h}e^{-\Delta F\ddagger/RT}$$

Making this substitution [2] becomes

$$\frac{du}{dr} = K\sinh f\alpha \tag{3}$$

The shearing stress from [1] may be substituted into [3] and the resulting expression integrated over the radius of the tube to get the velocity distribution in the tube. If the velocity is taken as zero at the tube wall as a boundary condition the results are:

$$u = \frac{2k}{\alpha P}\left(\cosh\frac{\alpha PR}{2L} - \cosh\frac{\alpha Pr}{2L}\right) \tag{4}$$

---

[3] This derivation utilizes the generalized theory of plastic flow as presented in reference 7 and is slightly different than the derivation presented by Tobolsky and Eyring in reference 6.

The flow rate may be obtained by considering the flow through an infinitesimal ring and integrating over the area of the tube.

$$Q = \int_0^R u2\pi r\,dr = \int_0^R \frac{2K}{\alpha P}\left(\cosh\frac{\alpha PR}{2L} - \cosh\frac{\alpha Pr}{2L}\right)2\pi r\,dr$$

$$Q = \frac{2\pi KR^2L}{\alpha P}\left(\cosh\frac{\alpha PR}{2L} - \frac{4L}{\alpha PR}\sinh\frac{\alpha PR}{2L} + \frac{16L^2}{(\alpha PR)^2}\sinh^2\frac{\alpha PR}{4L}\right) \qquad [5]$$

This equation expresses the volume rate of flow as a function of the pressure, the dimensions of the tube, and the physical constants for the material flowing. At sufficiently high pressures [5] may be approximated by

$$Q \approx \frac{\pi KR^2L}{\alpha P}\exp\left(\frac{\alpha PR}{2L}\right) \qquad [6]$$

The constants K and α for different materials may be obtained by fitting

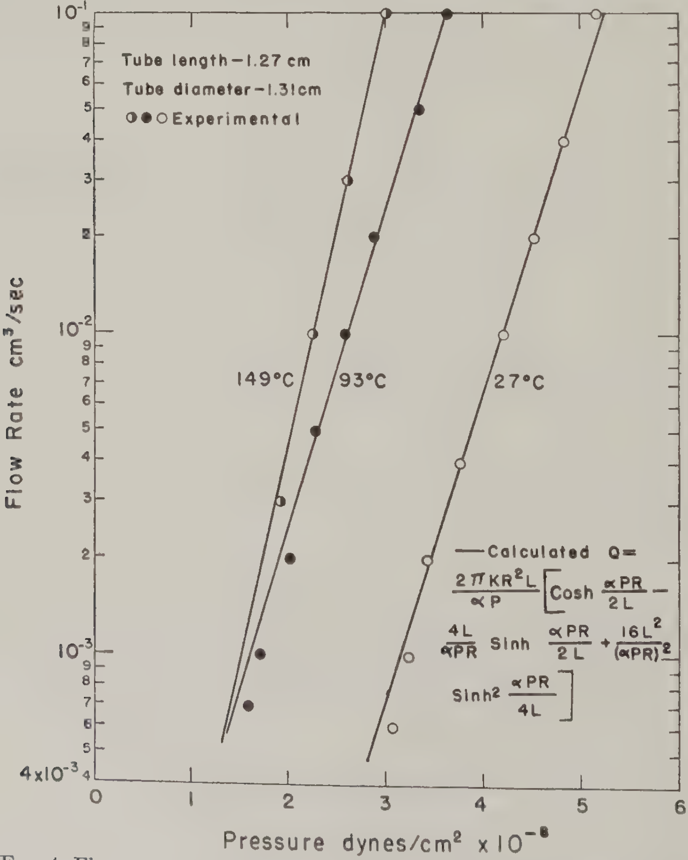

FIG. 4. Flow rate vs. pressure required to force lead through tube at various temperatures.

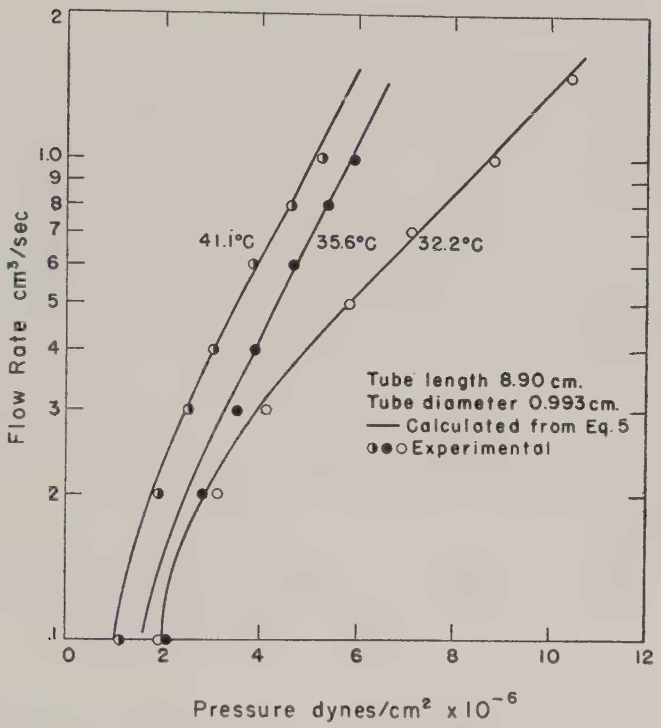

FIG. 5. Flow rate vs. pressure to force wax through tube at various temperatures.

the equation to experimental data. As previously pointed out by using dies with differing lengths of cylindrical throat pressure drop due to flow through the cylindrical throat may be isolated.

Figures 4 and 5 show the flow rate plotted as a function of the pressure drop across the length of the die. The solid line is a plot of Eq. [5]. The points represent experimental data. It may be noted that the curve is a straight line on the semilog plot at the high-pressure and as predicted by the approximate relation, Eq. [6].

The constant, K, free energy of activation, $\Delta F\ddagger$, and the constant α

TABLE I

Lead				Wax			
Temp.	K	$\Delta F\ddagger$	α	Temp.	K	$\Delta F\ddagger$	α
(°C.)	(sec.$^{-1}$)	(kcal/moles)	(dynes^{-1} cm.^{2})	(°C.)	(sec.$^{-1}$)	(kcal/moles)	(dynes^{-1} cm.^{2})
27	6.45×10^{-6}	25.0	4.59×10^{-8}	32.2	2.69	17.6	9.4×10^{-6}
93	1.31×10^{-4}	28.6	4.92×10^{-8}	35.6	1.33	18.3	1.91×10^{-5}
				35.6	1.12	18.5	1.91×10^{-5}
149	4.56×10^{-5}	33.9	6.72×10^{-8}	41.1	2.07	18.3	1.85×10^{-5}

were obtained from fitting the equation to the data. These parameters are constants for the materials at the specified temperature and are tabulated in Table I. Two sets of data are shown for the wax at 35.6°C. The second set of data was obtained from the difference between medium- and short-throated dies, and the other data apply to the long- and short throated dies.

As can be readily seen from the curves, the theory and the experimental data agree well at high pressures, but for some cases there appears to be a small discrepancy at low pressures. It is likely that a better fit in the low-pressure region could be obtained by applying one of the more elaborate models suggested by Ree and Eyring (8).

CONCLUSIONS

1. The major part of the pressure required for extrusion with dies of dimensions used in this work is due to the entrance effect.

2. Excluding the entrance effect, extrusion of lead and wax can be correlated by the Eyring plasticity equation.

3. At high flow rates the simplified expression, Eq. [6], gives a satisfactory correlation between flow rate, pressure, and temperature.

APPENDIX

Symbols used in this paper:

R = radius of uniform section of die, gas constant.
r = radius of flow element in die.
P = pressure.
f = shearing stress.
L = length.
u = velocity at radial distance r from center of die.
K = rate constant.
k = Boltzmann constant.
h = Planck's constant.
T = temperature.
$\Delta F^{\ddagger}$ = free energy of activation.
λ_1 = distance between slip planes.
λ = distance patch moves per jump.
f_0 = initial localized stress.
g = ratio of length of free vibration of patch to distance jumped.
a = $1/2f_0g$.
Q = volume flow rate.

ACKNOWLEDGMENTS

The authors gratefully acknowledge the helpful suggestions of Dr. Henry Eyring, Dean of the Graduate School, Dr. Samuel S. Kistler, Dean of the College of Engineering, and Dr. Mervin B. Hogan, Head of the Department of Mechanical Engineering.

REFERENCES

1. PEARSON, C. E., "The extrusion of metals," Wiley, New York, 1944.
2. SACHS, G., "Flow of metals," *Iron Age* **145,** Feb. 8 (1940).
3. WARD, N. F., "Energy model laws for extrusion of soft lead," *Proc. 5th Intern. Congr. Appl. Mechanics*, p. 249 (1939).
4. HILL, R., "A theoretical analysis of stresses and strains in extrusion and piercing," *J. Iron Steel Inst. (London)* **148,** 177 (1948).
5. PURCHASE, N. W., AND TUPPER, I. J., "Experiments with a laboratory extrusion apparatus under conditions of plane strain," *J. Mech. and Phys. of Solids* **1,** (4) 277 (1953).
6. TOBOLSKY, A., AND EYRING, H., "Mechanical properties of polymeric materials," *J. Chem. Phys.* **11** (3), 125 (1943).
7. EYRING, H., AND REE, A. T., "Generalized plasticity theory," *Proc. Natl. Acad. Sci. U.S.* **41** (3), 118–122 (1955).
8. REE, A. T., AND EYRING, H., "The theory of non-Newtonian flow, I. Solid plastic systems," *J. Appl. Phys.* **26** (7), 793 (1955).

JOURNAL OF COLLOID SCIENCE **12,** 204–229 (1957)

STRESS-RELAXATION BEHAVIOR OF POLYVINYL ACETATE FILMS

Kazuhiko Ninomiya and Hiroshi Fujita

Department of Fisheries, Faculty of Agriculture, Kyoto University, Maizuru, Japan

Received April 26, 1956

INTRODUCTION

According to the current theory of linear viscoelasticity (1), all time-dependent mechanical properties, such as the creep under constant stress, the relaxation of stress at constant strain, and the real and imaginary parts of the complex dynamic modulus, for a given substance under given experimental conditions, are correlated with each other through the rigorous mathematical relations involving a function called the "distribution of relaxation times" or more simply the "relaxation spectrum." Although numerous experimental data have recently been reported on linear viscoelastic behavior of high polymers, both in bulk and in solution, there are as yet few experimental studies which were attempted to check the validity of these theoretical interrelations using well-established high polymeric systems. In a series of publications Tobolsky and Catsiff (2) presented extensive stress-relaxation data on a National Bureau of Standards sample of polyisobutylene and compared dynamic properties predicted therefrom with the "best" dynamic mechanical data of Ferry and associates (3, 4) on the same sample. The results they obtained are highly satisfactory in all respects examined, and appear to confirm the validity of the theory of linear viscoelasticity, although they had to confine themselves to the comparison only in the region from rubbery to glassy consistency.

The purpose of the present paper is to describe the results of our study on a similar problem carried out with polyvinyl acetate. Stress-relaxation data are obtained on more than 10 samples of polyvinyl acetate over a wide range of temperature 10°–130°C. They are then combined, by the use of Tobolsky's time-temperature superposition principle (5) (equivalent to Ferry's reduced variables method (6)), to obtain a master stress-relaxation curve for each of the samples. The master curves so obtained all cover a range of relaxation modulus from 10^{10} to 10^4 dynes/cm.^{2}, and thus demonstrate well the general behavior of this transient mechanical property of polyvinyl acetate in the glassy state, in the rubbery state, and in the transition region in between. In addition to this, its dependence on average molecular weight is demonstrated clearly from these master curves. The second approximation method proposed by Ferry (7) is then used to determine the continuous distribution of relaxation times for each of the samples from the corresponding master stress-relaxation curve. It is found that the distribution curves so obtained are molecular weight-independent in and above the transition region and thus permit comparison with those obtained in the same region by previous workers on polyvinyl acetate samples of different molecular weights. In the present paper, the data obtained by Williams and Ferry (8) from dynamic measurement are chosen for this purpose, because their results are highly accurate and self-contained. The real and imaginary parts of the complex dynamic modulus as well as the mechanical loss tangent are calculated from the relaxation spectrum for one sample, and compared with the data of Williams and Ferry (8) in and above the transition region. No such comparison is made in and below the rubbery region, because no corresponding dynamic data are yet available.

Steady-flow viscosities, as calculated from all relaxation spectra obtained, are shown to increase linearly with $\bar{M}_v^{3.4}$, where $\bar{M}_v$ is the viscosity-average molecular weight, in agreement with the data by previous workers on various amorphous polymers (9).

Under some assumptions an equation is derived which represents the relaxation spectrum of the whole polymer as a sum of relaxation spectra associated with its components. It is shown, on the basis of this equation, that the shape of the relaxation distribution curve for a given polymer in and below the rubbery region is closely correlated with the weight distribution of molecular weights.

Materials and Methods

Samples

Two unfractionated samples of polyvinyl acetate (hereafter referred to as PVAc) were furnished from the Institute for Chemical Research, Kyoto University, through the kindness of Professor H. Kawai of the Department of Textile-Chemistry, Faculty of Engineering, Kyoto University. They had been prepared with a laboratory-scale low conversion. Their viscosity-average molecular weights, $\bar{M}_v$, determined from the intrinsic viscosities in acetone using Sakurada-Chiba's equation (10) (see below), were 358,000 and 144,000, respectively. For convenience, they were designated, respectively, as Sample O and Sample K. Sample O was fractionated by use of the method of successive fractional extraction, with methanol as solvent and a mixture of water and methanol as nonsolvent.

First, the sample was separated into 14 parts at 20°C. with an interval of successive fractionations of 2 to 3 days. The volume ratio, R, of two liquid phases in equilibrium was from 0.077 to 0.476 throughout this fractionation process. The corresponding yields of the fractions obtained were from 0.5% to 18%. The 14 fractions obtained in this process were designated, in order of fractionation, as FI, FII, – – – and FXIV. By using the same procedure, Sample O was separated into two crude fractions, S and P, in which case the R value was kept less than 0.01 and the supernatant phase was extracted 20 days after the nonsolvent had been added to the solution. To obtain more data to establish the molecular weight distribution in Sample O, a small portion of each fraction in the series from FVI to FXIV, except for FXII and FXIII, was further separated into two parts, using the same procedure as above, at 20°C. with the volume ratio R less than 0.005. The sample FXII was not fractionated further. Part of fraction FXIII was separated into five fractions, again using the same procedure under the same conditions. The sharper fractions thus obtained are designated, for instance, as FVI-I and FVI-II for those from fraction FVI. In this way, except for two crude fractions S and P, 25 fractions in total were derived from Sample O.

The molecular weights of these fractions and of the unfractionated samples, O and K, were evaluated from their intrinsic viscosities in acetone at 26°C., using Sakurada-Chiba's equation (10):

$$[\eta] = K\bar{M}_v^{\alpha}, \qquad [1]$$

where $[\eta]$, the intrinsic viscosity, is expressed in 100 ml./g., $\bar{M}_v$ is the viscosity-average molecular weight, and K and α are constants given, respectively, as

$$K = 4.53 \times 10^{-4} \qquad \text{and} \qquad \alpha = 0.62$$

in the molecular weight range 10^4–10^6. This equation had originally been determined at 30°C., but we applied it to our data at 26°C., assuming that this slight difference in temperature had a negligible influence on the values of K and α. A Ubbelohde-type viscometer having a flow time of 71.5 seconds for acetone at 26°C. was used, and the intrinsic viscosity values were determined, as usual, by extrapolating the reduced viscosity vs. concentration curves graphically to zero concentration. No kinetic energy correction was applied to the data obtained. It was found that the Huggins constant k' in the usual viscosity equation varied in the range 0.32–0.45 from fraction to fraction.

Preparation of Sample Films

For stress-relaxation measurements only twelve samples were used; they were fractions FVI, FVII, FVIII, FIX, FX, FXI, FXII, and FXIII, crude fractions S and P, and whole polymers O and K. Film samples for stress-relaxation experiments were prepared according to the following procedure.

The sample, dissolved in acetone and filtered through a sintered glass-filter, was precipitated by adding excess water to the solution. After the precipitate had been dried thoroughly, it was again dissolved in acetone to make up a solution of 5.0 g./dl. concentration, which was, in turn, allowed to stand for 24 hours at room temperature. The solution was then poured into a glass ring floating on mercury, and allowed to stand over P_2O_5 in a desiccator until the film formed became transparent. During this period the solvent was being removed by slowly drawing air through the desiccator. The ring with the film attached was then lifted off the mercury and placed in a leaching bath of distilled water. Finally, after a day's leaching the film was dried in air at room temperature until it became again transparent. The film thus obtained was allowed to stand in an air thermostat kept at 50°C. for a day, and then stored over P_2O_5 in a desiccator. For actual use in stress-relexation experiments a ribbon-shaped piece was cut out of the film prepared as above, using a razor blade. The film thickness was calculated from the known weight and area of the film, using 1.193 g./ml. for the density of polyvinyl acetate. The density was determined, using a flotation method, for all the samples having different molecular weights and found to be almost independent of molecular weight in the range studied. The value of 1.193 g./ml. was assumed from those data for the average density of this polymer at 23°C. Precisely speaking, the measured densities, ρ, increased slightly with molecular weight, M, according to the equation: $1/\rho = 0.8363 + (35/M)$ (23°C.).

Apparatus

The apparatus used for stress-relaxation measurements was an automatic chainomatic balance-relaxometer coupled with a self-recorder. It was essentially the same as the automatic relaxometer used by Guth (11) in a study of mechanical properties of cork; however, many modifications and improvements were added to Guth's original apparatus so that high sensitivity and stability could be obtained in measuring the stress over a wide interval of time and over a wide range of temperature concerned in the present work. The details of the apparatus and of the procedure in its actual use will be described elsewhere (12). The mechanical part, including the sample film, of the relaxometer was mounted tightly in the inner chamber of a double-layer thermostatted air bath constructed specially for the present work. The temperature in the inner chamber was regulated by means of a toluene-mercury thermoregulator in the range 10°–100°C. and of a liquid paraffin-mercury thermoregulator in the higher temperature range, both coupled with an electronic relay. The temperature in the outer chamber was controlled by means of a bimetallic thermoregulator and kept always somewhat below the desired temperature in the inner bath. When the system was properly adjusted, temperatures in the inner bath, measured with an accurate thermometer placed near the sample film, could be kept constant to within ±0.05°C. in the range below 100°C. and to within ±0.1°C. at the higher temperatures. It was found that accurate enough temperature control was extremely important to obtain reproducible stress-relaxation data in the transition region from rubbery to glassy consistency. Polyvinyl acetate is known to be slightly hygroscopic. However, it was found in the course of this work that the stress-relaxation curve at a given temperature is influenced markedly by relative humidity of the surrounding air; so bulks of P_2O_5 were placed in both chambers to maintain a moisture-free atmosphere during measurements.

The sample film was stretched manually by a predetermined amount within an interval of 3 to 4 seconds, and the resulting deformation was measured to within 0.001 cm. with the aid of a special screw gauge attached firmly to the main body of the apparatus. The sample length was about 5 cm. in all cases studied, so that strains could be determined correct to 0.02%. The strains used were less than 2% in and above the transition region, and less than 20% in and below the rubbery region. So the mechanical data obtained were believed to have been in the region of linear viscoelasticity. The sample width as well as the line density of the stress-supporting chain were varied properly, in accordance with the magnitude of stress to be measured, so that the desired stress-relaxation curve could be recorded with a reasonable magnification on the rotating drum. The stress was calculated with respect to the cross-sectional area of the unstrained sample.

It proved very important to use samples which had been sufficiently annealed, in order to obtain reproducible data at temperatures near the second-order transition point of the polymer. For the measurements in this region, therefore, the following annealing procedure was used before each relaxation run has been made: the sample film was allowed to stand at 40°C. for one week in a desiccator, after which it was gradually cooled down at a rate of 1°C. a day until the desired temperature was reached. The sample was then taken out of the desiccator and quickly introduced into the test chamber which had previously been regulated to the desired temperature. After the sample had been clamped, it was still allowed to stand for 24 hours, with the chamber kept at that temperature. We cannot claim that this annealing procedure was quite satisfactory to obtain reliable relaxation data in the region encompassing the transition point. In spite of careful treatments of the sample and the apparatus, peculiar data which were far out of line with the other results were obtained occasionally in this region, and had to be discarded for further discussion. A further investigation is apparently needed on this problem to establish a definite annealing procedure which permits reliable evaluation of the stress-relaxation behavior in the region encompassing the transition temperature.

RESULTS

Molecular Weight Distribution

The intrinsic viscosity values and the corresponding molecular weights, calculated from Eq. [1], of all the fractions separated from Sample O, including the crude fractions S and P, and of the unfractionated samples O and K are recorded in Table I. It is expected that the molecular weights of the fractions separated using the successive fractional extraction increase monotonical with the repetition of extraction. However, it is observed from the table that this was not the case with the results of the present fractionation, i.e., the molecular weight passes through a minimum when going from fraction FVI to fraction FVIII. This peculiar result may have been due to our insufficient fractionation technique. It should be mentioned that the yields of fractions FI to FV were so small that these fractions could not be used for relaxation measurements. Fraction FXIV was discarded for relaxation experiments, because it was probably much more heterogeneous than the earlier fractions.

The yield values and the molecular weights of the 25 fractions (indicated with asterisks in Table I) were combined, according to the usual procedure, to obtain the integral weight distribution of molecular weights in Sample O, as shown in Fig. 1. By differentiating graphically the smooth integral molecular weight distribution curve, A, drawn to best fit the experimental points, a curve, B, shown in the same figure was derived, which gives the differential weight distribution of molecular weights in Sample O, provided each fraction was sufficiently sharp. The sharpness of a given fraction may be checked by comparing its viscosity-average molecular weight with its number-average molecular weight determined osmotically; however, this was not attempted in this work. It is believed that the molecular weight distribution obtained here is not so markedly deviated from the true distribution, in view of the fact that fractionations were carried out with sufficiently small values of R (volume ratio of two liquid phases in equilibrium) (13). The weight-average, number-average, and viscosity-average molecular weights of Sample O, as calculated from the equations:

$$\begin{aligned}\bar{M}_w &= \int_0^\infty M\varphi(M)\,dM,\\ \bar{M}_n &= \left[\int_0^\infty \varphi(M)M^{-1}\,dM\right]^{-1},\\ \bar{M}_v &= \left[\int_0^\infty M^{0.62}\varphi(M)\,dM\right]^{1/0.62},\end{aligned} \qquad [2]$$

where $\varphi(M)\,dM$ is the normalized weight distribution of molecular weights shown in Fig. 1, are $\bar{M}_w = 418{,}000$, $\bar{M}_n = 233{,}000$, and $\bar{M}_v = 353{,}000$.

TABLE I

Intrinsic Viscosities $[\eta]$ *and Viscosity-Average Molecular Weights* $\bar{M}_v$ *of Polyvinyl Acetate Samples Studied*

Sample		$[\eta]$ (100 ml./g.)	$\bar{M}_v$
FI	*	0.580	103,000
FII	*	0.791	171,000
FIII	*	1.02	258,000
FIV	*	1.02	258,000
FV	*	0.750	157,000
FVI	○	0.509	83,600
FVI-I	*	0.460	71,400
FVI-II	*	0.900	209,000
FVII	○	0.466	72,600
FVII-I	*	0.449	68,300
FVII-II	*	0.800	172,000
FVIII	○	0.750	157,000
FVIII-I	*	0.700	139,000
FVIII-II	*	1.29	375,000
FIX	○	0.830	184,000
FIX-I	*	0.768	161,000
FIX-II	*	1.39	421,000
FX	○	1.09	286,000
FX-I	*	0.918	221,000
FX-II	*	1.52	489,000
FXI	○	1.39	420,000
FXI-I	*	1.15	376,000
FXI-II	*	1.91	701,000
FXII	*○	1.43	441,000
FXIII	○	2.04	784,000
FXIII-I	*	1.67	569,000
FXIII-II	*	1.69	581,000
FXIII-III	*	1.83	654,000
FXIII-IV	*	2.02	766,000
FXIII-V	*	2.42	1030,000
FXIV		2.44	1050,000
FXIV-I	*	1.80	929,000
FXIV-II	*	2.92	1400,000
O	○	1.26	358,000
S	○	1.07	277,000
P	○	1.66	562,000
K	○	0.715	144,000

* indicates fractions used to obtain the molecular weight distribution in Sample O.
○ indicates samples used in stress-relaxation measurements.

It is interesting to note that the calculated $\bar{M}_v$ is in excellent agreement with the value 358,000 obtained experimentally.

Stress-Relaxation Data

Typical experimental data are shown in Fig. 2, where we have plotted the observed relaxation curves for fraction FXI against time (minutes)

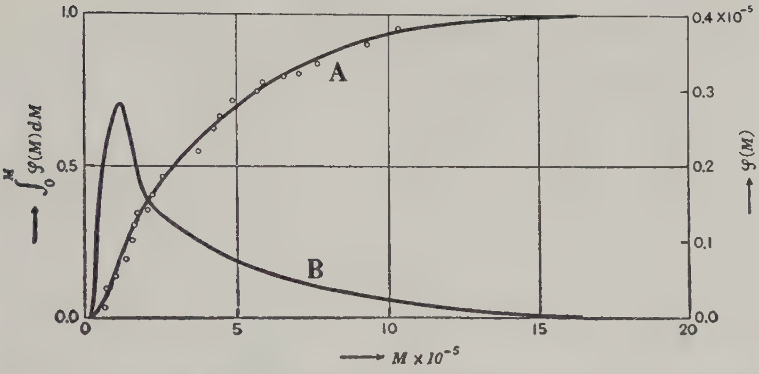

FIG. 1. Integral and differential weight distributions of molecular weights for Sample O.

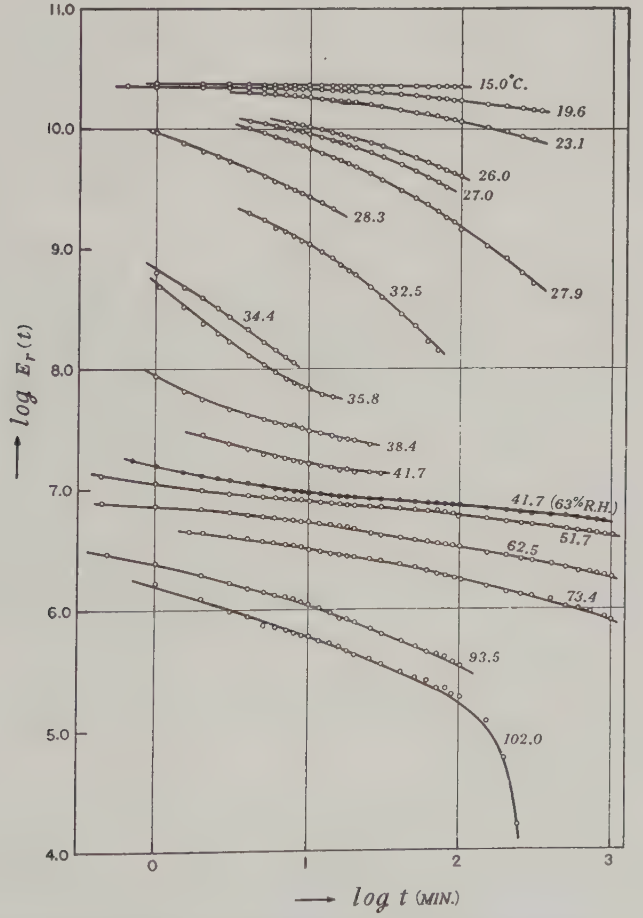

FIG. 2. Stress-relaxation data for sample FXI at various temperatures; $E_r(t)$ is the relaxation modulus in dynes per square centimeter.

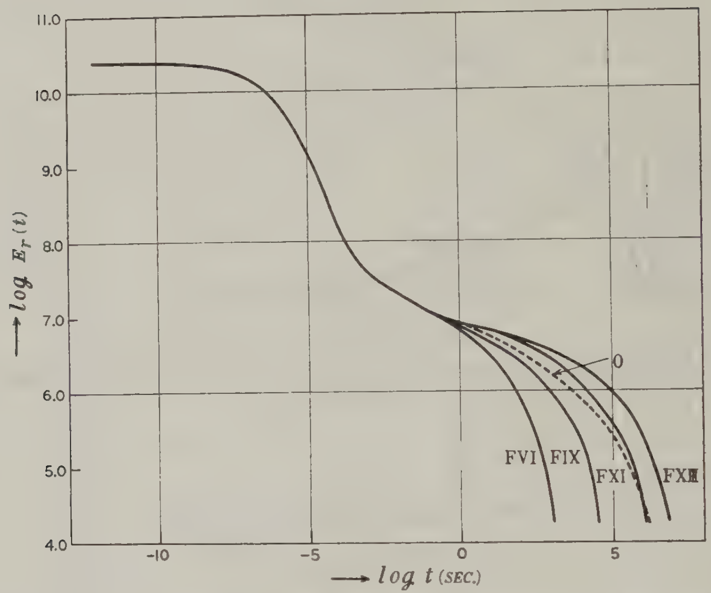

Fig. 3. Master stress-relaxation curves for several PVAc samples reduced to 75°C.

on a log-log graph. It is observed that the curves for various temperatures may be superposed to form a single composite curve, i.e., a master stress-relaxation curve, by shifting them horizontally along the log-time axis. Actually, small arbitrary vertical shifts were found necessary to apply to some of the observed curves, in order to make them superpose satisfactorily. These arbitrary shifts were used in place of the usual correction for the kinetic-theory dependence of the stress in a rubberlike material. It appeared less justified to apply this "theoretical" correction (6), because uncertainty in strain and stress measurements, imperfect annealing of the sample, and other unknown factors should have disturbed our experimental data more seriously. It was found that for all PVAc samples treated in the present relaxation measurements smooth master relaxation curves could be constructed satisfactorily in the manner described above. Figure 3 shows some of the master relaxation curves so obtained. The reference temperature for these time-temperature reduction processes was chosen as 75°C. to compare our data with Williams and Ferry's data (8) on an unfractionated PVAc sample.

It had previously been demonstrated for polyisobutylene (14, 15) and polymethyl methacrylate (16) that differences in molecular weight and molecular weight distribution had very little effect on the shape of relaxation distribution function in the transition region from rubbery to glassy consistency. This must also be the case with the shape of master relaxation function in the same region. Under the assumption that this condition holds for all the PVAc samples studied in this work, all the relaxation data covering the entire region from glassy consistency to rubbery flow were obtained only for a single sample, fraction FXI; and the composite relaxation curve derived therefrom was connected smoothly to those for other samples (which were determined only in and below the rubbery region) at lower terminal portions of the transition region, where all experimental master curves were found to converge to a single line, as shown in Fig. 3. It should be noted that the molecular weight-independent behavior of the master relaxation curve in the transition region is realized only in a certain limited range of molecular weight. As a matter of fact, the relaxation spectrum obtained by Harper *et al.* (17) for polyisobutylene of extremely low molecular weight does not superpose with that of Andrews and Tobolsky (15) for a high enough molecular weight polyisobutylene sample.

The factor a_T by which amount to shift the relaxation curve at temperature T along the log-time axis to form a composite master relaxation curve at the reference temperature was determined as a function of temperature for each of the samples studied, and found to be independent of molecular weight within a practical accuracy. Typical experimental a_T data will be presented in a later section of this paper.

DISCUSSION

Distribution of Relaxation Times

The overall trend of the master relaxation curves in Fig. 3 is of the familiar type which had been demonstrated by previous workers on various linear high polymers, both in bulk and in concentrated solutions. Different from the data of Tobolsky and associates on high molecular weight polyisobutylene (15) and polymethyl methacrylate (16), the present data on PVAc do not show any definite "plateau" in the rubbery region. The limiting glassy modulus may be estimated to be 2.5×10^{10} dynes/cm.^{2} from Fig. 3.

Relaxation spectra, $\Phi(\log \tau)$, were calculated for all the samples from their master relaxation curves E_r (log t), using the second approximation formula proposed by Ferry and Williams (7):

$$\Phi(\log t) = -\frac{1}{\Gamma(1+m)}\left[E_r(\log t)\,\frac{d \log E_r(\log t)}{d \log t}\right]_{t=\tau}, \qquad [3]$$

where Γ $(1 + m)$ is the Gamma function and m is given approximately by

$$m = \frac{d}{d \log t} \log\left[E_r(\log t)\,\frac{d \log E_r(\log t)}{d \log t}\right]_{t=\tau}. \qquad [4]$$

In calculating Φ in and above the transition region, use was also made of the second approximation formula of Schwarzl and Staverman (18) to check the values from Ferry's equation [3].

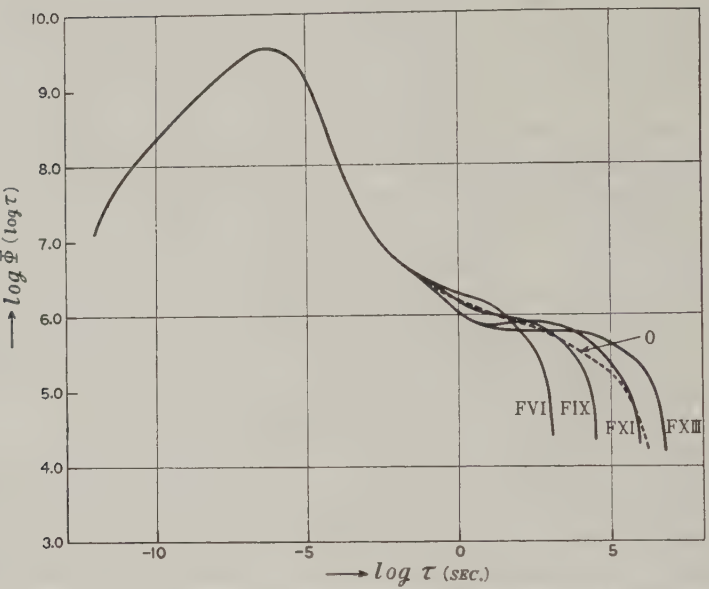

Fig. 4. Distributions of relaxation times for several PVAc samples at 75°C.; Φ (log τ) is the relaxation spectrum expressed in dynes per square centimeter.

By way of example, the Φ curves corresponding to the five master relaxation curves in Fig. 3 are presented in Fig. 4 on a log-log graph. The general trend and shapes of these curves are quite similar to those for many other linear high polymers, both in undiluted and diluted states. Different from high molecular weight polyisobutylene worked out in particular detail by Tobolsky (2) with transient measurements and by Ferry (3, 4) with dynamic measurements, PVAc demonstrates a very limited Rouse slope ($-\frac{1}{2}$ on the log Φ vs. log τ graph) (19) near the lower terminal zone of the transition region. Of interest is the systematic variation of the shape of relaxation spectrum brought about in the rubbery region by the change in molecular weight. It is seen that with increasing molecular weight a shallow minimum of Φ appears in the initial zone of the rubbery region and shifts slightly to longer times. The point at which the tail of the rubbery region drops off shifts to the right much more rapidly with increasing molecular weight, in agreement with the finding made by previous workers on many linear polymers. It is observed also that the present results indicate Φ at long relaxation times to depend to a considerable extent on molecular weight distribution. In fact, the Φ curves for fraction FXI and whole polymer O are significantly different in detailed shape over the rubbery region, particularly in its tail to rubbery flow, in spite of the fact that both samples have comparable viscosity-average molecular weights. There is a tendency for Φ at long relaxation times to have its shape become closer to the ideal "box-type" with increasing sharpness of molecular weight distribution. A similar tendency of Φ is observed in Ferry's data (20) on a sharply fractionated polyisobutylene sample in concentrated solutions, and also stated in Andrews and Tobolsky's paper (15) on undiluted polyisobutylene.

Williams and Ferry (8) have recently calculated the relaxation spectrum in shear $\Phi_s(\log \tau)$ at 75°C. for an unfractionated sample of PVAc ($\bar{M}_w = 420{,}000$ and $\bar{M}_n = 140{,}000$) from complex dynamic rigidities measured in the audiofrequency range at temperatures from 50° to 90°C. Their data cover the complete transition region from glassy to rubbery consistency. Under the assumptions that the relaxation spectrum at a given temperature is independent both of molecular weight and molecular weight distribution in the transition region and that Poisson's ratio for PVAc in this region is not different significantly from ½, Williams-Ferry's Φ_s values are compared with ours in Fig. 5. The open circles in the figure represent the values

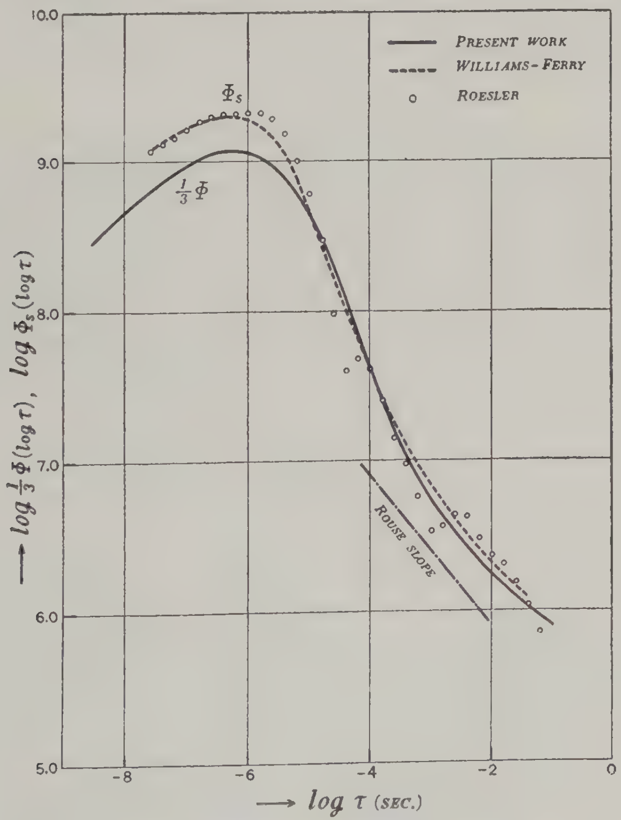

FIG. 5. Relaxation spectra in shear in the transition region from rubbery to glassy consistency; solid line, present result; dashed line, Williams-Ferry's result (obtained by smoothing their original data); open circles, values computed by Roesler from Williams-Ferry's data for the imaginary component of the complex dynamic rigidity.

calculated by Roesler (21) from Williams-Ferry's data for the imaginary component of the complex dynamic rigidity using the iteration method of Roesler and Twyman (22), and are included for comparison. Three sets of data agree quite satisfactorily in the central and lower zones of the transition region. In the upper zone of the transition region, encompassing the glassy zone, a considerable discrepancy is observed between our data and those of Williams and Ferry, although the location of the peak of Φ accords satisfactorily in both results. It is not clear to us why such a great discrepancy appeared in this high-modulus region. The difference appears too large to be accounted for by experimental errors only. In connection with this, it is important to note that our relaxation spectrum in this region was derived from the stress-relaxation data obtained at temperatures below the transition point (about 30°C.), whereas that of Williams and Ferry was from the dynamic data at temperatures far above the transition. As will be discussed below, the validity of the time-temperature superposition principle becomes less reliable beyond the upper central zone of the transition region. If so, the discrepancy as revealed here with the data on PVAc may be an indication of this phenomenon.

Predicted Dynamic Properties

Once the relaxation spectrum $\Phi(\log \tau)$ at constant temperature has been determined over a wide enough range of time-scale from stress-relaxation measurements, it is possible in principle to calculate dynamic mechanical properties at that temperature on the basis of the theory of linear viscoelasticity. Thus, for the real and imaginary parts, $E'(\omega)$ and $E''(\omega)$, of the complex dynamic modulus as functions of frequency ω, we have

$$E'(\omega) = 2.303 \int_{-\infty}^{\infty} \Phi(\log \tau) \frac{\omega^2\tau^2}{1 + \omega^2\tau^2} d(\log \tau), \tag{5}$$

$$E''(\omega) = 2.303 \int_{-\infty}^{\infty} \Phi(\log \tau) \frac{\omega\tau}{1 + \omega^2\tau^2} d(\log \tau), \tag{6}$$

and for the mechanical loss tangent

$$\tan \delta = \frac{E''(\omega)}{E'(\omega)}. \tag{7}$$

$E'(\omega)$ may be calculated from the known stress-relaxation modulus data, $E_r(t)$, by means of an approximate formula proposed by Catsiff (2) based on the more exact formula of Marvin (23):

$$E'(\omega) = [E_r(t) + B(m)\Phi(\log t)]_{t=1/\omega}, \tag{8}$$

where $B(m)$ is defined by

$$B(m) = \frac{\pi}{2} \operatorname{cosec}\left(\frac{\pi m}{2}\right) - \Gamma(m) \tag{9}$$

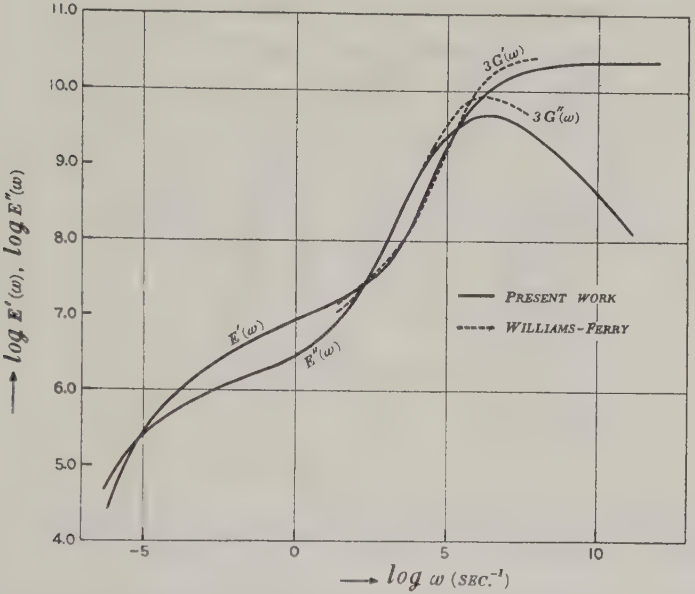

FIG. 6. Real and imaginary parts of the complex dynamic elasticity in dynes per square centimeter, $E'(\omega)$ and $E''(\omega)$, for Sample O; solid lines, predicted from the stress-relaxation data; dashed lines, Williams-Ferry's experimental curves.

and m is given approximately by Eq. [4]. A table of the function $B(m)$ is found in reference 2.

The values of $E'(\omega)$, $E''(\omega)$, and tan δ, computed for the whole polymer O, are presented graphically in Figs. 6 and 7, where the dynamic data of Williams and Ferry (8) cited above are included for comparison. Values of $E'(\omega)$ in the transition region were calculated by numerical integration of Eq. [5], and those in the rubbery region with the aid of Marvin's approximation. The overall agreement of the predicted values with the observed ones, where comparison is possible, is satisfactory for all—$E'(\omega)$, $E''(\omega)$, and the loss tangent. It should be noted that a slight discrepancy either in $E'(\omega)$ or $E''(\omega)$ is considerably magnified in computing the loss tangent. The marked deviations from the observed values, observed in the high-modulus portion of the transition region, noticeably at the peak of $E''(\omega)$, are no more than a reflection of the great discrepancy of our relaxation spectrum from that of Williams and Ferry in the corresponding region. The slight differences, as observed in the lower terminal zone of the transition region, may not be considered as too serious, being probably within the limits of experimental error.

The predicted loss tangent values are systematically lower than the observed values at frequencies higher than that at which the maximum

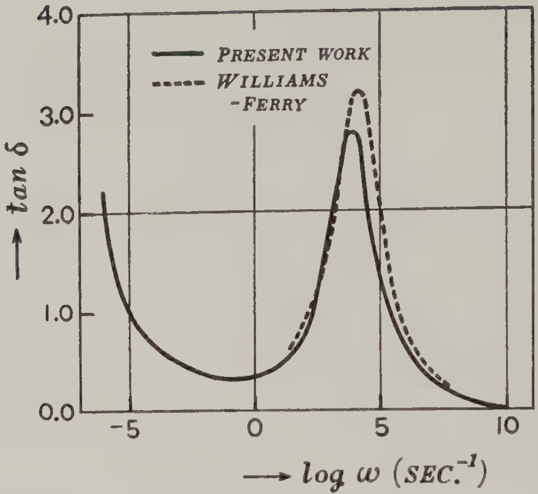

FIG. 7. Mechanical loss tangent, tan δ, for Sample O; solid line, predicted from the stress-relaxation data; dashed line, Williams-Ferry's experimental data.

dispersion occurs. Tobolsky and Catsiff (2) observed a similar disagreement in the loss tangent when they compared dynamic properties predicted from stress-relaxation data on a National Bureau of Standards polyisobutylene sample with Ferry's experimental dynamic data (3, 4) on the same sample. It is important to note the fact that the frequency at which the predicted loss tangent curves for PVAc begins to deviate systematically from the experimental curve lies well below the region of frequencies where both predicted $E'(\omega)$ and $E''(\omega)$ themselves are systematically lower than the respective experimental values. If we consider that a similar phenomenon was noted by Tobolsky and Catsiff for polyisobutylene (more definitely in their case), it appears that this phenomenon is rather common and suggests that the time-temperature superposition principle must, in general, cease to hold at earlier stages of the glassy-modulus region than usually presumed. Tobolsky and Catsiff (2) have stated, in line with this consideration: "Both theoretical and practical considerations indicate that the time-temperature superposition principle must fail at temperatures well below the glassy transition, T_g." However, it is obvious that much more data have to be accumulated on the mechanical behavior in this critical region before the definite answer to this problem can be derived.

No such comparison of predicted dynamic properties with observed ones as could be done in the transition region can be attempted in and below the rubbery region, because no experimental dynamic data are yet available there for any of the PVAc samples treated in this work. Since time-dependent mechanical properties in this region are affected pronouncedly by

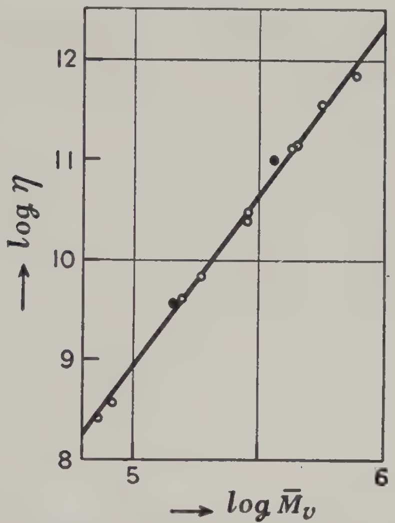

FIG. 8. Steady-flow viscosity in poises, η, plotted against viscosity-average molecular weight, $\bar{M}_v$ at 75°C.; open circles, data for fractionated samples; closed circles, data for unfractionated samples.

molecular weight and molecular weight distribution, data obtained for any other samples of this polymer are of no help for the comparison of interest. This condition imposes a rather serious limitation on any attempt to check the validity of the theory of linear viscoelasticity in the region of rubbery consistency.

Steady-Flow Viscosity

The steady-flow viscosity (in tension), η, of a given substance at constant temperature may be calculated from the relaxation spectrum (in tension), Φ (log τ), by means of the equation:

$$\eta = 2.303 \int_{-\infty}^{\infty} \tau\Phi(\log \tau)\, d(\log \tau). \qquad [10]$$

Values of η have been computed for all PVAc samples whose relaxation spectra were determined at 75°C. over wide enough ranges of time scale, and plotted against viscosity-average molecular weight $\bar{M}_v$ in Fig. 8 on a log-log graph. It is seen from the figure that the data are best represented by a linear equation of the form:

$$\log \eta = -8.05 + 3.4 \log \bar{M}_v \qquad [11]$$

over the range indicated. It is of interest to note that within the limits of practical accuracy the data for unfractionated samples (indicated specifically with closed circles) fall in line with the data for fractionated samples.

This indicates that the steady-flow viscosity is dependent primarily on viscosity-average molecular weight only and not affected significantly by molecular weight distribution (15). The molecular weight dependence of the steady-flow viscosity of PVAc as found here may be compared favorably with the results of Andrews and Tobolsky (15) on polyisobutylene, in which η varies linearly with the 3.3 power of viscosity-average molecular weight. Fox (9) has recently summarized published data for steady-flow viscosity on a number of high polymers, both in bulk and in concentrated solutions, and found that they are all best fitted by an empirical equation: $\log \eta = a + 3.4 \log \bar{M}_w$ (a is constant and $\bar{M}_w$ is weight-average molecular weight), in agreement in form with Eq. [11]. However, an important point must be pointed out which makes the reliability of the factor 3.4 in our Eq. [11] somewhat doubtful. We have adopted Sakurada-Chiba's formula in evaluating the viscosity-average molecular weights of PVAc samples from their intrinsic viscosities in acetone. Some reports on the viscosity-average molecular weight vs. intrinsic viscosity relation for this system indicate for α in Eq. [1] higher values than 0.62 appearing in Sakurada-Chiba's formula. The values of 0.66 and 0.68 have been reported by some authors (24, 25) and even a value of 0.74 by Chinai *et al.* (26). When any of these higher values is assigned to α in applying Eq. [1] to our intrinsic viscosity data, a higher slope than 3.4 is obtained for the $\log \eta$ vs. $\log \bar{M}_v$ plot. Thus, so far as the present data on PVAc are concerned, the reliability of the slope value 3.4 is not yet established firmly.

Effect of Molecular Weight Distribution

It has been shown in Fig. 4 that the shape of the relaxation spectrum in the rubbery region is dependent significantly on molecular weight distribution. As was pointed out by Ferry (27), it should, in principle, be possible to derive the molecular weight distribution for a given sample from its relaxation spectrum in this region. However, so far we have no adequate theory which makes this prediction carry through. This situation is due largely to the fact that no quantitative theory is yet available for the mechanical relaxation behavior of a molecularly homogeneous (non-cross-linked) polymer at long times. In what follows, under some assumptions a semiquantitative theory of correlating the mechanical behavior in the rubbery region with molecular weight distribution is presented and applied to the experimental data for Sample O.

The starting assumptions in this treatment are as follows: (*1*) the relaxation spectrum for a molecularly homogeneous polymer in the rubbery region can be approximated by a "box-type" function, and (*2*) any interactions arising from the mixing of polymers having different chain lengths can be neglected.

If we denote the relaxation spectrum of a given polymer and that of its

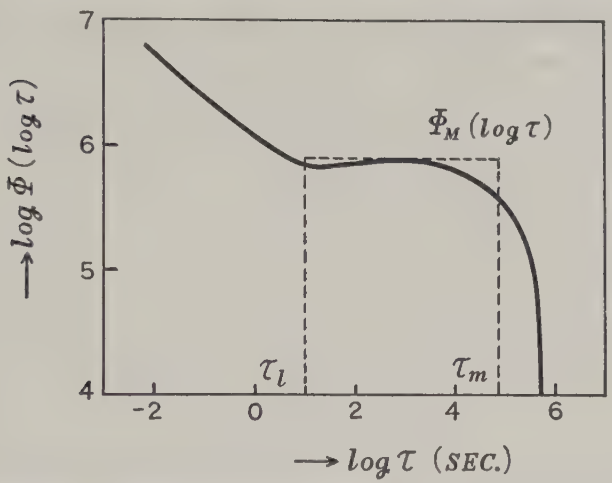

FIG. 9. Schematic diagram of the relaxation spectrum in the rubbery region, where the actual distribution curve is approximated by a "box-type" function.

component polymer with molecular weight M by $\Phi(\log\tau)$ and $\Phi_M(\log\tau)$, respectively, it is shown under the assumption (*2*) that

$$\Phi(\log\tau) = \int_0^\infty \Phi_M(\log\tau)\psi(M)\,dM, \qquad [12]$$

where $\psi(M)\,dM$ is the normalized volume distribution of component with molecular weight M. Since the density of polymer is practically independent of molecular weight in many systems, $\psi(M)\,dM$ is almost identical with the normalized weight distribution of molecular weights, $\varphi(M)\,dM$. Thus, Eq. [12] may be written

$$\Phi(\log\tau) = \int_0^\infty \Phi_M(\log\tau)\varphi(M)\,dM. \qquad [13]$$

The assumption (*1*) is very drastic; however, as has been noted in foregoing lines, there is a tendency for Φ in the rubbery region to have its shape become closer to the "box-type" with increasing sharpness of molecular weight distribution. The box-type distribution function may be characterized by three parameters τ_l, τ_m, and C, as shown graphically in Fig. 9. It is seen from the curves in Fig. 4 that, when each of them is approximated by an "equivalent" box function in the rubbery region (as shown schematically in Fig. 9), both τ_l and C are little affected by molecular weight, while τ_m is dependent very strongly on molecular weight. The steady-flow viscosity calculated for this box distribution from Eq. [11] is represented by

$$\log\eta = \log C + \log(\tau_m - \tau_l). \qquad [14]$$

Since for high enough molecular weights τ_l is very small compared with τ_m, Eq. [14] may be approximated to give

$$\log \eta = \log C + \log \tau_m. \tag{15}$$

The form of Φ_M $(\log \tau)$ for the box distribution is represented by

$$\Phi_M\ (\log \tau) = \begin{cases} 0\ (0 < \tau < \tau_l), \\ C\ (\tau_l < \tau < \tau_m), \\ 0\ (\tau_m < \tau < \infty). \end{cases}$$

Hence, Eq. [13] may be put in the form:

$$\Phi(\log \tau) = \int_{M_m}^{M_l} C\varphi(M)\, dM, \tag{16}$$

where M_m and M_l are functions of τ defined in such a way that

$$\begin{aligned} \tau &= \tau_m(M_m), \\ \tau &= \tau_l(M_l), \end{aligned} \tag{17}$$

when the molecular weight dependences of τ_m and τ_l are expressed, respectively, as $\tau_m(M)$ and $\tau_l(M)$.

Differentiating Eq. [16] with respect to log τ and arranging the resulting equation, we obtain

$$\Phi(\log \tau)\, \frac{\partial \log \Phi(\log \tau)}{\partial \log \tau} = C(M)\varphi(M)M\, \frac{\partial \log M}{\partial \log \tau}\Bigg|_{M=M_m}^{M=M_l}, \tag{18}$$

where $C(M)$ represents the condition that C is generally dependent on molecular weight. As has been noted above, τ_l is very little affected by molecular weight, so that Eq. [18] may be approximated to give

$$\Phi(\log \tau)\, \frac{\partial \log \Phi(\log \tau)}{\partial \log \tau} = -C(M_m)\varphi(M_m)M_m\, \frac{\partial \log M_m}{\partial \log \tau}. \tag{19}$$

Values of $C(M)$ may be obtained approximately from the heights of experimental relaxation spectra for a series of fractions in their horizontal zones of the rubbery region. It was found that for a series of fractions separated from Sample O, the $C(M)$ values can be fitted well by an equation of the form:

$$\log C(M) = 8.16 - 0.40 \log M \tag{20}$$

in the molecular weight range studied.

It was shown in the previous section that the steady-flow viscosities for all PVAc samples studied in this work, both fractionated and unfractionated, can be well represented by Eq. [11]. We have no information about the isothermal steady viscosity-molecular weight relation for a homologous series of ideally fractionated samples of PVAc. Since the power 3.4 appears to be considerably intrinsic to the molecular-weight dependence of melt viscosities of linear high polymers, it may not be too drastic to assume that η for a molecularly homogeneous sample is represented in the form:

$$\log \eta = -\alpha + 3.4 \log M, \tag{21}$$

where α is a molecular weight-independent parameter to be determined as follows.

By substituting Eqs. [20] and [21] in Eq. [14] we obtain

$$\log \tau_m = 3.8 \log M - (8.16 + \alpha),$$

which gives for the first equation of Eq. [17]

$$\log \tau = 3.8 \log M_m - (8.16 + \alpha). \tag{22}$$

Substitution of Eqs. [20] and [22] in Eq. [19] yields

$$\varphi(M_m) = 2.63 \times 10^{-8} M_m^{-0.60} \left[-\Phi(\log \tau) \frac{\partial \log \Phi(\log \tau)}{\partial \log \tau} \right]. \tag{23}$$

If we denote by M_l the lowest molecular weight up to which this relation may be applied, the following equation must be satisfied from the condition that $\varphi(M_m)$ is a normalized function:

$$\int_{M_l}^{\infty} \varphi(M_m)\, dM_m = 1. \tag{24}$$

Substituting Eq. [23] and arranging the resultant equation in terms of Eq. [22], there results

$$2.303 \cdot 10^{(0.4\alpha - 27.7)/3.8} \int_{\log \tau_l}^{\infty} \tau^{0.4/3.8} \left[-\Phi(\log \tau) \frac{\partial \log \Phi(\log \tau)}{\partial \log \tau} \right] \times d(\log \tau) = 1, \tag{25}$$

from which the value of α may be obtained if the value of τ_l and the relaxation spectrum Φ (log τ) for a given sample are known. For the samples of PVAc studied in this work, the value of α was chosen as $10^{1.25}$ seconds from the data presented in Fig. 4 and the relaxation spectrum for the whole polymer O (shown by dashed line in Fig. 4) was substituted in Eq. [25]. The value of α obtained is 8.81. Once α is evaluated in this way, it is possible to calculate the form of $\varphi(M)$ for Sample O by combining Eqs. [22] and [23]. The molecular weight distribution obtained in this way for Sample O is shown in Fig. 10 by solid line. The dashed line in Fig. 10 is the distribution curve determined directly by fractionation and has been reproduced from Fig. 1. The agreement of both curves is quite striking, except in the

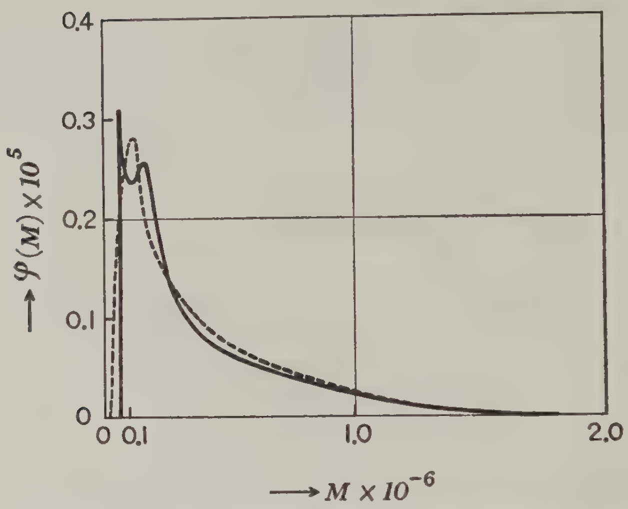

FIG. 10. Comparison of the molecular weight distributions for Sample O; solid line, from mechanical relaxation data; dashed line, from fractionation.

region of low molecular weights, where the procedure described above may not be considered as reliable. Although this agreement is probably more or less fortuitous, considering the many assumptions involved in the calculation, it is believed that the result is real and suggests the relaxation spectrum for a given polymer in the rubbery region to depend primarily, among the other factors, on the *weight distribution of molecular weights.*

Shift Factor and Apparent Activation Energy

The time-temperature superposition principle or its equivalent, the method of reduced variables, consists of two fundamental functions, i.e., the relaxation spectrum $\Phi(\log \tau)$ and the shift factor a_T. The dependence of mechanical behavior of a linear viscoelastic substance on time at constant temperature can be represented by Φ, and the dependence on temperature is best represented by a_T as a function of temperature T. The properties of Φ for PVAc at 75°C. over a wide range of time scale have been described fully in previous sections. We now in this section discuss about the behavior of a_T of this polymer.

It has already been mentioned that the form of a_T as a function of temperature is practically independent of molecular weight and molecular weight distribution in the range of temperatures treated in this work. As a typical example, the a_T data for fraction FXI are presented graphically in Fig. 11, where the logarithm of a_T is plotted against the absolute temperature T (in °K.) as well as the temperature in centigrade θ (in °C.). At 75°C. chosen as the reference temperature for the present reduction

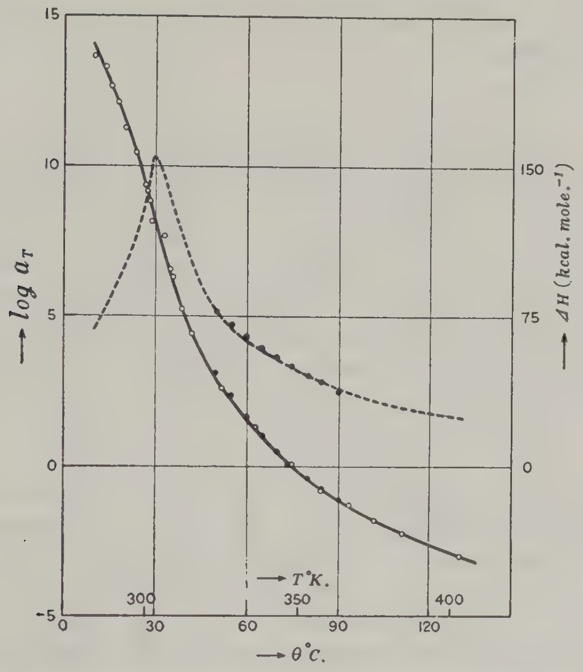

FIG. 11. Shift factor, a_T, and apparent activation energy for relaxation processes, ΔH, functions of temperature; open circles, present data; closed circles, Williams-Ferry's data.

processes the log a_T value vanishes because a_T takes unity here. In Fig. 11 the a_T data from Williams-Ferry's dynamic measurements (8) are also shown for comparison. Where the data overlap, those from our transient and their dynamic experiments agree remarkably well, supporting the validity of the time-temperature reduction principle of mechanical behavior in this temperature range. At lower temperatures the curve swings upward very sharply and eventually passes through an inflection point in the vicinity of 30°C. The overall trend of this shift factor curve is quite similar to those which have recently been found for many polymers both from transient and dynamic mechanical experiments (28). It is somewhat doubtful whether the shift factor data obtained from transient experiments at long time accord with those from dynamic experiments at high frequencies in the region below the second-order transition temperature, because, as has been noted before, the time-temperature superposition principle becomes less reliable in this region. No rigorous check on this point has yet been reported.

Williams, Landel, and Ferry (29) have shown that the shift factor data for a number of amorphous polymers and glass-forming liquids can be fitted very well, in the range $-50 < T - T_s < 50$°K., by a "universal" equation of the form:

$$\log a_T = -8.86 \frac{T - T_s}{101.6 + T - T_s}, \qquad [26]$$

where T_s is the reference temperature characteristic of a given system. A value of 349°K. was suggested for T_s of PVAc. The a_T curve calculated from this equation with $T_s = 349$°K. was found to follow our experimental data very closely except at temperatures below about 310°K., where the calculated curve deviated systematically below the observed values. To save the space the graph showing this comparison is not given here.

The apparent activation energy, ΔH, for relaxation processes may be calculated from data on a_T by means of the well-known equation:

$$\Delta H = 2.303\, R\, d \log a_T/d\,(1/T) = -2.303\, RT^2\, d \log a_T/dT, \qquad [27]$$

where R is the gas constant. The a_T curve in Fig. 11 was differentiated graphically at various temperatures, and the results were substituted in Eq. [27] to evaluate ΔH as a function of T. The ΔH vs. T curve so obtained is plotted also in Fig. 11 by dashed line, where the data of Williams and Ferry (8) are included for comparison. In the range where both data overlap, there is an excellent agreement as was the case with the shift factor itself. It is seen from Fig. 11 that the ΔH curve reaches a maximum at 29 (±1)°C., giving a maximum energy $(\Delta H)_{\text{max.}}$ of 154 kcal./mole. The temperature 29°C. at which the maximum activation energy appeared may be compared with the reported second-order transition temperatures (28–30°C.) for undiluted polyvinyl acetate (30, 31).

If the temperature at which the apparent activation energy for viscoelastic behavior reaches a maximum is denoted by T_d, we have, from Eq. [27],

$$(\Delta H)_{\text{max.}} = -2.303\, RT_d^2\, (d \log a_T/dT)_{T_d} \equiv KT_d^2. \qquad [28]$$

The proportionality factor K is 1.71×10^{-3} for the present data on PVAc. Tobolsky and Catsiff (2) reported that for seven polymers, including polyisobutylene, GR-S, butadiene-styrene copolymers, Paracril 26, and polymethyl methacrylate, the K values ranged from 1.51×10^{-3} to 2.03×10^{-3}. Bueche's (32) data on polymethyl methacrylate yield for K a value of 1.76×10^{-3}. These results indicate that the maximum apparent activation energy for viscoelastic behavior of a given polymer may be calculated, for most practical purposes, by means of an approximate formula:

$$(\Delta H)_{\text{max.}}\ (\text{kcal./mole.}) = 1.73 \times 10^{-3} T_d^2. \qquad [29]$$

Practically, T_d may be taken as the second-order transition temperature T_g (expressed in °K.) determined dilatometrically. The factor 1.73×10^{-3}

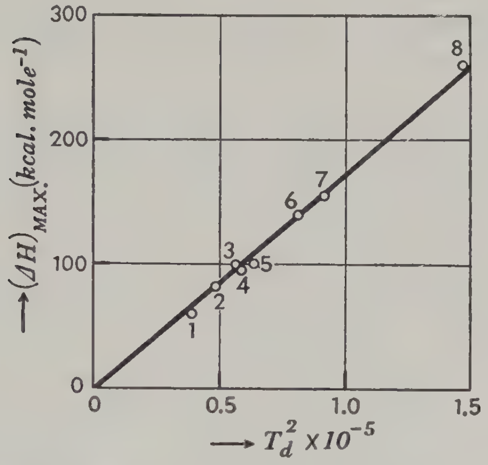

FIG. 12. Relations of maximum apparent activation energy and second-order transition temperature, T_d, for various linear high polymers: (*1*) polyisobutylene, (*2*) GR-S, (*3*) 60/40 butadiene-styrene copolymer (B-S), (*4*) Paracril 26, (*5*) 50/50 B-S, (*6*) 30/70 B-S, (*7*) PVAc, (*8*) PMMA.

was tentatively determined by plotting all available data of $(\Delta H)_{\max.}$ against T_d^2 and evaluating the slope of the resulting approximate straight line, as shown in Fig. 12.

ACKNOWLEDGMENTS

We wish to express our sincere appreciation to Professor John D. Ferry of the Department of Chemistry, University of Wisconsin, for his interest and support given in the course of this work. Thanks are also due Professor H. Kawai of the Department of Textile-Chemistry, Faculty of Engineering, Kyoto University, who supplied us with the unfractionated samples of polyvinyl acetate used in the present study.

SUMMARY

Extensive stress-relaxation data were obtained on twelve samples of polyvinyl acetate (including 8 fractionated, 2 roughly fractionated, and 2 unfractionated) over a wide range of temperature from 10° to 130°C. By making use of the time-temperature superposition principle they were combined to form a composite master relaxation curve for each of the samples, where all data were reduced to 75°C. chosen as the reference temperature. The master relaxation curves so obtained all cover the range from glassy consistency to rubbery flow as a function of time. From these, the relaxation distribution functions were calculated using the second approximation method proposed by Ferry, and compared with that derived by Williams and Ferry from dynamic mechanical measurements on

an unfractionated sample of polyvinyl acetate. It was found that in the transition region where the comparison could be made, both results agreed quite satisfactorily, except in its upper terminal zone encompassing the glassy state. The real and imaginary parts of the complex dynamic modulus and the mechanical loss tangent were computed as functions of frequency for one sample from its relaxation spectrum using the well-known equations in the theory of linear viscoelasticity. These predicted properties were found to agree fairly well with Williams-Ferry's experimental data in the transition region, again except in its portion near the glassy consistency. From these results, the validity of the time-temperature superposition principle in the high-modulus portion of the transition region was suspected, in line with a similar conclusion drawn by Tobolsky and Catsiff from their stress-relaxation study on polyisobutylene.

Steady-flow viscosities were calculated for all the samples studied from their relaxation spectra and found to increase with 3.4 powers of viscosity-average molecular weight, in agreement with the recent results on many other polymers.

The shift factor which represents the temperature dependence of viscoelastic behavior was obtained over the temperature range studied and found to be practically independent of molecular weight. The shape of the shift factor curve thus obtained is quite similar to those for many other linear high polymers and agrees closely with that derived by Williams and Ferry for an unfractionated polyvinyl acetate sample from dynamic measurements in the range 50°–90°C. The apparent activation energy for mechanical relaxation calculated from the shift factor data increases sharply with decreasing temperature and passes through a maximum at 29°C. This behavior is also entirely the same as those observed for other polymers. The temperature at which the apparent activation energy for mechanical relaxation appeared may be compared favorably with the second-order transition temperature determined dilatometrically on undiluted polyvinyl acetate.

Under the assumptions that the relaxation spectrum for a homogeneous (with respect to molecular weight) polymer in the rubbery region is represented by the so-called box-type function and that interactions between polymer molecules of different chain lengths are negligible, an equation was derived which represents the relaxation spectrum of a given heterogeneous polymer as the sum of relaxation spectra for its component polymers multiplied by its weight distribution of molecular weights. This equation was applied to the relaxation data for one unfractionated sample whose weight distribution of molecular weight had been determined using the successive fractional extraction method. It was found that the molecular weight distribution so derived from mechanical relaxation data is surprisingly close to the one from fractionation data except in the region of low molecular weights.

REFERENCES

1. GROSS, B., "Mathematical Structure of the Theories of Viscoelasticity," Hermann, Paris, 1953.
2. CATSIFF, E., AND TOBOLSKY, A. V., *J. Colloid Sci.* **10,** 375 (1955).
3. FITZGERALD, E. R., GRANDINE, L. D., JR., AND FERRY, J. D., *J. Appl. Phys.* **24,** 650 (1953).
4. FERRY, J. D., GRANDINE, L. D., JR., AND FITZGERALD, E. R., *J. Appl. Phys.* **24,** 911 (1953).
5. TOBOLSKY, A. V., AND ANDREWS, R. D., *J. Chem. Phys.* **13,** 3 (1945).
6. FERRY, J. D., *J. Am. Chem. Soc.* **72,** 3746 (1950).
7. FERRY, J. D., AND WILLIAMS, M. L., *J. Colloid Sci.* **7,** 347 (1952).
8. WILLIAMS, M. L., AND FERRY, J. D., *J. Colloid Sci.* **9,** 479 (1954].
9. FOX, T. G., AND LOSHAEK, S., *J. Appl. Phys.* **26,** 1080 (1955).
10. SAKURADA, I., AND CHIBA, T., *J. Chem. Soc. Japan (Ind. Chem. Sect.)* **47,** 135 (1944).
11. DART, S. L., AND GUTH, E., *J. Appl. Phys.* **17,** 314 (1946).
12. NINOMIYA, K., KISHIMOTO, A., AND FUJITA, H., *Chem. High Polymers (Japan)*, in preparation.
13. FLORY, P. J., *J. Chem. Phys.* **12,** 425 (1944).
14. BROWN, G. M., AND TOBOLSKY, A. V., *J. Polymer Sci.* **6,** 165 (1951).
15. ANDREWS, R. D., AND TOBOLSKY, A. V., *J. Polymer Sci.* **7,** 221 (1951).
16. MCLOUGHLIN. J. R., AND TOBOLSKY, A. V., *J. Colloid Sci.* **7,** 555 (1952).
17. HARPER, R. C., JR., MARKOVITZ, H., AND DEWITT, T. W., *J. Polymer Sci.* **8,** 435 (1952).
18. SCHWARZL, F., AND STAVERMAN, A. J., *Physica* **18,** 791 (1952); FUJITA. H., *Busseiron Kenkyu*, No. **63,** 48 (1953).
19. ROUSE, P. E., JR., *J. Chem. Phys.* **21,** 1271 (1953).
20. FERRY, J. D. JORDAN, I., EVANS, W. W., AND JOHNSON, M. F., *J. Polymer Sci.* **14,** 261 (1954).
21. ROESLER, F. C., Private communication to Prof. J. D. Ferry.
22. ROESLER, F. C., AND TWYMAN, W. A., *Proc. Phys. Soc. (London)* **B 68,** 97 (1955).
23. MARVIN, R. S., *Phys. Rev.* **86,** 644 (1952).
24. STAUDINGER, H., AND WARTH, H., *J. prakt. Chem.* [2] **155,** 261 (1940).
25. WAGNER, R. H., *J. Polymer Sci.* **2,** 21 (1947).
26. CHINAI, S. N., SCHERER, P. C., AND LEVI, D. W., *J. Polymer Sci.* **17,** 117 (1955).
27. FERRY, J. D., AND FITZGERALD, E. R., *Proc. 2nd Intern. Congr. Rheology, Oxford*, p. 140 (1953).
28. WILLIAMS, M. L., *J. Phys. Chem.* **59,** 95 (1955).
29. WILLIAMS, M. L., LANDEL, R. F., AND FERRY, J. D., *J. Am. Chem. Soc.* **77,** 3701 (1955).
30. JENCKEL, E., *Kolloid-Z.* **100,** 163 (1942).
31. KOKES, R. J., LONG, F. A., AND HOARD, J. L., *J. Chem. Phys.* **20,** 1711 (1952).
32. BUECHE, F., *J. Appl. Phys.* **26,** 738 (1955).

JOURNAL OF COLLOID SCIENCE **12**, 230–239 (1957)

FLOCCULATION, SUBSIDENCE, AND FILTRATION OF PHOSPHATE SLIMES[1]

IV. Flocculation by Gums, and Polyelectrolytes and their Influence on Filtration Rate

Victor K. La Mer,[2] Robert H. Smellie, Jr.,[3] and Pui-Kum Lee[4]

Received January 4, 1957

Abstract

The efficiencies of a large number of gums and polyelectrolytes as flocculants for improving flocculation and filtration of phosphate slimes have been investigated. Such factors as the speed of rotation and the total number of rotations in the mixing of flocculants and slimes, and the methods of adding the flocculants are discussed. The method of preparing stock solutions of flocculants and the age of such stock solutions significantly affect the flocculating efficiency in some cases.

All the flocculants tested produce an optimum (maximum) in flocculation and, hence, filtration rate within a very narrow increment of flocculant concentration. This behavior was previously observed with starches.

The pertinent data for 12 commercial products (out of about 150 tested), found to be the most effective flocculants for phosphate slimes, are summarized.

A. Introduction

In this paper we shall consider the efficiency of a number of gums and polyelectrolytes in improving flocculation and filtration. In a later paper further consideration will be given to the flocculating efficiency of essentially uncharged polymer molecules, such as the polyacrylamides.

B. Flocculation Process and Floc Structure

From previous considerations described in connection with potato starches (1) it seems reasonable that an effective flocculating agent must possess the following characteristics:

1. The molecules must possess a structure containing certain groups (OH or COO$^-$) which are physically or chemically adsorable on the surface of the particles.

---

[1] Supported by funds from Contract AT (30-1) 1189 between Columbia University and the U. S. Atomic Energy Commission. Progress Reports N.Y.O. 3289, 7402, and 7403.

[2] Dept. of Chemistry, Columbia University, New York 27, New York.

[3] Dept. of Chemistry, Trinity College, Hartford, Connecticut.

[4] Present Address: Minnesota Mining and Manufacturing Co., St. Paul, Minnesota.

2. The molecules must be of sufficient length to form a "bridge" between particles producing uniform flocs of the proper size and shape to give a filter cake having high porosity.

3. The flocculating agent must be soluble in water in order to be effective.

4. Concentration levels of these agents required to produce the "optimum" flocculation and, hence, the optimum filtration rate must be very small (up to a few hundred parts per million) in order to be competitive with potato starch in many cases.

In the simplest terms the effectiveness of a flocculating agent for the purpose of significantly improving filtration may be attributed to:

1). Scavenging ability, i.e., the ability to gather up all the primary particles into large flocs, leaving none to clog filters.

2). Binding ability, i.e., the ability to maintain a porous cake structurally strong enough to resist the compression effect in vacuum filtration.

The effectiveness of flocculating agents varies with concentration, composition of slime solid, per cent solids, particle size, and, in some cases, pH, and concentration of extraneous electrolytes. Consequently, all the comparisons in a series were made on a given slime at a given solid content. Such variants as pH and extraneous electrolyte content were constant in a given series, usually being maintained at the values found for the original (untreated) slime.

C. Agitation and the Method of Mixing Reagents; Reproducibility of Results

It has been observed that reproducible results cannot be obtained unless the amount of agitation and the method of adding the reagents are carefully controlled. The flocculating agents must be added in accurately measured doses, and the mixing by agitation must be controlled, within certain limits, as to the number of inversions of the container (shaking is not advisable) and the total time in which a given number of inversions is made.

1. Addition of Reagents

The flocculating agents were added to 50–100 ml. of the slime as 0.1 to 1% solutions in water. One milliliter of a 1% reagent solution gives a final concentration of 100 p.p.m. in a 100-ml. sample of slime (based upon total slime). If the reagent is added at one time and then mixed, the result is often different from that obtained when it is added dropwise and mixed after each addition, even if the total number of inversions of the container is the same in each case. The origin of this difference resides in the extent of adsorption of the flocculating agent in different parts of the slime. When all the reagent is added at once, the extent of adsorption at the top of the container will be greater than that below. In any case, the flocculating agent must be added in the same manner each time in order to obtain reproducible results with a given amount and timing of agitation.

2. *Method of Mixing-Agitation*

In mixing the flocculating agent the extent of agitation must also be controlled in order to obtain reproducible results. In earlier experiments where mixing was accomplished by inverting samples in 100-ml. graduated cylinders while held between the hands, it was observed that the number of inversions and the total time in which they were performed affected the reproducibility of the subsidence and filtration rates.[5]

The results using vacuum filtration were reproducible to within ±5% if a given number of inversions was performed within a given period of time. The number of inversions giving optimum results was 40 in 2 minutes. However, variation of the number of inversions between 10 and 40 in 2 minutes was permissible in some cases leading to a variation in filtration rates of about 10%. The vigor with which individual operators would carry out the manual inversions presented a possible uncontrollable variable, and for this reason a rotating device was constructed which rotated the cylinders at certain speeds (r.p.m.) which were determined by gearing. Using this device, we were able to eliminate the variation due to the manual technique of different operators.

With this mixing device using different slimes, flocculating agents, and solid contents, we have established that our mixing technique yields the reproducible filtration data illustrated in the figures. Floc size can be affected significantly by varying the agitation when all other factors are carefully controlled. This is evidenced in the filtration rates since differences in floc size lead to differences in the porosities of the filter cakes. The effect of the mechanical agitation is more dependent on the total number of revolutions than upon the r.p.m. for a given total number.

3. *Typical Results*

Figure 1 shows typical data on the effect of agitation on the filtration rate of Slime VIII (5.5% solids) after flocculation with different types of agents. The data are plotted on a log-log scale in order to take in the wide variations in the filtration time and the number of rotations of the cylinders, respectively. In each case the flocculant concentration is that producing the optimum in the filtration rate when the cylinders are inverted manually 40 times in 2 minutes. It is evident that the filtration of Slime VIII flocculated with Jaguar MD-4 is affected very little over a wide range of the number of rotations. The filtration rates with the other four flocculants

---

[5] Also observed independently by Dr. Scott Sears of the Virginia Chemical Company.

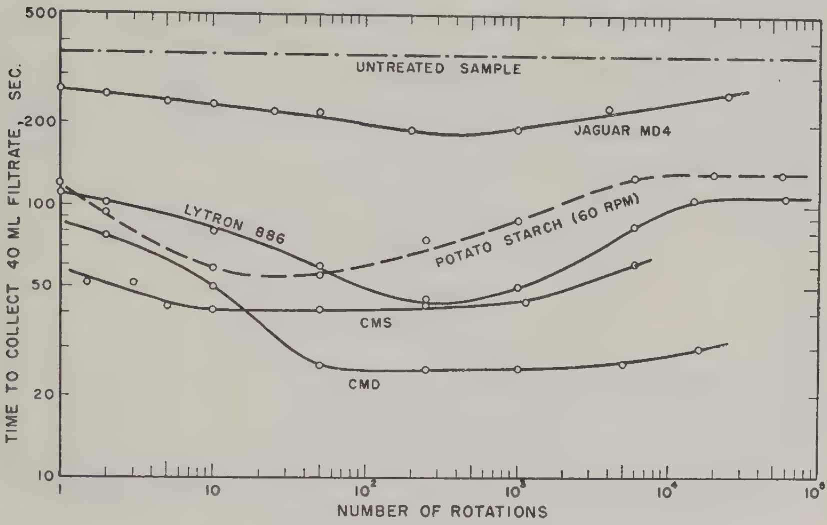

FIG. 1. Shows a log-log plot of the time to collect 40 ml. of filtrate (50-ml. sample) vs. the number of rotations at 15 r.p.m. (except for potato starch (60 r.p.m.)) for Slime VIII with several flocculants.

Jaguar MD4 (guar gum) is a product of Stein-Hall Company, New York, New York. CMS and CMD were, respectively, a carboxy methyl starch and a carboxy methyl dextran prepared by Drs. Beckmann and Roger at Columbia University. The other two flocculants used are described in the text. Slime VIII is a replica of the "leached zone" slime III described in reference 1.

shown are more dependent upon the number of rotations. They vary by factors of as much as fivefold.

The optimum number of revolutions varies with the rate of rotation, the composition, and amount of flocculant, the composition of the slime, and the per cent solids. Figure 2 shows the effect of agitation on filtration rate at different concentrations of Dow Separan 2610 using Slime XIII (5.5% solids). The times required to collect 50 ml. of filtrate from 100 ml. of slime are plotted against the number of rotations of the cylinder (at the constant rate of 15 r.p.m.) on a log-log scale. The effect varies considerably with the flocculant concentration with an optimum at about 250 p.p.m. The influence of agitation on the filtration rate will also be of great practical importance in any large-scale utilization of polymeric flocculating agents. At the present time each slime must be studied separately with each different type of flocculating agent.

Factors such as the rate of adsorption of the flocculating agent and the sizes and shapes of containers may also be of significance in determining the effect. However, by standardizing the rate and the number of inversions of the container at their optimum values the results become remarkably reproducible.

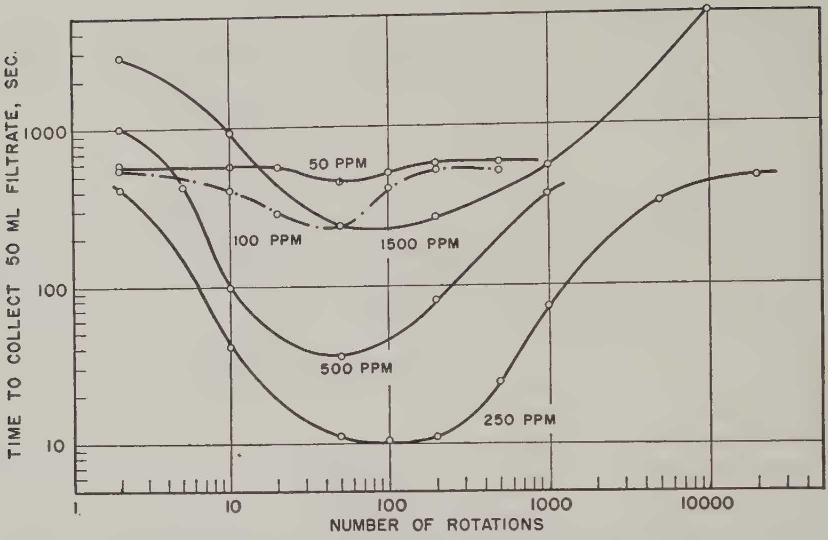

FIG. 2. Shows a log-log plot of the time to collect 50 ml. of filtrate (100-ml. sample) vs. the number of rotations at 15 r.p.m. for Slime XIII with different concentrations of Dow Separan 2610 as the flocculant. Separan 2610 is a product of the Dow Chemical Co., Midland, Michigan. Slime XIII is a replica of the "leached zone" slime III described in reference 1.

D. FILTRATION WITH VARIOUS FLOCCULATING AGENTS

In the earlier experiments with synthetic polyelectrolytes and natural gums the method of mixing the agents and slimes manually was used in the standardized procedure (a total of 40 inversions in 2 minutes). With further development of this technique reproducibility of filtration data to within 5% was demonstrated.

The three slimes used in the first complete study of several flocculating agents of the polyelectrolyte and gum types (1952–53) were supplied by the Virginia-Carolina Chemical Company and described as follows.

Slime R51. A sample of slimes from the debris overflow pump at Clear Springs, Florida, was taken over a period of 2 days. The samples were screened on 200 mesh, discarding the oversize to separate out the actual debris from the slimes. After settling the excess water was decanted and the solids resuspended by agitation and bottled.

% Solids—6.23[6]
% P_2O_5—17.01
% Fe_2O_3—5.58
% Al_2O_3—8.72
% CaO—18.56

---

[6] All these analyses represent only acid-soluble material.

Slime R52. A sample of Homeland, Florida, hydroseparator overflow which was sampled over two shifts each on 3 days. The material was not screened and may have contained some plus 200 mesh particles. This would be normal for slimes from the matrix. The excess water was removed as with Slime R51.

% Solids—5.65[6]
% P_2O_5—15.50
% Fe_2O_3—3.40
% Al_2O_3—5.97
% CaO—22.54

Slime R53. A sample of leached zone material from Clear Springs, Florida, was deslimed through a 200-mesh screen. The conditioning consisted of a 30-minute agitation in a cylindrical container. The minus 200 mesh material was permitted to settle and the excess water decanted.

% Solids—25.30[6]
% P_2O_5—27.04
% Fe_2O_3—3.26
% Al_2O_3—29.11
% CaO—5.62

The flocculating agents used in this series of experiments were:

1). Lustrex 886 (now Lytron 886)—a partial calcium salt of the copolymer of maleic anhydride and vinyl acetate—Monsanto Chemical Company. A 0.5% solution (in water) was used.

2). Guartec—a product of General Mills, Inc. It is believed to be primarily a starch of the galactomannan type prepared from Guar flour. About 85% of this material is dispersible while the remainder produces a brown insoluble residue. Since it was difficult to disperse Guartec in water, 1 g was first triturated with a few milliliters of 95% ethyl alcohol. This slurry was then poured into enough water at 95–100°C. and dispersed rapidly. The final dispersion was either 0.5 or 1% by weight.

3). NOPCO (formerly National Oil Products Corp., Harrison, New Jersey) soil conditioners, NOPCO A, B, and C. NOPCO-B was readily soluble in cold water, whereas NOPCO-A and NOPCO-C dissolved very slowly.

4). Potato starch—product of Goodman and Co., Long Island City, New York (reference to this starch was made in paper II of this series (1).

In general, heating during the preparation of stock solutions of Lustrex-X-886 and the NOPCO compounds decreased the flocculating power of

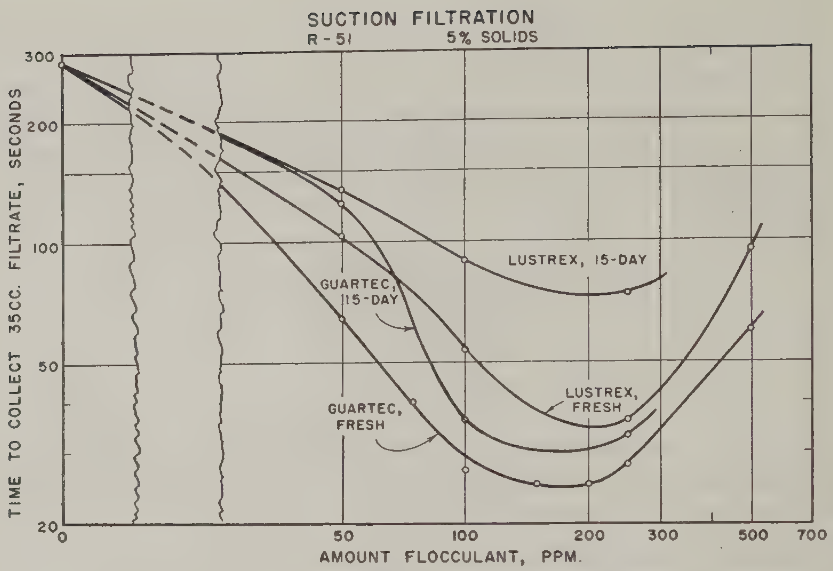

FIG. 3. Vacuum filtration of Slime R-51; 100-ml. samples. Time to collect 35 ml. of filtrate (in seconds) vs. parts per million of flocculant (based on total slime) on log-log scales. The flocculating agents were used in the following form: *A*. Freshly prepared Guartec solution. *B*. A Guartec solution 15 days old. *C*. Freshly prepared Lustrex X-886 solution. *D*. A Lustrex X-886 solution 15 days old.

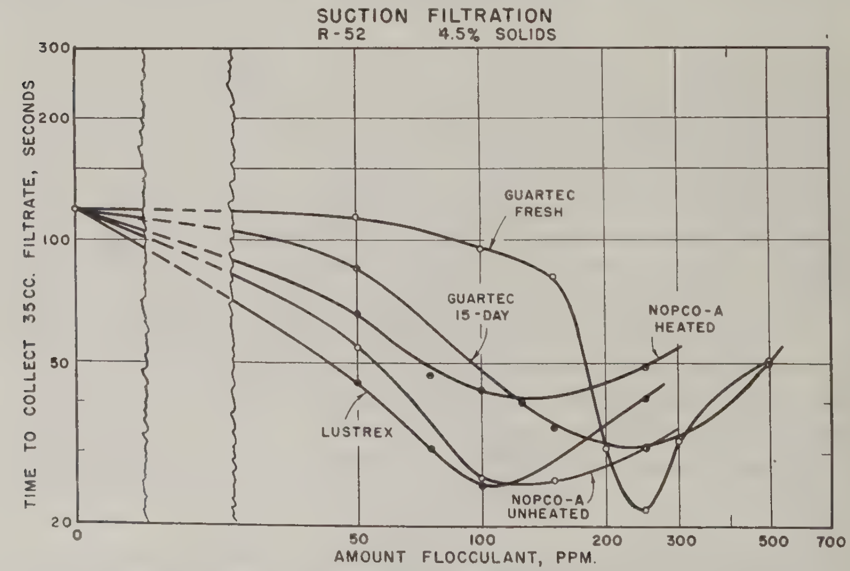

FIG. 4. Vacuum filtration of Slime R-52; 100 ml. samples. Time to collect 35 ml. of filtrate (in seconds) vs. parts per million of flocculant (based on total slime) on a log-log scale. The flocculating agents were used in the following form: *A*. Freshly prepared Guartec solution. *B*. A Guartec solution 15 days old. *C*. Freshly prepared Lustrex X-886 solution. *D*. A solution of NOPCO-A freshly prepared in the cold. *E*. A solution of NOPCO-A freshly prepared with hot water.

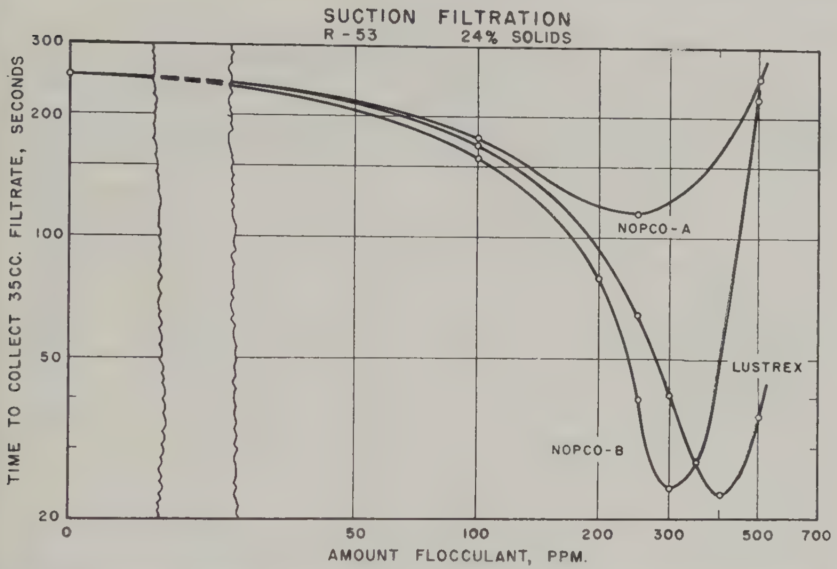

Fig. 5. Vacuum filtration of Slime R-53; 100-ml. samples. Time to collect 35 ml. of filtrate (in seconds) vs. parts per million of flocculant (based on total slime) on a log-log scale. The flocculating agents were used in the following form: *A*. Freshly prepared Lustrex X-886 solution. *B*. A solution of NOPCO-A freshly prepared in the cold. *C*. A solution of NOPCO-B freshly prepared in the cold.

these agents. Solutions of Lustrex X-886 and Guartec deteriorated on standing with significant reduction in the flocculating power within a few days after preparation. With all these agents fresh solutions prepared in the cold showed the highest efficiency for a given amount of flocculant. Hydrolysis, lactone formation, and possibly other chemical effects are involved in the deterioration of the flocculating agents.

Filtrations of the slimes were performed at a pressure difference of about 74 cm. Hg using the technique described in paper II of this series (1). The times required to collect 35 ml. of filtrate are plotted against the amounts of flocculating agent in parts per million (based on total slime) on a log-log scale. Figures 3, 4, and 5 show data for slimes R51, R52, and R53, respectively, with the flocculating agents described above.

E. Discussion

The optima in concentration for all flocculants producing the maxima in filtration rate (minima in time) are well defined. The efficiency of any particular flocculating agent varies with the characteristics of the slime. For example Guartec is more efficient than Lustrex X-886 with slime R51, but with R52 the order is reversed. It should also be noted that the "old" solutions of Guartec and Lustrex X-886 are significantly less effective than

TABLE I

Improvement in Filtration Rates Effected by Flocculants

Represents 12 of the best products out of a total of 150 commercial samples tested.

The Filtration Improvement Factor (F.I.F.) is the ratio of the filtration rate for a given flocculated slime to that of untreated slime.

Flocculant	F.I.F.	Optimum flocculant conc. in ppm.
Amer. Cyanamid Co.		
Reagent S-3000	16	200
Polyacrylamide PAM-50	20	400
Polyacrylamide PAM-75	12	250
Polyacrylamide PAM-100	50	250
Dow Chemical Co.		
Separan 2610	70	200
General Aniline & Film Co.		
PVM/MA (copolymer of methyl vinyl ether and maleic anhydride) series		
PVM/MA (sp. visc. 0.5–0.8) with 0.2% added $CaCl_2$	30	80
PVM/MA (sp. visc. 7.4) with 0.2% added $CaCl_2$	30	80
A. F. Goodman & Sons		
Potato starch	9.3	400
W. A. Scholten, Netherlands (agent Morningstar Nicol)		
Starch ether: Solvitose H4	8	800
Monsanto Chemical Co.		
Lytron 886 (partial Ca salt of copolymer of vinyl acetate and maleic anhydride)	9	30
Lytron 886 with 0.05% added $CaCl_2$	50	80
Lytron 887 (copolymer of vinyl acetate and maleic anhydride)	9	30
Morningstar Nicol Co.		
613-45 (cationic starch derivative)	8	1500

the freshly prepared solutions. In the case of NOPCO-A with R52, the solution prepared by heating is a less effective flocculant than the one prepared in the cold. Considerable improvement in filtration rates of flocculated samples over those of the untreated slimes were observed. These experiments were performed in triplicate.

The sharp decrease in flocculating efficiency with consequent decrease in filtration rates for flocculant concentrations greater than the optimum was noted in all cases (Figs. 3, 4, and 5). Observations under the microscope have shown that the average floc size decreases with the higher concentrations of polymeric flocculating agents. The protective action of flocculants arising from the more complete covering of the particle surfaces has also been observed with starches and was discussed in paper II. Our observations with polymeric flocculating agents have demonstrated that the region in which the optimum in flocculation and, hence, in filtration rate occurs is usually relatively narrow. Accordingly, experiments should be performed using small increments of flocculating agent.

Approximately 200 polymeric flocculating agents have been tested quantitatively over the past three years. The majority of these agents were commercially produced; the others were research samples provided by various companies or synthetic polymers prepared by Professor Beckmann and Dr. Roger of our staff. The pertinent filtration data using some of the commercial products tested are summarized in Table I.

The optimum concentrations of the various flocculants which produce the maximum filtration rates are given with a "filtration improvement factor" (F.I.F.), which represents the ratio of the filtration rate at the optimum concentration of the flocculant to that of the untreated slime. The slimes used in these experiments were replicas of Slime III prepared from "leached zone material" as described in paper II. The data for some of the agents prepared by Drs. Roger and Beckmann have been reported in part in reference 2.

Since all the polymeric agents exhibited the same pattern of behavior, although often differing considerably in effectiveness as flocculants, the interpretation of such factors as per cent solids and particle size in relation to the optimum in flocculant concentrations becomes feasible. In addition, it has been possible to explain the variation of the filtration rate with the concentration of flocculant by the means of a relatively simple theory relating the surface action of flocculating agents to the flocculant size and filtration rate. These findings will be reported in later papers of this series.

REFERENCES

1. LA MER, V. K., AND SMELLIE, R. H., JR., *J. Colloid Sci.* **11**, 710 (1956).
2. ROGER, M., AND BECKMANN, C. O., Reported at the National Meeting of the American Chemical Society, Minneapolis, Minnesota, September, 1955.

JOURNAL OF COLLOID SCIENCE **12,** 241–242 (1957)

IN MEMORIAM:

WOLFGANG PAULI, SR.

SEPTEMBER 11, 1869–NOVEMBER 4, 1955

Wolfgang Pauli, Sr., one of the world's leading colloid chemists, died on November 4, 1955, in Zurich, Switzerland.

Born at Prague (at that time a city of the Austrian Empire), Pauli received his doctorate in medicine at the German University of his native city in 1892. In the same year, he published his first paper on proteins at the laboratory of F. Hofmeister, who together with E. Fischer is considered the founder of the polypeptide theory of protein structure. Pauli became a successful diagnostician in Vienna but gave up his medical practice to devote himself entirely to research. In 1922, he was named full professor and Director of the Institute of Medical Colloid Chemistry of the University of Vienna. He left this position in 1939, when the Nazi invasion forced him into exile. The last 15 years of his life were spent in Zurich.

Pauli's long scientific career was devoted mainly to two endeavors. The first was the establishment of the correlation of the colloid-chemical and physicochemical behavior of proteins with their chemical constitution. The recent development of polymer chemistry, and especially the chemistry of polyelectrolytes, brought confirmation of many of the ideas he advanced. His studies on such subjects as the binding of small ions by proteins and its effect on optical rotation and viscosity show the breadth and depth of his vision. From 1917 on, Pauli devoted his main effort to the study of inorganic colloids. Here his thesis was that the electric charge of colloid particles is due to the electrolytic dissociation of complex compounds chemically bound to the surface. This encountered a great deal of skepticism but gradually found quite a general acceptance. In the course of his studies, Pauli developed many original methods. His electrophoretic apparatus (devised with Landsteiner) became the prototype of many others. He pioneered in the application of electrodialysis, and devised electrodecantation (electrophoresis-convection). The word "Gegenion" frequently used, even in English language publications, was coined by Pauli.

Two of Pauli's books have been translated into English. They are *Physical Chemistry in the Service of Medicine* (translated by Martin H. Fisher), New York, 1907, and *Colloid Chemistry of Proteins* (translated by P. C. L. Thorne), first edition, London and Philadelphia, 1922. Two others have appeared in German only: *Elektrochemie der Kolloide* (with E. Valko), Berlin, 1929, and *Kolloidchemie der Eiweisskörper* (with E. Valko), revised 2nd edition, Dresden-Leipzig, 1933.

Pauli was an inspiring teacher. Research workers from all parts of the world flocked to his laboratories, and many of his pupils gained prominence in science and industry.

Wolfgang Pauli, Jr., the physicist and Nobel prize winner of 1945, is his son.

W. Pauli, R. Zsigmondy, H. Freundlich, and Wo. Ostwald were considered, in the period between the two World Wars, the leaders of German colloid chemistry. Each of them created a distinct school of colloid chemistry and their mutual polemics, occasionally fought with a vehemence reminiscent of the early history of organic chemistry, enlivened the pages of the *Kolloid-Zeitschrift*. In the closing years of his long life, Pauli, the last of the group, witnessed the development of modern colloid chemistry, which brought a synthesis of their seemingly divergent ideas and is based, to more than a small extent, on the contributions they made.

Emery I. Valko

JOURNAL OF COLLOID SCIENCE **12**, 243–262 (1957)

PARTICLE MOTIONS IN SHEARED SUSPENSIONS

V. Rigid Rods and Collision Doublets of Spheres[1]

W. Bartok and S. G. Mason

Pulp and Paper Research Institute of Canada and Department of Chemistry,
McGill University, Montreal, Canada

Received October 4, 1956

LIST OF SYMBOLS

a = diameter of sphere.

C = orbital constant.

Δd = distance between particle centers measured along the xy-projection of major axis of doublet.

G = velocity gradient.

l' = projection of major axis of a cylinder on the xy-plane.

$p(\xi)$ = differential distribution function ξ.

$P(\xi)$ = integral distribution function $\int_0^\xi p(\xi)\,d\xi$, i.e., fraction of assembly having modes less than ξ.

r = axis ratio.

r_e = equivalent ellipsoidal axis ratio.

t = time.

T = period of rotation about Z-axis.

u, v, w = velocity components along X, Y, Z-axes.

u' = relative translational velocity of particle centers $= d(\Delta x)/dt$.

$\Delta x, \Delta y, \Delta z$ = distance between particle centers measured along coordinate axes.

$\Delta x_1, \Delta y_1, \Delta z_1$ = distance between outermost points of spheres measured along coordinate axes.

θ, ϕ = colatitudinal and azimuthal spherical polar coordinates (Z = polar axis).

θ_0, ϕ_0 = spherical polar coordinates of initial point of contact in collisions of spheres.

λ = azimuthal angle (Y = polar axis).

ψ = time variable in angular velocity plots.

τ = doublet life.

INTRODUCTION

Previous papers in this series have dealt with the rotation and interaction of spheres (1–3) and the rotation, interaction, and orientation of rods

---

[1] Conducted with financial assistance from the Defence Research Board of Canada (DRB Grant 9510-05).

(1, 4) caused by laminar shear of the suspending liquid. The experiments were performed in a field of flow defined by $u = Gy$, $v = 0$, $w = 0$, and the phenomena were observed along the Y-axis, i.e., across the planes of shear. In this paper we describe similar experiments on the rotation of rigid rods, and on fused and collision doublets of equal-sized rigid spheres, in which observations were made along the Z-axis, i.e., in the plane of shear of the field of motion defined above. The investigation was carried out to extend the earlier observations, particularly those on the behavior of collision doublets of spheres.

The phenomena can be considered most conveniently with reference to Jeffery's theoretical equations (5) for the periodic rotation of rigid prolate spheroids of axis ratio r_e:

$$\tan\phi = r_e \tan\frac{Gt}{r_e + 1/r_e} \qquad [1A]$$

$$= r_e \tan\frac{2\pi t}{T} \qquad [1B]$$

in the spherical elliptical orbit described by

$$\tan\theta = \frac{Cr_e}{(r_e^2\cos^2\phi + \sin^2\phi)^{\frac{1}{2}}} \qquad [2]$$

with a period

$$T = 2\pi(r_e + 1/r_e)/G, \qquad [3]$$

where ϕ and θ are the spherical polar coordinates shown in Fig. 1.

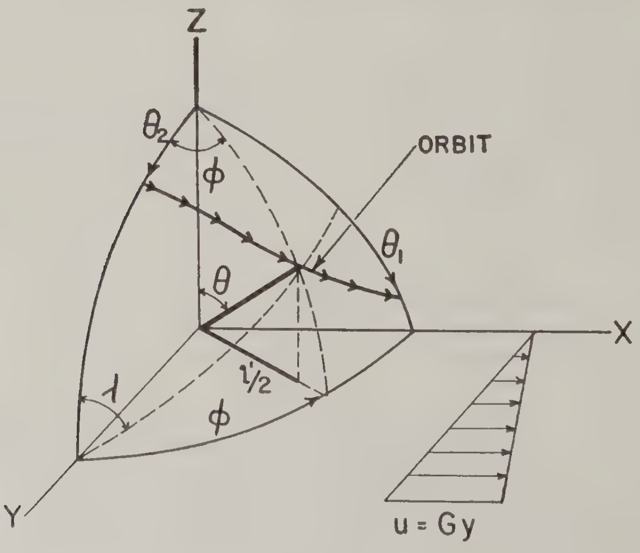

FIG. 1. Spherical polar coordinate system (after (1)).

In the earlier measurements ϕ and θ could not be measured directly; instead, the orbit was followed by measuring the angle λ (Fig. 1) using the following equation derived from [1] and [2]:

$$\tan \lambda = Cr_e \sin \frac{2\pi t}{T}. \qquad [4]$$

Equation [4] holds for rigid rods provided that the measured period of rotation and the equivalent ellipsoidal axis ratio r_e (smaller than the true axis ratio) calculated from [3] are used (1, 4). Equation [4] applies also to air bubble doublets (3).

The rate of formation, the rotational velocity, and the various lives of collision doublets have been found to agree well with calculations based upon rectilinear approach of the spheres up to the instant of contact when the doublet forms, and their subsequent rotation as a rigid dumbbell according to Eqs. [1], [2], and [3] with $r_e = 1$, until they separate at the mirror image of the initial position of contact (2). These experiments suggested the possibility of true physical contact between the spheres, but later experiments with doublets of spheres of different size ratios rendered this unlikely (3, 6).

In the experiments reported here the variation of ϕ of the various particles was measured directly to confirm the validity of [1]. In addition, a number of aspects of collision doublet behavior were investigated which were not possible by the earlier method; the observations have led to a modified picture of doublet behavior.

EXPERIMENTAL PART

A few measurements were made in the Couette double cylinder apparatus (1) in which particles were observed along the Y-axis of the field of flow. The rest were made in another apparatus employing the same principle but arranged to permit viewing along the Z-axis. Shown schematically in Fig. 2, it consisted of two concentric stainless steel cylinders rotating in opposite directions to establish laminar shear of the liquid placed in the annular gap between the two cylinders. The speeds of rotation, and hence $\dot{\gamma}$, were varied at will by means of two continuously and independently variable drives and were measured on two direct-reading tachometers.

To permit illumination of the field in the annulus from below, and observation from above, the outer cylinder had a bottom and a cover of plate glass. The observation microscope could be focused vertically and was mounted integrally with the light source so that the two could be rotated through 180° about the axis of the rotating cylinders and traversed across the annular gap.

The outer cylinder had an i.d. of 11.995 in.; two interchangeable inner cylinders of o.d. 9.017 and 10.515 in. were available, the smaller of which

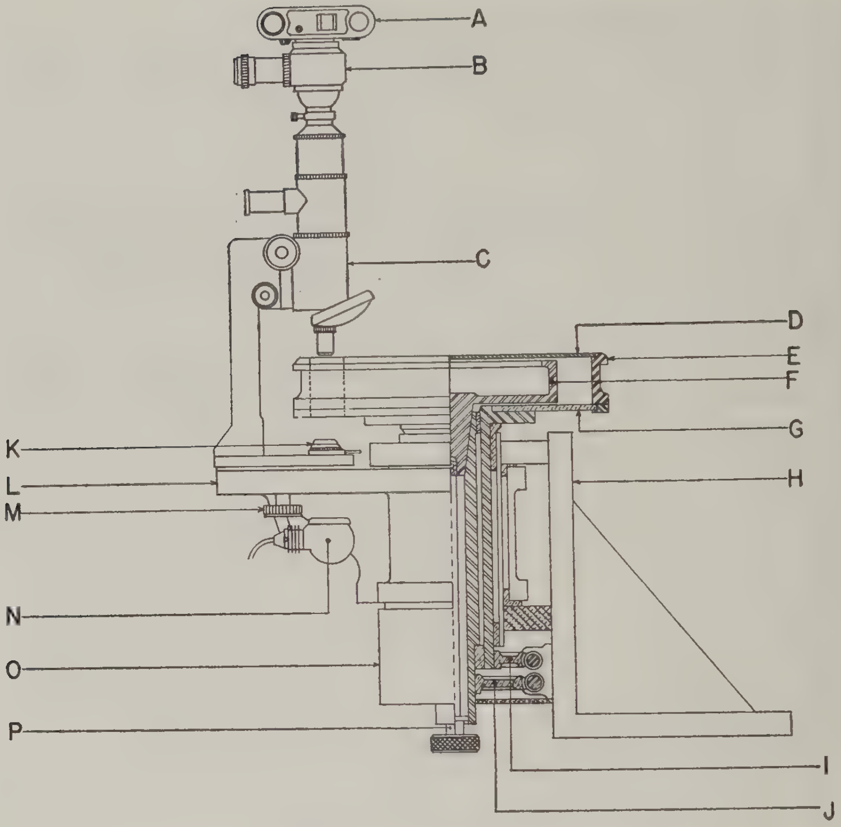

FIG. 2. Cross-sectional view of the concentric cylinder apparatus for observations along the Z-axis. Legend: A—camera; B—beam splitter; C—microscope; D—glass cover plate; E—outer cylinder; F—inner cylinder; G—bottom glass plate; H—apparatus mount; I—outer cylinder worm drive; J—inner cylinder worm drive; K—iris diaphragm; L—microscope swivel mount; M—traversing knob; N—light source; O—gear housing; P—inner cylinder release rod.

was used. With this combination the velocity gradient at the stationary layer, where all observations were made, became (1)

$$G = 0.2721\, N_1 + 0.4815\, N_2, \tag{5}$$

N_1 and N_2 being the speeds in r.p.m. of the inner and outer cylinders, respectively.

As in previous investigations, the liquid medium used was household corn syrup having a viscosity of about 50 poises and a density of about 1.3 gm./c.c.; viscosity measurements using falling spheres of various diameters indicated Newtonian behavior. To avoid "end" effects resulting from the drag exerted on the liquid by the bottom of the relatively shallow annulus (about 2 in. deep) of the new apparatus, the suspensions were floated on a liquid of low viscosity; carbon tetrachloride was chosen for this purpose.

The proper functioning of the apparatus, including the absence of end effects, was established by measuring the periods of rotation of single glass spheres. Measurements over a range of values of G on particles located at different positions in the annulus showed an agreement with [3] for $r_e = 1$ within several parts per thousand.

In most of the experiments the events were recorded photographically by means of a Robot Royal automatic camera mounted on the microscope. In this way, for example, the XY-projections of collision doublets were photographed for subsequent measurement without stopping the motion of the apparatus, as had been necessary in many of the earlier experiments (2). The time at which each exposure was made was measured from the play-back of a tape-recording of the audible clicks of the camera shutter.

Orlon particles having various lengths cut from 2.5 denier filament were used as rigid cylinders. The experiments on collision doublets were made with glass spheres (1), screen-fractionated to yield a fraction having a number-average diameter of 107μ with a standard deviation of 5μ. In the original stock of glass spheres many cases were found where two spheres had become fused together (during manufacture) at the surface without distorting the shape of either sphere. A number of these rigid dumbbells in which the two spheres had the same size were selected for study.

RESULTS

Rigid Cylinders

The rotation of rigid rods about the Z-axis was readily measured in the new apparatus using the photomicrographic technique. A typical result is shown in Fig. 3, where the variation of the azimuthal angle ϕ with time for a straight Orlon fiber is given and compared with Jeffery's theory. A more sensitive test of the theory is provided by plotting $\tan\phi$ against $\tan(2\pi t/T)$ as in Fig. 4. Both plots show excellent agreement with [1B], an equation which can be used to calculate the steady-state distribution of orientations with respect to ϕ in a suspension of rods (4).

A further test of Jeffery's equations was made from measurements of the projected length at various positions of the orbit. Let $l'(\phi)$ be the length of the XY-projection of the particle in the position ϕ, and θ_1 and θ_2, the respective co-latitudes when ϕ is $\pi/2$ and 0, corresponding to the major and minor axes of the spherical ellipse defined by [2].

The following relations are readily derived from [2]:

$$\tan\theta_1 = Cr_e; \qquad [6]$$

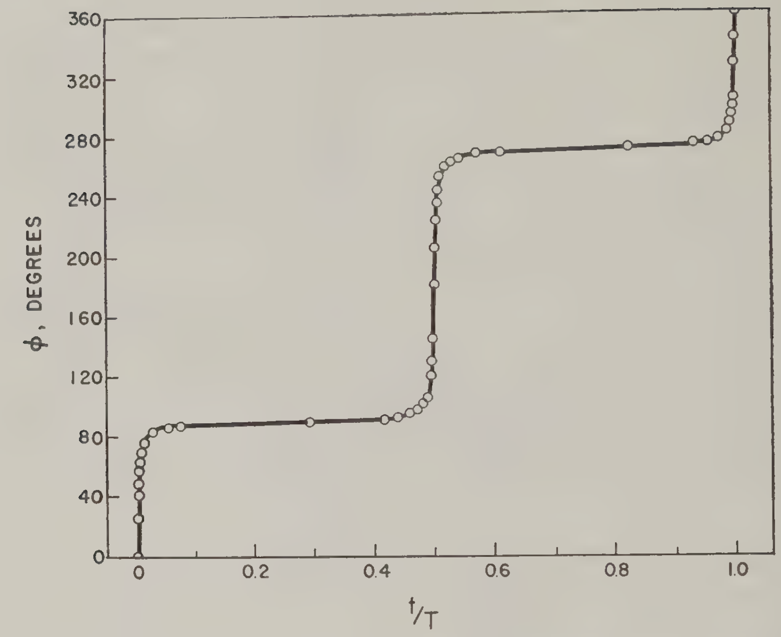

FIG. 3. The variation of ϕ with time for a rigid Orlon cylinder at $G = 0.448$ sec.$^{-1}$. The curve is calculated from [1], using $r_e = 45.5$ determined from [3].

$$\sin\theta_1 = \left[r_e^2 - \frac{l'(\pi/2)}{l'(0)}\right]^{\frac{1}{2}} \frac{1}{(r_e^2 - 1)^{\frac{1}{2}}}; \qquad [7]$$

$$\frac{l'(\phi)}{l'(\pi/2)} = \frac{Cr_e/\sin\theta_1}{(r_e^2\cos^2\phi + \sin^2\phi + C^2 r_e^2)^{\frac{1}{2}}}. \qquad [8]$$

The orbit constant C for a particle of known r_e can be calculated using [6] and [7] from the ratio $l'(\pi/2)/l'(0)$. Figure 5 shows a comparison of experimental values of $l'(\phi)/l'(\pi/2)$ with those calculated from [8] using the orbit constant determined in this manner. The agreement is good.

Rotation of Fused Doublets

The rotation of fused doublets of equal-sized spheres was studied as a matter of interest and for comparison with the collision doublets.

According to Eirich and Mark (7), the liquid contained in cavities and slots of a particle is immobilized and the hydrodynamic shape of such a particle is that contained by its outer contour. On this basis a fused doublet would correspond roughly to an ellipsoid of $r_e = 2$. In this case [3] becomes

$$\frac{TG}{2\pi} = \frac{5}{2}. \qquad [9]$$

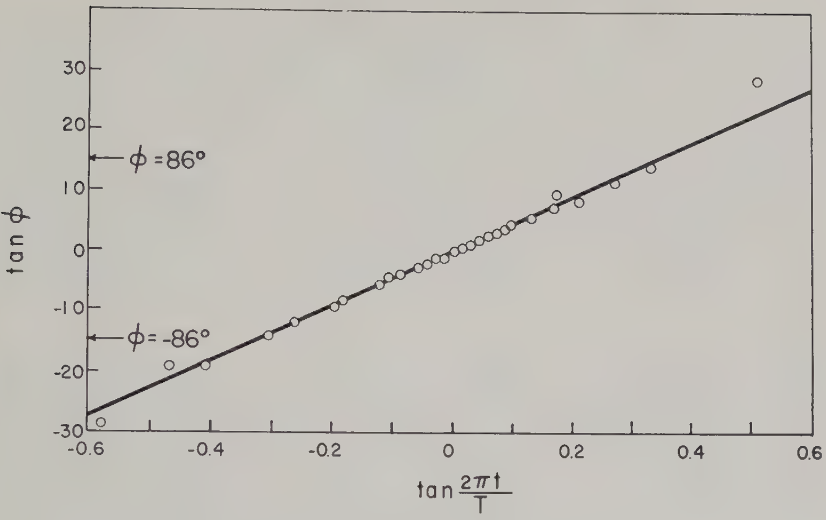

FIG. 4. Tan ϕ vs. tan $2\pi t/T$ for the same particle as in Fig. 3. The straight line is given by [3].

The measured periods of rotation summarized in Table I verify this behavior remarkably closely.

In Fig. 6 values of tan ϕ are plotted against t/T for a fused doublet rotation. In these experiments, the angles were measured visually using a goniometric ocular and are not as precise as the photographic measurements; nevertheless, the experimental points are in good agreement with the theoretical line calculated for $r_e = 2.00$ from [1].

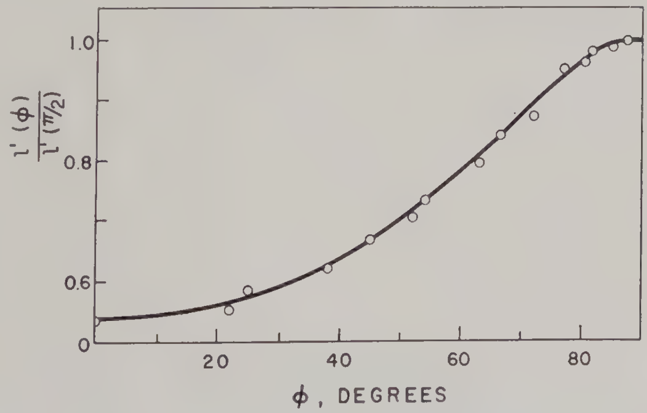

FIG. 5. The variation of $l'(\phi)/l'(\pi/2)$ with ϕ for a rigid cylinder. Here $r_e = 23.4$; $C = 0.63$; $G = 0.298$ sec.$^{-1}$. The curve is calculated from [8].

TABLE I

Periods of Rotations of Fused Doublets

Doublet	Range of G (*sec.*$^{-1}$)	No. of measurements	$TG/2\pi$ (mean)	Mean dev.
A	0.4–2.3	10	2.47	0.01
B	0.2–1.0	9	2.50	0.03
			Mean 2.49	0.02

Collision Doublets

General. The behavior of collision doublets of equal-sized spheres viewed along the Z-axis differs in several respects from that inferred from observations (2, 3) along the Y-axis: the collisions are not sharply defined, the paths of approach and recession are curvilinear, and θ and $d\phi/dt$ vary during the life of the doublet.

The discontinuity in relative motion of the two spheres which appears along the Y-axis to be visually real at "collision" and "separation" (2), and which was confirmed in a further series of experiments in the old Couette apparatus, is not observed along the Z-axis. Instead, the two spheres show a gradual approach until they begin to rotate as a rigid system. As before, separation and recession are observed as the mirror images through the plane $x = 0$ of the initial approach. The y-coordinate of each particle changes when the two are still visibly separated; thus the paths of approach and recession are curved. Finally, there is strong evidence that the spheres

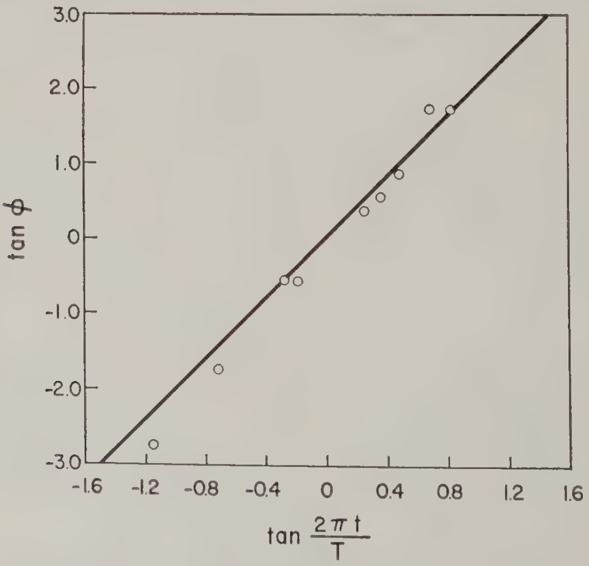

FIG. 6. Rotation of a fused doublet. The straight line is calculated from [1] for $r_e = 2$. $G = 0.330$ sec.$^{-1}$.

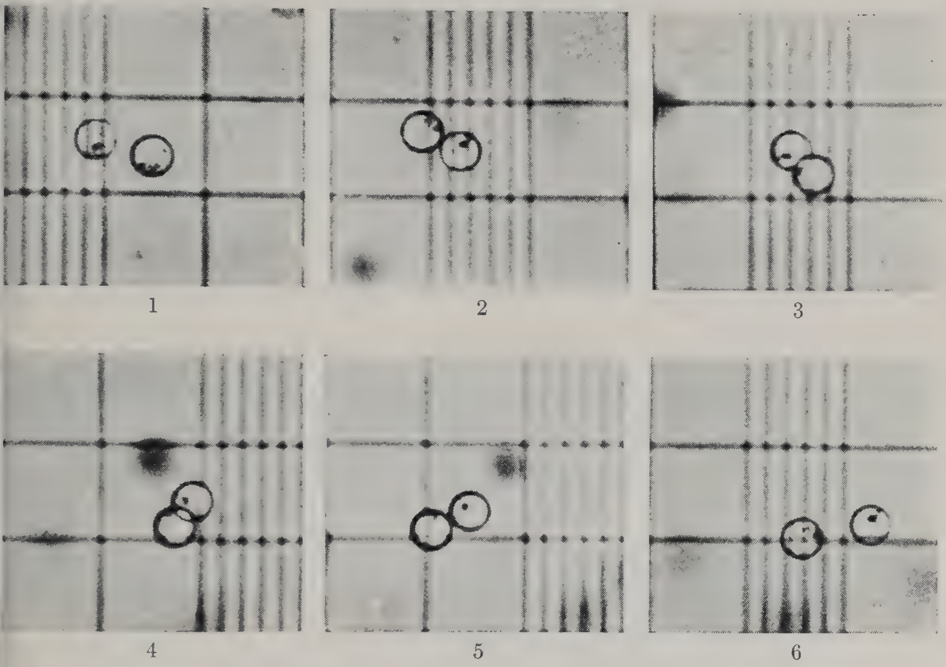

FIG. 7. Photomicrograph of formation and separation of collision doublet. Frames: 1—approach of spheres; 2—apparent contact; 3—before mid-point of collision ($\phi < 0$); 4—past mid-point ($\phi > 0$); 5—mirror-image separation; 6—recession of spheres.

of the doublet are not in true physical contact at any time. A series of photographs of a collision is shown in Fig. 7.

Angular Velocity. Visual observation suggested that during its life a collision doublet rotates with a variable angular velocity $d\phi/dt$ in much the same way as a fused doublet, i.e., as a particle of $r_e = 2$. Since the doublet exists only for a fraction of a complete rotation, T could not be measured. Therefore [1] was written for $r_e = 2$ in the alternative form

$$\tan \phi = 2 \tan \left(\frac{2tG}{5} \right). \qquad [10]$$

It was previously suggested (2) that $r_e = 1$ for a collision doublet, i.e., $d\phi/dt$ is constant and

$$\phi = \frac{2\pi t}{T'}. \qquad [11]$$

Figure 8 shows a plot of ϕ vs. ψ, where in this instance $\psi = tG/5\pi$ (the equivalent of t/T for $r_e = 2$) for five collision doublets. It is seen that the angular velocity is not constant but increases to a maximum at $\phi = 0$ and then decreases, and that the experimental points follow [10] rather than [11].

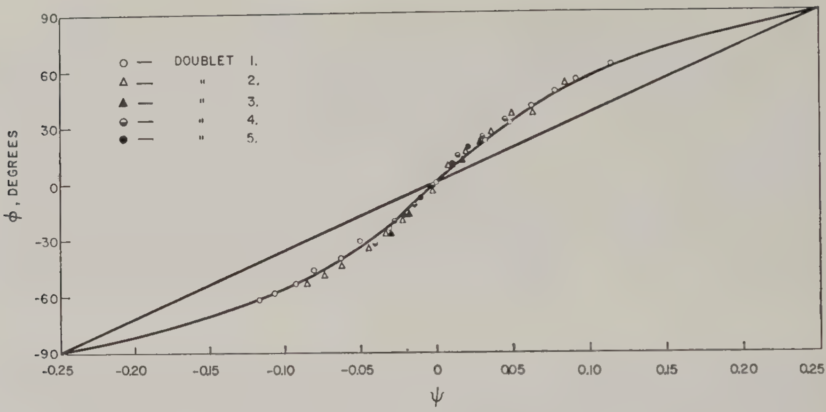

FIG. 8. The variation of ϕ with time for five different collision doublets having various orbit constants. The curve is calculated from [10] for $r_e = 2$, $\psi = Gt/5\pi$. The straight line is calculated from [11] for $r_e = 1$, $\psi = t/T'$. All doublets appeared visually to be in contact, except doublet 5. Orbit details are listed in Table II.

Further evidence of behavior according to [10] is provided by plotting $\tan \phi$ against $\tan (2tG/5)$; this should yield a straight line passing through the origin and having a slope = 2. The agreement between the experimental points for the five collisions given in Fig. 9 and the theoretical line is excellent. A straight line fitted to the experimental data by the method of least squares yields a slope of 2.07 and an intercept of 0.0049 on the ordinate with a standard deviation of 0.045 from this line.

It should be noted that in four of the doublets shown in Figs. 8 and 9, the particles appeared to be in contact. However, the two spheres of the fifth (doublet 5) could be seen to be slightly separated throughout the rotation.

The erroneous conclusion of a constant $d\phi/dt$ in the earlier work (2) is readily explained. The value of ϕ was calculated from the measured displacements Δx and Δz of the particle centers. These measurements proved to be very difficult to make; each pair of values was obtained visually by stopping the apparatus, so that inertial effects may have complicated the phenomena. More serious, however, was the omission of G from the measurements. Instead, a hypothetical period of rotation T' was calculated from the experimental values of the initial angle of contact ϕ_0 and of the doublet life τ using the equation derived from [11]:

$$T' = \frac{\tau\pi}{\phi_0}; \qquad [12]$$

and the values of ϕ calculated from the coordinate measurements were plotted against $\psi = t/T'$ to yield a straight line. When this procedure is followed using the data for the doublets in Fig. 8, the S-shaped curve is

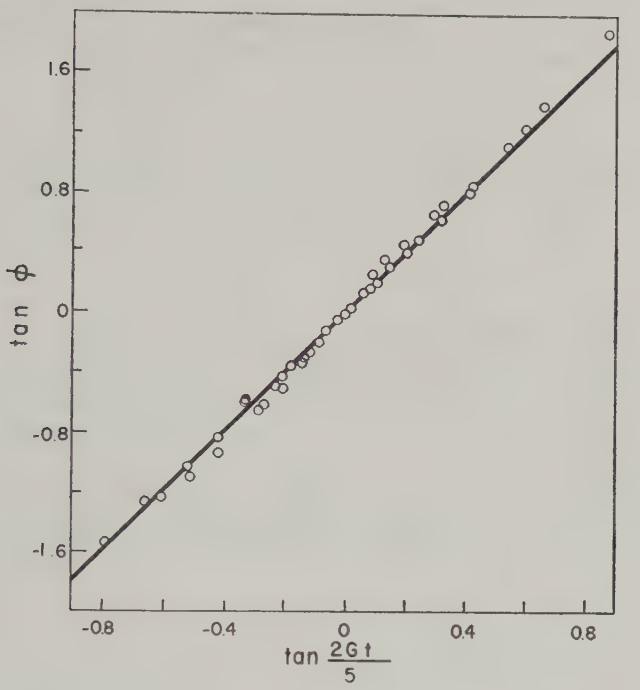

FIG. 9. Tan ϕ vs. tan $2Gt/5$ for the same five collision doublets as in Fig. 8. The straight line is calculated from [10].

expanded along the ψ-axis so that the initial and terminal points are made to lie on the straight line corresponding to $r_e = 1$; as a result of this expansion of the time scale, the remaining points fall close to the straight line, particularly when ϕ_0, as was the case previously (2), is small.

When $r_e = 2$, [2] becomes

$$\tan\theta = \frac{2C}{(4\cos^2\phi + \sin^2\phi)^{\frac{1}{2}}}. \qquad [13]$$

The vertical separation of the outermost points is given by

$$\Delta z_1 = a(1 + \cos\theta). \qquad [14]$$

In the earlier investigation it was reported that θ, and hence Δz_1, remain constant during the life of a doublet. Although both quantities may be expected to vary, the effect is small. Values of θ can be calculated from the measured XY-distance of separation Δd using

$$\Delta d = a\sin\theta \qquad [15]$$

where a is the diameter of each sphere, from which values of C can be obtained by insertion in [13]. Table II gives C and the maximum and

TABLE II

Doublet Orbits

Doublet	Measured values		Calculated values				
				$\phi = 0$		$\phi = \phi_0$	
	a Scale div.	ϕ_0 (*deg.*)	C	Θ_2 (*deg.*)	Δz_1 Scale div.	Θ_0 (*deg.*)	Δz_1 Scale div.
1	30.0	62	1.73	60	45.0	70	41.1
2	28.5	51	1.48	56	44.4	63	42.0
3	30.0	27	0.75	37	54.0	39	53.0
4	26.5	32	2.14	65	37.7	67	36.8

minimum values (corresponding to $\phi = 0$ and ϕ_0) of θ and Δz_1 calculated from [13] and [14], for the four "touching" doublets previously mentioned. It is seen that the variation of θ and Δz_1 is so small that the earlier observation that both were constant was correct within the limits of precision of the measurements.

Doublet History. The continuous approach and recession of two interacting spheres is shown by a typical example in Fig. 10 giving the variation with time of $\Delta x/a$ and $\Delta y/a$, both of which can be measured directly on the photomicrographs.

It is of interest to compare the observed variation of Δx and Δy with that calculated from Jeffery's equations.

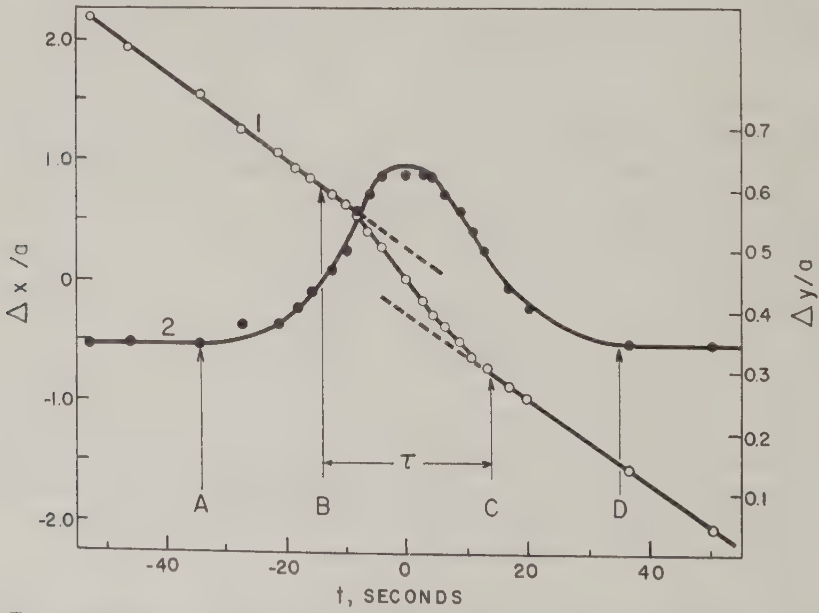

FIG. 10. Measured distance between particle centers along X – (Curve 1) and Y – (Curve 2) axes during approach, collision, separation, and recession. $G = 0.1171$ sec.$^{-1}$.

The variation of Δx is computed as follows:

1. Before and after interaction, the relative velocity of particle centers is

$$\frac{d(\Delta x)}{dt} = G \cdot \Delta y. \qquad [16]$$

2. During interaction, assuming that the distance between particle centers is a, it follows from the geometry (2) that

$$u' = \frac{d(\Delta x)}{dt} = \frac{d}{dt}(a \sin \theta \sin \phi). \qquad [17]$$

For $r_e = 2$, [10], [13], and [17] can be combined to yield u' explicitly as

$$u' = \frac{Ga}{5}\left(\frac{4 + \tan^2 \phi}{1 + \tan^2 \phi}\right) \cdot \left[\frac{6C \sin^2 \phi \cos \phi \cos\theta}{(4 \cos^2 \phi + \sin^2 \phi + 4C^2)(4 \cos^2 \phi + \sin^2 \phi)^{\frac{1}{2}}} + \cos \phi \sin \theta\right] \qquad [18]$$

At the mid-point of the collision, i.e., where $\phi = 0$, [18] reduces to

$$u' = \frac{4}{5} Ga \sin \theta_2 . \qquad [19]$$

The velocity at the mid-point calculated on the basis of the earlier assumption that $d\phi/dt$ and θ remain constant during the life of the doublet is (2)

$$u' = \frac{Ga}{2} \sin \theta_2 \qquad [20]$$

i.e., 5/8 the value given by [19]. Furthermore it was predicted, and appeared to be confirmed experimentally, that u' drops discontinuously at contact from $G \cdot \Delta y$ to $G \cdot \Delta y/2$ with the reverse occurring at separation; the present more reliable observations indicate that u' is continuous throughout the interaction.

Table III summarizes experimental values of u' at the estimated initial

TABLE III

Translational Velocity of Collision Doublets

Doublet	a Scale div.	G (*sec.*$^{-1}$)	ϕ_0 (*deg*)	C	u'/a						
					$\phi = 0$			$\phi = \phi_0$			
					Measured	Eq. [19]	Eq. [20]	Before interaction	After interaction	Eq. [16]	Eq. [18]
6	28.0	0.2111	50	1.73	0.140	0.139	0.087	0.065	0.065	0.068	0.063
7	32.0	0.1171	58	0.86	0.065	0.059	0.037	0.035	0.036	0.037	0.036

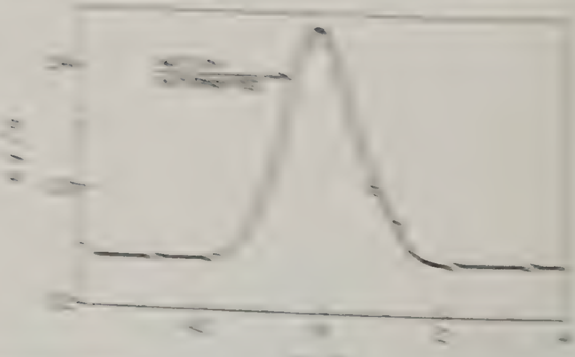

[illegible]

[illegible]

[illegible]	[illegible]	[illegible]
[illegible]	[illegible]	[illegible]
[illegible]	[illegible]	[illegible]
[illegible]	[illegible]	[illegible]
[illegible]	[illegible]	[illegible]
[illegible]	[illegible]	[illegible]
		[illegible]

[illegible]

[illegible]

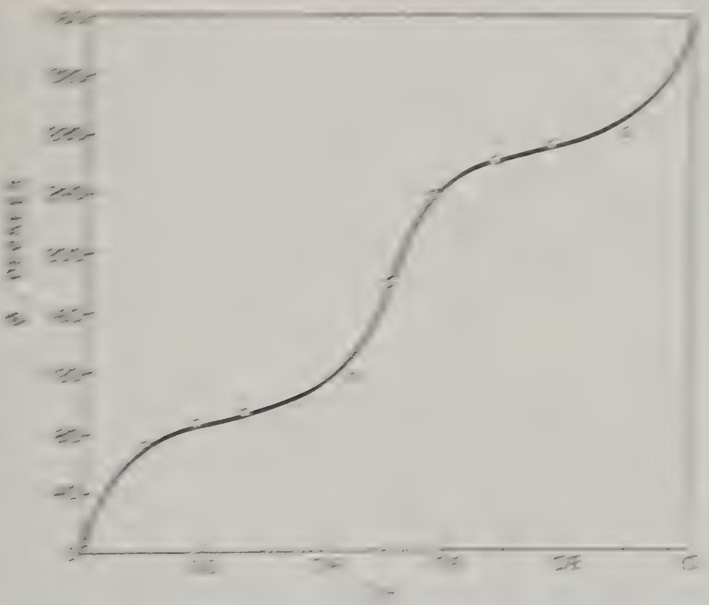

[illegible]

In this instance, however, it is close to the value 3.7 previously found for doublets of touching air bubbles which describe a number of rotations and then coalesce (3). It may be assumed that the mechanism of interaction for head-on collisions of both glass spheres and air bubbles is essentially the same, i.e., continued rotation is induced by the small u', which is insufficient to overcome the hydrodynamic interaction forces. In Fig. 12, ϕ is plotted against t/T for the rotation of a second head-on collision doublet. Here $TG/2\pi = 3.72$, which yields $r_e = 3.42$ from [3]. The graph shows good agreement between the experimental points and the curve calculated from [1]. Similar agreement was previously found for an air bubble doublet (3).

DISCUSSION

The collision mechanism can be summarized as follows:

1. The paths of approach and recession of two interacting spheres are curvilinear without any discontinuity in the motion at interaction. A gradual transition takes place until at sufficiently small distances of separation the doublet rotates as a rigid dumbbell having $r_e = 2$.

2. The doublet rotation is symmetrical about the plane $x = 0$ and after rotation each particle regains its original y- and z-coordinates.

3. The spheres are never in true physical contact. The thickness of the liquid film separating them probably decreases until $\phi = 0$ and then increases symmetrically.

The principal discrepancy in the earlier work (2) was the acceptance of a discontinuity in u' at initial contact and separation. This apparent discontinuity can be seen in the XZ- but not in the XY-plane. It makes interactions easy to observe and was confirmed in the course of making some additional measurements of collision frequency in the old apparatus. The effect must be attributed to an optical illusion probably caused by the manner in which the change in Δy is followed by the change in u' (Fig. 10). As before (2), the measured collision frequencies were within the random statistical error of the calculated values based upon rectilinear approach.

Mooney has stated (8), and has recently provided an analytic proof (9), that the paths of approach and recession are curvilinear and are mirror images of one another and that the spheres do not come into true physical contact. The experimental evidence is in agreement with these predictions.

The rotation of fused and collision doublets, in accordance with Jeffery's equations for prolate spheroids, provides evidence of the immobilization of liquid contained in the cavities (7). It is remarkable that in both cases, and for all orbits except those resulting from head-on collisions, r_e is almost exactly 2 even though the ends of the doublet are not ellipsoidal.

Since $d\phi/dt$ of a collision doublet is variable, it is necessary to revise some of the previously stated concepts concerning the doublet life (2). The expressions for the doublet life, its mean and maximum values, and the distribution function of doublet lives were all based on the assumption that collision doublets rotate as though $r_e = 1$, instead of 2.

The equations, amended to correspond to $r_e = 2$, are given below:

1. During its life the doublet must rotate through the angle $2\phi_0$. It follows from [10] that the corresponding life is

$$\tau = \frac{5}{G}\left[\tan^{-1}\left(\frac{1}{2}\tan\phi_0\right)\right]. \qquad [22]$$

Below $\phi_0 = 73°$ this yields a τ less than, and above it a τ greater than that for $r_e = 1$.

2. Assuming rectilinear approach at constant Δy, Δz until ϕ_0 is reached, the differential and integral distributions with respect to ϕ_0 of collisions (2), taking the limits of ϕ_0 to be 0 and $\pi/2$, are

$$p(\phi_0)d\phi_0 = \sin 2\phi_0 d\phi_0 \qquad [23]$$

and

$$P(\phi_0) = \sin^2\phi_0. \qquad [24]$$

Combining [22] and [23], we obtain for the mean life

$$\begin{aligned}\bar{\tau} &= \int_0^{\pi/2} \tau(\phi_0)\sin 2\phi_0 d\phi_0 \\ &= \frac{5\pi}{6G}.\end{aligned} \qquad [25]$$

3. The maximum life (corresponding to $\phi_0 = \pi/2$) is

$$\tau_{\text{max.}} = \frac{5\pi}{2G}. \qquad [26]$$

This is a hypothetical value only, since, as was discussed earlier, the doublet from a head-on collision behaves quite differently.

4. The integral distribution of lives is obtained by combining [22] and [24] to give:

$$P(\tau) = \sin^2\left[\tan^{-1}\left(2\tan\frac{\tau G}{5}\right)\right]. \qquad [27]$$

The relations for doublet lives corresponding to $r_e = 2$ are given in Table V, and are compared with the expressions previously derived (2). A comparison of $P(\tau)$ is made in Fig. 13.

It must be pointed out that the doublet lives calculated above for $r_e = 2$ apply only for the interval corresponding to BC in Fig. 10. Since a disturbance of Δy takes place well in advance of apparent contact, the above equations do not account for the entire interaction time. Furthermore [25] and [27] are only approximately true since the distribution with respect to ϕ_0 is based on rectilinear approach; for a given doublet this would yield a

TABLE V

Doublet Lives

	$r_e = 1^a$	$r_e = 2$
τ	$4\phi_0/G$	$5/G[\tan^{-1}(1/2 \tan \phi_0)]$
$\bar{\tau}$	π/G	$\frac{5}{6}\frac{\pi}{G}$
$\tau_{\text{max.}}$	$2\pi/G$	$\frac{5}{2}\frac{\pi}{G}$
$P(\tau)$	$\sin^2(\tau G/4)$	$\sin^2(\tan^{-1}[2 \tan (\tau G/5)])$

[a] See reference (2).

value of ϕ_0 greater than is actually observed. This introduces an uncertainty into the values of $\bar{\tau}$ and $P(\tau)$ which cannot be resolved at this time.

The experimental values of $\bar{\tau}$ and $P(\tau)$ previously determined (2) correspond closely to $r_e = 1$. It is believed that this arose from the optical illusion of discontinuous relative motion before ϕ_0 was attained, i.e., at some reproducible time in the intervals AB and CD in Fig. 10, which would tend to make τ larger than the time interval corresponding to BC and given by [22]. The $\bar{\tau}$ corresponding to $r_e = 2$ is 17 % less than for $r_e = 1$, yet in the earlier measurements ((2) Table IV) there was no measurable influence of collisions on the mean period of rotation of single spheres. According to [25] the mean period of rotation of a sphere which spends a portion of its time in doublet form should be decreased by collisions. The experimental results, therefore, suggest that the mean velocity of rotation throughout the entire interaction, i.e., between A and D in Fig. 10, is, within the limits of experimental error of the earlier measurements, the same as that of a free sphere.

In view of these considerations it is concluded that in calculations which involve the doublet life, e.g., the steady-state concentration of doublets (3), it is preferable to use the doublet equations based upon $r_e = 1$.

The distribution of orbital constants C among the collision doublets

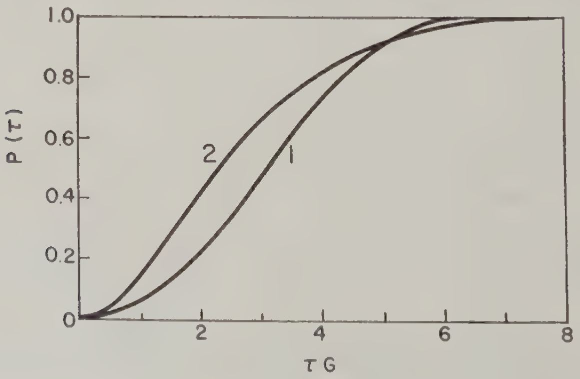

FIG. 13. Distribution $P(\tau)$ of collision doublets. Curve 1 is calculated for $r_e = 1$ (2). Curve 2 is calculated for $r_e = 2$ from [27].

TABLE VI

Distribution of Orbital Constants for Collisions

C	$P(C)$ Eq. [30]	$P(C)$ (Eisenschitz assumption)
0.00	0.000	0.000
0.20	0.001_9	0.044
0.50	0.004_5	0.170
1.00	0.206	0.398
1.50	0.366	0.550
2.00	0.494	0.644
3.00	0.650	0.752
5.00	0.785	—
10.00	0.903	—
∞	1.000	1.000

can be calculated assuming rectilinear approach. Considering for convenience the first octant only, the fraction of collisions in the interval $d\theta_0\, d\phi_0$ at θ_0, ϕ_0 is (2)

$$p(\theta_0, \phi_0)d\theta_0 d\phi_0 = \frac{3}{2}\sin^3\theta_0 \sin 2\phi_0 d\theta_0 d\phi_0 . \qquad [28]$$

Thus the fraction of collisions having orbits less than C is

$$P(C) = \int_0^{\pi/2}\int_0^{\theta_0(\phi_0)} p(\theta_0, \phi_0)d\theta_0 d\phi_0 , \qquad [29]$$

where $\theta_0(\phi_0)$ is given by [13]. On integration [29] yields

$$P(C) = \int_0^{\pi/2}\left[1 - \left(\frac{3\cos^2\phi_0 + 1}{A}\right)^{\frac{1}{2}}\left(\frac{2C^2}{A} + 1\right)\right]\sin 2\phi_0 d\phi_0 \qquad [30]$$

where

$$A = (3\cos^2\phi_0 + 1 + 4C^2).$$

Equation [30] was integrated graphically for various values of C. The numerical values of $P(C)$ are given in Table VI. The distribution calculated from the Eisenschitz assumption of isotropy using methods previously described for rigid ellipsoidal particles (4) is included in the table and is seen to be greater than given by [30].

The distribution $P(C)$ is of importance in refined calculations of the contribution of the collision doublets to the viscosity of a suspension of spheres (10–12). These calculations, however, will not be attempted here.

The interaction phenomena described here are also of interest in connection with particle aggregation, such as flocculation of fibers and coalescence and coagulation in emulsions and aerosols.

ACKNOWLEDGMENT

We wish to express our thanks to Dr. M. Mooney, General Laboratories, U. S. Rubber Co., Passaic, New Jersey, for his kindness in showing us, in advance of publication, his theoretical analysis of the approach and recession of spheres.

SUMMARY

The rotations executed by rigid rods, fused doublets of equal-sized spheres, and the transitory doublets formed by collision of equal-sized spheres suspended in a liquid subjected to laminar shear, have been studied by making observations along the planes of shear. In all cases there is excellent agreement with Jeffery's theoretical equations for rigid prolate spheroids when the equivalent axis ratio r_e is used. For fused and collision doublets, including those in which there is visible separation at all times, $r_e = 2$ except for nearly head-on collisions, when r_e is greater.

Unlike the earlier observations made across the shear planes, the collisions are not sharply defined. The paths of approach and recession are curvilinear and are mirror images of one another. The relative velocities of the two spheres vary continuously and the disturbance occurs well in advance of apparent particle contact. It is concluded that the spheres of the doublet do not touch. Doublets resulting from the rare occurrence of nearly head-on collisions show distinctive behavior with the two particles forming a doublet which executes a number of complete rotations.

The collision doublet behavior differs in several respects from that found in the earlier observations from which it was inferred that the two spheres approach one another on a rectilinear path until they make apparent contact and then rotate with $r_e = 1$ to the mirror-image position of separation. Equations are derived for the mean, maximum, and distribution of doublet lives corresponding to $r_e = 2$.

It is concluded, however, that for many calculations involving doublet life and collision frequency it is preferable to use the doublet equations based upon rectilinear approach and $r_e = 1$.

Finally, the distribution of orbit constants of collision doublets is calculated.

REFERENCES

1. TREVELYAN, B. J., AND MASON, S. G., *J. Colliod Sci.* **6,** 354 (1951).
2. MANLEY, R., ST. J., AND MASON, S. G., *J. Colloid Sci.* **7,** 354 (1952).
3. MANLEY, R. ST. J., AND MASON, S. G., *Can. J. Chem.* **33,** 763 (1955).
4. MASON, S. G., AND MANLEY, R. ST. J., *Proc. Royal Soc.* (*London*), **A238,** 117 (1956).
5. JEFFERY, G. B., *Proc. Royal Soc.* (*London*) **A102,** 161 (1922).
6. MANLEY, R. ST. J., ARLOV, A. P., AND MASON, S. G., *Nature* **175,** 682 (1955).
7. EIRICH, F., AND MARK, H., *Papier-Fabr.* **35,** 251 (1937).
8. MOONEY, M., *J. Colloid Sci.* **6,** 162 (1951).
9. MOONEY, M., Private communication.
10. MANLEY, R. ST. J., AND MASON, S. G., *Can. J. Chem.* **32,** 762 (1954).
11. VAND, V., *J. Phys. & Colloid Chem.* **52,** 277 (1948).
12. BURGERS, J. M., Second Report on Viscosity and Plasticity, pp. 113–184. Academy of Sciences, Amsterdam, 1938.

JOURNAL OF COLLOID SCIENCE **12**, 263-266 (1957)

OBSERVATION OF PROMOTORS FOUND IN CONTACT CATALYSTS

S. Yamaguchi and T. Takeuchi[1]

Scientific Research Institute, Ltd., Hongo, Tokyo, Japan

Received July 30, 1956

ABSTRACT

It is demonstrated by means of electron diffraction at 50 kv. and at 200 kv. that the promotor phase (MgO or NiO) predominates over the catalyst substrate phase (Cu) in the surface of the contact catalyst.

The harder electron waves (wavelength, about 0.02 A) are able to penetrate the rather thick particles (1). On the other hand, the softer electrons (wavelength, about 0.05 A) graze the surfaces of thick particles or penetrate the thin crystallites composed of the light atoms.

Powder of reduced copper combined with magnesium oxide (Mg, one atom %)[2] gave the diffraction patterns shown in Figs. 1(*a*) and (*b*). These two patterns correspond to the harder and the softer electrons (wavelengths, 0.0505 and 0.0266 A), respectively. They were obtained from the same spot in the sample. In Fig. 1(*a*), the diffraction rings characteristic of MgO are more intense than those of Cu. In Fig. 1(*b*), on the contrary, the intensities of the diffraction rings from Cu are stronger than those from MgO. The diffraction intensities estimated in Fig. 1(*a*) and (*b*) are illustrated in Fig. 2(*a*) and (*b*). Change of the diffraction intensity accompanied with that of wavelength is shown here. Figure 3(*a*) is an electron micrograph of the powder of the sample (driving voltage of electrons, about 50 kv.). Figure 3(*b*) is a micro-diffraction pattern observed from a limited field in Fig. 3(*a*). The characteristics of Fig. 3(*b*) are quite similar to those of Fig. 1(*a*) with the softer electrons.

Powder of reduced copper combined with nickel oxide (Ni, one atom %) gave the same diffraction patterns and micrograph as from that combined with MgO. It is concluded from the results here obtained that the MgO

---

[1] Toyama University, Japan.

[2] Reduced copper catalysts combined with the promotors have been prepared by one of the authors (Takeuchi). An aqueous solution containing copper and magnesium (or nickel) nitrates was dried and then calcinated. The mixture of the oxides obtained was reduced with hydrogen at 400°C.

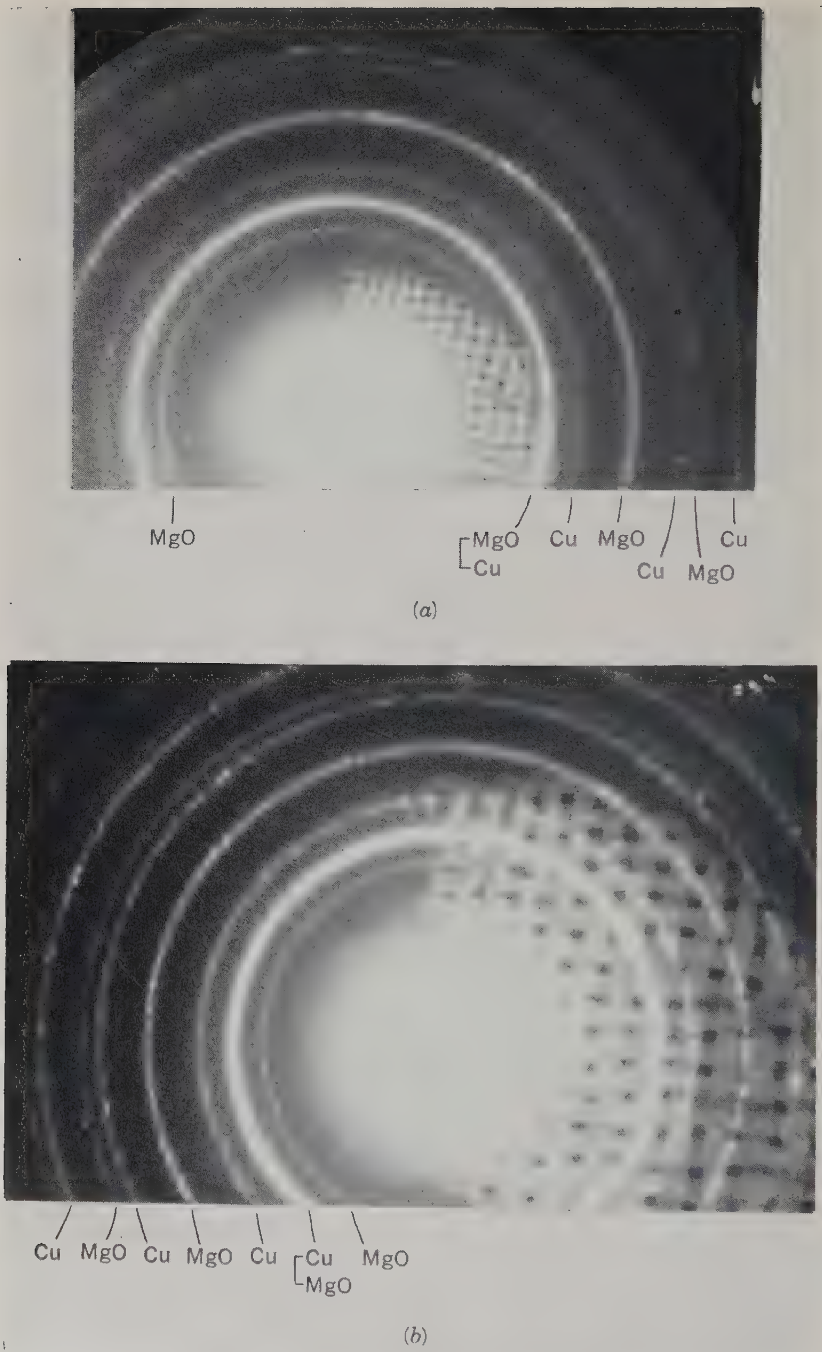

FIG. 1. (*a*) Diffraction pattern from Cu—MgO. Wavelength of electrons, 0.0505 A. Intensities of the rings from MgO are stronger than those from Cu. Camera length, 495 mm. Positive enlarged 2.3 times.

(*b*) Diffraction pattern from the same spot in the sample as for Fig. 1(*a*). Wavelength, 0.0266 A. Intensities of the rings of Cu are stronger than those of MgO. Positive enlarged 4.4 times.

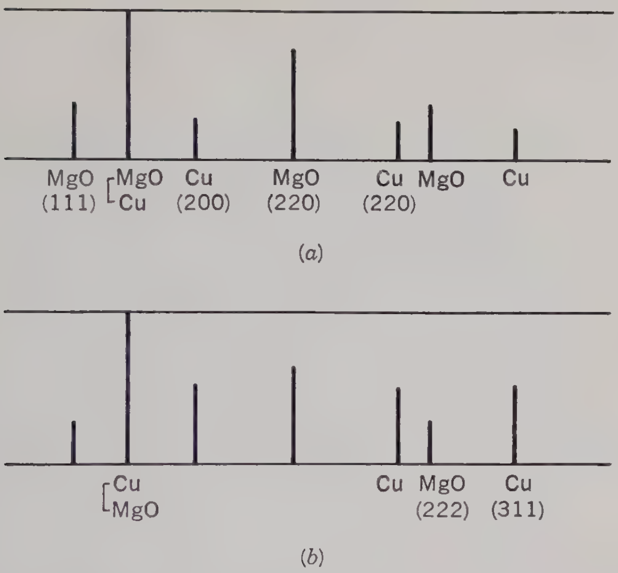

FIG. 2. (*a*) and (*b*) Change of the diffraction intensities accompanied with that of wavelength of incident electrons in Fig. 1(*a*) and (*b*).

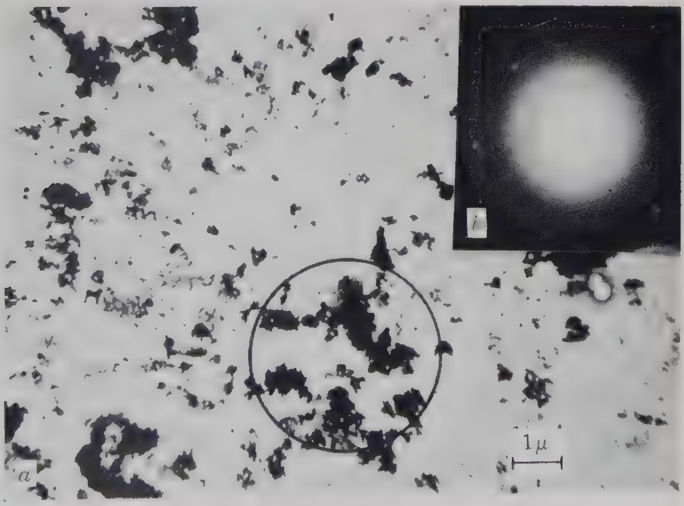

FIG. 3. (*a*) Electron micrograph of powder of Cu—MgO catalyst. (*b*) Micro-diffraction pattern from a limited field in (*a*).

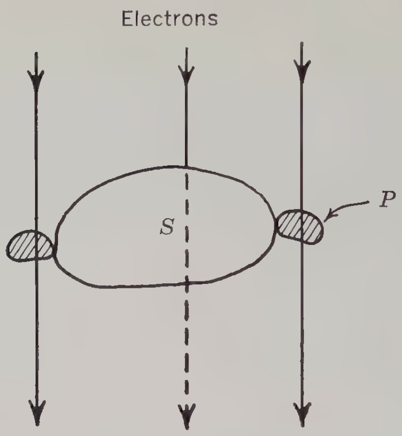

FIG. 4. Possible model of the contact catalyst with promotor. *S*, substrate of catalyst. *P*, promotor.

and the NiO crystallites are situated on the surfaces of the Cu substrates (see Fig. 4).

REFERENCE

1. YAMAGUCHI, S., *J. Appl. Phys.* **25**, 811 (1954).

JOURNAL OF COLLOID SCIENCE **12,** 267–270 (1957)

THE ELECTROVISCOUS EFFECT IN COLLOIDAL SYSTEMS

Pasupati Mukerjee

Department of Chemistry, University of Southern California, Los Angeles 7, California

Received July 31, 1956

Recent communications in this journal on the electroviscous effect in silver iodide (AgI) sols (1–4) and in emulsions (4, 5) have given rise to several important questions regarding the nature of the electroviscous effect in colloidal systems and the validity of its recent theoretical treatment by Booth (6). The present note is an attempt to answer some of these questions and to present a unified picture on the basis of a reinterpretation of experimental results.

The viscosity equation for a very dilute colloidal system can be written as

$$\overset{0}{\eta}_{\text{rel}} = 1 + 2.5\,\varphi\,(1 + f),$$

where $\overset{0}{\eta}_{\text{rel}}$ is the relative viscosity extrapolated to a zero value of φ, the volume fraction of the particles, and 2.5 is the value obtained by Einstein (7) for an ideal system of spherical particles; f measures the deviation from the ideal behavior. This may be caused by factors such as particle asymmetry, hydration, or the electroviscous effect in the case of charged colloids. The value of f obtained by Overbeek *et al.* for the AgI sol over a range of concentration of added electrolytes is 0.38–0.46. In the case of some oil-in-water emulsions van der Waarden obtained values in the range 0.04–1.0. We are concerned with the interpretation of these values.

It is important to mention at this point that we are interested in the first-order electroviscous effect only. This involves particle-solvent interactions alone and not particle-particle interactions. This effect must, therefore, be detected and estimated only at infinite dilution of the particles.

In the original paper (2) and its correction (3) Overbeek *et al.* attribute the deviation of the viscosity behavior from Einstein's relation in the case of the AgI sol to particle asymmetry. As the revised estimates of the corrections calculated according to Booth's theory are high (3), when reasonable values of the ζ-potential are assumed, the authors concluded that the theory fails for the AgI system. The electroviscous effect can be expressed as a power series in the ζ-potential of which the term in ζ is zero and the term in ζ^2 has been evaluated by Booth (6). The higher terms are unknown at present. Overbeek *et al.* ascribed the discrepancy between theory and experiment to Booth's neglect of the higher terms in the series. This suggests that some of the higher terms can compensate for the term in ζ^2 in such a fashion as to reduce the predicted value for certain values of the ζ-potential. This line of reasoning leads us to the extremely unlikely result of a decrease in the electroviscous effect with increasing values of the ζ-potential since the higher terms become progressively more important as the value of ζ increases. It is possible that still higher terms may exert enough influence to prevent this. But then one must conclude that Booth's treatment must be extremly inadequate since it treats only the first term of a series, which, at best, is poorly converging. But then it becomes difficult to explain the success with which Booth's theory applies to proteins (6, 8, 9), emulsions (as shown below), and micelles of sodium lauryl sulfate (10), for which values of f from 0.2 to 0.8 are predicted and experimentally verified for ζ-values of the order of 100 mv.

On the other hand, the explanation of the deviations for AgI sol in terms of particle asymmetry is not adequate. The experimental values of f (0.38–0.46) require average axial ratios between 2.5 and 3 (11) if the particles are ellipsoids of revolution. Such axial ratios can be detected easily in electron micrographs. The pictures published by the authors (1) show no such deviation from sphericity. The authors, themselves, concluded from their shadowing experiment that the particles are not far from spherical. We are thus forced to conclude that particle asymmetry cannot explain all the observed value of f, although it may make a small contribution, since the particles may be jagged or angular.

A second attempt has been made to explain the behavior of AgI sol in terms of an "apparent volume increase" during flow (4, 5). This idea originated with the work of van der Waarden with emulsions (5). It is suggested that this increase is due to an immobilization of the solvent around the particle as a result of the electric field present. van der Waarden discounted the possibility of any significant contribution to the factor f of a first-order electroviscous effect in the classical sense, as treated by Smoluchowsky (12), Krasney-Ergen (13), and Booth (6), on the grounds that the effects predicted by these theories, as calculated by Overbeek *et al.* for the AgI sol, are small (2). The revised calculations (3) are, however, far from small and indeed, for the emulsions studied by van der Waarden, the electroviscous effect expected according to Booth's theory is very large. This is because the electroviscous effect increases with increasing thickness of the double layer and hence decreasing electrolyte concentration. In the emulsions studied by van der Waarden the only electrolyte in the system, aside from contaminations, was in the form of the emulsifier, which was added as a fixed fraction of the emulsified oil. At infinite dilution of the latter, when this first-order electroviscous effect is estimated, the concentration of the electrolyte could only have been that present in the water as an impurity and must have been very small.

To illustrate further that Booth's theory of the first-order electroviscous effect can account for the experimental results sufficiently well we have computed the factor f according to Booth for several assumed values of electrolyte concentration and of ζ-potential. The emulsion which gave the highest value of f (0.92–1.00) and had a particle radius 138 A. was chosen. The critical micelle concentration of this emulsifier in water was reported to be 0.015% (5). The maximum concentration of the emulsifier in the aqueous phase was probably not much higher than this. The probable concentration for these dilute emulsions was much less and previous work of van der Waarden (14) indicates that it may have been lower than 0.001%. To calculate Booth's values the equivalent conductivity of sodium was taken to be 50 and that of the sulfonates to be the same as for the lauryl sulfate ion, 21.6 (15). Since the average molecular weight of the sulfonates was 475 (5) as compared to 288 for sodium lauryl sulfate, this is probably an overestimate which lowers the calculated f values.

Table I shows that for ζ-values between 75–125 mv. the Booth factor f can be as high as the experimental value even for relatively high concentrations of emulsifier in the aqueous phase. The emulsified oil had an ionized monolayer on its surface and thus resembled soap micelles for which ζ-values of over 100 mv. for about 0.01 *M* electrolyte concentration have been estimated (16). Such potentials are, therefore, not unlikely for the emulsions.

It is apparent from the above that the classical electroviscous effect and Booth's treatment of it can account for the maximum effects observed with emulsions under reasonable assumptions. It is, therefore, unnecessary to postulate any novel effect such as a volume increase during flow. It is also apparent that the effects are so large that a more detailed study of the emulsion system should be of great interest.

In the case of the AgI sol the observed values of f are of the same order as predicted by Booth's theory for reasonable values of the ζ-potential (3). The only reason why the observed effect has not been interpreted as an electroviscous effect seems to be the fact that the values of f obtained did not seem to decrease with electrolyte concentration as they must for an electroviscous effect. The experimental data, however, show wide scatter, especially at low concentrations of the sol. For the higher electrolyte concentrations [solution 6 or higher, ref. (1)] the f values show definite

TABLE I

The Factor f *According to Booth*

Emulsifier conc. in water	**ζ = 75 mv.**	**ζ = 100 mv.**	**ζ = 125 mv.**
0.015%	0.4	0.7	1.1
0.010%	0.4	0.8	1.2
0.005%	0.5	0.9	1.4
0.002%	0.7	1.2	1.8

and pronounced increases at low concentrations making extrapolation impossible. Even for solution 4 such an increase is discernible. For this solution, within the uncertainties estimated by the authors, it is possible to extrapolate so as to obtain an f value of 0.28. Because of such uncertainties coupled with the neglect of the non-Newtonian factor in the viscosities (1) it seems difficult to conclude definitely from the data whether f decreases with electrolyte concentration or not. Thus the only objection against the applicability of Booth's theory for the explanation of the viscosity behavior of AgI sol is uncertain. Since the alternative explanations offered are unsatisfactory, we feel that Booth's theory gives a sufficiently good account of the experimental results within the limits of the various uncertainties.

To summarize: The experimental results for emulsions and AgI sol can be interpreted as a first-order electroviscous effect; the values show that this effect can be large; the classical interpretation of the electroviscous effect and its theoretical treatment by Booth account for the experimental data satisfactorily as in the case of proteins (8, 9) and soap micelles (10); and it is unnecessary to postulate or reinterpret the electroviscous effect as a new phenomenon involving immobilization of solvent molecules around the charged colloidal particles.

This communication is based on a proposition submitted for the Ph.D. qualifying examination at the University of Southern California in 1954. The author acknowledges gratefully the help and encouragement of Professor Karol J. Mysels.

References

1. Harmsen, G. J., van Schooten, J., and Overbeek, J. Th. G., *J. Colloid Sci.* **8,** 64 (1953).
2. Harmsen, G. J., van Schooten, J., and Overbeek, J. Th. G., *J. Colloid Sci.* **8,** 72 (1953).
3. Harmsen, G. J., van Schooten, J., and Overbeek, J. Th. G., *J. Colloid Sci.* **10,** 120 (1955).
4. Harmsen, G. J., van Schooten, J., and van der Waarden, M., *J. Colloid Sci.* **10,** 315 (1955).
5. van der Waarden, M., *J. Colloid Sci.* **9,** 215 (1954).
6. Booth, F., *Proc. Roy. Soc.* (*London*) **A203,** 533 (1950).
7. Einstein, A., *Ann. Physik* **19,** 289 (1906); *ibid.* **34,** 592 (1911).
8. Tanford, C., and Buzzell, J. G., *J. Phys. Chem.* **60,** 225 (1956).
9. Buzzell, J. G., and Tanford, C., *J. Phys. Chem.* **60,** 1204 (1956).
10. Unpublished calculations to be communicated shortly.
11. Oncley, J. L., *Ann. N. Y. Acad. Sci.* **41,** 121 (1941); Alexander, A. E., and Johnson, P., Colloid Science, p. 367. Oxford University Press, 1949.
12. Smoluchowski, M. V., *Kolloid-Z.* **18,** 194 (1916).
13. Krasney-Ergen, W., *Kolloid-Z.* **74,** 172 (1936).
14. van der Waarden, *J. Colloid Sci.* **7,** 140 (1952).
15. Williams, R. J., Phillips, J. N., and Mysels, K. J., *Trans. Faraday Soc.* **51,** 728 (1955).
16. Stigter, D., and Mysels, K. J., *J. Phys. Chem.* **59,** 45 (1955).

JOURNAL OF COLLOID SCIENCE **12**, 271–282 (1957)

PHOTOCHEMICAL PROCESSES IN SOLIDS: THE KINETICS OF FREE RADICAL REACTIONS IN NYLON

Roger A. Ford

Research Department, British Nylon Spinners Ltd., Pontypool, Monmouthshire

Received September 28, 1956

ABSTRACT

The formation in nylon films of an absorption center at 2900 A. by the action of ultraviolet light is reported. The processes involved are found to be free radical in nature and the suggestion is made that this center is either an alkyl or acyl peroxy radical. The kinetics of absorption center formation have been studied using a spectrophotometric technique. It is found that the peculiarities of the system are the result of the difference in order between gaseous and radical diffusion rates in a high polymer. The usefulness of polychromatic light in this type of work is pointed out. Finally, the possibility of using nylon films as a matrix for the study of free radicals at room temperature is mentioned.

INTRODUCTION

The effects of radiation on high polymers have become a matter of considerable commercial importance. Much work has been carried out on the effects of ionizing radiation with a view to changing the physical properties of certain high polymers. Meanwhile, the deleterious effects of ultraviolet light on the weathering properties of sheets and fabrics of fiber-forming polymers have been a long-standing subject for industrial research. Although considerable success in reducing the photodegradation caused by sunlight has been achieved by empirical approaches, a more fundamental understanding of solid-state photochemistry is needed.

The embedding of the site of quantum absorption in a solid matrix is likely to exert a profound effect on both the primary photochemical and secondary thermal processes that result from such absorption. One might expect the quantum efficiency of dissociation in solids to be lower than in liquids or in the gas phase. The primary recombination effect of Franck and Rabinowitch (1a, b), which is a direct consequence of the interaction of encounter frequencies with the rates for transfer of kinetic energy in condensed media (in the gas phase collisions and encounters are identical), should be particularly effective in solids.

From the general values for diffusion coefficients in liquids and solids, calculation gives the encounter duration as $\sim 10^{-10}$ sec. in liquids, and $\sim 10^{-6}$ sec. in solids. Also Rabinowitch (2) has shown that the average frequency of collisions between two reference molecules increases with increasing density of the medium, though not steeply. Since encounter duration and the primary quantum yield, ϕ, should be inversely related, a reduction of ϕ by several orders of ten would appear normal for a change from the liquid to solid phase.

However, what small amount of work has been done in rigid media (3a, b) has shown that free radicals may be quite readily formed and subsequently trapped for long periods. Moreover, the periods of irradiation necessary and the primary quantum yields in all cases so far investigated seem comparable to those in the liquid phase (4). It would appear, therefore, that some anomalies may be expected in the rates of kinetic energy transfer in solids, to explain this discrepancy. Unfortunately, little can be said about this at the present time, as our knowledge of such energy transfer processes is virtually nonexistent.

The low diffusion rates in a solid should also influence the kinetics of the secondary thermal processes that occur after free radical formation. Here, nonuniform distribution of the reaction intermediates makes it necessary to derive the local rate equations for an infinitesimal volume dV, and then integrate over the irradiated volume to derive the expression for the observed rate. Wilson (5) has carried out a theoretical treatment on a set of such cases using the Laplace transformation technique. These considerations should be of particular importance in high polymeric solids. For here, the radicals may be attached to the end of polymer chains, which should have exceedingly low rates of diffusion. On the other hand, the rates of gaseous diffusion in high polymers are relatively high, being $\sim 10^{-5}$ cm.^{2} sec.$^{-1}$, for inert gases such as N_2, O_2, and CO_2 (6) (i.e., of similar order to diffusion processes in liquids). This, we shall suggest, may be the reason for further kinetic peculiarities.

During the course of some work recently reported (7), it was noted that nylon films developed a new absorption band at 2900 A. on irradiation by ultraviolet light. This new band increased in intensity when the films were stored in the dark after irradiation and decreased again on reirradiation to its value immediately prior to storage, before increasing further. From the presence of a dark reaction, it seemed most probable that this absorption center formation was controlled by free radical processes in the solid. Accordingly, experiments on the kinetics of absorption center formation were undertaken in the hope that they might yield information on the nature of the absorption center and on free radical processes in high polymers.

EXPERIMENTAL MATERIALS

To be suitable for our purpose, a polymer must be capable of forming a transparent glassy film to avoid the complication of radiation scattering.

Experience has shown that this is best obtained using copolyamides. Thus films were prepared from a 10% formic acid solution of a copolymer consisting of nylons 6.6, 6, and 6.10, in the proportions 40:30:30, respectively. This solution was spread on a glass plate and the solvent rapidly evaporated off in an air oven at 90°C. In this manner clear films, ~20 μ thick, were obtained, which could be stripped from the glass without damage.

Kinetics of Absorption Center Formation

The formation of absorption centers has been studied using the radiation from an unfiltered Hanovia S.250 Hg arc. Specimens were placed in a reproducible position, 1 foot distant from the source, inside a quartz vessel to prevent attack by ozone. Periods of irradiation up to 200 hours were used. The optical densities (O.D.) of the specimens were measured at various times using a Unicam SP.500. All O.D.'s were corrected for light scattering (by extrapolation of the transmission in the visible region

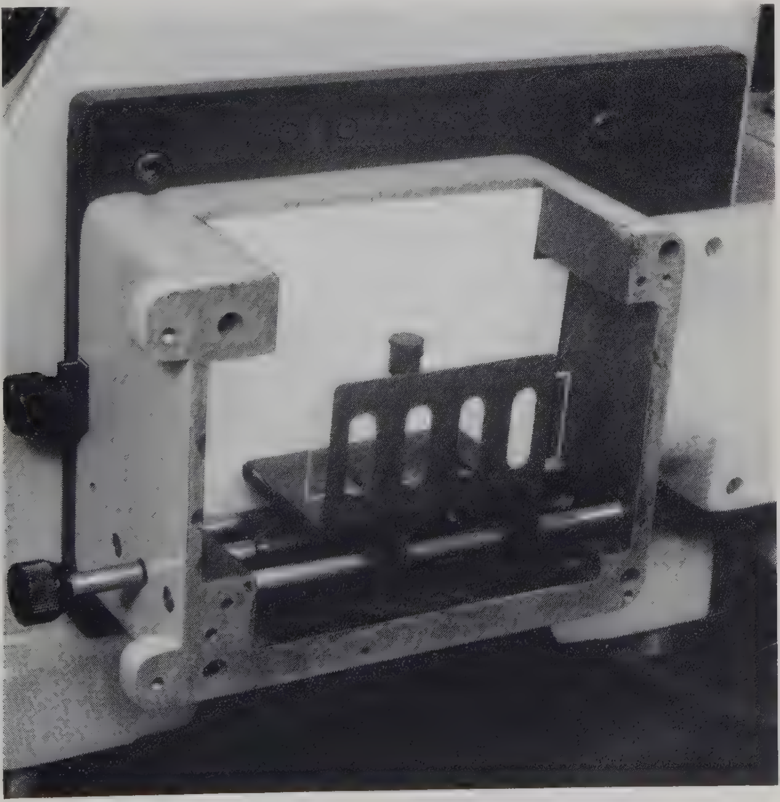

FIG. 1. Film holder for use with Unicam SP.500.

where no absorption bands exist). The specimens were mounted in aluminum foil holders, which were accurately placed in a special film holder built for use with the Unicam SP.500 (Fig. 1).

This has been designed to place the films as near as possible to the photocell window so that light-scattering losses may be minimized.

RESULTS

Spectrum of an Irradiated Nylon Film

Figure 2 shows the absorption spectrum of a nylon film *A*, before, and *B*, after, irradiation for 60 hours. Initially the film shows absorption only below 2400 A. owing to the singlet $\pi \rightarrow \pi$ and $n \rightarrow \pi$ transitions of the —CONH— group, which are centered around 1950 and 2100 A., respectively (11). On irradiation a new band appears around 2900 A., which is quite clearly resolved. There is also some increase in O.D. at shorter wavelengths. This may be associated with the band at 2900 A. or may be due to other products; at present it is impossible to decide. Spectrum *C* (Fig. 2) is of the same film after it has been stored in the dark until no further change in O.D. was detectable. One can see from these spectra that there is no suggestion of a different product's being formed during storage.

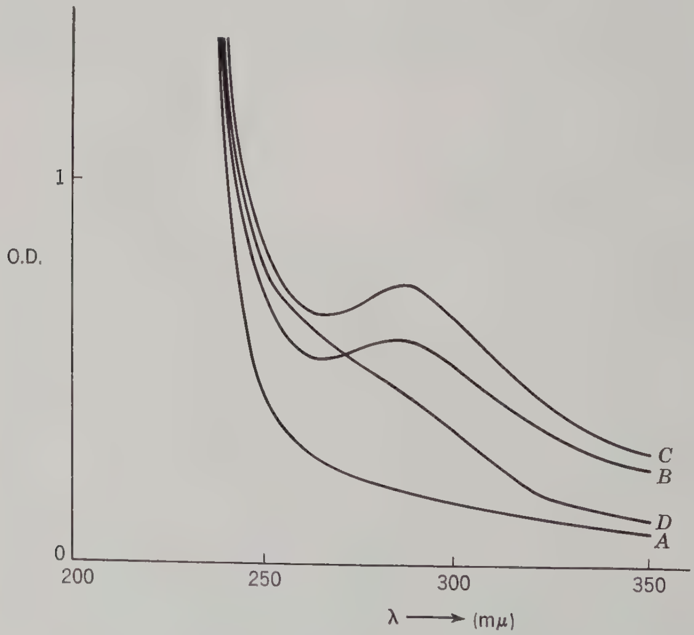

FIG. 2. Spectrum of nylon film: (*A*) before irradiation; (*B*) immediately after irradiation (80 hours); (*C*) after storage in the dark for 24 hours after irradiation; (*D*) irradiated film after dissolving and recasting from H·COOH.

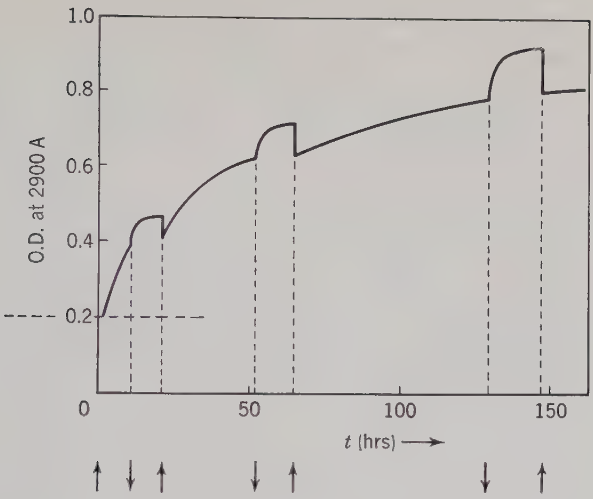

FIG. 3. Variation in O.D. of nylon film during periods of irradiation and storage in the dark. (Light on ↑ ; Light off ↓).

Kinetics of Absorption Center Formation

Measurements of O.D. at 2900 A. have been made at various intervals for irradiation periods up to 200 hours. After this the spectrum was changing only slowly with time. Readings were made at short intervals (~5 min.) during the periods immediately after the termination and recommencement of irradiation, because of the rapidity of the O.D. change over the periods. Figure 3 shows the values of O.D. at 2900 A. as a function of time during periods of irradiation and storage. The initial absorption at 2900 A. is due to the "tail" of the amide $\pi \rightarrow \pi$ and $n \rightarrow \pi$ transitions.

Four general features of absorption center formation may be drawn from the above data.

1. Irradiation causes the formation of a new band at 2900 A.

2. If, after irradiation, films are stored in the dark, this band increases in intensity with an initial rate greater than that immediately prior to storage.

3. On reirradiation the band intensity falls rapidly to a value corresponding to that immediately prior to storage.

TABLE I

Irradiation period (*hours*)	ΔO.D.$_{2900\text{ A.}}$ in light	ΔO.D.$_{2900\text{ A.}}$ in dark	$\dfrac{\Delta\text{O.D.}_{2900\text{ A.}}\text{ in light}}{\Delta\text{O.D.}_{2900\text{ A.}}\text{ in dark}} = R$
30	0.265	0.065	4.08
60	0.365	0.095	3.84
70	0.382	0.098	3.90
100	0.500	0.120	4.17
180	0.670	0.170	3.94

4. The increase of the band intensity during storage appears to be a constant fraction of its total intensity throughout the reaction, as shown in Table I. This behavior can be accounted for most satisfactorily in terms of the scheme detailed below.

Reactions	Rates
1. $A + h\nu_1, \xrightarrow{k_{\epsilon_1}} B° + C°$	$k_{\epsilon_1}I_1$
2. $B° + M \xrightarrow{k_2} BM°$	$k_2[B°][M]$
3. $BM° + h\nu_3 \xrightarrow{k_{\epsilon_3}} B° + M$	$k_{\epsilon_3}I_3[BM°]$

A is the nylon substrate, B° and C° free radicals, M some molecular species, BM° the absorption center at 2900 A., and I_1 and I_3 the light intensities at frequencies ν_1 and ν_3, respectively.

Then assuming Beer's law:

$$\frac{d[B°]}{dt} = k_{\epsilon_1} I_1 - k_2[B°][M] + k_{\epsilon_3} I_3[BM°] \qquad [1]$$

and

$$\frac{d[BM°]}{dt} = k_2[B°][M] - k_{\epsilon_3} I_3[BM°]; \qquad [2]$$

adding [1] and [2] and integrating, assuming $[BM°] = 0$ and $[B°] = 0$ at $t = 0$,

$$[B°] + [BM°] = k_{\epsilon_1}I_1 \cdot t \qquad [3]$$

Then

$$\frac{d[BM°]}{dt} = k_2[M]k_{\epsilon_1} I_1 \cdot t - [BM°]\,(k_2[M] + k_{\epsilon_3} I_3;$$

$$[BM°] = \frac{k_2[M]\, k_{\epsilon_1} I_1}{(k_2[M] + k_{\epsilon_3}I_3)^2}\{e^{-(k_2[M]+k_{\epsilon_3}I_3)t} + (k_2[M] + k_{\epsilon_3} I_3)t - 1\}; \qquad [4]$$

and

$$\frac{d[BM°]}{dt} = \frac{k_2[M]\, k_{\epsilon_1} I_1}{k_2[M] + k_{\epsilon_3} I_3}\{1 - e^{-(k_2[M]+k_{\epsilon_3}I_3)t}\}. \qquad [5]$$

When $(k_2\,[M] + k_{\epsilon_3}I_3)t \gg 1$, i.e., as t increases, the exponential terms in Eqs. [4] and [5] tend to zero (rapidly if $(k_2M + k_{\epsilon_3}I_3) \gg 1$) and from [5]

$$\frac{d[BM°]}{dt} = \left(\frac{1}{1 + k_{\epsilon_3} I_3/k_2[M]}\right) k_{\epsilon_1} I_1 . \qquad [6]$$

From [4]

$$[BM°] = \left(\frac{1}{1 + k_{\epsilon_3} I_3/k_2\,[M]}\right) k_{\epsilon_1} I_1 \cdot t. \qquad [7]$$

Substituting [3] into [7]

$$[\mathrm{B}^\circ] = k_{\epsilon_1} I_1 t \left(1 - \left(\frac{1}{1 + k_{\epsilon_3} I_3/k_2\,[\mathrm{M}]}\right)\right);$$

therefore

$$\frac{[\mathrm{BM}^\circ]}{[\mathrm{B}^\circ]} = \frac{k_2[\mathrm{M}]}{k_{\epsilon_3} I_3} = R. \qquad [8]$$

Effect of Intermittent Light

(Here we are dealing with periods of relatively long duration, i.e., not of the order of the mean lifetimes of the radicals involved, when different kinetic effects may result (8).)

Values of R may be determined since $[\mathrm{BM}^\circ]$ is proportional to the intensity of the 2900 A. band in the light, whilst $[\mathrm{B}^\circ]$ is proportional to the further increase in intensity of this band on storage in the dark. Values of R are given in Table I. The constancy we have found for R over irradiation periods from 30 to 180 hours shows that for such periods we are justified in using the approximate Eqs. [6] and [7].

When the light is cut off photoreactions 1 and 3 should cease, leaving reaction 2 to convert the remaining B° into BM° during storage. Then since $\frac{d\,[\mathrm{BM}^\circ]}{dt}$ initially increases on cutting off the light (see Fig. 3), $k_2\,[\mathrm{M}] > k_{\epsilon_1} I_1$ and $k_{\epsilon_3} I_3 > k_{\epsilon_1} I_1$ because $\frac{d\,[\mathrm{BM}^\circ]}{dt}$ initially goes negative on reirradiation after storage. Therefore reaction 1 will be rate-limiting during irradiation.

Effect of Light Intensity

For a fixed light intensity we have found R to be constant so we may rewrite [6] as

$$\frac{d[\mathrm{BM}^\circ]}{dt} = \left(\frac{1}{1 + KI_3}\right) k_{\epsilon_1} I_1, \qquad [9]$$

where

$$K = k_{\epsilon_3}/k_2\,[\mathrm{M}] = \text{a constant.}$$

Thus, it may readily be seen that with I_3 constant $\frac{d[\mathrm{BM}^\circ]}{dt}$ will be linear with respect to I_1. On the other hand, if I_1 is now constant, $\frac{d[\mathrm{BM}^\circ]}{dt}$ will be related to I_3 by the complex function $\left(\frac{1}{1 + KI_3}\right)$. A model showing the rate surface to be expected from this behavior is shown in Fig. 4.

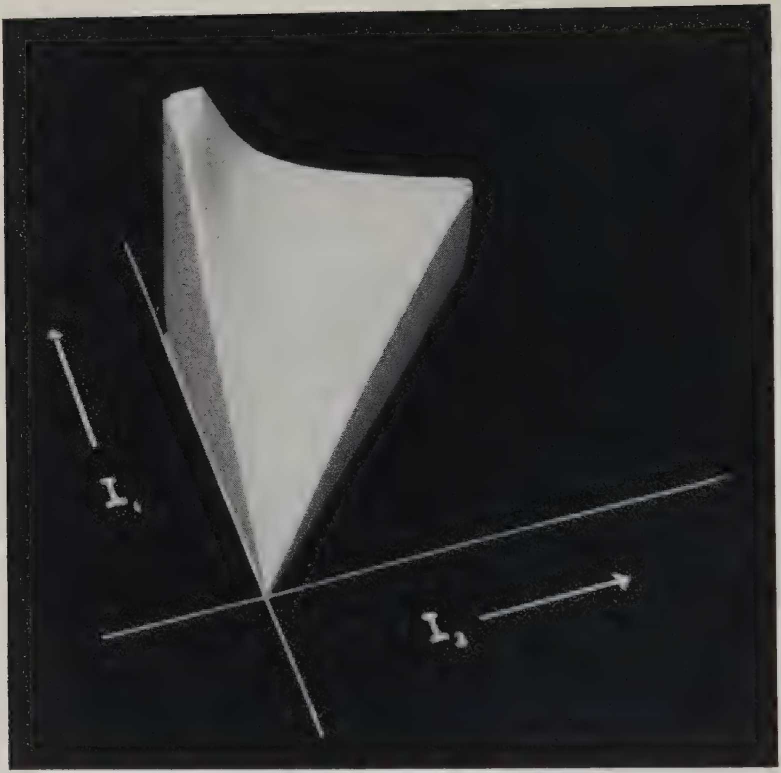

Fig. 4. Solid model showing the rate surface for BM° formation with variation of light intensities I_1 and I_3. The diagonal cross section describes the condition when I_1 and I_3 are varied in proportion.

Equation [9] also predicts that the overall rate of absorption center formation should be a constant at a given light intensity. However, Fig. 3 shows that the rate decreases with the period of irradiation. It is suggested that this is due to an optical "inner filter" effect as strongly absorbing products begin to compete with A for the incident light. The constancy of R shows that the decrease is not connected with reactions 2 and 3. If we are to test the above kinetic scheme by varying the light intensity it is necessary, therefore, to assume that for given periods of irradiation the concentration of the species causing the "inner filter" will be proportional to the incident intensity, i.e., the incident energy utilized by the initial photolysis reaction integrated over the period of irradiation will be proportional to the incident intensity. Since the formation of this species is almost certainly dependent on the free radicals formed in reaction 1, this appears to be a reasonable assumption.

The system we have to study is one in which two substances are under-going simultaneous photolysis. There is a difficulty here, in that it is unlikely that a separation of the two reactions will be possible using monochromatic light.

Unless the frequency difference between the two absorption processes is large, the ability of the dissociated particles to carry away increments of excess kinetic energy will result in the higher frequency radiation's being active for both reactions. Also, dissociation via the higher excited states of the molecule which absorbs at the lower frequency may be possible. Under such conditions the most practical procedure is (rather than working with monochromatic light) to work with polychromatic light so that I_1 and I_3 are varied in proportion. It may readily be seen from [7] that under these conditions [BM°] has a complex depending on light intensity, tending to a limit $\frac{k_{\epsilon_1} I_1}{K I_3} \cdot t$ at high light intensities. If I_1 and I_3 are varied so that $I_3/I_1 = \omega$ (a constant)

$$[\mathrm{BM}^\circ] = \left(\frac{1}{1 + KI_{1\omega}}\right) k_{\epsilon_1} I_1 \cdot t$$

and

$$\frac{[\mathrm{BM}^\circ]}{k_{\epsilon_1} I_1 \cdot t} = \frac{-k\omega[\mathrm{BM}^\circ]}{k_{\epsilon_1} \cdot t} + 1.$$

Thus for fixed periods of irradiation [BM] should show a linear dependency on $[\mathrm{BM}^\circ]/I_1$, which has the form of a quantum efficiency, ϕ. This we have observed to be the case with films of nylon as is shown in Fig. 5.

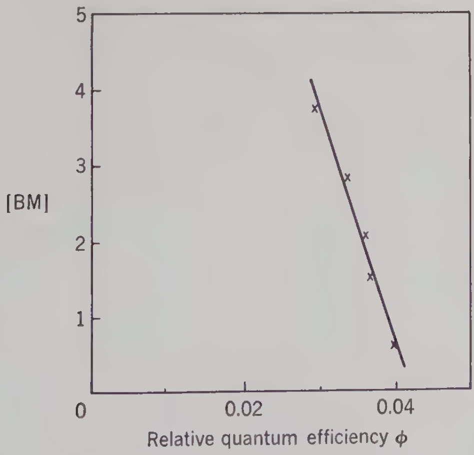

FIG. 5. Plot of [BM°] against [BM°]/I. ([BM°] measured as ΔO.D. at 2900 A. of irradiated nylon film.)

DISCUSSION

The Nature of the Absorption Center at 2900 A.

The presence of a "dark" reaction, together with the agreement of our results on light intensity variation with the proposed kinetic scheme, supports the view that the absorption center is free radical in nature. The problem is to ascertain the nature of the species M in reaction 2.

$$B^\circ + M \rightarrow BM^\circ$$

From our results we know that for a fixed light intensity, R, and therefore M also, is constant throughout the reaction. The possibility of M being another free radical is therefore removed. It remains that M is either the surrounding polymer matrix or some gaseous component such as oxygen.

Of these two alternatives, the latter appears more promising. We know that the rates of gaseous diffusion in high polymers are relatively high, and this would be consistent with the relative rapidity of reactions 2 and 3. In particular, if M were the polymer matrix, we should expect the photolytic reaction [3] to be hindered by diffusion similarly to reaction 1, but this is not observed. We suggest, therefore, that the absorption center is the peroxy radical BO_2°, where B is a long-chain alkyl or acyl group. Such radicals may be expected to show the photoinstability necessary to explain reaction [3].

Peroxy radicals have been postulated for many years as intermediates in organic oxidations (9a, b), but as yet it appears that they have never been detected spectroscopically. The possible identification of the 2900 A. band with this free radical is therefore of considerable interest.

We have attempted to confirm this assignment by carrying out the irradiation of films in a high vacuum cell to exclude oxygen. In this case a general increase in absorption was observed over the 2500 to 3000 A. region, which also showed a further increase in the dark. However, no clear peaking at 2900 A. was observed and the intensity did not fall on reirradiation after storage, as is shown in Fig. 6. We believe this general absorption to be due to the products of alternative free radical reactions that occur in the absence of oxygen, but this is being investigated further. Also, if the absorption center is a free radical, the 2900 A. band should disappear when the film is dissolved. The spectrum of an irradiated film that has been dissolved and recast from formic acid is shown in Fig. 2 (*D*). From this it may readily be seen that the band, apart from some general increase in absorption, has indeed disappeared. However, it should be mentioned that some finely divided gelatinous material separated out on dissolving, which could be associated with this band, but it seems impossible to check this directly.

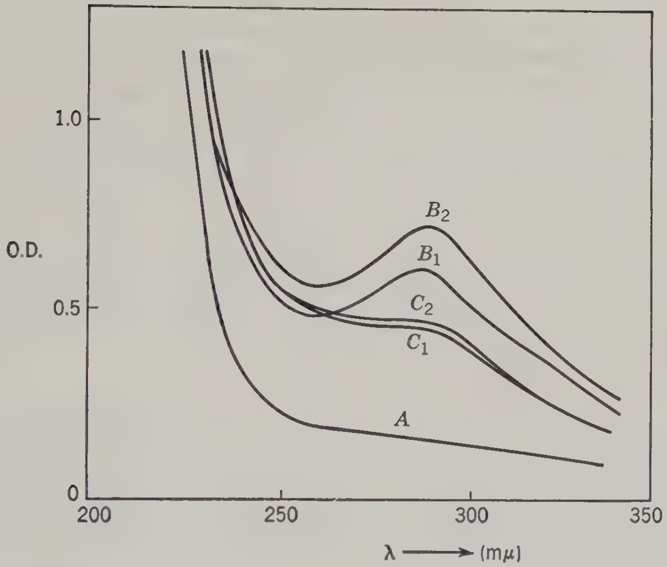

FIG. 6. Spectrum of nylon film: (*A*) before irradiation; (B_1) immediately after irradiation in air (90 hours); (B_2) after a further 24 hours storage in the dark; (C_1) immediately after irradiation in a vacuum cell (90 hours, 10^{-3} mm. Hg with liquid N_2 trap); (C_2) after a further 24 hours storage in the dark.

It seems, therefore, that our results are consistent with the assignment of the 2900 A. band to a peroxy free radical, but further confirmation is required. To this end, an attempt is being made to detect this radical by electron spin resonance in cooperation with Dr. D. J. E. Ingram of Southampton University.

Diffusion Processes in High Polymers

Our results suggest that in the case of high polymers, the diffusion processes involved in chemical reaction may be separated into two classes depending on their rates. First, gaseous diffusion processes with $D \sim 10^{-5}$ cm.^{2} sec.$^{-1}$ and second, polymer "chain" or "segment" diffusion processes, which will be very much slower. The difference in order between these classes is probably at least 10^6. Accordingly, we have shown that with free radical processes in such a system, "chain" or "segment" diffusion will be the rate-limiting step, the completion of gas absorption and evolution reactions being relatively instantaneous. This leads to a considerable simplification of the kinetics, but also, in the cases where gaseous equilibria are involved, to peculiar kinetic effects of the kind we have described above.

Finally, we wish to suggest that nylon offers considerable promise, as an alternative to rigid glasses at low temperatures, for the study of free radicals at room temperature. Films ~20 μ thick are quite suitable for spectroscopic work down to 2400 A. and our results suggest that hydrogenation of the radicals by reaction with the polymer matrix does not occur readily. Some work has been done already in "Perspex" but here free radicals were detected only at 77°K. (10), presumably because of reaction with unpolymerized monomer.

ACKNOWLEDGMENTS

The author takes pleasure in acknowledging several valuable discussions with Dr. E. J. Bowen, F.R.S., and Professor G. Porter. Also, he wishes to thank Dr. K. W. Kemp and Mr. C. G. Cannon of this laboratory for many helpful comments and British Nylon Spinners Limited for permission to publish.

REFERENCES

1. (*a*) FRANCK, J., AND RABINOWITCH, E., *Trans. Faraday Soc.* **30,** 120 (1934); (*b*) RABINOWITCH, E., AND WOOD, W. C., *Trans. Faraday Soc.* **32,** 1381 (1936).
2. RABINOWITCH, E., *Trans. Faraday Soc.* **33,** 1225 (1937).
3. (*a*) NORMAN, I., AND PORTER, G., *Proc. Roy. Soc.* (*London*) **230A,** 399 (1955); (*b*) WILLARD, J. E., *Ann. Rev. Phys. Chem.* **6,** 152 (1955).
4. PORTER, G., Private communication.
5. WILSON, J. E., *J. Chem. Phys.* **22,** 334 (1954).
6. BARRER, R. M., "Diffusion in and through Solids," p. 420. Cambridge University Press, 1941.
7. FORD, R. A., *Nature* **176,** 1023 (1955).
8. BERTHOUD, A., AND BELLENOT, M., *Helv. Chim. Acta* **7,** 302 (1923).
9. (*a*) WATERS, W. A., "The Chemistry of Free Radicals," Oxford University Press, 1948; (*b*) STEACIE, E. W. R., "Atomic and Free Radical Reactions," Reinhold, New York, 1954.
10. PORTER, G., Private communication.
11. (*a*) HUNT, H. D., AND SIMPSON, W. T., *J. Am. Chem. Soc.* **75,** 4540 (1953); (*b*) HAM, J. S., AND PLATT, J. R., *J. Chem. Phys.* **20,** 335 (1952).

JOURNAL OF COLLOID SCIENCE **12**, 283–293 (1957)

VISCOELASTIC PROPERTIES OF A HIGH-CONSISTENCY ASPHALT

A. B. Brown, J. W. Sparks, and F. M. Smith

Research Department, Standard Oil Company (Indiana), Whiting, Indiana

Received November 15, 1956

ABSTRACT

High-consistency asphalts behave, rheologically, in the complex viscoelastic pattern common to many macromolecular species such as synthetic plastics and elastomers. A correlation with accepted linear viscoelastic theory has been developed for the behavior pattern, under tensile test conditions, of a typical hard asphalt in creep, creep recovery, and stress relaxation. The same simple viscous and elastic moduli are found to determine these several action modes. The range and magnitude of discrete moduli have been determined from the empirical creep time and creep recovery time relations. Calculated values of stress relaxation, based on these moduli derived from creep and creep recovery, compare favorably with direct experiment.

Introduction

The prime duties of asphalt are mechanical: to transmit stresses to structurally stronger supporting members while maintaining itself as a continuous protective film impermeable to water. At any stage of chemical life, the actual failure of asphalt is basically a physical phenomenon, measurable in rheological units of stress, strain, and time.

Asphalt, by and large, has not enjoyed the benefits of such fundamental rheological studies because of its relative cheapness and freedom from acute competition. On the other hand, intense competition among the synthetic plastics and elastomers has led to very fruitful studies in their modes of rheological responses. High-consistency asphalts resemble these high-polymer materials physically, and a similar rheological behavior might be presupposed. This rheology is complex, but the complexity is constructed of simpler elements working in concert. The essential specifications of these unit elements are their moduli of viscosity and of elasticity. The effective use of such concepts should lead to more realistic specifications and more certain matching of the mechanical capabilities of the asphalt to its job requirements. In view of their very extensive use in roads and roofs, in particular, the specific rheological behavior pattern of high-consistency asphalts deserves particular attention at this time.

Asphalt is normally applied at low consistencies, obtained by use of volatile diluents or elevated temperatures. In this state, its flow characteristics are very nearly Newtonian and viscosity is a sufficient defining constant. However, its service life is normally lived at much higher consistencies, ranging upward through millions of poises, realized on evaporation of diluent or on cooling to ambient temperatures. In this condition, a time-dependent elasticity becomes increasingly prominent and complicates the simpler viscous flow pattern predominating at low consistencies. Analysis of the interactions of these viscous and elastic properties is our immediate goal.

Among the simpler approaches to such an analysis, the response pattern under tensile stressing conditions is particularly revealing. The functions to be resolved are: (*1*) creep, which is extension with time under constant stress, (*2*) creep recovery, which is retraction with time when the stress is removed, and (*3*) stress relaxation, which is the decrease with time of the stress required to impose a given extension and thereafter maintain it constant. This discussion develops the correlation of these three functions in terms of common discrete viscous and elastic moduli, and reveals that this typical hard and rheologically complex asphalt conforms very closely to linear viscoelastic theory. There is no need to ascribe peculiar non-Newtonian or non-Hookean viscous or elastic behavior to the unit rheological process postulated.

Experimental Method

The mechanics of measuring creep, creep recovery, and stress relaxation are relatively simple. For creep, a cylindrical bar of the asphalt is subjected to a constant stretching stress and the rate of elongation is measured. For creep recovery, this stress is released after some chosen degree of extension and the rate of length retraction is measured. For stress relaxation, some chosen degree of extension is imposed by a constant stress, and then the diminution with time of the stretching effort required to maintain this selected degree of elongation is measured.

Basically, the tensile apparatus used was a balance beam through which a load on one arm was transmitted as a tensile stress to the 25 × 100 mm. cylindrical asphalt sample attached to the other arm and anchored to a fixed base. Creep was measured by the movement of the core of a Shaevitz differential transformer and magnified on the chart of an electronic recorder. When load was removed, the same mechanism recorded creep recovery. At any predetermined creep, the balance beam could be made to contact the detector of a Statham strain gage by which stress relaxation of any load at a fixed strain could be measured and registered on a second electronic recorder. The instrumentation detected changes of about 0.5% of the applied stress, ranging downward from about 4×10^5 dynes/cm.^{2}, and of 0.2–0.3% of the absolute creep or creep recovery strains, which were limited to a maximum of 2.5% of the sample length. Test temperature was 60°F.

The particular high-consistency asphalt selected for study was one intermediate between the two major classifications of roofing and paving asphalts. It was made by conventional air blowing at 450–500°F. of a Mid-Continent sweet crude residuum to the following inspections:

Softening point, °F.	193
Penetration at 77°F.	50
Ductility at 77°F.	2.1

EXPERIMENTAL RESULTS

Figure 1 presents four creep curves obtained at the indicated loadings. Application of stress produces an immediate extension, with the rate rapid at first but decreasing as the action continues. The fact that these curves approach limiting slopes, but not limiting magnitudes, indicates an approach, after long action, to an ultimate pattern of simple or Newtonian viscous flow. The earlier pattern is not one of constant rate of shear at constant stress. For any given duration of creep, degree of creep is directly proportional to the applied stress. Thus, the different load curves coincide when the ordinate is expressed as per cent extension under unit stress. Such a relationship indicates that the controlling equations of motion in creep are linear even though not simple Newtonian.

Figure 2 is a plot of per cent of creep strain recovered vs. creep recovery time after the activating stress is removed. The several creep recovery curves are distinguished by the indicated creep times which preceded creep recovery. The rate is rapid at first and then decreases as creep recovery continues. The approach of these curves to limiting values under 100% indicates a residue of unrecoverable creep, usually called permanent

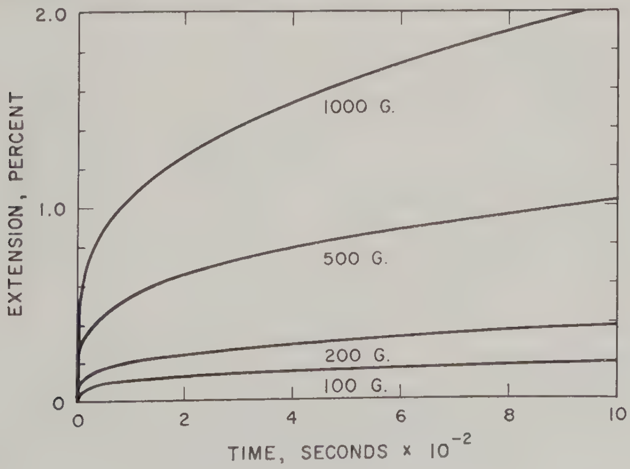

FIG. 1. Creep at varying loads.

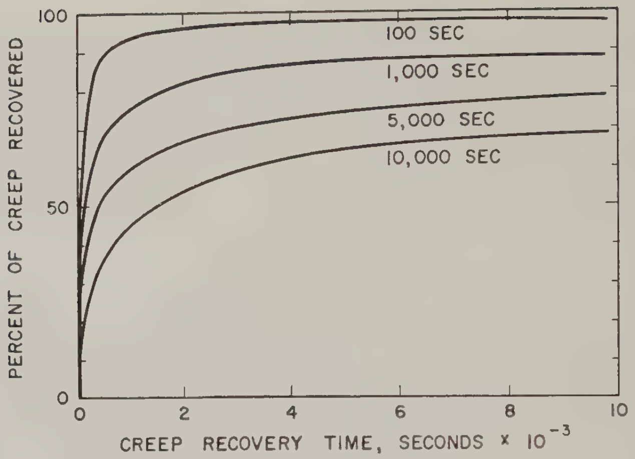

Fig. 2. Creep recovery as per cent of creep.

set. This is the greater, the longer the sample has been under load prior to creep recovery. The position of these recovery curves is independent of the magnitude of the applied stress, and, thus, of the magnitude of the creep strain, but is dependent on duration of creep.

That creep recovery occurs at all denotes a type of elastic action. This elasticity is predominantly time-dependent rather than Hookean or instantaneous. Coupled with this predominating damped elasticity is a small but real element of Hookean elasticity. Measurement of this requires a rather more precise technique. Thus, from the transmission velocities of ultrasonic compression and shear waves, Young's modulus for

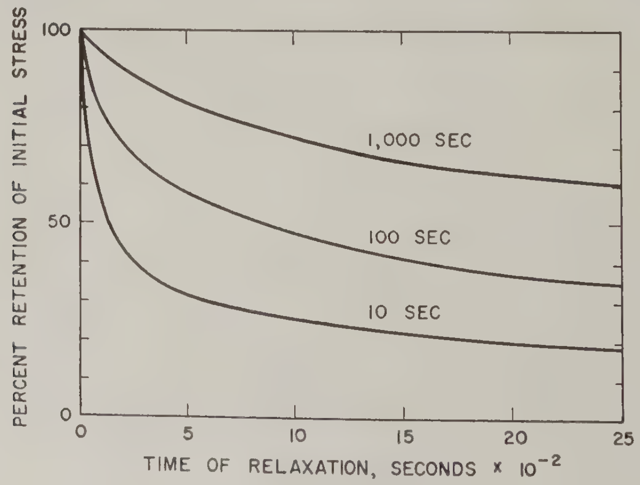

Fig. 3. Stress relaxation after varying creep times.

this asphalt is calculated as being 2.5 × 10^9 dynes/sq. cm. This corresponds to a Hookean elastic strain of 0.004, which is less than 1% of the total creep or creep recovery strains experimentally measured.

Figure 3 shows three stress relaxation curves, distinguished from one another by the time in creep prior to the start of the relaxation action. Plotted as per cent retention of initial stress versus relaxation time, these curves are invariant with respect to the magnitude of the stress applied in creep, but do vary with its duration. Here, too, the rate of stress relaxation is rapid at first, then decreases with time. These relaxation curves have been followed experimentally to 100,000 seconds and farther, and, in all cases, the limits appear to be complete stress relaxation.

Discussion of Results

These asphalt deformation patterns show the presence of both viscous and elastic effects. Though coincident with the patterns of neither a purely viscous Newtonian nor of a purely elastic Hookean material, they partake somewhat of the natures of both.

The theory underlying such steady-state viscoelastic behavior of macromolecules has been extensively developed by many investigators in recent years (1–4). Asphalts possess an array of macromolecular constituents, albeit of generally smaller dimensions than the synthetic plastics. They, too, may be expected to reveal a range of viscoelastic mechanisms, each with different response time under an applied stress. In such an array, all those mechanisms closely conforming to a Hookean elastic mode of action can be averaged or reduced to a single mechanism of some intermediate modulus; the same is true for all these mechanisms closely conforming to a Newtonian viscous mode of action. Only over restricted ranges, however, is it mathematically acceptable so to reduce an array of the hybrid viscoelastic mechanisms of the damped elastic type represented by the Kelvin pairs-in-parallel or the Maxwell pairs-in-series arrangements. Thus, a model of discrete units will usually retain a number of such reduced Kelvin or Maxwell mechanisms, with retardation and/or relaxation times spread over the action time zone of interest. By such reduction (5), the actual near infinite array of component viscoelastic mechanisms in the asphalt may be developed as a discrete few averaged mechanisms with some advantages in comprehension of the internal mechanics.[1] The more rheologically simple the asphalt, and the narrower the range of action time of interest, the fewer such reduced mechanisms are needed for an adequate rheological description (6–10). For this asphalt, under the given conditions of test, four retarded elastic elements are required to adequately describe the observed performance.

---

[1] More elegant mathematics might handle the creep, creep recovery, and stress relaxation phenomena as continuous functions but, in the more complex materials, the transforms from continuous creep to continuous relaxation functions may become mathematically difficult. For practical use, however, empirical continuous creep and relaxation functions may be employed, without the necessity of showing the relationship between the constants via the component viscous and elastic moduli (B. Gross: *Physics Today* **5**, No. 8, 6 (1952)).

In terms of such a reduced model, with one free spring, one free dash-pot, and four Kelvin elements, the equations of motion in creep and in creep recovery are (11),

$$\gamma_c = S/G_0 + \sum_{i=1}^{4} S/G_i(1 - e^{-t_c/\tau_i}) + St_c/\eta_5; \qquad [1]$$

$$\gamma_{cr} = S/G_0 + \sum_{i=1}^{4} S/G_i(1 - e^{-t_c/\tau_i})\,(1 - e^{-t_{cr}/\tau_i}). \qquad [2]$$

Equation [1] defines γ_c, the unit strain or fractional extension in creep, and Eq. [2] defines γ_{cr}, the unit strain or fractional retraction in creep recovery. In both cases, the definition is a summation of averaged mechanisms. In Eq. [2], each paired mechanism is defined by a term in which both creep time, t_c, and creep-recovery time, t_{cr}, appear. Thus, the action pattern in creep recovery depends in part on the past history of creep.

The first term on the right of either represents the near-instantaneous extension or retraction of the reduced springlike elastic mechanisms. The elastic modulus of this combination is G_0, and S is the applied stress.

The second term on the right of either equation represents the damped elastic movements in extension or retraction of the sum of four paired-in-parallel elements, each of which has an individual elastic modulus, $G_1 \cdots G_4$, and an individual viscosity modulus, $\eta_1 \cdots \eta_4$. The ratio of the η to the G of each pair is its τ-value and appears in the exponent of the Naperian e. This τ has the dimension of time and is called retardation time.

The last term on the right of Eq. [1] represents the viscous flow of the reduced Newtonian dash-pot. An equivalent term does not appear in Eq. [2] because this mechanism is inoperative in creep recovery.

The action time for a Hookean mechanism is near instantaneous. However, the response of the tensile tester lagged somewhat and, in effect, saw all movement of the first 1–2 seconds as instantaneous. For practical purposes, therefore, all action of 1 second or less was defined as Hookean. This measurable quantity determines S/G_0, and, at known stress, gives the practical free elastic modulus, G_0. The G_0 will be different from and generally smaller than Young's modulus, as it will include some time-dependent but, nevertheless, fast-acting Kelvin mechanisms. G_0 can be determined, from either creep or creep recovery, by photographic registration of the initial strain action which is picked up on an oscilloscope.

The τ-values are time dimensional and determine the pace of the response of the individual Kelvin elements. Because experimental interest is concerned with degree of response over some extended time range, the τ's may be chosen and spaced to cover this range. As the τ's occur exponentially, it is convenient to space such arbitrarily chosen τ's in successive logarithmic time decades, the first covering 1–10 seconds, the next, 10–100 seconds, and so on. Over the experimental conditions, the creep curves were found to attain a reasonable approximation to linearity beyond the action range of 10,000–20,000 seconds. By then, the damped elastic mechanisms may be regarded as having substantially attained equilibrium deformation. Thus, four such mechanisms of four such appropriately but arbitrarily chosen τ-values will reasonably approximate the damped elastic effects. All quantities on the right of Eq. [2] except G_1, G_2, G_3, G_4 are now fixed. By determining creep recovery strains at four different action times, following creep under a known stress for a known time, a set of four simultaneous equations results which may be solved for the several G's. The corresponding viscosity moduli, $\mathfrak{n}_1 \cdots \mathfrak{n}_4$, of the Kelvin pairs can then be calculated from the relation $\tau = \mathfrak{n}/G$.

By inserting these G's and τ's in Eq. [1] at some known creep strain determined at some relatively long creep time, the value of the term $St_c/\mathfrak{n}_5$ may be obtained, and, thus, the value of $\mathfrak{n}_5$, the viscosity modulus of the reduced unpaired dash-pots. The moduli values found are:

Elastic Moduli (dynes/cm.²)	*Viscosity Moduli (poises)*
$G_0 = 6.2 \times 10^7$	—
$G_1 = 14 \times 10^7$	$\mathfrak{n}_1 = 5.0 \times 10^8$
$G_2 = 4.1 \times 10^7$	$\mathfrak{n}_2 = 1.4 \times 10^9$
$G_3 = 3.8 \times 10^7$	$\mathfrak{n}_3 = 1.2 \times 10^{10}$
$G_4 = 0.7 \times 10^7$	$\mathfrak{n}_4 = 2.2 \times 10^{10}$
	$\mathfrak{n}_5 = 2.0 \times 10^{11}$

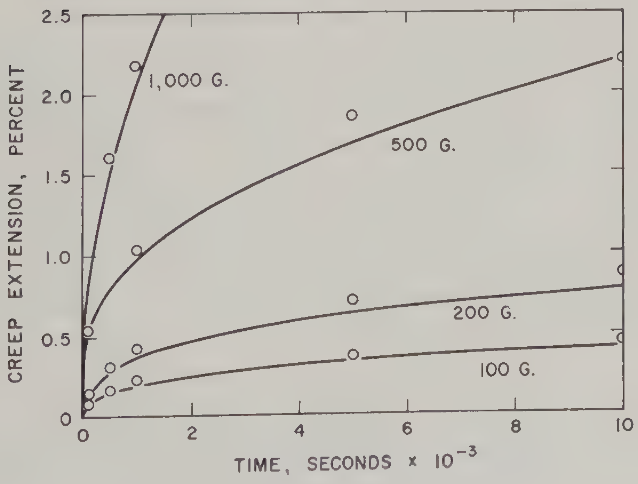

FIG. 4. Creep: experimental vs. theoretical.

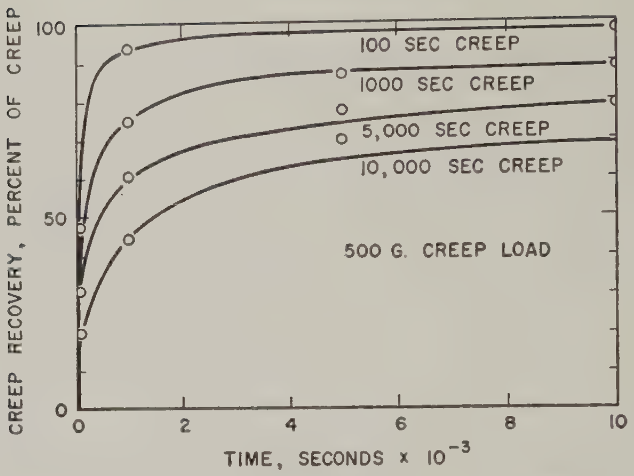

FIG. 5. Creep recovery: experimental vs. theoretical.

From these moduli and Eqs. [1] and [2], one may calculate creep and creep recovery values under any specified conditions within the general range of action time of the experiments in which the moduli were determined. Figure 4 shows such calculated creep values as circles, spotted along the best line experimental curves for four stress loadings. Similarly, in Figure 5, creep recovery values, similarly calculated, are spotted as circles along the best line experimental curves for four creep recoveries which follow creep actions of the indicated durations.

It now remains to correlate creep and creep recovery with stress relaxation. If the basic assumptions concerning the viscoelastic behavior of high-consistency asphalt are correct, then the same internal mechanisms must be at work in stress relaxation as in creep and creep recovery, and the viscous and elastic moduli controlling the latter must also control the former. Now, stress relaxation is mathematically a function in constant strain and variable stress, whereas creep and creep recovery are functions in constant stress and variable strain. Thus, a transformation is required to express the moduli of the former function in terms of those of the latter.

In terms of our mechanical analog, the transformation involves a transition from a pairs-in-parallel to a pairs-in-series model, since the former has the function form of creep and creep recovery and the latter that of stress relaxation. The equation defining the pairs-in-series model is (12):

$$S = Ae^{-t_{sr}/\tau_1'} + Be^{-t_{sr}/\tau_2'} \dots + Ee^{-t_{sr}/\tau_5'} \qquad [3]$$

where S is the amount of stress retained in the sample after relaxing for t_{sr} time. Here, the primed τ's are called relaxation times rather than retardation times but again represent the ratios of viscous to elastic moduli of the paired mechanisms. Like the τ's of the pairs-in-parallel model, these primed τ's are also time dimensional. The τ's of the two models are not related in any simple one-to-one manner, but each modulus of the one is a function of all the moduli of the other. The coefficients $A \cdots E$ are constants relating to the creep history of the sample prior to stress relaxation. These coefficients can be defined in terms of the moduli determined in creep or creep recovery. The theory of this definition has long been known (13–15), but the practical application to the empirical multi-element mechanism, as developed above, requires some mathematical legerdermain (16). We will not undertake a discussion of the mechanics of this here, as we hope soon to devote a paper to this procedure.

Matching of moduli between creep and creep recovery, on the one hand, and stress relaxation on the other for this asphalt is not entirely quantitative, but is close enough to identify the essential similarity of these two behavior patterns. The stress relaxation calculations are sensitive to the values for G_0 and for η_5 which are precisely the two creep moduli of an admittedly hybrid nature. Be it recalled that G_0 was developed as an approximate Hooke elastic modulus and included not only the true Hookean response but also all damped elastic response of action time faster than 1 second. Also, the η_5 viscosity modulus was developed by including not only the true Newtonian viscous flow but also the action of all damped mechanisms of slower response than the damped elastic elements of τ_4 retardation time. Thus, for best fit to the creep and creep recovery actions, G_0 and η_5 were determined here as being 6.2×10^7 dynes/cm.^{2} and 2.0×10^{11} poises, respectively, whereas for best fit to the stress relaxation experimental data, values of 3.1×10^7 and 1.0×10^{11} for G_0 and η_5 are

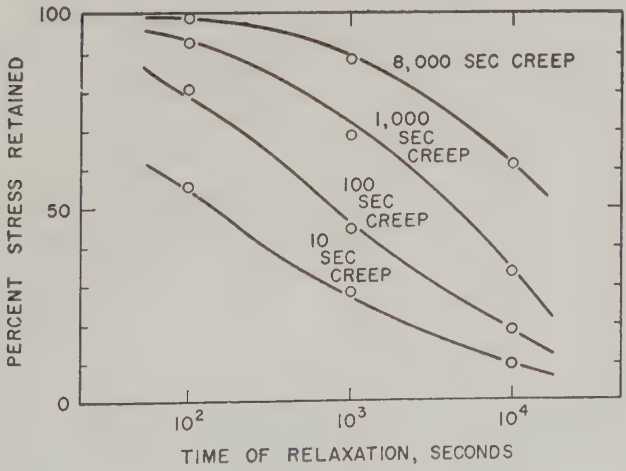

Fig. 6. Stress relaxation: experimental vs. theoretical.

needed in the transformation function. The other eight moduli, $G_1 \cdots \mathbf{n}_4$, require no modification.

Figure 6 shows the agreement between calculation and experiment for stress relaxation. The parameters are times of creep that precede relaxation. Continuous lines represent the best line curves of the experimental relaxation data and the circles represent stress relaxations calculated from creep moduli as described. Over this wide range of stress relaxation times the agreement is good.

These findings are qualitatively in agreement with those of other investigators cited who have reported data on asphaltic bitumens. This particular asphalt under the particular conditions of test shows itself as being rheologically more complex than heretofore reported in asphalt studies and requires a more complicated mechanical analog for its representation. It is of considerable interest to observe, however, that even such a behavior pattern, rheologically complex insofar as asphalts go, can still be described in terms of unit viscous and elastic moduli of the simplest form, i.e., Newtonian viscosity and Hookean elasticity.

Conclusion

These inquiries are continuing with variables of temperature, composition, and rates of action. It is to be hoped that the results of other investigations into the flow properties of hard asphalts will find their way into print. Such studies can eventually lead to preparation of asphalts of a much wider range of capabilities, and to technically sounder selection by the consumer of the best asphalt for any given service.

References

1. Extensive discussion and bibliographies appear in the following:
   Alfrey: "Mechanical Behavior of High Polymers" (1948).
   Houwink: "Elasticity, Plasticity, and the Structure of Matter" (1937).
   Mark: "The Physical Chemistry of High Polymeric Systems" (1940).
   Nadai: "Theory of Flow and Fracture in Solids" (1950).
   Reiner: "Twelve Lectures on Theoretical Rheology" (1949).
   Reiner: "Deformation and Flow" (1949).
   Scott-Blair: "A Survey of General and Applied Rheology" (1949).
   Pfeiffer: "The Properties of Asphaltic Bitumen" (1950).
2. Academy of Sciences at Amsterdam: First Report on Viscosity and Plasticity (1935).
3. Leaderman: *Textile Research* **11,** 171, (1941); *Ind. and Eng. Chem.* **35,** 374, (1943).
4. Dienes, G. J., *J. Colloid Sci.* **2,** 131 (1947).
5. Alfrey: "Mechanical Behavior of High Polymers," p. 171.
6. Saal, R. N. G., and Labout, J. W. A.: "Rheological Properties of Asphaltic Bitumens," *J. Phys. Chem.* **44,** 149 (1940).
7. Broome, D. C., and Bilmes, L.: "Rheology of Plastic Materials," *Nature* **147,** 176, 237 (1941).

8. Lethersich, W.: "Mechanical Behavior of Bitumens," *J. Soc. Chem. Ind.* **61,** 101 (1942); also, British Elec. and Allied Ind. Research Assoc., Tech. Report A/T83 (1941).
9. Mack, C.: "Plastic Flow, Creep, and Stress Relaxation", *J. Appl. Phys.* **17,** 1083, 1093, 1101 (1946).
10. Reiner, M.: Research on the Rheological Properties of Bitumen and Asphalts, Gov. of Palestine, Board for Scientific and Industrial Research (1948).
11. Alfrey, "Mechanical Behavior of High Polymers," pp. 54 ffl.; 116 ffl.
12. Alfrey, "Mechanical Behavior of High Polymers," p. 181.
13. Sinka, R., *J. Appl. Phys.* **13,** 201 (1942).
14. Alfrey, T., and Doty, P., *J. Appl. Phys.* **16,** 700 (1945).
15. Gross, R., Proc. Second Inter. Congress of Rheology, 221 (1953).
16. Graves, R. L., (Standard Oil Company (Indiana)). To be published.

JOURNAL OF COLLOID SCIENCE 12, 294–307 (1957)

EXPERIMENTAL INVESTIGATIONS ON THE EFFECT OF LIGHT SCATTERING UPON THE REFRACTIVE INDEX OF COLLOIDAL PARTICLES[1]

Wilfried Heller and Thomas L. Pugh

Chemistry Department, Wayne State University, Detroit, Michigan

Received December 3, 1956

I. Introduction

Reliable determinations of the size of colloidal spheres in a liquid medium from light-scattering measurements require the use of the Mie theory. The theoretical data (1) show that it is then necessary to know the refractive index of the particles very accurately if its value, relative to that of the medium, m, is larger than about 1.05. Taking for example a particle diameter of two-thirds micron and an m-value of 1.20, an uncertainty in m of 0.003 will produce an uncertainty of approximately 5% in the particle diameter calculated from the specific turbidity. Here, then, the refractive index of the scattering material should be known to four significant figures or better, if possible. It is advisable to take this as a standard whenever $m > 1.05$ and the particle size > 0.1 of the wavelength used in the experiments.

Two general methods suggest themselves for a suitable accurate determination of the refractive index: (*1*) The refractive index may be determined on a macroscopic specimen of the material cast into a transparent film or on a powder using suitable instrumentation. (*2*) From refractive index data obtained on the disperse system, itself, the refractive index of the dispersed material may be derived by means of a suitable mixture rule. The former method, which is not always applicable, has the intrinsic weakness that it may not give the exact refractive index of the colloidal particles which may be affected by the possibly different optical properties of third substances adsorbed at the very large particle surface area. Outright erroneous results may be obtained on using dry macroscopic specimens if the particles interact with the medium of dispersion. For example, it was recognized at an early date that the refractive index of aqueous protein solutions (2) depends on the degree of hydration of the protein (3).

The second method is, therefore, in general, preferable. However, even on using a suitable mixture rule, it is a priori not certain whether the refractive

---

[1] This work was supported by the Office of Naval Research.

index of the particles derived from it is the real or only an apparent refractive index. That it may be only an apparent quantity may be surmised on the basis of the following observations: Schoorl found that the coagulation of egg albumin was accompanied by a decrease in refractive index of the solution as well as by an increase in viscosity (4). Joshi and his co-workers (5) found that the refractive index of the solution of hydrophobic colloids changed during coagulation. They used these changes for a study of coagulation kinetics without attempting to investigate or elucidate the cause of the change in refractivity. Deile, Krämer, and Klause (6) similarly used refractive index changes as a measure of the effect of methylcellulose upon the stability of polystyrene latices. Their assumption was that aggregated polystyrene particles, formed as the coagulation progresses, are more opaque and consequently contribute less to the refractive index of the system. This assumption is obviously untenable, since polystyrene does not exhibit true absorption in the visible. Therefore, the minor spectral shift in absorption bands due to increased light scattering (7) and the simultaneous change in the absorption coefficient cannot possibly account for the effects observed.[2]

The present paper is concerned with a systematic investigation of this apparent effect of particle size on the refractive index of dispersed systems. On the basis of the results, suitable methods for evaluating the true refractive index of dispersed colloidal particles will be proposed.

II. Mixture Rules for the Derivation of the Refractive Index of Colloidal Particles from Refractometric Measurements on Colloidal Solutions

A. Theoretical Mixture Rules

The theoretical mixture rules available for evaluating the refractive index of colloidal particles from measurements of the refractive index of the entire system have been given and briefly discussed in a previous paper (8). The following two are of interest here: (*1*) the Lorentz-Lorenz equation which applies to solutes that can be approximated by spheres.

$$\frac{\mu_{12}^2 - 1}{\mu_{12}^2 + 2} = \frac{\phi_1(\mu_1^2 - 1)}{\mu_1^2 + 2} + \frac{\phi_2(\mu_2^2 - 1)}{\mu_2^2 + 2}. \qquad [1]$$

Here μ_{12}, μ_1, and μ_2 are the refractive index of the disperse system, of the medium, and of the dispersed particles, respectively, and ϕ is the respective volume fraction. The more general case of solutes of any shape was subsequently treated by Wiener (9). The field considered in the derivation of these equations is electrostatic so that one would expect neither to hold satisfactorily in the case of pronounced light scattering by the solute. In fact, an attempt to use Wiener's mixture rule in order to obtain information on the shape of nonspherical colloidal particles led to negative results (10). (*2*) A new mixture rule implicitly based upon the electromagnetic theory of light, is the following (8, 11)

---

[2] The work quoted, like that of many other workers, is of relatively little value because of the use of the Abbé refractometer. This instrument allows one to obtain only four significant figures for the refractive index of the solution and therefore only the first decimal for the refractive index of the particles themselves—unless high concentrations are used which, however, jeopardize the validity of the rule of additivity of the refractive indices of particles and medium.

$$\mu_2^2 = \frac{\mu_1^3 + 2b\mu_1^2(\mu_{12} - \mu_1)}{\mu_1 - b(\mu_{12} - \mu_1)} \qquad [2]$$

where $b = (2/3)\ \phi_2$. It may also be written as follows (12):

$$\frac{\Delta\mu}{c_2'} = \frac{3\mu_1}{2\rho_2}\left(\frac{m^2 - 1}{m^2 + 2}\right) \qquad [2a]$$

where $\Delta\mu = (\mu_{12} - \mu_1)$, c_2' is the concentration of the colloidal particles in g./cc., $m = \mu_2/\mu_1$, and ρ_2 is the density of the particles. Since the derivation of Eq. [2] made use of the Debye equation of light scattering (13), it was certain that the former would share the limitations of the latter equation. Thus, validity of Eq. [2] requires the particle size to be small relative to the wavelength used in the refractive index measurements. In addition, the refractive index of the particles should differ only slightly from that of the medium. An attempt was made to partially remove the latter limitation by establishing an empirical correction equation (8),

$$\mu_2\text{corr.} = \frac{\mu_2}{0.093(\mu_2 - \mu_1)^{1.99} + 1}, \qquad [3]$$

where μ_2 is the value derived from Eq. [2].

After the present work had been completed an interesting paper by Zimm and Dandliker (12) appeared which made it possible to obtain a theoretical mixture rule also based upon the electromagnetic theory of light (14), which does not have the limitations specified for Eq. [2]. This new mixture rule will be considered briefly at the end of this paper. Its application to the systems investigated here has been discussed more fully elsewhere (14).

B. Empirical Mixture Rule

Most generally used in the past was the following empirical mixture rule which simply states that the refractive index of a solution varies linearly with solute concentration (15).

$$\mu_{12} = \mu_1\phi_1 + \mu_2\phi_2 = \mu_1 - \phi_2(\mu_1 - \mu_2) \qquad [4]$$

There is no doubt that this mixture rule holds at sufficiently small concentrations as long as neither the particle size nor the degree of solvation—

in the case of solvated particles—changes with concentration. The basic prerequisite for validity of Eq. [4], volume additivity, was in fact proved rather recently (16) for systems like those investigated below. Nevertheless, as stated above, it is not certain whether the μ_2 as derived from Eq. [4] is the true or only an apparent refractive index. In the latter case,

$$\mu_{12} = \mu_1\phi_1 + \mu_2'\phi_2, \qquad [4a]$$

where μ_2' is an apparent quantity.

If $\mu_2' \neq \mu_2$ and if μ_2' should, in fact, vary with the size of nonsolvated particles, only complications arising from light scattering and/or surface adsorption could be responsible. Refractive index measurements represent, in the final analysis, measurements of the phase difference between the light traversing the disperse system or solution and that traversing the medium only. This phase difference may be different in the presence of light scattering, more so the stronger the scattering in the forward direction.

The question as to whether or not the particle size—on account of light scattering—affects the refractive index of colloidal particles can be answered by determining by means of Eq. [4*a*] the refractive index of nonsolvated particles, in monodisperse colloidal systems of systematically varied particle sizes. Extrapolation to zero particle size, that is to zero light scattering, should then yield the true refractive index, μ_2,[3]—needed in connection with particle size determinations from light-scattering measurements—if there is reasonable assurance that the size is the only pertinent variable.

III. The Systems Investigated

Dow polystyrene and polyvinyltoluene[4] latices were the systems investigated. Light-scattering data for several of these latices were also obtained in this laboratory (17). The original latices contained 30–50% solids, necessitating extensive dilution for the measurements of the refractive index. For that purpose, a small amount of latex was diluted to about 0.5–1.0% solids with freshly prepared double distilled water. The diluted latex was then centrifuged at about 350 g's for ½ hour to remove any agglomerates that might have been present. One hundred milliliters of the supernatant suspension were pipetted into a glass-stoppered pyrex flask. Its polymer concentration was determined by accurately weighing out (to 0.1 mg.) one or generally two 30-g. samples, evaporating them to dryness in a partial vacuum at 80°C., and then weighing the dried solids.[5] The concentration of the remainder of the centrifuged latex was reduced by two orders of magnitude by two successive volumetric dilutions. Five to seven samples of varied concentration were thus obtained. These samples were kept in pyrex glassware which had been carefully cleaned and subsequently steamed out for several minutes. All measurements were made on the samples within a period of one week after their preparation.

---

[3] Extrapolation to zero scattering can, of course, be accomplished also by systematically varying the refractive index of the medium. Application of this alternate method is under preparation.

[4] The latex samples were generously supplied by Dr. J. W. Vanderhoff of the Dow Chemical Company of Midland, Michigan.

IV. The Method of Refractive Index Measurements

A. Theoretical Remarks

As stated in section I, the refractive index of the colloidal particles should be known to four figures. This defines both the experimental method to be used and the precautions to be taken. From Eq. [4*a*] it follows on rearrangement that:

$$\Delta\mu = \mu_{12} - \mu_1 = (\mu_2' - \mu_1)\phi_2. \qquad [4b]$$

Using water at 25°C. and the green Hg-line, 5460.73 A., $(\mu_2' - \mu_1)$ has the value of 0.2668 if $m = 1.20$ (this m-value comes closest to that pertinent to the systems used). Consequently,

$$(\mu_{12} - \mu_1)/\phi_2 = 0.2668$$

In order to obtain four figures for μ_2', the third decimal of this number should be significant. The volume fraction that can be used—at intermediate particle sizes (diameter, D: 400 mμ)—at the given m-value without serious blurring of the optical field irrespective of the instrument used, is 1×10^{-4} on using a 1 cm. cell, or 1×10^{-3} on using a layer thickness of 1 mm., the latter representing about the limit of experimentally useful layer thicknesses. The refractive index of the solutions would therefore have to be measurable to the seventh decimal in order to fulfill the theoretical precision requirement. This excludes at once the use of any but differential instruments. The only instruments to be considered for the present purpose are either a differential refractometer modified for better than average precision or an interferometer. An interferometer, of the Haber-Loewe type, was used for the present work. The setting of the compensator plates was adjusted so that a path difference, Γ, of 31 A. (a phase difference of 2°) could be measured corresponding to a compensator drum reading of ± 0.25 units. Since the refractive index difference measured by the instrument

$$\Delta\mu = \mu_{12} - \mu_1 = \Gamma/d \qquad [5]$$

(d is the optical path in centimeters), a $\Delta\mu$-value with an uncertainty of only ±3 × 10^{-7} is obtained. Using a 1-cm. cell and the upper limiting volume fraction, defined above for $D = 400$ mμ, the largest measurable path difference was 2000 A. Since the value of ϕ_2 is known to four significant figures, μ_2' is obtained from Eq. [4*b*] with an uncertainty of $\pm 2.3 \times 10^{-3}$[6] (19). The upper limiting ϕ-value is, of course, dependent on the particle size. Therefore, the μ_2'-values obtained for particles with a diameter > 400 mμ may be as much as ten times less precise. Conversely it is possible to obtain four to five significant figures for particles with a diameter $<$ 400 mμ provided the concentrations used remain within the range of validity of Eq. [4*a*]. The number of significant figures to be expected for μ_2' (and for m derived from it) applies, as stated, to the use of the highest concentration applicable. The decrease in the number of significant figures with the decrease in concentration is, however, of relatively minor significance, since, as described below, μ_2'-values are derived from measurements of $\Delta\mu$ at a series of concentrations, i.e., from straight lines which go through the origin of $\Delta\mu$ (c)-plots.

---

[5] The nonpolymeric percentage of the dried solids was negligible as verified by centrifuging out the polymer from a latex and evaporating the supernatant liquid to dryness and weighing.

B. Experimental Procedure

The interferometer furnishes the phase or path difference between two coherent components of a light beam which traverse separately the two compartments of a twin cell. One component traversed in our case the latex and the other water, which could be used as the reference liquid in place of the latex serum without risking any error of consequence, as verified by experiments.

The experiments for the determination of $\Delta\mu$—by means of a 1-cm. twin cell—were all carried out at room temperature (23° ± 2° C). The data obtained apply to the green Hg-line, 5460.73, for which the instrument had been calibrated by means of a suitable interference filter. The calibration followed the conventional technique of correlating Γ and f_i, where f_i represents the displacement, by i fringes, of the variable interference pattern with respect to the stationary pattern ($\Gamma = i\lambda_0$, where λ_0 is the vacuum wavelength of the light used.) The calibration was carried out for the first 5 fringes and for two twin 1-cm. cells filled with fresh double distilled water.[7] The range experimentally used was generally limited to drum readings corresponding to the displacement of less than one fringe.

The $\Delta\mu$-values thus obtained were determined, on the average, for six systematically varied concentrations of a given latex. On plotting $\Delta\mu$ vs. ϕ_2, the slope would immediately yield $\mu_2' - \mu_1$. Practically, it is more convenient to plot $\Delta\mu$ vs. c_2 where c_2 is the weight fraction of the polymer. In

---

[6] The uncertainty in ρ_2 needed for the calculation of m is roughly ten times smaller (see ref. 19).

[7] The effective layer thickness of the two 1-cm. twin cells used in the experiments differed very slightly resulting in slightly different calibration factors. This difference was taken into account.

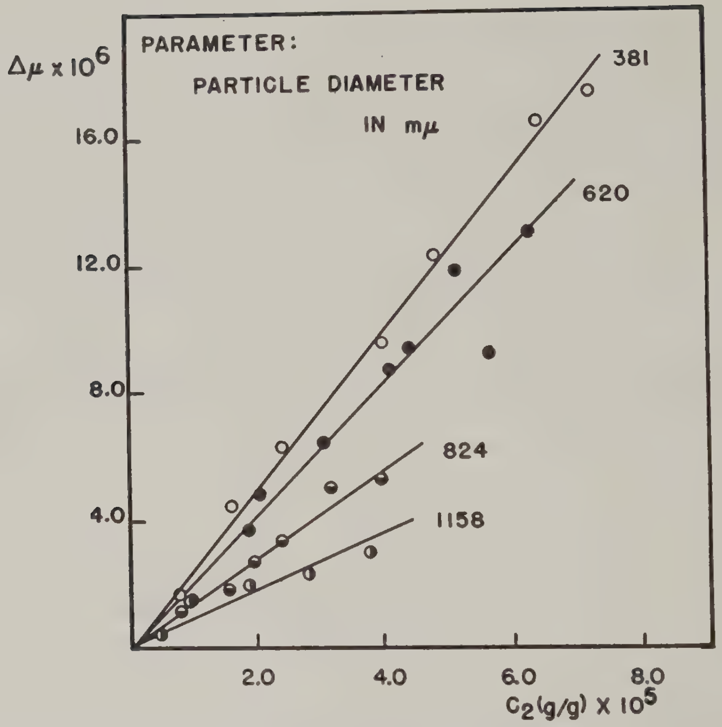

FIG. 1. Variation, with concentration, of the refractive index of polyvinyltoluene latex, relative to water.

view of the low concentrations used and the closeness of the ρ_1- and ρ_2-values (19), $\rho_{12}/\rho_1 \cong 1$, so that

$$\mu_2' = (\Delta\mu/c_2)\,(\rho_2/\rho_1) + \mu_1. \qquad [4c]$$

A few numerical checks showed that the error incurred in using Eq. (4c) was smaller than the overall error in μ_2'. The slopes of the $\Delta\mu$ vs. c_2 plots were determined as accurately as possible by using the method of least mean squares. Representative plots are given in Fig. 1. A compilation of the slopes for all the different polystyrene and polyvinyltoluene particle sizes can be found in Table I.[8] From these slopes the value of μ_2' is obtained on inserting for ρ_2/ρ_1 the value of 1.0600 and 1.0288 for polystyrene and

---

[8] This table allows for a quick approximate determination of the quantitative effect which a given amount of polymer of a particular particle size exerts on the refractive index of water. It is thus apparent that a latex must have a minimum concentration of 4 mg. per ml. in order to affect the third decimal place of the refractive index of water assuming $\Delta\mu/c_2 = 0.25$ and $\rho_{12} \rightarrow 1.0$. Similarly, it is seen at once that the interferometer, as used here, was capable of detecting a change in polymer concentration as small as 1 mg. per liter latex.

TABLE I

The Refractive Index Increment, Per Unit Weight Concentration, in Latices and Its Variation with Particle Size

D (mμ)	$\Delta\mu/c_2$
Polystyrene	
132	0.2457
135	0.2470
238	0.2585
240	0.2578
249	0.2455
268	0.2560
271	0.2587
280	0.2684
295	0.2387
514	0.2264
814	0.1244
953	0.1134
Polyvinyltoluene	
46	0.2571
163	0.2357
304	0.2371
381	0.2509
620	0.2059
824	0.1422
1158	0.0763

polyvinyltoluene, respectively, the values of ρ_2 having been secured by density determinations on the same systems (19).

IV. RESULTS AND DISCUSSION

The apparent refractive indices of the colloidal polyvinyltoluene and polystyrene spheres—as determined from Eq. [4*c*]—are given in Tables II and III and plotted against the particle diameter in Figs. 2*a* and 2*b*. The results show that the value of μ_2' decreases very strongly with increasing particle size if the particle diameter is in excess of approximately 400 mμ. A systematic change at lower diameters is not apparent from the data.

A decrease in μ_2' with increasing particle size is obtained also on using other mixture rules as shown in Table IV. The decrease is only slightly different on using Eq. [2] but very different on using the Lorentz-Lorenz Eq. [1]. In the latter case, the limiting values at very small diameters are unreasonably small, adding another argument to the contention that this equation is not applicable to colloidal solutions.

The practical independence of μ_2' of particle size—within the lower range of particle sizes—suggests that the mean of the values within this range is essentially equivalent to the refractive index expected at vanishingly small particle size, $(\mu_2')_0$.

TABLE II

The Apparent Refractive Index of Colloidal Polystyrene Spheres

D (mμ)	μ_2'	% Deviation from value at $D = 0$
0	($1.602_1 \pm .008_2$)[a]	—
132	1.594_4	−0.48
135	1.595_8	−0.39
238	1.607_9	+0.36
240	1.607_2	+0.32
249	1.594_2	−0.49
268	1.605_4	+0.21
271	1.608_2	+0.38
280	1.618_5	+1.02
295	1.587_0	−0.95
514	1.573_9	−1.77
814	1.465_9	−8.51
953	1.454_2	−9.24

[a] Average, and mean deviation from it, of all values for particles with diameters $\leqslant$ 295 mμ; standard deviation: $\sigma = 0.0092$.

TABLE III

The Apparent Refractive Index of Colloidal Polyvinyltoluene Spheres

D (mμ)	μ_2'	% Deviation from value at $D = 0$
0	($1.586_3 \pm .009_1$)[a]	—
46	1.598_5	+0.77
163	1.576_5	−0.62
304	1.577_9	−0.53
381	1.592_1	+0.37
620	1.545_8	−2.55
824	1.480_3	−6.68
1158	1.412_5	−10.96

[a] Average, and mean deviation from it, of all values for particles with diameters $\leqslant$ 381 mμ; standard deviation: $\sigma = 0.0093$.

These $(\mu_2')_0$-values of polystyrene are not identical with those of μ_2 obtained from direct measurements on a thin film of the bulk polymer (18). The comparison in Table V shows that the bulk data differ by approximately 0.3%, which is definitely, although only slightly, outside the limits of error of $(\mu_2')_0$. This small difference—the bulk values being slightly lower—may be accounted for by the effect of a surface film of stabilizer adsorbed on the latex particles which is bound to affect both their density (19) and refractive index. The agreement between $(\mu_2')_0$ and the bulk value is far better in the case of polyvinyltoluene. This comparison carries, however, far less weight, since it is uncertain whether the para/ortho ratio of colloid and bulk—originating from different batches—was really the same. It is clear, however, from these comparisons that the bulk values may be used in the case of *strongly hydrophobic* particles dispersed in water, if uncer-

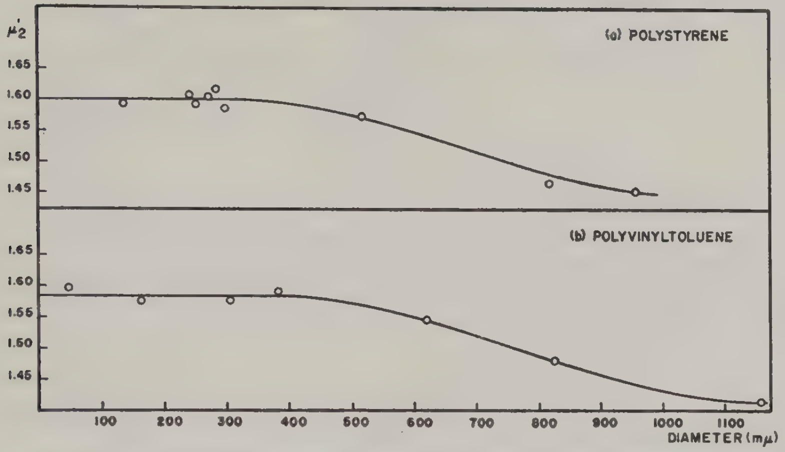

FIG. 2. Variation of the apparent refractive index μ_2' with particle diameter.

TABLE IV

The Apparent Refractive Index of Colloidal Polyvinyltoluene Spheres as Calculated from Various Theoretical and Empirical Equations

D mμ	$(\mu_2')_{[4c]}$	$(\mu_2')_{[1]}$	$(\mu_2')_{[2]}$
46	1.598_5	1.449_7	1.610_2
163	1.576_5	1.422_8	1.586_1
304	1.577_9	1.424_5	1.587_8
381	1.592_1	1.442_5	1.603_2
620	1.545_8	1.386_0	1.553_0
824	1.480_3	1.311_0	1.483_5
1158	1.412_5	1.233_3	1.413_4

Numbers in square brackets refer to equation used for calculating μ_2'.

tainties not exceeding 5–10% can be tolerated in particle size determinations from light scattering.

On using the value of $(\mu_2')_0$, for calculating the size of the polystyrene particles—ranging in diameter from 45 to 814 mμ—from the specific turbidity, on the basis of Mie theory, a most satisfactory agreement was found, for the entire colloidal range, with those obtained from electron microscopy (17).[9] In the case of polyvinyltoluene good agreement was reached on allowing for a possible error in $(\mu_2')_0$ of 0.25% for diameters ranging from 120 to 824 mμ. This seems to remove any doubt that the $(\mu_2')_0$-values represent, in fact, the true refractive index μ_2 of the respective polymers irrespective of particle size. This index includes the contribution

---

[9] Insertion of μ_2'-values obtained at very large particle sizes, on the other hand, led to particle sizes far too small. The variation of the latter deviations with further increase in particle size reflected very well the variation of the deviation of the μ_2'-values from the extrapolated μ_2'-value, i.e., from $(\mu_2')_0$.

TABLE V

Comparison of Results for Colloidal and for Bulk Polymer

(5461 A.)

	Bulk polymer μ_2 (20°C.)	Colloidal polymer (this paper) $(\mu_2')_0$ (25°C.)
Polystyrene	1.596_4[a]	1.602_1
Polyvinyltoluene	1.585_2[b]	1.586_3

[a] Data recalculated for 5461 A. from Cauchy's dispersion formula (18).

[b] Based on values of 1.5831 for pure meta and 1.5766 for pure para polyvinyltoluene and taking into account that the polymer in the latices probably contained 65% meta and 35% para vinyltoluene units.

of the surface layer. Absence of a systematic change of μ_2' with particle size below $D \sim 400$ mμ indicates that the change of this contribution, with D, is less than the experimental error.

Regarding the decline of μ_2' with increasing D, at D values > 400 mμ, changes in the relative contribution of the surface layer to the refractive index cannot account for it in view of the absence of a detectable effect at smaller diameters where it should be more pronounced. The decline is so strong that systematic changes in molecular weight or polymer structure, with D, too extensive to be likely, would have to be assumed if such an alternate explanation were to be attempted. The magnitude of a decline in μ_2' of this origin should be less and certainly could not exceed the very small and almost negligible decline of ρ_2 with increasing D, found for the same samples (19). Nevertheless, it appeared desirable to provide an independent check of this variation of μ_2' with D excluding interference of the latter two variables. To this effect, a very dilute polyvinyltoluene latex, containing particles with a diameter of 47 mμ, was allowed to coagulate slowly in an interferometer cell by adding a small amount of NaCl as coagulating agent. This experiment actually duplicated, on a more quantitative basis, that carried out by Deile, Krämer, and Klause on concentrated systems using an Abbé refractometer (6). The coagulating system was completely homogenized, by gentle agitation, just prior to each measurement. A decrease in the measured refractive index of the colloidal system, amounting to seven units in the sixth decimal,[10] was observed during the increase in average particle size to more than 0.5 micron, by aggregation rather than by particle growth. The results shown in Fig. 3 give the changes of refractive index of the colloidal solution, relative to water, as a function of the time elapsed since addition of the coagulating electrolyte. Since the concentration remained sufficiently constant,[11] the curve reflects the be-

---

[10] This also shows that highly precise interferometric measurements are necessary in this type of work.

[11] Evaporation of water from the interferometer cell, covered with a tightly fitting glass plate, could not be avoided over the 5-day period. The resulting error in the

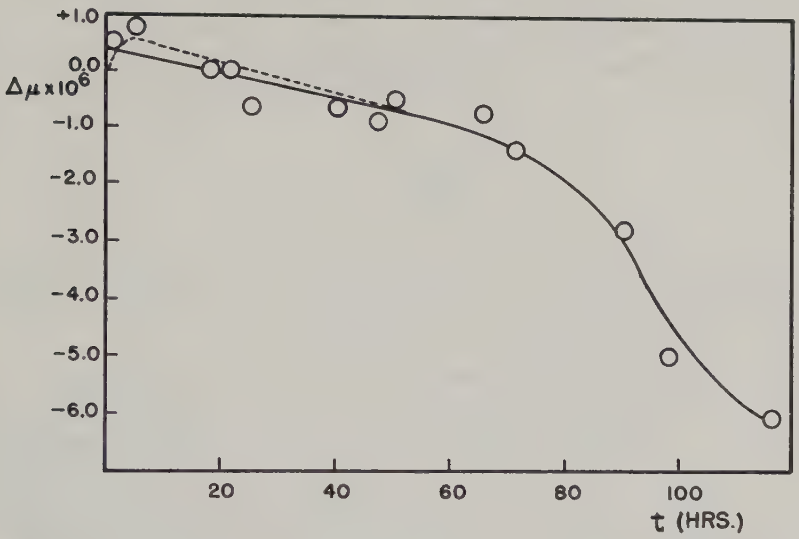

Fig. 3. Variation of the relative refractive index of a polyvinyltoluene latex with the progress of a very slow aggregation of the colloidal spheres. (D = 47 mμ). Coagulant: NaCl. t: time after adding electrolyte. T: 23° ± 2°C. Reference liquid: water. The ordinate represents the refractive index difference in excess of that found at $t = 0$.

havior of μ_2' also. The latter varied from an initial value of 1.599 to a final value of 1.474.[12]

The detailed features of the curve in Fig. 3 are of some interest. First of all, there appears to be a slight increase in the refractive index in the early stages of the growth of the particles by aggregation (dotted part of the curve). The increase observed is, however, not sufficiently far outside of the range of experimental error to be more than probable. After a sufficient period of time (approximately 100 hours in the example illustrated) the rate at which μ_2' decreases with increasing particle size seems to decline appreciably. This again is only probable and not certain, since the experiment was not extended beyond a period of 5 days.

The preceding experiments and their discussion show conclusively that the apparent refractive index of polymer spheres varies both with their size and on aggregation and that no nonoptical change can account for this optical change, particularly not in the latter instance. The increase in light scattering with particle size is, therefore, the only conceivable simultaneous, optical, variable which could be the cause of the change in μ_2'.

Upon conclusion of the experiments reported here, a very interesting paper by Zimm and Dandliker (12) appeared concerning the quantitative

---

quantitative data is not of importance for the present purpose, since in its absence the decrease in $\Delta\mu$ with time would have been even more pronounced.

[12] A very definite increase in turbidity was noted 40 hours after the addition of the electrolyte and the actual formation of discrete flocs set in after about 63 hours.

TABLE VI

True Refractive Index of Polystyrene Spheres as Derived from a New Mixture Rule

Polystyrene

No.	D (mμ)	μ_2
1	135	1.58_6
2	249 (238)[a]	1.58_5
3	238 (249)[a]	1.59_7
4	271	1.59_7
5	514	1.59_1

[a] Electron microscope samples 2 and 3 seem to have been inverted. The probably correct diameters are given in brackets.

effect of light scattering on the refractive index of colloidal particles. A new mixture rule was derived on the basis of the equation given by Zimm and Dandliker (14). General features of the μ_2' versus D curve as established theoretically on the basis of the new mixture rule are remarkably similar to the curves given in Figs. 2*a*, 2*b*, and 3. By means of a graphical interpolation method—also described elsewhere (14)—it became possible to calculate the true refractive index, μ_2, from the μ_2'-data reported here in conjunction with the turbidity data obtained on the same samples (17). These μ_2-values are given in Table VI for polystyrene. It is seen from this table that the true refractive index of the polymer spheres, i.e., the refractive index obtained on excluding the contribution of light scattering, is, as expected, independent of particle size. The agreement of the various μ_2-values pertinent to widely different particle diameters must be considered as remarkably good since the results are affected by the combined uncertainties inherent in interferometric, light-scattering, and density measurements, in concentration determinations, and in the application of the graphical method employed for the derivation of μ_2. On averaging the μ_2-values of Table VI one obtains 1.59_1 for polystyrene (complete polyvinyltoluene data not being available). This value agrees within better than 1% with the $(\mu_2')_0$ given in Table II, which must be considered as very satisfactory. Obviously, the new graphical method for obtaining μ_2 from μ_2', with the aid of turbidity data, is less accurate than the extrapolation method described here. It has, on the other hand, the advantage that μ_2' needs to be determined only on a single system.

SUMMARY

Interferometric measurements on a series of monodisperse polyvinyltoluene and polystyrene latices of systematically varied particle size show that the refractive index of colloidal particles derived from experiment by means of mixture rules is an apparent quantity. It decreases with increasing particle size, and also with increasing aggregation, at constant size of the primary particles. It is shown that this effect can be caused only by the

effect of light scattering upon the experimentally measured quantities. An experimental extrapolation method is described by means of which the true refractive index of the colloidal particles can be obtained. The latter is independent of particle size.

REFERENCES

1. HELLER, W., AND PANGONIS, W., *J. Chem. Phys.* **26**, 498 (1957).
2. See, for instance: ROBERTSON, T., *J. Phys. Chem.* **13**. 469 (1909); *J. Biol. Chem.* **7**, 359 (1910); *ibid.* **8**, 287, 441, 507 (1910).
3. This interaction is, as is to be expected, negligible for lyophobic particles (see the numerous examples in Ostwald's survey on work prior to 1915; OSTWALD, WO., "Licht und Farbe in Kolloiden," T. Steinkopff, Dresden und Leipzig, 1924, and therefore does not enter for the systems investigated here.
4. SCHOORL, N., *Rec. trav. chim.* **43**, 205 (1924).
5. JOSHI, S. S., *et al.*, *J. Indian Chem. Soc.* **13**, 141, 217, 309 (1936).
6. DEILE, O., KRÄMER, H., and Klause, W., *Kolloid-Z.* **130**, 105 (1953).
7. HELLER, W., *Compt. rend.* **205**, 971 (1937).
8. HELLER, W., *Phys. Rev.* **68**, 5 (1945).
9. WIENER, O., *Physik. Z.* **5**, 332 (1904); *Ber. Akad. Wiss. Leipzig* **61**, 113 (1909); *ibid.* **62**, 256 (1910); *Abhandl. sächs Akad. Wiss.* Leipzig **33** (No. 6) (1912).
10. FREUNDLICH, H., AND ROGOWSKI, F., *Kolloid-Beih.* **37**, 215 (1933).
11. EWART, R. H., ROE, C. P., DEBYE, P., AND MCCARTNEY, J. R. (*J. Chem. Phys.* **14**, 687 (1946)) and also BOUTARIC, A. (*Compt. rend.* **228**, 79 (1949)) subsequently gave mixture rules equivalent to that in ref. (8).
12. ZIMM, B., AND DANDLIKER, W., *J. Phys. Chem.* **58**, 644 (1954).
13. DEBYE, P., *J. Appl. Phys.* **15**, 338 (1944).
14. NAKAGAKI, M., AND HELLER, W., *J. Appl. Phys.* **27**, 975 (1956).
15. See, for instance: CHRISTIANSEN, C., *Ann. Physik* **23**, 298 (1884); *ibid.* **24**, 439 (1885).
16. KAHLER, H., AND LLOYD, B., Jr., *Science* **114**, 34 (1951).
17. TABIBIAN, R., HELLER, W., AND EPEL, J. N., *J. Colloid Sci.* **11**, 195 (1956); HELLER, W., EPEL, J. N. AND TABIBIAN, R., *J. Chem. Phys.* **22**, 1777 (1954).
18. BOUNDY, R., AND BOYER, R., "Styrene," p. 524. Reinhold, New York, 1952.
19. PUGH, T. L., AND HELLER, W. *J. Colloid Sci.* **12**, 173 (1957).

JOURNAL OF COLLOID SCIENCE **12,** 308–320 (1957)

MECHANICAL PROPERTIES OF A POLYURETHANE ELASTOMER IN THE RUBBER-TO-GLASS TRANSITION ZONE

Robert F. Landel

Jet Propulsion Laboratory, California Institute of Technology, Pasadena 3, California

Received December 13, 1956

ABSTRACT

The complex shear compliance of a polyurethane elastomer has been measured in the transition region from rubbery to glasslike properties with a Fitzgerald transducer. Values for the real and imaginary components of the complex shear compliance J' and J'' are reported over a frequency range of 45 to 6000 cycles/sec. and a temperature range of -16 to 39°C. Composite curves of J' and J'' reduced to a standard temperature were obtained by the method of reduced variables. The temperature shift factors followed the WLF equation. The data do not extend to high enough reduced frequencies to approach the glassy compliance, but at low frequencies the dynamic compliance is essentially equal to the equilibrium rubbery value. The loss tangent J''/J' passes through an extremely broad maximum with increasing frequency. The shape of the retardation distribution function resembles that of polyisobutylene; however, the value of the ratio of the maximum in the retardation distribution function to the equilibrium compliance is not the same for the two polymers. The value for the polyurethane agrees instead with that previously found for cellulose tributyrate and polyvinyl chloride gels (which are crosslinked by crystallization). For several decades at the long time end of the transition zone the relaxation distribution function has the slope of $-\frac{1}{2}$ prescribed by the Rouse theory, as does a 20.4% cellulose tributyrate gel. At shorter times the experimental curve rises more steeply than predicted by theory, just as do the corresponding curves for vinyl polymers. However, the total deviation from the linear theoretical curve is small and the overall shape of the relaxation distribution function for the polyurethane more nearly resembles that found for disubstituted than for monosubstituted vinyls.

INTRODUCTION

The dynamic mechanical properties of a number of amorphous uncrosslinked vinyl polymers have been studied in recent years (1). Above the glass transition temperature T_g, the time dependence of these properties has been interpreted in terms of the Rouse (2) and Bueche (3) molecular theories of viscoelasticity and the temperature dependence in terms of the WLF (4) equation, a near-universal function of T_g.

The time dependence originates in cooperative modes of motion of segments of the coiled polymer molecules as the disturbed coils strive to return to their equilibrium configuration under the influence of Brownian motion. The primary molecular parameters characterizing these modes of motion are the average frictional resistance to motion encountered by a monomer unit (5), the effective bond length of the monomer (5), and, for sufficiently long chains, the amount of intermolecular entanglement with neighboring molecules (5, 6). The temperature dependence of mechanical properties is due primarily to the temperature dependence of the frictional resistance factor, which is a function of the free volume of the system.

With the broad outlines of mechanical properties thus well understood, attention is now turning to the fine structure of the distribution functions of relaxation or retardation times. Watkins, for instance, has recently reported on the effects of molecular weight distribution (7) and chain branching (8). Ferry and co-workers are studying the effects not only of increasing the length of side chains on vinyl polymers (alkyl methacrylates) (9, 10) but also of changing the backbone structure itself, by comparing the properties of vinyls and cellulose derivatives (11, 12).

In view of the differences between the behavior of the cellulosic and vinyl systems, it is of interest to study polymers whose backbone structure is intermediate in complexity. Such studies should serve to delineate more clearly the effect on mechanical behavior of changes in the basic structure. One readily available class of polymers of this type is the polyurethane. Since these polymers are generally utilized as crosslinked rubbers, only the transition zone from rubbery to glasslike behavior is of immediate interest, although Offenbach and Tobolsky (13) have shown that at long times and high temperatures these materials undergo chemical stress relaxation.

MATERIALS AND METHODS

The polyurethane elastomer selected for study was a sample of Vulcollan 18/40 provided by the Mobay Chemical Co.[1] It is apparently the same material as the Vulcollan B used by Tobolsky. Vulcollan 18/40 is prepared from a low molecular weight polyester which is extended and crosslinked to form an elastomer by reacting it with naphthalene 1,4-diisocyanate and 1,4-butanediol. The polyester has a molecular weight of approximately 2000 and is prepared from adipic acid and a mixture of ethylene and propylene glycols.

Measurements of the complex shear compliance ($J^* = J' - iJ''$) were made at frequencies between 45 and 6000 cycles per second with a Fitzgerald Transducer[2] (14). The commercial instrument differs from the original model in having two transducers in the housing rather than one. These transducers will be referred to as Side I and Side II.

The apparatus was tested after calibration by measuring the compliance of the National Bureau of Standards sample of polyisobutylene (15) at 0,

---

[1] Mobay Chemical Co., St. Louis, Missouri.

[2] Atlantic Research Corp., Alexandria, Virginia.

20, 50, and 80°C. and comparing the results with the published values of Fitzgerald, Grandine, and Ferry (16). The agreement was satisfactory.

The disklike samples of Vulcollan used in the transducer were cut from $\frac{1}{16}$ in. sheets with either a cylindrical cutter or a specially constructed knife-blade tool mounted in a drill press. During cutting, the samples were lubricated with glycerine which was subsequently washed off with tap water. The samples were then stored in a desiccator for 2 to 7 days before use. Once the samples had been inserted in the apparatus, a very gentle stream of tank nitrogen was continuously passed through the housing in order to minimize the effects of moisture and oxygen.

Three pairs of samples were used. Samples 7 and 10, approximately $\frac{1}{16}$ in. (thickness) by $\frac{3}{8}$ in. (diameter), were inserted in Sides I and II. Their sample coefficients[3] were calculated to be 10.9 and 10.4 cm., respectively. Sample 9, $\frac{1}{16}$ in. by $\frac{5}{32}$ in., was run concurrently with sample 10 and had a nominal sample coefficient of 29.8 cm. However, it did not adhere perfectly to the driving tube surfaces, as evidenced by the fact that values of both J' and J'' were higher than those obtained from samples 7 and 10. On the other hand, the loss tangents, which are independent of the sample coefficient, were in full agreement. The application of an empirical correction factor of 0.76 gave results which essentially duplicated those of sample 10. Therefore, the data obtained on sample 9 are not reported here. Although the sample coefficients of 7 and 10 are admittedly nearly identical, the fact that these two samples were studied in separate sides of the transducer lends credence to the validity of the sample coefficients used. All samples were compressed about 9%, which produced a slight bulging. However, compression tests made outside the transducer showed that the sample coefficients could not be in error by more than 0.4% so that no correction for bulging was necessary. The values of the sample coefficients at the various temperatures were calculated using an experimentally determined thermal expansion coefficient of 6.80×10^{-4} deg.$^{-1}$.

RESULTS

The temperature sequence followed in making measurements on sample 7 was: 11.5, 9.7, 0.4, −6.1, −11.1, 13.9, 6.2, −16.2, and a check run at 14.0; that for sample 10 was 14.2, 0.9, 25.3, and 39.4. As mentioned above, the values of both J' and J'' for sample 10 agreed with those of sample 7 at the overlapping temperatures. The values of J' and J'' are plotted logarithmically in Figs. 1 and 2.

Logarithmic plots of the reduced compliance $J_p' = J'[(T\rho/T_0\rho_0) + (J_\infty/J')(1 - T\rho/T_0\rho_0)]$ and $J_p'' = J''(T\rho/T_0\rho_0)$ were prepared to test the method of reduced variables (17). Here ρ and ρ_0 are the densities at the absolute temperature of measurement T and the standard temperature T_0. The limiting high frequency compliance J_∞, was assumed to be

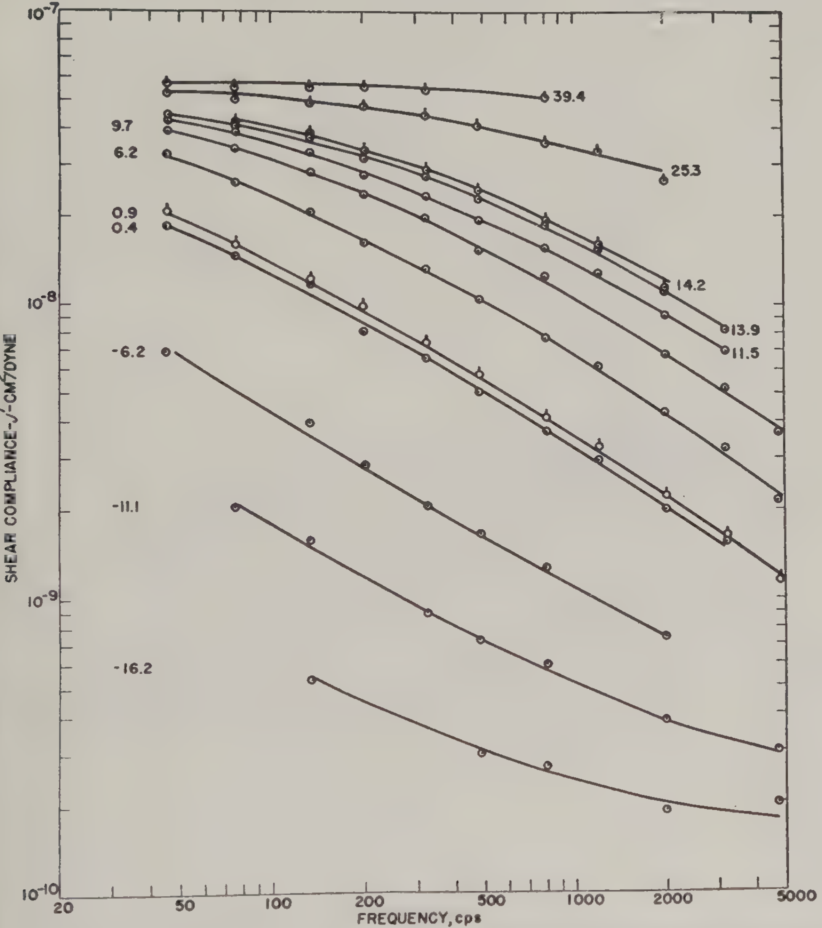

FIG. 1. Variation of the real part of the complex shear compliance of Vulcollan at the indicated temperatures. Tag up: Sample 10; no tag: Sample 7.

10^{-10} cm.$^{-2}$/dyne, and T_0 was chosen as 273.6°K. While 287°K. might have been a better choice of standard temperature, because data on both samples were obtained there, J'' passes through its maximum at this temperature, and the resulting flat curves are not suitable as a basis for obtaining a_T values. If the method of reduced variables is applicable, then all relaxation times depend identically on temperature. An identical horizontal shift for both J_p' and J_p'' on a logarithmic frequency scale should force the reduced compliance curves to coincide and form two master curves. By using the values of the shift factor a_T given in Table I, satisfactory superposition of J_p' and J_p'' was obtained as shown in the composite plots of Figs. 3 and 4.

TABLE I

Temperature Shift Factors

Temp.. °C.	Log a_T
39.4	−2.67
25.3	−2.05
14.2	−1.29
13.9	−1.27
11.5	−1.09
9.7	−0.88
6.2	−0.54
0.9	−0.09
0.4	0.00
−6.1	0.80
−11.1	1.54
−16.2	2.38

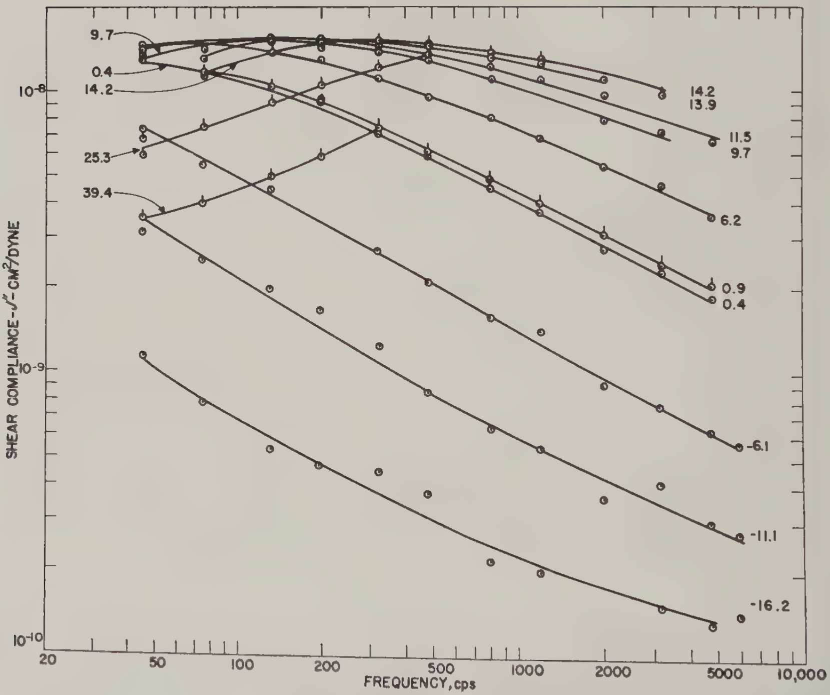

FIG. 2. Variation of the imaginary part of the complex shear compliance of Vulcollan at the indicated temperatures. Tag up: Sample 10; no tag: Sample 7.

DISCUSSION

Temperature Dependence

The values of a_T are plotted against $T - T_0$ in Fig. 5 for comparison with one form of the WLF equation (4):

$$\log a_T = -8.86\,(T - T_s)/(101.6 + T - T_s),$$

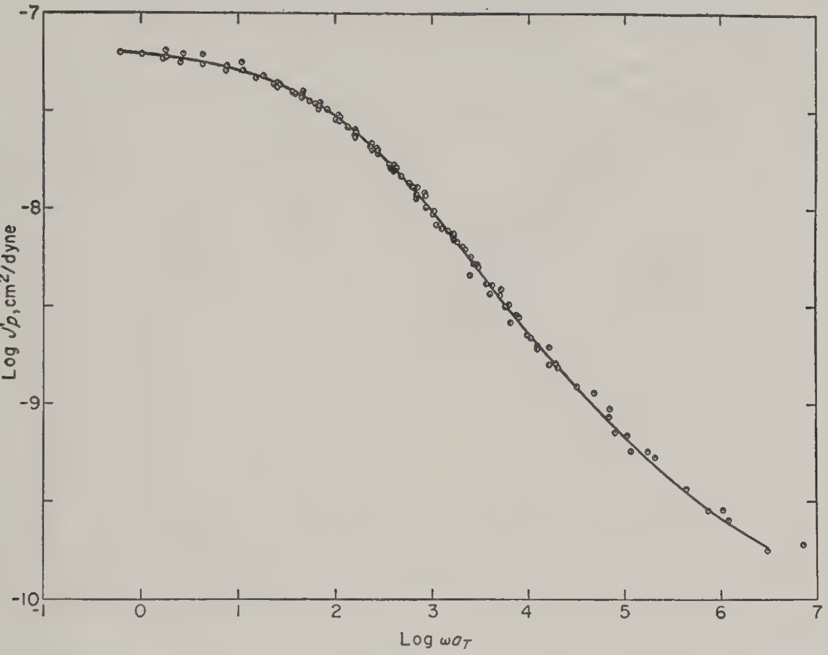

FIG. 3. Real part of the complex compliance reduced to 0.4°C., plotted logarithmically against reduced frequency. Sample 10 is not distinguished from Sample 7. Temperature key same as in Fig. 1.

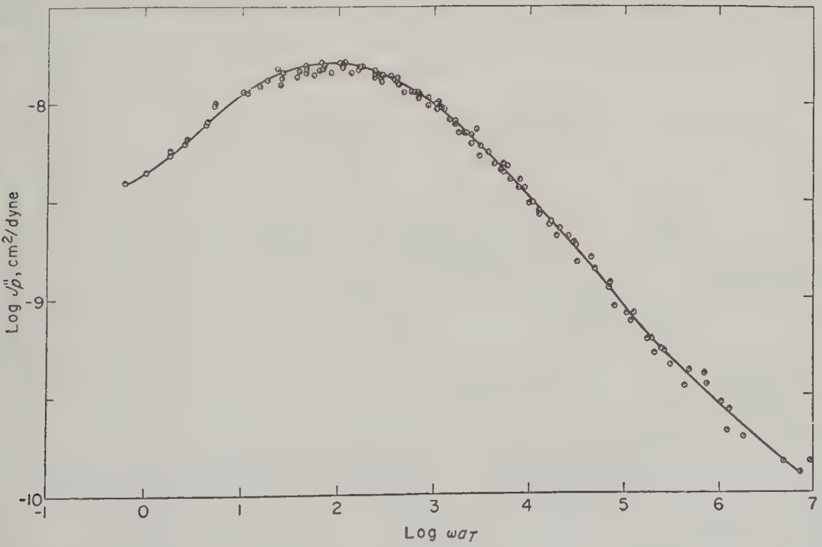

FIG. 4. Imaginary part of the complex compliance reduced to 0.4°C., plotted logarithmically against reduced frequency. Sample 10 is not distinguished from Sample 7. Temperature key same as in Fig. 2.

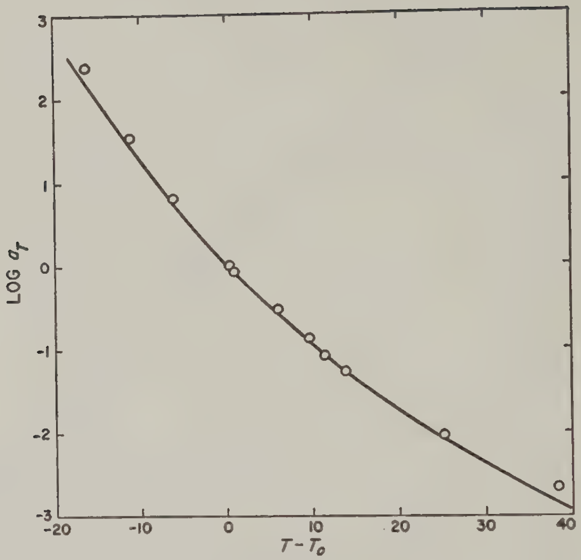

FIG. 5. Temperature reduction factors plotted logarithmically against $T-T_0$. The curve is from the WLF equation.

where T_s is a standard reference temperature which should be about 50° higher than the glass transition temperature T_g. By fitting the data to this equation, T_s for the system is found to be 283°K. and T_g should therefore by very nearly −40°C. Preliminary measurements of the linear expansion of Vulcollan strips give a value of −35°, in reasonable agreement.

Magnitude of Mechanical Properties

The measurements did not extend to high enough reduced frequencies to give J_∞ directly. The sample sheets available were too thin to give sample coefficients sufficiently small to enable precise measurements to be made in this region. The transducer is so designed that the sample admittance Y_M' is given by $Y_M' = Y_{AB} - Y_M''$, where Y_{AB} is a measured admittance and Y_M'' is an apparatus admittance. Since $Y_M' = i\omega J^*/C$, a small value of C is required when the samples are hard and J^* is small in order to avoid losing precision when calculating the difference $Y_{AB} - Y_M''$.

Vulcollan is crosslinked by primary valence bonds and thus has a true equilibrium rubbery modulus G_E. Therefore G', the real part of the complex shear modulus G^* $(= 1/J^* = G' + iG'')$, is actually the sum of a time-independent modulus, G_E, and a time-dependent modulus, $G' - G_E$. It is G' which is calculated directly from J' and J'', but it is $G' - G_E$ which is determined by the distribution function of relaxation times and

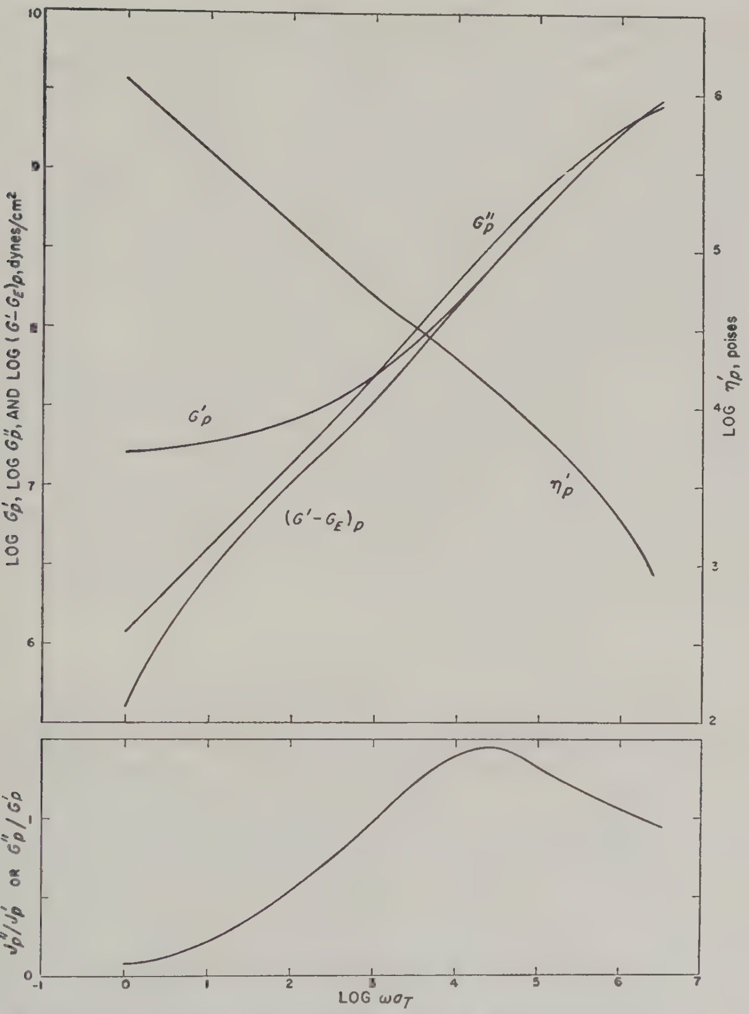

FIG. 6. Total real and time-dependent real parts of the complex shear modulus, G_p' and $(G'-G_E)_p$, imaginary part of the modulus, G_p'', and real part of the complex shear viscosity, η_p', all reduced to 0.4°C. and plotted logarithmically against reduced frequency. Reduced loss tangent plotted against log reduced frequency.

is therefore a function of the molecular relaxation processes. Values of G', G'', and the real part of the complex viscosity η' $(= G''/\omega)$ were calculated from the composite curves of Figs. 3 and 4 and are plotted logarithmically against the reduced frequency in Fig. 6. The limiting value of G' at low frequencies is G_E. The value of G_E at 0.4°C. was estimated from the curve to be $10^{7.20}$ dynes/cm.^{2} and the quantity $G' - G_E$, also shown in Fig. 6, was calculated accordingly. The corresponding room temperature value of G_E is 1.47×10^7 dynes/cm.^{2}, in excellent agreement with a value of 1.44×10^7 dynes/cm.^{2} obtained by direct measurement under static conditions. The slope of the G' curve is less for the polyurethane than for non-crosslinked amorphous polymers. This is due in part to the fact that the value of G' at high reduced frequencies is the glassy modulus, which is nearly independent of the system. However, the limiting value at low frequencies is G_E and since the equilibrium modulus will be higher for a crosslinked system, the G' slope will be less. The Vulcollan is thus similar in this respect to cellulose tributyrate gels which are crosslinked by crystallization of the polymer (11).

The loss tangent J''/J' $(= G''/G')$, also plotted in Fig. 6, follows a very broad curve with a low maximum, again resembling the behavior of the cellulose tributyrate gels rather than vinyl polymers. The only vinyl derivative which shows a similar loss tangent curve is polyisobutylene (18). Indeed, the very gentle descent from the maximum at higher reduced frequencies is reminiscent of the shoulder observed with polyisobutylene. In the present case, however, the shape of the curve beyond the maximum may be an artifact due to experimental inaccuracies at higher reduced frequencies.

Retardation Distribution Function

The distribution function of retardation times L was calculated from the composite curves of Figs. 3 and 4 by the usual second approximation methods (19). The values are tabulated in Table II and plotted in Fig. 7. Those calculated from J' are in good agreement with those from J''.

The ratio of the maximum value of L to the equilibrium compliance is 0.14, essentially the same as the value of 0.13 found for cellulose tributyrate (CTB) and polyvinyl chloride gels (11). On the other hand, L peaks more sharply for the Vulcollan than it does for the gels and in this respect closely resembles the shape of L for polyisobutylene, where $L_{\max}/J$ is 0.20. The relative shapes are indicated in Fig. 8, where the distribution functions of CTB and PIB have been shifted by an arbitrary amount to give a common value of $L_{\max}$ for all three systems.

Relaxation Distribution Function

The distribution function of relaxation times Φ was calculated from the plots of G' and G'' of Fig. 6 by the second approximation methods. Since Φ is independent of G_E, the G' plot was used in the calculation instead of $G' - G_E$ because of its greater accuracy. Values of Φ are also given in Table II and plotted in Fig. 7. Again the values calculated from the real and imaginary components of the modulus are in reasonable agreement.

The Rouse theory predicts a slope of $-\frac{1}{2}$ for Φ in the region of the time scale where cooperative motion involves segments long enough to be

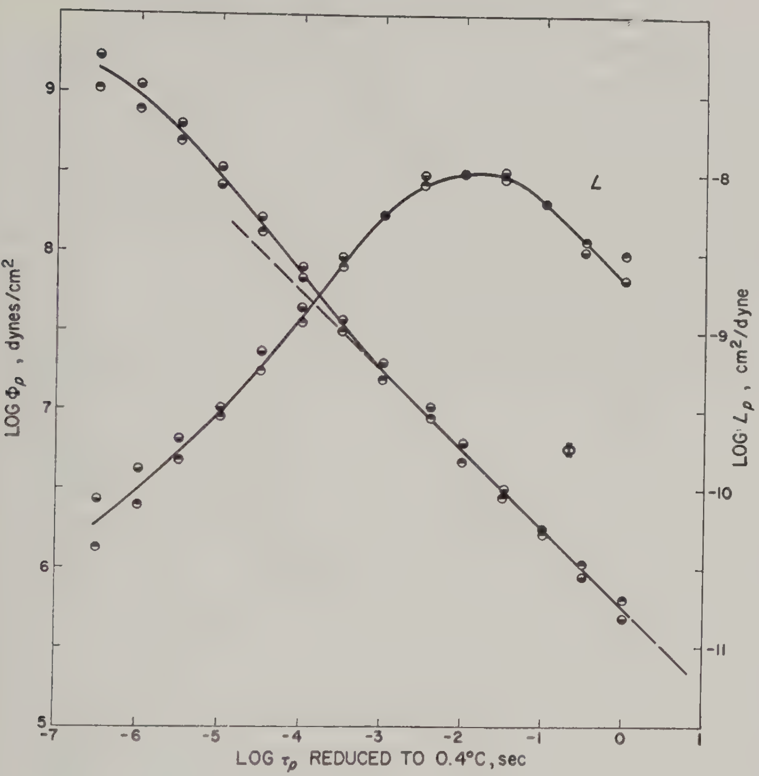

FIG. 7. Distribution functions of relaxation times, Φ, and retardation times, L, reduced to 0.4°C. and plotted logarithmically against reduced time. Key: top black circles, calculated from G_p' or J_p'; bottom black, from G_p'' or J_p''. Dashed line indicates the slope of $-\frac{1}{2}$ predicted by the Rouse theory.

independent of short-range effects, such as steric hindrances to rotation about bonds, but not so long as to be influenced by the behavior of chain ends, whether free or immobilized in crosslinks. Relaxation distribution functions for vinyl polymers follow this slope at the long-time end of the transition zone in the region where $\log \Phi = 6$ but have higher slopes at shorter times. A 20.4% CTB gel shows the predicted slope over several decades, but the more concentrated gels exhibit lower slopes. The Vulcollan resembles the dilute CTB system in that Φ follows the form predicted over 3½ decades of log time but then rises more steeply as it does with vinyls. The correlation with the Rouse theory implies that the polyester chain behaves more like a free-draining coil than do the carbon-carbon chains of the vinyl polymers studied thus far.

On the other hand, even though the chain behaves as if it were a free-draining coil, the monomeric friction coefficient (5) is of the order of

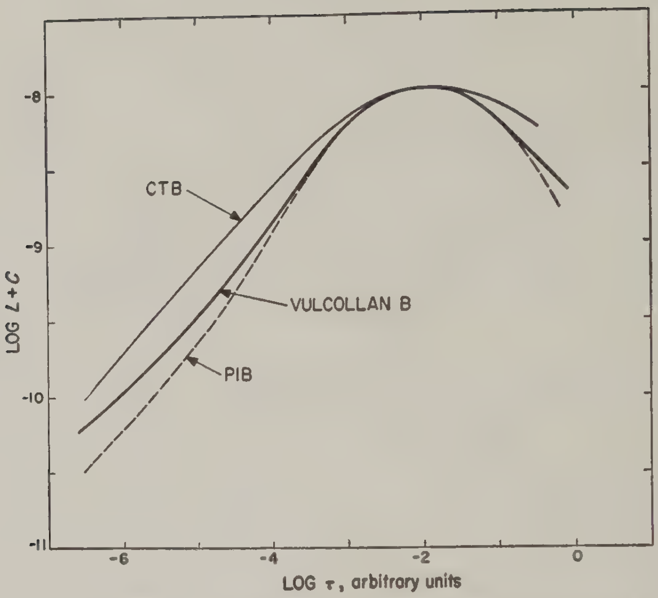

FIG. 8. Relative shapes of distribution functions of retardation times for Vulcollan B, polyisobutylene, and a 20.4% gel of cellulose tributyrate in dimethyl phthalate. The CTB and PIB curves have been shifted by an arbitrary amount, C, to give a common value of L_{max}.

TABLE II

Retardation and Relaxation Distribution Functions Reduced to 0.4°C.

	Log L		Log Φ	
Log τ	From J'	From J''	From G'	From G''
0.0	−8.51	−8.67	5.80	5.68
−0.5	−8.43	−8.49	6.03	5.94
−1.0	−8.18	−8.17	6.25	6.23
−1.5	−8.03	−7.98	6.45	6.51
−2.0	−8.00	−8.00	6.67	6.79
−2.5	−8.07	−8.01	6.96	7.02
−3.0	−8.27	−8.27	7.19	7.30
−3.5	−8.59	−8.53	7.50	7.57
−4.0	−8.95	−8.85	7.83	7.91
−4.5	−9.26	−9.13	8.13	8.22
−5.0	−9.55	−9.49	8.42	8.53
−5.5	−9.82	−9.68	8.69	8.81
−6.0	−10.11	−9.87	8.89	9.04
−6.5	−10.38	−10.07	9.02	9.23

magnitude found for vinyl derivatives (20). The monomeric friction coefficient of homopolymers, ζ_0, can be calculated from the following equation (5):

$$\zeta_0 = 24\pi^2 \Phi^2 \tau \times 10^{16} (M_0/a\rho)^2/kTN_0^2$$

where M_0 is the monomer molecular weight, a is the equivalent bond length of the monomer unit in A, ρ is the density at the temperature T, k is the Boltzmann constant, and N_0 is Avogadro's number. Although the value of a is unknown, the quantity M_0/a, the molecular weight per equivalent bond length, is probably close to 12 g./mole/A, the average value found for vinyl derivatives. The value of ρ at 0°C. is 1.26 g./cm.^{3}, so that $\log \zeta_0 = -2.76$ at that temperature or 4.60 at T_g, 233°K. A much smaller value of M_0/a is obtained if the estimation is made somewhat differently. If the ester were prepared from adipic acid and ethylene glycol, and the length of the carbon-oxygen bond along the chain were equivalent to that of the carbon-carbon bond in the bimethylene groups, then the monomer length would be equivalent to five C-C units of a vinyl polymer. The average value of a for such units is 6 A. The equivalent monomer molecular weight is $M_0/5$, and M_0/a is reduced to 5.73 g./mole/A. Nevertheless $\log \zeta_0$ is decreased by only 0.32 log unit. Since $\log \zeta_0$ is roughly proportional to T_g, these values are in accord with those found for PIB (T_g = 202°K., $\log \zeta_0 = 4.04$) and polymethyl acrylate ($T_g = 276$, $\log \zeta_0 = 6.24$) (20). The value for the 20.4% CTB gel at T_g (about 195°K.) is of the order of 9.3.

CONCLUSIONS

The change in backbone structure from a vinyl to a polyester containing several adjacent methylene groups does not modify the mechanical properties to any great degree. The crosslinks modify the response primarily in their effect on the equilibrium modulus, although the higher value of the latter affects the response over several decades of logarithmic time. The resulting changes in the dynamic modulus or compliance are in accord with those observed in gels crosslinked by crystallization.

ACKNOWLEDGMENTS

The raw data pertaining to the Vulcollan were taken by Mr. V. H. Howard; the calculation of J' and J'' from these data was carried out on an Electrodata Computer by Mr. M. J. Seamons of the Computer Service Group of the Jet Propulsion Laboratory.

REFERENCES

1. For a recent review, see FERRY, J. D., Chapter 6 in Stuart, "Die Physik der Hochpolymeren," Vol. 4, Springer, Berlin, 1955.
2. ROUSE, P. E., JR., *J. Chem. Phys.* **21,** 1272 (1953).
3. BUECHE, F., *J. Chem. Phys.* **22,** 603 (1954).

---

[3] The sample coefficient, C, is equal to twice the ratio of the sample area to the sample thickness. It is a proportionality factor relating the complex mechanical admittance of the sample Y_M' to its complex compliance: $J^* = -i\,CY_M'/\omega$ where $i = \sqrt{-1}$ and ω is the frequency in radians/sec.

4. Williams, M. L., Landel, R. F., and Ferry, J. D., *J. Am. Chem. Soc.* **77,** 3701 (1955).
5. Ferry, J. D., Landel, R. F., and Williams, M. L., *J. Appl. Phys.* **26,** 359 (1955).
6. Bueche, F., *J. Chem. Phys.* **20,** 1959 (1952).
7. Watkins, J. M., Spangler, R. D., and McKannan, E. C., *J. Appl. Phys.* **27,** 685 (1956).
8. Watkins, J. M., Paper presented at the 129th meeting of the American Chemical Society at Dallas, Texas, April 11, 1956.
9. Child, W. C., Jr., and Ferry, J. D., Presented at the meeting of the American Physical Society, Pittsburgh, Pennsylvania, March 15, 1956.
10. Ferry, J. D., Child, W. C., Jr., Zand, R., and Stern, D. M., Presented at the meeting of The American Physical Society, Pittsburgh, Pennsylvania, March 15, 1956.
11. Landel, R. F., and Ferry, J. D., *J. Phys. Chem.* **59,** 658 (1955); *ibid.* **60,** 294 (1956).
12. Plazek, D. J., and Ferry, J. D., *J. Phys. Chem.* **60,** 289 (1956).
13. Offenbach, J. A., and Tobolsky, A. V., *J. Colloid Sci.* **11,** 39 (1956).
14. Fitzgerald, E. R., and Ferry, J. D., *J. Colloid Sci.* **8,** 1 (1953).
15. Marvin, R. S., "The Dynamic Mechanical Properties of Polyisobutylene," Proceedings of the Second International Congress on Rheology, Academic Press Inc., New York, 1954.
16. Fitzgerald, E. R., Grandine, L. D., Jr., and Ferry, J. D., *J. Appl. Phys.* **24,** 650 (1953).
17. Ferry, J. D., and Fitzgerald, E. R., *J. Colloid Sci.* **8,** 224 (1953).
18. Ferry, J. D., Grandine, L. D., Jr., and Fitzgerald, E. R., *J. Appl. Phys.* **24,** 911 (1953).
19. Williams, M. L., and Ferry, J. D., *J. Polymer Sci.* **11,** 169 (1953).
20. Ferry, J. D., and Landel, R. F., *Kolloid-Z.* **148,** 1 (1956).

JOURNAL OF COLLOID SCIENCE **12**, 321–324 (1957)

RATE CONSTANTS IN THE POLYMERIZATION OF METHYL METHACRYLATE

U. S. Nandi

Indian Association for the Cultivation of Science, Calcutta 32, India

Received October 24, 1956

ABSTRACT

Kinetic constants, e.g., δ and C_M for methyl methacrylate polymerization within the range of 20°C. to 115°C. are presented from work carried out with a wide variety of initiators and under varying conditions.

The general equation correlating the number-average degree and rate of polymerization in a catalyzed system may be easily deduced (1, 2) as

$$1/\bar{P} = C_M + C_I I/M + R_p\delta^2/M^2 \qquad [1]$$

where $\bar{P}$ = number-average degree of polymerization;
C_M, C_I = chain transfer for monomer and initiator ($C_M = k_{trM}/k_p$);
I, M = catalyst and monomer concentrations;
R_p = rate of polymerization;
$\delta = k_t^{1/2}k_p$; k_t and k_p are the rate constants for termination and propagation of the polymer chain.

From the general equation [1] δ and C_M can be evaluated by the existing methods already described in our previous publications (3–5). The values of δ and C_M, especially the former, are very important as they occupy a unique position in the correct determination of the initiation rate of a polymerizing system.

$$R_i\,(1 + x) = 2\,R_p^{\,2}\,\delta^2/M^2, \qquad [2]$$

where x is the ratio of disproportionation to the overall termination process.

In an earlier publication Ferington and Tobolsky (6) have compiled data for δ^2 and C_M at various temperatures. In the present paper we have tried to supplement data obtained, over a wider range of temperature and with a wide variety of catalysts, in our own laboratory. The results are represented in Table I.

From the above table it may be observed that values for δ and C_M obtained by us are in excellent agreement with those of Baysal and Tobolsky (2) and other workers in the field. In the case of C_M the older literature values of Schulz and Harborth (7) appear to be somewhat high. The value

TABLE I

δ and C_M for Methyl Methacrylate at Various Temperatures

Temp. (°C.)	δ	$C_M \times 10^5$	Catalyst	Reference
20	17.64	*0.3*	Azo	*a*
25	17.09	1.5	Azo	*b*
30	13.27	1.2	Azo	*a*
	13.89	1.5	BZ_2O_2	*c*
35	—	*0.2*	H_2O_2	*h, i*
50	10.15	4.0	BZ_2O_2 and Azo	
	11.62	0.8	H_2O_2	*h, i*
60	8.20	1.0	Azo	*e*
	8.08	—	Azo	*f*
	8.43	1.0	H_2O_2	*h, i*
	8.32	1.0	Azo, 1,1′ Azobis cyclohexane carbonitrile, Azo, 2 methylbutynitrile, 2,2′ Azo 2, 4 dimethylbutyronitrile, 2,2′ Azo 2 methyl 3,3 dimethylbutyronitrile, 2,2′ Azo 2 methyl butyronitrile	*j*
	7.55	0.90	*o*-Cl BZ_2O_2	*k*
	7.22	1.0	*p*-methoxy BZ_2O_2	*k*
	8.25	0.97	Palmitoyl peroxide	*k*
	8.12	1.0	*m*-Cl BZ_2O_2	*k*
	7.66	1.05	*p*-NO_2 BZ_2O_2	*k*
	7.22	1.10	*o*-CH_3 BZ_2O_2	*k*
	7.95	1.01	Cinnamoyl peroxide	*k*
	7.80	1.03	*p*-Cl BZ_2O_2	*k*
	7.55	1.20	*m*-NO_2 BZ_2O_2	*k*
70	6.63	6.0	BZ_2O_2	*d*
80	5.26	1.6	H_2O_2	*h, i*
98	4.05	3.1	DTBP	*g*
115	2.48	5.5	H_2O_2	*h, i*

Azo—2,2′ Azobisisobutyronitrile; BZ_2O_2—Benzoyl peroxide, DTBP—di-*t*-butylperoxide.

[a] Levy, J. A., Senior thesis, Princeton University, Princeton, New Jersey, 1954.

[b] Hseih, H., Unpublished results (cited by Ferington, T. E., and Tobolsky, A. V., *J. Colloid Sci.* **10,** 536 (1955).

[c] Ferington, T. E., *J. Colloid Sci.* **10,** 536 (1955).

[d] Schulz, G. V., and Harborth, G., *Makromol. Chem.* **1,** 106 (1947).

[e] Baysal, B., and Tobolsky, A. V., *J. Polymer Sci.* **8,** 529 (1952).

[f] O'Brien, J. L., and Gornick, F., Presented at Philadelphia meeting of American Chemical Society, Jan. 29, 1953.

[g] Offenbach, J., Unpublished results (cited by Ferington, T. E., and Tobolsky, A. V., *J. Colloid Sci.* **10,** 536 (1955)).

[h] Nandi, U. S., and Palit, S. R., *J. Polymer Sci.* **17,** 65 (1955).

[i] Nandi, U. S., and Palit, S. R., Proceedings of the International Macromolecular Symposium, 1954, published in *La Reserca Scientifica.*

[j] Saha, N. G., Nandi, U. S., and Palit, S. R., Unpublished results from this laboratory.

[k] Saha, N. G., Nandi, U. S., and Palit, S. R., *J. Chem. Soc.* **85,** 427 (1956).

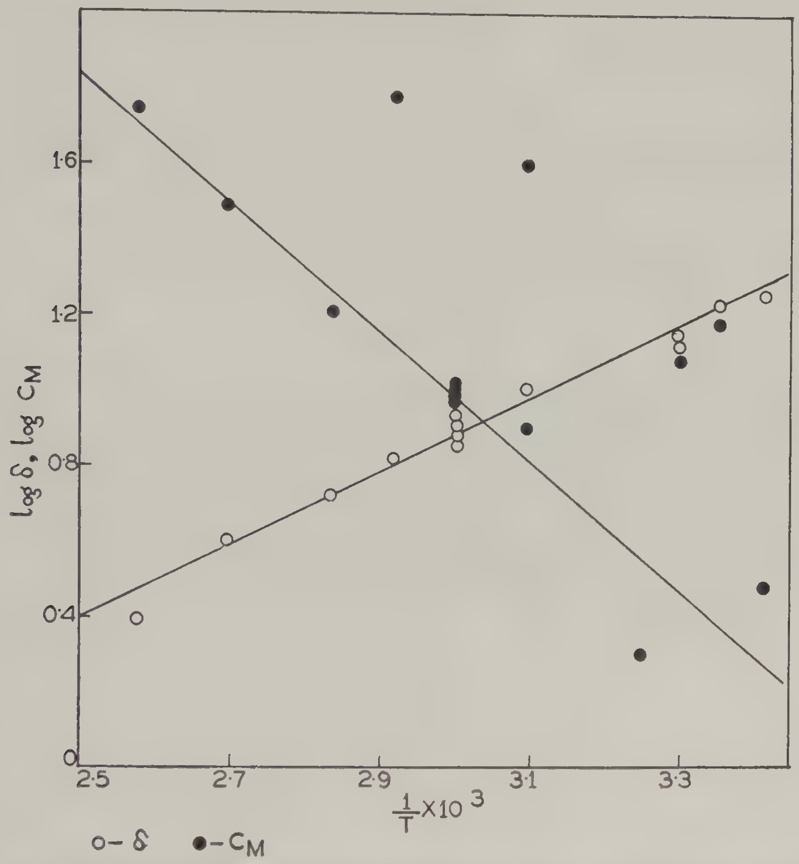

FIG. 1. Dependence of δ and C_M on temperature in methyl methacrylate polymerization.

of C_M has been carefully determined, and our extensive work at 60°C. conclusively proves the validity of our data.

The values of log δ and log C_M are plotted as a function of $1/T$ in Fig. 1 and the best straight line drawn through these points. The best fit of the data is given by the equations

$$\delta = 9.4 \times 10^{-3} \exp^{4.4 \text{ kcal.}/RT}$$

and

$$C_M = 9.1 \times 10^5 \exp^{-7.6 \text{ kcal.}/RT}$$

This result may be compared with the results obtained from Ferington and Tobolsky's (6) compiled data:

$$\delta = 17.31 \times 10^{-3} \exp^{4.1 \text{ kcal.}/RT}$$

From absolute rate constants of Matheson *et al.* (8) the equation may be calculated as

$$\delta = 16.1 \times 10^{-3} \exp^{4.9 \text{ kcal.}/RT},$$

and the latter result is in excellent agreement with our equation which incidentally covers a wider range of temperature.

The author is indebted to Prof. Santi R. Palit for his keen interest and helpful suggestions in the work and thankfully acknowledges the grant of a National Research Fellowship.

REFERENCES

1. PALIT, S. R., NANDI, U. S., AND SAHA, N. G., *J. Polymer Sci.* **14,** 295 (1954).
2. BAYSAL, B., AND TOBOLSKY, A. V., *J. Polymer Sci.* **8,** 529 (1952).
3. NANDI, U. S., AND PALIT, S. R., *J. Polymer Sci.* **17,** 65 (1955).
4. NANDI, U. S., AND PALIT, S. R., Proceedings International Symposium on Macromolecules, 1954, Published in *La Reserca Scientifica.*
5. SAHA, N. G., NANDI, U. S., AND PALIT, S. R., *J. Chem. Soc.* **85,** 427 (1956).
6. FERINGTON, F. E., AND TOBOLSKY, A. V., *J. Colloid Sci.* **10,** 536 (1955).
7. SCHULZ, G. V., AND HARBORTH, G., *Makromol. Chem.* **1,** 106, (1947).
8. MATHESON, M. S., AUER, E. E., BEVILACQUA, E. B., AND HART, E. J., *J. Am. Chem. Soc.* **71,** 497 (1949).

JOURNAL OF COLLOID SCIENCE **12**, 325–326 (1957)

RATE CONSTANTS IN THE POLYMERIZATION OF METHYL METHACRYLATE

T. E. Ferington and A. V. Tobolsky

Frick Chemical Laboratory, Princeton University, Princeton, N.J.

Received January 3, 1957

U. S. Nandi (1) has given further experimental values for rate constants in the polymerization of methyl methacrylate. These should be compared not only with the results of Ferington and Tobolsky (2), as he suggests, but also with those of O'Driscoll and Tobolsky (3), in which the temperature range was extended to −40°C. by using benzoyl peroxide plus dimethyl aniline as the initiator. The combined data from these three papers are plotted in Fig. 1. One may draw either three lines through the points as indicated or a smooth curve.

It has been shown previously (4) that

$$\delta^2 = \frac{2k_{td} + k_{tc}}{k_p^2} \qquad [1]$$

where: k_{td} is the rate constant for termination of the polymer chain by disproportionation;

k_{tc} is the rate constant for termination of the polymer chain by combination;

k_p is the rate constant for the propagation step in polymerization.

Thus one would expect to obtain a curved line on plotting log δ against $1/T$ if both disproportionation and combination were important in the reaction. If a curved line is drawn, then the equation for δ derived from Matheson's absolute rate constants may be approached as closely as desired, depending on the temperature range used.

In considering these data, however, one must note that according to Nandi's references 3, 5 the relation between molecular weight and dilute solution viscosity which he uses is

$$\bar{P}_n = 2.81 \times 10^3 \, [\eta]^{1.32} \qquad [2]$$

which is the equation given by Baxendale *et al.* (5) for fractionated polymethyl methacrylate, rather than the one they give for unfractionated material, namely,

$$\bar{P}_n = 1.99 \times 10^3 \, [\eta]^{1.46}. \qquad [3]$$

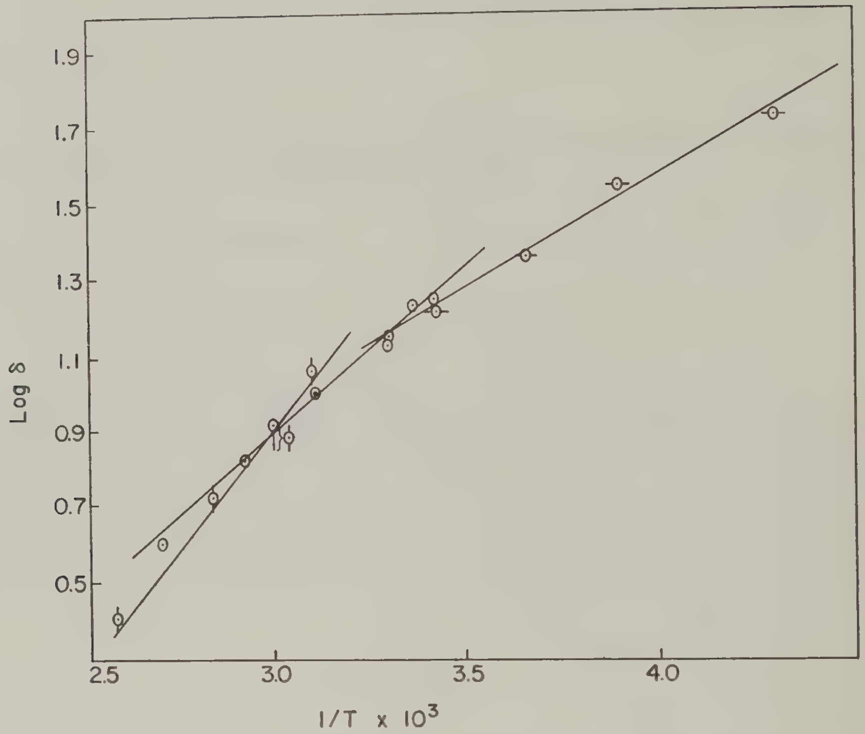

FIG. 1. Assemblage of values of δ from the literature. ⊙ T. Ferington and A. V. Tobolsky. -⊙- K. O'Driscoll and A. V. Tobolsky. ⏀ U. S. Nandi.

If the latter equation had been used in determining δ, the values obtained would have been somewhat different.

The same remarks about molecular weight apply to Nandi's equation for C_M. Here, since

$$C_M = 1/\bar{P}_n \qquad (\text{at } R_p = 0) \tag{4}$$

one can modify his given equation

$$C_M = 9.1 \times 10 \ \exp(-7.6 \text{ kcal.}/RT) \tag{5}$$

to

$$C_M = 4.0 \times 10^6 \exp(-8.0 \text{ kcal.}/RT) \tag{6}$$

by obtaining $[\eta]$ from his C_M values and Eq. [2] and then using this value in Eq. [3] to get the true $\bar{P}_n$ and hence C_M.

REFERENCES

1. NANDI, U. S., *J. Colloid Sci.* **12,** 321 (1957).
2. FERINGTON, T. E., AND TOBOLSKY, A. V., *J. Colloid Sci.* **10,** 536 (1955).
3. O'DRISCOLL, K., AND TOBOLSKY, A. V., *J. Colloid Sci.* **11,** 244 (1956).
4. TOBOLSKY, A. V., AND BAYSAL, B., *J. Polymer Sci.* **11,** 471 (1953).
5. BAXENDALE, J. H., BYWATER, S., AND EVANS, M. G., *J. Polymer Sci.* **1,** 237 (1946).

JOURNAL OF COLLOID SCIENCE **12,** 327–341 (1957)

DYNAMIC MECHANICAL PROPERTIES OF POLY-*n*-BUTYL METHACRYLATE[1]

William C. Child, Jr.,[2] and John D. Ferry

Department of Chemistry, University of Wisconsin, Madison, Wisconsin

Received January 7, 1957

INTRODUCTION

Continuing an investigation of methacrylate polymers synthesized and characterized at Samuel Feltman Ammunition Laboratories, Picatinny Arsenal, we now report data on the mechanical properties of two fractions of poly-*n*-butyl methacrylate. Several fractions of this polymer have already been studied in dilute solution by Chinai and Guzzi (1), and measurements of dielectric properties in the undiluted state have been made by Strella and Zand (2). The dynamic mechanical properties through the transition from rubberlike to glasslike consistency, which are reported here, reveal anomalies attributable to side-chain motions, as previously adduced for polyethyl methacrylate (3).

MATERIALS AND METHOD

The synthesis and fractionation of the polymer have been described (1). The two fractions used in this study, FF-1 and FF-2, had weight-average molecular weights of 3.05 and 0.37×10^6, respectively. They had been dried from frozen benzene solution, and were stored over silica gel desiccant.

Measurements of the complex shear compliance ($J^* = J' - iJ''$) were made between 24 and 2400 cycles with the Fitzgerald Apparatus manufactured by Atlantic Research Corporation, Alexandria, Virginia. Three pairs of disc-shaped samples of each fraction were employed, molded at 225°–240°F. and 10,000 lb./sq. in. The samples were quite clear and light brown in color. The method of insertion and the calculation of the sample coefficients have been described previously (3). For this calculation, the density of the polymer was taken as 1.055 at 25°C. The thermal expansion coefficient was estimated to be 6×10^{-4} deg.$^{-1}$ above the glass transition temperature (27°C.), later confirmed by measurements of Mandelkern and Quinn (4). Detailed descriptions of the samples follow.

---

[1] Part XXVI of a series on Mechanical Properties of Substances of High Molecular Weight.

[2] Now at Carleton College, Northfield, Minnesota.

Fraction FF-1. Samples 67, approximate dimensions 11/16 in. diam. by 3/32 in. thickness, were compressed in the apparatus about 4% and the sample coefficient was 24.32 cm. at 90°C. Measurements were made at approximately 5° intervals from 65° to 110°, followed by check runs at (approximately) 100°, 85°, and 70° which agreed satisfactorily with the initial results. (The exact temperatures are given in the legend of Fig. 1.)

Samples 69, approximate dimensions 11/16 in. by 1/32 in., were compressed about 7%, and the nominal sample coefficient was 54.8 cm. at 90°C. Measurements were made at approximately 5° intervals from 90° to 130° (excluding 100°). The exact temperatures were the same as those employed for Samples 67 (the two pairs being in opposite ends of the apparatus), and all the data agreed quite closely at the 4 overlapping temperatures. However, still closer agreement could be obtained by an empirical adjustment of the sample coefficient by a factor of 1.03. Since the coefficient is more difficult to determine for very thin samples, this correction was applied to the data from Samples 69.

Samples 70, approximate dimensions 1/8 in. by 5/16 in., had to be inserted twice to achieve correct centering, with successive compressions of 7% and 6%. The nominal sample coefficient was 4.511 cm. at 80°C. Measurements were made at approximately 5° intervals from 54° to 80°, followed by 49°, 44°, and a check run at 54° which agreed well with the initial measurements. The values of J' and J'' were smaller, at overlapping temperatures, than those for Samples 67 by about 7%, but the ratios J''/J' were in good agreement. As usual, therefore, the difference was attributed to an error in the sample coefficient and all the data were corrected by an empirical factor of 1.07.

Fraction FF-2. Samples 80, approximate dimensions 11/16 in. by 1/32 in., were compressed about 8%, and the sample coefficient was 63.3 cm. at 100°C. Measurements were made at approximately 5° intervals from 90° to 100° and from 110° to 135°, followed by a check run at 90° which agreed with the initial results. (The exact temperatures are given in the legend of Fig. 2.)

Samples 81, approximate dimensions 11/16 in. by 3/32 in., were compressed about 3%, and the nominal sample coefficient was 17.1 cm. at 100°C. They experienced the same temperature sequence as Samples 80. Measurements were made at approximately 90°, 95°, 100°, 110°; after exposure to higher temperatures up to 135°, a check run at 90° gave values of J' and J'' 4% lower than initially, attributed to some sag of these thicker samples as observed when the apparatus was opened; subsequent measurements were made at 80°, 70°, and 75°, with a final check run at 90° which agreed with the preceding results. At overlapping temperatures, the initial J' and J'' values were about 4% higher than those for Samples 80.

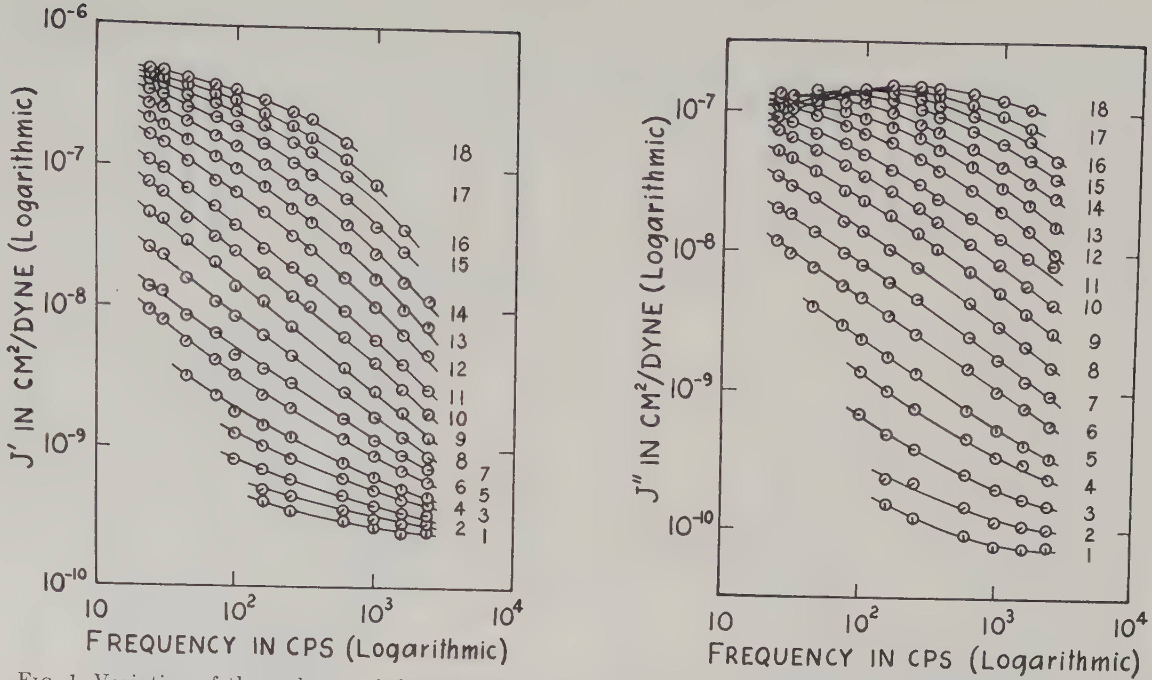

FIG. 1. Variation of the real part of the dynamic shear compliance, J' (left) and the imaginary part, J'' (right) with frequency for poly-n-butyl methacrylate FF-1 at 18 temperatures; numbers correspond to the temperature sequence 43.7°, 48.7°, 53.8°, 59.7°, 64.2°, 70.2°, 74.8°, 80.0°, 85.3°, 89.8°, 94.6°, 99.9°, 105.1°, 109.7°, 115.2°, 120.4°, 125.1°, and 130.1°C.

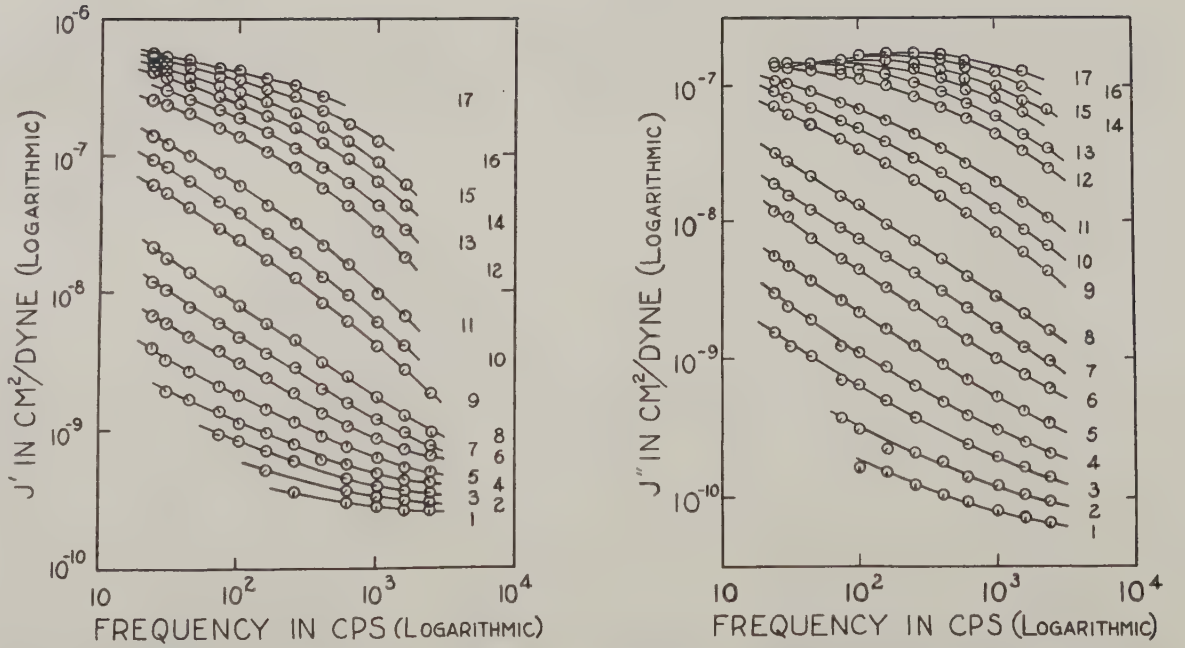

FIG. 2. Variation of the real part of the dynamic shear compliance, J' (left) and the imaginary part, J'' (right) wth frequency for poly-n-butyl methacrylate FF-2 at 17 temperatures; numbers correspond to the temperature sequence 45.0°, 49.8°, 55.0°, 59.5°, 64.7°, 70.3°, 74.9°, 79.8°, 90.0°, 94.4°, 99.3°, 110.0°, 115.0°, 120.4° 125.0°, 130.7°, and 135.2°C.

Samples 82, approximate dimensions $\frac{5}{16}$ in. by $\frac{3}{16}$ in., were compressed about 5%, and the nominal sample coefficient was 3.25 cm. at 80°C. Measurements were made at approximately 5° intervals from 70° to 80°, and then from 65° to 45°, with a final check run at 70° which agreed with the initial results. The values of J' and J'' were about 10% higher than those for Samples 80, but the ratios J''/J' were in good agreement.

In calculating final absolute values of J' and J'', it was assumed that the correct values lay between those for Samples 80 and 82, and the following empirical correction factors were applied: 80, 1.05; 81 before sag, 1.09, after sag, 1.05; 82, 0.95.

Results

The original data for J' and J'', measured at 18 temperatures from 44° to 130° for Fraction FF-1, and at 17 temperatures from 45° to 135° for Fraction FF-2, are shown in Figs. 1 and 2, respectively. Where data on different samples were taken at the same frequencies and temperatures, the values have been averaged.

The values for the two fractions at corresponding temperatures are closely similar, thus confirming the expectation, as previously found for polyethyl methacrylate, that the mechanical properties in the transition region between rubberlike and glasslike consistency are essentially independent of molecular weight so long as the latter is fairly high. Here the molecular weights differ by a factor of over eightfold.

For reduction to a standard temperature, chosen as 100°C., J_p' and J_p'' were calculated by the usual formulas (5), using the thermal expansion coefficient given above. The value of J_∞, the limiting high frequency compliance, was chosen as 10^{-10} cm.^{2}/dyne, but its choice was not critical.

Logarithmic plots of the reduced functions could be superposed quite well by the usual arbitrary shift factors a_T, identical for both real and imaginary components, except for a range between 55° and 80° for J_p' and between 110° and 135° for J_p''. The first anomaly can be attributed to a secondary (β) mechanism involving side chain motions, as previously concluded for polyethyl methacrylate and further analyzed below. The second, which appears as a temperature dependence of the height of the maximum of J_p'', while its position on the reduced time scale remains unaltered, is a new type of deviation from the usual superposition with reduced variables.

Outside the anomalous regions, the empirical a_T values followed closely an equation of the WLF form (6):

$$\log a_T = -c_1^0(T - T_0)/(c_2^0 + T - T_0) \qquad [1]$$

and values of a_T calculated from this equation, with the coefficients given in Table I, were actually used for the final plots against reduced frequency

268, 2 tables, 8 figs., Child & Ferry

TABLE I

Parameters for Temperature Dependence of α Mechanism

		Fraction FF-1	Fraction FF-2
Reference T_0 = 373°K.:	c_1^0	14.53	9.70
	c_2^0	255	169.6
Reference T_g = 300°K.:	c_1'	20.4	17.0
	c_2'	182	96.6
	f_g	0.021	0.026
	α_f	1.2×10^{-4}	2.6×10^{-4}

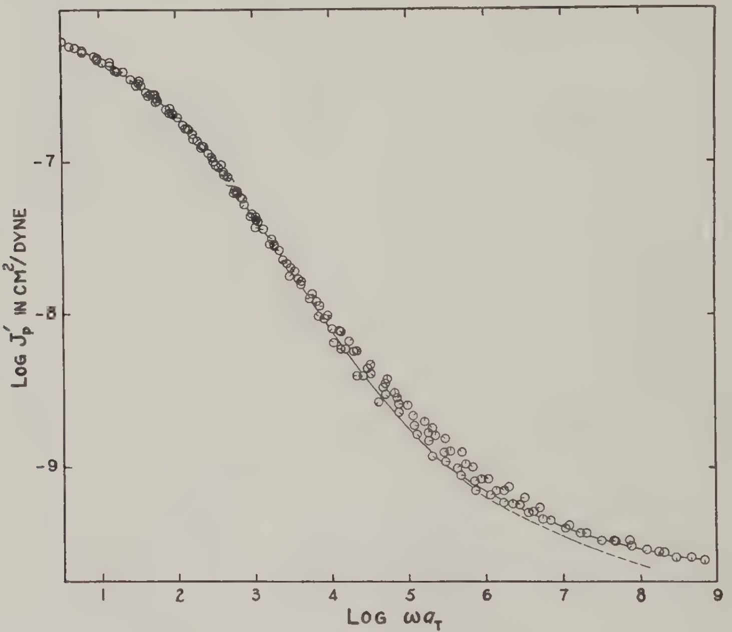

Fig. 3. Real part of the complex compliance, J', for Fraction FF-2 reduced to 100°C. and plotted logarithmically against reduced frequency. Reduction factors a_T calculated from coefficients in Table I. Pip down at right 45.0°C.; successive 45° or 90° relations clockwise correspond to increasing temperatures at approximately 5° or 10° intervals, respectively (exact temperatures given under Fig. 2). Dashed line gives reduced real compliance for Fraction FF-1. The solid curve represents the probable compliance of the α mechanism.

(ωa_T) shown in Figs. 3 and 4. Here the points for Fraction FF-2 are shown; the corresponding plots for Fraction FF-1 coincide exactly except for a small divergence at high reduced frequency, shown by dashed curves.

With knowledge of the glass transition temperature, T_g = 300°K. (4), the values of c_1' and c_2' appropriate to T_g as reference temperature may be calculated from formulas previously given (6), and from these the parameters f_g and α_f which represent the fractional free volume at T_g and its

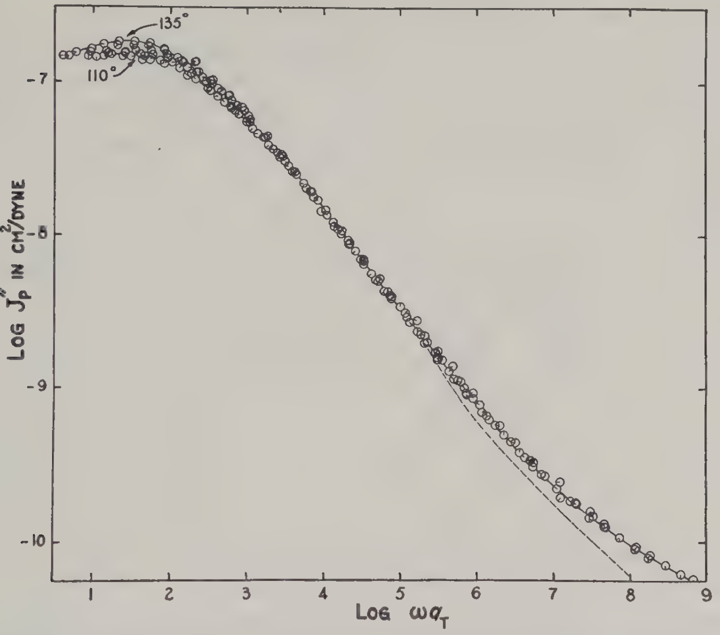

FIG. 4. Imaginary part of the complex compliance, J'', for Fraction FF-2, reduced to 100°C. and plotted logarithmically against reduced frequency. Reduction factors a_T calculated from coefficients in Table I. Temperature key same as in Fig. 3. Dashed line gives reduced imaginary compliance for Fraction FF-1.

expansion coefficient relative to the total volume (7). All these values are given in Table I. Though the values for the two fractions differ somewhat, f_g is in the range (0.02 to 0.03, most frequently 0.025) observed for polymers uncomplicated by anomalies in the application of reduced variables (7); and though α_f is smaller than usual, the value for FF-2 agrees exactly with the increase in macroscopic thermal expansion coefficient at T_g (4). It may be concluded, therefore, that Eq. [1] correctly describes the temperature dependence of the chain backbone motions which dominate and usually wholly determine mechanical behavior in the transition region.

ANALYSIS OF α AND β MECHANISMS

The fanning out of points at individual temperatures in Fig. 3 may be attributed to a β or side-chain mechanism whose contributions to compliance shift differently with temperature from those of the α mechanism associated with chain backbone motions. The absence of such an anomaly in the J_p'' plot means that the β contributions to J'' are everywhere negligible compared with the α contributions. Hoff (8) has in fact concluded from some measurements at approximately constant frequency that there is a β mechanism in poly-n-butyl methacrylate which is largely obscured by the α mechanism because the latter occurs at lower temperatures than in the methyl or ethyl methacrylate polymers. The present data substantiate this conclusion and, since both frequency and temperature have been varied, offer the opportunity of separating the two contributions to J'.

The analysis is similar to that previously made for polyethyl methacrylate (3) but it is far simpler because the anomaly is confined to the center of the reduced frequency range. Only Fraction FF-2 was selected for treatment because the data cover a somewhat wider temperature range and the coefficients in Table I indicate that the temperature reduction was more successful for this fraction. On the J_p' plot, the lower envelope of the points was assumed to represent the α contributions, and these were subtracted point by point from J' to give J_β'. The latter was then plotted logarithmically against ωa_T, but of course curves at different temperatures did not superpose. However, as in the earlier case of polyethyl methacrylate, these curves could be superposed by empirical horizontal shifts representing $\log a_{T\beta} - \log a_T$, where $a_{T\beta}$ is the reduction factor for the β mechanism. From such shifts, accompanied by values of $\log a_T$ derived from Eq. [1], $\log a_{T\beta}$ was calculated. From 55° to 75°, $\log a_{T\beta}$ was a linear function of the reciprocal absolute temperature with a slope corresponding to an apparent energy of activation of 24 kcal.

Strella and Zand (2) have studied the dielectric dispersion of the same two fractions of poly-n-butyl methacrylate over a wide temperature range. Their principal dispersion, which corresponds to the β mechanism, changes in shape at lower temperatures, preventing the direct application of reduced variables; but from 65° to 114° the shape is nearly independent of temperature and the dielectric data can be reduced in the usual manner (5). Reduction factors b_T obtained in this way fall on the same logarithmic plot against $1/T$ as the above-described $a_{T\beta}$ factors, lending confidence to the value of 24 kcal. for the apparent activation energy of this mechanism.

Figure 5 shows J_β' reduced to 100° in this way. The superposition is fairly good and the dispersion is moderately sharp.

HIGH-TEMPERATURE REDUCTION ANOMALY

While the separation into α and β mechanisms resolves the lack of superposition in J_p' at intermediate temperatures, the failure in superposition of J_p'' at high temperatures has not yet been discussed. The maximum in J_p'' sharpens and rises somewhat with increasing temperature, following the empirical equation $\log J_p''$ (at max.) $= A + B(t - 100)$, where t is Centigrade temperature. The constant A is -7.11 for both fractions; B is 0.0040 and 0.0047 for FF-1 and FF-2, respectively, probably

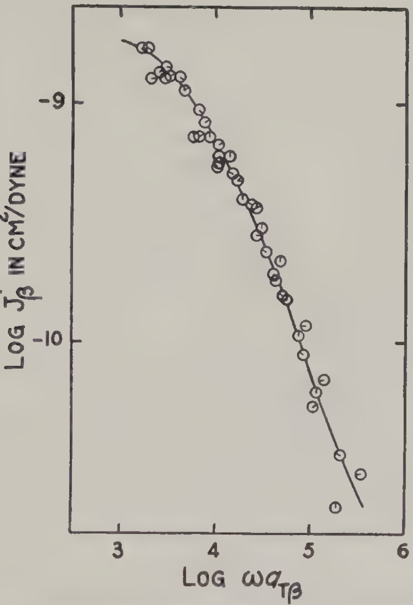

FIG. 5. Real part of the complex compliance of the β mechanism for Fraction FF-2, reduced to 100°C. on the basis of a constant apparent activation energy of 24.4 kcal. and plotted logarithmically against reduced frequency. Temperature key to points same as in Fig. 3.

not significantly different. The location of the maximum on the reduced frequency scale is not affected by temperature. The sharpening in J'' must be associated with a similar sharpening in the retardation spectrum L (which in zero approximation equals J'') near its maximum. This should of course in turn affect J' as well, but the familiar equations relating these quantities (e.g., Eqs. [2] and [3] of reference (3)) show that J' is weighted by contributions from L at shorter times where the anomaly is absent. This explains why the magnitude of J' is not affected to a perceptible extent.

Near this maximum in J'' and L, the mechanical properties of a high molecular weight polymer reflect the widely spaced entanglements discussed by Bueche (9, 10). The sharpening of the maximum with increasing temperature is probably caused by a change in the disposition of these entanglements. A similar anomaly appears in poly-n-hexyl methacrylate (12).

DISTRIBUTION FUNCTIONS

The retardation spectra or distribution functions, L, have been calculated for the two mechanisms from the data of Figs. 3–5 by the second approximation formulas of Williams and Ferry (13); they are given in

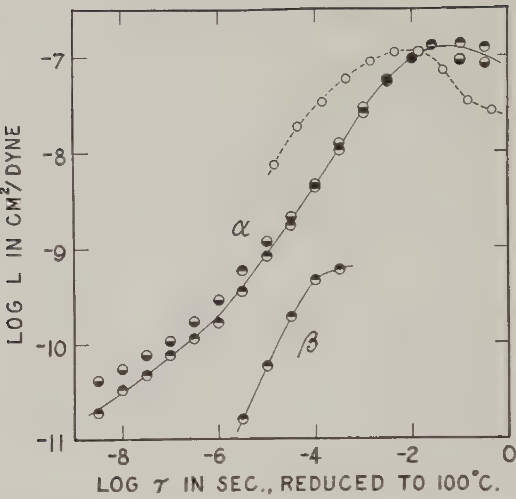

Fig. 6. Retardation spectra of the two mechanisms for Fraction FF-2 reduced to 100°C. Points top black, from J'; bottom black, from J''. Open circles calculated from creep data of Bueche on another sample of polybutyl methacrylate.

TABLE II

Relaxation and Retardation Distribution Functions Reduced to 100°C. Calculated for Fraction FF-2

log τ_p (*sec.*)	log L_p in cm.²/dyne		log H_p in dynes/cm.²	
	from J'	from J''[a]	from G'	from G''
	α Mechanism			
−8.5	−10.72	−10.39	8.64	8.77
−8.0	−10.49	−10.26	8.69	8.80
−7.5	−10.33	−10.11	8.76	8.85
−7.0	−10.12	−9.96	8.80	8.83
−6.5	−9.94	−9.76	8.71	8.81
−6.0	−9.77	−9.52	8.52	8.66
−5.5	−9.45	−9.24	8.21	8.35
−5.0	−9.09	−8.93	7.84	7.94
−4.5	−8.76	−8.66	7.55	7.51
−4.0	−8.36	−8.28	7.16	7.16
−3.5	−7.98	−7.90	6.84	6.87
−3.0	−7.60	−7.53	6.51	6.58
−2.5	−7.28	−7.25	6.24	6.23
−2.0	−7.02	−7.03	5.94	5.93
−1.5	−6.89	−6.92	5.67	5.66
−1.0	−6.87	−6.96	5.47	5.36
−0.5	−6.91	−7.08	5.41	5.03
	β Mechanism			
−5.5	−10.78			
−5.0	−10.23			
−4.5	−9.72			
−4.0	−9.33			
−3.5	−9.23			

[a] Low frequency values taken from measurements at 135°.

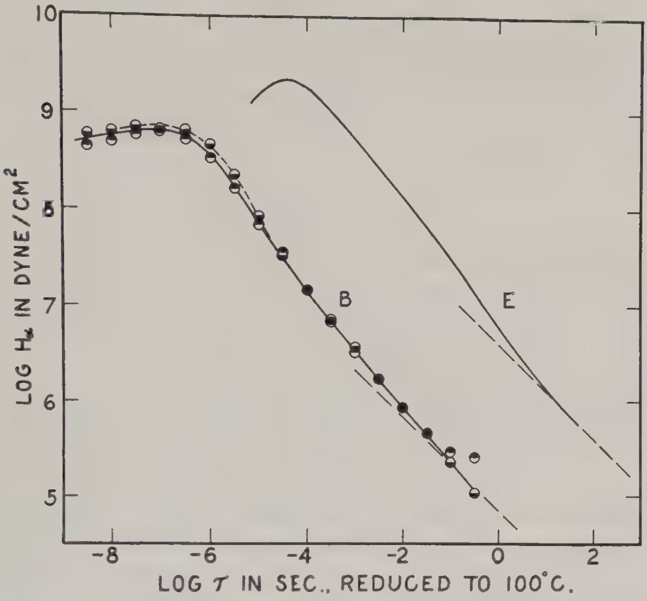

FIG. 7. Relaxation spectrum of the α mechanism for Fraction FF-2 at 100°C. Points top black, from G'; bottom black, from G''. Dashed curve gives relaxation distribution function for Fraction FF-1. Curve E is for polyethyl methacrylate at 100°C. (Reference 3).

Table II and plotted in Fig. 6. For the α mechanism at low frequencies, where J_p'' depends somewhat on temperature even after reduction, values from the measurements at the highest temperature (135°) were chosen. The agreement between calculations from real and imaginary components for the α mechanism is quite good except at the short time end. For the β mechanism, only the real calculation is of course available. At 100°C., L_β lies so far below L_α that their sum, the total retardation spectrum, would scarcely be distinguishable from L_α on the logarithmic plot shown here. At lower temperatures, L_β, shifting less rapidly to longer times, would lie closer to L_α and make relatively greater contributions to L. Their relative positions are, however, consistent with the absence of a detectable anomaly in J'' within the temperature range of our experiments.

The retardation spectrum of the α mechanism for Fraction FF-1 deviates slightly from that for Fraction FF-2 at short times, but the differences are less than the discrepancies between the real and imaginary component calculations.

The relaxation spectra or distribution functions[3], H, for the α mechanism have also been calculated from corresponding plots of the complex shear modulus and are also given in Table II. Again, the agreement between calculations is very good. The spectrum is plotted in Fig. 7. The relaxation spectrum for the α mechanism of Fraction FF-1 coincides with that for Fraction FF-2 except at short times, where the former is shown by a dashed curve. Even here the deviations are quite small.

---

[3] Our former symbol for this function, Φ, has been replaced by H to conform to the recommendations of the Committee on Nomenclature of the Society of Rheology.

DISCUSSION

Temperature Dependence

The temperature dependence of relaxation times in the α mechanism, following the WLF equation, is given by the parameters in Table I. The differences between the two fractions are magnified in the derived calculations; the actual log a_T values are 10 to 15% higher in Fraction FF-2 than in FF-1. In view of previous experience (3, 14, 15), it seems unlikely that this is a real effect of molecular weight, although its source is not understood. The parameters for FF-2 are closer to those found for other polymers, though the value of α_f is somewhat smaller than usual.

The temperature dependence of relaxation times in the β mechanism corresponds to an apparent activation energy of 24 kcal., somewhat smaller than that of 31 kcal. observed for polyethyl methacrylate. The apparent activation energies of the two mechanisms would be equal at 190°C., so at this temperature, well above the experimental range studied here, the two contributions would be shifting together along the time scale.

Time and Frequency Dependence

The retardation and relaxation spectra associated with the α mechanism are similar in shape to those of other polymers, particularly those with disubstituted carbon chains (7). The α relaxation spectrum of polyethyl methacrylate is also reproduced in Fig. 7 for comparison. The shapes are almost identical but the maximum in the n-butyl polymer is broader and lower (log H = 8.81) than in the ethyl (log H = 9.36). Similarly, the maximum in the retardation spectrum (log L = -6.90, from measurements at the highest temperature) appear to be *higher* than that of polyethyl methacrylate (3), although the latter was not quite encompassed by our earlier measurements. Qualitatively, the differences in heights of both spectra are probably associated with the smaller number of monomer units per unit volume in the n-butyl polymer, which has a higher monomer molecular weight and also a lower density.

Figure 6 also shows for comparison the retardation spectrum calculated by second approximation methods from creep measurements of Bueche (10) at lower temperatures on a sample of polybutyl methacrylate, reduced to 100°C. by the reduction factors for our Fraction FF-2. This spectrum resembles ours closely in shape and in the height of the maximum, but is displaced to shorter times by about a factor of ten. The difference is very probably associated with the fact that T_g for Bueche's sample was quoted

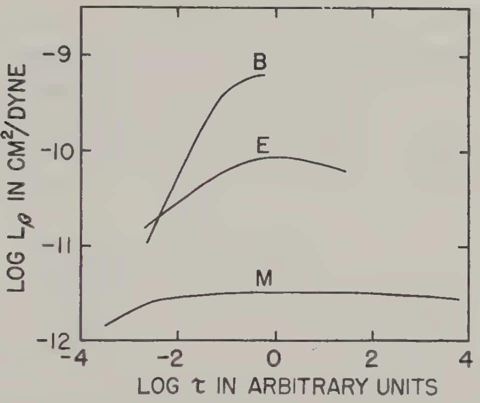

FIG. 8. Retardation spectra of β mechanisms with arbitrary logarithmic time scale, for three methacrylate polymers, M, methyl; E, ethyl; B, n-butyl.

as 8°C., the lower value suggesting the presence of a trace of diluent or unreacted monomer. Otherwise the similarity of the spectra gives encouraging support of the Boltzmann superposition principle and the applicability of reduced variables, on which all these analyses are based.

A tangent drawn to the H curve with the theoretical slope (16, 11) of $-\frac{1}{2}$, as indicated in Fig. 7, provides the usual calculation of the monomeric friction coefficient ζ_0. For this purpose, a, the root-mean-square end-to-end distance per monomer unit, is taken as 6.4 A., derived from light-scattering measurements in a Θ-solvent (1). Log ζ_0 is -3.51 at 100°C. Reduction to T_g, using the data for Fraction FF-2 in Table I, gives log $\zeta_0 = 3.74$. This is considerably smaller than the values for several other polymers at T_g (3, 7), though it is larger than an earlier estimate for poly-n-butyl methacrylate (7). Even though the fractional free volume at T_g is about the same for each of these polymers (7), a more favorable disposition of local free volume around the monomer unit may be responsible for the greater mobility of poly-n-butyl methacrylate (7).

The retardation spectrum of the β mechanism is moderately sharp. It is of interest to compare its shape with those of polyethyl and polymethyl methacrylate. The polyethyl β spectrum is available from the preceding paper of this series (3), while the polymethyl can be calculated from torsional creep measurements by Iwayanagi (17) at $-51°$ to 37°C. and Lethersich (18) at 18° to 20°C., far below the glass transition temperature where the α mechanism makes no contribution to compliance. The results of Iwayanagi and Lethersich agree rather well and indicate a very broad maximum, practically a plateau over many decades of logarithmic time. The shapes of the β spectra for the three polymers are compared in Fig. 8.

The broad plateau in polymethyl methacrylate is reminiscent more than anything else of the retardation spectrum of crystalline polyethylene

(19), which is effectively rather densely cross-linked. This suggests that the motion of the methyl ester side chain requires cooperation of chain backbones of *neighboring* molecules, and that such cooperation can extend over rather large domains, leading to a very broad distribution. With increasing side chain length, there is less coupling to the motions of neighboring backbones, presumably because of the looser local packing, and the spectrum becomes progressively sharper.

Influence of Molecular Weight

The dashed curves for J_p' and J_p'' of Fraction FF-1 deviate slightly from those for Fraction FF-2, at high reduced frequency, but it is doubtful whether these differences are really attributable to an effect of molecular weight. If the temperature reduction factors for FF-2 are applied to the data for FF-1, the reduced compliance curves are practically coincident. The differences seem therefore to be associated with some peculiarity in the temperature reduction of FF-1, though the source is obscure. The differences are, in any case, barely perceptible in the retardation and relaxation spectra.

ACKNOWLEDGMENTS

This work was supported by Picatinny Arsenal, Ordnance Corps, Department of the Army. We are grateful to Professor Edwin R. Fitzgerald, Pennsylvania State College, for supervising maintenance of the Fitzgerald Apparatus, and to Mrs. Garrett Droppers for making most of the calculations. We are indebted to Messrs. Stephen Strella and Robert Zand for the opportunity of examining their dielectric data in advance of publication.

SUMMARY

The real (J') and imaginary (J'') components of the complex compliance have been measured between 24 and 2400 cycles/sec. in the temperature range from 44° to 135°C. for two fractions of poly-*n*-butyl methacrylate of weight-average molecular weights 3.05 and 0.37×10^6. The data were closely similar for the two fractions. The method of reduced variables gave superposed curves for J' and J'' except for two anomalies: one near the center of the dispersion of J' which could be analyzed in terms of two additive mechanisms (α and β), and one near the maximum of J'' which appeared as a slight sharpening of the maximum with increasing temperature, attributed to a change in the disposition of chain entanglements. For the α mechanism, the temperature dependence of the reduction factors a_T followed an equation of the WLF form. For the β mechanism, the temperature dependence of the reduction factors $a_{T\beta}$ corresponded to a constant apparent activation energy of 24 kcal. The retardation and relaxation spectra for the α mechanism, attributed to the usual chain backbone motions, resemble in form those for other disubstituted vinyl chains;

the friction coefficient per monomer unit in backbone motion, calculated from the extended Rouse theory, is smaller at T_g than usual. The retardation spectrum for the β mechanism is considerably sharper than for polymethyl or polyethyl methacrylate, probably because side chain motions are less coupled to those of neighboring chain backbones.

REFERENCES

1. CHINAI, S. N., AND GUZZI, R. A., *J. Polymer Sci.* **21,** 417 (1956).
2. STRELLA, S., AND ZAND, R., *J. Polymer Sci.*, in press.
3. FERRY, J. D., CHILD, W. C., JR., ZAND, R., STERN, D. M., WILLIAMS, M. L., AND LANDEL, R. F., *J. Colloid Sci.* **12,** 53 (1957).
4. MANDELKERN, L., AND QUINN, F. A., JR., private communication.
5. FERRY, J. D., AND FITZGERALD, E. R., *J. Colloid Sci.* **8,** 224 (1953).
6. WILLIAMS, M. L., LANDEL, R. F., AND FERRY, J. D., *J. Am. Chem. Soc.* **77,** 3701 (1955).
7. FERRY, J. D., AND LANDEL, R. F., *Kolloid-Z.* **148,** 1 (1956).
8. HOFF, E. A. W., ROBINSON, D. W., AND WILLBOURN, A. H., *J. Polymer Sci.* **18,** 161 (1955).
9. BUECHE, F., *J. Chem. Phys.* **20,** 1959 (1952).
10. BUECHE, F., *J. Appl. Phys.* **26,** 738 (1955).
11. FERRY, J. D., LANDEL, R. F., AND WILLIAMS, M. L., *J. Appl. Phys.* **26,** 359 (1955).
12. CHILD, W. C., JR., AND FERRY, J. D., *J. Colloid Sci.*, in press.
13. WILLIAMS, M. L., AND FERRY, J. D., *J. Polymer Sci.* **11,** 169 (1953).
14. BROWN, G. M., AND TOBOLSKY, A. V., *J. Polymer Sci.* **6,** 165 (1951).
15. NINOMIYA, K., AND FUJITA, H., *J. Colloid Sci.*, **12,** 204 (1957).
16. ROUSE, P. E., JR., *J. Chem. Phys.* **21,** 1272 (1953).
17. SATO, K., NAKANE, H., HIDESHIMA, T., AND IWAYANAGI, S., *J. Phys. Soc. Japan* **9,** 413 (1954).
18. LETHERSICH, W., *Brit. J. Appl. Phys.* **1,** 294 (1950).
19. FERRY, J. D., in H. A. STUART, "Die Physik der Hochpolymeren", Vol. 4, p. 425. Springer, Berlin, 1956.

JOURNAL OF COLLOID SCIENCE **12:** 342–343 (1957)

LETTER TO THE EDITOR

ON MICELLE FORMATION OF DODECYLAMMONIUM SALTS OF FATTY ACIDS IN NONPOLAR SOLVENTS

Micelle formation in nonaqueous solvents has been reported by many authors (1–5). However, it has not been determined whether a critical concentration or a concentration range for micelle formation exists in these cases. Singleterry and co-workers reported the existence of a critical concentration range (1, 3, 4). Pink and Nelson reported that aggregation occurs at an extrapolated zero concentration (5). Hence, it seems that a study of the existence of a critical concentration or a critical range for micelle formation in a nonpolar solvent should be made with various methods and materials.

The reaction products of fatty acids and dodecylamine were used as detergents because of their relatively high solubilities in various nonpolar solvents (6). The existence of a critical micelle concentration for solutions of these detergents in benzene has been suggested (7, 8).

To determine whether or not a critical concentration for micelle formation exists in a nonpolar solvent, the behavior of these detergent solutions was studied by solubilization of water.

Equivalent mixtures of fatty acid and dodecylamine were shaken in hexane at room temperature. Butyric acid and caprylic acid were used as fatty acids. Crystals, precipitated by cooling in ice or ice-salt baths, were recrystallized from the same solvent. The products were white with m.p. 39–41°C. and 43–45°C., respectively. The products of fatty acid and amine have acid-amine ratios of 1 to 1, 2 to 1, or 3 to 1 according to the species of amine (9–12). It appears from these papers that equimolar mixtures of primary amine and fatty acid form 1:1 compounds. The product of butyric acid and dodecylamine had a nitrogen content of 5.01% (calculated for the acid-amine ratio of 1 to 1 is 5.13%), and that of caprylic acid and dodecylamine had a nitrogen content of 4.25% (calculated for a 1:1 compound is 4.26%). Their structures were shown to be ammonium salts, at least in the solid state, by means of infrared measurements (7). Hence the products are dodecylammonium butyrate and dodecylammonium caprylate. Benzene, cyclohexane, and carbon tetrachloride, used here as solvents, were purified and care was taken to remove all water.

Measurements of solubilization of water were made by a method reported previously (7). The relation between the limiting amount of water

TABLE I.

The Apparent CMC (Moles per Liter) and the Solubilizing Power (SP) (Moles of Water per Mole of Detergent) from Solubilization Experiments

Temperature 26° ± 1°C.

Detergent / Solvent	Dodecylammonium butyrate CMC	SP	Dodecylammonium caprylate CMC	SP
Benzene	0.016 ± 0.002	4.6	0.030 ± 0.002	2.8
Cyclohexane	0.002 ± 0.001	24	0.016 ± 0.002	3.0
Carbon tetrachloride	0.016 ± 0.002	4.3	0.072 ± 0.004	1.9

solubilized and the concentration is linear within the concentration range used here. Values were corrected for the solubility of water in pure solvent. The linearity was also observed at various temperatures in benzene (8). Extrapolation to zero solubilization was used to obtain an apparent critical micelle concentration (CMC). The slope of the linear line was taken to be the solubilizing power. The apparent CMC and the solubilizing power expressed by the numbers of moles of water per mole of detergent are collected in Table I. In these systems, at least, the solution containing a detergent of a longer hydrocarbon chain has the higher CMC.

The results obtained above are for micelle formation in nonpolar solutions saturated with water. Behavior of related systems in the absence of water is being studied by another method (13).

REFERENCES

1. Arkin, L., and Singleterry, C. R., *J. Am. Chem. Soc.* **70**, 3965 (1948).
2. van der Waarden, M., *J. Colloid. Sci.* **5**, 448 (1950).
3. Kaufman, S., and Singleterry, C. R., *J. Colloid. Sci.* **7**, 453 (1952).
4. Kaufman, S., and Singleterry, C. R., *J. Colloid. Sci.* **10**, 139, (1955).
5. Nelson, S. M., and Pink, R. C., *J. Chem. Soc.* **1952**, 1744.
6. Palit, S. R., and Venkateswarlu, V., *Proc. Roy. Soc. (London)* **A208**, 542 (1951).
7. Kitahara, A., *Bull. Chem. Soc. Japan* **28**, 234 (1955).
8. Kitahara, A., *Bull. Chem. Soc. Japan* **29**, 15 (1956).
9. Prideaux, E. B. R., and Coleman, R. N., *J. Chem. Soc.* **1937**, 4.
10. Pool, W. O., Harwood, H. J., and Ralston, A. W., *J. Am. Chem. Soc.* **67**, 775 (1945).
11. Kaufman, S., and Singleterry, C. R., *J. Phys. Chem.* **56**, 604 (1952).
12. Yeager, E. N., and Barrow, G. M., *J. Am. Chem. Soc.* **77**, 6206 (1955).
13. Kitahara, A., *Bull. Chem. Soc. Japan*, in press.

Ayao Kitahara

Department of Chemistry,
Toho University,
Narashino, Chiba, Japan

Received April 2, 1957

ERRATUM

Volume 11, Number 6, in the article entitled "Flocculation, Subsidence, and Filtration of Phosphate Slimes. III. Subsidence Behavior" by Robert H. Smellie, Jr., and Victor K. La Mer, on page 730, line 3 should read:

$\left(\text{It is evident from the above and from Eq. [4] that } v = v_0 \cdot \frac{\rho_0^2}{\rho^2}.\right)$

JOURNAL OF COLLOID SCIENCE **12**, 345–355 (1957)

THE ADSORPTION OF SODIUM LAURYL SULFATE AND LAURYL ALCOHOL AT THE AIR-LIQUID INTERFACE

A. Wilson,[1] M. B. Epstein,[2] and John Ross

Colgate Palmolive Company, Jersey City, New Jersey

Received October 15, 1956

ABSTRACT

Measurements have been made of the changes in concentration accompanying formation of large surface areas from solutions of pure sodium lauryl sulfate. The adsorption rises until the critical micelle concentration is reached and then remains constant with a maximum area per molecule of 40 A^2.

In the three-component system sodium lauryl sulfate, lauryl alcohol, and water, no distinction could be shown above or below the surface transition temperature for the adsorption of lauryl alcohol and sodium lauryl sulfate.

Only a monolayer of the two adsorbed materials is necessary to give slow draining films below the transition temperature.

This paper describes a direct measurement of adsorption at the surface of aqueous solutions of pure sodium lauryl sulfate. An account is also given of the adsorption of lauryl alcohol (LOH) dissolved in aqueous solutions of sodium lauryl sulfate (SLS). A comparison is made of the adsorption above and below the sharp and reversible transition temperatures known to occur in the rate of drainage of foams and single films given by solutions of these two surface-active agents (1, 2).

The general approach has been the measurement of the decrease of concentration which accompanies the formation of a large known surface area through the generation of a column of equilibrated single bubble-size foam, using pure materials. In earlier work in this laboratory such foams were employed to show that minima in surface tension-concentration curves could be removed by preferential adsorption of the alcohol (3) and also to demonstrate the existence of sharp transition temperatures in foam drainage (4).

Other approaches to adsorption measurements in the past have been the "moving bubble" method of Donnan and Barker (5) and the microtome method of McBain and his co-workers (6). More recent work has involved the use of radiotracers (7).

---

[1] Present address: American Cyanamid Co., Bound Brook, New Jersey.

[2] Present address: Onyx Oil and Chemical Co., Jersey City, New Jersey.

EXPERIMENTAL

Materials and Preparation of Solutions

The SLS used in this investigation was prepared by the method of Dreger *et al.* (8). The absence of minima in the surface tension-concentration curve indicated that it was free of higher homologs. The nonformation of slow draining films at concentrations below the critical micelle concentration (CMC) and at temperatures down to 0°C. showed it to be free of LOH or similar surface-active impurities (2). We consider the absence of slow draining films to be equivalent to the absence of material conferring high surface viscosity, and our examination was directed to the region most sensitive to surface-active impurities. This view is in agreement with the recent findings of B. C. Blakey and A. C. S. Lawrence (9).

The LOH was a portion of the material used in the sulfation and therefore free of higher homologs, as shown by the surface tension-concentration curves of the SLS.

The solutions were prepared gravimetrically on an analytical balance using water which had been redistilled from an all-Pyrex apparatus.

Description of Foam Adsorption Apparatus

Foam was generated in a cylindrical column while being continuously wetted by circulation of the solution (Fig. 1). All parts in contact with the solution and foam were made of Pyrex glass with the exception of the platinum-rhodium spinneret used to form the bubbles. The stopcocks were smoothly ground and not greased. The spinneret of thimble shape had 40 holes 0.003 inch in diameter and was fitted on a male glass tapered joint.

The air used to generate the foam was obtained by displacement from a 20-liter carboy through flow of water from a constant-level reservoir. The air was passed through Ascarite and then scrubbed by passage through distilled water. A manometer gave the pressure at the entrance to the spinneret.

Procedure

A sample of solution of known weight was placed in the bubbler vessel at the lower part of the column and the system closed. Pumping of the solution through the recycling system was started as soon as the air was admitted to the spinneret. Alternate compression and release of the rubber bulb connected to the all-glass pump caused solution to be pushed up the capillary tubing and through the overflow cup at the top of the column. Solution did not pass beyond the safety bulb between the glass pump and the rubber bulb. The overflow cup prevented the formation of bubbles in the capillary during the decompression stroke of the pump. The liquid flowed down the solid Pyrex rod which served to carry and distribute the solution to the

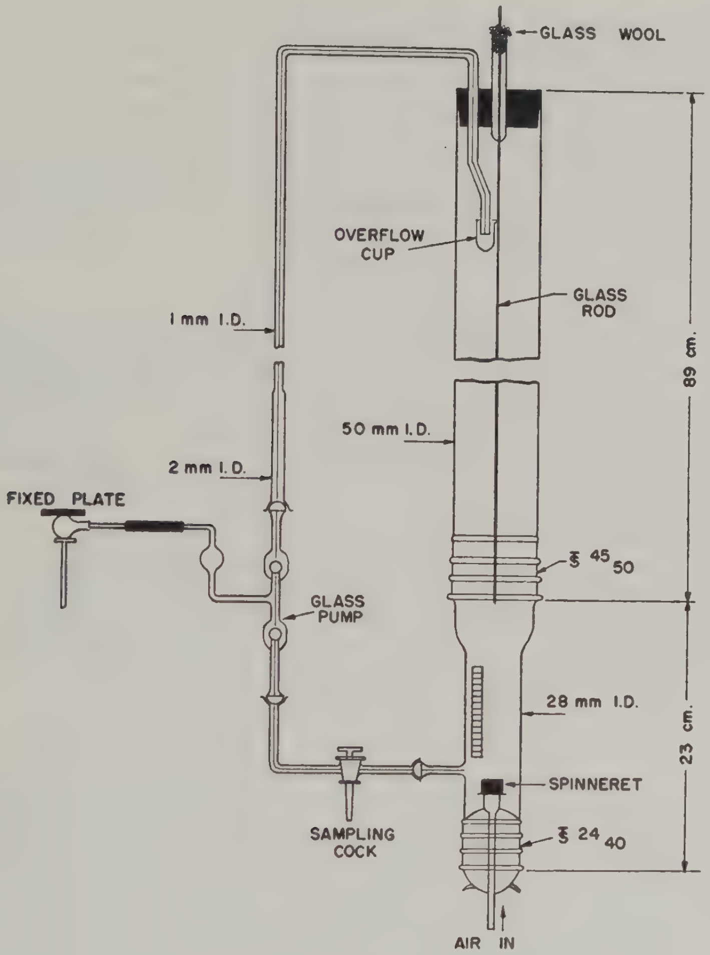

FIG. 1. Foam adsorption apparatus.

foam. The solution recycling rate used was about 4 ml./min. and the total liquid in the pumping system was 5 ml. No part of the liquid failed to circulate and in all experiments thorough mixing for several minutes before withdrawal of a sample of bulk liquid was found adequate.

Bubble Size Measurement; Volume of Foam

Bubble size was measured by photographing the wet foam against a scale calibrated in millimeters on the column and then determining the average bubble diameter from photographic enlargements. The parallax due to the differing positions of the plane of the scale and the plane of the measured bubbles was negligible. With the spinneret over a wide range of concentrations and flow rates the variation in bubble size was negligible. At the pumping speeds employed the foam was sufficiently wet to keep the bubbles essentially spherical. Any correction for distortion would be exceedingly small under these conditions, since they were very far from being polyhedra (10). The amount of foam at the top which was not efficiently rewetted with the recirculating solution was negligible and there was no visible heterogeneity. The total error in the volume of the air in the foam is estimated to have been less than 0.5%.

Analysis of Solutions

Calibration curves over the range of concentrations of SLS studied were obtained with a Zeiss interferometer using gravimetrically prepared solutions. To avoid band skipping the concentrations were closely spaced (11). The plots of units of refraction against concentration were fitted well by straight lines above and below the CMC and gave as its value 0.234% (0.813×10^{-2} moles/liter), in excellent agreement with the values obtained by other methods (12).

The change in concentration of SLS was determined by comparison with the initial solution or with a standard solution. In the experiments with SLS alone the change in concentration was of the order of 0.007 g./100 g. solution, and this change could be measured on the interferometer with an accuracy of about ±0.00014 g./100 g. solution.

Experiments with Added LOH

In the first series of experiments with added LOH two optical windows with engraved scales were provided so that the bubbles could be photographed accurately. The column was jacketed and the outside tubing was thermostatted to the same temperature as the column by means of well-lagged electrical wrapping supplied with thermocouples. A jacketed coil was inserted just above the bubble trap and was regulated by the same source as the column jacket. The central rod was replaced with a closed tube carrying a thermocouple which reached the bulk solution below.

For the second series of experiments with added LOH the bubble chamber and all parts for pumping were removed in order to reduce the volume of liquid. By means of standard tapers the spinneret and a sampling tube were attached to opposite ends of the column. Equilibrium was established by manual rocking and rotation of the column. The expansion ratio attained was greater than 750 cm.^{2} area/ml. solution.

Analysis for LOH was based upon the separate determination of the film drainage transition temperature for the given sample, the relation to the concentration of each component having been calibrated previously (2). In the final series described, cationic titration with methylene blue as indicator was used for chemical determination of SLS with an accuracy of about 2 parts in 300.

TABLE I

Adsorption of Sodium Lauryl Sulfate

	S	P	R	O	T	Q	W
Concentration initial soln. (moles/liter) $\times 10^2$	0.4356	0.6548	0.8701	1.053	1.393	1.741	2.671
Change in concentration, (moles/liter) $\times 10^2$	0.023	0.026	0.028	0.027	0.029	0.029	0.035
Volume of soln., ml.	70.0	70.0	70.0	65.0	70.0	70.0	60.0
Average bubble diameter, mm.	1.30	1.30	1.30	1.30	1.30	1.30	1.30
Volume of air in foam, ml.	1040	1040	1040	1040	1060	1040	1070
Surface area of foam, cm.^{2}	48000	48000	48000	48000	48920	48000	49385
Moles adsorbed $\times 10^5$	1.62	1.87	1.97	1.85	1.99	1.99	1.98
Moles adsorbed per cm.^{2} of surface $\times 10^{10}$	3.37	3.88	4.10	4.00	4.07	4.15	4.00
Area/molecule, A^2	49.3	42.8	40.5	41.5	40.7	40.0	41.5

RESULTS AND DISCUSSION

Adsorption of SLS

In Table I the results of seven adsorption runs at 24° to 26°C. are given for various concentrations of SLS. The derived values for the moles adsorbed per square centimeter of surface and the area per molecule are plotted in Fig. 2 as a function of concentration. The adsorption rises until the CMC is reached, where the values of adsorption and the corresponding areas per molecule become essentially constant. The value 4.06×10^{-10} moles/cm.^{2} taken as the average over the flat portion of the curve, corresponds to a surface area per molecule of 40 A^2 as compared with the value of approximately 20 A^2 assigned to a closely packed monolayer of oriented hydrocarbon chains. It appears that an adsorbed film of SLS is of the expanded or gaseous type, both below and well above the CMC—a conclusion also reached by Brady through the consideration of surface tension and surface viscosity data (13).

By combining according to the Gibbs adsorption theorem careful surface tension measurements and activity coefficients calculated from the Debye-Hückel theory, Brady arrived at the value 38 A^2 for highly purified SLS near the CMC.

The values we have found are at variance with the radiotracer values of Ruyssen and Maebe (14) which continued to increase beyond the CMC. We do not know why the two techniques have produced such different results. It is clear that all methods must meet common requirements of purity of materials and exacting care in the prevention of surface contamination. It is our feeling that the restricted surface areas employed until now with radiotracer techniques may introduce difficulties which are avoided by the techniques we have adopted.

Constancy of pH on Exhaustive Foaming

It has long been known that the common soaps hydrolyze in aqueous solutions and that the weak acid is selectively adsorbed at an air-solution interface. On the other hand, the sodium alcohol sulfates being strong electrolytes do not undergo hydrolysis in solution to the alkyl sulfuric acid except possibly at very low pH. It has been suggested that surface hydrolysis may take place, in particular with dilute SLS solutions of pH range 5.5–7.9 (15). Several measurements of the pH of unbuffered SLS solutions before and after exhaustive foaming with carbon dioxide-free nitrogen are

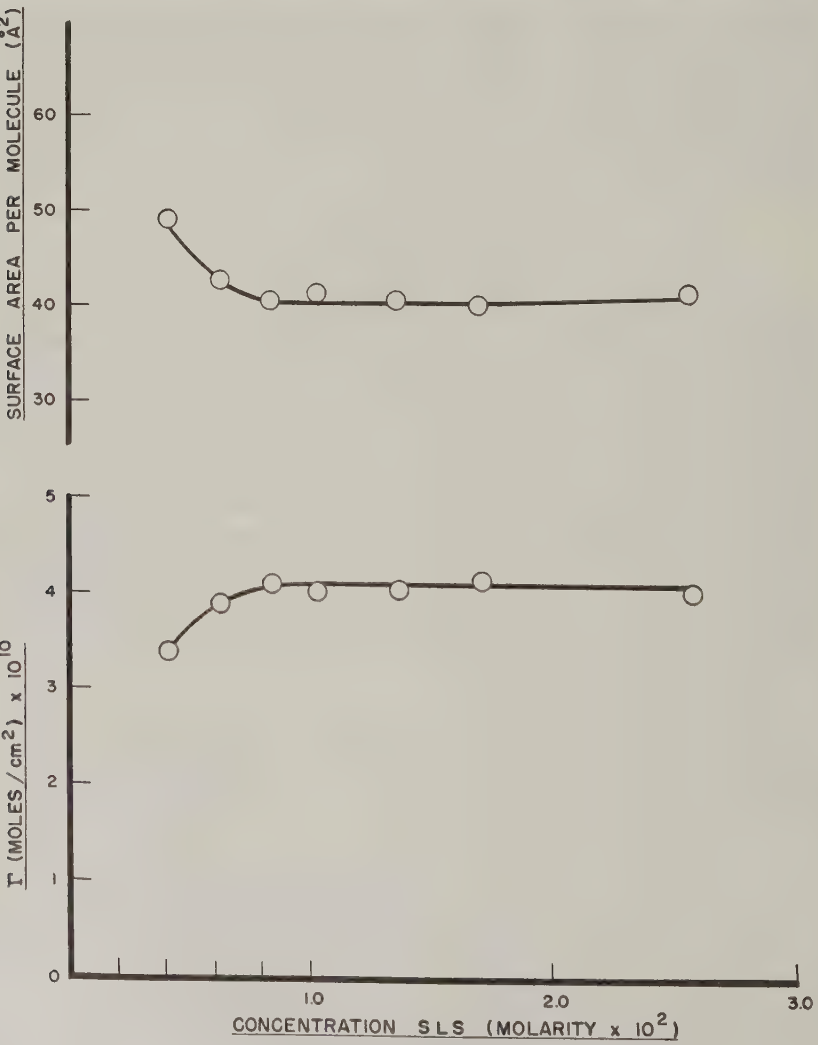

FIG. 2. Surface adsorption of sodium lauryl sulfate.

TABLE II

pH Changes of Exhaustive Foaming[a]

Vol. Soln. *(ml.)*	Initial conc. SLS,(%)	Vol. foam, *(liters)*[b]	pH before foaming	pH after foaming
60	0.324	14.2	5.62	5.76
60	0.362	15.3	5.90	5.89

[a] Final concentration approximately 0.10%.

[b] Bubble diameter 1.3 mm.

reported in Table II. The changes in pH that were observed in these experiments are negligible, and similar results were obtained when air was used instead of nitrogen for foaming. We were unable to confirm the result of Cooke and Talbot, who state that "however the hydrolytic adsorption may perhaps be due to fatty acid impurity in sodium lauryl sulfate" and report the presence of definite minima in their surface tension curves.

Adsorption of LOH in Presence of SLS

Sporck (16) has pointed out the importance of measuring the adsorption of the two surface-active components in both the slow and fast draining foams. For the SLS, he obtained values from which those given below do not differ significantly. For the LOH Sporck used radiotracer methods which he felt were not entirely satisfactory. The film drainage transition temperature being a definite physicochemical property which is a sensitive function of the concentration in the bulk of the two surface-active components, we have used it as a satisfactory tool for measuring changes in the composition of the bulk solution.

Two different approaches were chosen in the foam experiments. In the first, a large surface area of foam was generated in increments at constant temperature from a solution of known mass and composition. The conditions were such that the foam passed from slow to fast draining during the course of the foam generation by depletion of the alcohol in the bulk liquid (*cf.* Fig. 1, Ref. 2). After each increment, a sample of liquid was removed for analysis, and the sum of these samples was both small and known. Such an experiment gave a value of the foam expansion needed to yield a transition under the given conditions and a preliminary estimate of the magnitude of the adsorption.

Three experiments were carried out at a temperature of 25°C. The initial concentrations were 0.200% SLS and 0.002% LOH; final concentrations were approximately 0.197% SLS and 0.00015% LOH. In each experiment the region of transition was noted.

On either side of the transition the amount of LOH adsorbed was of the order of 4×10^{-10} moles/cm.^{2}. It was therefore inferred that with respect to the LOH all that is needed to sustain the slow draining condition is a monolayer.

TABLE III

Adsorption above and below the Transition Temperature

SLS, initial, g./100 g. soln.	0.3003			
LOH, initial, g./100 g. soln.	0.0118			
FDTT, initial soln., °C.	30.3			
Weight of solution taken, g.	49.7[a]	49.7[b]	40.0[a]	40.0[b]
Volume of foam, ml.[c]	700	700	750	700
Mean diameter of bubbles, mm.	1.7	1.5	1.5	1.7
Jacket temp. at 1st sampling, °C. (before transition)	22	31	22	30.5
Weight 1st sample, g.	10	10	10	10
FDTT, 1st sample, °C.	27.8	27.5	25.4	25.9
SLS by titration, g./100 g. soln.	0.2946	0.2935	—	0.2917
Jacket temp. at 2nd sampling, °C. (after transition)	30	22	30.5	23.5
FDTT, 2nd sample, °C.	27.9	27.7	25.7	25.9
SLS by titration, g./100 g. soln.	0.2898	0.2945	—	0.2878
LOH, after foaming, g./100 g. soln.[d]	0.0076	0.0074	0.0055	0.0058
LOH adsorbed, moles × 10^{10}/cm.^{2}	4.6	3.9	4.5	4.6
SLS adsorbed (average), moles × 10^{10}/cm.^{2}	5.7	3.7	—	5.2

[a] Rising temp. expt.

[b] Falling temp. expt.

[c] Maintained unchanged with temperature by keeping system closed.

[d] From average FDTT of samples.

The results facilitated planning a second approach in which a foam with a known large area was examined at temperatures which bracketed the transition temperature, a small sample of liquid being withdrawn at each temperature. Using the simplified procedure described in the experimental section, it was found by numerous experiments not recorded here that it was of first importance to establish equilibrium.

Four experiments are given in Table III. In these a concentration of SLS was selected which was above the CMC to ensure complete solubility of the lauryl alcohol, yet sufficiently low to obviate the necessity for very large volumes (surface areas) of foam. The lower temperature of the experiments was chosen as sufficiently high to be above the temperature at which solid adduct of SLS and LOH is precipitated (Ref. 2, Fig. 4).

The drop in transition temperature accompanying foam formation was 2.5° to 5.0°C. This drop accompanies the change in bulk concentration of both surface-active components. The SLS concentration was determined by chemical analysis, and this knowledge in turn permitted the determination of the LOH concentration from the known curves relating composition to transition temperature (Ref. 2, Fig. 2).

In the first of each pair of experiments (Table III) the transition was from slow to fast draining; in the second in the opposite direction. The

TABLE IV

Adsorption Results below the Transition Temperature[a]

SLS, initial, g./100 g. soln.	0.250	0.300[b]	0.400
LOH, initial, g./100 g. soln.	0.0098	0.0118	0.0157
FDTT of foamed soln., °C.	31.6	27.8	24.6
LOH adsorbed, moles $\times 10^{10}$/cm.^{2}	3.9	4.6	4.0
SLS adsorbed, moles $\times 10^{10}$/cm.^{2}	3.4	5.7	5.1

[a] Bubble size, weight of solution, and volume of foam were the same as in the first column of data, Table III.

[b] From Table III.

agreement of the data was accepted as satisfactory evidence of the attainment of equilibrium.

It appears from the calculated values given in Table III that the adsorption of the two surface-active components is of the same order. However, only limited significance is attached to the values given for the SLS because the change in concentration (8 parts in 300) is close to the precision of the titrations (2 parts in 300). With respect to the adsorption of LOH, the change in concentration which occurred during foaming was very large compared to the precision of the method of analysis.

Upon transition there was no observed change in the magnitude of adsorption of the LOH, as shown by the closeness of the transition temperatures for the first and second samples.

The experiment was repeated using other concentrations of SLS and different ratios of LOH. The results are summarized in Table IV, and it appears that over the region examined no differences in the adsorption above and below the transition were revealed.

These results may be expected to have a bearing on the surface tension behavior of the system. The suggestion has been made that the transition is a phase change at the surface (2) and has been discussed in terms of thermodynamic equilibria among a system of quasi-phases, namely, surface, aqueous medium, and micelles (17). The transitions observed are for a reversible change occurring at constant pressure in a system at equilibrium, and the free energy of the process is zero. With rather simple assumptions, it may be considered that no change in surface tension occurs on transition. Respecting the slope of the surface tension-temperature curve, it is in general very small for solutions of surface-active agents over the micellar region, and in the light of the results given in Table IV, an observable change in slope at the transition is not to be expected. Observation by the pendant drop method of limited accuracy showed this probably to be the case, the value of the slope being less than 0.1 dyne/cm./°C. over a wide range of temperatures bracketing a transition.

We consider, however, that significant changes in surface potential may occur on transition.

It is recognized that the adsorption of the LOH will be a function of the amount available. Data on the very interesting question of the relations at more widely differing transition temperatures were not obtained. We have shown that in solutions of pure SLS alone adsorption falls off below the CMC. This region, however, is the one over which solubilization of LOH is small. It is to be expected that strong adsorption of the LOH will persist below the CMC, and in fact foam fractionation can be most efficient in this region (3). With respect to the behavior of SLS below the CMC in the presence of LOH, we have no data of sufficient accuracy to be revealing. It may, however, be speculated that the LOH enhances the adsorption of the SLS, as indicated by the observation of high transition temperatures in this region and by the penetration experiments of Schulman and his coworkers *e.g.* (18).

The authors appreciate the valued discussions and continued interest of L. Shedlovsky and G. D. Miles during the course of this work.

Conclusions

1. Direct adsorption measurements have been made in the system sodium lauryl sulfate-water. The adsorption rises until the critical micelle concentration is reached and then remains constant. The maximum value corresponds to a gaseous film with an area per molecule of 40 A^2.

2. At neutral pH surface hydrolysis does not occur in the foregoing system.

3. In the system sodium lauryl sulfate-lauryl alcohol-water, to sustain either the slow or the fast draining condition, a monolayer of the two components is sufficient.

References

1. Miles, G. D., Ross, J., and Shedlovsky, L., *J. Am. Oil Chemists' Soc.* **27,** 268 (1950).
2. Epstein, M. B., Wilson, A., Jakob, C. W., Conroy, L. E., and Ross, J., *J. Phys. Chem.* **58,** 860 (1954).
3. Miles, G. D., *J. Phys. Chem.* **49,** 71 (1945).
4. Epstein, M. B., Ross, J., and Jakob, C. W., *J. Colloid Sci.* **9,** 50 (1954).
5. Donnan, F. G., and Barker, J. T., *Proc. Roy. Soc.* (*London*), **A85,** 557 (1911).
6. Confer McBain, J. W., and Wood, L. A., *Proc. Roy. Soc.* (*London*) **A174,** 286 (1940).
7. Reviewed by Dixon, J. K., Judson, C. M., and Salley, D. J., "Study of adsorption at a solution-air interface by radiotracers" in "Monomolecular Layers" (H. Sobotka, ed.), American Association for the Advancement of Science, 1954.
8. Dreger, E. E., Keim, G. I., Miles, G. D., Shedlovsky, L., and Ross, J., *Ind. Eng. Chem.* **36,** 610 (1944).
9. Blakey, B. C., and Lawrence, A. C. S., *Discussions Faraday Soc.* **No. 18,** 270 (1954).
10. Matzke, F. B., *Proc. Natl. Acad. Sci. U. S.* **31,** 281 (1945).

11. Bauer, N., and Fajans, K., "Refractometry" in "Physical Methods of Organic Chemistry," Vol. 1, Part 2, p. 1228. Interscience Publishers, New York, 1949.
12. Williams, R. J., Phillips, J. N., and Mysels, K. J., *Trans. Faraday Soc.* **51**, 728 (1955).
13. Brady, A. P., and Brown, A. G., in "Monomolecular Layers."
14. Ruyssen, R., and Maebe, J., *Mededeel. Koninkl. Vlaam-Acad. Wetenschap. Belg. Kl. Wetenschap.* **15**, 5 (1953).
15. Cook, M. A., and Talbot, E. L., *J. Phys. Chem.* **56**, 412 (1952).
16. Sporck, C. R., *J. Am. Oil Chemists' Soc.* **30**, 190 (1953).
17. Epstein, M. B., Wilson, A., Gershman, J., and Ross, J., *J. Phys. Chem.* **60**, 1051 (1956).
18. Goddard, E. D., and Schulman, J. H., *J. Colloid Sci.* **8**, 329 (1953).

JOURNAL OF COLLOID SCIENCE **12**, 356–362 (1957)

THERMAL FORCES ON AEROSOL PARTICLES IN A THERMAL PRECIPITATOR

C. F. Schadt and R. D. Cadle

Stanford Research Institute, Menlo Park, California

Received November 12, 1956

Abstract

The generally accepted theory of thermal precipitation predicts that aerosol particles having high thermal conductivity would be very difficult to collect. However, no such difficulties have been reported in the literature. Accordingly, a study has been undertaken of the thermal forces on aerosol particles under greatly differing conditions of particle size, thermal conductivity of the particles, and temperature gradient. Thermal gradients were produced with a commercially available (Casella) thermal precipitator, using a ribbon filament. Thermal forces were calculated from the width of deposit, using the Stokes-Cunningham equation.

The thermal forces on stearic acid particles were almost precisely those predicted by radiometer theory (Epstein's equation). The effect of particle size and of magnitude of thermal gradient were essentially those expected. However, the thermal forces on sodium chloride and iron particles were 20 to 40 times the values predicted by theory, although there was a decrease in thermal force with increasing thermal conductivity. Possible reasons for these results are discussed.

The chemical analysis of aerosol particles is generally a two-step process. The first step involves collecting the particles from a sample of the aerosol. The second step involves the analysis of the collected material, as by the methods described by Cadle (1), Lodge (2), and Crozier (3). One of the most useful methods for collecting aerosol particles, especially in the size range of 0.1 to 10 μ diameter, is by thermal precipitation. A number of so-called thermal precipitators are commercially available. All of them depend for their action on the force on a particle in a thermal gradient. The thermal gradient is produced by a source of heat, which may be a wire or ribbon filament, or plate, and a colder surface, usually a microscope slide or cover slip, on which the particles are collected.

At least two theories have been proposed to explain the thermal forces. One is that a particle in a thermal gradient is subjected to a stronger molecular bombardment from the direction of the heat source. Cawood (4) developed a mathematical relationship based on this concept. Another explanation is based on radiometer theory. According to this theory, if a temperature gradient exists along a surface, desorbed molecules have a greater component of velocity in the direction of increasing temperature than in the absence of a temperature gradient. If the surface is that of a particle, the particle moves down the temperature gradient as a result of the reaction force. Epstein (5) derived the following expression, based on radiometer theory, for the force on a sphere:

$$F_t = 9\pi a \left(\frac{k_a}{2k_a + k_i}\right) \frac{\eta^2}{\rho T} G \qquad [1]$$

where F_t = thermal force, dynes
a = radius of particle, cm.
k_a = thermal conductivity of the gas, cal./sec. cm. °K.
k_i = thermal conductivity of the sphere, cal./sec. cm. °K.
η = viscosity, g./cm. sec.
ρ = density of gas, g./c.c.
T = absolute temperature, °K.
G = temperature gradient prevailing in the gas, °K./cm.

Rosenblatt and La Mer (6), using tricresyl phosphate droplets, and Saxton and Ranz (7), using paraffin oil and castor oil droplets, found satisfactory agreement between experimental data for thermal forces and Epstein's equation. There was marked disagreement with Cawood's equation.

The thermal conductivities of the materials used in the above investigations were relatively low. Epstein's equation predicts that aerosol particles having high thermal conductivity would be very difficult to collect by thermal precipitation because of the low thermal forces. However, no such difficulties have been reported in the literature, although thermal precipitators have been used for many years for many types of aerosols. Since the implications of Epstein's equation impose a severe limitation on the usefulness of an important analytical tool, a study was undertaken of the thermal forces on aerosol particles under greatly different conditions of particle size, thermal conductivity of the particles, and temperature gradient. Each aerosol had a narrow particle size distribution. The dispersed phase of the aerosols consisted of stearic acid, sodium chloride, or carbonyl iron. Thermal gradients were produced with a commercially available (Casella) thermal precipitator using a ribbon filament. Thermal forces were calculated from the width of deposit using the Stokes-Cunningham equation.

EXPERIMENTAL

The stearic acid was obtained from the Eastman Kodak Company and was redistilled. Aerosols of stearic acid were prepared using a condensation-type generator (8). Particle sizes were determined using the "owl" (9) and microscopic examination of the collected particles. Most of the aerosols exhibited higher order Tyndall spectra, indicating that they were nearly monodisperse.

The sodium chloride was reagent grade and was not further purified. Aqueous solutions were dispersed using an aspirator-type aerosol generator similar to that described by Cadle and Magill (10). The newly formed aerosols were passed through a bed of glass beads to remove the larger particles. Evaporation of the water droplets left an aerosol of sodium chloride crystals. Size distributions of the aerosol particles were determined by preparing electron micrographs of particles collected with the thermal precipitator. The size of the suspended salt crystals was varied by varying the concentration of the salt solution. A typical size distribution is shown in Fig. 1.

Carbonyl iron was obtained from the General Dyestuff Corporation. Chemical analysis showed that it contained 97.3 % iron. The iron dust was

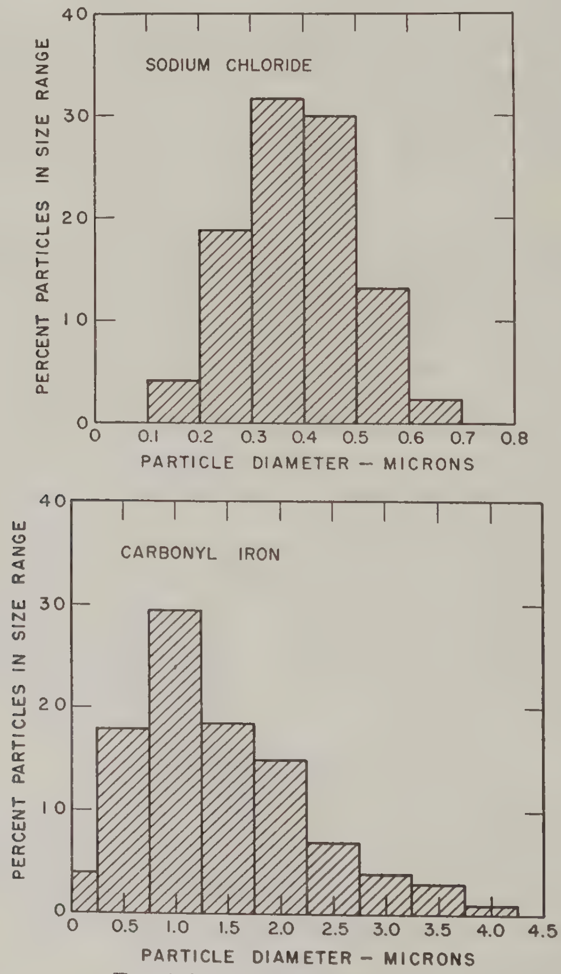

Fig. 1. Particle size distribution.

TABLE I

Dimensions of Thermal Precipitator

Filament width	1.4 mm.
Length of exposed filament	10 mm.
Distance from filament to each cover slip	0.15 mm.

dispersed using dust-dispering apparatus previously described (10). A single particle size distribution was used, which was determined by microscopic examination of the collected particles (Fig. 1).

A line drawing of the thermal precipitator has previously been published (11). The usual wire heating filament was replaced with a ribbon filament. The aerosol was drawn past the hot filament by allowing water to flow from the lower chamber. The particles were collected on microscope cover slides located on opposite sides of the hot filament. Some of the dimensions of the precipitator are shown in Table I. Temperature gradients were determined using a copper-constantan thermocouple made from 1-mil wire.

A typical run consisted of generating the aerosol, drawing it through the thermal precipitator using a predetermined air flow rate and thermal gradient, and measuring the widths of the deposits on the two cover slides.

Heat flow calculations indicated that a linear temperature variation was achieved between the warm and cold surfaces.

RESULTS AND CALCULATIONS

The results, expressed as the average width of deposit on the two cover slides, are presented in Table II. So long as the width of deposit was less than the width of the ribbon, the width of deposit was controlled by the time required for the particles nearest the filament to travel to the cover slides. For a given air flow rate this time was determined by the thermal forces on the particles.

Theoretical deposit widths were calculated, making the assumptions that the flow between the filament and the cover slips was laminar, and that the thermal gradient was uniform across the filament. Thermal forces were calculated using Epstein's equation. Terminal velocities normal to the filament were then calculated from the Stokes-Cunningham equation:

$$v = F_t(1 + AL/a)/6\pi\eta a \tag{2}$$

where v = velocity of particle normal to the filament, cm./sec.

A = constant related to the coefficient of slip. AL taken to be 0.82×10^{-5} cm.

L = mean free path of air molecules, cm.

Theoretical deposit widths were then calculated from the values of v and of the rate of air flow through the precipitator. The theoretical widths are included in Table II. In order to facilitate comparison of the different types of aerosol materials, values of F_t/aG were calculated from observed deposit widths using Eq. [2] and are shown in Table II.

TABLE II

Theoretical and Observed Widths of Particle Deposits

Approximate particle diameter (*microns*)	Thermal gradient (*°K./cm.*)	Sampling rate (*c.c./min.*)	Average observed width of deposit (*cm.*)	Theoretical width of deposit (*cm.*)[a]	F_t/Ga (*dynes/°K.*)	
					Experimental	Theoretical
			Stearic Acid			
5	2230	3.2	0.16	0.12	2.69×10^{-7}	3.68×10^{-7}
	4230	3.2	0.10	0.063	2.29	
	4230	6.7	0.15	0.13	3.14	
	6730	6.7	0.11	0.083	2.94	
2	2230	3.0	0.11	0.105	3.54	
	9800	3.0	0.06	0.024	1.46	
	6730	7.5	0.12	0.088	2.66	
	6730	15.0	0.17	0.174	3.76	
1	2230	2.2	0.08	0.073	3.30	
	2230	3.0	0.12	0.098	3.03	
0.3	8270	2.2	0.037	0.015	1.43	
	1600	3.0	0.056	0.104	6.66	
	2230	3.0	0.070	0.074	3.94	
	8270	4.0	0.047	0.027	2.06	
			Sodium Chloride			
0.4	2230	3.2	0.13	3.06	2.40	9.85×10^{-9}
	5360	3.2	0.077	1.35	1.70	
	5360	6.4	0.082	2.70	3.20	
	8270	6.4	0.066	1.74	2.58	
	8270	16.7	0.12	4.57	3.72	
0.2	2230	2.5	0.13	1.94	1.49	
	2230	5.0	0.11	3.92	3.52	
	4230	7.7	0.056	3.14	5.46	
	5360	7.3	0.092	2.36	2.50	
	8270	7.1	0.068	1.49	2.15	
			Iron			
1	8300	5	0.168	12.8	0.96	9.55×10^{-10}
	8300	2	0.132	5.1	0.48	
	8300	1	0.084	2.6	0.38	
	8300	1	0.085	2.6	0.38	
	5400	1	0.144	3.9	0.36	
	5400	0.5	0.060	2.0	0.40	
	5400	0.5	0.095	2.0	0.25	

[a] Based on Epstein's theory of thermal force and on Stokes' law with Cunningham correction.

The following values for thermal conductivities were used in making the calculations:

Stearic acid	3.0×10^{-4} cal./cm. sec. °K.
Sodium chloride	1.55×10^{-2} cal./cm. sec. °K.
Iron	0.16 cal./cm. sec. °K.
Air	5.9×10^{-5} cal./cm. sec. °K.

Discussion

Quite good agreement was obtained between the observed and calculated deposit widths for stearic acid aerosols. As would be expected, increasing the thermal gradient and decreasing the sampling rate decreased the width of the deposit. Decreasing the particle size likewise decreased the deposit width. The effect of particle size agrees with theory; when the expression for F_t from Eq. [1] is substituted in Eq. [2], a cancels out except in the term AL/a representing the Cunningham correction.

The calculated deposit widths for the sodium chloride particles averaged nearly 30 times the observed widths, although again increasing the thermal gradient and decreasing the sampling rate decreased the deposit width. Similar results were obtained with the iron, the calculated deposit widths averaging about 40 times the observed widths.

If Eq. [1] and [2] are correct, the values of the parameter F_t/aG calculated from the observed deposit widths should be nearly constant for a given material, but decrease with increasing thermal conductivity of the particles. Such a decrease was in fact observed, but it was much less than the decrease in

$$9\pi\left(\frac{k_a}{2k_a + k_i}\right)\frac{\eta^2}{\rho T}$$

which, by Eq. [1], should equal F_t/aG (Table II). The average experimental values for F_t/aG for stearic acid, sodium chloride, and iron were 3.07×10^{-7}, 2.87×10^{-7}, and 0.45×10^{-7} dynes/°K., respectively.

The possibility that electrical forces were responsible for the discrepancies between observed and calculated deposit widths was considered. This possibility was essentially eliminated by the following considerations:

1. One end of the filament was grounded to the metal head; thus the potential difference between the filament and the collecting surface (brass block) varied along the filament from nearly zero at one end of the sampling region to about 2 volts at the other end. There was no significant variation in the width of deposit from one end to the other.

2. The width of deposit was nearly the same whether particles were collected directly on the brass blocks or on glass cover slips. Thus there was no electrostatic effect due to the presence of a glass surface.

3. With no thermal gradient, but with glass cover slips in place, no particles were deposited except for a very weak general background.

The reason for the large discrepancies between the values for the thermal forces calculated from the experimental results and those calculated from Epstein's equation is not known. Possibly the sodium chloride and iron particles had smaller thermal conductivities than the bulk material. However, it is also possible that Epstein's equation gives very low results for the thermal forces when the thermal conductivities of the particles are relatively high. There are several possible explanations. One is that simplifying assumptions used in the derivation of Eq. [1] are not justified. These assumptions were discussed by Saxton and Ranz. Another possibility is that the force resulting from differential molecular bombardment of particles in a thermal gradient is sufficiently large that it is a major part of the thermal force when the thermal conductivity of the particles is relatively high.

From a practical standpoint, the results indicate that thermal precipitation is a much more generally satisfactory method for collecting aerosol particles prior to analysis than commonly accepted theory would indicate.

References

1. Cadle, R. D., *Anal. Chem.* **23,** 196 (1951).
2. Lodge, J. P., Jr., and Fanzoi, H. M., *Anal. Chem.* **26,** 1829 (1954).
3. Crozier, W. D., and Seely, B. K., "Some techniques for sampling and identifying particulate matter in the air." *Proc. 1st Natl. Air Pollution Symposium, Pasadena, Calif.*, 1949.
4. Cawood, W., *Trans. Faraday Soc.* **32,** 1068 (1936).
5. Epstein, P. S., *Z. Physik* **54,** 537 (1929).
6. Rosenblatt, P., and La Mer, V. K., *Phys. Rev.* **70,** 385 (1946).
7. Saxton, R. L., and Ranz, W. E., "Thermal force on an aerosol particle in a temperature gradient." *Univ. Illinois, Eng. Expt. Sta., Tech. Report* **No. 6,** December, 1951; *J. Appl. Phys.* **23,** 917 (1952).
8. Sinclair, D., and La Mer, V. K., *Chem. Revs.* **44,** 245 (1949).
9. Sinclair, D., "Measurement of particle size and size distribution," in "Handbook on Aerosols," U. S. Atomic Energy Commission, Washington, D. C., 1950.
10. Cadle, R. D., and Magill, P. L., *Ind. Eng. Chem.* **43,** 1331 (1951).
11. Cadle, R. D., "Particle Size Determination," p. 77. Interscience, New York-London, 1955.

JOURNAL OF COLLOID SCIENCE **12**, 363–377 (1957)

THE DYNAMIC MECHANICAL BEHAVIOR OF SOME NYLONS[1]

A. E. Woodward, J. A. Sauer, C. W. Deeley, and D. E. Kline

College of Chemistry and Physics, The Pennsylvania State University,
University Park, Pennsylvania

Received January 25, 1957; revised April 25, 1957

ABSTRACT

The dynamic mechanical properties of 6-6 nylon, 6-10 nylon, and a nylon copolymer have been studied in the audio-frequency region over a temperature range extending from about 80°K. to near the melting point by driving rodlike samples in their first transverse mode of oscillation. In all nylon types tested, four dispersion regions are observed, the first three being at temperatures of approximately 170°, 250°, and 350°K. These dispersion regions appear both as peaks in the absorption curve and as relatively sharp drops in the resonance frequency curve. The magnitude and temperature positions of the damping maxima are dependent on the specific nylon type. Over parts of the temperature region the damping of 6-6 nylon depends on the thermal history and water content of the sample. Possible assignments for each of the observed dispersion regions in terms of molecular motion are given. Correlations between the dynamic mechanical data and the results of other physical measurements on the nylons are pointed out.

I. INTRODUCTION

A relatively new method for the elucidation of internal structure and atomic movement in solids involves the study of the internal friction or mechanical damping as a function of temperature and frequency. A variety of solid high polymers has been investigated to date.

The most complete study of mechanical damping in the nylons is that of Schmieder and Wolf (1) using a torsional pendulum at low frequencies. All members of the series of nylons investigated by these authors showed four dispersion regions over the temperature range from 80° to 530°K. The loss peaks arising at temperatures below the main melting region were interpreted in terms of cooperative movement of groups of atoms along the polymer chain residing in stressed and nonstressed amorphous areas.

In addition to the investigation of various polyethylenes and other polymers carried out in these laboratories (2–4), the resonance frequency and damping behavior as a function of temperature from 80°K. to about 550°K. of a number of nylon samples have been observed using a transverse

---

[1] This work was supported in part by a research contract with the Atomic Energy Commission.

vibration method. Samples of 6-6 nylon (polyhexamethylene adipamide), 6-10 nylon (polyhexamethylene sebacamide), a copolymer containing 6-6, 6-10, and 6 (caproamide) units, and irradiated 6-6 nylon were used. Some effects of thermal history and water content on the mechanical properties of 6-6 nylon samples were also observed.

In this paper the results of this investigation will be presented and discussed; an attempt will be made to correlate the observed changes in the mechanical loss with those changes observed in x-ray (5), dielectric loss (6), coefficient of expansion (7), heat capacity (8), nuclear magnetic resonance (9), and retractive force (10) measurements.

II. Experimental

1. *Specimens*

The samples of 6-6 nylon, 6-10 nylon, and a copolymer containing 6, 6-6, and 6-10 units were supplied by the Polychemicals Department, E. I. du Pont de Nemours and Company. The copolymer was received as a ½ inch thick molded sheet, the other two types as rods of ½ inch and ¼ inch diameter. Specimens from two separate 6-6 nylon batches were used. Samples 1, 3, 4, 5, 7, and 8 were machined on a lathe to dimensions of 11.17 cms. in length and 0.762 cms. in diameter; sample 2 had the same length but was 0.635 cms. in diameter, and sample 6 was machined to a length of 10.49 cms. and a diameter of 0.863 cms. All samples except numbers 2 and 3 were then stored in a desiccator prior to use. Densities of the three polymer types after extended desiccation and heating to 90°C. for 13 hours, measured by a displacement method with ethyl alcohol as the liquid at 25°C., were found to be 1.150, 1.082, and 1.104 g./c.c. for the 6-6, 6-10, and copolymer samples, respectively. From the densities, per cent crystallinities of 57 and 40 were calculated for the 6-6 and 6-10 nylons using amorphous densities of 1.069 and 1.042 g./c.c., respectively, and crystalline densities of 1.22 and 1.152 g./c.c., respectively, given by Starkweather and Moynihan (11). The per cent crystallinity of the copolymer was estimated from x-ray diffraction measurements at the Polychemicals Department of E. I. du Pont de Nemours and Company as $<10\%$; the approximate number-average molecular weights, measured in the same laboratories, are 17,000 for the 6-6 nylon and 12,000 for the 6-10 nylon.

Two of the 6-6 nylon specimens were irradiated in hole number 12 of the X-10 graphite reactor at Oak Ridge, Tennessee. The slow neutron flux was 8.8×10^{11} n/cm.^{2}/sec., the cadmium ratio $\simeq 30$, and the associated γ-flux 6.9×10^5 r/hr.; the average γ-ray energy was 9 Mev. Sample number 4 received a dosage of 5.1×10^{16} n.v.t. and sample number 5 a dosage of 1.1×10^{18} n.v.t., where the n.v.t. value is the integrated thermal neutron flux in neutrons/cm.^{2}.

Two thermal treatments were given samples 1, 4, and 5 prior to certain test runs. These treatments were: (*1*) heating to 475°K. in a prior test, then cooling back to room temperature in the oven over a period of about 12 hours, (*2*) annealing at 450°K. for 1 hour in an inert medium, then air quenching at room temperature (samples 4 and 5), and (*3*) heating to 450°K. and cooling back to room temperature over about a 12-hour period (sample number 1). The heat treatments which each sample received are noted in the figures given in Section III.

Prior to testing, sample number 3 was conditioned at 100% humidity at 75°–80°C. for 32 days. An increase in weight of 5.4% was found after about 15 days of this treatment, with no further increase being observed during the remaining time.

2. Procedures

Each sample rod was hung in a horizontal position from cotton threads and was driven by a transducer attached to one thread while its response was noted at the other thread. An auto-recording apparatus, discussed elsewhere (12), was employed for measuring the resonance frequency and damping of the specimen. Temperatures below 300°K. were attained by using liquid nitrogen. Dewar flasks or a conventional oven provided the thermal isolation necessary. A drift method (12) was employed to permit measurements at any temperature in this region. Above 300°K. electrically heated ovens, permitting automatic or manual temperature control, were employed.

III. RESULTS

The results expressed in terms of the resonance frequency, f_0, and the internal friction, Q^{-1}, as functions of temperature are given for a number of specimens in Figs. 1–8. ($Q^{-1} = \Delta f/f_0$, where Δf is determined by measuring the width of the resonance curve at the half-power points.) As is evident from the figures, the damping curves for all three nylon types show four dispersion regions over the temperature range from 80°K. to the temperature where sagging of the samples prevented further measurement. These dispersions are found at about 170°, 250°, 350°K. and near to the melting or final softening temperature. Generally the heights of the loss peaks and the specific temperatures at which these maxima occur are found to differ from one type of nylon to another; noticeable differences are also seen for samples of the same nylon which have undergone different thermal pretreatments or which contain different amounts of water. It is found that the occurrence of a damping peak is generally accompanied by a drop in the resonance frequency, the rate of this decrease being greater when the rate of increase of the damping is greater and/or the peak is higher. This behavior has been noted previously for some polyethylene samples (4).

In Fig. 1 the data obtained for a 6-6 nylon sample are given. By com-

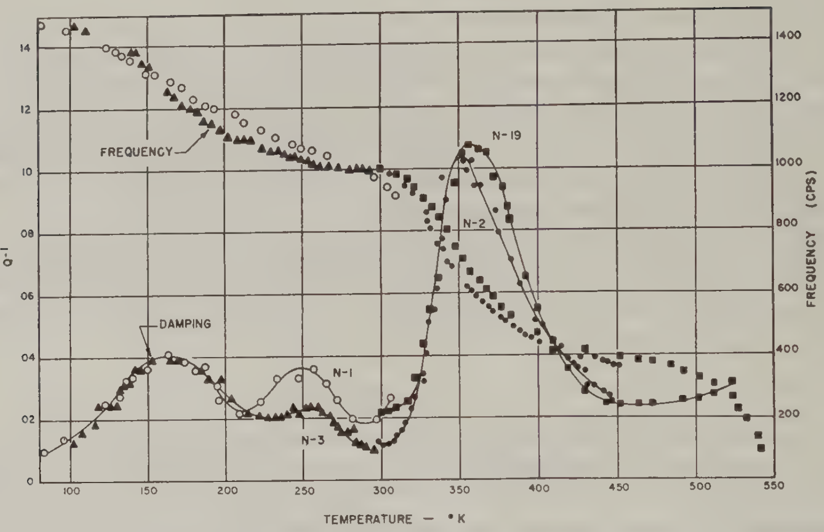

FIG. 1. Resonance frequency and damping versus temperature for 6-6 nylon.
Sample 1: (○) after 1 month in desiccator (test *N*-1), data taken from reference 13;
(●) after 16 months in desiccator (*N*-2);
(▲) after slow cooling from 475°K. (*N*-3);
(■) after slow cooling from 450°K. (*N*-19).

parison of curves *N*-1 and *N*-2 it is noted that storing this sample in a desiccator for 16 months over a drying agent has caused a shift of about 20° to higher temperatures in the damping curve around the room temperature region. After continuing test *N*-2 to 475°K., the sample was allowed to cool slowly to room temperature and a new run (*N*-3) was made over the temperature region of 100° to 300°K. Although the 170°K. dispersion region was essentially the same, a marked decrease in the height of the 250°K. peak had taken place. The sample was again heated (to 450°K.) and allowed to cool slowly to room temperature. Its dynamic mechanical behavior was then studied from room temperature to near its melting point. The results indicate (run *N*-19 vs. run *N*-2) a small increase in the peak temperature in the 350°K. region accompanied by a small increase in the damping maximum. The fact that in the 300°K. region the damping values for this run (*N*-19) do not coincide with the values first obtained for the heat-treated sample (run *N*-3) is not explainable at this time. This type of behavior was also observed for a nylon copolymer, as pointed out below.

Since earlier tests indicated that the water content of 6-6 nylon had an effect on the dynamic mechanical behavior, a nondesiccated sample (sample number 2) and a sample conditioned at 100% relative humidity (sample number 3) were run. In Fig. 2 the damping data for these two samples are compared with the results obtained for the desiccated sample. The resonance frequencies for sample 2, not shown in Fig. 2, were essentially the same over this temperature range as found for sample 1, test *N*-2. The resonance frequency for sample 3 dropped from 1150 to 550 c.p.s. over the range from 246° to 305°K. The room temperature shift of the damping mentioned above was verified, and in addition the 350°K. peak was found to shift to lower temperatures accompanied by an increase in the damping maximum as the water content of the polymer was increased.

The damping results for a 6-6 nylon specimen modified by a pile irradiation of 5.1×10^{16} n.v.t. (sample 4) are shown in Fig. 3. A shift of the curve to higher temperatures in the room temperature region, analogous to that for the nonirradiated samples, was found after extended desiccation (see curves *N*-10 and *N*-11). A rerun on the same sample after taking it to 475°K. and slow cooling to room temperature gave a decrease in the 250°K. peak (*N*-12) which is, however, not as great a one as found for the unirradiated sample; the curve from around 300° to 350°K. also shifts to higher tem-

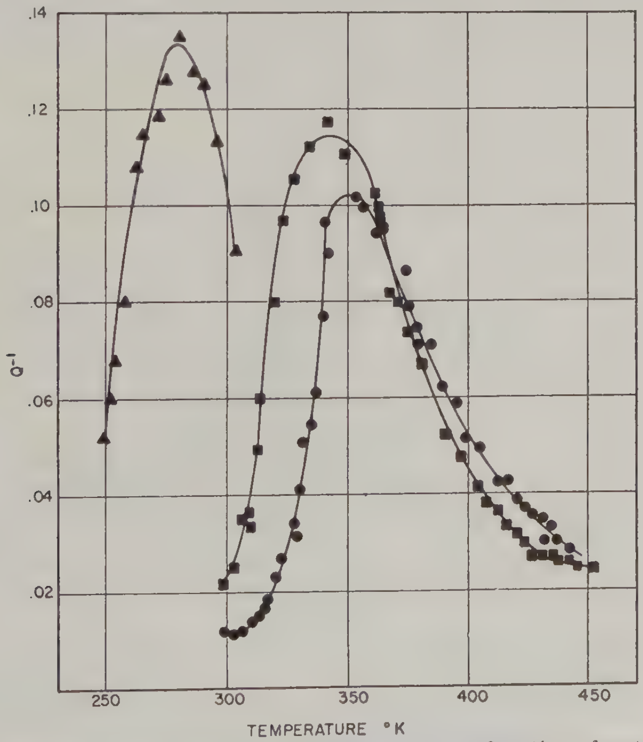

FIG. 2. Damping versus temperature for 6-6 nylon as a function of water content.
Sample 1: (●) 16 months in desiccator (*N*-2).
Sample 2: (■) as received (*N*-4).
Sample 3: (▲) 3 weeks at 100% relative humidity (*N*-18).

peratures. Further treatment of this sample by heating to 450°K. and air quenching causes the 250°K. dispersion region (see curve N-13) to exhibit a damping maximum which is larger than that found following slow cooling from 475°K. but is smaller than the original value. In the 350°K. region a marked increase in the peak height, an increase of area under the curve, and a shift of the peak to a higher temperature is found when the curve (N-13) is compared with the earlier test (N-11) made on this sample. However, a slower cooling rate accompanied by a higher annealing temperature appears to shift this peak to a still higher temperature (compare N-12 and N-13).

A series of tests similar to those described in the preceding paragraph was also made using a 6-6 nylon sample which had received a 1.1×10^{18} n.v.t. dosage in the Oak Ridge reactor. These results are shown in Fig. 4. A shift in the damping in the room-temperature region upon long desiccation, as was found for the 6-6 nylon samples described above, is apparent upon comparison of runs N-14 and N-15; the shift in this case, however, is less, being about 10°. Following annealing at 475°K. a slow cooling to room temperature no further shift is observed (test N-16) in this region—a different result from that found for the other irradiated 6-6 nylon sample. Cooling of this sample from 475°K. (N-16) or this treatment plus air

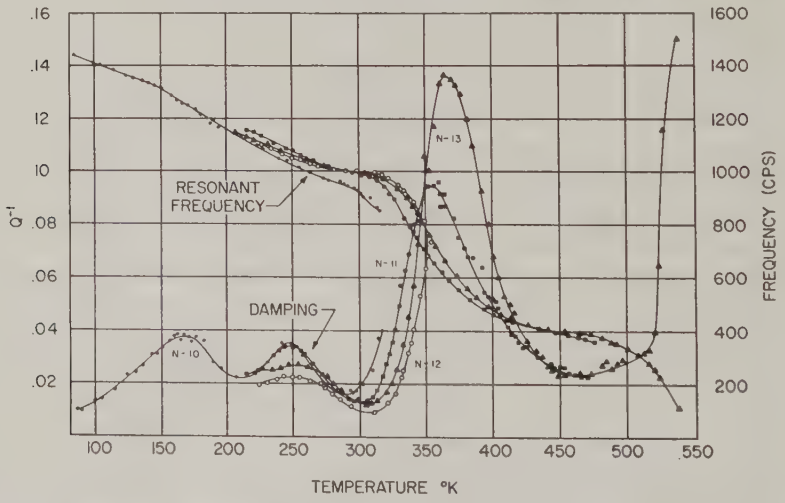

FIG. 3. Resonance frequency and damping versus temperature for irradiated 6-6 nylon (5.1×10^{16} n.v.t.).

Sample 4: (●) after 1 month in desiccator (N-10), data taken from reference 13;

(■) after 16 months in desiccator (N-11);

(○) after slow cooling from 475°K. (N-12);

(▲) after annealing at 450°K. and room-temperature quenching (N-13).

quenching from 450°K. (*N*-17) appear to impart about the same effect on the damping in the 250°K. dispersion region. Both treatments cause a lowering of the maximum damping value, although this effect is not as marked as the similar one in the other 6-6 samples. The effect of the heat treatment on the 350°K. peak is to produce a marked increase, as revealed by comparison of the data for *N*-17 and *N*-15. In the region above 500°K. the resonance frequency, and therefore the modulus, shows an increase with increasing temperature, whereas the damping appears to pass through a sharp maximum and then level off.

The difference in the damping for the 6-6 nylon and the two irradiated samples can best be illustrated by plotting the data on a common graph (Fig. 5). Little change is noted with irradiation dose in the low-temperature region. Near room temperature, the 10^{18} n.v.t. sample shows a definite shift to higher temperatures—an effect which occurred in the other samples upon extended desiccation. Although the damping is similar for the unirradiated and the 5.1×10^{16} n.v.t. samples in the region from 300°K. to 470°K. a dosage of 10^{18} n.v.t. causes an increase in the height. Above 470°K. marked differences are found for the three samples, the rise in the damping occurring at lower temperatures as the irradiation dosage is increased.

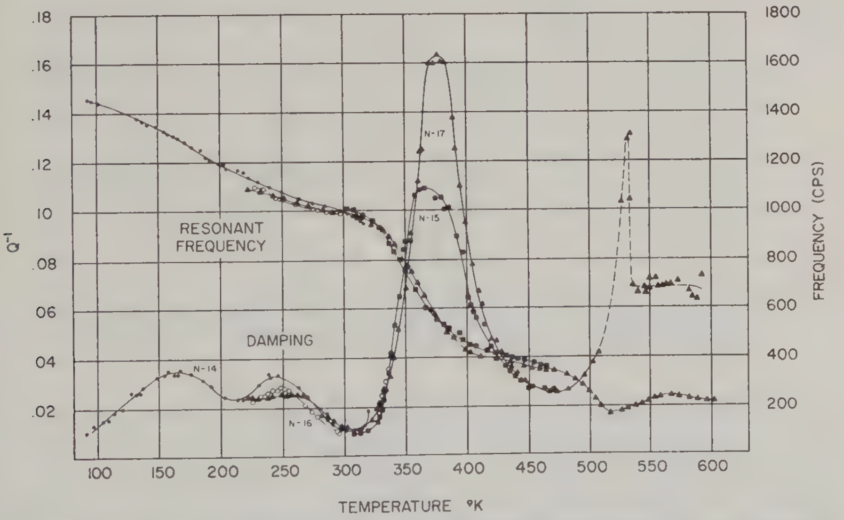

FIG. 4. Resonance frequency and damping versus temperature for irradiated 6-6 nylon (1.1×10^{18} n.v.t.).
Sample 5: (●) after 1 month in desiccator (*N*-14), taken from reference 13;
(■) after 16 months in desiccator (*N*-15);
(○) after slow cooling from 475°K. (*N*-16);
(▲) after annealing at 450°K. and room-temperature quenching (*N*-17).

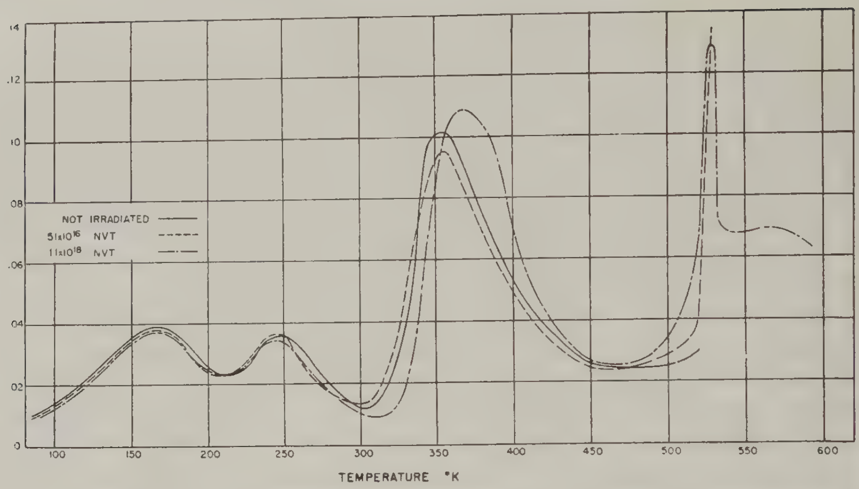

Fig. 5. Effect of pile irradiation on the damping as a function of temperature for 6-6 nylon. Data taken from tests *N*-1, -2, -10, -11, -13, -14, -15, -17, and -19.

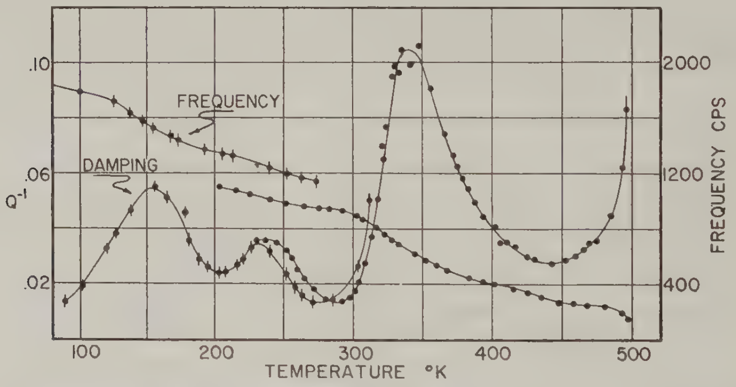

Fig. 6. Resonance frequency and damping versus temperature for 6-10 nylon. Sample 6: (◆) 1 month in desiccator (*N*-6), data taken from reference 13; Sample 7: (●) 18 months in desiccator (*N*-7).

In Fig. 6 the damping as a function of temperature for two 6-10 nylon samples is reproduced. Storing the 6-10 specimens in a desiccator causes only a slight shift to higher temperatures of that portion of the curve around the room-temperature region in contrast to the shift of 10°–20° for the 6-6 nylon samples. The two 6-10 nylon samples also show some differences in the high side of the 250°K. peak.

To investigate further the effect of structure on the internal friction of the nylons, a copolymer of 6-6 and 6-10 containing caproamide units was tested; the results are given in Fig. 7. The time in the desiccator between the two runs was only three months. It is seen that the shift to higher temperatures found for 6-6 nylon has not occurred for the copolymer. Instead in the second run higher damping values than those found in the first run were indicated between 250° and 300°K. This unexplainable change causes the maximum value for the 250°K. region to be somewhat in doubt.

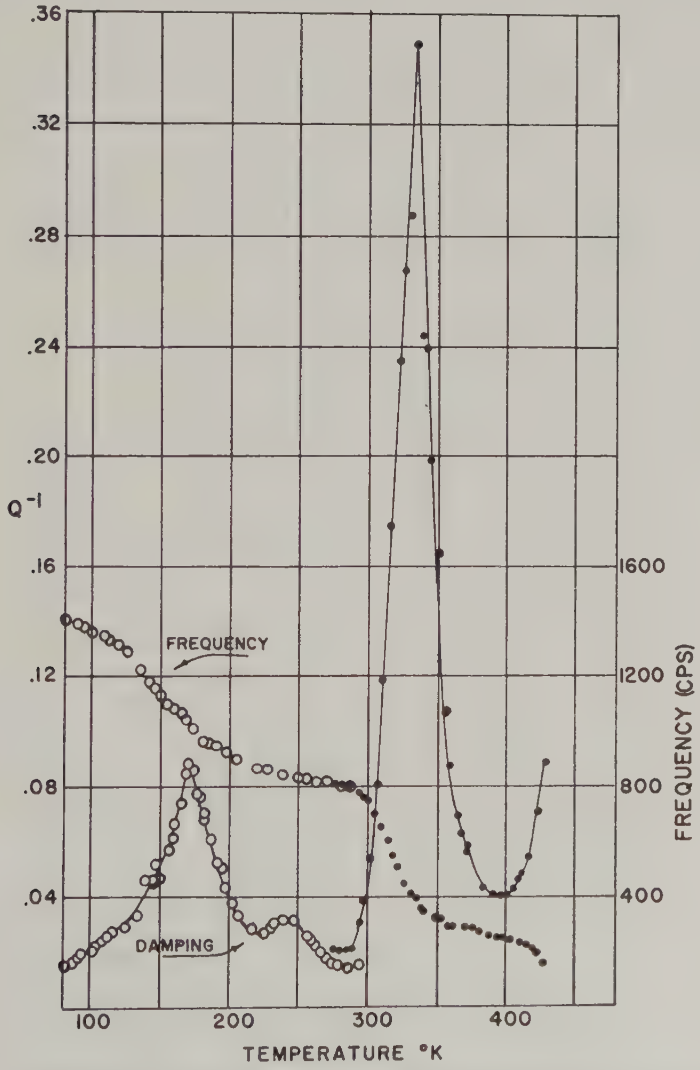

FIG. 7. Resonance frequency and damping versus temperature for a copolymer of 6-6, 6-10, and 6 nylon.
Sample 8: (○) after 1 month in desiccator (*N*-8);
(●) after 3 months in desiccator (*N*-9).

To facilitate comparison of the results for the three nylon types Fig. 8 is given (3). Owing to the differences in the damping found by runs on the same sample or on two samples of the same type, the exact nature of the curves around room temperature is in doubt. It can be seen in Fig. 8 that considerable differences exist in all four dispersion regions for the three nylon types. In the lowest temperature region where a peak is found, the damping maximum and the area under the curves increase in the order: 6-6 nylon, 6-10 nylon, copolymer. In the next highest temperature range (about 250°K.) all three peaks show approximately the same height; however, a shift in the damping maximum to lower temperatures for the 6-10

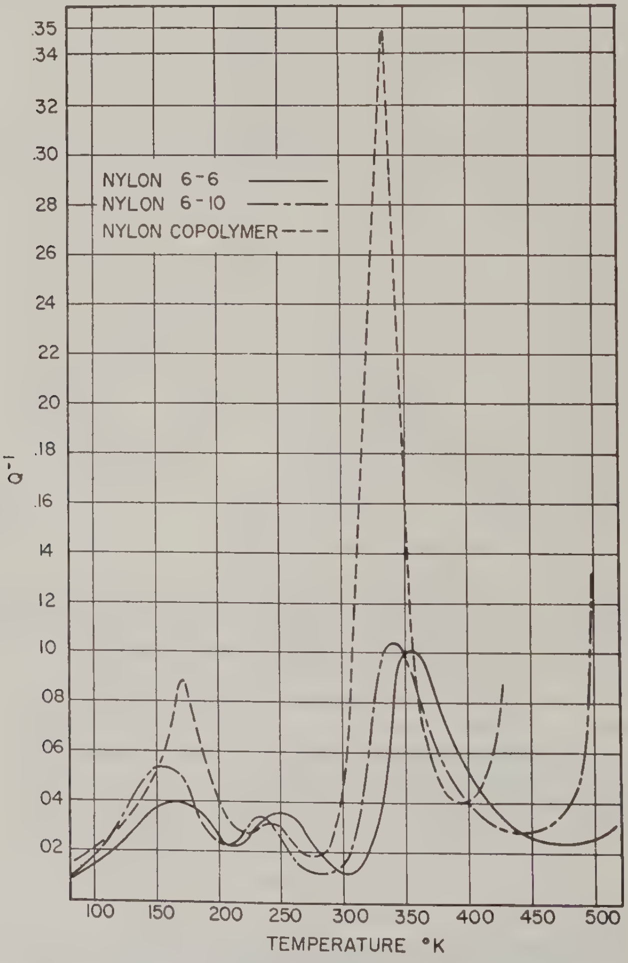

FIG. 8. Damping as a function of temperature for three nylons. Data taken from tests *N*-1, -2, -6, -7, -8, -9, and -19.

sample is indicated as compared to the others. In the next dispersion region around 340°K. a large increase in the height is shown for the copolymer as contrasted to the other two types, which show similar results. There is also a shift to lower temperatures for this peak in the order: 6-6, 6-10, copolymer. Finally, the temperature at which the highest temperature dispersion becomes apparent decreases in the order: 6-6, 6-10, copolymer.

IV. Discussion

A comparison of the damping curves given herein for 6-6 and 6-10 nylons with those published by Schmieder and Wolf (1) shows agreement concerning their general features, although the peak around 350°K. for 6-6 and that for 6-10 nylons were found to be approximately equal in height and area in the present work as contrasted with the reported differences; differences in the thermal history of the samples may account for this. The essentially amorphous copolymer shows similar behavior to that reported (1) for a quenched polyhexamethylene methyl pimelamide sample with little crystallinity. The four dispersion regions found in both investigations to occur in the vicinity of 500°, 350°, 250°, and 170°K. are designated herein as α, α', β, and γ, respectively. The higher temperatures found consistently for the loss peaks in this work as compared to Schmieder and Wolf's are expected owing to the higher frequencies employed. On the assumption that the dispersions are rate processes, activation energies were calculated from the frequencies and temperatures at the maximum damping in the α', β, and γ regions found in the two investigations. The activation energies in kilocalories for 6-6 and 6-10 nylons, respectively, were found to be 73 (run N-2) and 163 for the α' dispersion, 21 (run N-1) and 19–27 (runs N-7 and N-6, respectively) for the β dispersion, and 21 (run N-1) and 20 for the γ dispersion. Since data at only two frequencies are available and the thermal histories of the samples used in the two investigations are possibly different, these values are considered to give an order of magnitude only.

The α region in the damping curves reflects the large amount of mobility that the polymer chains acquire upon melting of the crystalline portions. The shift in this region to lower temperatures as the number of CH_2's between amide groups becomes larger or more irregular agrees with known changes in melting points (14).

The mechanisms advanced by Schmieder and Wolf (1) to account for the three loss peaks occurring at around 170°K. (γ), 250°K. (β), and 350°K. (α') essentially involve cooperative movement of either unstressed or stressed segments of the polymer chains in the amorphous regions. The data given here support their proposals to a certain extent, but to account for all the observations made during other types of measurements as well as dynamic mechanical ones, these mechanisms must be expanded and modified.

Recent retractive force measurements on 6-6 nylon (10) have indicated that two second-order transitions, one at 323°K., reported earlier (7), and the other near 383°K., take place in the temperature region encompassed by the α' damping peak. (See Fig. 1.) Also, a crystalline transition which is complete at 436°K. has been reported from x-ray (5) and heat capacity (8) studies.

Other experimental techniques have demonstrated that definite changes take place in the α' region for the nylons. Dielectric loss maxima at high frequencies for 6-10 nylons (6) and relatively sharp decreases in line width in nuclear magnetic resonance measurements for 6-6, 6-10, and a 6-6, 6-10 copolymer (9) have been reported in this temperature range. A "transition map" of temperature versus log frequency (15) for nylon 6-10 appears to correlate the electrical loss and the NMR transition with the mechanical loss peak at 340°K. A recent study by Boyd (16) has shown similar dielectric loss results for 6-6 nylon which also correlate well with the mechanical data.

It has been proposed (1) that the lower temperature portion of the α' peak in the vicinity of 330°K. is related to the onset of motion of large chain parts in the amorphous regions as the temperature is increased. The large activation energies for the α' process in both 6-6 and 6-10 nylons indicate that large chain portions are involved. Other data given herein add further support to this contention. Since the magnitude of the damping in this region for the three polyamides (see Fig. 8) is in approximate accordance with the amounts of amorphous material present and the large number of hydrogen bonds which can form in amorphous areas (17), the motion occurring at these temperatures is probably a result of the breaking of hydrogen bonds in the amorphous parts (10). The decrease in the α' transition temperature in the order: 6-6, 6-10, copolymer as noted in both the mechanical and nuclear magnetic resonance (9) measurements is in agreement with this interpretation; the decrease in the crystallinity which takes place in that order would be accompanied by a decrease in the restraints which prevent the separation of the amide groups on adjacent chains in the amorphous areas.

There is the possibility that the change in the crystalline structure reported as completed at 436°K. for 6-6 nylon (5) is reflected in the dynamic mechanical measurements accounting for part or all of the peak asymmetry in this region. A mechanical dispersion might be expected owing to axial rotation in the crystalline domains which must necessarily precede the transition (5). Part of the asymmetry found in 6-6 and 6-10 nylons may also be caused by the chain motion which is responsible for the second-order transition for 6-6 nylon at about 380°K. (10). This motion, thought to be an axial rotation of chain segments in the amorphous areas (10), could account for the slight asymmetry in the α' peak for the essentially amorphous copolymer. Stressing of the amorphous portions of polymers brought about by crystalline restraints might be responsible for the broadening of dispersion regions, a phenomenon shown to occur in polyethylene terephthalate yarns (18). Although this may also happen in the nylons, this explanation does not necessarily account for the total asymmetry in the α' dispersion, as proposed (1).

The presence of water in 6-6 nylon was found to cause a decided shift of the maximum α' damping to a lower temperature while increasing the height of the maximum. This effect may be due to a plasticization of the amorphous chain parts (19). An analogous shift has been noted in dynamic electrical measurements for both 6-6 and 6-10 nylons (6, 16). The greater magnitude of the shift in the α' peak with a decrease in the water content for 6-6 nylon as compared to 6-10 nylon (see Figs. 1 and 6) is in accord with the larger equilibrium water absorption of the former (20).

In the next lower dispersion region, designated herein as β, a second-order transition has been reported at about 250°K. for 6-6 nylon (10). A transition at this temperature might be attributed to the development of movement of the $-CH_2-$ units between amide groups in the amorphous areas, but this explanation is not consistent with the thermal history dependence of the β peak reported here and the occurrence of a still lower temperature peak. It is seen in Figs. 1 and 3 that when a sample is given thermal treatments which would be expected to favor the formation of intermolecular hydrogen bonds across the amide groups, the peak height and area decrease with a corresponding increase in the α' peak. This leads to the proposal that the β region in the polyamides is due to segmental motion involving amide groups in the amorphous regions which are not hydrogen-bonded to other amide groups. If this is the case then an electrical loss peak should occur in this region, as has been found recently by Boyd (16).

The dependence of the γ peak on the polyamide type tested and its proximity to the low-temperature peak in the polyethylene (1, 4, 21) and certain methacrylate esters (22) is in agreement with the proposal (1) that it is caused by the onset of cooperative movement of $-CH_2-$ groups between amide linkages in the amorphous parts. Owing to the increase in amorphous content, the increase of the area under this curve is expected to be: copolymer $>$ 6-10 $>$ 6-6, which is found. The association of a higher temperature with the onset of chain motion involving amide groups (the β peak) as compared to that for similar movements of hydrocarbon units (the γ region) follows from the higher polarity of the amide groups and the increase of stiffness in that part of the polymer chain. Both of these transitions might be expected to involve a much smaller number of chain segments than the number cooperating in the α' process owing to the much smaller activation energies for the β and γ processes.

Some preliminary results from a study of the effect of irradiation on the dynamic mechanical properties of 6-6 nylon have been presented in the preceding section. Since the exact nature of the changes taking place in the nylons upon irradiation is in doubt (23, 24), only a short and necessarily qualitative discussion of these results will be given at this time.

One of the first effects expected upon introduction of enough cross-links into a crystalline polymer to give a three-dimensional system is that above the temperature where the remaining crystalline regions melt the polymer will exhibit rubber-like behavior. In mechanical measurements the rubbery state is usually characterized by a positive temperature coefficient for the modulus as is found from 530° to 560°K. for the 6-6 nylon sample which had been given a 1.1×10^{18} n.v.t. irradiation dose (Fig. 4). Owing probably to decomposition of this polymer the resonant frequency and therefore the modulus decrease again at higher temperatures. Since this rubbery behavior was not evident for the sample exposed to a 5.1×10^{16} n.v.t. dosage, any cross-links introduced have acted principally to increase the molecular weight of the material to a point short of forming an infinite network.

Below the crystalline melting temperature the introduction of cross-links which involve regular covalent bonds, as distinguished from those involving hydrogen bonds in the crystalline areas, would be expected to reinforce any effects due to the presence of crystallites alone. As the dosage is increased, however, the increase in the number of cross-links would cause a decrease in the crystalline order, as has been found for polyethylene (25). Cross-linking the solid polymer might also freeze the sample in a state determined by its previous thermal history. Heat treatment of such materials would then be unable to bring about as great a rearrangement of chains and alignment of dipoles as it would for an unirradiated sample with an identical thermal history. On the assumption that the β region is caused by movements of segments which include non-hydrogen-bonded amide groups, this freezing in of the structure would account for the result that the magnitude of the decrease in the β peak height after annealing is smaller for the 10^{18} n.v.t. sample. The larger increase in the α' peak for the irradiated samples as compared to the unirradiated upon heat treatment appears to reflect a decrease in the crystallinity due to rearrangements of the branched or network system to relieve strains introduced by the cross-linking reaction.

References

1. Schmieder, K., and Wolf, K., *Kolloid-Z.* **134,** 149 (1953).
2. Sauer, J. A., and Kline, D. E., *J. Polymer Sci.* **18,** 491 (1955).
3. Sauer, J. A., and Kline, D. E., Paper given at IX International Conference of Theoretical and Applied Mechanics, Brussels, Belgium, September, 1956.
4. Kline, D. E., Sauer, J. A., and Woodward, A. E., *J. Polymer Sci.* **22,** 455 (1956).
5. Brill, R., *J. prakt. Chem.* [2] **161,** 49 (1942).

6. Baker, W. O., and Yager, W. A., *J. Am. Chem. Soc.* **64,** 2171 (1942).
7. Boyer, R. F., and Spencer, R. S., *J. Appl. Phys.* **15,** 398 (1944).
8. Wilhoit, R. C., and Dole, M., *J. Phys. Chem.* **57,** 14 (1953).
9. Slichter, W. P., *J. Applied Phys.* **26,** 1099 (1955).
10. Roseveare, W. E., Private communication.
11. Starkweather, H. W., Jr., and Moynihan, R. E., *J. Polymer Sci.* **22,** 363 (1956).
12. Kline, D. E., *J. Polymer Sci.* **22,** 449 (1956).
13. Kline, D. E., Thesis for Ph.D. degree, The Pennsylvania State University, University Park, Pa., 1954.
14. Baker, W. O., and Fuller, C. S., *J. Am. Chem. Soc.* **64,** 2399 (1942).
15. Deutsch, K., Hoff, E. A. W., and Reddish, W., *J. Polymer Sci.* **13,** 565 (1954).
16. Boyd, R. H., Private communication.
17. Bunn, C. W., and Garner, E. V., *Proc. Roy. Soc. (London)* **A189,** 39 (1947).
18. Wood, D. W., *Nature,* **174,** 753 (1954).
19. Baker, W. O., Fuller, C. S., and Pape, N. R., *J. Am. Chem. Soc.* **64,** 776 (1942).
20. Starkweather, H. W., Jr., Moore, G. E., Hansen, J. E., Roder, T. M., and Brooks, R. E., *J. Polymer Sci.* **21,** 189 (1956).
21. Oakes, W. G., and Robinson, D. W., *J. Polymer Sci.* **14,** 505 (1954).
22. Hoff, E. A. W., Robinson, D. W., and Willbourn, A. H., *J. Polymer Sci.* **18,** 161 (1955).
23. Little, K., *Nature* **173,** 680 (1954); *ibid.* **170,** 1075 (1952).
24. Charlesby, A., *Nature* **171,** 167 (1953); Lawton, E. J., Bueche, A. M., and Balwit, J. S., *Nature* **172,** 76 (1953).
25. Charlesby, A., and Ross, M., *Proc. Roy. Soc. (London)* **A217,** 122 (1953).

JOURNAL OF COLLOID SCIENCE **12,** 378–388 (1957)

THEORY OF EVAPORATING WATER CLOUDS

Richard H. Milburn*

Fort Detrick, Frederick, Maryland

Received August 20, 1956; revised April 24, 1957

Abstract

The mass and heat transfer processes within finite clouds of water droplets are studied. Vapor concentration, temperature, and droplet size are described by continuous field functions. A simple nonlinear differential equation is developed to govern the propagation of these fields in space and time. Solutions of an approximate linear equation are found in order to describe the initial stages of cloud evaporation and to illustrate two different types of boundary condition.

I. Introduction

Many studies have been made of the formation of clouds of water droplets in the atmosphere (e.g., Findeisen (1) and Howell (2)), and of the breakup and dissipation of such clouds as the result of precipitation (e.g., Findeisen (3)) and radiational energy transfer (4). These investigations have been concerned primarily with large-scale clouds existing under the relatively turbulent conditions provided by atmospheric temperature-lapse and wind patterns.

It is of interest for micrometeorological and laboratory aerosol studies to examine in greater detail the heat conduction and vapor diffusion processes existing within small and newly created clouds of volatile materials. The following paper will discuss, in Section II, the heat and vapor balance within idealized nonturbulent and initially homogeneous clouds of water droplets. In Section III a simple nonlinear differential equation will be derived to describe the progress of droplet evaporation in the various regions of the cloud. Although the emphasis in these two sections will be on spherical clouds, the basic results will be of general applicability. A linearized form of the cloud equation derived in Section III will be solved in Section IV for spherical clouds using two representative boundary conditions. In Section V some illustrative numerical examples will be given.

II. Heat and Vapor Transfer within the Cloud

a. Discussion

Most of the vapor and temperature gradient surrounding an evaporating spherical drop lies within a few radii of the drop surface. As is customary, it will be assumed in the following paper that the individual cloud droplets are sufficiently far apart for the average vapor pressure and temperature of the immediately surrounding medium into which they evaporate to be described by simple scalar "field" functions of space and time. This requirement that the drop separation be large relative to the drop radii will be seen in Sections III, *b* and V, *a* to be satisfied for a variety of clouds. This assumption permits the use of differential vapor and heat diffusion equations to describe the propagation of the vapor and temperature fields.

---

* Now at Dept. of Physics, Harvard University, Cambridge, Mass.

The average single-droplet mass in a particular region of the cloud is also introduced as a scalar field function of space and time, and acts as a distributed source for the vapor and temperature fields. The value of the droplet mass function at any point and time is related to the vapor and temperature fields at the same point and time by the use of the familiar quasistatic equations describing the evaporation of single drops (*cf.* Luchak and Langstroth (5) and Langstroth *et al.* (6)). Thus it is assumed that individual droplets will be able to reach a steady-state condition with respect to their immediate surroundings in a time short compared with the duration of processes affecting the cloud as a whole. This assumption will also be discussed further in Section III, *b*.

A third assumption, implicit in the following work, is that the individual water droplets remain fixed in space so that the number of such drops in a unit volume is a constant. This requirement, which excludes turbulent clouds from consideration, effects in return a great simplification in the theory.

b. The Field Equations

The notation and units of Table I will be used. Using the first of the assumptions of Section II, *a* the cloud will be described by the following equations of bulk vapor diffusion

$$\partial_t c(\mathbf{r}, t) = D\nabla^2 c(\mathbf{r}, t) - n\partial_t m(\mathbf{r}, t) \qquad [1]$$

and bulk heat diffusion

$$\partial_t T(\mathbf{r}, t) = K\nabla^2 T(\mathbf{r}, t) + (Ln/\rho_a c_p)\partial_t m(\mathbf{r}, t). \qquad [2]$$

Using the second major assumption leads to the equations (*cf.* Luchak and Langstroth (5) and Langstroth *et al.* (6)) of droplet mass transfer

$$\partial_t m(\mathbf{r}, t) = 4\pi D(3m/4\pi\rho_w)^{1/3}[c(\mathbf{r}, t) - C_0(\mathbf{r}, t)] \qquad [3]$$

and droplet heat transfer

$$L\partial_t m(\mathbf{r}, t) = -4\pi k(3m/4\pi\rho_w)^{1/3}[T(\mathbf{r}, t) - T_0(\mathbf{r}, t)]. \qquad [4]$$

To these must be added the equation for the saturated vapor pressure of water

$$C_0(\mathbf{r}, t) = C_0[T_0(\mathbf{r}, t)]. \qquad [5]$$

TABLE I

Basic Notation and Units

Independent Variables:

$\mathbf{r}$: spatial position; in spherical clouds the distance from the cloud center (cm.)
t: time, relative to an initial time of cloud dissemination (sec.)

Dependent Variables:

$T(\mathbf{r}, t)$: temperature at $(\mathbf{r}, t)$, not near drop surface (°K.)
$T_0(\mathbf{r}, t)$: temperature of droplets at $(\mathbf{r}, t)$, (°K.)
$c(\mathbf{r}, t)$: water vapor concentration at $(\mathbf{r}, t)$, not near drop surface (g. cm.$^{-3}$)
$C_0(\mathbf{r}, t)$: water vapor concentration at drop surface at $(\mathbf{r}, t)$ (g. cm.$^{-3}$)
$m(\mathbf{r}, t)$: droplet mass at $(\mathbf{r}, t)$ (g.)

Constants:

T_i: temperature of the air initially, and at large distances from the cloud (°K.)
C_i: water vapor concentration in air initially, and at large distances from the cloud (g. cm.$^{-3}$)
n: droplet density in cloud (cm.$^{-3}$)
m_0: initial mass of individual droplets (g.)
r_0: initial radius of individual droplets (cm.)
R: cloud characteristic length, for spherical clouds the radius (cm.)
L: latent heat of vaporization of water (cal. g.$^{-1}$)
k: thermal conductivity of air (cal cm.$^{-1}$ sec.$^{-1}$ °K.$^{-1}$)
K: molecular heat diffusivity of air (cm.^{2} sec.$^{-1}$)
D: diffusivity of water vapor through air (cm.^{2} sec.$^{-1}$)
ρ_a: density of air (g. cm.$^{-3}$)
ρ_w: density of water (g. cm.$^{-3}$)
c_p: specific heat of air at constant pressure (cal. g.$^{-1}$ °K.$^{-1}$)

Operators:

∇^2: Laplacian (cm.$^{-2}$)
∂_t: partial time derivative (sec.$^{-1}$)

The five equations [1]–[5] permit, in principle, solution for the five fields c, C_0, T, T_0, and m, with suitable boundary conditions.

c. The Psychrometric Equation

Equation [2] may be made more convenient if the relationship $\rho_a c_p = k/K$ is used. It is also useful to observe that for water vapor in air at room temperature K is about equal to D. Making these substitutions and eliminating $\partial_t m$, Eqs. [1] and [2] yield

$$(\partial_t - D\nabla^2)[c + (k/LK)T] = 0. \qquad [6]$$

Similarly Eqs. [3] and [4] give

$$[c + (k/LK)T] = [C_0 + (k/LK)T_0]. \qquad [7]$$

Now Eq. [6] holds everywhere, both inside and outside the cloud. Also c, T. and their gradients are continuous at the boundary. Since the function $[c + (k/LK)T]$ is initially everywhere equal to the spatially constant value $[C_i + (k/LK)T_i]$, it will remain so for all times. Thus, using Eqs. [5] and [7],

$$[C_i - C_0(T_0)] = -(k/LK)(T_i - T_0). \qquad [8]$$

This is the familiar psychrometric equation, and shows that all the cloud droplets will be at the constant wet bulb temperature appropriate to the initial conditions, which are also the ambient conditions external to the cloud. This is a reflection of the familiar constancy of wet-bulb temperatures as air becomes saturated adiabatically (*cf.* Hewson and Longley (7), and also Marshall and Langleben (8) for pertinent discussion).

III. THE CLOUD EQUATION

a. Derivation

Since C_0 and T_0 have been found in the preceding Section to be spatial and temporal constants, determinable from Eq. [8], Eqs. [1] and [3] remain to be solved for $c(\mathbf{r}, t)$ and $m(\mathbf{r}, t)$. Then $T(\mathbf{r}, t)$ may be found from Eq. [2], or better, Eq. [7]. Applying the operator $(\partial_t - D\nabla^2)$ to Eq. [3] and eliminating $c(\mathbf{r}, t)$ with Eq. (1),

$$-n\partial_t m = (\tfrac{3}{8}\pi D)(4\pi\rho w/3)^{1/3}(\partial_t - D\nabla^2)\partial_t m^{2/3}, \qquad [9]$$

which is seen to be nonlinear in the field $m(\mathbf{r}, t)$. Define

$$\alpha = (8\pi D/3)(\tfrac{3}{4}\pi\rho_w)^{1/3}. \qquad [10]$$

Shortly after the cloud is formed, but before the evaporation has proceeded far enough for there to be appreciable influence of one drop upon another, the droplet masses will obey the familiar law, derivable from Eq. [3],

$$m^{2/3} = m_0^{2/3} - \beta t, \qquad [11]$$

with

$$\beta = \alpha(C_0 - C_i). \qquad [12]$$

If Eq. [9] is integrated with respect to t, and Eq. [11] is used for small values of t,

$$n\alpha m(\mathbf{r}, t) + (\partial_t - D\nabla^2)m^{2/3}(\mathbf{r}, t) = n\alpha m_0 - \beta. \qquad [13]$$

It is seen that for a very sparse cloud $n \simeq 0$, and Eq. [11] is the solution of Eq. [13] for all times.

It is convenient to write Eq. [13] and similar equations in dimensionless form. Let

$$m(\mathbf{r}, t) = m_0 f^{3/2}(\mathbf{x}, s),\ \mathbf{x} = (\mathbf{r}/R),\ s = (\pi^2 D/R^2)t, \qquad [14]$$

$$\gamma = 1 - (C_0 - C_i)/nm_0\,, \qquad [15]$$

and

$$\delta^2 = 3n\alpha m_0^{1/3}R^2/2\pi^2 D = (4/\pi)nR^2 r_0 . \qquad [16]$$

These substitutions yield the basic cloud equation

$$[\partial_s - (1/\pi^2)\nabla^2]f(\mathbf{x}, s) = (2\delta^2/3)[\gamma - f^{3/2}(\mathbf{x}, s)] , \qquad [17]$$

with the initial condition $f(\mathbf{x}, 0) = 1$. It should be observed that Eq. [17] will hold at every point independently of the shape of the cloud. For a spherical cloud, besides the symmetry condition at $x = 0$, $f(x, s)$ need satisfy only one additional requirement at $x = 1$, to specify the conditions of ventilation at the cloud surface.

The simple parameter δ^2 in Eq. [16] may be termed the "cloudiness" since it determines, as will be seen, whether the cloud evaporates primarily at its surface (when $\delta^2 \gg 1$) or more or less throughout its body (when $\delta^2 \ll 1$). The other parameter, γ, reflects the total water content of the cloud. Were there no vapor loss at the cloud boundary, γ would equal unity when no droplet evaporation at all can occur, zero when it is just possible for all droplets to evaporate completely to produce saturation, and negative values when the droplets are insufficient in size and numbers to saturate the air at all. Of course, in general, a finite cloud will always evaporate away eventually owing to diffusion of vapor from the boundary.

b. Range of Validity of the Cloud Equation

A major assumption in the development of Eq. [17] has been that the individual droplets attain a quasistatic equilibrium with respect to their immediate surroundings in a time short relative to the time scale of the cloud as a whole. Since the usual wet-bulb temperature is of the order of 10 °K. below the ambient temperature, and the latent heat of vaporization of water is about 585 cal. g.$^{-1}$, it is easily estimated that the evaporation of about 2% of a droplet's mass will suffice to reduce the drop temperature from ambient to the wet-bulb value. Even at 90% relative humidity water drops in the 1- to 50-μ range will reach this temperature within a few seconds. Cloud life times will generally be much longer. Only clouds having a very high overall water content will not be able to evaporate enough prior to saturation for the wet-bulb temperature to be reached. If the cloud is disseminated at a drop temperature different from ambient, analogous estimates will apply. These conditions may be expressed by the approximate inequality $(C_0 - C_i) > 0.02\, nm_0$.

It is also assumed in Section II that the interparticle distance, say d, is large relative to the drop radii r_0. Thus let it be required that $d > 10r_0$. Since each droplet occupies an average volume of $d^3 > 10^3 r_0^3$, the average density of water in droplet form must be $nm_0 < 4 \cdot 10^{-3}$ g. cm.$^{-3}$. The overall conditions for the validity of Eqs. [1]–[4] and the equations derived therefrom may be expressed as

$$nm_0 < 50 \text{ min. } [(C_0 - C_i), 8 \cdot 10^{-5} \text{ g. cm.}^{-3}]. \tag{18}$$

Of course, the linear equations to be developed in Section IV from Eq. [17] will be of a much more restricted validity.

IV. Linear Approximations to the Cloud Equation

a. The Linear Equation

The nonlinearity of Eq. [17] makes it difficult to solve in detail analytically. For this reason it is instructive to linearize Eq. [17], or equivalently the system of Eqs. [1] and [3], under the assumption that $f(\mathbf{x}, s)$, in Eq. [17], does not differ too much from unity over the range of interest. For the specification of boundary conditions it is most convenient to derive and solve equations in $c(\mathbf{r}, t)$, and then to determine $m(\mathbf{r}, t)$ by integration of Eq. [3]. Let $m^{2/3}(\mathbf{r}, t) = m_0^{2/3} - g(\mathbf{r}, t)$. The linearization assumption is that g is small enough with respect to $m_0^{2/3}$ for the approximation

$$\partial_t m(\mathbf{r}, t) = m_0 \partial_t [1 - g(\mathbf{r}, t)/m_0^{2/3}]^{3/2} \simeq -\tfrac{3}{2} m_0^{1/3} \partial_t g(\mathbf{r}, t) \tag{19}$$

to hold reasonably well. Also $\partial_t m^{2/3}(\mathbf{r}, t) = -\partial_t g(\mathbf{r}, t)$. Substituting Eq. [19] in Eq. [1], and eliminating with Eq. [3], the linear equation

$$[\partial_s - (1/\pi^2)\nabla^2] c(\mathbf{x}, s) = \delta^2 [C_0 - c(\mathbf{x}, s)] \tag{20}$$

is obtained, where dimensionless space and time coordinates have again been used. With a spherical cloud Eq. [20] holds for the region $0 \leq x < 1$. Outside the cloud, $x > 1$, a similar equation holds, and is obtained by taking $\delta^2 = 0$ in Eq. [20].

b. Boundary Conditions

In all cases the initial condition on $c(\mathbf{x}, s)$ will be taken to be

$$c(\mathbf{x}, 0) = C_i, \ \textit{all } \mathbf{x}. \tag{21}$$

Also, it is expected that

$$c(\infty, s) = C_i, \tag{22}$$

and for a spherical cloud

$$\partial_x c(x, s)]_{x=0} = 0. \tag{23}$$

At $x = 1$ two cases will be considered, for spherical clouds.

(*1*) *Clamped Boundary.* The condition is that

$$c(1, s) = C_i. \tag{24}$$

This condition corresponds to an unphysically sharp convection maintaining the vapor concentration at the boundary fixed at the ambient value. In this case the complete solution for $c(x, s)$ is found by standard methods to be (*cf.* Carslaw and Jaeger (9))

$$c(x, s) = C_0 - (C_0 - C_i)\left\{\frac{\sinh \delta\pi x}{x \sinh \delta\pi} + \frac{2\delta^2}{\pi x}\sum_{p=1}^{\infty}\frac{(-1)^{p+1}\exp[-(p^2+\delta^2)s]}{p(p^2+\delta^2)}\sin p\pi x\right\}. \qquad [25]$$

The summation term is seen to represent the initial transient, which rapidly dies out relative to the other terms. If $\delta^2 \gg 1$, the remainder of Eq. [25] is approximately equal to C_0, from $x = 0$ out to nearly $x = 1$, whence c rapidly drops to the ambient value C_i. Hence for such a cloudiness δ^2 the cloud will be expected to evaporate primarily at its outer surface. Using Eqs. [3] and [10],

$$m^{2/3}(r, t) = m_0^{2/3} + \alpha(R^2/\pi^2 D)\int_0^{(\pi^2 D/R^2)t} ds\,[C(r/R, s) - C_0]. \qquad [26]$$

Integration of Eqs. [25] and [26] is readily performed. The nontransient terms alone yield

$$m^{2/3}(r, t) = m_0^{2/3} - \beta t \cdot \frac{\sinh \delta\pi(r/R)}{(r/R)\sinh \delta\pi}. \qquad [27]$$

(*2*) *Free Boundary.* The conditions are that $c(x, s)$ and $\partial_x c(x, s)$ be continuous at $x = 1$, and $c(x, s)$ satisfy Eq. [20] with $\delta^2 = 0$ for $x > 1$. In this case vapor and heat transfer outside the cloud proceed according to tha laws of free diffusion. The solution of Eq. [20] for this case may also be readily determined. If the transient terms are omitted, this solution is, inside the cloud,

$$c(x, s) = C_0 - (C_0 - C_i) \cdot \frac{\sinh \delta\pi x}{\delta\pi x \cosh \delta\pi}, 0 \le x \le 1. \qquad [28]$$

In addition, the solution outside is

$$c(x, s) = C_i - (C_0 - C_i)\left[\frac{\sinh \delta\pi}{\delta\pi \cosh \delta\pi} - 1\right]\frac{1}{x}, x \ge 1. \qquad [29]$$

For large δ^2, Eq. [28] is similar to the steady-state part of Eq. [25], except that the vapor concentration at the cloud boundary is higher in the free-boundary case, nearly equalling C_0 instead of C_i. The droplet mass change may be found from Eq. [26] to be

$$m^{2/3}(r, t) = m_0^{2/3} - \beta t\,\frac{\sinh \delta\pi(r/R)}{\delta\pi(r/R)\cosh \delta\pi}. \qquad [30]$$

Comparing Eqs. [30] and [11], it is seen that particles at the edge of clouds having $\delta^2 \gg 1$ will evaporate about $(1/\delta\pi)$ times as fast as free particles, assuming the present boundary conditions. Equation [30] has also been obtained by Bade (10) from an integral equation developed by Keller using quite different methods.

V. DISCUSSION

a. *Parameters for a Particular Cloud*

Consider a typical cloud having a density $n = 10^3$ cm.$^{-3}$ of drops of disseminated radius $r_0 = 10^{-3}$ cm. Let the cloud be spherical of radius $R = 10^3$ cm. Then, from Eq. [16], $\delta^2 = 1.27 \cdot 10^6$, showing that even in a moderately dense cloud the "cloudiness" is much larger than unity. Also, if the initial humidity is 50% saturated at 25 °C., then $C_i = 1.16 \cdot 10^{-5}$ g. cm.$^{-3}$, $T_0 = 18$ °C., and $C_0 = 1.50 \cdot 10^{-5}$ g. cm.$^{-3}$. Thus $m_0 = 4.2 \cdot 10^{-9}$ g., and from Eq. [15] it is determined that $\gamma = 0.187$. Also, the inequality in Eq. [18] is well satisfied, showing that the theory applied to the present cloud should be approximately valid. It is evident from the value of γ that the cloud will evaporate quickly to about 20% of its original mass. At this point the air becomes saturated and further evaporation will proceed only near the boundary.

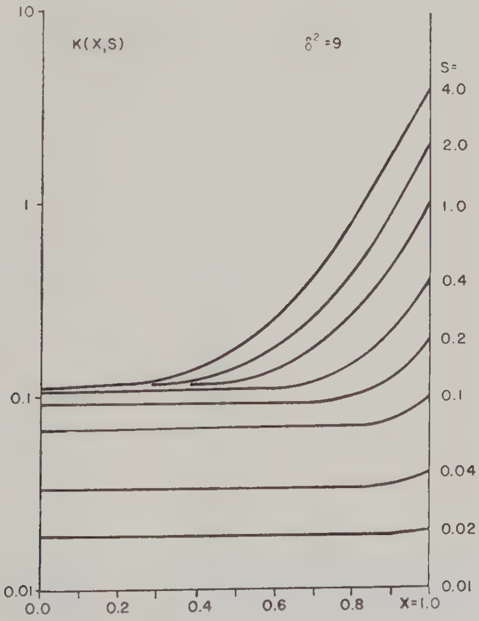

FIG. 1. Plot of Eq. [32].

b. The Linear Clamped Boundary Solution for $\delta^2 = 9$

The transient terms in the linear solution to the cloud equation are illustrated by calculating the clamped boundary equation [25] for a particular case of intermediate cloudiness, $\delta^2 = 9$. Writing out the integral in Eq. [26], in terms of dimensionless variables, it is easily found that

$$m^{2/3}(x, s) = m_0^{2/3} - \beta(R^2/\pi^2 D)K(x, s), \tag{31}$$

where

$$K(x, s) = s\frac{\sinh \delta\pi x}{x \sinh \delta\pi} + \frac{2\delta^2}{\pi x}\sum_{p=1}^{\infty}\frac{(-1)^{p+1}\{1 - \exp[-(p^2 + \delta^2)s]\}}{p(p^2 + \delta^2)^2}\sin p\pi x. \tag{32}$$

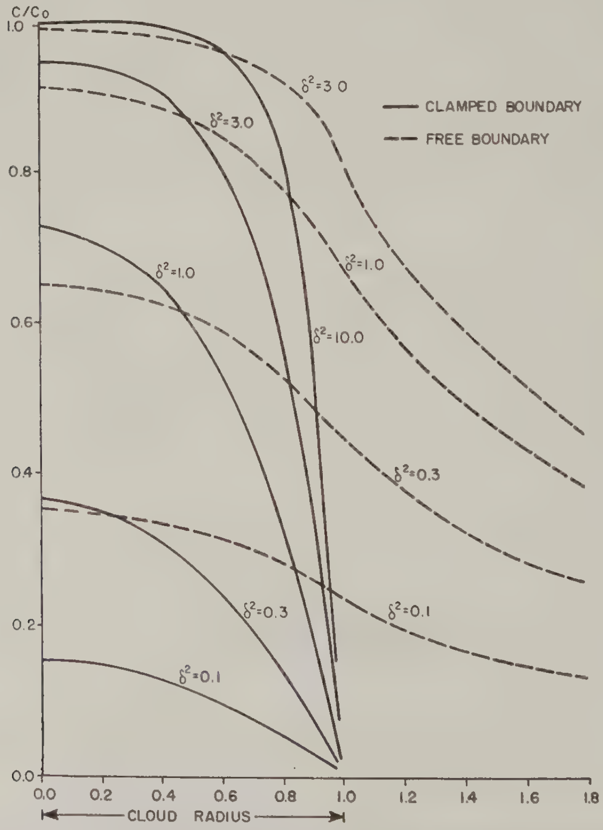

FIG. 2. Plot of vapor concentrations inside and outside cloud, relative to saturation vapor concentration. Quasistatic equilibrium is assumed. The linear theory is used.

The function $K(x, s)$ is plotted for $\delta^2 = 9$ and various times s in Fig. 1. It is seen that saturation conditions are reached in the center of the cloud for times s of the order of 0.4, where the evaporation stops, while at the boundary the evaporation proceeds apace. The free boundary case will exhibit similar behavior, although the numerical calculations will be much more complicated. It must be emphasized here that the linear solutions do not accurately describe the evaporation process beyond the first 20% or so of droplet mass reduction.

c. Linear Steady-State Solutions for Various Degrees of Cloudiness

In Fig. 2 are plotted the steady-state vapor concentrations, Eqs. [25], [28], and [29], for $C_i = 0$ and for various degrees of cloudiness δ^2. This figure illustrates clearly the difference between the free and clamped boundary cases. It is to be observed that to obtain a vapor concentration equilibrium in the region $x \geq 1$ in the free boundary case requires the expenditure of an infinite amount of vapor, as is seen by integrating Eq. [29] over the volume from $x = 1$ to $x = \infty$. Hence this cannot strictly occur during the early life of a finite cloud, and Eq. [29] is at best approximate.

VI. CONCLUSION

The cloud theory described in this paper is based upon the three primary assumptions discussed in Section II, *a*. The first of these is that the drops be widely separated relative to their radii. An assumption of this nature will be necessary in any theory which attempts to describe the behavior of clouds by means of the continuous functions required for convenient analysis. Moreover it was seen in Sections III, *b* and V, *a* that this assumption, along with the "quasistatic" assumption of Section II, *a*, will be indeed applicable to a variety of physical clouds.

The third assumption, limiting the discussion to strictly nonturbulent clouds, represents a severe idealization of nature. Were turbulence included, it would lead to the motion of individual droplets within the cloud, and to the addition of an extra "field" describing the density of various sized drops in the cloud. The complication inherent with such an addition is considered beyond the scope of the present paper.

Subject to the restrictions just outlined, it has been shown in this paper that it is possible to describe the evaporation and heat transfer within an aqueous cloud by means of a nonlinear differential equation which is simple in form and subject in principle to detailed solution for a variety of cloud densities and shapes. By applying a linearized form of this equation to spherical clouds, some of the more salient features of cloud evaporation have been examined in detail.

Acknowledgments

The author is indebted to Mr. K. L. Calder and Dr. W. L. Bade for their critical examination of this manuscript.

References

1. Findeisen, W., *Beitr. Phys. frei Atmos., Leipzig* **20,** 157 (1933).
2. Howell, W. E., *J. Meteorol.* **6,** 134 (1949).
3. Findeisen, W., *Met. Z., Braunchweig* **56,** 365, 453 (1939).
4. Hewson, E. W., *Quart. J. Roy. Meteorol. Soc.* **74,** 243 (1948).
5. Luchak, G., and Langstroth, G. O., *Can. J. Research* **A28,** 574 (1950).
6. Langstroth, G. O., Diehl, C. H. H., and Winhold, E. J., *Can. J. Research* **A28,** 580 (1950).
7. Hewson, E. W., and Longley, R. W., "Meteorology, Theoretical and Applied," p. 60. Wiley, New York, 1944.
8. Marshall, J. S., and Langleben, M. P., *J. Meteorol.* **11,** 104 (1954).
9. Carslaw, H. S., and Jaeger, J. C., "Conduction of Heat in Solids," Chapters 11, 12. Oxford University Press, 1947.
10. Bade, W. L., Private communications, 1955.

JOURNAL OF COLLOID SCIENCE **12**, 389–399 (1957)

DYNAMIC MECHANICAL PROPERTIES OF POLY-*n*-HEXYL METHACRYLATE[1]

William C. Child, Jr.,[2] and John D. Ferry

Department of Chemistry, University of Wisconsin, Madison, Wisconsin

Received March 19, 1957

INTRODUCTION

Following previous reports on the dynamic mechanical properties of polyethyl methacrylate (1) and poly-*n*-butyl methacrylate (2) in the transition from rubberlike to glasslike consistency, we now present similar data for poly-*n*-hexyl methacrylate. These measurements were part of a cooperative investigation with the Samuel Feltman Ammunition Laboratories, Picatinny Arsenal.

MATERIALS AND METHOD

The synthesis and fractionation of the polymer have been described elsewhere by Chinai (3). The fraction used in this study, with a weight-average molecular weight of 4.0×10^6, had been dried from frozen benzene solution and stored over silica gel desiccant. In studies of the lower members of this homologous series (1, 2), fractions of widely different molecular weight were employed, but since the mechanical properties depended very little on molecular weight in the transition region (as expected), a single fraction was considered sufficient for poly-*n*-hexyl methacrylate.

Measurements of the complex shear compliance ($J^* = J' - iJ''$) were made between 15 and 2400 cycles/sec. with the Fitzgerald Apparatus manufactured by Atlantic Research Corporation, Alexandria, Virginia. Three pairs of disc-shaped samples were employed, molded at 165°F. The samples were quite clear and almost colorless, and were sufficiently tacky to adhere readily to the driving surfaces in the apparatus. The sample coefficients were calculated as described before (1), taking the density of the polymer as 1.01 g./cm.^{3} at 25°C. and the thermal expansion coefficient as 6.5×10^{-4} deg.$^{-1}$ above the glass transition temperature. (Rogers and Mandelkern have since reported 1.01 g./cm.^{3} and 6.6×10^{-4} deg.$^{-1}$) (4). Detailed descriptions of the samples follow.

---

[1] Part XXVII of a series on Mechanical Properties of Substances of High Molecular Weight.

[2] Now at Carleton College, Northfield, Minnesota.

Samples 83, approximate dimensions 1¹⁄₁₆ in. diam. by ³⁄₃₂ in. thickness, were compressed in the apparatus about 4% and the sample coefficient was 15.2 cm. at 40°. Measurements were made at approximately 5° intervals from 35° to 60°, followed by a check run at 35° which agreed with the initial results. (The exact temperatures are given in the legend of Fig. 1.)

Samples 84, approximate dimensions 1¹⁄₁₆ in. by ¹⁄₃₂ in., were compressed about 7%, and the sample coefficient was 55.7 cm. at 100°. They were mounted at the same time as samples 83 and experienced the same temperature sequence. Measurements were made at approximately 5° intervals from 50° to 95°, followed by a check run at 50° which agreed with the initial results, and then one at 100°. At overlapping temperatures, the values of J' and J'' agreed very well with those from samples 83, so that no empirical correction was needed.

Samples 87, approximate dimensions ⁵⁄₁₆ in. by ⅛ in., were compressed about 4%, and the nominal sample coefficient was 2.97 cm. at 40°C. Measurements were made at approximately 5° intervals from 25° to 50°C. and then from 20° down to 5°C., with a final check run at 25°C. which agreed with the initial results. The values of J' and J'' were about 13% higher than those for samples 83 and 84, so an empirical correction factor of 0.87 was applied to these data.

Finally, samples 84 were reinserted (numbered now 89) to obtain additional results at higher temperatures. When recompressed, the nominal sample coefficient was 52.1 cm. at 100°C. Measurements were made at 95°, 100°, 105°, 115°, and 125°C. with a check run at 100°C. which agreed with the initial results. The values of J' and J'' were about 3% lower at overlapping temperatures than those from samples 84, so an empirical correction factor of 1.03 was applied to these data.

RESULTS

The original data for J' and J'', measured at 23 temperatures from 5° to 125°C., are shown plotted logarithmically in Fig. 1. Where data on different samples were taken at the same frequencies and temperatures, the values have been averaged.

For reduction to a standard temperature, 100°C. was chosen in conformity with the other members of the series; J_p' and J_p'' were calculated by the usual formulas (5), using the thermal expansion coefficient given above. The value of J_∞, the limiting high-frequency compliance, was chosen as 10^{-10} cm².&#47;dyne, but its choice was not critical.

Logarithmic plots of the reduced functions could be superposed quite well by the usual arbitrary shift factors a_T, identical for both real and imaginary components, except for a range between 15° and 50°C. for J_p' and between 105° and 125°C. for J_p''. The respective anomalies closely resemble those found in poly-n-butyl methacrylate and will be further

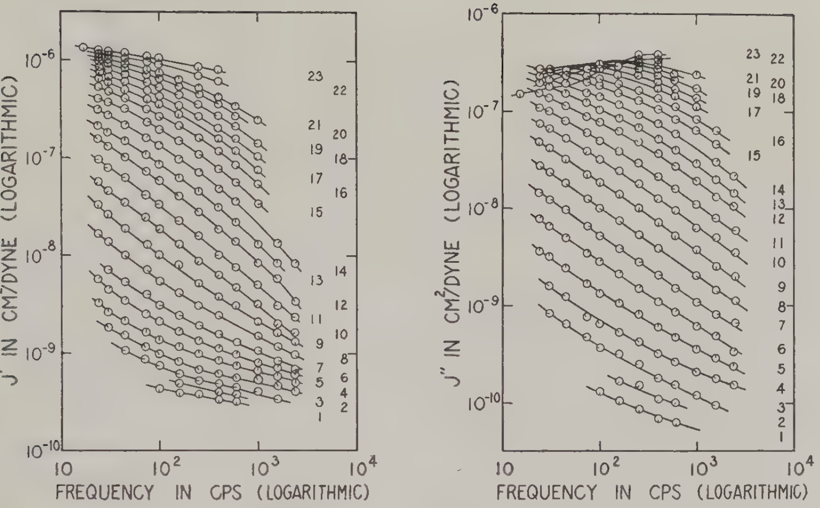

FIG. 1. Variation of the real part of the dynamic shear compliance, J' (left) and the imaginary part, J'' (right) with frequency for poly-*n*-hexyl methacrylate at 23 temperatures; numbers correspond to the sequence 4.7, 9.7, 14.6, 19.4, 24.7, 29.9, 34.7, 40.0, 45.1, 50.0, 55.0, 60.4, 64.5, 69.5, 74.7, 80.2, 85.3, 89.4, 94.6, 99.9, 104.8, 114.8, and 125.0° C.

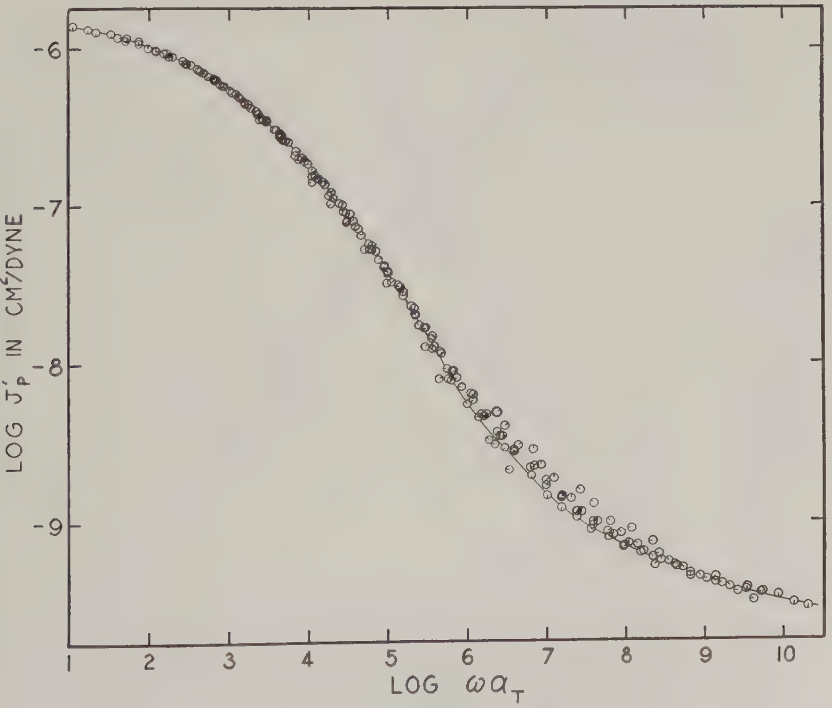

FIG. 2. Real part of the complex compliance, J', reduced to 100° C. and plotted logarithmically against reduced frequency with reduction factors calculated from WLF equation. Pip down at right 4.7° C.; successive 45° or 90° rotations clockwise correspond to increasing temperatures at approximately 5° or 10° intervals (exact temperatures given under Fig. 1). The solid curve is the assumed compliance of the α mechanism.

discussed below. Outside the anomalous regions, the empirical a_T values followed very closely an equation of the WLF form (6):

$$\log a_T = -c_1^0(T - T_0)/(c_2^0 + T - T_0)$$

with $c_1^0 = 9.80$ and $c_2^0 = 234.4$ for $T_0 = 373.2°\text{K}$. Values of a_T calculated from this equation were actually used for the final plots against reduced frequency (ωa_T) shown in Figs. 2 and 3.

With knowledge of the glass transition temperature, $T_g = 268°\text{K}$. (4), the values of c_1' and c_2' appropriate to T_g as reference temperature may be calculated from formulas previously given (6), and from these the parameters f_g and α_f. For f_g, interpreted as the fractional free volume at T, we obtain 0.024_5, identical with the average "universal" value for numerous amorphous polymers. For α_f we obtain 1.9×10^{-4}, reasonable in magnitude though somewhat smaller than usual. The change in macroscopic thermal expansion coefficient at T_g, which has been sometimes identified with α_f, is reported by Rogers and Mandelkern (4) to be between 2.0 and 2.8×10^{-4} deg.$^{-1}$.

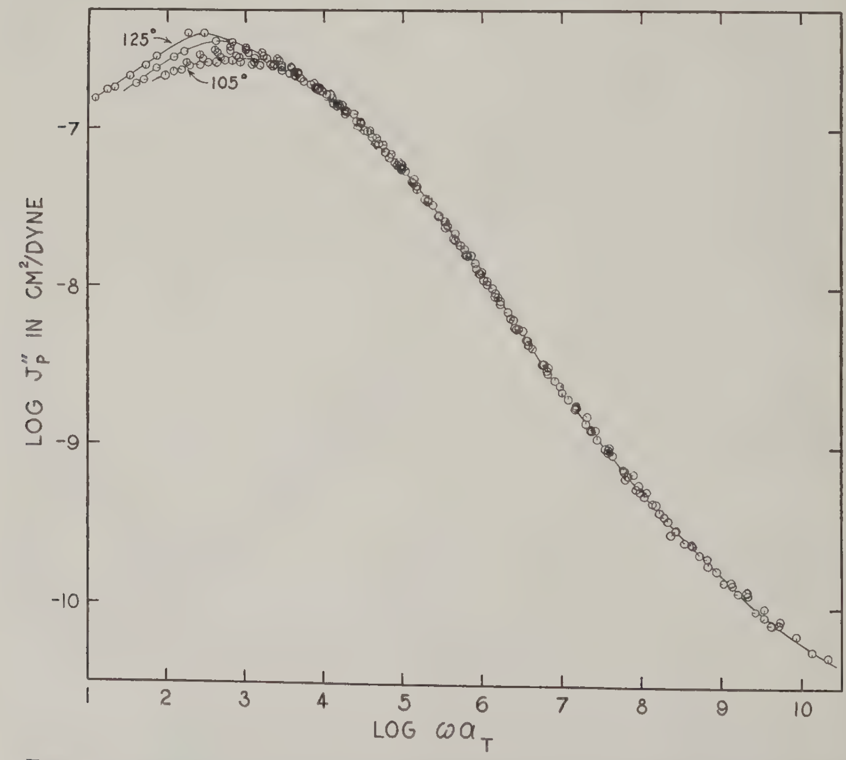

FIG. 3. Imaginary part of the complex compliance, J'', reduced and plotted as in Fig. 2, with the same temperature key.

DISCUSSION

Analysis of α and β Mechanisms

The fanning out of points at individual temperatures in Fig. 2 may be attributed to a β or side-chain mechanism just as in the case of poly-*n*-butyl methacrylate (2), and the data have been analyzed to separate the α and β contributions exactly as for the latter polymer. The lower envelope represented by the curve was taken as the α contribution, and the β contributions were obtained by subtraction point by point. Logarithmic plots of J'_β were superposed by empirical shift factors $a_{T\beta}$, and the superposition was reasonably satisfactory as shown in Fig. 4. From 15° to 40°C., log $a_{T\beta}$ was a linear function of the reciprocal absolute temperature with a slope corresponding to an apparent activation energy, ΔH_β, of 13 kcal. Although dielectric dispersion data are not yet available to compare with this figure as for the previous polymers in this series (1, 2), it presents a reasonable decrease with increasing side-chain length when compared with

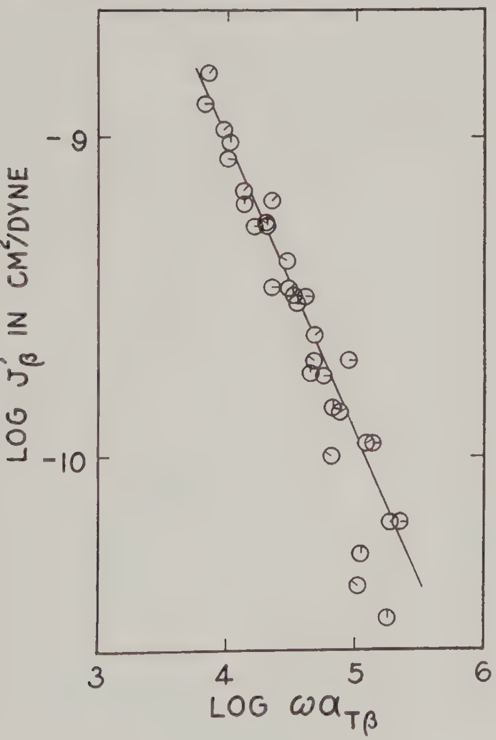

FIG. 4. Real part of the complex compliance of the β mechanism reduced to 100° C. on the basis of an apparent activation energy of 13 kcal. Temperature key same as in Fig. 2.

the values for the β mechanism of the ethyl (31 kcal.) and n-butyl (24 kcal.) polymers.

Because of the somewhat arbitrary choice of the envelope for J'_α, and the small differences involved in obtaining J'_β, the information thus obtained for the β mechanism is only semiquantitative, but sufficient to determine its location on the temperature and frequency scales. For comparison with other polymers in the methacrylate series, it is instructive to reduce J' for each to its own glass transition temperature. Using the WLF equation for shifting the α contribution and the Arrhenius equation for shifting the β contribution on the frequency scale, with the appropriate parameters for each polymer, and then adding the contributions at each frequency, we obtain the result shown in Fig. 5. At T_g, the α and β dispersions predicted in this manner are clearly separated, but the gap between them decreases with increasing side-chain length. With increasing temperatures, the α dispersion shifts to higher frequencies faster than the β dispersion, and the gap becomes closed 20° to 50°C. above T_g, depending on the width of the gap at T_g and the values of f_g, α_f, and ΔH_β. Near the

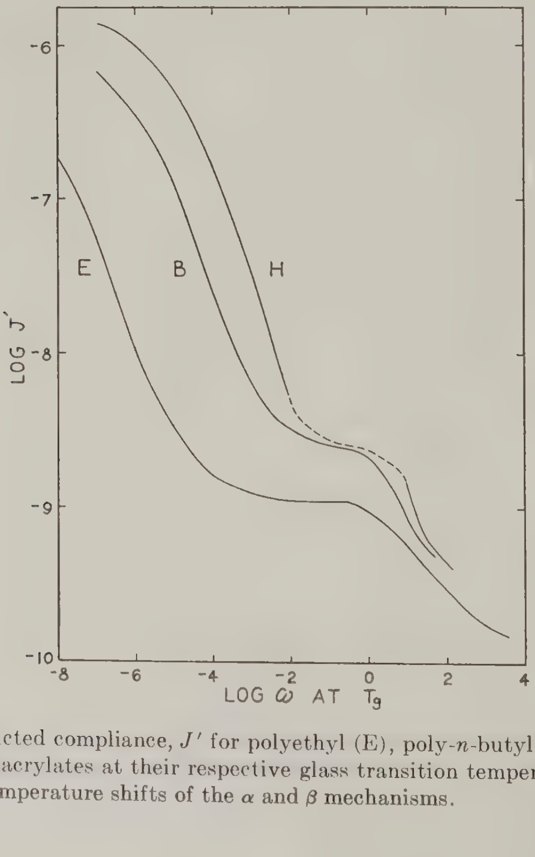

FIG. 5. Predicted compliance, J' for polyethyl (E), poly-n-butyl (B), and poly-n-hexyl (H) methacrylates at their respective glass transition temperatures, based on extrapolated temperature shifts of the α and β mechanisms.

temperature where the gap is closed, the failure of reduced variables will be most evident.

High-Temperature Reduction Anomaly

Between 105° and 125°C. the height of the maximum in log J'' increases with temperature, being given approximately by $-6.53 + 0.0052\ (t - 100)$, where t is Centigrade temperature. This behavior closely resembles that of the n-butyl polymer, where the corresponding temperature coefficients were 0.0040 and 0.0047 for the two fractions studied. Future measurements at lower frequencies will help to clarify this anomaly, which is attributed to changes in the disposition of the widely spaced entanglements discussed by Bueche (7).

Distribution Functions

The retardation (L) and relaxation (H) spectra, calculated by the second approximation formulas of Williams and Ferry (8) from Figs. 2–4 and corresponding plots of the shear moduli G' and G'' of the α mechanism, are given in Table I. At low frequencies, where J_p'' depends somewhat on

TABLE I

Relaxation and Retardation Distribution Functions Reduced to 100°C.

$\log \tau_p$	Log L_p (*cm.*²/*dyne*)		Log H_p (*dynes*/*cm.*²)	
(*sec.*)	From J'	From J''	From G'	From G''
	α *Mechanism*			
−10.0	−10.47	−10.50	8.55	8.57
−9.5	−10.38	−10.34	8.67	8.62
−9.0	−10.17	−10.15	8.71	8.69
−8.5	−9.97	−9.92	8.69	8.66
−8.0	−9.85	−9.70	8.60	8.65
−7.5	−9.60	−9.35	8.46	8.51
−7.0	−9.21	−9.15	8.00	8.15
−6.5	−8.91	−8.85	7.58	7.62
−6.0	−8.57	−8.58	7.16	7.27
−5.5	−8.08	−8.05	6.80	6.89
−5.0	−7.65	−7.65	6.57	6.60
−4.5	−7.35	−7.29	6.29	6.28
−4.0	−7.05	−7.01	5.97	6.00
−3.5	−6.80	−6.83	5.76	5.80
−3.0	−6.71	−6.72	5.58	5.63
−2.5	−6.68	−6.60	5.27	5.37
−2.0	−6.68	−6.76	4.99	5.04
−1.5	−6.79	−6.93	4.90	4.74
−1.0	−6.90	−7.09	4.71	4.49
	β *Mechanism*			
−5.0	−10.14			
−4.5	−9.69			
−4.0	−9.22			

temperature even after reduction, values from the measurements at the highest temperature (125°C.) were chosen. The agreement between calculations from real and imaginary components is quite good.

The retardation spectra are plotted in Fig. 6. For the β mechanism, only a fragment is provided which resembles in slope that for poly-n-butyl methacrylate. For the α mechanism, also, the shape closely resembles that

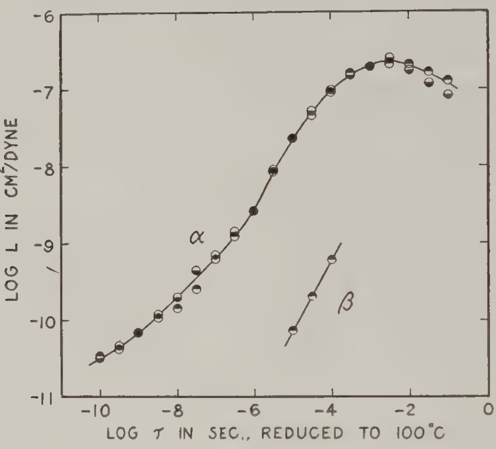

FIG. 6. Retardation spectra of the α and β mechanisms reduced to 100° C. Points top black, from J'; bottom black, from J''.

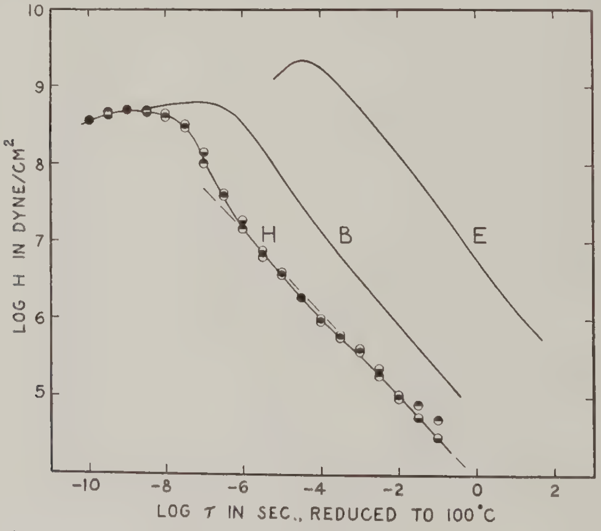

FIG. 7. Relaxation spectrum of the α mechanism reduced to 100° C. (Curve H). Points top black, from G'; bottom black, from G''. Curves E and B are for polyethyl and poly-n-butyl methacrylates at 100° C.

of poly-*n*-butyl methacrylate, though the maximum is substantially higher ($\log L_{\max} = -6.64$ as compared with -6.90 for the *n*-butyl).

The relaxation spectrum of the α mechanism is plotted in Fig. 7, together with those of the ethyl and *n*-butyl polymers all reduced to 100°C. With increasing side-chain length, the spectrum naturally shifts to shorter times and it also changes in shape; the lower portion of the transition zone conforms more closely to the theoretical (9–11) slope of $-\frac{1}{2}$, and the upper portion curves up more sharply; while the maximum becomes lower and broader. For interpretation of these changes, a more detailed molecular theory of viscoelastic properties is needed.

Backbone and Side-Chain Motions

By fitting the lower portion of the relaxation spectrum to the theoretical slope, as shown by the dashed line, the monomeric friction coefficient ζ_0 can be calculated (11). For this purpose, the root-mean-square end-to-end distance per square root of the number of monomer units, a, is taken as 7.54 A, derived from light-scattering measurements in a Θ-solvent (3). At 100°C., $\log \zeta_0 = -5.21$. Reduced to T_g, $\log \zeta_0 = 2.63$. This is the smallest value thus far reported for an undiluted polymer at its glass transition. When the ethyl, *n*-butyl, and *n*-hexyl polymers are compared all at 100°C., their monomeric friction coefficients are in the ratios $10^5:50:1$; when they are compared each at its own T_g, the coefficients are in the ratios $4000:13:1$.

These figures are a measure of the effect of side chains on facilitating chain backbone motions. The higher mobility in the hexyl polymer even near T_g can be illustrated by other comparisons. Thus, the magnitude of J' at 500 cycles/sec. is $10^{-9.5}$ cm.^{2}/dyne for poly-*n*-hexyl methacrylate 10° above T_g. But for polyethyl methacrylate this compliance is not attained until the temperature is 28° above T_g. As another example, the extrapolations represented by Fig. 5 indicate that perceptible mechanical response due to backbone motions should be achieved in the hexyl polymer at its T_g within a time scale of hours. In the ethyl polymer at its T_g, a time scale of weeks would be required.

In polymethyl (12, 13) and polyethyl (1) methacrylate, compliance attributable to side-chain motions persists somewhat above T_g in a region of time (or frequency) where the ordinary segmental backbone motions do not contribute. But this compliance is associated with a rather broad retardation spectrum, caused probably by the necessity of local cooperative motions of neighboring backbones to permit the side chains to rearrange (13, 14). In poly-*n*-butyl and poly-*n*-hexyl methacrylate, on the other hand, our analysis of the β-anomaly implies that somewhat above T_g the backbone contributions to compliance persist to higher frequencies (shorter times) than do the side-chain contributions. At the higher frequencies, these longer side chains seem to plasticize the main chain by virtue of their bulky volume without responding by wriggling themselves. At lower frequencies where they do respond, their retardation spectrum appears to be rather sharp, and presumably less cooperation of neighbors is needed for their rearrangements. These interpretations are somewhat speculative, however, because the α and β mechanisms are really identified only by their temperature dependences.

ACKNOWLEDGMENTS

This work was supported by Picatinny Arsenal, Ordnance Corps, Department of the Army. We are indebted to Mrs. Garrett Droppers for making most of the calculations.

SUMMARY

The real (J') and imaginary (J'') components of the complex compliance have been measured between 15 and 2400 cycles/sec. in the temperature range from 5° to 125°C. for a fractionated poly-*n*-hexyl methacrylate with molecular weight 4.0×10^6. The method of reduced variables gave superposed curves for J' and J'' except for the same two anomalies observed for poly-*n*-butyl methacrylate: the maximum in J'' increased slightly with increasing temperature, and near the bottom of the dispersion of J' the data corresponded to two additive mechanisms with different temperature dependences. For the principal (α) mechanism, the temperature dependence of retardation times follows the WLF form with f_g (relative free volume at the glass transition temperature, T_g) $= 0.025$ and α_f (thermal expansion coefficient of free volume) $= 1.9 \times 10^{-4}$ deg.$^{-1}$. For the β mechanism, the temperature dependence of retardation times corresponds to an apparent activation energy of 13 kcal. The retardation and relaxation spectra of the α mechanism resemble those for other methacrylate polymers, but certain progressive effects of increasing side-chain length on the position and detailed shape of the spectra are apparent. The logarithm of the monomeric friction coefficient (in dynes-sec./cm.) is -5.21 at 100°C. and 2.63 at -5°C. (T_g). At their respective T_g's, the friction coefficients of polyethyl, poly-*n*-butyl, and poly-*n*-hexyl methacrylates are in the ratios 4000:13:1, though the relative free volume at T_g as deduced from the WLF equation is the same for all three polymers.

REFERENCES

1. FERRY, J. D., CHILD, W. C., JR., ZAND, R., STERN, D. M., WILLIAMS, M. L., AND LANDEL, R. F., *J. Colloid Sci.* **12,** 53 (1957).
2. CHILD, W. C., JR., AND FERRY, J. D., *J. Colloid Sci.* (in press).
3. CHINAI, S. N., *J. Polymer Sci.* (in press).

4. Rogers, S. S., and Mandelkern, L., *J. Phys. Chem.* (to be submitted).
5. Ferry, J. D., and Fitzgerald, E. R., *J. Colloid Sci.* **8,** 224 (1953).
6. Williams, M. L., Landel, R. F., and Ferry, J. D., *J. Am. Chem. Soc.* **77,** 3701 (1955).
7. Bueche, F., *J. Chem. Phys.* **20,** 1959 (1952).
8. Williams, M. L., and Ferry, J. D., *J. Polymer Sci.* **11,** 169 (1953).
9. Rouse, P. E., Jr., *J. Chem. Phys.* **21,** 1272 (1953).
10. Bueche, F., *J. Chem. Phys.* **22,** 603 (1954).
11. Ferry, J. D., Landel, R. F., and Williams, M. L., *J. Appl. Phys.* **26,** 359 (1955).
12. Iwayanagi, S., *J. Sci. Research Inst.* (*Tokyo*) **49,** 4 (1955).
13. Heyboer, I., *Kolloid-Z.* **148,** 36 (1956).
14. Koppelmann, J., *Kolloid-Z.* **144,** 12 (1955).

JOURNAL OF COLLOID SCIENCE **12**, 400–411 (1957)

VISCOSITIES OF CONCENTRATED POLYMER SOLUTIONS. IV. CELLULOSE TRIBUTYRATE

Robert F. Landel[1], John W. Berge, and John D. Ferry

Department of Chemistry, University of Wisconsin, Madison, Wisconsin

Received April 3, 1957

INTRODUCTION

Earlier papers in this series have reported viscosities of concentrated solutions of polyvinyl acetate (1), polyisobutylene (2), polystyrene (3), and a copolymer of styrene and maleic acid (3). In the present communication, viscosity data are given for solutions of six fractions of cellulose tributyrate in 1,2,3-trichloropropane. The results are compared with the above earlier measurements as well as with some on solutions of cellulose trinitrate (4) and sodium deoxyribonucleate (5) which have recently been obtained in this laboratory.

MATERIALS AND METHODS

The cellulose tributyrate was fractionated from samples generously provided by Dr. C. J. Malm of the Eastman Kodak Co. The stocks and three of the fractions (H, L, and R2b) have been described in a previous report of dynamic mechanical properties (6). The other three fractions were obtained by a new fractionation of Stock II, following the earlier procedure (6). The intrinsic viscosities in acetone, and the molecular weights calculated therefrom by the relation (6) $[\eta] = 4.80 \times 10^{-5} M^{0.88}$, are given in Table I.

The 1,2,3-trichloropropane was shaken with sulfuric acid, washed with water, dried, and distilled at 60 mm. pressure through a 30-plate Oldershaw bubble cap column.

The polymer solutions were made up by weight. Their densities were in most cases measured pycnometrically with water as a confining liquid; in some cases, especially with fractions H, L, and R2b, densities were interpolated. Viscosities were measured by the capillary and falling ball methods as before (1, 2).

RESULTS

The viscosities (η) of solutions of the six fractions at various weight fractions (w_2) up to 0.41 and various temperatures between −5° and 50°C.

---

[1] Now at Jet Propulsion Laboratory, Pasadena, California.

TABLE I

Characterization of Cellulose Tributyrate Fractions

Fraction	$[\eta]$ (dl./g.)	Mol.wt.
L	0.70 ± .02	55,000
10C	1.10 ± .02	90,000
8C	1.56 ± .03	134,000
R2b	—	152,000[a]
4E	2.43 ± .03	222,000
H	3.15 ± .02	300,000

[a] Molecular weight calculated from osmotic pressure ($= \bar{M}_n$).

TABLE II

Viscosities of Fraction L, $\bar{M}_\eta$ = 55,000

w_2	Method	log η in poises at								Q_η (kcal.)
		−5.0°C.	10.0°C.	15.0°C.	20.0°C.	25.0°C.	30.0°C.	40.0°C.	50.0°C.	
0.0068	C	—	—	−1.269	—	−1.381	—	−1.526	—	3.87
0.0236	C	—	—	−0.740	—	−0.896	—	−1.068	—	5.27
0.0475	C	—	—	−0.456	—	−0.616	—	−0.812	—	5.90
0.0845	C	—	—	0.418	—	0.223	—	−0.018	—	7.26
0.124	C	—	—	0.644	—	0.441	—	0.185	—	7.63
0.168	C	—	—	—	—	1.265	—	0.970	—	8.21
0.226	C	—	—	—	—	1.534	—	1.225	—	
0.226	F	2.301	—	1.732	—	1.537	—	1.233 1.318	1.124 1.117	8.26
0.280	F	2.734[a] 2.798[b]*	2.351	—	—	1.968	—	1.641	1.441[c]	9.61
0.312	F	3.123 3.092	2.628	—	—	2.234	—	1.903	1.665[d]	10.08
0.345	F	3.301[e]* 3.348[e]*	2.890	—	2.605	—	2.350	—	—	10.88
0.409	F	—	—	—	3.754* 3.640* 4.337*	—	2.846	2.581	2.350[f]	11.5

* Solution was crystallizing or contained crystallites.

C = Capillary, F = Falling Ball.

[a] −4.8°C. [d] 50.2°C.

[b] −4.1°C. [e] −1.3°C.

[c] 49.2°C. [f] 49.5°C.

are given in Tables II to VII. An example of the temperature dependence is given in Fig. 1, where log η is plotted against reciprocal absolute temperature for fraction 4E at nine concentrations (expressed here as c, grams polymer per cubic centimeter solution). The lines are straight within experimental error, as was also found for the other fractions over the rather limited temperature range available. Values of Q_η, the apparent heat of

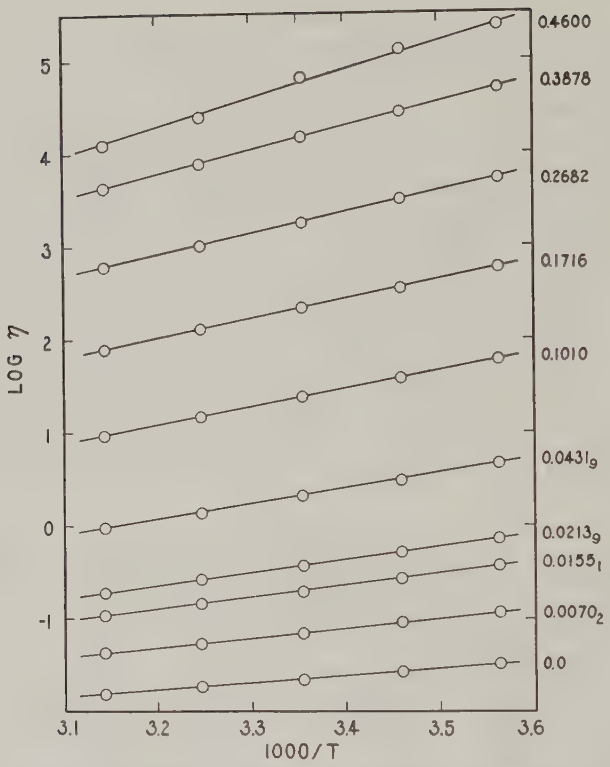

Fig. 1. Logarithm of viscosity plotted against reciprocal absolute temperature for solutions of Fraction 4E. Figures at right denote concentration in grams per cubic centimeter.

those obtained for vinyl polymers (1–3). The latter are nearly linear or somewhat concave upward, and in good solvents the slope is small, so that at moderate concentrations Q_η is not much higher than that of the pure solvent; also, at constant concentration the dependence of Q_η on molecular weight (M) is small. The cellulose tributyrate curves rise sharply at low concentrations and are concave downward; an extrapolation to zero from higher concentrations would give a value considerably higher than that of the pure solvent, as noted also for cellulose trinitrate solutions (4). Moreover, there is considerable molecular weight dependence, especially at low concentrations.

The disposition of the curves in Fig. 3 suggested that at low concentrations Q_η might be a unique function of the product cM, and this was indeed found to be the case, as shown in Fig. 4. It is evident that the principal contribution of the polymer to Q_η, about 5 kcal., is rather rapidly developed as cM increases to 20,000. Above this point, Q_η is no longer a function of cM alone and increases more slowly.

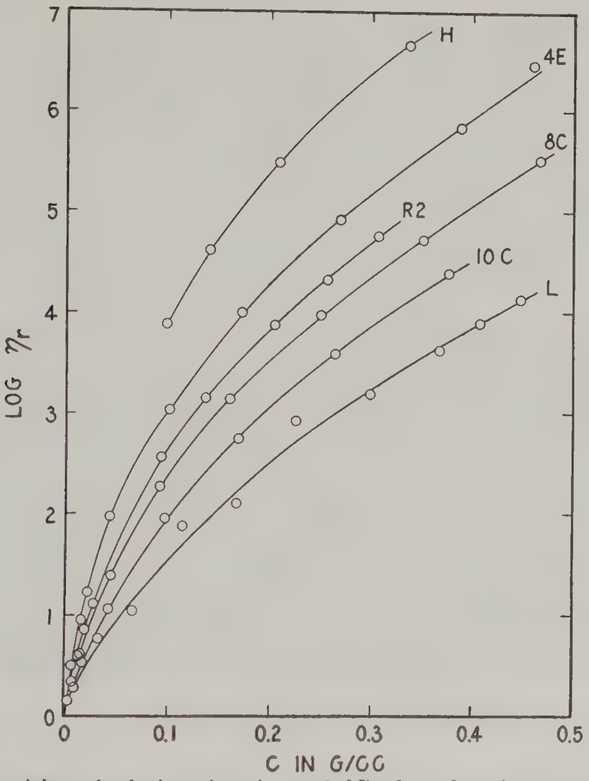

FIG. 2. Logarithm of relative viscosity at 25°C. plotted against concentration for the six fractions. (Points for R2b include additional values for dilute solutions, obtained in connection with intrinsic viscosity measurements.)

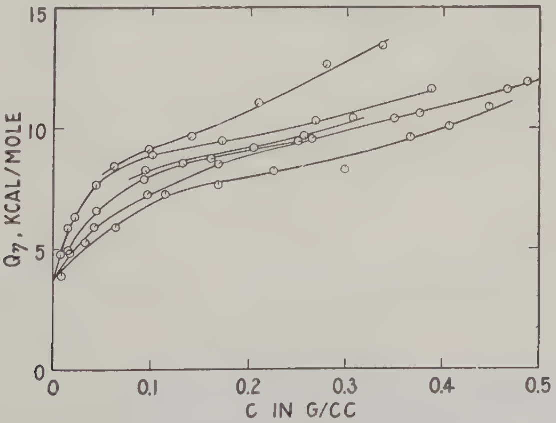

FIG. 3. Apparent activation energy for viscous flow plotted against concentration. Pip up, fraction L; successive 45° rotations clockwise, fractions 10C, 8C, R2b, 4E, and H.

The abscissa cM is a measure of the average number of Bueche entanglements (7) per molecule. The average molecular weight between entanglements, M_e, is M_{ep}/v_2, where v_2 is the volume fraction of polymer and M_{ep} a constant regarded as M_e extrapolated to the hypothetical undiluted polymer in an uncrystallized, unvitrified state (8). Since $v_2 = c/\rho$, where ρ is the density of the undiluted polymer, the number of entanglements per molecule is $\xi = M/M_e = cM/\rho M_{ep}$. If the critical value of cM is interpreted as the onset of a continuous network with $\xi = 2$, this corresponds to a value of M_{ep} of about 8500. Another estimate of M_{ep} will be made below.

The presence of this sharp rise in Q_η over a narrow concentration range in cellulose tributyrate solutions, in contrast to the behavior of several vinyl polymers where it is not observed, is probably related to the change in molecular dimensions with temperature as observed by intrinsic viscosity measurements in a Θ-solvent (9). With increasing temperature, steric barriers to free rotation are overcome and the mean-square end-to-end distance $\overline{r_0^2}$ decreases, thereby shrinking the domain swept out by each molecule. The resulting drop in viscosity (and corresponding magnitude of Q_η) would be expected to be much more exaggerated in the region of cM where the viscosity is determined by entanglements than at lower cM where the continuous entanglement network has not been established.

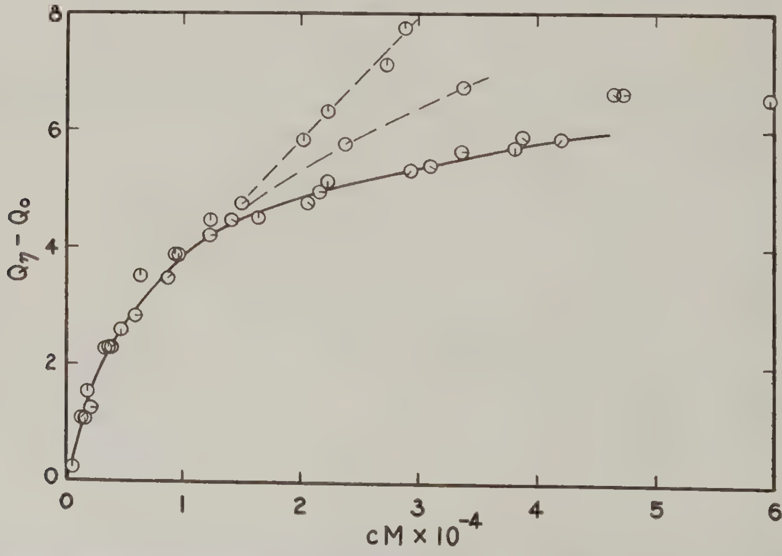

FIG. 4. Apparent activation energy for viscous flow minus that of solvent, plotted against product of concentration and molecular weight. Key to fractions same as in Fig. 3.

Concentration and Molecular Weight Dependence of Viscosity

In previous analyses (2, 3) it has been possible to interrelate the dependence of viscosity on concentration and on molecular weight by showing that, over a considerable range of these variables at constant temperature, the relative viscosity η_r is a single function of $c^5M^{3.4}$ or the equivalent. At moderately high concentrations of polyisobutylene in decalin and in xylene, η_r is directly proportional to the above product. The exponent of 3.4 for M has, of course, been found for many polymers and their solutions above the critical value of M for onset of an entanglement network (8). In Fig. 5, $\log \eta_r$ for the cellulose tributyrate solutions at 25°C. is plotted against $5 \log c + 3.4 \log M$. A single composite curve is obtained with remarkably good coincidence for all the fractions except H, which lies above the others. At high values of the argument, the function of $(c^5M^{3.4})$ is simply direct proportionality, the logarithmic plot approximating a straight line with slope of unity. Thus cellulose tributyrate resembles other polymers of simpler structure in the common exponent of 3.4, which has been interpreted theoretically by Bueche (7, 10).

For comparison, similar plots are shown in Fig. 5 for solutions of polyisobutylene of various concentrations and molecular weights (2), cellulose trinitrate of one molecular weight and various concentrations (4), and sodium deoxyribonucleate (SDNA) of one molecular weight and various

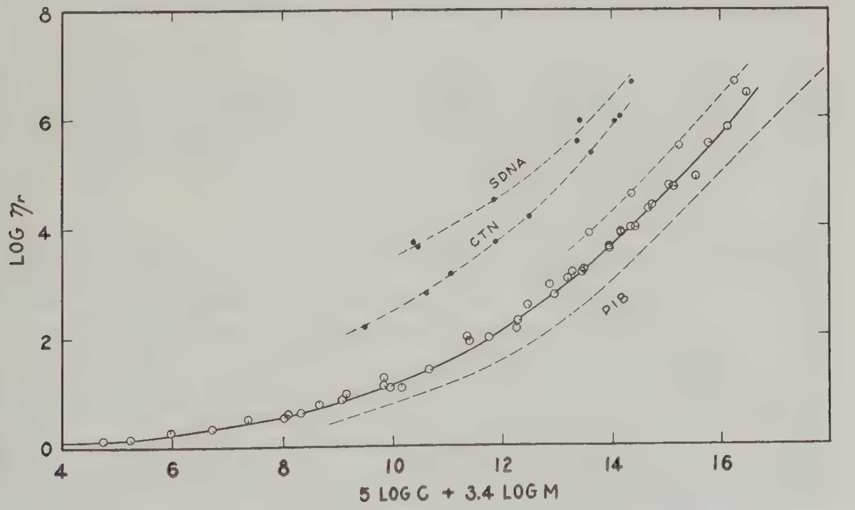

FIG. 5. Relative viscosity plotted logarithmically against $c^5M^{3.4}$. Key to fractions same as in Fig. 3. Other polymers for comparison: SDNA, sodium deoxyribonucleate in water; CTN, cellulose trinitrate in isophorone; PIB, polyisobutylene in xylene and in decalin.

concentrations (5). The curves are all rather similar in shape, and it may be inferred that with this type of plot the concentration dependence of viscosity can be estimated from the molecular weight dependence or vice versa, even though an analytical formulation for the curve is lacking.

Comparisons of Different Polymers

At equal values of the abscissa in Fig. 5, different polymers have very different relative viscosities. In the preceding paper of this series (3), a more reasonable comparison was attempted by substituting the number of chain bonds for the molecular weight in the abscissa; this brought several vinyl polymers into fairly close concordance. The data of Bueche (11) for various fractions of polymethyl methacrylate at one concentration in diethyl phthalate, when plotted in this manner, fall on a curve of similar shape, but it lies far above those for polyisobutylene, polystyrene, and polyvinyl acetate. And the cellulose derivatives and SDNA, with their different backbone structures, cannot be accommodated at all in such a scheme.

In seeking a better basis of comparison, we note that the viscosity in these concentrated solutions is certainly dominated by the Bueche entanglements, and that the effect of molecular size should therefore be governed not by M nor by the number of chain bonds but rather by the number of entanglements per molecule, ξ. For a given polymer, $M = \xi M_{ep}/v_2 = \xi M_{ep}\rho/c$. It follows that the linear portions of the plots in Fig. 5 correspond to the relation

$$\eta = k\eta_s\rho^5 M_{ep}{}^{3.4}\xi^{3.4}v_2{}^{1.6}, \qquad [1]$$

where k is an unspecified constant; or the equivalent relation where all quantities characteristic of a given polymer have been combined into a single dimensionless constant A:

$$\eta = A\eta_s\xi^{3.4}v_2{}^{1.6}. \qquad [2]$$

The value of A is not universal; $\log A = 3.57$, 3.20, and 3.86 for cellulose tributyrate, polyisobutylene, and polymethyl methacrylate solutions, respectively. Thus, plots of η_r against $\xi^{3.4}c^{1.6}$ would not give exact coincidence of data for all polymers. However, the order of magnitude of A is the same for all, and exact coincidence can scarcely be expected, since the choice of a temperature of 25°C. for comparison is arbitrary.

Further information may be obtained by comparing the form of [2] with an extension of the theory of Bueche (7), in which the absolute value of the viscosity depends on the monomeric friction coefficient ζ_0, representing the force per monomer unit required for translation of a polymer segment through its surroundings at unit velocity (12):

$$\eta = \zeta_0 a^2 n Z^2 (f/f_0)/36. \qquad [3]$$

Here $a^2 = \overline{r_0^2}/Z$, Z is the degree of polymerization, n is the number of molecules per cubic centimeter, and f/f_0 is the factor by which the effective friction coefficient is increased by entanglement. In a previous discussion of the effect of entanglements on viscoelastic properties (12), it was proposed that f/f_0 can be approximated by $(\xi/2)^{2.4}$. Using this relation together with the facts that $n = cN_0/M$ (where N_0 is Avogadro's number), $Z = M/M_0$ (where M_0 is the molecular weight of a monomer unit), and $M_0/N_0\rho = v_0$, the volume of a monomer unit, we obtain from [3]

$$\eta = \zeta_0 a^2 M_{ep}(\xi/2)^{3.4}/18M_0v_0. \qquad [4]$$

Finally, comparison of [2] and [4] gives for the friction coefficient

$$\zeta_0 = 18 \times 2^{3.4}A\eta_s v_0 v_2^{1.6}/\overline{r^2}_{ep}, \qquad [5]$$

where $\overline{r^2}_{ep}$ is the mean-square distance between entanglement points in the (hypothetical) undiluted polymer. It is certainly reasonable that ζ_0 should be proportional to η_s and v_0, though analogy with Stokes' law would place the cross-section area of the monomer unit in the denominator rather than $\overline{r^2}_{ep}$. The dependence on $v_2^{1.6}$, as well as absolute values of ζ_0 calculated from [4], may be tested subsequently by determining ζ_0 from viscoelastic measurements (12). It may be noted that the overall approximate fifth-power concentration dependence of viscosity is resolved by this treatment into a dependence of the local friction coefficient on a much lower power of concentration, and this should be more easily susceptible of theoretical explanation.

If $\overline{r^2}_{ep}$ is independent of temperature, the elevation of Q_η shown in Fig. 4 can be attributed to the change in ξ associated with the temperature dependence of $\overline{r_0^2}$. Since $\xi = \overline{r_0^2}/\overline{r_e^2}$ and it enters Eq. [4] to the 3.4 power, the additional contribution to Q_η should be 6.8 Q_r, where Q_r is the effective activation energy for changes in $(\overline{r_0^2})^{\frac{1}{2}}$. From the data of Mandelkern and Flory (9), the latter is about 1.2 kcal., leading to about 8 kcal. for the contribution to Q_η; this agrees in order of magnitude with the observed value of about 5 kcal.

Effect of Entanglements on Magnitude of Viscosity

At a given concentration, a plot of log η against log M should show an abrupt change of slope where $M = 2M_e$ (7, 8, 11), the value of M_e being of course inversely proportional to concentration. For the cellulose tributyrate solutions, the slope changes too gradually to identify the critical value, but the latter can be revealed by a somewhat different method of plotting. The abscissa is chosen as log M + log c, so that the critical value will be the same for all concentrations (*cf.* Fig. 4); the ordinate is then taken as log η − 1.6 log c so that *above* the critical value of cM all the data should coincide (*cf.* Fig. 5 and Eq. [1]). For clarity, values of η were interpolated

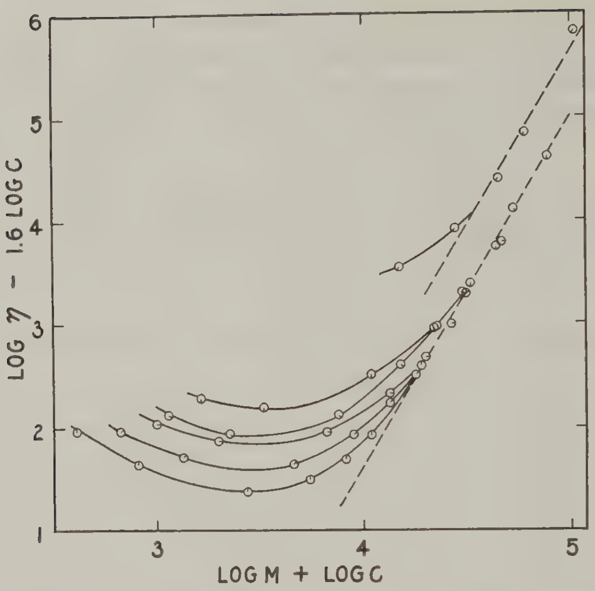

Fig. 6. Log η − 1.6 log c plotted against log M + log c, points interpolated for different molecular weights at fixed concentration intervals, to determine the critical molecular weight for entanglements. Dashed lines drawn with slope of 3.4.

from Fig. 2 at fixed concentration intervals. The result is shown in Fig. 6. Except for fraction H, the data do fall on a single line with slope of 3.4, and the individual fractions diverge from this line in the range of cM of 24,000 ± 6,000. This corresponds to M_{ep} = 10,000, in reasonable agreement with the estimate from Fig. 4, although both values are very rough.

Acknowledgments

This work was part of a program of research on the physical structure and properties of cellulose derivatives and other polymers supported by the Allegany Ballistics Laboratory, Cumberland, Maryland, an establishment owned by the United States Navy and operated by the Hercules Powder Company under Contract NOrd 10431. It was also supported in part by the Research Committee of the Graduate School of the University of Wisconsin from funds supplied by the Wisconsin Alumni Research Foundation. We are indebted to Miss Elinor A. Williams for most of the viscosity measurements on fraction L.

Summary

Viscosities of solutions of six fractions of cellulose tributyrate in 1,2,3-trichloropropane have been measured over a wide range of concentrations up to a weight fraction of 0.41 and at several different temperatures between −5° and 50°C. The apparent activation energy for viscous flow was a single function of the product of concentration in grams per cubic

centimeter (c) and molecular weight (M) over the range of cM from 0 to 20,000, and in this range it increased by about 5 kcal., but at higher concentrations comparatively little. At 25°C., the relative viscosity was a single function of $c^5M^{3.4}$, and at high values of this argument was directly proportional to it. The results of these and measurements on other polymers are discussed in relation to the average number of entanglement points per molecule in Bueche's sense. The average molecular weight between entanglement points in cellulose tributyrate, extrapolated to the undiluted state, is estimated as about 10,000. It is concluded that the monomeric friction coefficient for translation of a polymer segment is proportional to the solvent viscosity and to the 1.6 power of the polymer concentration.

REFERENCES

1. FERRY, J. D., FOSTER, E. L., BROWNING, G. V., AND SAWYER, W. M., *J. Colloid Sci.* **6**, 377 (1951).
2. JOHNSON, M. F., EVANS, W. W., JORDAN, I., AND FERRY, J. D., *J. Colloid Sci.* **7**, 498 (1952).
3. FERRY, J. D., GRANDINE, L. D., JR., AND UDY, D. C., *J. Colloid Sci.* **8**, 529 (1953).
4. PLAZEK, D. J., AND FERRY, J. D., *J. Phys. Chem.* **60**, 289 (1956).
5. HELDERS, F. E., AND FERRY, J. D., *J. Phys. Chem.* **60**, 1536 (1956).
6. LANDEL, R. F., AND FERRY, J. D., *J. Phys. Chem.* **59**, 658 (1955).
7. BUECHE, F., *J. Chem. Phys.* **20**, 1959 (1952).
8. FOX, T. G., AND LOSHAEK, S., *J. Appl. Phys.* **26**, 1080 (1955).
9. MANDELKERN, L., AND FLORY, P. J., *J. Am. Chem. Soc.* **74**, 2517 (1952).
10. BUECHE, F., *J. Chem. Phys.* **25**, 599 (1956).
11. BUECHE, F., *J. Appl. Phys.* **26**, 738 (1955).
12. FERRY, J. D., LANDEL, R. F., AND WILLIAMS, M. L., *J. Appl. Phys.* **26**, 359 (1955).

JOURNAL OF COLLOID SCIENCE **12**, 412–416 (1957)

LIGHT-SCATTERING CALIBRATION WITH LUDOX[1]

D. A. I. Goring, M. Senez, B. Melanson, and M. M. Huque

Physical Chemistry Division, Pulp and Paper Research Institute, Montreal, Canada

Received March 22, 1957

Several authors (1–8) have reported successful use of Ludox colloidal silica for absolute calibration in light scattering. In a recent study with the semi-micro apparatus described previously (9), reproducibility of calibration data was poor from sample to sample of Ludox. Calibration constants for old samples (1–2 years) differed considerably from those of fresh solutions. Also, it was found that erratic results were obtained when solutions were diluted with distilled water as opposed to dilute aqueous sodium chloride. A further study with a Brice-Phoenix photometer has now been completed which elucidates some of the earlier discrepancies.

EXPERIMENTAL

Five samples of Ludox were studied. These either were fresh or had been stored for periods up to 2 years. The concentration of solids was determined by evaporation and weighing. Stock Ludox was diluted to a concentration of approximately 6%. Motes were removed by filtration through sintered discs. By dilution of the filtered 6% solution, a range of six or more concentration between $\frac{1}{2} \rightarrow 6\%$ was obtained for spectrophotometric and light-scattering measurements.

Dilution of stock Ludox was carried out with distilled water or 0.05 M NaCl. The electrical conductivity of 0.05 M NaCl was approximately equivalent to that of the Ludox sol. It is probable that small variations in the small ion concentration of stock Ludox would be swamped by the initial, fivefold dilution with 0.05 M NaCl.

The spectrophotometric turbidity, τ_s, was measured in a Beckman DU spectrophotometer using 10 cm. cells. Values of $(c/\tau_s)_{c=0}$ were obtained by extrapolating the graphs of c/τ_s vs. c to zero concentration.

Initial light-scattering observations were made in the semimicro apparatus (SMA) described previously (9). Later measurements were carried out with a Brice-Phoenix apparatus (BPA) using the normal-width beam and a 40 × 40 mm. semioctagonal cell (10). The light-scattering turbidity, τ_L, was computed from the 90° intensity, I_{90}, from the data supplied for the instrument; $(c/\tau_L)_{c=0}$ was obtained by extrapolating the graphs of c/τ_L vs. c to zero concentration.

---

[1] This work was begun at the Atlantic Regional Laboratory of the National Research Council, Halifax, N.S., and completed at the Pulp and Paper Research Institute of Canada, Montreal, Quebec.

The accuracy of the absolute values of τ_L was checked by a light-scattering determination of the Rayleigh ratio of benzene and the turbidity of Debye's standard polystyrene[2] in toulene. For benzene, a Rayleigh ratio of 49.6×10^{-6} cm.$^{-1}$ was found at $\lambda = 436$ mμ, in excellent agreement with the value of 49.7×10^{-6} cm.$^{-1}$ reported by Maron and Lou (12, *cf.* 10, 11). For the standard polystyrene solution, an excess turbidity of 3.25×10^{-3} cm.$^{-1}$ was found at $\lambda = 436$ mμ; the value quoted in the instructions for use of the sample was 3.30×10^{-3} cm.$^{-1}$.

The above procedure was not possible with the SMA, because no absolute method of determining τ_L was available. A calibration constant, C, was obtained from

$$\left(\frac{c}{\tau_s}\right)_{c=0} = C\left(\frac{c}{I_{90}}\right)_{c=0}$$

and trends in C were noted.

Dissymmetries at zero concentration were less than 1.05. With Ludox no correction was necessary for this effect, because the 90° intensity from a slightly dissymmetrical envelope, generated by spherical scatters, is very nearly equal to the 90° intensity from a Rayleigh system with the same τ_s (*cf.* 9). Depolarization at $c = 0$ was negligible.

RESULTS AND DISCUSSION

At least two separate experiments were performed for each set of conditions (e.g., sample, diluent, wavelength). With the SMA, reproducibility of intercepts obtained by extrapolation was ±6% for spectrophotometric data and ±7% for light scattering. Considerably greater care was taken for the measurements with the BPA in which reproducibility for spectrophotometric and light-scattering data were ±1.7% and ±1.3%, respectively.

In the initial experiments with the SMA, some calibrations were attempted using pure water as a diluent. Results were extremely erratic and are not reported. Dilution with 0.05 *M* NaCl was then found more satisfactory. With the BPA, dilution with water and with 0.05 *M* NaCl was compared. In general, greater regularity of data was found when the electrolyte was used. For example, the average error in duplicate determinations of $(c/\tau_L)_{c=0}$ was 2.7% for dilution with water and 0.5% with 0.05 *M* NaCl.

---

[2] We are indebted to Prof. P. Debye for the sample of standard polystyrene.

Variation of c/τ_L with c can be affected by:

a). attenuation of the incident beam and scattered light (c/τ_L increases with c) (6);

b). secondary scattering (c/τ_L decreases with c) (7);

c). intermolecular interaction (c/τ_L increases with c).

In the BPA, attenuation is compensated by comparison of the scattered intensity with the transmitted beam. A similar correction was made for the SMA. However, there was no simple way to separate the effect of interaction and secondary scattering. A quantitative analysis (particularly of the latter) would be extremely complex and was not attempted. However, as emphasized by Maron and Lou (6), and Kraut and Dandliker (7), these effects are eliminated if extrapolation to zero concentration is possible.

With the BPA, certain trends were noted in the concentration dependence of both c/τ_s and c/τ_L, examples of which are shown in Fig. 1. If secondary scattering is assumed to be a negligible effect in the spectrophotometric measurements, the slope of the c/τ_s vs. c curve must be due to interaction alone. Slopes were greater in the case of dilution with water. For example, in Fig. 1 the slope of c/τ_s vs. c increased from 0.7 cm. for 0.05 M NaCl to 2.3 cm. for water. This effect is probably due to the increased ionization of the silica at lower counter ion concentrations.

At finite concentrations c/τ_L was less than c/τ_s owing to the increase of τ_L by secondary scattering. This is in agreement with the results of Kraut and Dandliker (7). As shown in Fig. 1, the effect was appreciable, and it emphasized the need for extrapolation to zero concentration. With BPA an error of 20% could result in working at a concentration of 1% silica. For dilution with 0.05 M NaCl, c/τ_s and c/τ_L usually varied linearly with c. This facilitated extrapolation. In aqueous solution, the graphs were often slightly curved and extrapolation was more uncertain.

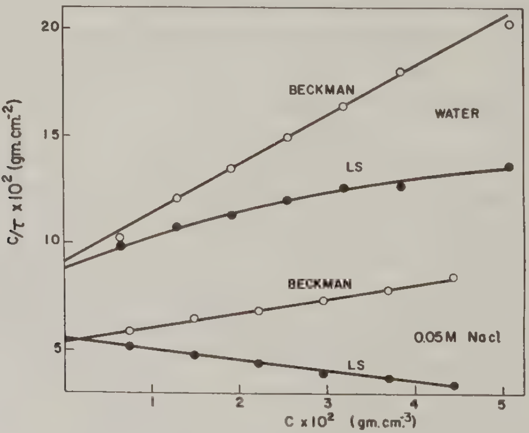

FIG. 1. Graphs of c/τ_s (Beckman) and c/τ_L (light scattering) vs. c at $\lambda = 436$ mμ for Ludox 5 (Table II) diluted with water and 0.05 M NaCl.

TABLE I

Values of C from Transmission and Light-Scattering Data with the SMA. Dilution Was with 0.05 M NaCl. The Wavelength Was 5461 A.

Sample	Age (*years*)	C
1	2	203
2	1	222
3	0	241

TABLE II

Values of $(c/\tau)_{c=0}$ *from Transmission and Light-Scattering Data with the BPA*

			1000 $(c/\tau)_{c=0}$ g. cm.$^{-2}$			
			λ = 436 mμ		λ = 546 mμ	
Sample	Age (*years*)	Diluent	Trans.	LS	Trans.	LS
Ludox 4	1	Water	111	126	268	298
Ludox 5	0	Water	89	90	237	220
Ludox 4	1	0.05 M NaCl	89	100	211	222
Ludox 5	0	0.05 M NaCl	67	69	160	162
PS		Water	0.457	0.479	1.183	1.207

The values of C for the first three samples of Ludox are given in Table I. It is clear that a 20% decrease in C occurred from the fresh to the older sample. This decrease is confirmed by the results in Table II, in which $(c/\tau_s)_{c=0}$ is about 10% less than $(c/\tau_L)_{c=0}$ for the 1-year old sample but equal to $(c/\tau_L)_{c=0}$ for the fresh solution. Such an effect is probably due to the development of light absorption on aging which would give an erroneously high value for τ_s in the older samples. It is also possible that the differences in light scattering and spectrophotometric behavior may be due to manufacturing variations in the samples used; however, the regularity of the trends suggests an aging effect.

It is interesting to note that there is no critical criterion of nonabsorption of light by the calibrating solution. For a Rayleigh system of small isotropic spheres, $\lambda^4\tau$ (more correctly $\frac{\lambda^4\tau}{(n_0\,dn/dc)^2}$ (9)) is constant for change in λ; a number of workers have observed such constancy for Ludox suspensions (1, 2, 3, 5, 8, 9). But the fourth power relationship could obtain approximately in spite of appreciable absorption at all wavelengths. The absence of absorption in the fresh solution of Ludox is suggested by the agreement between $(c/\tau_s)_{c=0}$ and $(c/\tau_L)_{c=0}$; and the reliability of τ_L is supported by the correctness of the Rayleigh ratios for benzene and Debye's standard polystyrene. But there is no proof of nonabsorption for fresh Ludox, and the results suggest that aged Ludox solutions absorb light.

Light absorption in silica suspensions is probably associated with impurities in the dispersed phase. Thus its effect would be diminished if a similar scattering intensity could be achieved at a much lower concentration. A monodisperse polymer latex of suitable particle size $\left(\simeq \frac{\lambda}{10}\right)$ seemed a logical alternative to Ludox. Accordingly, exploratory calibration experiments were carried out with a monodisperse polystyrene latex[3] of spherical particles 88 mμ in diameter (13). A suitable range of concentration was 0.005 → 0.03% compared with 1 → 6% necessary with Ludox. Dissymmetries were $(1.36)^{c=0}_{\lambda=436}$ and $(1.23)^{c=0}_{\lambda=546}$; but factors correcting I_{90} to the value for the equivalent Rayleigh envelope were only 1.021 and 1.005, respectively. Values of c/τ_s were constant for change in c showing negligible interparticle interaction. As shown in Table II, fair agreement was found between $(c/\tau_s)_{c=0}$ and $(c/\tau_L)_{c=0}$.

CONCLUSIONS

In conclusion, it may be said that Ludox is suitable for light-scattering calibration when

a). Dilution is made with 0.05 M NaCl instead of water.

b). Results are extrapolated to zero concentration.

c). Fresh solutions are used.

A polystyrene latex of suitable particle size can also be used, considerably lower concentrations being necessary.

REFERENCES

1. TIETZE, F., AND NEURATH, H., *J. Biol. Chem.* **194**, 1 (1952).
2. OSTER, G., *J. Polymer Sci.* **9**, 525 (1952).
3. MOMMAERTS, W. F. H. M., *J. Colloid Sci.* **7**, 71 (1952).
4. EDELHOCH, H., KATCHALSKI, E., MAYBURY, R. H., HUGHES, W. L., AND EDSALL, J. T., *J. Am. Chem. Soc.* **75**, 5058 (1953).
5. OTH, A., OTH, J., AND DESREUX, V., *J. Polymer Sci.* **10**, 551 (1953).
6. MARON, S. H., AND LOU, R. L. H., *J. Polymer Sci.* **14**, 29 (1954).
7. KRAUT, J., AND DANDLIKER, W. B., *J. Polymer Sci.* **18**, 563 (1955).
8. HUGHES, W. J., JOHNSON, P., AND OTTEWILL, R. H., *J. Colloid Sci.* **11**, 340 (1956).
9. GORING, D. A. I., *Can. J. Chem.* **31**, 1078 (1953).
10. BRICE, B. A., HALWER, M., AND SPEISER, R., *J. Opt. Soc. Amer.* **40**, 768 (1950).
11. CARR, C. I., AND ZIMM, B. H., *J. Chem. Phys.* **18**, 1616 (1950).
12. MARON, S. H., AND LOU, R. L. H., *J. Polymer Sci.* **14**, 273 (1954).
13. BRADFORD, E. B., AND VANDERHOFF, J. W., *J. Appl. Phys.* **26**, 864 (1955).

---

[3] Kindly supplied by Dr. J. W. Vanderhoff of the Dow Chemical Company.

JOURNAL OF COLLOID SCIENCE **12,** 417–418 (1957)

AN EQUATION OF STATE FOR LECITHIN MONOLAYERS

D. G. Hedge

Chemistry Department, The University, Nottingham, England

Received July 30, 1957; revised April 12, 1957

In a recent paper by Phillips and Rideal (1) a general equation of state for a monolayer was derived. For the case of an uncharged monolayer this equation reduced to

$$\pi - E_r - A\frac{dE_r}{dA} + \frac{kT}{c_s}\frac{dc_s}{dA} = 0, \qquad [1]$$

where π is the surface pressure, A is the surface area, k is the Boltzmann constant, T is the absolute temperature, c_s is the surface concentration, and E_r is the cohesive attraction energy. The equation was shown to hold for a film at the oil/water interface, where $E_r = 0$ owing to the fact that the hydrocarbon chains anchored at the interface are indistinguishable from the hydrocarbon oil molecules displaced from the interface.

At the air/water interface, however, $E_r \neq 0$, and cohesive forces must be considered. Langmuir (2) included a force constant π_0 in his equation for liquid films:

$$(\pi - \pi_0)(A - A_0) = kT. \qquad [2]$$

In Eq. [2] A_0 is the limiting area of the film molecules. An equation similar in form to the Langmuir equation may be derived from Eq. [1] by allowing for the cohesive energy. By analogy with three-dimensional systems the cohesive energy may be taken to be proportional to the square of the surface density, or inversely proportional to A^2. If a is the proportionality constant, then substituting $E_r = a/A^2$ in Eq. [1] gives

$$\pi - \frac{a}{A^2} - \frac{Ad}{dA}(a/A^2) + \frac{kT}{c_s}\frac{dc_s}{dA} = 0. \qquad [3]$$

Since $c_s \propto 1/A$,

$$\frac{kT}{c_s}\frac{dc_s}{dA} = -\frac{kT}{A} \qquad [4]$$

and Eq. [3] becomes

$$\pi - \frac{a}{A^2} + \frac{2a}{A^2} - \frac{kT}{A} = 0$$

TABLE I

A (A^2/molecule)	π_0 (dynes/cm.)	$10^{-4}\,a$
65.0	13.6	5.7
62.14	13.9	5.4
60.73	14.1	5.2
57.91	14.9	5.0
55.08	15.7	4.8
52.97	17.1	4.8
52.26	17.9	4.9
51.55	18.8	5.0
49.43	23.1	5.6

or

$$\left(\pi + \frac{a}{A^2}\right)A = kT. \qquad [5]$$

For a liquid film the areas are not large enough for the area occupied by the molecules themselves to be neglected. The area A must then be reduced by the limiting area of the film molecules, A_0, giving the equation

$$\left(\pi + \frac{a}{A^2}\right)(A - A_0) = kT. \qquad [6]$$

Equation [6] has been tested using films of a sample of lecithin similar to that used in a previous paper (3). At pH 7 lecithin is effectively uncharged, and it is liquid up to considerably high surface pressures. Since lecithin has two saturated n-long-chains A_0 was taken to be 40 A^2. Table I shows values of the constant a over a range of areas; also shown are values of π_0 from Eq. [2].

The improvement of Eq. [6] over the Langmuir equation is shown in Table I since, whereas π_0 varies considerably, a is around 5×10^4 for quite a large range of areas. Although the equation has been tested only with lecithin its application to other uncharged liquid monolayers is intended.

REFERENCES

1. PHILLIPS, J. N., AND RIDEAL, E. K., *Proc. Roy. Soc. (London)* **A232,** 149 (1955).
2. LANGMUIR, I., *J. Chem. Phys.* **1,** 756 (1937).
3. ELEY, D. D., AND HEDGE, D. G., *J. Colloid Sci.*, in press.

JOURNAL OF COLLOID SCIENCE **12**, 419–429 (1957)

THE ENERGETICS OF LIPID–PROTEIN INTERACTIONS

D. D. Eley and D. G. Hedge

Department of Chemistry, The University, Nottingham

Received July 30, 1956; revised April 12, 1957

ABSTRACT

A detailed study of the interactions between monolayers of stearic acid and cholesterol and dissolved proteins has been carried out from a theoretical point of view. In addition to measurement of the activation energy of the adsorption an attempt has been made to investigate the thermodynamics of the systems. Changes in surface pressure as a result of injecting a lipid film with protein have been attributed to penetration of the film by the larger nonpolar side chains of the first adsorbed layer of protein. An equilibrium has been thought to exist between those side chains penetrating the lipid monolayer and those immediately beneath the surface. By this means it has been possible to compare the adsorption energies of different proteins and to calculate the number of side chains penetrating the lipid. It has been shown that a little under half the available side chains penetrate stearic acid films, but far less are able to penetrate cholesterol films.

INTRODUCTION

A technique has recently been developed (1) for spreading proteins at a lipid monolayer/water interface, using stearic acid and cholesterol as the lipids. The work has been extended to include more complex substances (2) such as lecithin and cephalin, and the nature of the lipid was found to have a pronounced effect upon the structure of the lipoprotein layer formed. By studying the effect on the surface pressure of injecting various quantities of protein under a lipid monolayer it was possible to obtain isotherms from which the structures of two adsorbed layers of protein could be deduced. Evidence was provided for an interaction between the peptide bonds of the first sublayer of protein and the polar groups of the lipid, an exception to this rule being lecithin, where the active groups of the protein were the negatively charged side chains.

It was suggested in the previous papers that the rise in surface pressure following injection of a lipid film by a protein was caused by penetration of the film by some of the nonpolar side chains of the protein. The object of the present paper is to test this postulate by carrying out a thermodynamical study of the interactions. A comparison of the adsorption energies for different proteins was effected, and an estimate was made of the number of side chains penetrating the lipid monolayer. In addition to this the effect of temperature was investigated, so enabling the activation energy of the process to be determined. By these means a more detailed picture of the mechanism of the interaction and of the structure of the lipoprotein layer was obtained.

Experimental

The interactions studied from the point of view of varying the temperature were those between stearic acid films and bovine plasma albumin (BPA), insulin, and lysozyme at pH 7.4 and ionic strength 0.15. The film balance and materials were similar to those described in the earlier work (1).

Variation of temperature was carried out by enclosing the surface trough in an insulated box and circulating water from a thermostat round the walls of the box and through a glass snake which fitted into the trough and was completely immersed. In this way the temperature of the air was kept near that of the water, which was constant to ±0.1°C. The presence of the glass snake was shown to have a negligible effect on the results obtained.

The temperature was varied from about 3°C. to 30°C., and marked differences in the initial rate of increase of surface pressure, $d\pi/dt$, were noted. The procedure used to measure $d\pi/dt$ was to start the stop watch at the beginning of the injection and take readings of the surface pressure

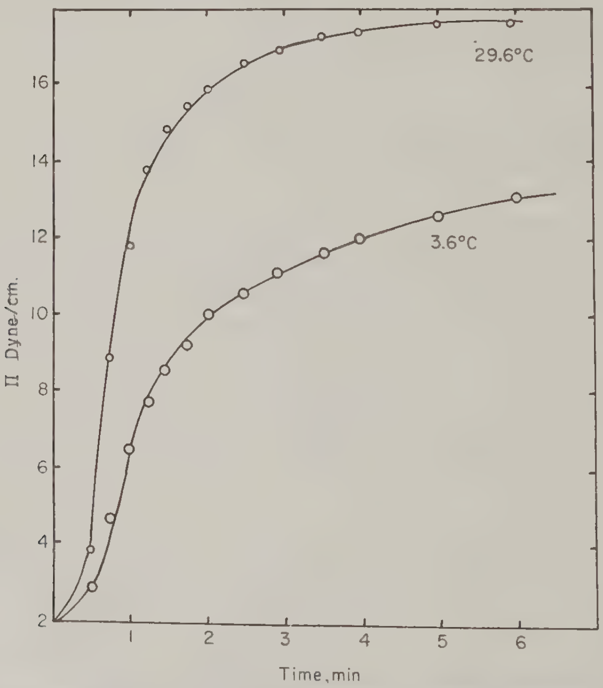

Fig. 1. Surface pressure/time curve for injection of stearic acid films by insulin at various temperatures.

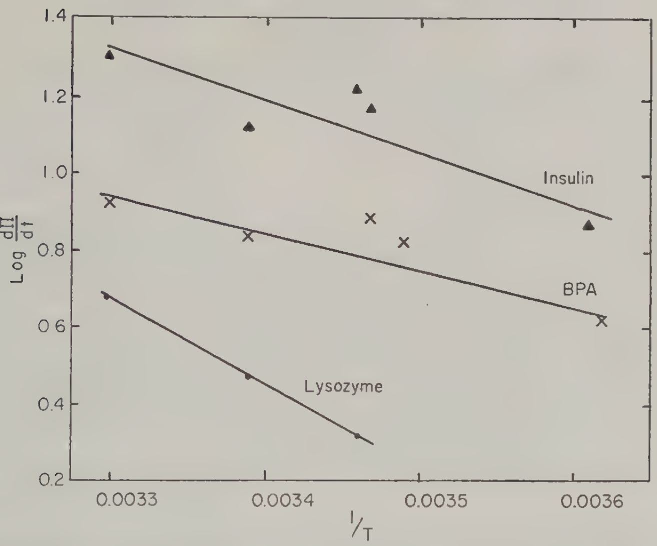

FIG. 2. Temperature dependence of the rate of adsorption by stearic acid films.

every 30 seconds, or in the case of insulin, every 15 seconds.[1] The amount of protein injected was always 0.02 mg.

ACTIVATION ENERGY OF ADSORPTION

Examples of the increase of surface pressure π with time t are shown in Fig. 1. Since the total rise in surface pressure $\Delta\pi_e$ at equilibrium was found proportional to the number of molecules injected, all of which were assumed to be adsorbed, i.e., $\Delta\pi_e = kn_{ads}$, it is assumed that the rate of adsorption is given by

$$\frac{dn_{ads}}{dt} = \frac{n_{ads}}{\Delta\pi_e} \cdot \frac{d\pi}{dt}, \text{ molecules sec}^{-1}.$$

In fact $\Delta\pi_e/n_{ads}$ was found to be a constant independent of temperature, so that activation energies can be derived to a first approximation from a plot of log $d\pi/dt$ vs. $1/T$. The data are shown in Fig. 2, where the $d\pi/dt$ values are taken as the maximum slopes of the curves in Fig. 1, and scales have been adjusted to bring all three curves onto one diagram.

Table I shows the values to lie in the range 7000 ± 3600, and the scatter of points to be such that, at least in the first two cases, the differences in E are not significant.

COMPARISON OF ADSORPTION ENERGIES

It has been assumed in the thermodynamical study that the rise in surface pressure following injection of a protein under a lipid film, is caused

---

[1] The stearic acid film was brought to an initial surface pressure of 2 dynes/cm. before injection, the total film area being 0.025 m.^{2}.

TABLE I

Activation Energies for Adsorption on Stearic Acid Monolayers

Protein	*E* (*kcal./mole*)
BPA	4,200
Insulin	6,000
Lysozyme	10,600

by penetration of the monolayer by the nonpolar side chains of the protein. Work by Cumper and Alexander (3) and Davies (4, 5) suggests that the only side chains likely to penetrate the lipid film would be those of such amino acids as valine, leucine, isoleucine, proline, phenylalanine, tryptophan, and tyrosine. The proteins have then been taken to consist only of these amino acids, and the basic postulate for the thermodynamical study is that an equilibrium exists between the side chains penetrating the lipid film and those immediately beneath the surface.

Langmuir (6) has shown that there is a constant arithmetical increase in the work done when a molecule passes from the interior to the surface layer for each additional CH_2 in the chain. Owing to the varying amino acid composition of the proteins used, the nonpolar side chains (NPS) will have slightly different average chain length. This provides a method of testing the theory of penetrating side chains. The number of amino acids in the proteins used, taken from the tables of Tristram (7), and the average chain length per NPS are shown in Table II, in which R is the total number of amino acid residues. The units of molecular weight for BPA, fibrinogen, insulin, and lysozyme are taken to be 69,000, 100,000, 12,000, and 15,000, respectively.

In order to compare the free-energy changes for two proteins it is necessary to consider the sublayer concentration of NPS required to give the same change in surface pressure.

Since it has been shown that, for the first adsorbed layer, the rise in surface pressure is proportional to the amount of protein injected (1), the concentrations to be compared may be taken to be $c/\Delta\pi$, where c is the total number of NPS injected for the formation of the first sublayer and $\Delta\pi$ is the corresponding rise in surface pressure. The difference in the free-energy changes for the adsorption of two proteins, denoted by subscripts 1 and 2, is then given by

$$\Delta G_1 - \Delta G_2 = RT \ln \frac{\Delta\pi_1 c_2}{\Delta\pi_2 c_1}. \quad [1]$$

TABLE II

Amino Acid Composition of Proteins

Protein	*R* per unit	NPS per unit	Average CH_2 per NPS
BPA	588	188	4.3
Fibrinogen	845	250	4.6
Insulin	103	42	4.3
Lysozyme	127	37	5.0

TABLE III

Comparison of Adsorption Energies for Proteins and Stearic Acid

Proteins	$\Delta G_1 - \Delta G_2$ (*cal./mole*)	Energy change per CH_2 (*cal./mole*)
BPA(1)—insulin(2)	34	—
Fibrinogen(1)—BPA(2)	143	477
Lysozyme(1)—BPA(2)	308	440
Lysozyme(1)—insulin(2)	342	489
Lysozyme(1)—fibrinogen(2)	165	412
Fibrinogen(1)—insulin(2)	177	590

The values of $\Delta\pi$ used in these calculations were, where possible, those given by the uncharged molecule, when the maximum value is obtained (1). In all cases except BPA these were the same as those quoted for the first sublayer at pH 7.4 in the earlier paper (1). With BPA $\Delta\pi$ at the isoelectric point (pH 4.9) was found to be 13.85 dynes/cm. for stearic acid and 8.4 dynes/cm. for cholesterol.

Consider stearic acid adsorption of BPA and insulin. The weight of BPA required to form the first sublayer is 0.021 mg. (1), or 3.05×10^{-10} mole. Since there are 188 NPS per molecule of BPA the concentration c in Eq. [1] is 5.73×10^{-8}. For BPA then, where $\Delta\pi$ is 13.85 dynes/cm. $\Delta\pi/c$ is 2.42×10^8. Similarly, for insulin $\Delta\pi/c$ is 2.57×10^8. Substituting in Eq. [1] at 17°C., with $RT = 580$ cal./mole

$$\Delta G_1 - \Delta G_2 = 580 \times 2.303 \times \log \frac{2.42}{2.58}.$$

Table III shows $\Delta G_1 - \Delta G_2$ for stearic acid adsorption. Using the difference in the average number of CH_2 groups per NPS for the two proteins the energy change is shown also for each CH_2 group. The corresponding quantities for cholesterol adsorption are given in Table IV.

NUMBER OF PENETRATED SIDE CHAINS

The isotherm usually employed for the problem of adsorption at an interface is that of Gibbs. The modification made by Pethica (8) to allow for the presence of an insoluble monolayer and excess neutral electrolyte takes the form

$$d\pi = \phi RT\Gamma d \log m, \qquad [2]$$

where Γ is the surface concentration of the penetrating species, m is the bulk concentration,[2] and ϕ is given by

$$\phi = A/(A - \bar{A}). \qquad [3]$$

In Eq. [3] A is the spread area per molecule of the insoluble monlayer and

---

[2] In our work m is the effective concentration of nonpolar side chains in the solution immediately under the monolayer, proportional to the weight of protein injected for our standard conditions.

TABLE IV

Comparison of Adsorption Energies for Proteins and Cholesterol

Proteins	$\Delta G_1 - \Delta G_2$ (*cal./mole*)	Energy change per CH_2 (*cal./mole*)
Insulin(1)—BPA(2)	25	—
Fibrinogen(2)—insulin(2)	192	670
Fibrinogen(1)—BPA(2)	217	702

$\bar{A}$ is the partial molar area of the spread molecules. Owing to the low compressibility of the lipid monolayers, $\bar{A}$ at a given surface pressure is taken to be the same as the area of lipid in a monlayer of pure lipid at that pressure.

It follows from Eq. [2] that a plot of π against log m should give a straight line. Such a relationship was obtained by Pethica (8) for absorption of sodium dodecyl sulfate by cholesterol films, and by Crisp (9) for adsorption of amines by acid films. The curve in Fig. 3 shows that in the present systems a straight line is obtained only up to the completion of the first layer, after which it curves over sharply. The Gibbs equation may then be applied for the first sublayer of protein, enabling a calculation of Γ, and hence the number of penetrating side chains, to be effected. In Eq. [2] A and $\bar{A}$ may be obtained from the π/A curves of the lipids.

The force/area curves for stearic acid and cholesterol are shown in Figs.

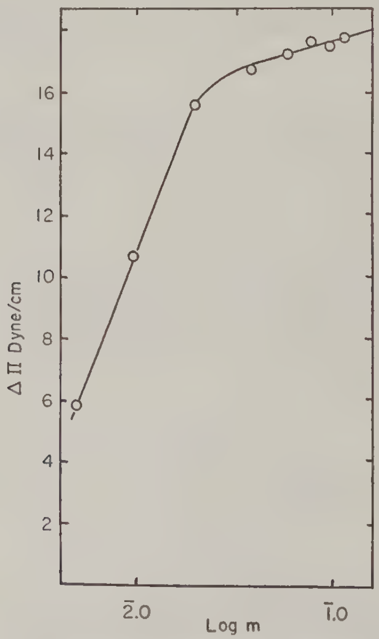

FIG. 3. Plot of surface pressure rise, $\Delta\pi$, against log m for injection of stearic acid films by insulin.

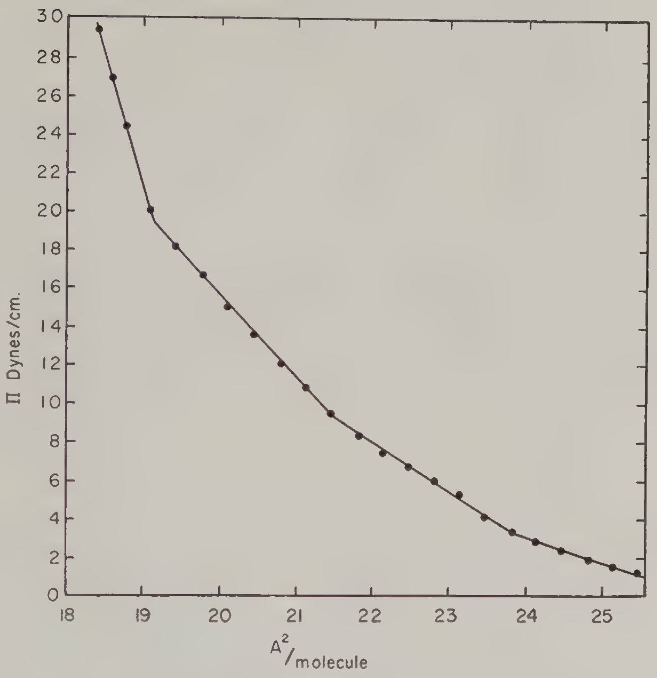

FIG. 4. Force/area, π/A, curve of stearic acid.

4 and 5, respectively. In each case the substrate was a 0.04 *M* phosphate buffer of pH 7.4, with the ionic strength made up to 0.15 with sodium chloride, the temperature being 16.7°C. The presence of three condensed phases in the stearic acid curve may be due to the salt in the substrate, since a similar effect was observed by Harkins (10) for octadecyl alcohol, though a curve similar to that in Fig. 4 was obtained by Ries and Cook (11) for stearic acid on distilled water.

A second method of calculating the number of penetrated NPS is by considering a geometrical model. The "free space" available on compressing the lipid film from the initial surface pressure to the final one is given by $(A - \bar{A})$ per molecule of lipid. This space can then be considered to be occupied by penetrating side chains, and since there is one amino acid residue per lipid molecule (1), the proportion of the available NPS which penetrate can be determined. Most of the hydrocarbon groups are rather bulky, and the average cross-sectional area may be taken to be that of an isobutyl chain (30 A^2).

The calculations using the Gibbs equation and the geometrical model were carried out using the same conditions of pH as in the comparison of free energies of adsorption. Taking the case of stearic acid and insulin, the slope of the straight portion of the curve of π against log m is 16.5, thus

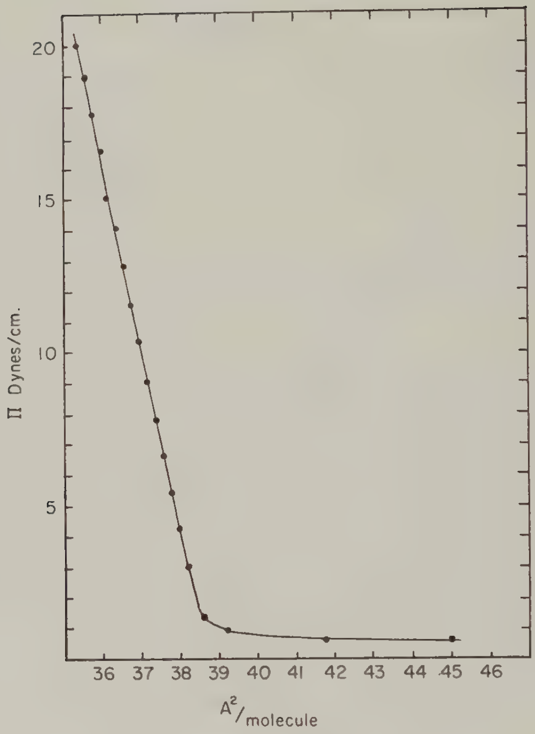

FIG. 5. Force/area, π/A, curve of cholesterol.

giving $A/(A - \bar{A})\ RT$. Since the initial area of the stearic acid film is 24.6 A^2/molecule and the partial molar area $\bar{A}$ at the completion of the first sublayer is 19.37 A^2/molecule, ϕ is $24.6/5.23 = 4.71$. The concentration of NPS, Γ, is then $16.5/4.71 \times 580 = 0.006$ molecule/A^2. The previous work (1) showed that for the first sublayer of protein there is one amino acid residue per stearic acid molecule; thus the total area per amino acid residue is 24.6 A^2. It follows that the ratio of the number of amino acids to the number of penetrated NPS is $1/0.006 \times 24.6$, and since the total number of amino acid residues per molecule of insulin is 103 the number of penetrated side chains per molecule is $103 \times 0.006 \times 24.6 = 15$. Calculating the

TABLE V

Number of Penetrated Side Chains for Stearic Acid

Protein	A (A^2/molecule)	$\bar{A}$ (A^2/molecule)	Penetrated NPS	
			Geometry	Gibbs
BPA	24.6	19.94	92	89
Insulin	24.6	19.37	18	15
Fibrinogen	24.6	21.13	98	57
Lysozyme	24.6	21.54	14	7

TABLE VI

Number of Penetrated Side Chains for Cholesterol

Protein	A (A^2/molecule)	$\bar{A}$ (A^2/molecule)	Penetrated NPS	
			Geometry	Gibbs
BPA	37.1	35.7	28	26
Insulin	37.1	35.5	5	4
Fibrinogen	37.1	36.2	25	11

corresponding number by the geometrical method the free space is 5.23 A^2 per molecule of stearic acid or 103 × 5.23 = 540 A^2 per molecule of insulin. If each penetrating chain has a cross-sectional area of 30 A^2 the number able to penetrate from each protein molecule is 540/30 = 18. The results of these calculations are shown for stearic acid in Table V and for cholesterol in Table VI.

Discussion

It is evident from the values of the activation energy that only a weak interaction exists in these systems, since all the figures in Table I are small. In order of magnitude they are comparable with the activation energy for the self-diffusion of water, for which Davies (12) quotes a value of 5300 cal./mole. Since the activation energies for adsorption of BPA and insulin are close to this figure it would appear that the rate-determining process, at least in the case of these proteins, is the diffusion of water away from the surface. If the higher activation energy of lysozyme is true, it would suggest the presence of an additional energy barrier, possibly derived from the much smaller tendency of this protein to form a monolayer. In the case of cholesterol this extra energy barrier is sufficient to prevent any adsorption at all (1). Stearic acid at pH 7.4 is negatively charged, however, whereas lysozyme is positively charged, so this electrostatic attraction will lower the energy barrier sufficiently for adsorption to take place.

When the free energies of adsorption are considered it is seen that the energy changes per CH_2 group are fairly constant for the same lipid, being about 500 cal./mole for stearic acid, and about 700 cal./mole for cholesterol. It is interesting to compare these figures with the values obtained by previous workers. Langmuir (6) obtained a value of 625 cal./mole for adsorption of a methylene group at the air/water interface, thus agreeing with the above figures. However, Pankhurst (13), who studied penetration of short-chain polar substances into monolayers of fatty acids and sterols, obtained adsorption energies which varied from 700 to 1100 cal./mole CH_2. He concluded that ΔG is larger for penetration of an insoluble monolayer than for adsorption at an air/water interface. This was supported by Crisp (9), who obtained a value of 800 cal./mole for the energy per CH_2 of penetration by amines of acid monolayers. Since these figures are close to those found for the partition of compounds between nonpolar liquids and water, Crisp concluded that an ion with a hydrocarbon chain is adsorbed with all its methylene groups present in the nonpolar region of the monolayer.

The conditions operating in the present systems are rather different from those described in the papers of Crisp and Pankhurst, since the hydrocarbon chains are joined to the peptide chains of the protein. This could prevent some of the methylene groups from penetrating the lipid monolayer and so lower the apparent energy per CH_2 group.

A consideration of the number of penetrated side chains enables the detailed structure of the lipoprotein layer to be obtained. In comparing Tables V and VI with Table II it is noticed that in the complexes formed with stearic acid a little under half the total number of NPS penetrate the lipid film. With cholesterol, on the other hand, far fewer side chains penetrate. One reason for this is probably the higher initial surface pressure used for cholesterol adsorption; another is possibly the much larger bulk of the cholesterol hydrocarbon group, preventing penetration for stearic reasons. In effect, the overall explanation for the difference in behavior of two lipids may be found by comparing the compressibilities of two monolayers over the region of the π/A curve used for the adsorption. From Figs. 4 and 5 it is seen that the adsorption occurs over the liquid condensed region of the stearic acid curve, but in the region of lowest compressibility with cholesterol. There is consequently less free space in compressing a film of cholesterol over a given range of surface pressures.

Comparing the two methods of calculating the number of penetrating NPS it is seen that, although there is quite good agreement with BPA and insulin, the values derived from a geometrical model are larger than those obtained from the Gibbs equation. A similar effect was observed by Pethica (8), and it is probably due to the limitations of the geometrical method. It has been assumed that the π/A curve of the lipid is followed also by the complex film, the same cohesive forces existing. This will not be true however, since the hydrocarbon content of the penetrating side chains is far less than that of both stearic acid and cholesterol. The cohesive forces will therefore be less than those operating in films of the pure lipids, and the number of penetrating side chains calculated by this method correspondingly high.

The foregoing thermodynamical treatment of these systems not only gives information about the mechanism of formation and structure of the lipoprotein layer, but the consistency of the adsorption energies provides a justification for the theory of penetrating side chains. In view of this it is most unlikely that protein molecules are penetrating the lipid film in their entirety. A further point against a "patchwork-type" mixed film formation is that each protein should exhibit the same behavior towards all lipids, and the maximum surface pressure reached should be the collapse pressure of the protein. Consideration of the case of BPA at pH 7.4 shows that the nature of the lipid had a considerable effect on the results, since the maximum surface pressures reached with stearic acid, cholesterol (1), and lecithin (2) were 10, 17, and 9 dynes/cm., respectively, compared to a collapse pressure of 16 dynes/cm. for BPA. The differences here are not due to the state of the lipid film since, whereas stearic acid has some solid character, cholesterol and lecithin films are liquid.

Acknowledgment

The authors wish to express their thanks to the Department of Scientific and Industrial Research for a maintenance grant to D. G. H.

References

1. Eley, D. D., and Hedge, D. G., *Discussions Faraday Soc.*, April, 1956.
2. Eley, D. D., and Hedge, D. G., *J. Colloid Sci.*, in press.
3. Cumper, C. W. N., and Alexander, A. E., *Trans. Faraday Soc.* **46,** 235 (1950).
4. Davies, J. T., *Trans. Faraday Soc.* **49,** 680, 949 (1953).
5. Davies, J. T., *Biochem. J.* (*London*) **56,** 509 (1954).
6. Langmuir, I., *J. Am. Chem. Soc.* **39,** 1848 (1917).
7. Tristram, G. R., "The Proteins" (H. Neurath and K. Bailey, eds.), Vol. 1, Part A, p. 181. Academic Press, New York, 1953.
8. Pethica, B. A., *Trans. Faraday Soc.* **51,** 1402 (1955).
9. Crisp, D. J., "Surface Chemistry," p. 65. T. Butterworth, London, 1949.
10. Harkins, W. D., "Physical Chemistry of Surface Films," (Reinhold, New York, 1952).
11. Ries, W. E., and Cook, R., *J. Colloid Sci.* **9,** 535 (1954).
12. Davies, J. T., *Advances in Catalysis* **6,** 1 (1954).
13. Pankhurst, K. G. A., *Proc. Roy. Soc.* (*London*) **A179,** 393 (1942).

JOURNAL OF COLLOID SCIENCE **12,** 430–432 (1957)

BOOK REVIEWS

Steric Effects in Organic Chemistry. Edited by MELVIN S. NEWMAN. John Wiley & Sons, Inc., New York, 1956. 710 pp. Price $12.50.

Thirteen chapters are included in this valuable and timely book:

1. Conformational Analysis (60 pp.) by W. G. Dauben and K. S. Pitzer;
2. Substitution at Saturated Carbon Atoms (103 pp.) by E. L. Eliel;
3. Steric Effects in Aromatic Substitution (38 pp.) by G. S. Hammond and M. F. Hawthorne;
4. Additions to Unsaturated Functions (48 pp.) by M. S. Newman;
5. Intramolecular Rearrangements (54 pp.) by D. J. Cram;
6. Olefin Forming Elimination Reactions (44 pp.) by D. J. Cram;
7. Cleavage Reactions of the Carbon-Carbon Bond (89 pp.) by H. H. Wasserman;
8. Steric Effects among the Common Organometallic Compounds (29 pp.) by G. F. Wright;
9. Steric Effects on Equilibrated Systems (46 pp.) by G. S. Hammond;
10. Molecular Complexes and Molecular Asymmetry (12 pp.) by M. S. Newman;
11. Steric Effects on Certain Physical Properties (44 pp.) by L. L. Ingraham;
12. Calculation of the Magnitude of Steric Effects (32 pp.) by F. H. Westheimer;
13. Separation of Polar, Steric and Resonance Effects in Reactivity (119 pp.) by R. W. Taft, Jr.

These chapters have been written by chemists who are very active in research. Indeed, the first impulse of the reviewer is to commend Professor Newman for the selection of collaborators and to congratulate him for getting the job completed within a reasonable period of time, considering the active publication record of most of the contributors.

One is not surprised to find a fresh and inquisitive approach to the subject matter in many of the chapters. The material is obviously alive in the minds of the writers. Of course, one finds variations in depth and, in spite of a thorough editorial job, in style among the chapters. Some of them, for example, Chapters 1, 2, and 13, discuss material extensively covered in the recent literature; however, in the case of Chapters 2 and 13 the present treatment is so thorough as to justify the duplication of effort. In some cases, for instance, Chapters 7, 8, 10, and 11, the emphasis on steric factors should be novel and stimulating to many readers. Other classical playgrounds of steric vs. polar factors have been properly covered, i.e., in such chapters as 3, 4, 5, 6, and 12. The effort to avoid superficiality in the treatment of inherently complex situations is apparent in many of these, for instance, in the discussion of the large ortho/para ratios in compounds bearing certain meta-substituents (p. 178).

The book is beautifully printed. A thorough study of it is earnestly recommended.

FAUSTO RAMIREZ, New York, New York

The Chemistry of Phenolic Resins. By ROBERT W. MARTIN. John Wiley & Sons, Inc., New York, 1956. 298 pp. Price $9.50.

This book deals not only with the chemistry of the resins from phenols and aldehydes and ketones but for the first time emphasizes the use of the chemicals from such condensations in various other fields. Thus the author has tabulated in very convenient form such products as the phenol alcohols and the bisphenols many of which find only minor resin uses.

All libraries and all research groups which touch upon the phenols and polyphenols or the aldehydes and the ketones should have this book as a valuable reference volume. The literature coverage for the various chapters is quite adequate and is a valuable part of the book. The general picture of the phenolic resin reaction series is given in somewhat more detail than is available in any previous volume. The effects of phenolic substitutents, phenolic functionality, phenol-aldehyde ratio, and the catalysts used are quite well presented. The complications due to high reactivity of the reaction are intermediates, but in a separated form.

Scattered throughout the book are sufficient new and unpublished data (for instance, p. 21, line 15) to intrigue the expert worker in phenolic materials. The author's analysis of the competing reaction problems will be of interest (p. 22) to chemists in many fields. His own improved separation method has added to the chemical knowledge of these materials.

The chapter on bisphenols is quite complete and calls attention to a field which is destined to grow to large volume usage even beyond the resin field.

Chapter 4 on the phenolic resins shows a good understanding of this complicated subject. Here the distinction between one-step and two-step resins comes not entirely from the catalyst but is a combination of the catalyst and the phenol-formaldehyde ratio. Thus alkaline catalysts for novolac resins are used with considerable production difficulty as is noted on p. 111. In the same way acids will give heat-hardening resins with much difficulty as to control. As a comment on an omission the problems of stability of the methylene linkage are not fully covered.

The heat cure of phenolic resins is well described as a complex process. The acid cure is somewhat oversimplified. It should be said that the first part of the acid set can be reversed by an addition of alkali, indicating that the first effect is a solubility effect. However, the next step is a water release (or a vapor release) which is not so easily reversed.

The chapter on reactions of phenol-aldehyde products gives hints as to important present uses with unsaturated compounds and as to many future uses with halogens, acids, bases, oxygen, and hydrogen which should be of interest to most organic chemists.

The reviewer considers that this volume has covered a rather difficult subject in a very effective manner. It will enable all polymer chemists to be up to date on the oldest condensation polymer field viewed from the organic chemical angle.

The data covered by this chapter are being rapidly expanded by current literature so for this section the literature past 1954 should be periodically reviewed.

HOWARD L. BENDER, Bloomfield, New Jersey

Chemical Engineering Practice. Vol. 1: General; Vol. 2: Solid State. Edited by HERBERT W. CREMER AND TREFOR DAVIES. Academic Press Inc., New York, 1956. Vol. 1, 494 pp. Vol. 2, 632 pp. Price $17.50/volume (subscription price $13.30/volume).

These volumes are the first two of a series of twelve intended to present "the various stages of development of a manufacturing process from the laboratory bench to the completed factor." Most of the contributors are British, as are the editors. The approach is akin to the engineering science method, "the classification employed being based on underlying physicochemical principles rather than upon the actual operations which give effect to them."

Volume 1, entitled *General*, contains a review of the history of chemical engineering together with chapters on material and energy balances and other basic chemical engineering calculations. The economics of production and pilot-plant design are also considered, the latter in some detail.

Of more interest to the colloid scientist or surface chemist is Volume 2, entitled *Solid State*. Two rather different subjects are treated in this volume: The first part begins with a chapter on the fundamental concepts of the solid state and then goes on to treat at some length the properties of metals and metallic alloys. It is pointed out that it is still not possible to apply many of the fundamentals to practical problems of structures. After a chapter on the properties of glasses, this section concludes with a broad, qualitative review of the corrosion of metals.

The second major subject treated in Volume 2 is the behavior of packed beds and porous masses and their applications in filtration, combustion, and transpiration cooling. Included also is a section on powder metallurgy. The treatment of flow through porous systems constitutes a thorough résumé. In addition to the usual material found in such discussions, information on two-phase and molecular flow is also presented. It can be argued, however, that much of the subject matter of this section might be better included in the volumes on fluid flow promised for the future. This, of course, is the conventional method of categorization; it has merit in that the properties of the solid material itself are usually of secondary importance compared with the fluid properties and nature of the channels.

This series will constitute a valuable addition to the fundamental reference literature of chemical engineering.

S. K. Friedlander, New York, N. Y.

F. G. Donnan

IN MEMORIAM:

FREDERIC G. DONNAN

DECEMBER 16, 1956

F. G. Donnan, F.R.S., emeritus professor of the University College, London, died on December 16th, 1956, in Canterbury Hospital. He was 86 years old and died of old age.

Born in Northern Ireland he had the warmth and temperament of the Irish. He was known as the great man in physical chemistry, and his interest covered a wide area from chemical thermodynamics to colloids.

His pioneer contributions to colloid science were of fundamental value and remain so today. He investigated emulsification (1), interfacial tension (Donnan's pipette) (2), ionic equilibria across semipermeable membranes (3), and the stability of hydrophobic dispersions (4). It is stated in this latter paper of 1912, that it is the electrical double layer which prevents particles from coagulating if their kinetic energy is insufficient to pierce the double layer. His interest was not restricted to the study of fundamental phenomena (in which he published about 40 papers), but overlapped into the industrial applications, making industry aware of the value of colloidal science (5). His imaginative mind was deeply touched by the problems of biological phenomena. He kept in close contact with eminent biologists and physiologists (A. V. Hill, Jacques Loeb), to find a way to apply his field, physical chemistry, to Life. His address on the "Mystery of Life" summarized his creed (6). "The last product of development [of Universe] is the mind of man" and "Science, truly understood, is not death, but the birth of mystery, awe, and reverence." In addition to his experimental contributions in the field of physiology he made several attempts to find theories governing Life (7). He contributed in editing with Arthur Haas *The Commentary on the Scientific Writings of J. Willard Gibbs* (8), whose writings he greatly admired.

Paul Stamberger

Bibliography

1. *Z. physik. Chem.* **31,** 42 (1899).
2. *Engineering* **99,** 551–2 (1915).
3. *Z. Elektrochem.* **17,** 572 (1911).
   J. Chem. Soc. **105,** 1040–63 (1914).
4. *Z. physik. Chem.* **80,** 597 (1912).
5. *Brit. Assoc. Advance. Sci. Rept.* **1918,** ibid. **1920.**
6. *Smithsonian Inst. Ann. Rept.* **1929,** 309–21.
7. "Specific laws of theoretical biology." *Z. angew. Chem.* **52,** 467–71 (1939). "Linkage of physikochemical process in biology." *Nature* **148,** 723–4 (1941). "Application of thermodynamics to the phenomena of Life." *J. Gen. Physiol.* **8,** 685–88 (1927).
8. Donnan, F. G., and Haas, A., "The Commentary on the Scientific Writings of J. Willard Gibbs." Yale University Press, New Haven, 1936.

JOURNAL OF COLLOID SCIENCE 12, 434–451 (1957)

BEHAVIOR OF ADSORBED PROTEIN IN CANE SUGAR JUICE

M. C. Bennett

Department of Sugar Chemistry & Technology, Imperial College of Tropical Agriculture, Trinidad

Received January 15, 1957; revised June 3, 1957

ABSTRACT

Sugar cane juice is an electrophoretically homogeneous suspension of particles. Protein adsorbed at the particle surface is stabilized by the high concentration of sucrose present, but on dilution, there is an increase in pH of the isoelectric point and denaturation takes place. Centrifugal washing completely removes adsorbed protein from the chloroplasts but not from the wax particles present in the system.

Some of the protein in juice is rendered soluble in 70% alcohol, and not available for adsorption, below pH 3. Adsorption curves in the cold show minimum protein solubility near the isoelectric point and an increase in area of adsorbent due to calcium phosphate precipitation above pH 6. Protein coagulation on boiling masks the latter effect, and the curve of N/particle against pH is still further changed by the loss of amide N from adsorbable material. Some effects of formaldehyde are mentioned.

INTRODUCTION

In biological fluids such as latex and milk which contain a system of suspended particles, electrophoresis and coagulation experiments have provided evidence that protein and other substances are adsorbed at the particle surface (1). Sugar cane juice is another natural colloid system known to contain much material in suspension (this being removed during the commercial clarification process) and known to be rich in soluble protein and polysaccharide (2, 3); there is, however, little published information concerning the physical relationship between these various constituents.

The suspended particles in cane juice which may be seen under the microscope have diameters up to 6μ, and they have been observed to be present in densities ranging between 2.5×10^8 and 1.2×10^9 particles/ml. A study of the sediments and supernatant liquids obtained by centrifuging juice samples at 1000 *g* has shown that about 85 % of the particles present have diameters around 2μ, whereas only 5 % have diameters of 4μ or greater; this size distribution is apparently quite general for the juices so far studied (4).

Investigations into the nature of the suspended particles (4) have shown that two main types are present:

1. Wax particles, composed mainly of a mixture of esters of ceryl alcohol with long-chain fatty acids, but also containing appreciable quantities of the free acids and alcohols, some sterols, phospholipids, and unidentified resins, the mixture having a specific gravity (*ca.* 1.2) greater than that of the dispersion medium.

2. Chloroplasts and polysaccharide—or starch—containing plastids released from ruptured cane cells. Sediments of particles in the 4–6 μ diameter range have a high mineral (mainly silicate) content, and therefore suspended minerals must form a third type of particle present in cane juice, though only in small amount. Results indicate that between 50% and 75% of all particles in raw juice are of the wax type.

The total quantity of dispersed phase is small (*ca.* 0.25% w/w) and puts cane juice in the range of "dilute suspensions" or sols in which an added stabilizer is not necessary to prevent spontaneous flocculation. Nevertheless in a system so complex as the extract from crushed plant tissue, it is to be expected that a variety of substances, present in solution in the continuous phase, would be adsorbed at the particle surface and thereby mask to a certain extent the true nature of the particle surface. The heterogeneous particle system in cane juice is, in fact, found to be electrophoretically homogeneous and can therefore be compared with the classical system in which a variety of particles (for instance, quartz, carbon, oil drops, and even wool fibers) are introduced into a gelatin solution. Just as in this case it is inferred that electrophoretic homogeneity is observed because the particles all carry a surface film of gelatin, so in the cases of natural latex, milk, and now sugar juice it may be inferred that all particles carry a film of material adsorbed from the aqueous dispersion medium.

In this work attention is focused upon the proteinaceous constituents of sugar juice, and the term "adsorbed" is used to describe that protein which is present as a film at the particle surface. However, it has been noted that there are three distinct particle types present in juice, and it is quite possible that the interaction between particle and protein layer is not in all cases purely physical; indeed it has been possible to show that the plastid type of particle can be stripped free of its adsorbed layer by repeated washing but the wax type can not.

In the present investigation it has been possible to follow changes in the electrophoretic behavior of the system with changes in the extent and nature of protein adsorption, and certain physical effects have been found which, although not reported, may well take place in other biological colloid systems under the appropriate conditions.

EXPERIMENTAL

The sugar cane used for this study was of variety B37172, grown under normal field conditions at the College Farm. Cane stalks were crushed in a laboratory three-roller mill, and the juice was filtered through loosely packed cotton wool to remove fibrous debris and flakes of cuticle wax. All determinations on the juice were made within 5 hours after the milling, although effects due to decomposition can be detected only after 10 hours (5). Unless otherwise stated, all work was carried out at the temperature of the laboratory 26° ± 1°C.

Particle density determinations were made by direct counting using a Levy counting chamber of a standard hemocytometer. A rather more convenient method was based on the measurement of the optical density of the suspension, the O. D. being corrected for the small (2%–3%) contribution of the pigments present in juice, this being determined on a bentonite clarified sample. A study was made of the change in O. D. with pH and wavelength, and subsequent determinations were carried out in 0.1 *M* acetate buffer at pH 4.5 using light of wavelength 650 mμ. For particle densities lower than 10^7/ml. there was shown to be a linear relation between O.D. and counted particle density.

Electrodialyses of juice were carried out using a Marsden cell (6) with continuous water flow through the electrode compartments. One hundred milliliter samples were electrodialyzed at an initial current of *ca.* 150 ma., and after 4 hours the juice had a specific conductance of *ca.* 5×10^{-4} ohm^{-1} cm.$^{-1}$.

Particle electrophoretic mobility determinations were made on diluted samples of both electrodialyzed and raw juice as described in the relevant section below. Measurements were generally made in phosphate buffers or NaCl at a total ionic strength of 0.01. Using NaCl, the pH was adjusted using HCl or NaOH, and no difference was detected between mobilities in this electrolyte and those in phosphate buffer at the same pH. Suspensions were adjusted to a particle density of *ca.* 10^7 particles/ml. by centrifuging particles (under 1000 *g*) from the juice sample until the required dilution gave the required density. After dilution the suspension was allowed to stand for 30–60 min. before introduction into the electrophoresis cell, though no time effects were detected over this period. Salts used to determine the reversal of charge concentrations of various cations were the nitrates of Th, Ce, Al, Pb, UO_2, Zn, Cu, and Sr, and the chlorides of La, Ca, Ba, Mg, Li, Na, and K.

Mobility measurements were made by the microelectrophoresis technique under a magnification of 250 using a Mattson type single tube cell (7) of internal diameter 2 mm., of length 10.7 cm., and fitted with platinum wire electrodes. Particle velocities were measured over a distance of 135μ at the satationary level which was located using the method of Henry (8). The potential gradient was determined from the current flowing and the specific conductance of the suspension in the cell by the method of Abramson, Moyer, and Gorin (1); with suspensions in media of low ionic strength it was found that the potential gradient could be determined with sufficient accuracy by means of a voltmeter across the tube electrodes. Mobilities quoted are the means of ten measurements in each direction, and the reproducibility of determinations in the various systems studied is given in the results below.

Measurements of pH were made using a Cambridge pH meter, and conductance measurements using a Mullard conductivity bridge (type E7566).

The change in the extent of protein adsorption with a change in pH was followed by centrifuging particles from a given sample of raw juice and determining both the N content and the number of particles in the sediment. In practice 200 ml. samples of juice were adjusted to the required pH using HCl and NaOH, allowed to equilibrate for 1 hour, and then centrifuged at 1000 *g* for 1 hour. The sediment obtained after decantation was allowed to drain for a further 30 min. (the error introduced by the very small volume of equilibrium solution remaining in the sediment was less than 1 %) and then redispersed in N-free distilled water. The suspension was made up to a known volume and a sample pipetted off for a total N determination. Particle counts were carried out on the juice sample before and after centrifuging, and the number of particles removed under these conditions was found to vary between 50 % and 100 % of the original number present: the number of particles in the sediment was generally of the order of 10^{11} while the total N content determined using the micro-Kjeldahl technique was of the order of 10 mg. The significance of these and other N determinations is discussed more appropriately in a later section.

Inorganic phosphate in juice was determined by a molybdenum blue colorimetric method (9), and calcium and magnesium determinations were made both on ashed samples and directly on the juice by ethylenediamine tetraacetate titration using Eriochrome Black T indicator after the method of Schwarzenbach (10).

All chemical reagents used throughout the investigation were of A.R. quality.

Results and Discussion

Electrophoretic Behavior

1. Dilution Effects. A preliminary investigation of the variation of particle mobility with pH in raw juice diluted 1:10 showed that all particles in the system behaved in the same manner and that they were isoelectric at pH 3.25. Subsequently the curve shown in Fig. 1 (curve i) was obtained using electrodialyzed juice diluted 1:10, and the curve is seen to be similar to those obtained from electrophoretic studies on natural latex particles (1) which have demonstrated the presence of adsorbed layers at the particle surface. Mobilities were measured in this system with a reproducibility of 2 %–3 %.

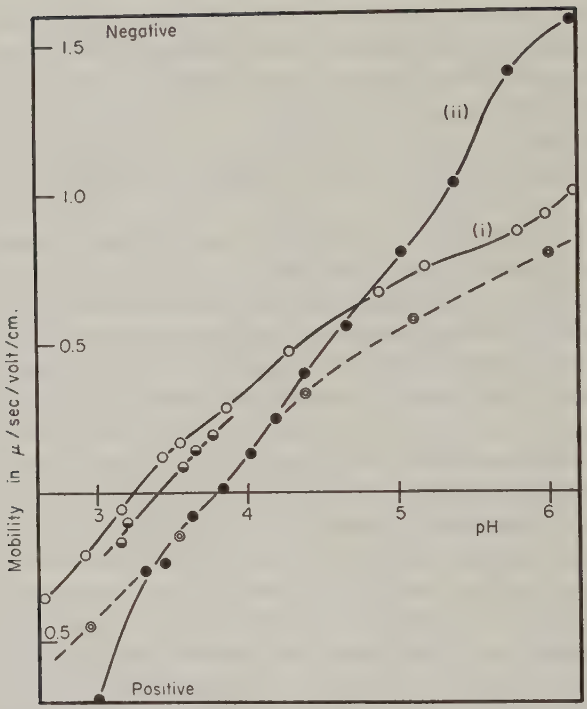

FIG. 1. Mobility-pH curves determined at three different dilutions of electrodialyzed juice; ○ (curve i) at 1:10, ◒ at 1:20, ● (curve ii) at 1:100. Dashed curve (◎) determined on alcohol-denatured protein (see text). All mobilities determined in NaCl, μ = 0.01 at a density of *ca.* 10^7 particles/ml.

Moyer (11), studying the fat droplets in milk, has shown that it is possible to strip the casein layer from the droplet surface by repeated washing and centrifuging. When a raw juice sample was centrifuged under 1000 g and the sediment resuspended in 0.01 M NaCl (that is, after only one centrifugal washing), it was found that a cataphoretically homogeneous system was produced which was isoelectric at pH 3.80. An identical pH-mobility curve was given by the particles present in raw juice diluted 1:100, and this finding led to a study of the change in isoelectric point with the dilution of juice sample.

Nine different samples of juice were used, after electrodialysis, in the determination of mobility curves at five dilutions, and three of these curves are shown in Fig. 1. The change in isoelectric point with dilution is shown in Fig. 2. The reproducibility with which mobilities could be determined decreased with increasing dilution (to *ca.* 6 % at 1:100).

The range of isoelectric points measured (pH 3.80–3.25) is rather lower than that usually found for pure proteins, but there can be little doubt that proteinaceous substance is present at the particle surface, since a complete protein hydrolyzate may be obtained from the adsorbed material (see below). Further, it is generally found that a protein in aqueous solution has minimum solubility near its isoelectric point, and this is certainly found in the adsorption studies described later in which maximum protein adsorption is measured at the isoelectric points recorded above.

Protein layers adsorbed at the solid-liquid interface are usually considered to consist of unfolded or surface-denatured molecules (12), but in considering the present system it should be noted at once that the solution contains an appreciable concentration (*ca.* 0.4 M) of sucrose which might well have the effect of substantially increasing the stability of proteins present in their folded or native form (13, 14).

The increase in isoelectric point (0.55 pH unit) found on dilution is of the same order as that measured upon denaturation of a pure protein (1), and the hypothesis may therefore be put forward that the above effect is related to the sucrose concentration in the diluted system, the reduction in sucrose concentration on dilution leading to reduced stability and hence denaturation of the outermost adsorbed protein layer.

The hypothesis was tested simply by repeating the dilutions using 0.01 M NaCl in 0.05 M sucrose (a concentration chosen to be slightly larger than that present in raw juice diluted 1:10, but not large enough to affect appreciably the viscosity of the system). Mobility curves were obtained at two dilutions, 1:50 and 1:100, and were both found to be coincident with curve i, Fig. 1, having an isoelectric point at pH 3.25.

Some further support for the hypothesis was derived from the fact that particles carrying alcohol-denatured protein showed an isoelectric point at

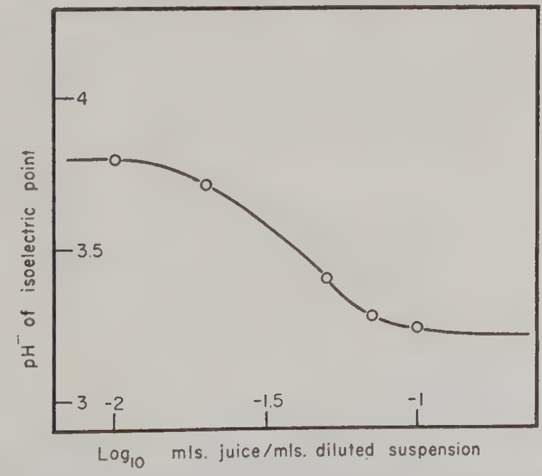

FIG. 2. The variation of isoelectric point with dilution. Mobility curves determined as the three shown in Fig. 1.

pH 3.80. The mobility curve is shown in Fig. 1 (dashed curve) and was obtained using the precipitate of particles and protein thrown down from the raw juice by the addition of alcohol to 70% v/v, this being redispersed, after washing free of alcohol, in 0.01 *M* NaCl of volume equal to that of the original juice sample.

2. The Removal of Adsorbed Layers. It has been suggested that all particles still have some proteinaceous material adsorbed at their surface after one centrifugal washing. However, on repeating the process a number of times it was found that the suspension became electrophoretically heterogeneous, a number of particles now showing no isoelectric point over the pH range studied.

In this experiment, the juice was first centrifuged at 500 *g* for 5 min. to remove the very largest particles (most of which were presumed to be mineral), and thereafter the washing process was carried out on the particles remaining in suspension by centrifuging at 1000 *g* for 1 hour and resuspending the sediment in distilled water using a blender. After ten such washing operations a suspension was obtained in which *ca.* 60% of the particles gave the mobility-pH curve (i), Fig. 3, most of the remainder showing an isoelectric point at pH 3.8 and giving curve (ii) (which is seen to be identical to curve ii, Fig. 1). No change in the system was observed after three more washing operations.

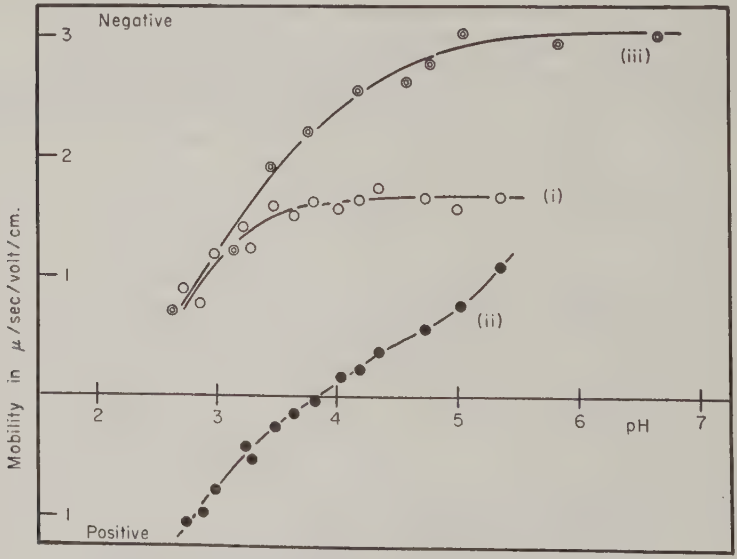

Fig. 3. Mobility-pH curves for various particle systems. Curves i and ii, the particle types present in juice sediment washed ten times (see text). Curve iii, particles in the dispersion of toluene-extracted cane wax. Curves determined under same conditions of those shown in Fig. 1.

It is well known that proteins are very strongly adsorbed at the oil-water interface, and since it has been shown that the fatty droplets of cream may not be stripped completely free from proteinaceous material by repeated centrifugal washing (11), it would appear that the same is true of the wax particles in cane juice. On the other hand, the plastids present in this system might reasonably be expected to have a polysaccharide surface, at which protein would be only loosely held, and therefore which would be exposed after repeated washing.

Some measure of support for this explanation was derived from the study of a wax-in-water suspension prepared by steam-jet dispersion of the crude wax obtained by toluene extraction of commercial clarification mud (15). The dispersion was made directly into NaCl solution containing no added stabilizer, the large quantity of free fatty acids (*ca.* 0.3 meq./g. crude wax) presumably being sufficient. Particle diameters varied between 1 and 3 μ, and suspensions could be made to contain as many as 3×10^8 particles/ml. The variation with pH of the mobility of these particles was measured under the same conditions as before and gave curve iii in Fig. 3, though owing to a greater spread in the mobilities of individual particles in a given suspension, the determined values were reproducible only to 9%–10%. The curve is almost identical with that quoted by Growney (16) for oil drops containing stearic acid, studied in the same medium.

When some (about half the number originally present) of the particles in raw juice were removed by centrifuging and these replaced by the wax particles prepared by steam-jet dispersion, the whole system was observed to be electrophoretically homogeneous and to behave in a manner identical with the original juice sample, i.e., according to the curves shown in Fig. 1. Repeated centrifugal washings carried out on this system did not yield particles showing the high mobilities of the original "naked" wax particles (curve iii, Fig. 3), but gave a suspension of the two mobility types shown by curves i and ii in Fig. 3. Apparently the proteinaceous material adsorbed at the surface of the introduced wax particles may not be removed by centrifugal washing.

Bungenburg de Jong (17) has shown that there is a specific sequence in the concentrations of different inorganic cations required to reverse the charge on certain colloid types with an acidic nature. Thus carboxyl colloids, such as arabinate and pectinate, may be distinguished from phosphatides and sulfate colloids, while the carboxyl group of a long-chain fatty acid gives rise to yet another cation sequence or spectrum. The method has recently been applied in a study of the bacterial surface of *E. coli* (18).

It was hoped that some further information concerning the nature of the surface of particles in the various systems described above could be gained from the spectra of reversal of charge concentration of different cations; the spectrum obtained using the steam-jet dispersed wax system is shown

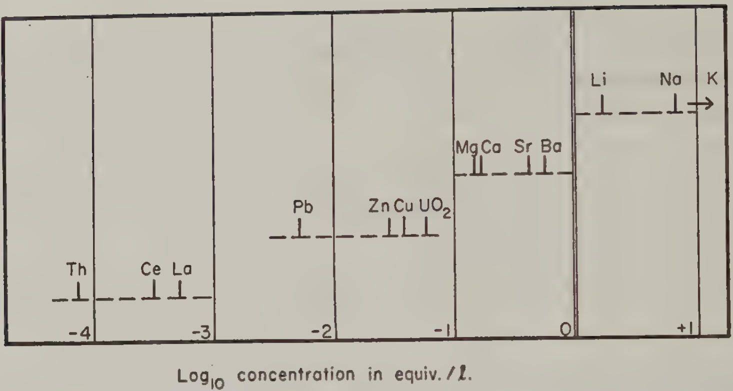

Fig. 4. Reversal of charge spectrum (see text) for particles in the dispersion of toluene-extracted cane wax.

in Fig. 4. It is seen to be very similar to that obtained by Bungenburg de Jong using oleate (17), and the data are consistent with the view that essentially only carboxylate ions are present at the wax-water interface in this system.

With regard to this system, it may be shown that the quantity of free fatty acid in the wax sample used for the dispersion (0.25 meq./g., as determined by alcoholic KOH titration) is equivalent to 6×10^8 carboxyl groups available in each particle, assuming a particle diameter of 2 μ. This is substantially more than the number which might reasonably be expected to occupy the available surface area (12×10^8 A^2) of particles of this diameter. The charge density σ may be determined from the horizontal part of curve iii, Fig. 3, where the particle mobility is 3μ/sec./volt/cm., using the approximate relationship,

$$\sigma = v\kappa\eta$$

(where v is mobility, η viscosity, and $1/\kappa$ the thickness of the double layer). The value of σ obtained is 2.5×10^3 e.s.u./cm.^{2}, and assuming a particle diameter of 2μ, the total electronic charge would be 6.5×10^5 e/particle. It is clear that only a very small fraction of fatty acid available must be ionized at the wax-water interface in order to account for the calculated particle charge.

In the case of the system obtained by the repeated centrifugal washing of particles present in raw juice, the heterogeneity of the system precluded a satisfactory determination of the mobility curves in different salt solutions, and hence a reversal of charge spectrum was not obtained.

The Measurement of Protein Adsorption

1. Protein N Distribution. Protein-nitrogen concentrations in juice have been determined (3) as the difference between total juice nitrogen and the sum of amino, amide, and nitrate nitrogen, values of approximately 1 g./l. being obtained for the protein concentration as 6.3 × N. In the light of the present findings, it is seen that some of this protein must be intrinsically part of the chloroplasts and similar plastids present and therefore cannot be regarded as available for adsorption: the N value, important from the standpoint of this investigation, is that which gives a measure of adsorbable nitrogenous material. The total protein N in a given juice sample must therefore be considered to be made up of three terms: (*1*) intrinsic particle protein N; (*2*) adsorbed layer protein N; (*3*) dissolved protein N; and it is clear that if these three quantities are expressed in terms of the number of particles present, then term (*1*) and the sum of terms (*1*) + (*2*) + (*3*) must represent the lower and upper limits, respectively, of the quantity of protein N associated with each particle in the juice sample under any set of conditions.

Because of the heterogeneous nature of the juice suspension it is possible to obtain only a rough estimate of the average protein N content of the particles themselves (term (*1*)). This N value was determined on the sediment obtained after ten centrifugal washings of particles removed from raw juice, the result being in error by the quantity of adsorbed protein N which, it has been shown electrophoretically, the wax particles still carry. The average value determined during the course of experiments described below was $0.85 \pm 0.18 \times 10^{-10}$ mg. N/particle, while it may be noted that particles prepared by steam-jet dispersion of toluene-extracted wax had a nitrogen content of *ca.* 0.2×10^{-10} mg. N/particle. It seems reasonable to conclude from the latter figure that the wax particles in juice must also contain an appreciable quantity of nonprotein N, and hence it would be more accurate to define term (*1*) as "average particle N content."

The addition of alcohol to raw juice, to give 70% v/v final concentration, produces an immediate flocculation which completely clarifies the juice. The precipitate may be removed and washed with 70% alcohol by centrifuging and a total nitrogen determination carried out on the sediment. Since no further nitrogenous precipitate can be obtained by the addition of $(NH_4)_2SO_4$ to saturation or of trichloroacetic acid to the clear supernatant liquid either before or after alcohol removal, all protein is apparently thrown down in 70% alcohol and the N content of the precipitate must therefore be a measure of the particle N + total protein N content of the juice sample, that is, the sum of terms (*1*), (*2*), and (*3*).

It is convenient to express the N content of the alcohol precipitate in terms of the number of particles present, and values obtained from 23 different samples of juice lie between 1.90 and 2.55×10^{-10} mg. N/particle; it is seen that the average N content of the particles themselves accounts for about a third of this quantity.

The pH of juice samples used in this study was generally around 5.5, but on lowering the pH of a sample to below 3 it was found that the N con-

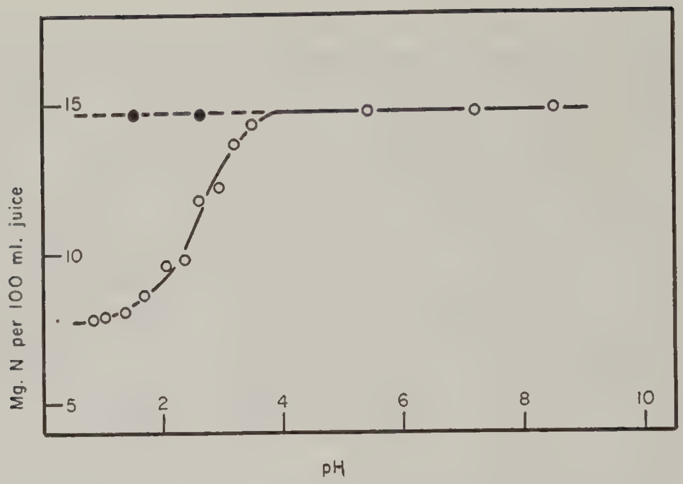

Fig. 5. The change in the N content of material precipitated from juice by the addition of alcohol to 70% v/v with pH of juice sample. ○ in the cold, ● samples heated *before* pH adjustment.

tent of the 70% alcohol precipitate was substantially reduced, as shown in Fig. 5. The points shown are the N contents of the alcoholic precipitates from 100 ml. aliquots of the same raw juice adjusted to various pH values using only HCl or NaOH, purposely avoiding the use of buffers in which the effect of the anion was unknown (19). The effect produced by the addition of acid was complete within 2 min. (the shortest time in which samples could be prepared and the precipitation carried out), and no further change was detected when samples were allowed to stand for times up to 1 hour at the low pH before precipitation. The effect was reversible in that samples allowed to stand 5 min. at pH values below 3 and then readjusted to pH values above 5 gave alcoholic precipitates of N content corresponding with the higher pH values. It is seen that the effect has the characteristics of an ionization of pK_a 2.5 which confers alcohol solubility upon a large proportion of the protein in juice. Two points are shown in Fig. 5 which indicate that the effect is removed by heating the sample above 90°C. (at which temperature heat coagulation of juice protein is complete (20)) prior to pH adjustment.

The effect is further discussed in a later section, after evidence has been presented which suggests that it is also reflected in the adsorption studies.

2. The Extent of Adsorption. If a number of samples of a raw juice be adjusted to different pH values between 1 and 9, it will be seen that flocculation takes place over two distinct ranges, around pH 3.5 and above pH 6. From Fig. 2 it appears that in undiluted raw juice the suspended particles carry no net charge at *ca.* pH 3.2, and so it might be expected that spontaneous flocculation would take place within 0.5 pH unit of this isoelectric point. The flocculation observed at pH values greater than 6 is that which is made use of commerically in the clarification process, and it has been known for many years that this is associated with the precipitation of calcium and magnesium phosphates. Trinidad raw juices contain Ca^{2+} and Mg^{2+} in 10–25 mM total concentration and phosphate up to 10 mM. The flocculation above pH 6 may be prevented altogether either by electrodialyzing raw juice until free from inorganic phosphate or by adding a suitable chelating agent, for instance, ethylenediamine tetraacetic acid (EDTA).

The visible effects which take place on changing the pH of a juice sample are accompanied by marked changes in the quantity of nitrogen associated with each particle (i.e., with changes in the sum of terms (*1*) and (*2*) above). The complete curve of N/particle against pH is shown in Fig. 6, in which the upper dashed line represents the total alcohol-precipitable N/particle in the sample (see Fig. 5) and the lower horizontal dashed line refers to the average N content of particles stripped, as far as possible, of their proteinaceous adsorbed layers by ten successive centrifugal washings (term (*1*)).

Kemp and Twiss (21) have shown that in latex systems the isoelectric point of protein in solution is the same as that of the adsorbed protein, and it must be inferred that this holds in the case of raw juice, since the point of

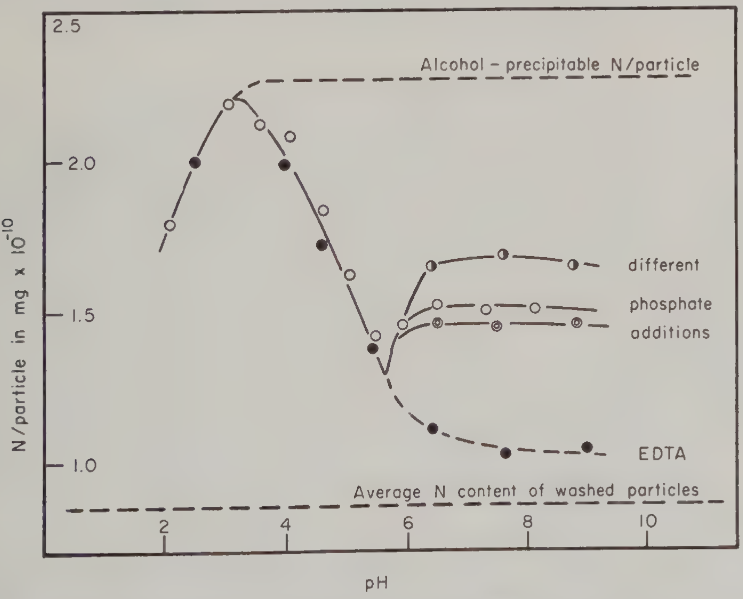

FIG. 6. The change in protein adsorption in cold raw juice with pH. Ca^{2+} + Mg^{2+} 19.2 mM, phosphate 3.9 mM, $\mu \sim 0.1$, particle density 61×10^7 per ml. ○ raw juice, ● in presence of 20 mM EDTA, ◑ in presence of 9.3 mM phosphate, ◎ in presence of 13.3 mM phosphate.

maximum adsorption (or minimum solubility) is very close to the expected isoelectric point from Fig. 2. It would follow that in the case of sugar juice we are dealing with the adsorption of protein in its native configuration.

The sharp rise to a plateau in the adsorption curve between pH 5.5 and 6 is undoubtedly associated with phosphate precipitation, for the addition of sufficient EDTA to chelate all calcium and magnesium present removed the plateau and completed the smooth curve as shown in Fig. 6. The height of the plateau above the EDTA curve was found to be dependent upon the extent of phosphate precipitation and passed through a maximum with increase in original phosphate concentration. The precipitation of calcium and magnesium phosphates in this system and the adsorption of this precipitate on the particles previously in free suspension has been studied in detail (22), and although the work is incomplete, it is clear that the formation of a plateau in the N/particle curve shown above is an expression of the increase in area available for protein adsorption.

The shape of the curves shown in Fig. 6 is quite general for all juice samples which have been studied. It is interesting to note, however, that the maximum in the adsorption curve has always been found close to, but never above, the alcohol-precipitable N/particle curve, whereas the smooth curve obtained in the presence of EDTA has always been found to approach, but never fall below, the line representing the N content of the particles themselves.

Protein Adsorption in Boiled Juice

1. Protein-N Distribution. In 1916 it was reported (20) that the coagulation of sugar juice proteins is complete at 90°C. At that time little was known of the stabilization of protein by sugars, and it was later found that only 70% of the nondialyzable nitrogenous material was coagulated on boiling (23). This finding is certainly borne out by the adsorption experiments described below, and, in fact, a rather smaller quantity (about 50%) of the total protein present was found to be heat-coagulable in the juice samples used here.

In calculating the percentage of heat-coagulable protein in a given sample, it is not correct, however, simply to compare the N content of heat-coagulated material with that of the 70% alcohol precipitate, for the boiling process produces the further effect of measurably reducing the N content of alcohol-insoluble material.

This loss in alcohol-precipitable N is a slow process which is almost independent of pH and is shown plotted against time of boiling in Fig. 7. The points shown were determined at four pH values, and it is seen that at zero time (before boiling) they form a curve similar to that shown in Fig. 5. The points represent the N content of alcoholic precipitates from 100 ml. aliquots of juice adjusted to the required pH value and then boiled under

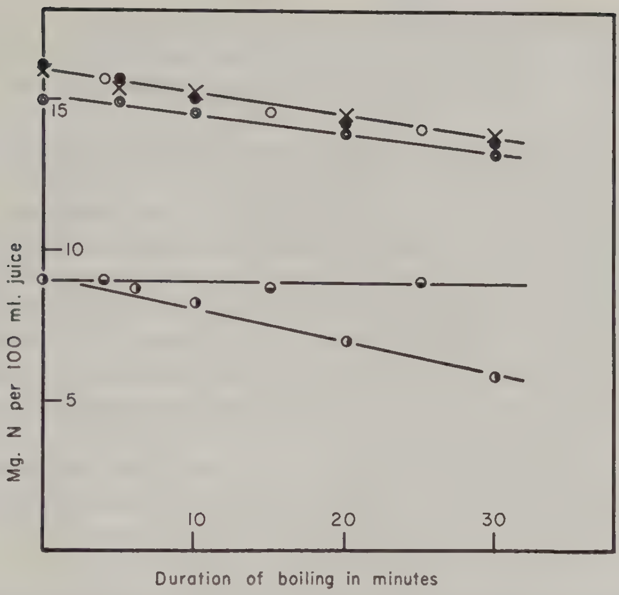

FIG. 7. The change in the N content of material precipitated from juice by the addition of alcohol to 70% with time of boiling after pH adjustment. ● pH 7.0, × pH 5.5, ◎ pH 3.2, ◑ pH 1.8. In the presence of 0.3% formaldehyde, ○ pH 7, ◑ pH 1.8.

reflux for the required period. The maximum pH change measured after 30 min. boiling was 0.4 unit in the sample originally at pH 7.0.

Further investigation showed that the loss in precipitable N was accompanied by an increase in the ammonia content of the filtrate, and hence the effect might be interpreted as a loss of amide N. Such an effect has certainly been observed with glutamine, which is readily hydrolyzed to glutamic acid on boiling at all pH values (24), and perhaps the same process may take place when glutamine residues form part of a polypeptide chain. Glutamic acid has been identified in juice protein hydrolyzates (see below), and the slight decrease in the rate of N loss at the measured isoelectric point (pH 3.2) shown in Fig. 7 is in accordance with the results recorded for the hydrolysis of pure glutamine at its isoelectric point.

Some further support for this interpretation may be gained from a study of the effect of formaldehyde. At neutral pH values, formaldehyde reacts rapidly and reversibly with proteins (25, 26) to form amino-methylol groups, and therefore cannot be expected to influence an amide hydrolysis. At acid pH values, however, formaldehyde is capable of cross-linking pairs of amide and amino groups in a manner which is not reversible, and although this condensation is usually found to be a slow process, it might be expected to confer a certain degree of stability upon those amide groups against hydrolysis. The results shown in Fig. 7 reveal that in the presence of formaldehyde, no loss of precipitable N takes place on boiling at low pH values, while the reagent produces no change in the effect of boiling at pH 7.

It is interesting to note that the isoelectric point of particles in a sample of raw juice boiled for 30 min. and then diluted 1:20 was found to be pH 3.05, for if the boiling process only brought about denaturation of the protein present, an isoelectric point at *ca.* pH 3.8 might have been expected.

2. The Extent of Adsorption. A typical curve of N/particle against pH for samples of juice boiled 10 min. under reflux after pH adjustment is shown in Fig. 8, where it is compared with the curve obtained in the cold. The curve of alcohol-precipitable N/particle against pH for the boiled samples lies below that obtained from samples not heated, as expected from the result expressed in Fig. 7.

Additions of phosphate and EDTA did not change the value of N/particle at any pH, so that the extent of protein adsorption was not dependent upon calcium phosphate precipitation or indeed upon the presented surface area of adsorbent. The value of adsorbed N/particle above pH 5 is clearly a measure of the amount of heat-coagulable protein per particle present.

Below pH 5 the interpretation of the adsorption curve is not quite so

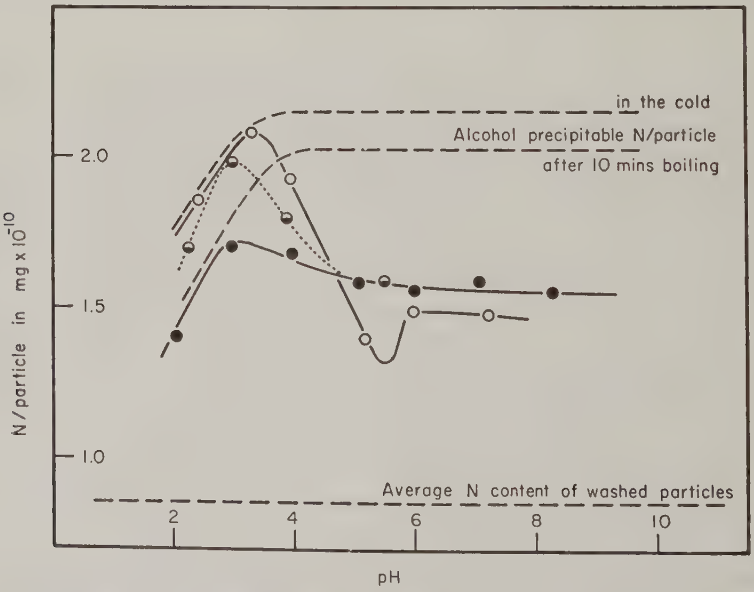

FIG. 8. The effect on protein adsorption of boiling the juice sample after pH adjustment. Ca^{2+} + Mg^{2+} 19.5 mM, phosphate 8.7 mM, $\mu \sim 0.1$, particle density 71 × 10^7 per ml. ○ in the cold, ● after 10 min. boiling, ◒ after boiling in presence of 3% formaldehyde.

straightforward. It has already been noted that the isoelectric point of particles in a juice sample boiled 30 min. was pH 3.05, and hence a maximum in the adsorption curve might be expected at this point; in fact, no sharp peak appears in the determined curve. Apparently, from Fig. 8, the curve of alcohol-precipitable N/particle represents the maximum quantity of N which is available to each particle, and this maximum value has been attained around (and below) pH 3.

Some support for this view was gained from the adsorption curve obtained using samples boiled in the presence of formaldehyde (dotted curve, Fig. 8). In this case there was no loss of (amide) N on boiling the acidified samples (see Fig. 7), and hence the curve of alcohol-precipitable N/particle is coincident with that obtained in the cold (the upper dashed curve, Fig. 8) at pH values, say, below 4. Upon the above hypothesis, in acid media, the maximum available N/particle in samples boiled with formaldehyde is now the same as that in samples not heated, and hence both adsorption curves show pronounced maxima near the isoelectric point.

CONCLUDING OBSERVATIONS

If a sample of juice is clarified by treatment with bentonite suspension, or by precipitation of calcium phosphate at pH 7, a clear amber solution is obtained which still contains an appreciable concentration of protein. The solution is quite stable even after boiling for 30 min. or freezing overnight, presumably owing to the sucrose present, but proteinaceous material may be precipitated by the addition of $(NH_4)_2SO_4$, alcohol, or acid to pH 3.2.

Stevens (27) is studying the hydrolyzates obtained from some of the above fractions by paper chromatography. The two-dimensional chromatograms of the hydrolyzate from juice material insoluble in 70% alcohol and from the precipitate formed in raw juice at pH 3.2 were found to be identical, and of the amino acids present, the following have so far been identified: alanine, aspartic acid, glutamic acid, glycine, leucine, lysine, proline, serine, threonine, and valine.

Treatment of the alcoholic precipitate from raw juice with 2:4-dinitrofluorobenzene (28), followed by hydrolysis, yielded ϵ-2:4 dinitrophenyl lysine; α-substituted dinitrophenylamino acids were not detected, the experiment indicating the presence, in the original juice, of high molecular weight or cyclic protein structures.

However, the electrophoretic and adsorption data presented above suggest that we are dealing not with the behavior of a simple protein structure, but rather with that of a conjugated system in which acid characteristics are conferred upon the protein by the linkage of another molecule, for instance, a polysaccharide. Polyuronic acid derivatives have certainly been identified in cane juice (2), and there can be little doubt that pectins exist in solution. Upon the above hypothesis, it may be suggested that it is the conjugated system which is alcohol-insoluble and which has an isoelectric point at pH 3.25.

Further, it would appear that the linkage is made through an ionized (possibly carboxylate) group, for on the addition of acid to below pH 3, the conjugated system might be considered to be broken down, leaving an alcohol-soluble protein which is apparently so strongly stabilized in sugar juice that it may not be regarded as available for adsorption. Such a protein, soluble in both alcoholic and aqueous media, has been isolated from *Hevea* latex (29) and since in the adsorbed state it too has an isoelectric point below pH 4, it is possible that this also exists in the natural latex as a conjugated system.

Acknowledgments

The author would like to thank Professor L. F. Wiggins, Mr. N. O. Schmidt, and Dr. R. Stevens for their interest and advice in this work, which forms part of a program of research carried out under the aegis of the British West Indies Sugar Research Scheme.

The author is also indebted to Sir Eric Rideal F.R.S. for his help in the final preparation of the manuscript.

References

1. Abramson, H. A., Moyer, L. S., and Gorin, M. H., Electrophoresis of Proteins. Reinhold, New York, 1942.
2. Binkley, W. W., and Wolfrom, M. L., *Advances in Carbohydrate Chem.* **8,** 291 (1953).
3. Honig, P., ed., "Principles of Sugar Technology." Elsevier, Amsterdam, 1942.
4. Bennett, M. C., *Intern. Sugar J.* **59,** 176, 208 (1957).
5. Schmidt, N. O., *Proc. Brit. West Indies Sugar Technol. Conf.*, 182 (1954).
6. Marsden, A. W., *J. Soc. Chem. Ind.* **59,** 60 (1940).
7. Mattson, S., *J. Phys. Chem.* **37,** 223 (1933).
8. Henry, D. C., *J. Chem. Soc.*, 997 (1938).
9. Williams, J. Howarth, *Proc. B.W.I. Sugar Technol. Conf.*, p. 167 (1954).
10. Schwarzenbach, G., Biedermann, W., and Bangerter, F., *Helv. Chim. Acta* **29,** 811 (1946).
11. Moyer, L. S., *J. Biol. Chem.* **133,** 29 (1940).
12. Davies, J. T., *Biochim. et Biophys. Acta* **11,** 165 (1953).
13. Ball, C. D., Hardt, C. R., and Duddles, W. J., *J. Biol. Chem.* **151,** 163 (1943).
14. Seegers, W. H., *Arch. Biochem.* **3,** 363 (1941).
15. Balch, R. T., *Sugar Research Foundation, Technol. Rept. Ser.* **No. 3** (1947).
16. Growney, G., *Trans. Faraday Soc.* **37,** 148 (1941).
17. Bungenburg de Jong, H. G., in "Colloid Science" (H. R. Kruyt, ed.), Vol. 2, p. 259. Elsevier, Amsterdam, 1949.
18. Davies, J. T., Haydon, D. A., and Rideal, Eric, *Proc. Roy. Soc. (London)* **B145,** 375 (1956).
19. Klotz, I. M., and Ayers, J., *Discussions Faraday Soc.* **No. 13,** 189 (1953).
20. Deerr, N., *Intern. Sugar J.* **18,** 558 (1916).
21. Kemp, I., and Twiss, D. F., *Trans. Faraday Soc.* **32,** 890 (1936).

22. Bennett, M. C., and Schmidt, N. O., unpublished work.
23. Farnell, R. G. W., *Intern. Sugar J.* **26,** 48, 420 (1924).
24. Vickery, H., Pucher, G., Clark, H., Chibnall, A. and Westall, R., *Biochem. J.* (*London*) **29,** 2710 (1935).
25. French, D., and Edsall, J. T., *Advances in Protein Chem.* **2,** 277 (1946).
26. Fraenkel-Conrat, H., in *Amino Acids and Proteins* (Greenberg, D. M., ed.), p. 532. Charles C Thomas, Springfield, Illinois, 1951.
27. Stevens, R., private communication.
28. Sanger, F., *Biochem. J.* (*London*) **39,** 507 (1945).
29. Bondy, C., and Freundlich, H., *Compt. rend. trav. lab. Carlsberg* **22,** 89 (1937)

JOURNAL OF COLLOID SCIENCE **12,** 452–459 (1957)

PURIFICATION AND SURFACE TENSION PROPERTIES OF ALKYL SODIUM SULFOSUCCINATES

E. F. Williams, N. T. Woodberry, and J. K. Dixon

American Cyanamid Company, Research Division, Stamford, Connecticut

Received January 28, 1957; revised June 24, 1957

Abstract

Methods of purifying a series of dialkyl sodium sulfosuccinates by crystallization and slurry adsorption are described. These procedures are useful for purification of relatively large quantities. The relationship of critical micelle concentration to chain length of the alkyl group is described. A consideration of the nature of the surface tension-concentration curve near the critical concentration indicates that micelle formation and surface hydrolysis occur below the critical micelle concentration.

Introduction

Miles and Shedlovsky (6) observed in early 1944 that the purity of a surface-active agent is suspect when its surface tension curve shows a minimum. Their later studies and those of many other workers (1, 7, 8) have confirmed the validity of their observation and have indicated that the quantitative physical chemical measurements on surface-active agents may be greatly affected by traces of impurities in these agents. Therefore, it was decided to repeat on a broad scale, measurements on the well-known dialkyl sodium sulfosuccinates with purified materials[1] so that the effects of variations in ester, chain length, branching, etc., could be properly evaluated. This was of particular interest to us because of the extensive past work carried out in these Laboratories on those agents. Methods of purification presented in this paper indicate not only methods of purifying the sulfosuccinates but also means for removing impurities from other surface-active agents on a relatively large scale. The effects of chain length and branching on critical micelle concentration, as measured by surface tension, have been determined.

---

[1] It is obvious that the purer the surface-active agent, the easier it may be to purify to high degree. Thus the use of pure starting materials will reduce the complexity of the purification steps for the surface-active agent in question. Methods of preparation (9) have been published elsewhere and need not be repeated here.

METHODS OF PREPARATION

Early workers were able to demonstrate that as the impurities were removed from a solution of an impure agent by foam fractionation, the surface tension curve of the resulting solution of purified agent showed no minimum. Measurement of surface tension by the du Nuöy ring method has been used throughout this work to detect and follow the presence and removal of impurities during the purification of an agent. Quantitative estimations of free acid, half ester, and combined sulfite and sulfate were obtained by potentiometric titration. Confirmatory quantitative data on these impurities and the half esters were obtained by polarographic measurements.

Both of the methods of purifying sodium alkyl sulfosuccinates used in this work are capable of producing relatively large quantities of pure sulfosuccinates and may find general usefulness for other agents. The first procedure involved crystallization of the sulfosuccinate as a hydrate from a suitable solvent. The second involved the adsorption of impurities on a solid adsorbent by a slurry adsorption method. It was often preferable to use both methods together.

A. Crystallization

Attempts to crystallize the anhydrous sulfosuccinates from solvents other than water failed in spite of all precautions. However, all the sulfosuccinates, di-methyl- through di-*n*-octyl-, form one or more hydrates. These, with the exception of several branched-chain compounds, can be obtained crystalline from the system water-methyl alcohol-sulfosuccinate. The following methods used for the crystallization of the di-*n*-butyl (short-chain) and the di-*n*-octyl (long-chain) compounds serve to illustrate the crystallization procedure:

1. Crystallization of Di-n-butyl Sodium Sulfosuccinate. A sample of 50 g. of the *dry* sulfosuccinate was dissolved in 90 ml. of *dry* methyl alcohol. After filtration, to remove extraneous solids, 8 g. of water (equivalent to a trihydrate) was added and the sample cooled to about 0°–5°C. If necessary, the solution was seeded and after 1 hour the crop was recovered by filtering through a coarse sintered-glass funnel. The funnel was cooled before filtration. If any sulfonated monoester is present it can usually be removed in a small first crop. The small amount of sulfate which is present usually remains in the mother liquor. The procedure is quite flexible. The losses are a function of the technique of the operator. The di-*n*-butyl sodium sulfosuccinate under the conditions presented crystallizes as the monohydrate. The method, with slight modifications made necessary by the change in solubility due to change in alcohol chain length, applies equally well to the di-*n*-amyl and di-*n*-hexyl compounds.

2. Crystallization of Di-n-octyl Sodium Sulfosuccinate. A sample of 390 g. of the di-*n*-octyl sodium sulfosuccinate was dissolved in 800 ml. of *dry* methyl alcohol and filtered through washed Hyflo Supercel. The filter was washed with 50 ml. of dry methyl alcohol. At least 5 moles (*ca.* 80 ml.) of water was added to the filtrate which was allowed to stand at 8°–12°C. for 1½ hours. To this was added with stirring 200 ml. of methyl alcohol containing 25 ml. of water at 5°C. The mixture was centrifuged quickly in a basket centrifuge refrigerated to 10°–15°C. The crop, after vacuum drying, was 300–325 g., approximately 80%.

B. Purification by Adsorption

The sulfosuccinates may be purified by adsorbing impurities on a solid adsorbent of suitable surface area and surface characteristics. It has been found that activated carbon is best for these particular surface-active agents, thus providing an efficient means of removing unsulfonated maleic ester, colored materials, and adsorbable impurities. The sulfosuccinate was made up at 5–10% concentration in polar solvents, such as water or a water-alcohol mixture. This was treated with activated carbon (Darco G-60) using about 3–5% based on the total weight of solution. The surface-active agent was recovered from the filtered solution by freeze drying. *It is preferable to carry out the purification on a solution of concentration near the critical micelle concentration.*

The application of the adsorption purification is well illustrated by the case of diisobutyl sodium sulfosuccinate (AEROSOL IB Surface Active Agent). The surface tension curve of the starting material showed a marked minimum which can be attributed to the unsulfonated ester present (determined polarographically to be 0.136%). Soxhlet extraction for 48 hours with ether, two crystallizations from methyl alcohol, treatment with 5% Darco G-60 at 25% concentration, and foam fractionation at 2% concentration were each ineffective in removing the ester completely. When this material was made up to 10% concentration in water and treated with 5% Darco G-60 and this followed by dilution to 5% concentration and subjected to a second Darco treatment, the surface tension curve no longer showed a minimum, indicating that the removal of impurities was complete. After one carbon treatment at 10% concentration, the solution could also be diluted to 2.5% and cleaned up by foam fractionation. Without the carbon treatment, foam fractionation was ineffective at concentrations of 2% or higher (Fig. 1).

C. Surface Tension Data

Measurement of the surface tension of aqueous solutions of the purified alkyl sulfosuccinates proved to be an excellent means of determining the efficiency of each purification procedure as it was carried out. The presence

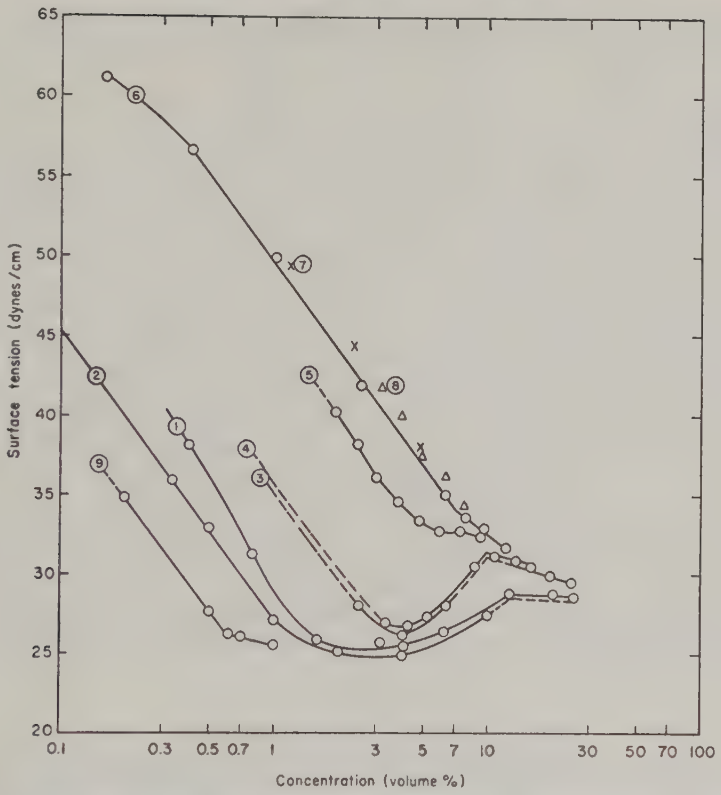

FIG. 1. Surface tension curves of diisobutyl sodium sulfosuccinate (*AEROSOL IB Surface Active Agent*)

Curve:

(*1*) Commercial Sample, Lot H-100, Bridgeville, as received.
(*2*) Commercial Sample, Lot H-436, Bridgeville, as received.
(*3*) (*1*) treated with 5% Darco G-60 at 25% concentration in benzene—subsequently crystallized twice from methyl alcohol-water.
(*4*) (*1*) extracted 48 hours in Soxhlet with ether.
(*5*) Residue from foam fractionation of (4) at 2% concentration.
(*6*) Residue of second foam fraction of recrystallized (*1*). Fractionation at 2% concentration.
(*7*) (*2*) treated with 5% Darco G-60 at 10% concentration followed by 5% Darco G-60 at 5% concentration and finally foam fractionation at 2% concentration.
(*8*) Sample differs from (*7*) only in that it was not foam fractionated.
(*9*) Foam fraction from (*6*).

of impurities was indicated by changes in the minimum and slope of the surface tension curve near the critical micelle region. Also, the lack of reproducibility of, and the time effects in, the surface tension determinations made on a particular solution gave an indication of purity. After performing the purification procedures outlined above, it was possible to obtain in

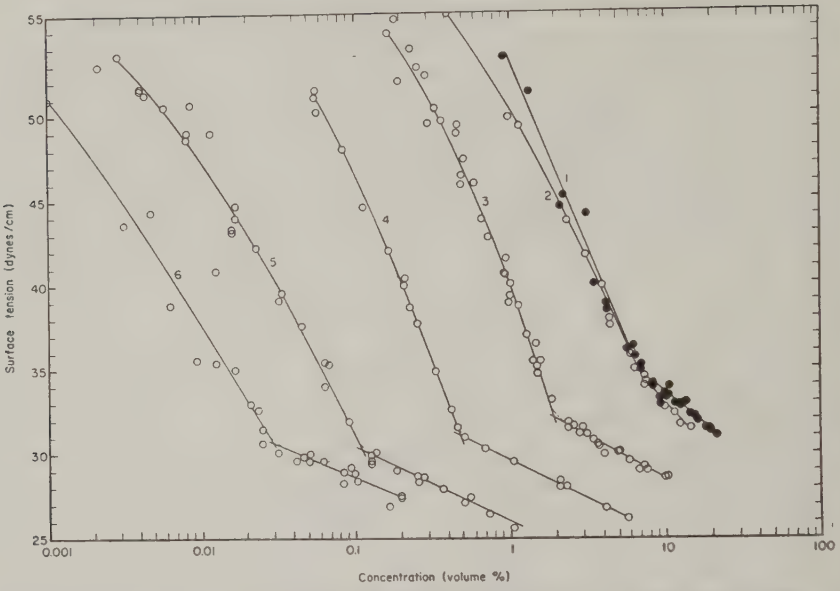

FIG. 2. Surface tension curves of dialkyl sodium sulfosuccinate below CMC, regression equation used. (*1*) *n*-Butyl; (*2*) Isobutyl; (*3*) *n*-Amyl; (*4*) *n*-Hexyl; (*5*) 2-Ethylhexyl; (*6*) *n*-Octyl.

TABLE I

Regression Equations

Butyl	$\gamma = 72.890 - 8.321\,\psi + 0.169\psi^2$;	(0.673 g. – 6.911 g./100 ml.)
Amyl	$= 57.233 - 3.921\,\psi - 1.536\psi^2$;	(0.167 g. – 1.868 g./100 ml.)
Hexyl	$= 46.527 - 8.495\,\psi - 0.858\psi^2$;	(0.0115 g. – 0.503 g./100 ml.)
IB	$= 63.351 - 4.303\,\psi - 0.596\psi^2$;	(0.161 g. – 6.292 g./100 ml.)
OT	$= 31.140 - 8.458\,\psi - 0.611\psi^2$;	(0.00106 g. – 0.0919 g./100 ml.)

γ = dyne/cm. $\psi = \ln_e(10c)$ c = g./100 ml.

a high state of purity, as indicated by physical and chemical determination, the following di-*n*-alkyl and branched-chain sodium sulfosuccinates: di-*n*-butyl, di-*n*-amyl, di-*n*-hexyl, di-*n*-octyl, diisobutyl (AEROSOL IB Surface Active Agent), and di-2-ethylhexyl (AEROSOL OT Surface Active Agent).

Surface tension curves of the above pure sulfosuccinates are presented in Fig. 2. The data for each agent below the critical micelle region have been treated by the mothod of least squares. The regression equation for each is given in Table I and the curves in Fig. 2 are drawn using these equations. The standard deviation for these measurements below the critical micelle region is ±0.45 dyne/cm.

D. Discussion of Surface Tension

It is evident from Fig. 2 that as the chain length of the alkyl group decreases, the critical micelle concentration is marked by a much less abrupt break in the surface tension curve. Thus in the case of the di-*n*-butyl derivative it is difficult to determine a critical micelle concentration. If we refer to a recent treatment of Debye (2), we note that a smaller chain length leads to a micelle containing a smaller number of monomer units. Unpublished work of this Laboratory, however, has shown that the formation of micelles starts at a concentration relatively lower with respect to the critical concentration for those agents of shorter chain length and thus micelle formation takes place over a more extended range.

An additional factor promoting the curvature up to the critical micelle region might be the occurrence of surface hydrolysis. The occurrence of such hydrolysis was described in earlier work from this Laboratory (3, 5) where the radiotracer technique was used to study the adsorption of the sodium and of the sulfosuccinate ions in solutions of di-*n*-octyl sodium sulfosuccinate. This work was carried out over a wide range of concentrations and showed that in dilute solutions surface hydrolysis occurred with little or no sodium ion being present in the surface. However, as the concentration increased toward the critical micelle region, the sodium replaced the hydrogen in the surface layer.

That these conditions would lead to a curvature of the surface tension curve becomes apparent when one considers the Gibbs adsorption equation in some detail:

$$d\gamma = -RT\sum_i \Gamma_i d \ln c_i$$

where γ is the surface tension, R and T have the usual significance, Γ_i is the surface excess in moles/cm.^{2} and c_i the bulk concentration of the i species. Concentration is used instead of activity, which is valid for the dilute concentration range under consideration.

For a dialkyl sodium sulfosuccinate ($\mathrm{Na}^+\mathrm{A}^-$) there is the possibility of A^-, Na^+, and H^+ adsorption in the monolayer; therefore

$$-d\gamma = RT\Gamma_{\mathrm{Na}^+}\, d \ln c_{\mathrm{Na}^+} + RT\Gamma_{\mathrm{A}^-}\, d \ln c_{\mathrm{A}^-} + RT\Gamma_{\mathrm{H}^+}\, d \ln c_{\mathrm{H}^+}$$

Since these agents are the sodium salts of strong acids and do not hydrolyze appreciably in dilute solution, the pH of the *bulk* solutions does not change markedly with changes in concentration;[2] hence $d \ln c_{\mathrm{H}^+} = 0$ and this term may be omitted. Stoichiometrically $d \ln c_{\mathrm{Na}^+} = d \ln c_{\mathrm{A}^-} = d \ln c_{\mathrm{NaA}}$. Therefore $\Gamma_{\mathrm{Na}^+} = \Gamma_{\mathrm{A}^-} = \Gamma_{\mathrm{NaA}}$ and $-\dfrac{1}{RT}\dfrac{d}{d \ln c_{\mathrm{NaA}}} = 2\Gamma_{\mathrm{A}^-}$

On the other hand, if H^+ is adsorbed rather than Na^+ then $\Gamma_{\mathrm{Na}^+} = 0$, $\Gamma_{\mathrm{H}^+} = \Gamma_{\mathrm{A}^-} = \Gamma_{\mathrm{HA}}$, and $-\dfrac{1}{RT}\dfrac{d}{d \ln c_{\mathrm{NaA}}} = \Gamma_{\mathrm{A}^-}$.

Thus to describe the surface tension curve for a particular agent mathematically, both of the equations shown above should be employed. If both conditions exist, a change in slope (curvature) in surface tension curve

---

[2] Checked experimentally by the authors.

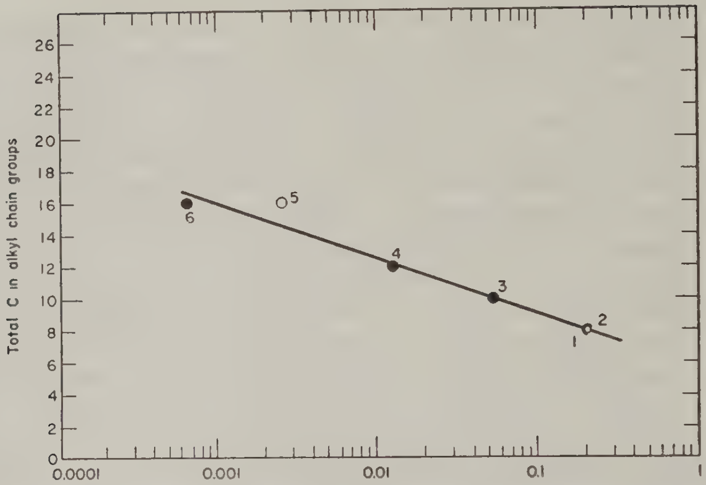

Fig. 3. Effect of chain length on critical micelle concentration (line drawn to Hobbs' equation log CMC = 0.290β − 1.63). (*1*) *n*-Butyl; (*2*) Isobutyl; (*3*) *n*-Amyl; (*4*) *n*-Hexyl; (*5*) 2-Ethylhexyl; (*6*) *n*-Octyl.

TABLE II

Critical Micelle Concentration (CMC) as a Function of Alkyl Chain Length

Compound	Molecular weight (theoretical)	CMC (*g./l.*)	CMC (*moles/l.*)
n-Butyl	332.351	67	0.20
n-Amyl	360.403	19.2	0.53
n-Hexyl	388.455	4.8	0.0124
n-Octyl	444.559	0.30	0.00068
Isobutyl	332.351	68	0.20
2-Ethylhexyl	444.559	1.12	0.0025

would not be unexpected. Therefore, the slight curvature obtained for the surface tension curves of the highly purified agents reported herein (see Fig. 2) in the region between the knee of the curves and the critical micelle region is given as experimental proof that surface hydrolysis does occur for all these agents.

Hobbs (4) has made a theoretical derivation of the following equation:

$$\log \text{CMC} = -0.290\,\beta - 1.63$$

where CMC is the critical concentration (mole/l.) and β is the number of carbon atoms in the alkyl chain group (for the sulfosuccinates, of course, it is the sum of the carbon atoms in the two alkyl chains). This equation was derived on the assumption that each charge on the micelle had an activity of roughly 0.5 *e*, where *e* is the charge on the electron. This assumption was made to take account of the work necessary to introduce an additional ion in the micelle surface layer with its associated ion atmosphere and the adsorbed oppositely charged ions. It is interesting to note that even with this assumption the experimental points for the straight-chain sulfosuccinates obey this equation. (See Fig. 3, Table II.) As one would expect, the CMC for the branched-chain sulfosuccinates occurs at higher concentration than the total number of carbon atoms in the alkyl chain would indicate, since the "effective" chain length is less than that of the straight-chain sulfosuccinate containing the same number of carbon atoms.

Acknowledgments

Acknowledgment is made to Miss Ellen Schiff for purifying some of these agents, to Mr. George F. Yates for carrying out the surface tension measurements, and to Dr. Robert De Baun and Miss Marcia Fuhrer for determining the regression equations.

References

1. Brady, A. P., *J. Phys. & Colloid Chem.* **53,** 56 (1949).
2. Debye, P., *Ann. N. Y. Acad. Sci.* **51,** 575 (1949).
3. Dixon, J. K., Judson, C. M., and Salley, D. J., "Monomolecular Layers," published by American Association for the Advancement of Science, 1954.
4. Hobbs, M., *J. Phys. & Colloid Chem.* **55,** 675 (1951).
5. Judson, C. M., Lerew, A. A., Dixon, J. K., and Salley, D. J., *J. Phys. Chem.* **57,** 916 (1953).
6. Miles, G. D., and Shedlovsky, L., *J. Phys. Chem.* **48,** 47 (1944).
7. Shedlovsky, L., *Ann. N. Y. Acad. Sci.* **49,** 279 (1948).
8. Shedlovsky, L., Ross, J., and Jakob, C. W., *J. Colloid Sci.* **4,** 25 (1949).
9. U. S. Patent 2,441,341.

JOURNAL OF COLLOID SCIENCE **12**, 460–464 (1957)

ON THE MEASUREMENT OF CONCENTRATION GRADIENTS IN THIN FILMS

S. H. Bauer

Department of Chemistry, Cornell University, Ithaca, New York

Received March 19, 1957

Professor F. A. Long pointed out to me an interesting problem which follows the solution of the rather difficult equations for diffusion of low molecular weight molecules into thin polymer sheets (1). What experimental procedures are available for checking directly the computed variation of concentration of the diffusing species with depth, $c(x)$? One possibility which appears to be simple experimentally is suggested in this note.

Label the diffusing species with a radioactive tracer which emits "soft" radiations, H^3, S^{34}, or C^{14}. At the termination of the diffusion period scan the intensity of radiation by means of a narrow angular aperture counter, as a function of the angle measured from the normal to the film surface. The desired function $c(x)$ may be computed by inverting an integral equation for $N(1/\cos\theta)$, as demonstrated below.

Refer to Fig. 1. The counter is pivoted about a line in the surface, at $x = 0$. Neglect for the present the matter of finite resolution in angle, $\Delta\theta$, and consider first the umbra ($abcd$) seen by the collimator. Its area is $z_0y_0/\cos\theta$, at any depth x. The effective solid angle of counter seen by an element of volume ($dxdydz$) in that layer is $z_0y_0/\left[4\pi\left(2A + B + \dfrac{x}{\cos\theta}\right)^2\right]$. Now, if there are n_0 disintegrations expected at that instant, at unit initial concentration, per unit volume, per unit time, then for the entire film depth the number of such disintegration products passing into the counter per unit time at an angle θ, due to the umbra is:

$$N_U\left(\frac{1}{\cos\theta}\right)$$
$$= 4n_0\int_0^{z_0/2} dz\int_0^{y_0/2\cos\theta} dy\int_0^{x_0} dx\, c(x)e^{-\mu x/\cos\theta}\,\frac{z_0y_0}{4\pi\left(2A + B + \dfrac{x}{\cos\theta}\right)^2}.$$

Here μ is the specific linear absorption coefficient of the polymer for the radiation emitted. It is assumed that the region between the film and the counter is nonabsorbing, that secondary scattered radiation does not get by the collimator, and, of course, that the concentration is a function of depth only.

The fact that the counter admits radiation over a finite angle, such that $\tan \Delta\theta = y_0/2A \doteq \Delta\theta$, reduces the resolution of this experiment. This appears in two places:

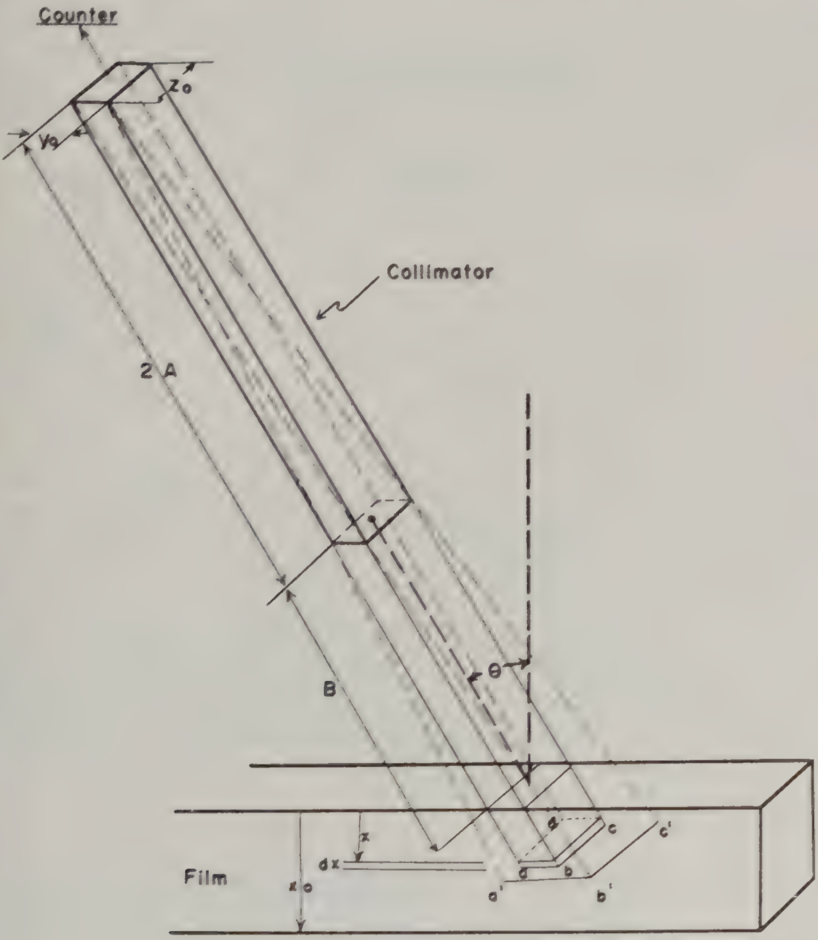

FIG. 1.

a). The counter sees a region of the sheet dx at x which is larger than the umbra delineated by ($abcd$).

b). The contribution from each element of volume $dzdydx$ should be weighted by $\exp\left[-\mu x/\cos(\theta + \delta\theta)\right]$ and integrated over $\Delta\theta$ around each θ, rather than by the average factor $\exp\left[-\mu x/\cos\theta\right]$ used above. The correction for the radiation which gets into the counter due to the penumbra is readily introduced. The latter extends from $a' \to b' \to c' \to d'$ with total dimensions

$$z_0 \left(\frac{A + B + \dfrac{x}{\cos\theta}}{A} \right) \cdot \frac{y_0}{\cos\theta} \left(\frac{A + B + x/\cos\theta}{A} \right) \left(\frac{1}{1 + (y_0/2A)\tan\theta} \right).$$

This gives:

$$N_{PU}(\alpha) = \frac{4n_0}{\mu} \int_{z_0/2}^{z_0\epsilon} dz \, \frac{(1 + A/B)\, z_0 - (2A/B)z}{\sqrt{4\pi}\,(2A + B + x\alpha)}$$
$$\cdot \int_{y_0\alpha/2}^{y_e} dy \left\{ y_0 + \frac{1}{\gamma} \frac{y - y_0\alpha/2}{y - \beta/\sin\theta} \right\} \times \frac{1}{\sqrt{4\pi}\,(2A + B + x\alpha)}$$
$$\cdot \int_0^{\beta_0} d\beta \; c(\beta/\mu) e^{-\alpha\beta}.$$

$$\alpha \equiv \frac{1}{\cos\theta}; \qquad \epsilon \equiv (A + B + x/\cos\theta)/2A; \qquad \gamma = \tan\theta/2A;$$

$$y_e = \frac{y_0\,\epsilon\alpha}{1 + y_0\gamma}; \qquad \beta \equiv \mu x; \qquad \beta_0 = \mu x_0.$$

Note that since $x_0 \cong 10^{-2}B$, for $\theta < 80°$ $(\alpha\beta/\mu)$ is negligible compared to B or $(A + B)$. Hence $\epsilon \cong B/2A$, etc. This is valid even when x_0 is very large, provided μ is sufficiently large; i.e., for very soft radiation only emanations from the top thin layer of material get out.

$$\frac{1}{\alpha} N(\alpha) = \tfrac{1}{2}(N_U + N_{PU}) = \frac{G}{\mu} \int_0^{\beta_0} c(\beta/\mu) e^{-\alpha\beta} \, d\beta \qquad [1]$$

is the integral equation to be inverted. Here G is, for all practical purposes, a geometric factor provided θ does not approach $\pi/2$.

$$G = \frac{n_0}{4\pi} \frac{z_0^2 y_0^2}{(2A + B)^2} + \frac{n_0}{4\pi} \frac{z_0^2 (B/A)}{2(2A + B)^2}$$
$$\cdot \left\{ (y_0^2 + y_0/\gamma) \left(\frac{1 + B/A}{1 + y_0\gamma} - 1 \right) \right.$$
$$\left. \times \frac{1}{\gamma} (B/2A - y_0) \ln \left(\frac{y_0\alpha \dfrac{1 + B/A}{1 + y_0\gamma} - 2B/\sin\theta}{y_0\alpha - 2B/\sin\theta} \right) \right\}.$$

The contribution due to the penumbra diminishes when (B/A) is made small, as expected, and the angular dependence of G is small except for large angles. In Eq. [1] μ and β_0 are parameters of the experiment and

$N(\alpha)$ is the measured corrected counting rate. Obviously, any computed $c(x)$ can be readily checked this way, as can the sensitivity of this method.

The computation of loss in resolution due to item (*b*) is considerably more involved. However, if one starts with the condition that

$$y_0/(2A + B) \ll 1,$$

a simplified treatment permits one to estimate an order of magnitude. To this approximation treat the radiation from all elements *dxdydz* for any specified x, as being uniformly modulated. Thus, in the umbra, for any such element, the maximum range in absorbing path allowed is that which corresponds to $\pm\phi$ in the vicinity of θ:

$$\tan \phi = \frac{\sqrt{y_0^2 + z_0^2}}{2A + B} \doteq \phi.$$

Thus at any θ, the intensity which reaches the counter, due to a layer dx at x, is to a first approximation given by an average absorption:

$$\frac{n_0 z_0^2 y_0^2}{4\pi(2A + B)^2} \frac{c(x)}{2\phi} \int_{-\phi}^{+\phi} e^{-\mu x/\cos(\theta+\nu)}\, d\nu \doteq \frac{n_0 z_0^2 y_0^2}{4\pi(2A + B)^2} c(x) \frac{e^{-\mu x \alpha}}{2\eta}$$
$$\cdot \left\{ (e^{+\eta} - e^{-\eta}) + \frac{2\alpha^2 - 1}{\alpha(\alpha^2 - 1)} \left(\frac{e^{-\eta} - e^{+\eta}}{\mu x} + \sqrt{\alpha^2 - 1}\,\phi[e^{-\eta} + e^{+\eta}] \right) \right\},$$

where

$$\eta \equiv \mu x \alpha \sqrt{\alpha^2 - 1}\, \frac{\sqrt{y_0^2 + z_0^2}}{2A + B}.$$

For good resolution, i.e., when ϕ is very small, the leading term reduces to that used initially for the idealized case. For the contribution from the penumbra, a somewhat larger angular range must be considered. The maximum departure from θ can be $\pm\psi$, where

$$\tan \psi = \frac{\sqrt{y_0^2 + z_0^2}}{2A} \doteq \psi.$$

A strictly similar analysis follows.

It is clear that unless the experiment is set up with inherently good resolution, the corrections which must be introduced get so involved that it becomes dubious whether the suggested scan with angle can lead to meaningful data for inversion. Two additional points should be made. First, although the counting efficiency may be low when a single narrow-angle collimator is used, a number of such tubes may be stacked in parallel to produce "Soller slits"; the counting rate will then be proportional to that number with no loss in resolution. Second, the assumed exponential decay law may not give the correct decrement with thickness (2), particularly when "soft" emitters are used, and the corrections listed above are considered. The proper absorption law may be checked by counting at a selected α films of different thicknesses which have been exposed to the diffusing species for so long a time as to make $c(x) = c_0$. Then

$$\frac{1}{\alpha} N(\alpha) = \frac{Gc_0}{\mu} \int_0^{\beta_0} F(\alpha\beta)\, d\beta; \tag{2}$$

$$\frac{d}{d\beta_0}\left[\frac{1}{\alpha} N(\alpha)\right] = \frac{Gc_0}{\mu} F(\alpha\beta_0). \tag{3}$$

The inversion of [1] or of the corresponding Eq. [2] with the experimentally determined kernel [3] can be carried out via the approximation methods developed by Zemanian (3).

REFERENCES

1. PRAGER, S., *J. Chem. Phys.* **19,** 537 (1951).
2. KATZ, L., AND PENFOLD, A. S., *Revs. Mod. Phys.* **24,** 28 (1952).
3. ZEMANIAN, A. H., *J. Appl. Phys.* **25,** 262 (1954).

JOURNAL OF COLLOID SCIENCE **12**, 465–479 (1957)

EFFECT OF THE CATION ON MICELLE FORMATION BY SULFONATES IN BENZENE[1]

Samuel Kaufman and C. R. Singleterry

Chemistry Division, U. S. Naval Research Laboratory, Washington 25, D. C.

Received May 21, 1957

ABSTRACT

The states of aggregation of dinonylnaphthalene sulfonates of ten cations (Li, Na, Cs, NH_4, Mg, Ca, Ba, Zn, Al, and H) have been studied in benzene by fluorescence depolarization, cryoscopy, viscometry, and densimetry. The micelles observed by fluorescence depolarization contained 9 to 14 acid residues each. Their aggregation number was usually independent of concentration and almost independent of the water content of the system, although moisture moderately increased the aggregation of the zinc salt. The relative insensitivity of the sulfonate micelle size to influences of the cation and moisture contrasts sharply with the behavior of the phenylstearate soaps, whose aggregation depends critically upon these variables. This indicates that the size of the dinonylnaphthalene sulfonate micelles depends primarily on the geometry of the acid residue. However, the apparent volume of the anion was inversely related to the coordinating tendency of the cation, suggesting that coordination forces are a factor in micelle stability. The acid is associated principally to the dimer, but in the presence of water some larger aggregates are formed.

Viscosities of the sulfonate solutions exceeded those predicted by the Einstein relation for spherical particles. This anomaly corresponded to an asymmetry of the order of 2, or a solvation of 10% to 20%. It might also have resulted from surface irregularities of the micelles. Present evidence does not justify a choice among these explanations.

Cesium dinonylnaphthalene sulfonate was shown cryoscopically to have an aggregation number of 6 or more. It differed from the other micelle-forming sulfonates, however, in not solubilizing enough Rhodamine B to permit determination of micelle size by the fluorescence depolarization technique. The micelle size found cryoscopically for the magnesium salt agreed with that derived from fluorescence depolarization measurements.

INTRODUCTION

Micelle formation by barium and sodium dinonylnaphthalene sulfonates in benzene has been described previously (1). The micelles were found to be small and to predominate at concentrations greater than 10^{-6} mole of sulfonate per liter. Evidence was presented to indicate that these sulfonate micelles were approximately isodimensional and that their size was not strongly dependent on the water content of the system. These latter results contrast strongly with those reported for the phenylstearates of seven alkali and alkaline earth elements (2–4), which form extensive linear aggregates, the size and stability of which, in the presence of water, alcohols, or acids depend upon the specific cation present. To ascertain whether this difference between the behaviors of sulfonates and carboxylates in benzene is general, the dinonylnaphthalene sulfonates of eight additional cations have been studied by the fluorescence depolarization and cryoscopic techniques.

---

[1] Presented before the Symposium on the Structure of Micellar Solutions, Division of Colloid Chemistry, 131st meeting of the American Chemical Society (April 7–12, 1957, Miami, Florida).

The cations investigated were lithium, sodium, cesium, ammonium, magnesium, calcium, barium, zinc, aluminum, and hydrogen. Primary data from the fluorescence measurements reported previously for the sodium and barium compounds are combined with the new data. For all ten compounds precise measurements have been made of the apparent volume and the viscometric contribution of the sulfonate in dilute benzene solutions.

EXPERIMENTAL

Materials

The sulfonates described here were prepared by metathesis or by neutralization of a naphtha solution of a special grade of dinonylnaphthalene sulfonic acid (HDNNS). This acid and its sodium and barium salts (NaDNNS and $Ba(DNNS)_2$) have been described previously (1). In each case, after completion of the preparative reactions, the compound was isolated from all but traces of alcohol and naphtha by repetitive dilution in benzene and evaporation at reduced pressure. Final preparation for storage comprised filtration of a benzene solution of the substance and lyophilization in ampoules (1). During the lyophilization, when evolution of solvent vapors appeared to cease, the temperature was cautiously raised to a maximum below the softening point of the compound to expel residual traces of moisture, alcohol, or high-boiling fractions of naphtha. When there was evidence of appreciable alcohol or naphtha evolved at this stage, the lyophilization was repeated. The compounds were sealed under nitrogen and refrigerated until used.

It was observed that before preparation of the salts a further purification of the acid could be effected by mixing its naphtha solution with an equal volume of methanol. The mixture separated readily into two liquid phases, the upper layer being darker and comprising about 8% of the combined volume. This phase, which was rejected, contained about 4% of the nonvolatile matter of the original HDNNS solution, but only 0.2% of its acid. The neutral rejected matter is believed to be unsulfonated hydrocarbon or inert resinous matter of high molecular weight. This purification step was used in preparing the acid for direct study, and for use as a starting material in the preparation of the cesium, ammonium, magnesium, aluminum, and zinc salts. The remaining sulfonates were prepared prior to the development of this refinement.

The HDNNS used for direct study was purified as described, and freed of alcohol by repeated addition and evaporation of benzene. This acid is a highly viscous fluid at room temperature. Thus there was little advantage in raising its temperature higher than 25° to 30°C. during the final evacuation, because any residual solvent could not escape readily from the viscous mass. Further, the concentrated acid is subject to decomposition at elevated temperatures. The final pressure during lyophilization was 3 μ Hg.

Cesium and ammonium dinonylnaphthalene sulfonates (CsDNNS and NH_4DNNS) were prepared by potentiometric titration of the acid solutions (diluted with isopropanol and methanol, respectively) with aqueous solutions of the respective bases, with appropriate precautions for exclusion of carbon dioxide. In both cases a small quantity of gelatinous precipitate formed at the approach to neutrality. The solid was separated centrifugally and was found to contain aluminum, iron, and silica, probably derived from containers during preparation and storage. Ultimate temperature and pressure in lyophilization were: for CsDNNS, 96°C. and 2 μ Hg; and for NH_4DNNS, 60°C. and 7 μ Hg. Analyses: Cs, 21.6 %(theory 22.43 %); N, 2.85 % (theory 2.93 %).

Lithium and calcium dinonylnaphthalene sulfonates (LiDNNS and $Ca(DNNS)_2$) were prepared by neutralization of the acid by solid LiOH and CaO, respectively. The HDNNS solution was diluted with isopropanol and a quantity of water which was soluble in the mixture, then agitated with the appropriate base until the solution was alkaline. The mixture was back-titrated with HDNNS, using an external indicator, and then centrifuged to clarity. Ultimate temperatures and pressures during lyophilization were: LiDNNS, 80°C. and 10 μ Hg; $Ca(DNNS)_2$, 88°C. and 10 μ Hg. Analyses: Li, 1.48 % (theory, 1.49 %); Ca, 4.19 % (theory, 4.18 %).

Magnesium dinonylnaphthalene sulfonate ($Mg(DNNS)_2$) was prepared by successive equilibrations of HDNNS with a methanolic solution of $MgCl_2 \cdot 6H_2O$ and subsequent addition of water, which caused a separation of phases. The aqueous layer, which was rejected, contained HCl formed in the reaction. The hydrocarbon phase was washed free of chloride ion with water, and potentiometrically titrated to neutrality with a small quantity of saturated aqueous $Mg(OH)_2$ solution. Ultimate temperature and pressure during lyophilization were 90°C. and 3 μ Hg. Analysis: Mg, 2.47 % (theory, 2.56 %).

Aluminum dinonylnaphthalene sulfonate ($Al(DNNS)_3$) was prepared by metathetic reaction between $Al_2(SO_4)_3$ and NaDNNS. The NaDNNS used for this reaction was made by neutralization of the acid with NaOH by the procedure described for CsDNNS, in which a small quantity of impurity was rejected as a gelatinous precipitate. The NaDNNS was diluted with isopropanol and water, and equilibrated with successive portions of aqueous $Al_2(SO_4)_3 \cdot 18H_2O$. The mixture separated into two phases, and the aqueous layer was rejected. The hydrocarbon phase was washed free of sulfate ion with water. Ultimate temperature and pressure during lyophilization were 80°C. and 1 μ Hg. Analysis: Al, 1.87% (theory, 1.93% for $Al(DNNS)_3$). Aluminum tri-salts of carboxylic acids cannot be prepared by metathesis in the presence of water; the ready preparation of the trisulfonate was to be expected from the greater acid strength of HDNNS.

Zinc dinonylnaphthalene sulfonate ($Zn(DNNS)_2$) was prepared analogously to $Al(DNNS)_3$. Ultimate temperature and pressure during lyophilization were 85°C. and 1 μ Hg. Analysis: Zn, 6.30% (theory 6.63%).

Discrepancies between theoretical and analytical values of cation content of the sulfonates described above are attributed to traces of unsulfonated hydrocarbon or to the presence in the alkylnaphthalene of some hydrocarbon of higher molecular weight. Deviations from theoretical values are reasonably consistent with this assumption. Tests of the salts indicated that they were precisely neutral.

The benzene and Rhodamine B used in this study have been described previously (1).

Measurements

The methods used for measurements of fluorescence and spectral absorption have been described previously (1, 5, 6).

Densities of liquids were determined in duplicate at 25 ± .003°C. with a 10 ml. modified Ostwald-Sprengel pycnometer capped at both ends, using a matched counterpoise. The average observed difference in weight between the duplicates was 0.16 mg. Observed weights were corrected for atmospheric buoyancy. From the solution density, the sulfonate and water concentrations, and the observed density of the anhydrous benzene, the apparent density of the dissolved sulfonate was computed. The average concentration of these sulfonate solutions was about 1 gram per 100 ml.

Viscometric observations were made in triplicate or quadruplicate at 25 ± .003°C. in an Ostwald-Fenske series 50 viscometer. Flow times were approximately 220 seconds, and the average maximum difference between any two observations of flow time for a given liquid was 0.1 second. The maximum difference was 0.2 second.

Observations of both density and viscosity for each liquid were made on portions taken from the same batch of solution. Relative uncertainties in concentrations were of the order of 0.01%. To preclude interferences from minute particles of lint or other solid in the determinations of flow time, each liquid was filtered through a Millipore filter whose effective pore size is rated at 0.45 μ.

Cryoscopic observations were made as described in an earlier publication (7).

RESULTS AND DISCUSSION

Fluorescence Depolarization

The results of fluorescence depolarization measurements, interpreted in terms of the corresponding volumes of spherical micelles, are presented graphically with respect to concentration in Fig. 1 for the eight compounds amenable to investigation by this technique. The curves represent data on solutions containing 0.5 mole (3.0 moles for NaDNNS) of water per equivalent of sulfonate plus 15% of the water required to saturate the benzene present. This procedure was established arbitrarily to provide a systematic water content which was low, yet sufficient to make the system insensitive to exchanges of trace amounts of water with the environment during the measurements. By inspection of the best smooth curves through the data of Fig. 1, representative values of the gram micelle volumes were selected. The aggregation number (expressed as acid residues per aggregate) was computed for each compound from the micelle volume, the apparent den-

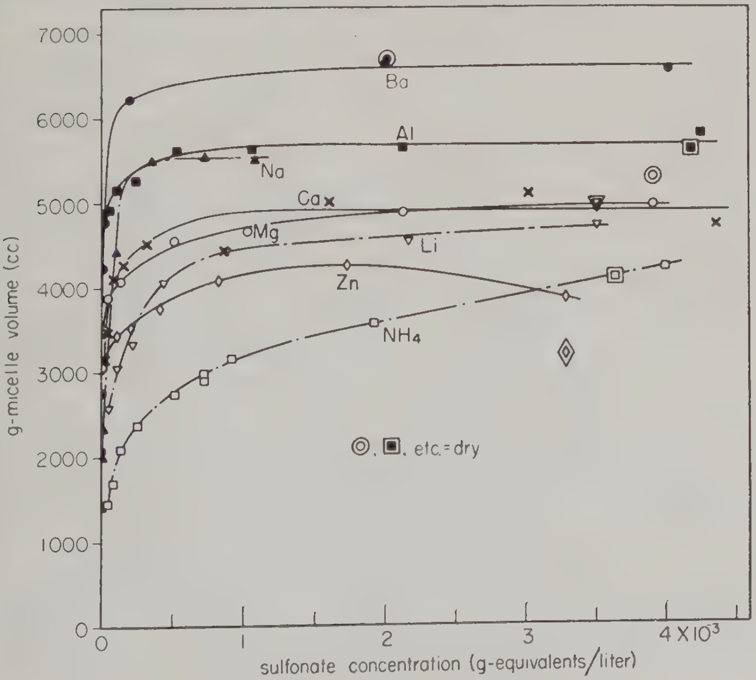

FIG. 1. Micelle size of dinonylnaphthalene sulfonates.

TABLE I

Summary of Properties of the Dinonylnaphthalene Sulfonates

Cation	Equivalent wt.	Apparent density (g./ml.)	Gram-micelle volume (c.c.)	Aggregation number $\left(\frac{\text{acid residues}}{\text{aggregate}}\right)$
Li	466.63	1.055	4700	10
Na	482.69	1.079	5530	10
Cs	592.60	1.293	—	6[a]
Mg	471.85	1.096	4950	11
Ca	479.73	1.094	4900	10
Ba	528.37	1.189	6600	14
Zn	492.38	1.126	3200–5150	7–10
Al	468.68	1.088	5660	13
NH_4	477.73	1.045	4200	9
H	460.70	1.039	—	2[a]

[a] Minimum possible aggregation number from cryoscopic results.

sity of the salt, and the total water content of the system, with the assumption that all water present was associated with the micelle. The pertinent data appear in Table I.

It is evident from Fig. 1 and Table I that in the concentration range between 2×10^{-4} and 4×10^{-3} equiv. per liter the micelles of salts of these widely varying cations fall within a rather narrow range of 9 to 14 acid residues per micelle. The acid itself and possibly cesium sulfonate, neither of which was a satisfactory subject for fluorescence depolarization measurements, are exceptions. In most cases the micelle size found is remarkably constant over a 20-fold concentration range. At high concentrations the apparent micelle volume approaches a limiting value which is considered the actual micelle size. In the very dilute range the apparent micelle size falls off in a way which has been attributed earlier (1) to the presence of a small amount of the dye in the form of a nonmicellar dye-sulfonate complex. Analysis of the data shows that for all the sulfonates of Fig. 1 except the ammonium salt micelles were certainly present at concentrations as low as 10^{-5} equiv. per liter, although the actual cmc's were not established.

The curve for ammonium sulfonate is atypical in that it develops no plateau in the concentration range studied. It was suspected that this behavior resulted from appreciable dissociation in these dilute solutions to ammonia and the free acid, which interacts with the dye to form a colored and fluorescent, but nonmicellar compound. Addition of a 10% excess of ammonia, however, did not suppress the effect. (Double point on NH_4 curve of Fig. 1.) Further work will be required to explain these results.

The curve for the zinc salt is atypical in that the apparent micelle volume decreases with increasing concentration above 1.7×10^{-3} equiv. per liter. This trend is attributed to the arbitrary scheme for controlling the water content of these systems. Within experimental uncertainties micelle

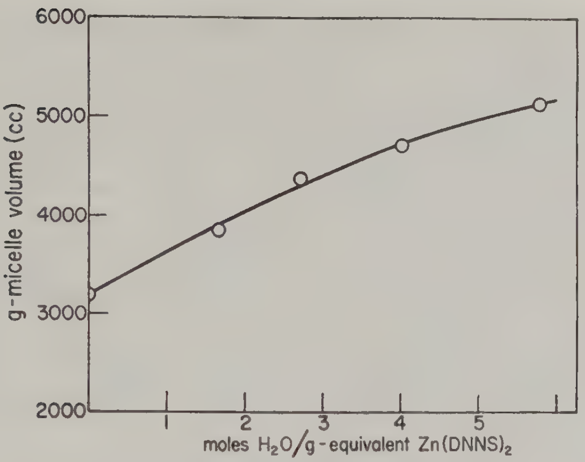

FIG. 2. Effect of water on size of $Zn(DNNS)_2$ micelles.

TABLE II

Effect of Moisture on Size of $Zn(DNNS)_2$ Micelles

Concentration: 3.3×10^{-3} g.-equiv./l.

Moles H_2O / g.-equiv. sulfonate	Observed g.-micellar volume (c.c.)	Expected g.-micellar volume (c.c.)	Observed increase / Expected increase
0	3192	3192	—
1.66	3856	3410	3.05
2.71	4379	3548	3.33
4.00	4724	3718	2.91
5.78	5156	3951	2.59

volumes were generally insensitive to the presence of moisture, as indicated in Fig. 1, where results for the dry systems are appropriately coded. However, the micelle volume in the anhydrous zinc sulfonate system is significantly less than that in the moist system. Therefore the effect of water was explored further by a study of the micelle volume of $Zn(DNNS)_2$ as a function of the total moisture present. The micelle size increased with increasing water-sulfonate ratio, as the plot in Fig. 2 demonstrates, but the effect is less marked beyond 4 moles of water per equivalent of salt. The observed increase in micelle size was approximately treble the total volume of water introduced per anhydrous micelle, as is shown in Table II. This corresponds to the entry of up to three more acid residues into each micelle as the system becomes moist. As the core of water forms and grows in the micelle, the geometry changes to permit each monomer to occupy a smaller solid angle of the swollen aggregate, thereby accommodating the entry of these additional monomer units. Similar but more pronounced growth of dioctyl sodium sulfosuccinate micelles on addition of water has been reported (8, 9). The shape of the $Zn(DNNS)_2$ curve may now be explained as follows. The $Zn(DNNS)_2$ micelles must be strongly hygroscopic, so that much more than 0.5 mole of water per equivalent of sulfonate is required to establish equilibrium with a benzene solvent 15% saturated with water. With decreasing sulfonate concentration, the water-sulfonate ratio increases without limit. In the more dilute solutions, therefore, the additional water may be taken from the solvent phase with a negligible change in the water content of the latter; the resulting high water content of the micelles leads to a relatively large size, in accordance with Fig. 2. With increasing sulfonate concentration, however, the water-sulfonate ratio approaches the limit 0.5. In a concentrated solution, therefore, the total water available from the solvent is insufficient to raise the water content of the micelles much above the original value of 0.5 mole per equivalent of sulfonate, and progressively smaller micelles result as one passes to higher concentrations of the sulfonate.

Cryoscopic Phenomena

Measurements of the micelle size of HDDNS and CsDNNS by the fluorescence depolarization method were attempted, but complications were encountered which made interpretation of the data uncertain. Several times the normal amount of Rhodamine B was required to develop measurable color and fluorescence in the solution. The absorption and emission peaks in the presence of both CsDNNS and HDNNS were ill-defined, and shifted so strongly in wavelength that the procedure for estimating the excited life of the dye (1, 5) became questionable.

To obtain more valid information concerning these two compounds, their benzene solutions were studied cryoscopically. The cryoscopic method was also applied to $Mg(DNNS)_2$, a sulfonate yielding well-defined data by the fluorescence depolarization method. This provided an independent validation of the optical method, supplementing the confirmation obtained earlier by osmotic pressure measurements (5).

The cryoscopic measurements were necessarily made on more concentrated (0.07 equiv. per liter) solutions than were studied optically. Determinations were made with the anhydrous solutions of all three compounds. Water was then dispersed ultrasonically in the solutions of HDNNS and $Mg(DNNS)_2$ for additional determinations immediately following measurements on the dry solutions. Despite the addition of water, which increased the solute content of the system, the observed freezing point of the wet HDNNS solution was higher than that for the anhydrous one. Further addition of water accentuated this effect. Addition of water to the anhydrous $Mg(DNNS)_2$ system depressed the freezing point, but only slightly in comparison to the amount theoretically expected from the independent cryoscopic effect of the water. Values for the degree of aggregation computed from the cryoscopic data appear in Table III. These values are

TABLE III

Cryoscopic Behavior of Dinonylnaphthalene Sulfonates

Cation	Aggregation number $\left(\frac{\text{acid residues}}{\text{aggregate}}\right)$		
	Anhydrous	$\frac{\text{1 Mole } H_2O}{\text{g.-equiv.}}$	$\frac{\text{2 Moles } H_2O}{\text{g.-equiv.}}$
Mg	11.5	8.8 (0.92)[a]	—
Cs	5.8	—	—
H	1.7	2.4 (0.63)[a]	2.6 (0.38)[a]

[a] Values in parentheses are predicted, assuming all water independently dispersed n the solvent.

derived with the assumption that none of the water is in simple solution, but is all bound to aggregates of sulfonate molecules. Quantities in parentheses represent the aggregation numbers to have been expected if all the water had been molecularly dispersed and cryoscopically active, but the total freezing point depression had been attributed to the sulfonate in calculating the aggregation number.

It is clear that the assumption of association of water with the aggregates of sulfonate molecules is substantially valid. The cryoscopic and optical results with $Mg(DNNS)_2$ are in satisfactory agreement, deviating from each other by less than one acid residue per micelle in the anhydrous solution. For the moist condition the cryoscopic value of 8.8 is somewhat lower than 11, found optically, but this deviation could easily result from the oversimplified assumption that all the water is in the micelle. Had all the water been dispersed molecularly in the benzene, the aggregation number found cryoscopically would have been 0.92; the observed aggregation number of 8.8 corresponds to the independent cryoscopic activity of 3% of the water present in the system.

Aggregation numbers derived cryoscopically for the acid strongly suggest dimerization in the anhydrous solution. The value 1.7 is consistent with an equilibrium in which about 20% of the acid is monomeric and 80% is dimeric. Water, however, associates itself with the acid and also clearly increases the degree of aggregation, as the results in Table III demonstrate. The equilibrium concept requires that at least a small fraction of the water be independently dispersed, but it is evident that most of it is associated with the acid in such a manner as to increase the aggregation tendency of the latter. Although the optical results for HDNNS cannot be considered definitive, the combination of data from both sources could be taken to imply that the hydrated acid could form an aggregate of more than two molecules by a hydrogen-bonding mechanism. The wet HDNNS system could then be considered to contain monomer and dimer and a few larger units in equilibrium.

Exact agreement between the results of fluorescence depolarization and cryoscopic measurements, which in this case refer to temperatures 20 degrees apart, is not to be expected if the association equilibrium is temperature-sensitive.

Although the questionable fluorescence depolarization data for the cesium sulfonate indicated that the dye was present only as free molecules or as a 1–1 complex with the sulfonate (volumes of 450 to 650), the cryoscopic data indicate an average aggregation number of 5.8 in the anhydrous solution. The cesium sulfonate micelles, then, differ from those of the other salts studied in being unable to solubilize and activate Rhodamine B to fluorescence. A similar lack of affinity for Rhodamine B has been noted for cesium phenylstearate (3). It appears that the polar forces within the cesium-containing micelles are weaker or different in nature from those encountered in the other micelles examined. This may result because the cesium ion has the least tendency to coordination of all cations included in this study. The cryoscopic aggregation number of 5.8 is a minimum value because it averages the effect of any molecularly dispersed solute present.

Viscometric Properties

In the foregoing presentation, particle sizes were derived from fluorescence depolarization measurements on the assumption that the micelles were smooth unsolvated spheres. This assumption may be questioned, and to assess its uncertainty all the sulfonates were studied viscometrically in moist benzene solution. The moisture level was controlled systematically by the same formula used in the optical study. The resulting data were used to compute asymmetry functions in a manner described by Honig and Singleterry (3), who used the mathematical treatment originated by Simha (10, 11). The asymmetries are listed in Table IV and are expressed as the ratio, J, between the major and minor axes of prolate ellipsoids of revolution. The axial ratios found ranged from 1.85 to 2.56. It was impractical to

TABLE IV

Viscometric Behavior of Dinonylnaphthalene Sulfonates

Cation	Concentration $\left(\frac{\text{grams}}{100\text{ ml.}}\right)$	Viscosity ratio $\frac{\eta}{\eta_0}$	Viscosity number $\frac{\eta - \eta_0}{\eta_0 c}$	Axial ratio J
Li	1.0682	1.031	2.86	2.05
Na	0.6668	1.018	2.74	1.95
Cs	0.9619	1.022	2.33	2.02
Mg	1.0977	1.033	3.04	2.45
Ca	1.4140	1.039	2.78	2.08
Ba	0.9717	1.024	2.43	1.85
Zn	0.9668	1.028	2.92	2.38
Al	0.9428	1.030	3.15	2.56
NH_4	1.0233	1.032	3.16	2.41
H	1.0111	1.030	3.01	2.19

measure viscosities at decreasing concentration for extrapolation to the limiting viscosity number (12) because of the uncertainty as to comparability of the micellar water contents, as well as because of the low viscosity ratios encountered. It has been estimated (3) that in solutions having viscometric properties and concentrations similar to those studied here the viscosity numbers differ from the values at infinite dilution by less than 3%.

If the viscometric behavior is considered to reflect exclusively a departure from sphericity, all the axial ratios found lie essentially between 2.45 and 1.85, which are the values for $Mg(DNNS)_2$ and $Ba(DNNS)_2$, respectively. Methods for computing the volume of a prolate ellipsoid of given asymmetry from fluorescence data have been discussed in the literature (3, 13). Applying the necessary equations to the data for the magnesium compound, the gram micelle volumes computed for the ellipsoids and spheres are 3410 and 4950, respectively; the barium system yields values of 5410 and 6560, respectively. The differences between the volumes of the spheres and ellipsoids in these two extreme cases correspond to differences of 2 to 3 acid residues per micelle. Comparable discrepancies would prevail for the other species excepting the cesium salt and the acid, for which no suitable optical results were obtained.

There is no conclusive evidence that the viscometric behavior is strictly a manifestation of particle asymmetry. The same behavior could be exhibited by solvated spherical micelles. If it is assumed that the departure from the Einstein behavior for smooth spheres results strictly from solvation of the spheres by benzene, 23% and 11% of the micelle volume must be assigned to solvation for $Mg(DNNS)_2$ and $Ba(DNNS)_2$, respectively. These percentages correspond approximately to 13 and to 8 benzene molecules per micelle. The radii of the micelles computed from the optically determined volumes were 12.5 A and 13.8 A, respectively. The solvation estimated is sufficient only to form enveloping sheaths 1.0 A and 0.5 A thick, respectively, considerably less than 2.3 A, the thickness of a benzene molecule. If, on the other hand, the solvate molecules are intercalated with the DNNS radicals in the micelle structure the number of solvate molecules is comparable with the number of sulfonate molecules present.

Another shape factor which might be responsible for the observed behavior is the presence of surface irregularities resulting from the nonyl groups attached to the naphthalene nuclei of the sulfonate. If these highly branched groups are extended radially, rather than folded down to present a smoothly curved surface, such protrusions would increase the viscous interaction between micelle and solvent both because of the greater surface exposed and because of the larger maximum dimensions of the micelle.

The viscometric behavior, then, can be viewed as a manifestation of asymmetry, solvation, surface irregularities, or a combination thereof. Although the available evidence does not permit definitive assessment of

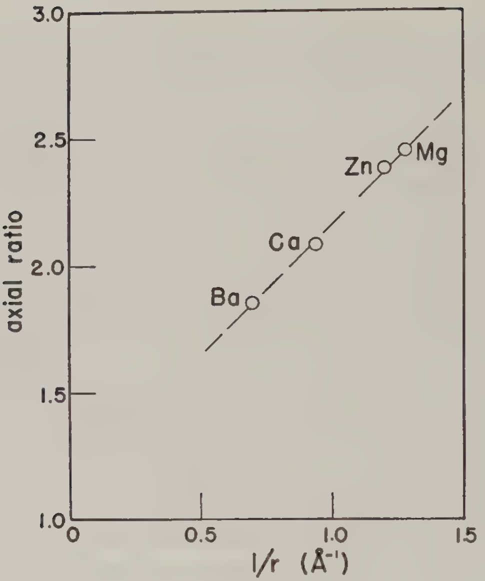

FIG. 3. Correlation of asymmetry with radius of cation.

the relative importance of each factor, the data suggest that asymmetry makes a major contribution. For the divalent cations, the axial ratio computed from the viscosity data increases linearly with the reciprocal of the cation radius, *r* (Fig. 3). Such an increase may be conceived to result from the increase in lateral pressure in the hydrocarbon sheath of the micelle as the polar core is contracted, because of smaller cationic radius and greater coordinating forces. It has been pointed out elsewhere (14) that such a lateral compression may be relieved by a change in micelle shape from spherical to ellipsoidal, and that for a given value of *J* the prolate form provides a greater increase in surface-to-volume ratio than the oblate. The existence of such a lateral compression in the hydrocarbon portion of the micelle is demonstrated by the data on the apparent volume of the anion when combined with various cations, as reported below.

It is also recognized that there is doubt (15, 16) concerning the validity of the Einstein equation and Perrin's equations (17) for rotational diffusion for particles as small as those studied here. As the particle size of the solute approaches that of the solvent molecules the solvent can no longer be considered a continuum. Sadron (18) suggests that the equations are valid if the ratio of solute to solvent dimensions is greater than 10. The ratio for the systems studied here is about 4.

However, the results derived independently by cryoscopic and optical methods agree very satisfactorily in the case of the $Mg(DNNS)_2$ solutions. The cryoscopic effects are independent of particle shape or particle size ratio, and effectively independent of solvation in the concentration studied. The agreement therefore indicates that the results obtained by the fluorescence depolarization method with the simple assumption of spherical par ticles are valid within the limits of experimental uncertainty.

Honig and Singleterry (2–4) found viscosity numbers of the phenylstearate micelles in moist benzene to vary over a wide range as a function of the water-soap ratio and the cation. The anhydrous alkali phenylstearates formed increasingly viscous systems with decreasing radius of the cation and the reverse was true of the alkaline earth compounds. The viscosity effects, which were extremely moisture-sensitive, were interpreted to be a manifestation of extensive linear aggregation. The size of the dinonylnaphthalene sulfonate micelles, on the other hand, was comparatively insensitive to the water content or the cation present.

Apparent Volume of the Anion

The density measurements required for the computation of aggregation numbers from the optically determined micelle volumes were made with more refinement than was required for this purpose. The more exact data permitted calculation of precise apparent equivalent volumes of the sulfonates and the sulfonate ions in the aggregated state. The latter value was derived from the former by subtracting the volume of the cation in the crystalline state, in accordance with the method used by Honig and Singleterry (3). Further study of crystal data has shown that the volume estimated for a given cation by this method is relatively independent of the anion or the crystal system taken.

The results of these calculations are summarized in Table V. In Fig. 4, the apparent gram equivalent volume of the dinonylnaphthalene sulfonate ion is plotted against the reciprocal of e^2/r for the cation present, where e and r are the charge and radius of the cation, respectively. Born (19) suggests e^2/r to be proportional to the energy of solution (hydration) of

TABLE V

Apparent Volumes of the Dinonylnaphthalene Sulfonate Ion

Cation	Ionic radius (A)	Crystal data used	Vol. assigned to cation (c.c./g.-ion)	Vol. assigned to anion (c.c./g.-ion)
Li	0.78	LiF	1.6	440.6
Na	0.98	NaF	4.2	443.2
Cs	1.65	CsF	21.4	437.0
Mg	0.78	MgF_2, MgS	1.8	429.6
Ca	1.06	CaF_2, CaS	5.0	436.1
Ba	1.43	BaF_2, BaS	13.7	437.5
Zn	0.83	ZnF_2, ZnS	2.3	436.1
Al	0.83	Al_2O_3	1.7	430.2
NH_4	1.42	NH_4Cl	11.3	445.9
H	—	—	(3.)	440.5

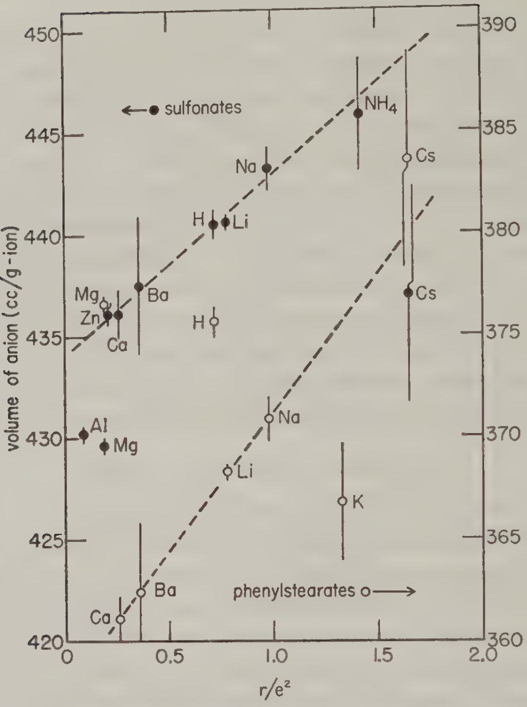

FIG. 4. Effect of the cation on the apparent volume of the dinonylnaphthalene sulfonate ion.

gaseous spherical ions; the stability of coordination complexes is also proportional to this quantity (20). The data of Honig and Singleterry for the apparent molal volume of the phenylstearate ion (3) are also included in Fig. 4 (on a displaced scale) for comparison. The vertical bars associated with the data points correspond to ±25% uncertainty in the estimate of the cation volume.

Although there was only a 4% spread in the apparent anion volumes of the sulfonates, the data show a clear linear relation between the apparent anion volume and the reciprocal of e^2/r, except for deviations at the ends of the range studied. The less precise data for the phenylstearate soaps show a similar relation. The data of Fig. 4 indicate that for the sulfonates as well as the carboxylates coordination between metal ions and the oxygen of the anion plays a major but not necessarily an exclusive role in the formation of micelles in a hydrocarbon solvent. The differences in apparent volume of the sulfonate ion are visualized as compression effects resulting from the different coordinating energies of the cations binding the $—SO_3^-$ radicals together in the micelle core.

The data available are not adequate for an explanation of the pronounced deviation of aluminum, magnesium, and cesium sulfonates from the linear relation shown by the other compounds. Magnesium and cesium also exhibited anomalies in the carboxylate study, although the anion volumes deviated in the opposite direction from that found for the sulfonates. A part, at least, of the inconsistencies noted for these compounds may have resulted from unsuitable choice of the water content of the system. A minor error may have arisen from the oversimplified assumption (9) in the volume calculations that the density of the water present was that of bulk water at 25°C. The effective volume occupied by the water will certainly be less when it is strongly coordinated to an ion such as aluminum or magnesium.

References

1. Kaufman, S., and Singleterry, C. R., *J. Colloid Sci.* **10,** 139 (1955).
2. Honig, J. G., and Singleterry, C. R., *J. Phys. Chem.* **58,** 201 (1954).
3. Honig, J. G., and Singleterry, C. R., *J. Phys. Chem.* **60,** 1108 (1956); Report 4472, Naval Research Laboratory (1956).
4. Honig, J. G., and Singleterry, C. R., *J. Phys. Chem.* **60,** 1114 (1956).
5. Singleterry, C. R., and Weinberger, L. A., *J. Am. Chem. Soc.* **73,** 4574 (1951).
6. Kaufman, S., and Singleterry, C. R., *J. Colloid Sci.* **7,** 453 (1952).
7. Kaufman, S., and Singleterry, C. R., *J. Phys. Chem.* **56,** 604 (1952).
8. Mattoon, R. W., and Mathews, M. B., *J. Chem. Phys.* **17,** 496 (1949).
9. Mathews, M. B., and Hirshhorn, E., *J. Colloid Sci.* **8,** 86 (1953).
10. Simha, R., *J. Phys. Chem.* **44,** 25 (1940).
11. Simha, R., *Proc. Intern. Congr. Rheology,* Part II, 70 (1948).
12. The rheological nomenclature and notation used in this publication are those recommended by the International Union of Chemistry; *J. Polymer Sci.* **8,** 257 (1952).
13. Weber, G., *Biochem. J. (London)* **51,** 145 (1952).
14. Singleterry, C. R., *J. Am. Oil Chemists' Soc.* **32,** 446 (1955).
15. Smyth, C. P., *J. Phys. Chem.* **58,** 580 (1954); *J. Am. Chem. Soc.* **78,** 20 (1956).
16. LeFevre, R. J. W., and Tardif, J., *Chemistry & Industry* **1955,** 1674.
17. Perrin, F., *J. phys. radium,* VII, **5,** 497 (1934).
18. Sadron, C., in "Flow Properties of Dispersed Systems," J. J. Hermans, ed., p. 195. Interscience Publishers, New York, N. Y., 1953.
19. Born, M., *Z. Physik* **1,** 45 (1920).
20. Martel, A. E., and Calvin, M., "Chemistry of the Metal Chelate Compounds," Ch. 5. Prentice-Hall, New York, N. Y., 1952.

JOURNAL OF COLLOID SCIENCE **12,** 480–495 (1957)

THE FORMATION OF MICELLES OF SOME AZO DYES[1]

H. P. Frank [2]

Institute of Polymer Research, Polytechnic Institute of Brooklyn, Brooklyn, New York

Received May 27, 1957

ABSTRACT

The solution behavior of two azo dyes, orange II and benzopurpurin 4B, was studied by means of conductance, viscosity, and light-scattering measurements. It was established that micellar particles of large size are formed only in the presence of added salt. The degree of association for benzopurpurin is much greater than for orange II. The conclusion is reached that the micelles represent rodlike particles, and it is believed that the dye ions are associated in the manner of a stack of coins. For benzopurpurin a particle weight (weight average) of 1,900,000 was determined at 25°C. and 0.04 *M* KCl; for orange II the particle weight varies with concentration and temperature reaching a value of 37,000 at 5°C. and 0.4 *M* KCl. Micelle formation of benzopurpurin takes place also in the absence of salt if the pH approaches IEP.

INTRODUCTION

The field of micellar electrolytes comprises essentially two families of compounds: soaps and dyestuffs. A great deal of work has been devoted to the clarification of the solution behavior of soaps during the past decades. Very few studies (1), on the other hand, have been carried out in the field of dye solutions since the publication in 1937 of Valko's book (2), which contains an excellent review of the state of knowledge at that time. In the course of our studies on the interaction of some azo dyes with the water-soluble polymer polyvinyl pyrrolidone (3), it became inevitable to study the behavior of dye solutions as such.

The dyes orange II (O-II) and benzopurpurin 4B (BP) were chosen as typical representatives of the family of azo dyes. The solution properties of these dyes were studied by means of various physical methods in the absence and presence of salt and at different temperatures. The objective of this investigation was to gain some information on the conditions under which micelle formation takes place and on the size and shape of the micelles.

---

[1] This work was supported by the office of the Surgeon General, Department of the Army.

[2] Chemistry Department, Illinois Institute of Technology, Chicago, Illinois.

EXPERIMENTAL

Reagents

O-II (Eastman Kodak), twice recrystallized from water:

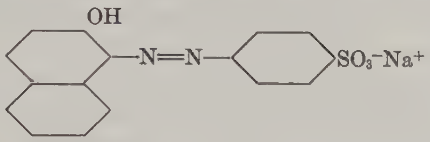

BP (Allied Chemical and Dye Corp., National Aniline Division), twice recrystallized from water:

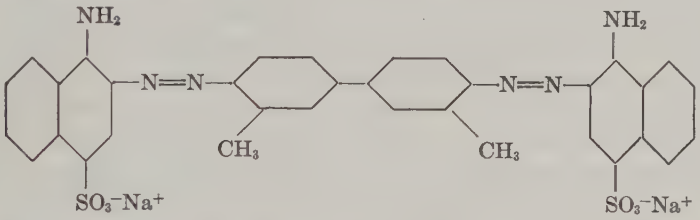

Potassium chloride used was Mallinckrodt (A.R. grade).

The water used for conductance measurements was twice distilled in the presence of potassium permanganate. The specific conductance is not particularly low but sufficient for the purpose: approximately $2 \times 10^{-6}\ \Omega^{-}$ cm.$^{-1}$ at 25°C. All conductance values reported are corrected for water conductance.

Conductance

The experimental conditions of conductance measurements are the same as described previously (3).

Viscosity

An Ubbelohde dilution viscometer was used. The efflux time for water was 158.0 sec. at 25°C., at which temperature all measurements were carried out unless otherwise noted. The kinetic energy correction was neglected. For BP in salt solutions a special multibulb viscometer (4) was used which permits viscosity measurements at varying velocity gradients and extrapolation to zero gradient.

Light Scattering

The instrument was a BS Phoenix light-scattering photometer. In order to measure strongly absorbing dye solutions certain deviations from the conventional procedure became necessary. It was found that light of the yellow Hg line (actually two lines: Hg_{y1} at 5790.66 and Hg_{y2} at 5769.60 A;

the distance between the two lines can be neglected, and the mean wavelength of 5780 A was used for calculations) can be used as incident beam. Neither O-II nor BP absorbs very strongly at this wavelength, and the intensity of the line and the sensitivity of the photomultiplier are sufficiently large to compensate for some light attenuation due to absorption. At still higher wavelengths beyond the absorption range, there are no practical and sufficiently intense monochromatic light sources available, the sensitivity of photomultipliers (RCA 1 P 21) drops off sharply, and the scattering intensity decreases rapidly with increasing wavelength. A mercury AH 3 lamp with a Corning cutoff filter (no. 2324) was used as the light source. The filter does not eliminate light of higher wavelength. This, however, does not cause any disturbing effects because the intensity of the red Hg lines is quite small, the photomultiplier becomes insensitive, and the scattering intensities are rapidly reduced at increasing wavelengths. The instrument was calibrated at 5780 A by a Ludox solution (5). Most measurements were taken at room temperature (25° ± 2°C.). A few measurements were taken at low temperature by cooling the liquid in the cell to 5°C. and taking readings before the liquid could warm up beyond 7°C. Dissymmetry measurements were made in a semioctagonal cell, and the entire scattering envelope (25°–135°) was determined in a cylindrical cell with flat front and rear faces. The absorption at the wavelength used was sufficiently small to neglect absorption corrections (6). The comparatively small absorption is, however, sufficient to make any reflection effect negligible (7).

Optical clarification of all solutions was achieved by pressure filtration at approximately 70°C. through ultrafine fritted discs.

The refractive index increment was measured in an interferometer and in a simple Abbe refractometer using the Na_D line.

Results

Conductance

The conductance results were plotted in the conventional manner (Fig. 1). Figure 1 contains also some literature data (8) which probably represent the best conductance measurements on dye solutions. It is apparent that the conductance values of this investigation are somewhat higher than reported data (8); this is probably due to traces of unremoved electrolyte in BP. This, however, does not affect any of the basic conclusions.

The data in Fig. 1 which represent measurements in salt solutions have been obtained by subtracting the conductance values for equally concentrated KCl solutions from the total conductance, thus producing a value for the conductance contribution of the dye. It is obvious that the accuracy of these results is greatly reduced compared with the conductance data in salt-free solutions. It is practically impossible to obtain any meaningful results at very small dye concentrations.

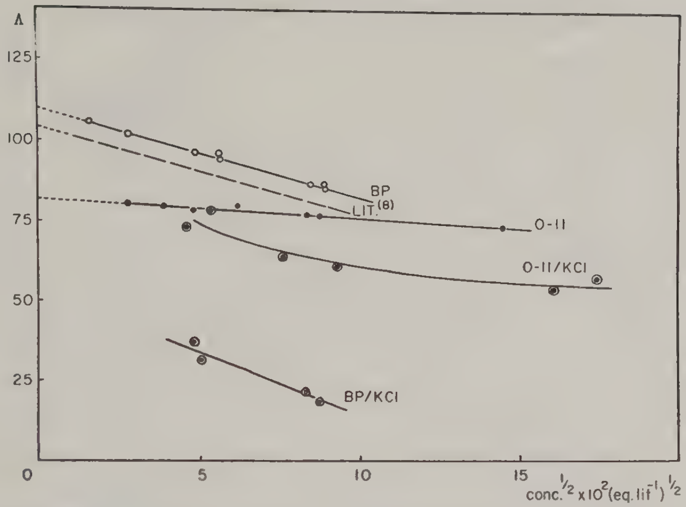

FIG. 1. Equivalent conductance Λ vs. square root of equivalent concentration for O-II and BP in the absence and presence of KCl at 25°C.

It remains doubtful whether a linear extrapolation to obtain Λ_0 is permissible. Some authors have observed a conductance maximum at very small dye concentrations (8). Linear extrapolation of O-II conductances leads to $\Lambda_0 = 82$, which is of a plausible magnitude (2), and for BP $\Lambda_0 = 110$ (considering the electrolyte impurities more likely 104), which appears somewhat high.

Viscosity

The viscosity results are presented in Fig. 2. O-II and BP in salt-free water produce only small viscosity increases, and within the limit of error the intrinsic viscosity is identical with the Einstein value of 2.5 for rigid spheres. The same is true for O-II at low salt concentrations (0.04 *M* KCl). At 0.4 *M* KCl a marked viscosity increase can be observed which is even greater at lower temperatures (3°C.). Evidently there is a critical salt concentration between 0.04 and 0.4 *M* above which the viscosity will increase considerably. Extrapolation to zero concentration, however, leads to approximately 2.5 at both temperatures. The data were obtained in a viscometer of a velocity gradient of approximately 2000 sec.$^{-1}$ (depending on the absolute viscosity of the solution). The viscosities of O-II in salt solution will probably be gradient-dependent, but in view of the only moderately high values of the reduced viscosities (not above 120) this effect is not likely to be very significant.

The behavior of solutions of BP in the presence of salt (0.04 *M* KCl; at still higher salt concentration the dye is salted out) is entirely different from that of O-II. In the first place it is important to assure equilibrium

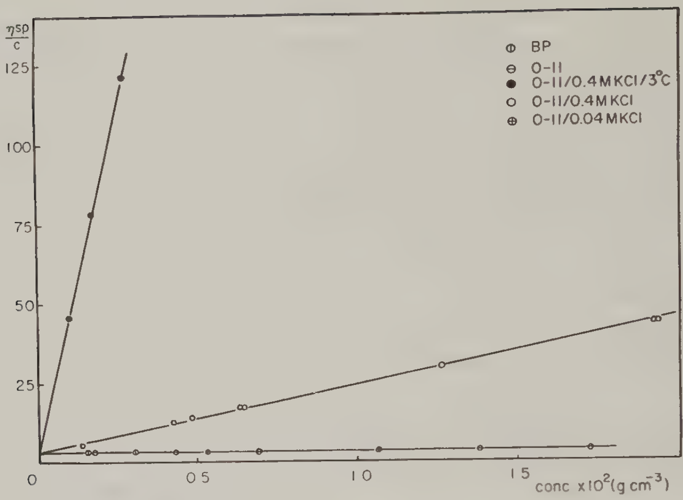

FIG. 2. Reduced viscosity η_{sp}/c vs. concentration for O-II in water and salt solutions and for BP in water at 3°C. and 25°C.

conditions for all measurements on BP solutions. BP is known to form large micelles in salt solutions (2, 9, 10). If BP is dissolved in a salt solution at elevated temperatures, it takes usually several days after cooling the solution to room temperature before the steady rise of the viscosity ceases and a time-independent viscosity is reached. At elevated temperatures (60°–70°C.) the reduced viscosities are very small, and the solutions are obviously molecularly disperse or very nearly so. One can go through several heating-cooling cycles and show the complete reversibility of this effect: the viscosity drops immediately to a very small value on heating and takes several days to rise after cooling. The formation of BP micelles is apparently a very slow process which may be diffusion-controlled, and may have a very small steric factor. Such a condition may exist if, for instance, the ends of a large micelle having a structure resembling a stack of coins adds additional dye ions. The rate of micelle formation may also be affected by a large activation energy which may be required to overcome electrostatic repulsion as additional dye ions are added to the growing micelle. On the other hand, the breakdown of micelles appears to be a rapid process in which only the binding affinities between dye ions have to be overcome. In view of these complications, which apply to all physical measurements on BP solutions (1), it is necessary to allow the system sufficient time for equilibration after dissolving and diluting.

The viscosity measurements were carried out over a velocity gradient range between 1000 and 3000 sec.$^{-1}$. The gradient used in this investigation is the so-called maximum gradient Q (11).

$$Q = Rpg/2L\eta. \qquad [1]$$

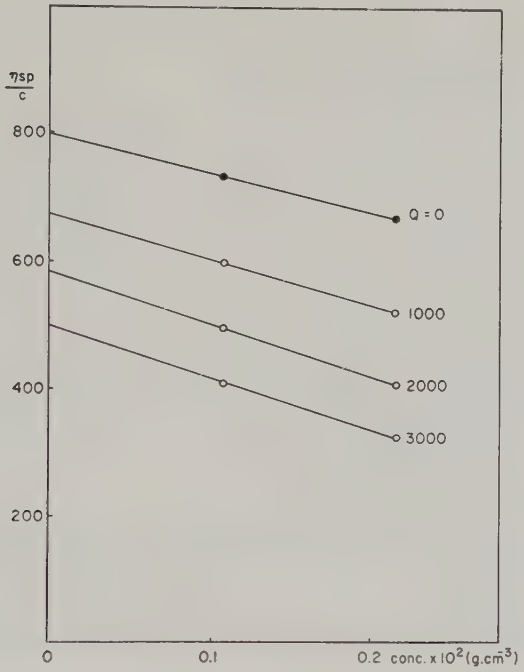

FIG. 3. Reduced viscosity η_{sp}/c vs. concentration of BP at different velocity gradients, 0.04 *M* KCl, 25°C.

TABLE I

Refractive Index Increments of O-II and BP in Water

Dye	Instrument	Wave length (*A*)	*dn/dc*	
O-II	Interferometer	5780	0.469	0.45 avg.
	Abbe refractometer	5893	0.429	
BP	Abbe refractometer	5893	0.575	

The data were treated in the manner suggested by Fuoss (11) and are presented in Fig. 3. The gradient dependence of [η] is very considerable. In contrast to O-II there is no decreasing tendency of the reduced viscosity at lower BP concentrations. Any extrapolation, uncertain as it may be, will certainly not lead to an intrinsic viscosity value in the neighborhood of 2.5. Other viscosity data which are not reported because of the uncertainty of the gradient, cover a greater concentration range and agree qualitatively with the above results and do not show any decrease of the reduced viscosities at concentrations as low as 0.02×10^{-2}.

Light Scattering

The refractive index increments *dn/dc* of O-II and BP in water are listed in Table I. For all further calculations the average value of 0.45 for O-II was used. This value is in contrast with a value of 0.2 in the literature (1).

BP solutions could not be measured in the interferometer because of the darkness even of dilute solutions. The value of 0.575 is in fair agreement with one reported previously (1): 0.545.

Solutions of O-II in water produce very small scattering intensities. The results are therefore numerically rather unreliable and can be considered only as an indication of the order of magnitude of the particle weight (PW). The concentration ranges from 0.049 to 0.289 × 10^{-2}(g.cm.$^{-3}$), and the scattering function Hc/τ is essentially concentration-independent and indicates a particle weight of about 3000, i.e., a degree of association (DA) of about eight. Whereas it may be possible that DA is actually lower than eight, one can exclude with certainty the possibility of existence of micelles with much greater DA under these conditions. The analogous results of BP in water are even less accurate (BP absorbs stronger at 5780 A) and seem to indicate a particle weight of about 2000, i.e., DA about three, in a concentration range from 0.025 to 0.250 × 10^{-2}.

The scattering intensities in salt solutions are much greater, and the results are accordingly more reliable. The results on O-II are shown on Fig. 4. All O-II solutions show a small depolarization ($\leqslant$0.1). No depolarization correction was applied. Dissymmetries at 25°C. were essentially unity. At 5°C. a small but measurable dissymmetry of 1.08 was observed in the con-

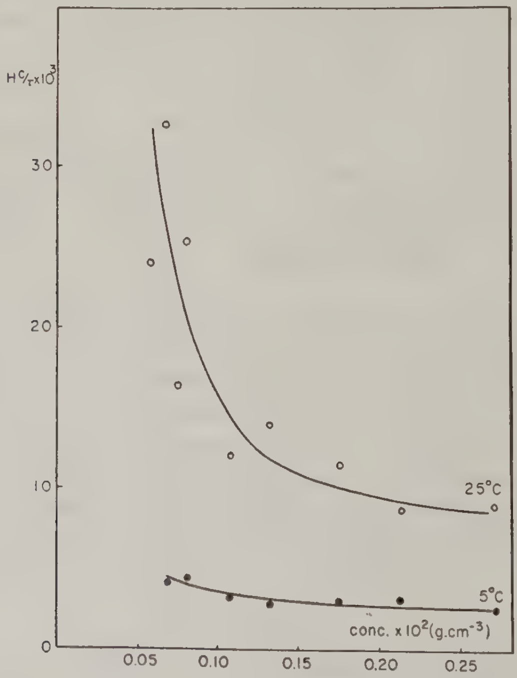

FIG. 4. Light scattering of O-II in 0.4 *M* KCl at 5°C. and 25°C.

TABLE II

Particle Weight and Degree of Association of O-II in 0.4 M KCl at 5°C. and 25°C.

	5°C.		25°C.	
Conc. × 10^2 (g.cm.$^{-3}$)	PW	DA	PW	DA
0.07	22,000	63	4,000	11.5
0.10	28,000	80	6,850	19.5
0.15	32,000	91	9,100	26
0.20	35,000	100	10,000	28.5
0.25	37,000	106	11,100	32

TABLE III

Size of O-II Micelles from Light-Scattering Dissymmetries

Conc.: 0.2×10^{-2}, $z = 1.08$, DA = 100, $\lambda' = \lambda/n = 4350$ A

Spherical	Rodlike
Density: 1.49,[a] Micelle volume: 3.9×10^{-23} cm.^{3}	$\overline{L}_z/\lambda' = 0.16$, $\overline{L}_z = 700$ A
Diameter: 42 A $\cong \lambda'/100$, $z_{\text{calc}} = 1.00$	$\overline{L}_z/\overline{DA}_w = 7$ A per O-II unit

[a] Determined by a flotation method in chloroform-cyclohexane.

centration range between 0.2 and 0.3×10^{-2}. No dissymmetry correction was used for the calculation of the particle weight. The experimentally determined dissymmetry was used for calculation of particle size. In view of the smallness of the dissymmetry its numerical value is rather uncertain, and the calculations supply information only on the order of magnitude of the size of the micellar particles. If one neglects all interaction effects between dye ions and micelles at finite concentrations, one can calculate PW and DA as a function of concentration and temperature (Table II).

The results of some calculations on the size of the micelles assuming either a spherical or rodlike physical model are presented in Table III. The calculations of Table III were carried out with the help of the tables of Doty and Steiner (12). It can be seen that a spherical micelle of DA = 100 would have a diameter which is incompatible with a value of 1.08 for the dissymmetry. A rodlike micelle, however, could be formed by stacking O-II ions together. A characteristic length of 7 A per O-II unit is not unreasonable and within molecular dimensions. It should be pointed out that in a polydisperse system the length of rodlike particles as calculated from dissymmetry represents a z-average, whereas DA is a weight average. The numerical ratio of the two experimentally obtained parameters (7 A per O-II unit) for a polydisperse system will be greater than if the ratio had been formed from identical averages, which, however, are experimentally not available.

Light scattering of solutions of BP in 0.04 *M* KCl was measured at room temperature only. Proper precautions were taken to assure equilibration after preparation of the solutions and after dilution. The scattering intensities of such solutions and the angular dependence are considerable. Therefore it was necessary to measure the entire scattering envelope (25°–135°) rather than dissymmetries. The scattering intensities obtained in the cylindrical cell were calibrated by comparative 90° measurements in an ordinary dissymmetry cell. Depolarization was measured at 90° with the incident beam being either unpolarized, or vertically or horizontally polarized. The average value of ρ_u is 0.48; ρ_v is 0.32; ρ_h is 1.24. The magnitude of all three values of ρ indicates the presence of very large electrically anisotropic particles (13), and their relation to each other obeys the theoretical requirement (Krishnan's reciprocity law):

$$\rho_u = \frac{1 + 1/\rho_h}{1 + 1/\rho_v}. \qquad [2]$$

The 90° scattering intensities which were used for calibration of the readings obtained with the cylindrical cell were corrected for depolarization by an appropriate Cabannes factor $(2\rho_v/1 + \rho_v)$.

A reciprocal intensity plot (Zimm plot) is shown in Fig. 5, and the important results are compiled in Table IV. This table also contains number-

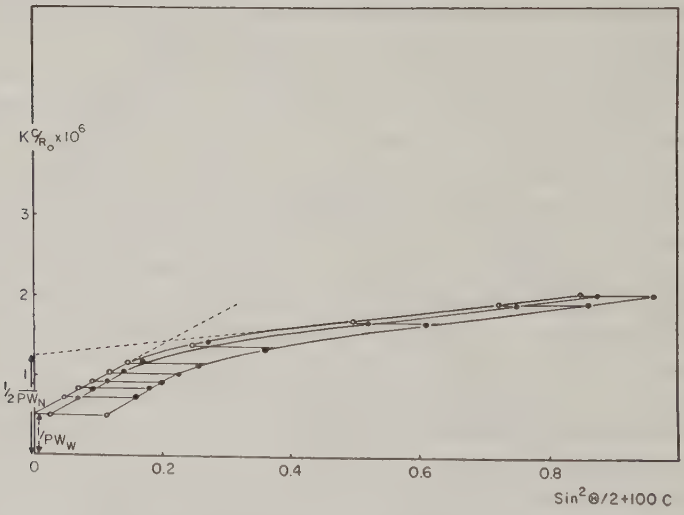

FIG. 5. Reciprocal intensity plot, BP in 0.04 *M* KCl, Kc/R. vs. $\sin^2\Theta/2 + 100\,c$

TABLE IV

Light-Scattering Results on BP in 0.04 M KCl

Intercept: $(Kc/R_\theta)_0 = 0.52 \times 10^{-6}$, $\overline{PW}_w = 1{,}900{,}000$, $\overline{DA}_w = 2620$.
$\bar{R}_z = 4240$ A, $\bar{L}_z = 6\bar{R}_z/\sqrt{3} = 14{,}700$ A.
Asymptotic intercept: $(Kc/R_\theta)_{180} = 1.25 \times 10^{-6}$, $\overline{PW}_n = 400{,}000$, $\overline{DA}_n = 550$.
$\bar{R}_n = 680$ A, $\bar{L}_n = 2360$ A.
$\bar{L}_z/\overline{DA}_w = 5.6$ *A*, $\bar{L}_n/\overline{DA}_n = 4.3$ A per BP unit.

average parameters obtained from extrapolation of the asymptotic slope ($\theta \rightarrow 180°$) (14).

$\bar{R}_z$ stands for the z-average of the root-mean-square radius of gyration and $\bar{R}_n$ for the number average; $\bar{L}_z$ and $\bar{L}_n$ stand for the length of the corresponding rodlike particle.

The general relation between the radius of gyration R of a rod and its length L which has been used in Table IV to calculate L, is as follows:

$$A = Lh, \qquad I = AR^2, \qquad dI = x^2h\,dx, \qquad I = \int_{-L/2}^{+L/2} hx^2\,dx = hx^3/3 \Big|_{-\,L/2}^{+\,L/2} = L^3/12.$$

$$I = L^3h/12, \qquad I/A = L^2/12 = R^2, \qquad R = L\sqrt{3}/6.$$

Here A is the area Lh in Fig. 6, and I is the moment of inertia with respect to axis y.

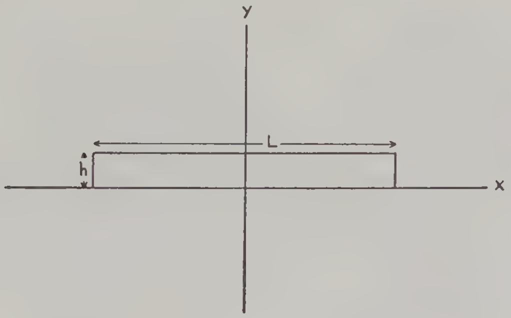

FIG. 6. Geometry of a rod-shaped particle.

DISCUSSION

From the results obtained a fairly consistent picture of the micellar behavior of the two azo dyes can be presented.

Conductance data generally do not furnish much information on association, as has been pointed out by Valko (2). The conductance data of O-II in water (Fig. 1) do not show any anomalies as compared with other strong electrolytes. An equivalent conductance of 82 would lead to an anion conductance of 31, which is entirely plausible in the absence of association. The slope of the O-II curve is entirely normal for a strong 1.1 valent electrolyte and is practically identical with that of KCl. The conductance data of BP would lead to an anion conductance of 53, which is higher than one could expect for molecularly disperse ions. The slope of the BP curve is unusually steep, which is probably indicative of counter ion retention.

In the presence of added salt the conductance of O-II is considerably reduced, which, however, is to be expected simply owing to greatly increased ionic strength of the solutions. In the case of BP the conductance reduction is much greater than can be explained by increased ionic strength. Extrapolation to a comparable ionic strength would lead to conductance values of the order of 50, whereas the experimental values are as low as 20. This large effect is evidently due to the formation of large particles which retain a large fraction of the counter ions, thus reducing the effective charge and the mobility of the micellar anions.

The viscosity data on O-II and BP in water seem to indicate the presence of spherical or nearly spherical particles which lead to an Einstein viscosity of 2.5. This evidence together with the low light-scattering intensities of such solutions seems to prove either the absence or the very small size of micelles (micelles containing about five or less ions cannot be excluded; such micelles may well have a more or less spherical shape if the dye ions are put together like a stack of coins, as will be discussed below). The viscosity increase of O-II in salt solution at 25°C., and even more at 3°C., strongly suggests formation of large-size anisotropic micelles. It is generally known for all kinds of micellar electrolytes that increasing salt concentration reduces electrostatic repulsion between ions of equal sign, and thus favors formation of micelles under the influence of intermolecular forces which are overshadowed by electrostatic forces in the absence of salt (2). The viscosity increase of O-II solutions must be due to formation of anisotropic particles with the length or degree of association increasing with concentration.

Neglecting hydrodynamic interaction between these particles one can calculate their axis ratio $f = L/h$ and length by using Simha's equation for rotational ellipsoids (15):

$$\eta_{sp}/c = 2.33f^{1.7}/10d, \qquad [3]$$

where d is the density of the solute (1.49 for O-II). The equation has been used on some results of O-II solutions (Table V). The length of the micellar particles represents a viscosity average

$$\bar{L}\eta = (\sum N_i L_i^{2.7}/\sum N_i L_i)^{1/1.7} \qquad [4]$$

and was calculated in the following fashion: O-II ions can assume a perfectly flat configuration (Fig. 7). The size of the O-II anion is 13.3 A length, 6.5 A width, and probably not more than 3 A thickness (2). The only plausible arrangement of O-II ions in the micelle will be such that the ions arrange themselves parallel to each other in the manner of a stack of coins (Fig. 8). The dispersion forces between the aromatic systems can exercise maximum interaction (16), and at the same time the hydrophilic polar groups can interact with the aqueous solvent. The pH of the O-II solutions was between 6 and 7, indicating complete ionization of the sulfonate group and no ionization of the phenolic hydroxyl group. The mean of the length

TABLE V

Particle Dimensions from Viscosity Data

Conc. × 10^2 (g. cm.$^{-3}$)	η_{sp}/c (cm.^{3} g.$^{-1}$)		$\bar{L}\eta$ (A)	$\overline{DA}_w$	$\bar{L}\eta\sqrt{\overline{DA}_w}$ (A per O-II)
		3°C.[a]			
0.1	47	28.5	285	80	3.6
0.2	90	42	420	100	4.2
0.3	132	53	530	120	4.5
		25°C.			
0.1	4.8	7.53	75.3	19.5	3.8
0.2	7	9.35	93.5	28.5	3.3
0.3	9.3	11.0	110	33.5	3.3
0.6	15.5	14.9	149		
1.0	24	19.3	193		
2.0	45	27.9	279		

[a] Light-scattering data were obtained at 5°C.

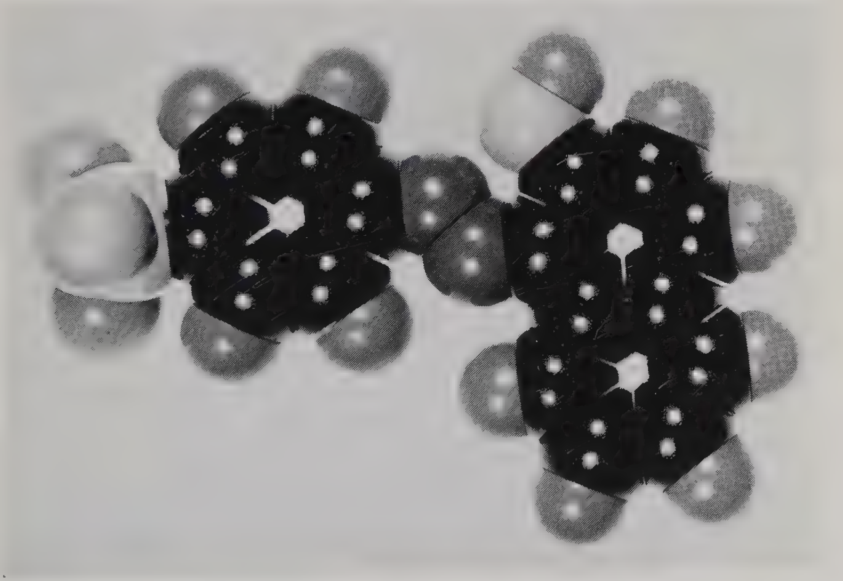

FIG. 7. O-II molecular model in flat configuration.

and width of the O-II ion would be approximately 10 A which can be taken to represent the short axis of the rotational ellipsoid. From this value and the value of *f* the length *L* can be obtained. If the length *L* is divided by DA from light scattering, the thickness of one unit can be obtained. Again this value is obtained by relating two different averages with each other, but the viscosity average of *L* will not differ greatly from the weight average. In the last column of Table V it can be seen that the numerical value is only slightly greater than the expected thickness of the O-II ion, and it is

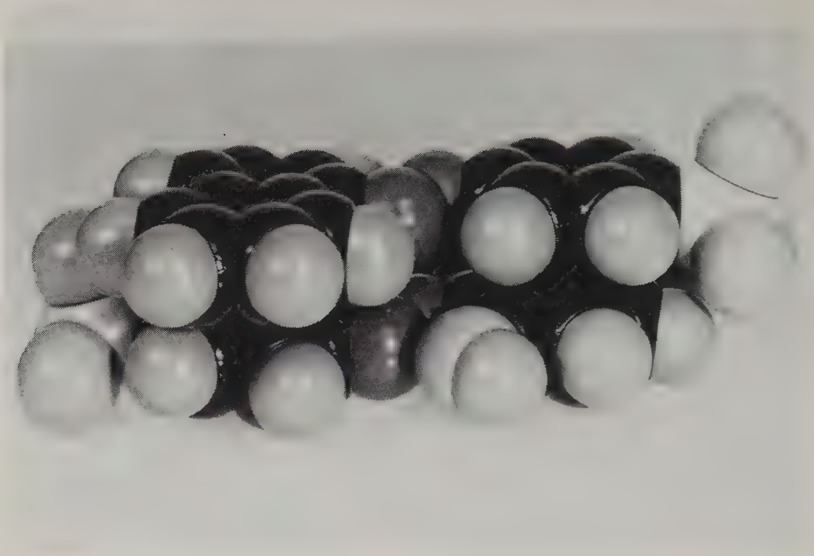

FIG. 8. Two O-II ions arranged parallel to each other (stack of coins arrangement).

fairly constant, proving the viscosity results to be consistent with the light-scattering data. Any variation will have to be attributed to the assumptions made such as neglecting interaction effects at finite concentrations.

From light-scattering data alone a length of 700 A was obtained (Table III) to be compared with 420 in Table V. It should be kept in mind that the length from light scattering represents a *z*-average which will be larger than the viscosity average for a polydisperse system. Also, the light-scattering size has not necessarily the same physical significance as the viscosity size, the former referring to a volume of different refractive index relative to the surrounding medium and the latter to a hydrodynamically effective volume. The short axis of the micelle could be greater than 10 A owing to hydration or counter ion retention which would lead to a greater length for a given axis ratio from viscosity data.

Another significant conclusion from viscosity data is that the reduced viscosity η_{sp}/c is proportional to $L^{1.7}$, and, on the other hand, proportional to the first power of the concentration (Fig. 2). Therefore, L has to be proportional to the 0.6 power of the concentration (neglecting $[\eta]$, which is small compared with most values of the reduced viscosities). If one makes the reasonable assumption that the probably accidental linearity between η_{sp}/c and the concentration contains a contribution from hydrodynamic interaction, and that the increase of η_{sp}/c due to increasing length of the micelle is therefore proportional to somewhat less than the first power of the concentration, one might obtain a relation between L and the 0.5 power of the concentration. A square-root relationship of this kind can be rationalized in the following manner: If one considers either side of the flat O-II ion as a reactive site with respect to association, one can write

$$s = 2c, \tag{5}$$

where s is the molar concentration of reactive sites and c the concentration of O-II. The fraction of associated and unassociated sites will be p and $(1 - p)$, respectively. The rates of association and dissociation as second- and first-order reactions will have to be proportional to $s^2(1 - p)^2$ and sp, respectively. One can then formulate an equilibrium constant:

$$K = sp/s^2(1 - p)^2. \tag{6}$$

Substituting Eq. [5] and solving for c leads to:

$$c = \frac{p}{(1 - p)^2} \frac{1}{2K} = \frac{p}{(1 - p)^2} K'. \tag{7}$$

Substituting $\overline{DA}_n = 1/1 - p$ into Eq. [7] one obtains

$$(\overline{DA}_n)^2 = c/pK'. \tag{8}$$

For $1 - p \ll 1$ one obtains

$$\overline{DA}_n = (c/K')^{1/2}. \tag{9}$$

Equation [9] indicates a square-root relationship between the number-average degree of association and the concentration, with the proportionality factor being a measure for the equilibrium constant. A relation between other averages of DA, such as the viscosity average and the concentration, will differ from Eq. [9] only by a constant factor which will be contained in K' and which will depend on the prevailing distribution.

BP solutions form very large micelles in the presence of salt. The pH of all BP solutions used was about 7, indicating complete ionization of the sulfonate groups and no ionization of the amino groups.[3] The viscosity data

---

[3] It was observed that BP solutions in pure water seem to age and tend to undergo association upon standing. It could be shown that absorption of CO_2 is responsible for this effect. A freshly prepared BP solution (concentration 0.256×10^{-2}) was heated to 80°C. for 30 min. in order to remove CO_2. After cooling to 25°C. viscosity and pH were determined: $\eta_{sp}/c = 2.6$, pH = 6.95. Both values can be considered normal. CO_2 was bubbled through the solution at 25°C. for 1 hour and again viscosity and pH measured: $\eta_{sp}/c = 5.9$, pH = 5.10. The solution also appears much darker than before CO_2 absorption. As the pH is reduced it approaches the IEP pH, which leads to increasing ionization of the amino groups and thus to formation of zwitter ions. It is assumed that electrostatic attraction between the zwitter ions is responsible for the formations of aggregates of this kind which are not being formed at neutral pH in the absence of zwitter ions. This observation may be the cause of some contrasting reports on BP behavior in the literature.

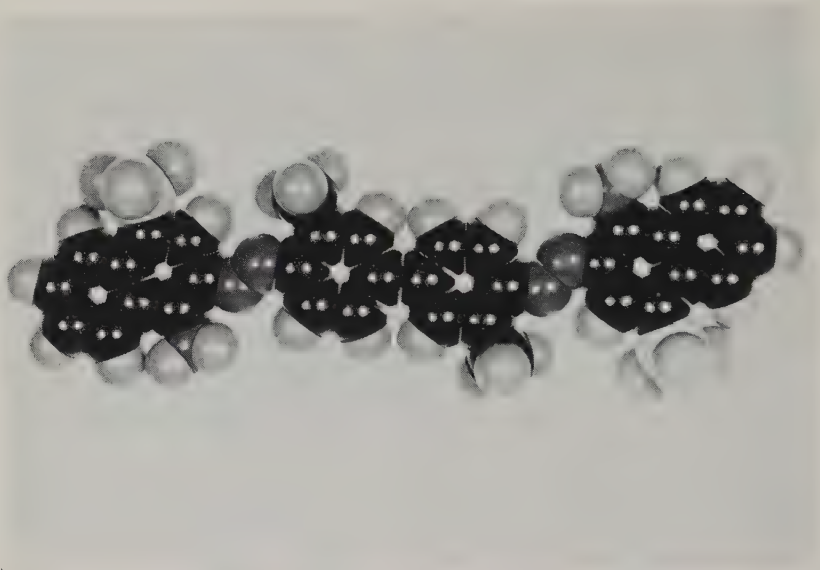

FIG. 9. BP molecular model in flat configuration.

of Fig. 3 indicate a behavior different from that of O-II. No disassociation seems to take place upon dilution within the concentration range studied. BP can also assume a flat configuration (Fig. 9), and the characteristic dimensions are as follows: length 24 A, width 10 A, and thickness again about 3 A. If the micelles are formed analogous to the O-II system application of Simha's equation leads to the following results:

$$[\eta] = 800, \qquad f = 150, \qquad \bar{L}_\eta = 2600 \text{ A},$$
$$\overline{DA}_w \text{ (light scatt.)} = 2620, \qquad \bar{L}_\eta/\overline{DA}_w = 1 \text{ A}.$$

The length is again obtained by using the mean of length and width of one BP anion as the short axis of the rotational ellipsoid, i.e., 17 A. The resulting thickness of 1 A of one BP unit appears to be too small to be plausible and is in contrast with the considerably greater values obtained from light-scattering data (Table IV). An analogous discrepancy applies to the lengths. Even with the obvious polydispersity of the solutions (Fig. 5, Table IV) taken into account, it seems doubtful whether the micellar dimensions from viscosity data are compatible with those from light scattering. It should, however, be pointed out that the only result for thickness of one BP unit which was obtained by combining parameters of corresponding average, is the number-average ratio in Table IV with 4.3 A, which is comparable to the thicknesses obtained for O-II. The complicating factors which have been pointed out for O-II solutions apply of course also to BP. Thus it may well be that the hydrodynamically effective dimensions of one BP ion exceed 10 or 25 A, respectively.

ACKNOWLEDGMENTS

The author is greatly indebted to Drs. F. R. Eirich and R. Ullman for helpful suggestions and stimulating discussions.

REFERENCES

1. ALEXANDER, P. AND STACEY, K. A., *Proc. Roy. Soc. (London)* **A212,** 274 (1952).
2. VALKO, E., "Kolloidchemische Grundlagen der Textilveredlung." J. Springer, Berlin, 1937.
3. FRANK, H. P., BARKIN, S., AND EIRICH, F., *J. Phys. Chem.*, 31st National Colloid Symposium June 1957, New York, N. Y.
4. SCHURZ, J., AND IMMERGUT, E., *J. Polymer Sci.* **9,** 279 (1952).
5. OSTER, G., *J. Polymer Sci.* **9,** 525 (1952).
6. FRANK, H. P., AND ULLMAN, R., *J. Opt. Soc. Amer.* **45,** 471 (1955).
7. SHEFFER, H., AND HYDE, J. C., *Can. J. Chem.* **30,** 817 (1952).
8. ROBINSON, C., AND MOLLIET, J. L., *Proc. Roy. Soc. (London)* **A143,** 630 (1934).
9. ROBINSON, C., AND MILLS, H. A. T., *Proc. Roy. Soc. (London)* **A131,** 576 (1931).
10. PAPKOVA-KWITZEL, T. P., *Kolloid-Z.* **69,** 57 (1934).
11. GOLDBERG, P., AND FUOSS, R., *J. Phys. Chem.* **58,** 648 (1954).
12. DOTY, P., AND STEINER, R. F. *J. Chem. Phys.* **18,** 1211 (1950).
13. ZIMM, B. H., STEIN, R. S., AND DOTY, P., *Polymer Bull.* **1,** 90 (1945).
14. BENOIT, H., *J. Polymer Sci.* **11,** 507 (1953).
15. SIMHA, R., *J. Phys. Chem.* **44,** 25 (1940).
16. DE BOER, J. H., *Trans. Faraday Soc.* **32,** 10 (1936).

JOURNAL OF COLLOID SCIENCE **12**, 496–509 (1957)

X-RAY SMALL-ANGLE SCATTERING OF CARBON BLACKS

Haruo Kuroda

Department of Chemistry, Faculty of Science, The University of Tokyo,
Tokyo, Japan

Received June 4, 1957

ABSTRACT

The intensity curves for the X-ray small-angle scattering of several carbon blacks are analyzed by Hosemann's theory and by Porod's theory. The particle size distribution is estimated from the small-angle scattering and is compared with the electron micrograph data. A serious disagreement is found between them. However, the average particle size, and the parameter, l_c, in Porod's theory are always of the same magnitude as the electron micrograph data. The meaning of these results is discussed.

INTRODUCTION

Carbon black is one of the materials which give strong small-angle scattering of X-rays. Since the early study of Krishnamuruti (1), this scattering has been investigated by many authors. However, the nature of this scattering is still under discussion.

Warren and his collaborators (2–4) have studied the X-ray diffraction pattern of carbon black in detail, and have thrown light on its structure. Graphite-like layers are stacked roughly parallel to one another, without such an orientation as in graphite about the normal of the layer, single graphite-like layer is in the order of 20 A, and the thickness of a parallel layer group is usually in the order of 10 A. In the course of these investigations, Biscoe and Warren (3) tried to obtain information on the clustering of parallel layer groups by a rough analysis of small-angle scattering. The logarithm of the observed intensity of small-angle scattering was plotted against the square of the corresponding scattering angle, and particle size was estimated according to Guinier's method from the slope of this curve. The results were in the order of 100–1000 A, which is many times larger than the dimensions of parallel layer groups, and of the same magnitude as the particle sizes observed by the electron microscope. This fact has been considered to indicate that many parallel layer groups aggregate to make a spherical cluster, which is the particle in the electron micrograph.

In contrast, the results of recent studies on the small-angle scattering of carbon blacks by Brusset (5) and Brusset *et al.* (6) led to the conclusion that the particle sizes measured by the electron microscope are several times larger than those from small-angle scattering. They suggested that the small-angle scattering of carbon black could be attributed to the substructure of the particles. For some carbon blacks, the small-angle scattering was considered to be due to the micropores in the carbon black particles.

However, there remain some questions about the procedure of analysis adopted by these authors. It may not be justifiable to estimate particle size using only a restricted part of the intensity curve for a polydisperse colloidal system such as carbon blacks. The limit of the applicability of Guinier's formula must be taken into account. Further, although these authors neglected the effect of inter-particle interference, it has long been a point of discussion in the theory of small-angle scattering by polydisperse colloidal systems. Recently two theories have been elaborated for small-angle scattering, the one due to Porod (7, 8) and the other due to Hosemann (9). The purpose of this study is to interpret the small-angle scattering of X-rays by carbon blacks with the aid of these theories, and to compare the data with those obtained by independent methods.

EXPERIMENTAL PROCEDURES

The details of the apparatus were described in the previous paper (10). X-rays were collimated to a pin-hole beam by two apertures separated by 50 cm. The specimen was packed into a circular cavity of 10 mm. diameter in a flat metal plate of 0.5 mm. thickness, and placed immediately behind the second aperture. The specimen film distance was 549 mm. The apparatus was evacuated except in the neighborhood of the specimen. Ni-filtered Cu K_α radiation was used.

About twenty diagrams were registered photographically for each specimen, with various exposure times and with different aperture sizes. Individual films were microphotometered by means of a Riken-B-type microphotometer. To obtain an intensity curve from them, only a restricted range of photographic density was used, so that a linear relation could be assumed between the incident energy of the X-rays and the corresponding photographic density. A series of intensity curves for each specimen were combined by graphical matching to a complete scattering curve extending from 4′ to 2° of the scattering angle.

The materials used were six commercial carbon blacks: Royal Spectra (H.C.C., Columbian Carbon Co.), Philblack E (S.A.F., Phillips Petroleum Co.), Peerless Mark II A (Peerless Carbon Co.), Tokyo Gas Carbon (Tokyo Gas Co.), Statex B (F.F., Columbian Carbon Co.), and Philblack O (H.A.F., Phillips Petroleum Co.).

After the experiments with small-angle scattering, the apparent density of each specimen under the experimental conditions was measured. Packing densities were estimated from these data, using the densities of the carbon

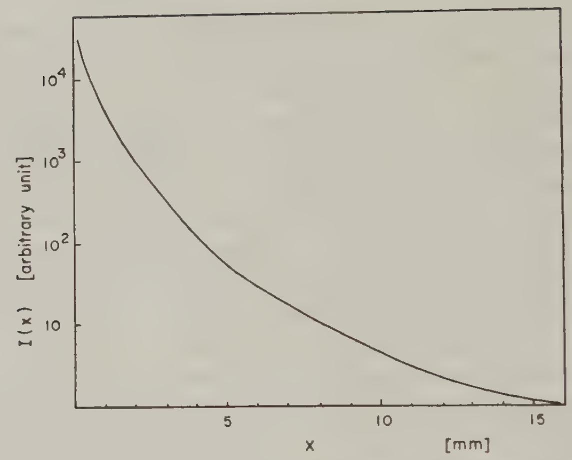

FIG. 1. Intensity curve of the small-angle scattering by Tokyo Gas Carbon.

black particle. Wide angle X-ray diffraction patterns were investigated with a Geiger counter X-ray diffractometer, made by Rigakudenki Co.

RESULTS

a) Interpretation of Scattering Curves by Hosemann's Theory

A typical example of observed intensity curves is shown in Fig. 1, where the logarithm of the observed intensity is plotted against x, which is the distance from the center of the direct beam on the film. Neither maximum nor inflection point can be observed, and the intensity increases rapidly with decreasing scattering angle. This is the type of intensity curve which is usually found in small-angle scattering by a polydisperse colloidal system.

The effects of interparticle interference in such a case have been investigated theoretically by Hosemann (9). Some simplifying assumptions are used in the theory. The square of the structure factor of a spherical particle of radius R, $F(h)^2$, is approximated by an exponential function of Guinier's formula,

$$F(h)^2 = N^2 \exp. [-h^2R^2/5], \qquad [1]$$

where N is the number of electrons in the particle, $h = 4\pi \sin \theta/\lambda$ where 2θ is the corresponding scattering angle, and λ is the wavelength of the X-rays.[1] The mass distribution of particle sizes is assumed to be a Maxwellian type, thus,

$$M(R) = \frac{2}{R_0^{n+1}\Gamma\left(\frac{n+1}{2}\right)} \cdot R^n \exp. [-R^2/R_0^2], \qquad [2]$$

---

[1] Under the present experimental condition,

$$h = 4\pi \sin \theta/\lambda = 7.439 \times 10^{-3}x.$$

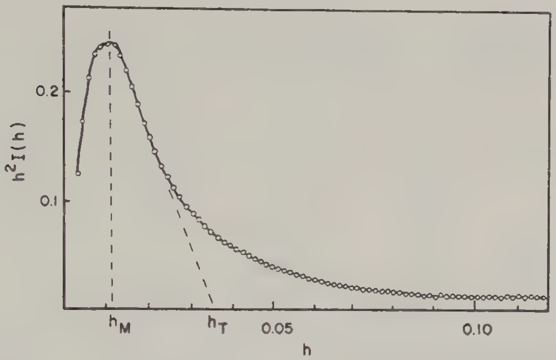

FIG. 2. Plot of $h^2I(h)$ versus h for Tokyo Gas Carbon.

TABLE I

Packing Density of the Specimens for Small-Angle Scattering

	Density of particle [g./cm.³]	Apparent density of specimen [g./cm.³]	Packing density of specimen	g.
Royal Spectra	1.68	0.136	0.08	0.52
Philblack E	1.76	0.549	0.31	0.64
Peerless II A	1.82	0.442	0.24	0.38
Tokyo Gas Carbon	1.68	0.239	0.14	0.67
Statex B	1.81	0.754	0.42	0.95
Philblack O	1.81	0.609	0.34	1.11

where n and R_0 are the parameters determining the distribution. Further, it is assumed that each particle is surrounded by an empty space, the volume of which is proportional to that of the corresponding particle. The theory shows that the interparticle interference would be negligible, if the mean relative statistic fluctuation of particle size, g, is not smaller than the packing density of particles in the specimen, c; i.e.,

$$g \geq c. \tag{3}$$

When we plot the observed intensity multiplied by h^2 against h, we can find a maximum on such a curve for all specimens. An example of these curves is shown in Fig. 2. It is seen that the shape of the curve is in good agreement with Hosemann's theory. In these cases, g can be derived from the following relation,

$$g = \frac{h_T}{2h_M} - 1 \cong \frac{1}{\sqrt{2(n+1)}}, \tag{4}$$

where h_M is the position of the maximum point, and h_T is the intersection with the h-axis of the tangent at the inflection point in the $h^2I(h)$-curve. The values of g calculated by Eq. [4] are presented in Table I with the observed values of the packing density. The condition expressed in the in-

TABLE II

Results Obtained by Hosemann's Method

	n	Average diameter [A]	Diameter by E. M. [A]	Dimension of parallel layer group	
				L_a [A]	L_c [A]
Royal Spectra	0.85	166	180	13.1	27.7
Philblack E	0.22	201	230	12.0	24.6
Peerless II A	1.21	292	300	14.2	26.8
Tokyo Gas Carbon	0.13	237	350	13.4	28.2
Statex B	−0.44	349	440	16.9	24.5
Philblack O	−0.50	400	350	13.3	27.5

equality [3] is found to be satisfied for all specimens. Therefore, according to the theory, interparticle interference can be neglected, and the mass averaged particle diameter $\bar{D}$ can be calculated by Eq. [5].

$$\bar{D} = \frac{2}{h_M}\sqrt{\frac{10}{n+2}}\,\frac{\Gamma\left(\frac{n+2}{2}\right)}{\Gamma\left(\frac{n+1}{2}\right)}. \tag{5}$$

The results are given in Table II.

We shall compare them with the particle sizes measured by the electron microscope, and with the dimensions of parallel layer groups. In the fourth column of Table II, the most frequently observed particle diameter in the electron micrograph of each specimen is shown. The dimensions of parallel layer groups are given in the last two columns of the same table. The dimension of a single graphite-like layer, L_a, was calculated from the breadth of (10)-reflection at half the maximum intensity, using Warren's formula for the random layer lattice:

$$L_a = 1.84\ \lambda/\beta \cos\theta, \tag{6}$$

and the thickness of the parallel layer group, L_c, was calculated from the breadth of (002)-reflection by Eq. [7].

$$L_c = 0.89\ \lambda/\beta \cos\theta. \tag{7}$$

The mass averaged particle diameters from small-angle scattering are of the same magnitude as the electron micrograph data, and are many times the dimensions of the parallel layer groups. In this respect, the results seem to agree well with the opinion stated by Biscoe and Warren (3). However, it must be noted that the parameter n, which determines the sharpness of the distribution curve, is smaller than 1, except with Peerless Mark II A. It is negative even in the cases of Statex B and Philblack O. It is obvious that there is a serious disagreement between the results just mentioned and the electron micrograph data, since the number fraction of the particles with radius R must increase regularly with decreasing R, unless the parameter n in the corresponding mass distribution of particle size is greater than 3. A number of reasons can be considered for this disagreement. The assumption concerning the distribution function is one point to be examined.

If we assume a discrete distribution instead of a continuous one, the scattering intensity will be expressed as

$$I(h) = K \sum_i M(R_i) R_i^3 \exp. (-h^2 R_i^2/5), \qquad [8]$$

where K is a constant and $M(R_i)$ is the mass fraction of the particles with radius R_i. The graphical analysis of the curve of log $I(h)$ versus h^2 in terms of Eq. [8] has been frequently used in order to evaluate $M(R_i)$. This method is due to Jellinek and Fankuchen (11).

The observed intensity curves were treated by this method. The results for Tokyo Gas Carbon and Statex B are shown in Tables III and IV. In Table III, the largest value of $M(R)$ occurs at the smallest particle size. The value of $M(R)$ decreases with increasing particle size, but rises again above 20% at D = 328 A. In Table IV, $M(R)$ is also largest for the smallest particle, the diameter of which is 32.8 A. This seems to coincide with the result for Statex B by Brusset *et al.* (6). They analyzed the Guinier

TABLE III

Results of Analysis of the Curve of log $I(h)$ versus h^2 by Fankuchen's Method (Tokyo Gas Carbon)

Diameter D [A]	Mass fraction $M(R)$ [%]
31.7	27.6
102	13.3
160	13.5
213	9.7
328	22.6
568	9.4
983	3.8

Average diameter, $\bar{D}$ = 230 A

TABLE IV

Results of Analysis of the Curve of Log $I(h)$ versus h^2 by Fankuchen's Method (Statex B)

Diameter D [A]	Mass fraction $M(R)$ [%]
32.8	28.7
108	9.2
186	13.2
275	11.0
418	17.9
710	13.4
1145	7.0

Average diameter, $\bar{D}$ = 324 A

plot of small-angle scattering into two components, the diameters being 33 A and 69 A, respectively. Considering the fact that the average diameter was 446 A by the electron microscope, and 463 A from the specific surface area determined by nitrogen adsorption, they attributed the observed small-angle scattering to micropores in carbon black particles. However, the present result shows the existence of a second maximum at about 400 A, which is almost equal to the average diameter by other methods. Such a second maximum was always found, while the value of $M(R)$ was largest at the smallest particle size for all specimens. The particle sizes corresponding to the second maxima, and the average diameters, $\bar{D} = \sum_i 2R_iM(R_i)/\sum_i M(R_i)$, are given in Table V. Both values are of the same magnitude as the corresponding electron micrograph data.

In order that the observed intensity curves be sufficiently approximated by

$$I(h) = K \int_0^\infty M(R)R^3 \exp.\,(-h^2R^2/5)\, dR, \tag{9}$$

$M(R)$ can be expected to have the characteristics mentioned above. Therefore, it seems incorrect to use a Maxwellian distribution function for $M(R)$. Instead $M(R)$ is considered to be composed of two parts; one can be closely correlated with the observations by the electron microscope, and the other cannot.

b) *Interpretation of Intensity Curves by Porod's Theory*

In order to expose the true physical meaning of the present results, it is hoped to treat the intensity curves from the more general viewpoint, without assuming *a priori* such an interpretation as Eq. [9]. Porod (7, 8) has elaborated a general theory on the basis of the Debye theory of X-ray scattering, which is applicable to the small-angle scattering of polydisperse colloidal systems. According to this theory, the scattering intensity can be expressed by the following integration,

$$I(h) = I_e(h)V\rho^2c(1 - c) \int_0^\infty H(r) \frac{\sin hr}{hr} 4\pi r^2\, dr, \tag{10}$$

TABLE V

Results Obtained by Fankuchen's Method

	Average diameter $\bar{D}$ [A]	Diameter at the second maximum of $M(R)$ [A]
Royal Spectra	181	125 or 130
Philblack E	203	320
Peerless II A	278	280
Tokyo Gas Carbon	230	330
Statex B	324	418
Philblack O	391	570

where $I_e(h)$ is the intensity of X-rays scattered by one electron, V is the total volume of the specimen irradiated by the X-ray, ρ is the mean electron density in the particles, c is the packing density of the specimen, and $H(r)$ is the characteristic function of the specimen. A number of essential relations have been derived from Eq. [10], without ambiguous assumption except as to the constancy of electron density in the particles. For instance, the theory shows that the scattering intensity at the higher scattering angles should be inversely proportional to the fourth power of the corresponding scattering angle,

$$\text{Lim.}\ [I(h)] = 2\pi\rho^2 S I_e(h)/h^4, \tag*{[11]}$$

where S is the total surface area of the specimen in the X-ray pass.

Porod has proposed a few functions as the useful parameters to describe the characteristics of the scattering. Among them a parameter l_c, which is called the distance of heterogeneity, is defined as

$$l_c = 2 \int_0^\infty H(r)\, dr. \tag*{[12]}$$

This quantity can be derived directly from the observed intensity curve using the following equation:

$$l_c = \pi \int_0^\infty \frac{hI(h)}{I_e(h)}\, dh \Bigg/ \int_0^\infty \frac{h^2 I(h)}{I_e(h)}\, dh \tag*{[13]}$$

In order to calculate the integrations in Eq. [13], it is necessary to estimate the values of integrands to the smaller scattering angle by extrapolation. The upper limits of the integrations were laid at $h = 0.12$. These procedures were considered to yield no serious errors. The results are given in Table VI.

The values of l_c are a little smaller than the particle sizes observed by the electron microscope. It is not easy to picture the geometrical significance of l_c in general. We shall consider, however, one special case where

TABLE VI

Results Obtained by Porod's Method

	Distance of heterogeneity l_c [Å]	Specific surface area ($\times 10^6$ cm.^{2}/g.)		
		By Eq. [11]	From particle size	(N_2 adsorption)
Royal Spectra	152	3.73	1.76	
Philblack E	172	2.15	1.49	(1.426[a])
Peerless II A	234	0.74	1.06	
Tokyo Gas Carbon	261	2.27	1.03	
Statex B	325	0.88	0.77	(0.70[b])
Philblack O	381	1.60	0.65	(0.751[a])

[a] Kraus, G., *J. Phys. Chem.* **59**, 343 (1955).

[b] Brusset, H., Lerat, B., and Makki, M., *Ann. chim. (Paris)* **9**, 447 (1954).

the interparticle interference is perfectly negligible, and all particles are spherical. In this case, the scattering intensity will be expressed by Eq. [14], using the exact structure factor for spherical particles (12),

$$I(h) = I_e(h) \sum_i (\tfrac{4}{3}\pi R_i^3)^2 \rho^2 \left(\frac{9\pi}{2}\right) [J_{3/2}(hR_i)/(hR_i)^{3/2}]^2, \qquad [14]$$

and the following relations can be derived:

$$\int_0^\infty \{I(h)/I_e(h)\} h\, dh = \rho^2 \sum_i (\tfrac{4}{3}\pi R_i^3)^2 \left(\frac{9\pi}{2}\right) \int_0^\infty [J_{3/2}(hR_i)/(hR_i)^{3/2}]^2 h\, dh$$
$$= \rho^2 \sum_i (\tfrac{4}{3}\pi R_i^3)(3\pi R_i);$$

and similarly,

$$\int_0^\infty \{I(h)/I_e(h)\} h^2\, dh = \rho^2 \sum_i (\tfrac{4}{3}\pi R_i^3)^2 \left(\frac{9\pi}{2}\right) \int_0^\infty [J_{3/2}(hR_i)/(hR_i)^{3/2}]^2 h^2\, dh$$
$$= \rho^2 \sum_i (\tfrac{4}{3}\pi R_i^3)(2\pi^2).$$

Thus

$$l_c = \tfrac{3}{2} \sum_i (\tfrac{4}{3}\pi R_i^3) R_i / \sum_i (\tfrac{4}{3}\pi R_i^3)$$

or

$$l_c = \tfrac{3}{4}\bar{D}, \qquad (15)$$

where $\bar{D}$ is the mass averaged diameter. The correlation between the observed values of l_c and the particle sizes measured by the electron microscope is shown in Fig. 3. A linear relation is seen between them. If the

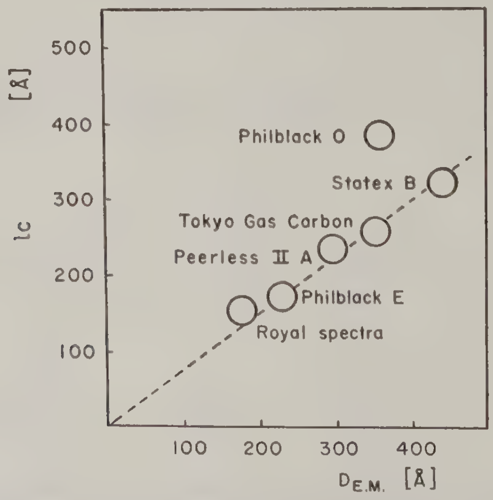

FIG. 3. Correlation between the distance of heterogeneity calculated from the intensity curve and the corresponding particle size by electron microscope.

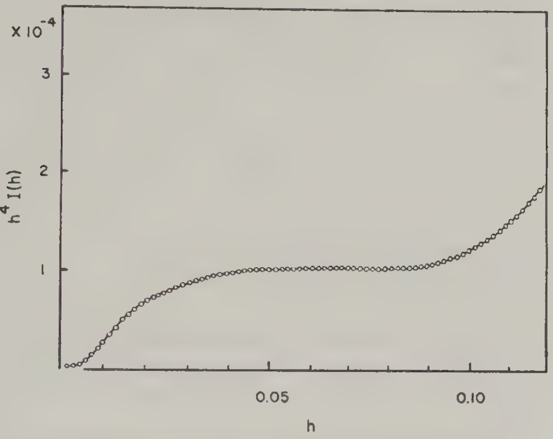

FIG. 4. Plot of $h^4I(h)$ versus h for Tokyo Gas Carbon.

mass averaged diameters are estimated from l_c according to Eq. [15], the values will be of the same magnitude as the electron micrograph data. This means that the observed small-angle scattering is due certainly to the particles which can be observed under the electron microscope. Probably the interparticle interference is not important under the conditions of the present study, at least to a first approximation.

We shall examine next the relation represented in Eq. [11]. The observed intensity was multiplied by h^4, and the product was plotted against h. Figures 4 and 5 are two typical cases of these curves. In Fig. 4, $h^4I(h)$ remains nearly constant in the region from $h = 0.04$ to $h = 0.08$. A horizontal region like this appears with every specimen. Philblack E offers an extreme case in this respect. This region can not be observed clearly, as is seen in Fig. 5, where the curve has only an inflection point.

If it is possible to interpret these horizontal regions by Eq. [11], the specific surface area S_{sp} can be evaluated by means of Eq. [16].

$$S_{sp.} = \pi \frac{(1 - c)}{d} \lim. [h^4 I(h)] \Big/ \int_0^\infty h^2 I(h)\, dh, \qquad [16]$$

where d is the density of the particle. The results are shown in Table VI.[2] The specific surface areas obtained by Eq. [16] are larger than the values estimated from the particle size.[3] However, they are still not unreasonable

---

[2] The value of $h^4I(h)$ at the inflection point was substituted instead of the value of $\lim[h^4I(h)]$ in such cases as Philblack E.

[3] This was evaluated assuming the following equation,

$$S_{sp.} = \frac{6}{d \cdot \bar{D}},$$

the value of $(4/3)l_c$, being used for $\bar{D}$.

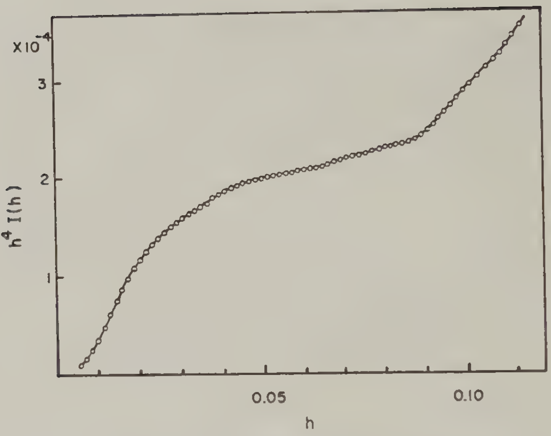

FIG. 5. Plot of $h^4I(h)$ versus h for Philblack E.

values. Therefore, it may be allowable to accept Eq. [11] as an explanation of the horizontal region in the $h^4I(h)$ curves. These regions should extend to larger scattering angles as far as they obey Porod's theory, but the observed curves rise again after a relatively short period. This is a point of disagreement with Porod's theory, which can not be explained simply as the result of experimental error. It seems that there is a definite reason for this fact connected with the substructure of the carbon black particle.

DISCUSSION

Different treatments of the observed small-angle scattering of carbon blacks give the same conclusion; there is a correlation between the results for small-angle scattering and those for the electron micrograph. However, there is one point which is inconsistent between the procedures of analysis by Porod's theory and those by the others. The exact structure factor of spherical particles can be approximated with an exponential function, Guinier's formula, only within the range of small-scattering angles where hR does not exceed 3. Out of this range, there is a deviation. The square of the structure factor shows a damped oscillation. Its principal term is $2\pi\rho^2 S/h^4$, and oscillating terms are added to it. In the polydisperse colloidal system, the scattering intensity in this region will be proportional to h^{-4}, in consequence of the superposition of the scattered radiation from particles of different size. This is the relation represented by Eq. [11]. Therefore, the small-angle scattering in the region where the intensity is proportional to h^{-4} must not be interpreted by Guinier's formula. In other words, the application of Eq. [9] must be limited to scattering angles smaller than this. If we reexamine the results by Fankuchen's method with this restriction, it is evident that the fractions of very small particle size can be given no physical meaning. For example, the fractions corresponding to the diameter 31.7 A, 102 A, and 160 A must be removed from the results for Tokyo Gas Carbon in Table III. Similarly, the fractions with diameters smaller than 190 A must be removed from the results for Statex B in Table IV. In this way, the obtained particle size distributions must be modified greatly. This will lead to a more satisfactory agreement with the observations by the electron microscope.

It is interesting to see that the treatment assuming Eq. [10] succeeded in yielding reasonable values for the average diameter, in spite of the great faults in the resultant particle size distributions. This seems to be due to the following reason. If the observed intensity curve can be sufficiently approximated by Eq. [9] disregarding its physical meaning, by using a suitable function for $M(R)$, it is possible to derive a simple relation between the average diameter and l_c by substituting Eq. [9] into Eq. [13],[4]

$$l_c = 2\left(\frac{\pi}{5}\right)^{1/2} \int_0^\infty RM(R)\,dR \Big/ \int_0^\infty M(R)\,dR = \left(\frac{\pi}{5}\right)^{1/2} \bar{D}, \qquad [17]$$

which shows that the average diameter will be always proportional to l_c, whenever no serious error is introduced in the procedure of analysis. Furthermore, comparing Eq. [17] with Eq. [15], it is evident that the average diameter estimated by the method of analysis which assumes Eq. [9] will be of the same magnitude as the value which is to be obtained using the exact structure factor.

The analysis based on Eq. [9] has been justified because the average particle size agrees with that by other methods (13). However, the discussion mentioned above seems to indicate that such a comparison can not be a criterion for the accuracy of the resultant particle size distribution.

The overestimation of the weight of the smaller particles in the particle size distribution is due not entirely to the incorrect application of Guinier's

---

[4] This relation can be derived as follows:

$$l_c = \frac{\pi \int_0^\infty h \left[\int_0^\infty M(R)R^3 \exp.\,(-h^2R^2/5)\,dR \right] dh}{\int_0^\infty h^2 \left[\int_0^\infty M(R)R^3 \exp.\,(-h^2R^2/5)\,dR \right] dh}$$

$$= \frac{\pi \int_0^\infty M(R)R^3 \left[\int_0^\infty h \exp.\,(-h^2R^2/5)\,dh \right] dR}{\int_0^\infty M(R)R^3 \left[\int_0^\infty h^2 \exp.\,(-h^2R^2/5)\,dh \right] dR}$$

$$= 2\left(\frac{\pi}{5}\right)^{1/2} \left\{ \int_0^\infty RM(R)\,dR \Big/ \int_0^\infty M(R)\,dR \right\}.$$

formula, but is also due partly to the high intensity of scattering in the intermediate angle range. A deviation from the relation represented by Eq. [11] is actually observed. In Porod's theory, the electron density in the particles is assumed to be constant, but this may be not always true, especially in carbon blacks. Various causes may be found for the heterogeneity of the electron density in the particles. For example, it may be caused by micropores, as discussed by Brusset *et al.* (6). If the electron density ρ at the point defined by a vector $\mathbf{x}$ is expressed as

$$\rho(\mathbf{x}) = \rho_0 + \eta(\mathbf{x}), \tag{18}$$

where ρ_0 designates the average electron density of the specimen, the intensity of the observable small-angle scattering from this system will be given by the following integration:

$$I(h) = I_e(h)\overline{\eta^2}V \int_0^\infty \gamma(r)\,\frac{\sin hr}{hr}\,4\pi r^2\,dr, \tag{19}$$

where $\gamma(r)$ is the following function,

$$\gamma(r) = \frac{1}{\overline{\eta^2}V}\int_V \eta(\mathbf{x})\eta(\mathbf{x}+\mathbf{r})\,d\mathbf{x}, \tag{20}$$

and

$$\overline{\eta^2} = \int_V \eta(\mathbf{x})\eta(\mathbf{x})\,d\mathbf{x},$$

and its properties assumed to depend only on the magnitude of r. This equation has been given by Debye and Bueche (14), and it has been pointed out that Eq. [11] is a special case of Eq. [19] (15). In general, $\eta(\mathbf{x})$ can be described as a summation of the two terms,

$$\eta(\mathbf{x}) = \eta_0(\mathbf{x}) + \Delta\eta(\mathbf{x}). \tag{21}$$

In the particle, $\eta_0(\mathbf{x})$ is taken to be equal to the average value of $\eta(\mathbf{x})$, and $\Delta\eta(\mathbf{x})$ represents the small fluctuation of $\eta(\mathbf{x})$ about $\eta_0(\mathbf{x})$. For a point outside the particle, $\eta(\mathbf{x})$ takes a constant value, and $\Delta\eta(\mathbf{x})$ is always zero. Then, Eq. [20] can be expanded as follows,

$$\begin{aligned}\gamma(r) = \frac{1}{\overline{\eta^2}V}\Big\{&\int_V \eta_0(\mathbf{x})\eta_0(\mathbf{x}+\mathbf{r})\,d\mathbf{x} + \int_V \eta_0(\mathbf{x})\Delta\eta(\mathbf{x}+\mathbf{r})\,d\mathbf{x}\\ &+ \int_V \Delta\eta(\mathbf{x})\eta_0(\mathbf{x}+\mathbf{r})\,d\mathbf{x} + \int_V \Delta\eta(\mathbf{x})\Delta\eta(\mathbf{x}+\mathbf{r})\,d\mathbf{x}\Big\}.\end{aligned} \tag{22}$$

The first term in this expansion is the component that has been discussed by Porod. It is certain that $\gamma(r)$ at large values of r can be sufficiently approximated by the first term only. However, the contribution from the other terms must be taken into account at the smaller value of r, and the scattering intensity at the higher scattering angle depends predominantly on the shape of $\gamma(r)$ at the smaller values of r. Therefore, the disagreement of the observed intensity distribution at the intermediate angles with the theory seems to be reasonable. The components corresponding to the first term and the last term can be separately observed by selecting suitable ranges of scattering angle only when the period of the fluctuation of $\eta_0(\mathbf{x})$ is sufficiently greater than that of $\Delta\eta(\mathbf{x})$. In the present case, the contribution of the first term was estimated to be more than 20% of the total intensity at 2°. Furthermore, the scattering due to the fine structure of carbon black cannot be neglected for the scattering angle higher than 3°. Accordingly it is questionable to analyze the intensity curve in the intermediate angle range by the usual method, for example, by Guinier's method. As a matter of fact, no correlation could be found between the slope of the curves of log $I(h)$ versus h^2, at 2°, and the dimensions of the parallel layer group. The same situation was confirmed in the study of the small-angle scattering for a series of specimens, which were heat-treated at various temperatures up to 3000°C. The details of this will be found in a separate report.

ACKNOWLEDGMENTS

The author wishes to express his thanks to Prof. H. Akamatu for his kind direction, and to Mr. H. Takahashi for his constant advice and criticism.

REFERENCES

1. Krishnamuruti, P., *Ind. J. Phys.* **5,** 475 (1930).
2. Warren, B. E., *J. Chem. Phys.* **2,** 551 (1934).
3. Biscoe, J., and Warren, B. E., *J. Appl. Phys.* **13,** 364 (1942).
4. Houska, C. R., and Warren, B. E., *J. Appl. Phys.* **25,** 150 (1954).
5. Brusset, H., *Compt. rend.* **225,** 1002 (1947).
6. Brusset, H., LeRat, B., and Makki, M., *Ann. chim.* (*Paris*) **9,** 474 (1954).
7. Porod, G., *Kolloid-Z.* **124,** 83 (1951).
8. Porod, G., *Kolloid-Z.* **125,** 51 (1952).
9. Hosemann, R., *Kolloid-Z.* **117,** 13 (1950).
10. Kuroda, H., *J. Chem. Soc. Japan* **77,** 1298 (1956).
11. Jellinek, M. H., and Fankuchen, I., *Ind. Eng. Chem.* **37,** 158 (1945).
12. Rayleigh, Lord, *Proc. Roy. Soc.* (*London*) **A90,** 219 (1914).
13. Shull, C. G., and Roess, L. C., *J. Appl. Phys.* **18,** 295 (1947).
14. Debye, P., and Bueche, A. M., *J. Appl. Phys.* **20,** 518 (1949).
15. Guinier, A., and Fournet, G., "*Small-Angle Scattering of X-rays.*" J. Wiley, New York, 1955.

JOURNAL OF COLLOID SCIENCE **12**, 510–522 (1957)

DEFLOCCULATION IN HYDROCARBON OILS

A. Bondi and H. Diamond

Shell Development Company, Emeryville, California

Received July 12, 1957

The increasing use of surface-active substances as deflocculants in non-aqueous solvents has called for better ways to measure the deflocculation of suspended solids in oils. The present investigation was undertaken to develop such a technique covering the temperature range of prospective industrial applications, viz., from room temperature to 200°C. The usual methods, nephelometry and sedimentation, did not appear sufficiently promising to justify the very elaborate instrumentation required. Of the remaining two methods, viscosity and electrical properties, the latter was finally chosen, primarily because accurate electrical measurements can easily be performed over a wide range of conditions.

Among the various possible electrical measurements, direct-current conductivity (at low potential gradients) is the simplest to carry out and to interpret if the solid particles of the system are electronic conductors. However, the following basic limitations are then incurred: (*a*) independent evidence is necessary to show whether a change in conductivity is due to flocculation or deflocculation of the system; (*b*) a quantitative correlation needs to be established between electrical conductivity and the manifestation of deflocculation that is specifically of interest, e.g., viscosity, sedimentation, or some complex use characteristic.

CHOICE OF SYSTEMS

The most important feature of a two-phase system that will give reproducible measurements, namely, the maintenance of uniform particle distribution throughout each volume element, is easily obtained if the particles comprising the disperse phase are small and do not differ in density very greatly from the fluid phase. Graphitized carbon blacks are the only readily available electronic conductors that meet these requirements; moreover, they are available with sufficiently wide variations in surface structure to permit examination of specific interaction effects with surface-active solutes.

Significant physical and chemical properties of the carbon blacks selected are shown in Table I. The intrinsic conductivity of the particles has not been determined and probably does not matter greatly, since the decisive

TABLE I

Properties of Carbon Black

Type	Specific surface area (m.^{2}/g.)[a]	pH Value
Shawinigan Acetylene Black	53	6.2
Spheron 9 (Channel Black)	115	4.3

[a] By nitrogen adsorption.

[b] Determined as the pH value of a 1%w aqueous suspension of the carbon black against a glass electrode. The acid reserve (or binding capacity for strong base) of both blacks is about the same under these conditions (0.6 to 0.7 mg. KOH/g., or approximately 0.1 to 0.2 micromole of acid groups per m.^{2} of surface area).

TABLE II

Properties of Oils (*8*)

	From Texas neutral oil					From Calif.
	White oil	Saturates fraction	Mono-aromatics fraction	Poly-aromatics fraction	Mixed fraction	Mixed fraction
Density		0.855	0.8877		0.875	0.896
n_D^{20}		1.4702	1.4931		1.4855	1.4920
M, average	450	470	470	400	460	430
Kinematic viscosity						
at 38°C., c.s.		38.6	49.2	694	57	117
at 100°C., c.s.		6.3	6.8	18.8	—	9.6
Monoaromatics, %m	0	None	90	30	18	20
Polyaromatics, %m	0	None	1.2	70	17	None

TABLE III

Nature of Additives

Symbol	Name	Molecular weight of hydrocarbon radical
A	Basic[a] calcium petroleum sulfonate[b]	*ca.* 400
C	Calcium alkyl phenate polymer (D.P. = 8)	*ca.* 220 (per chain link)
D	Nonionic polyfunctional polymer (D.P. = 40)	*ca.* 330 (per chain link)

[a] "Basic" signifies that the sulfonate contains more than the stoichiometric amount of calcium hydroxide, partly as colloidal dispersion (identifiable by X-ray diffraction pattern) and perhaps partly as soluble complex.

[b] Primarily alkyltetralin sulfonic acids.

conducting path is located on the particle surface, especially the interparticle contact.

Properties of the liquids employed are presented in Table II. Only oils reasonably free of surface-active impurities were chosen so as not to confuse interpretation of the data.

Chemical description of the deflocculants is given in Table III. No effort was made to obtain pure or better defined chemical substances as deflocculants for this exploratory investigation. Their preparation is very difficult, and only few pure compounds of suitable molecular structure are sufficiently soluble in hydrocarbons. Work on such a model substance may perhaps be reported in the future. One serious disadvantage of mixed adsorbates is their fractional adsorption and the consequent dependence of the results on the adsorbent/adsorbate ratio as well as on the absolute solute concentration. Extrapolation of the data presented to widely different ratios would depend upon knowledge of the equilibrium concentration of adsorbate in the free oil. The few such measurements carried out may be regarded as of only semiquantitative validity, since the composition of the surfactant mixture in the solution certainly differs from that adsorbed on the particle surface.

These deficiencies detract substantially from the value of the experimental data and should be seriously considered in any future investigations. Nevertheless, the many novel phenomena encountered are worth recording, even if only as a challenge. A correlation of the deflocculation data with performance of some of the deflocculants in automotive engines has also been reported (2).

Experimental Procedure

A stock suspension of 15% carbon black in base oil was prepared in a ball mill and its electrical conductivity checked at regular intervals. Whenever the conductivity began to decrease (owing to formation of surface-active oil oxidation products) the stock suspension was discarded. A solution of surface-active agent in base oil was added so as to yield a final blend at the desired additive concentration containing 10%w carbon black. The general relation between electrical conductivity and carbon black concentration has been described (4); a level of 10%w was chosen because the resulting soft gel would then not separate on standing. At room temperature, one week generally sufficed to equilibrate the additive blend which was then charged to the rotating-electrode cell. Equilibration in the apparatus at the higher temperatures was checked by extended replication of measurements and found to be quite rapid. The electrical measuring technique and equipment have been described elsewhere (3, 9).

Experimental Results

Physical meaning may be attached to the arithmetic as well as the geometric increase in electrical resistance occasioned by the action of the surface-active agents. Increase in resistance is a measure of the decrease in steady-state concentration of continuous (and therefore conducting) particle chains across the electrode gap. The ratio of the increase in resistance (caused by the deflocculant) to the resistance of the flocculated-particle system is proportional to the ratio of shear-induced particle collisions not leading to the formation of conducting chains to those that do. (See derivation in Appendix.) Degree of deflocculation is herein expressed as (the logarithm of) the resistance ratio, designated pD^w. The superscript indicates that the reference state of "complete flocculation" is the given carbon black suspension (at rest) in a medicinal white oil.

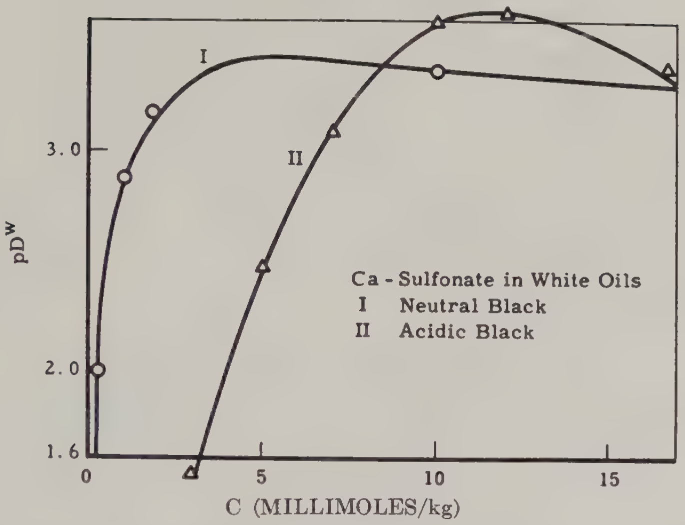

FIG. 1. Effect of Ca petroleum sulfonate (additive A) on deflocculation in saturated hydrocarbon oils at 30°C. *Curve I:* In white oil against acetylene black (multiply concentration scale by 10). *Curve II:* In saturates fraction against channel black.

A typical plot of pD^w (at a definite shear rate) against additive concentration is given in Fig. 1. As a standard procedure, actual data are extrapolated down to a shear rate of 2 sec.$^{-1}$ (1 r.p.m.), since control is poor at very low speeds. The maximum resistance (or resistance ratio) indicates the optimum deflocculation achievable with a given additive, and the corresponding concentration (C_B) is likewise a significant characteristic; both, of course, are a function of temperature.

As long as there is appreciable conduction through the particle chains formed by even transient contact (flocculation), shearing action increases electrical resistance through disruption of the chains. Once all particles have been covered with an electrically insulating monolayer of additive, electrical conduction in the suspension takes place primarily by charge transfer through particle collisions and electrical resistance decreases with increasing rotor speed (3). (Such charge transfer by particle collision has previously been observed in the same rotating-electrode apparatus with suspensions of nonconducting silica particles (3).) This reversal in effect of shear is a further, very sensitive, measure of deflocculation[1] and, as indicated in Fig. 2, generally precedes the resistance maximum, if only by a small concentration increment.

Typical resistance-vs.-concentration curves (with temperature as parameter) are given in Figs. 3 to 8. The peculiar maxima in certain systems result

---

[1] The criterion for deflocculation is that $dR/d\dot{e} < 0$ for the entire range (i.e., $\dot{e} > 5$ sec.$^{-1}$), not only at high shear rates; $dR/d\dot{e} < 0$ at high values of $\dot{e}$ (> 500 sec.$^{-1}$) even for flocculated systems because of extensive collisions of disrupted chain fragments.

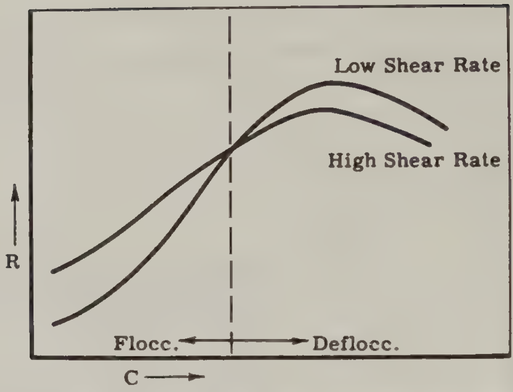

FIG. 2. Schematic drawing indicating the effect of shear rate and additive concentration (*C*) on the electrical resistance (*R*) of carbon black suspensions in oil.

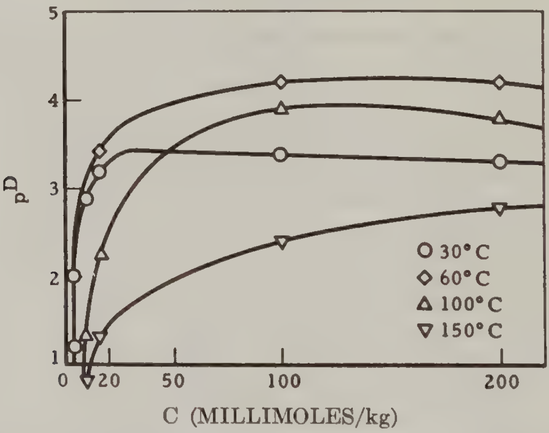

FIG. 3. Effect of concentration (additive A) and temperature on deflocculation of acetylene black in white oil.

from the contribution of ionic conductance of the unadsorbed additive, detailed in Fig. 9, which becomes important when complete surface coverage of the carbon particles has thoroughly suppressed electrical conduction through the particle chains.

The conductance of the free additive reduces the maximum observable resistance of the system and thereby obscures the measurement of the maximum degree of deflocculation, especially of channel blacks. Fortunately, this conductivity effect is relatively small (for reasons which will be discussed later on). The depression of the resistance maximum may therefore be insignificant and will be ignored for the present.

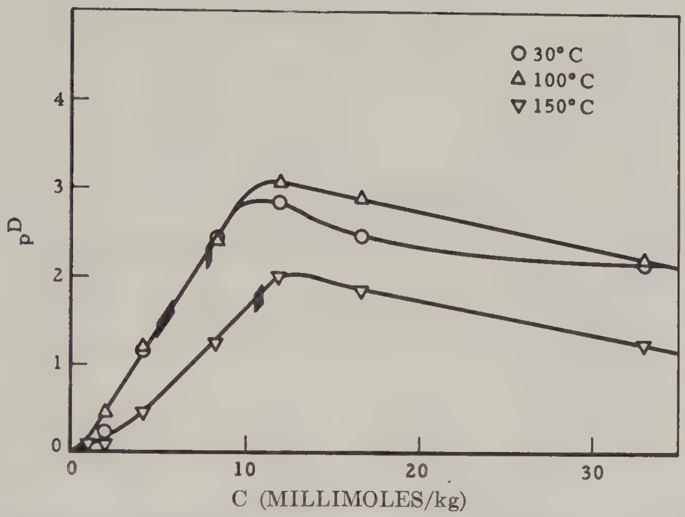

FIG. 4. Effect of concentration (additive A) and temperature on deflocculation of channel black in saturates fraction. The shaded areas denote "crossover" region.

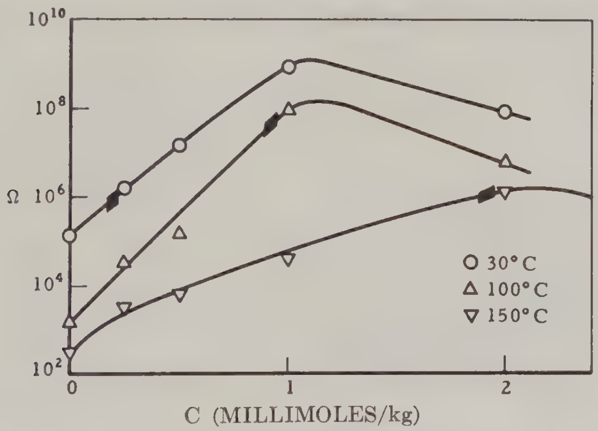

FIG. 5. Effect of polymeric additive D on deflocculation of acetylene black in mixed California fraction.

DISCUSSION

a) General Phenomena

The effect of chemical structure on deflocculation (as measured by electrical conductivity) may be better understood after consideration of the mechanism of conductance. Under static conditions, current flow through a fixed number of particle junctions depends largely on the mechanical history of the system. Under dynamic conditions, junctions are constantly

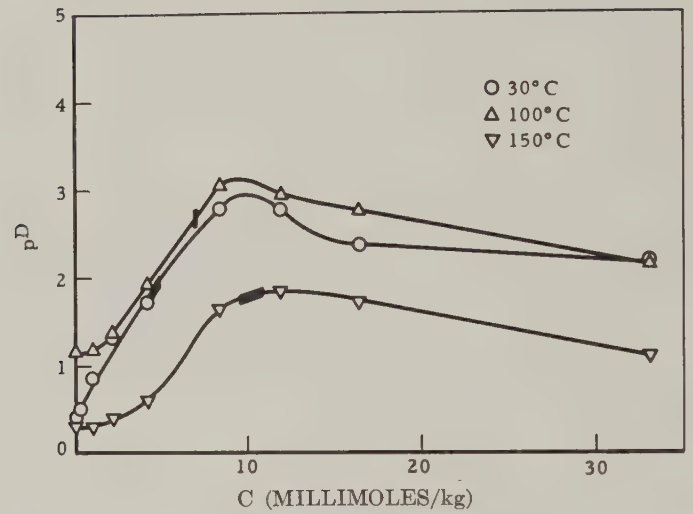

FIG. 6. Deflocculation effect of additive A in saturates fraction containing 15% monoaromatic hydrocarbons with channel black. Shaded area: crossover region.

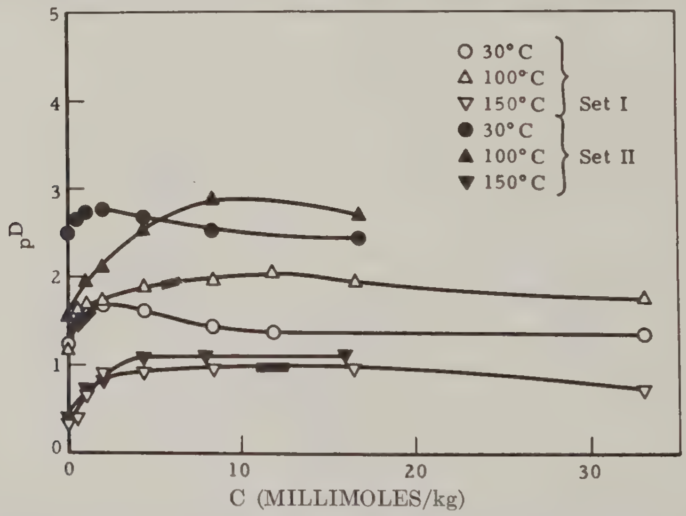

FIG. 7. Deflocculation effect of additive A with channel black: Set I in saturates fraction containing 10% polyaromatics; Set II mixed California fraction.

broken and re-formed; current intensity is then a measure of the steady-state concentration of junctions leading to continuous chains across the electrode gap. The rate of re-formation of the junctions depends upon the possibility of displacement of adsorbed molecules from the surfaces of the colliding particles, and is therefore inversely proportional to the lifetime τ_m of a molecule of fluid (or adsorbate) in the solid-fluid interface. If $\tau_m > \tau_c$ (the

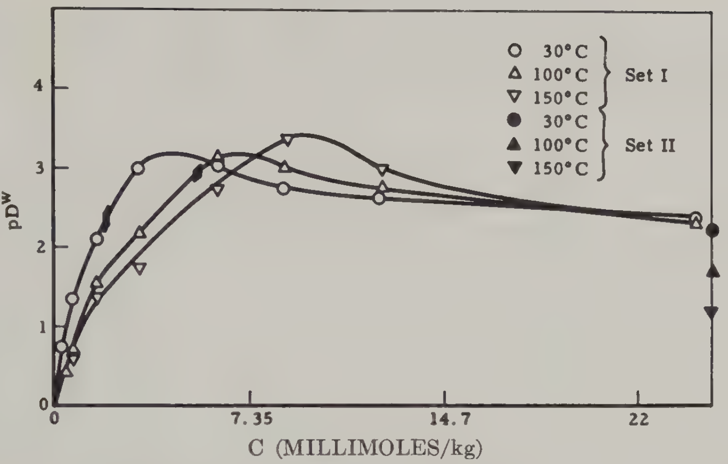

FIG. 8. Deflocculation effect of additive C on channel black in white oil. The point Set II indicates the location of maxima for acetylene black deflocculation in this additive.

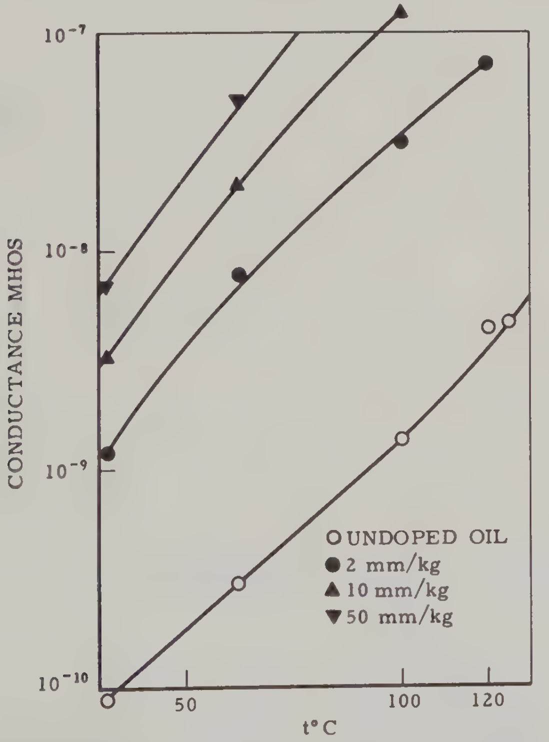

FIG. 9. Electrical conductivity of additive A solutions in motor oil stock in the cell used for the measurements in the carbon black system.

lifetime of a collision), then the probability for the incidence of a chain-forming collision is very small and becomes zero when $\tau_m \rightarrow \infty$, as when the adsorbate is held by strong chemical bonds. In principle,

$$\tau_m = \tau_0 \exp (\Delta H_a/RT)$$

where τ_0 (the reciprocal of the thermal vibration frequency of the atom in the surface) $\sim 10^{-13}$ sec. and ΔH_a is the heat of adsorption (out of solution) (5).

A long lifetime in the interface is necessary for an adsorbate to cause deflocculation. A few crude experiments showed that, at room temperature, the additive concentration in equilibrium with the layer giving maximum degree of deflocculation on 10%w of carbon black in the oil is quite small, viz., less than 10 micromoles/kg. of oil for a calcium petroleum sulfonate.[2] This figure is at best correct to within an order of magnitude and awaits confirmation by improved analytical techniques.

b) *Specificity of Interaction with Neutral and with Acidic Carbon-Black Surfaces*

A peculiar feature of the acidic carbon black is the low surface coverage (less than 70%) at which maximum deflocculation appears to be achieved. Since for this carbon black the N_2-adsorption area is identical with the electron microscope area, inaccessible pores cannot be responsible for the result. In the presence of aromatic oil components, the surface coverage by the additive is particularly small owing to the well-known (10) strong adsorption of the (basic) aromatic hydrocarbons on acidic carbon black (see Table IV).

Adsorption of the additives on the neutral surface of acetylene black is more "normal" than on the acidic channel black. The surfactant thoroughly displaces the oil molecules from the interface. Consequently, the low-temperature coverage is in approximate agreement with the assumption of dense packing of the adsorbate of known molecular structure. The adsorption of aromatic oil components (as evident from deflocculation) is practically negligible on acetylene black. The presence of aromatic components in the oil here increases the amount of additive required to maintain a given degree of deflocculation through the better "solubility," i.e., reduced thermodynamic activity and thereby reduced driving force for adsorption of the additive out of solution.

The higher concentration of additive required to deflocculate a neutral

---

[2] Determined from spreading-pressure measurements on the supernatant liquid, (by Dr. W. M. Sawyer). It is indicated that surface saturation (of the acidic black) occurs at 0.6 millimole/*kg* with respect to electrical deflocculation and at 1.5 millimole/*kg* according to adsorption isotherm measurements where conc. is determined by spreading pressure at the oil/water interface.

TABLE IV

Relative Surface Coverage at Maximum Degree of Deflocculation at 30°C.

Additive	Oil	Black	$\theta_c{}^b$	$\theta_m{}^b$
A[a]	Saturates fraction	Acidic	0.34	0.67
A	Saturates fraction + 1.5% monoaromatics	Acidic	0.38	—
A	Saturates fraction + 15% monoaromatics	Acidic	0.31	0.62
A	Saturates fraction + 1.5% polyaromatics	Acidic	0.16	—
A	Saturates fraction + 10% polyaromatics	Acidic	0.034	0.18
A	Mixed fraction, Texas	Acidic	0.034	0.034
A	Mixed fraction, California	Acidic	0.085	0.1
C[c]	White oil	Acidic	0.13	0.17
A	White oil	Neutral		1
D[d]	White oil	Neutral		1
D	White oil	Acidic		0.4

[a] Based on an area per molecule of 125Å², determined at the water/oil interface by Dr. F. M. Fowkes.

[b] Fraction of surface covered, θ_c at crossover (where $dR/d\dot{e} = 0$) and θ_m at resistance maximum.

[c] Based on an area per chain link of 80Å², determined at the water/air interface by Dr. W.M. Sawyer.

[d] Based on area per chain link of 46.3 Å², determined at the water/air interface by Dr. M. J. Schick.

TABLE V

Deflocculation by Aromatic Oil Components (in Additive-Free Oils)

Base oil	Aromatics	Conc. %w	Carbon black type	pD^{b*} at		
				30°C.	100°C.	150°C.
Mixed fraction, Calif.	Mixed aromatics[a]	20	Neutral	0.7	0.	0
Mixed fraction, Calif.	Mixed aromatics[a]	20	Acidic	1.5	0.9	0.8
Saturates fraction, Texas	Monoaromatics[b]	15	Acidic	0.3	0.3	0.2
Saturates fraction, Texas	Polyaromatics[b]	10	Acidic	1.4	1.0	0

* Degree of deflocculation relative to aromatic-free base components.

[a] Indigenous mixture.

[b] Chromatographically separated components added to the saturates fraction from the same fractionation procedure.

as compared to an acidic black, especially at high temperatures, (*cf.* Figs. 3 and 4) is noteworthy. Complete deflocculation of the neutral carbon black (in terms of the change in sign of the resistance/shear velocity relation mentioned above) is obtained with the nonionic polymeric additive D (Fig. 5) but not with most of the lower-molecular weight "detergents."

The effect of aromatic hydrocarbons on the deflocculating activity of the calcium sulfonate additive vs. acidic black can be recognized from a comparison of the curves of Figs. 4, 6, and 7. Monoaromatic hydrocarbons have a relatively small effect, but polyaromatic hydrocarbons severely depress the maximum achievable degree of deflocculation, especially at high temperatures. The molecules in the previously mentioned layer of coadsorbed (poly)aromatic hydrocarbon and additive apparently have a relatively small average lifetime in the adsorbed state. This may have less to do with the phenomenon of coadsorption than with the reduced activity of the additive in the polyaromatics as compared with the pure saturated hydrocarbon solution.

A rather striking case of specific chemical interaction between additive and carbon black is presented in Fig. 8, showing the deflocculation of acidic black by the strongly alkaline calcium phenate polymer. Especially noteworthy here is the temperature independence of the deflocculating effectiveness. The neutral black, by contrast, is deflocculated only very slightly by this additive, even at very high concentration.

c) *Multilayer Adsorption*

The maxima in the resistance-vs.-additive concentration curves appearing in most deflocculation measurements discussed above permit an approximate estimate of the amount of additive that is immobilized by adhesion to the fully deflocculated carbon-black particles. Nearly all the conductivity of the system, at moderate electrode speeds, is then derived from the ionic conductivity of the additive solution. If it is assumed that partial adsorption of the additive causes no fractionation by conductivity, then it becomes possible to estimate the amount of free additive in the solution by comparison of the observed conductivity beyond the maximum with a calibration curve of carbon-free blend conductivity-vs.-additive concentration (Fig. 9). The origin of the additive conductance is obscure at present.

The results of such a calculation may be summarized as follows. In oils containing fairly large concentrations of aromatic hydrocarbons, the observed excess conductivity is very nearly that predicted from the excess of additive over the amount adsorbed on the black. However, in oils containing no aromatics or only small amounts of monoaromatic hydrocarbons, the conductivity calculated on the basis of estimated unadsorbed additive is 5 to 50 times as great as the observed value.

The most obvious explanation, and one that seems irrefutable in spite of its mental inconvenience, is that many layers of adsorbate are being deposited at concentrations in excess of C_B (defined earlier). In agreement with previous observations in this laboratory (1), multilayer deposition is here also associated with the incidence of micelle formation. The maximum in the pD^w-vs.-temperature curve may also be the result of this competitive adsorption process.

In the case of polymers, the positive temperature coefficient of pD^w may be ascribed to the thermally induced dangling of long loops of partially attached chains, which very effectively prevent the mutual approach of carbon particles (7). The theory of polymer adsorption predicts that the loops between surface anchor points should become larger with increasing temperature (6). When a temperature is reached where most of the chain dangles off the surface and leaves it barren much of the time, the degree of deflocculation must decrease rapidly with further increases in temperature, as is indeed observed. It is noteworthy that very strongly adsorbed polymers displace oil molecules (including aromatics) more effectively from carbon-black surfaces than do low-molecular weight dispersants.

A detailed interpretation of these exploratory data in terms of relations between adsorption lifetime of the adsorbates, the molecular structure, temperature, etc. would be tempting but should await better understanding and control of the measurement itself.

SUMMARY

Exploratory electrical conductivity experiments on the deflocculation of neutral and acidic carbon blacks in hydrocarbon solvents have demonstrated the importance of specifying the nature of the surface of a suspensoid in dispersion tests.

All the additives examined in aromatic-free solvent deflocculated acidic carbon black more effectively than neutral carbon black.

The composition of the hydrocarbon solvent had a far greater effect on deflocculation of acidic than of neutral black, presumably because the intrinsically basic aromatics were strongly adsorbed by acidic surfaces.

Multilayer adsorption of a few conventional deflocculants out of essentially paraffinic oils has been indicated. The dispersant performance of a strongly adsorbed polymeric deflocculant may be explained in terms of partial detachment in the form of chain loops that "dangle" from the interface into the oil.

The chemical reasons for the observed effects may now be understood in a qualitative manner, but detailed quantitative explanations will require more refined experimental techniques.

APPENDIX

Derivation of an Expression for the Degree of Deflocculation

Assumptions:

1. The total number of collisions $N_c = N_e + N_i$, where N_e, N_i are the collisions which are effective and ineffective, respectively, in bringing about the formation of conducting particle chains.

2. The electrical current $i \propto \dot{N}_e = \dot{N}_c - \dot{N}_i$ (the dot indicating the time derivative).

Hence, $(i(f) - i(d)) \propto (\dot{N}_i(d) - \dot{N}_i(f))$, where (f), (d) refer to the flocculated and the deflocculated system. Now, in the cases of interest, $\dot{N}_i(d) \gg \dot{N}_i(f)$, or $(i(f) - i(d)) \propto \dot{N}_i(d)$, and

$$\frac{i(f) - i(d)}{i(d)} \propto \frac{N_i(d)}{N_e(d)}.$$

Acknowledgments

The authors are indebted to Dr. F. M. Fowkes and his collaborators for supplementary surface chemical information on the additives used in this work. Much of the experimental work was carried out by Messrs. R. F. Fraatz, W. E. Kerlin, and K. R. Williams.

References

1. Barnum, E. R., Larsen, R. G., and Wachter, A., *Corrosion* **4,** No. 9 (1948).
2. Bondi, A., Beaubien, S. J., and Diamond, H., *Lubrication Eng.* **12,** 267 (1956).
3. Bondi, A., and Penther, C. J., *J. Phys. Chem.* **57,** 72 (1953).
4. Bondi, A., *Proc. 2nd Intern. Conf. Rheology*, p. 274 (1953).
5. Brophy, J. E., and Zisman, W. A., *Ann. N. Y. Acad. Sci.* **53,** (4) 836 (1951).
6. Frisch, H. L., and Simha, R., *J. Phys. Chem.* **57,** 584 (1953); *ibid.* **58,** 507 (1954).
7. Mackor, E. L., and van der Waals, J. H., *J. Colloid Sci.* **7,** 535 (1952).
8. Moore, R. J., Shell Development Company, private communication.
9. Penther, C. J., and Bondi, A., *J. Phys. Chem.* **57,** 540 (1953).
10. van der Waarden, M., *J. Colloid Sci.* **5,** 317 (1950).

JOURNAL OF COLLOID SCIENCE **12**, 523–525 (1957)

Letter to the Editor

HENRY'S LAW CONSTANTS OF BUTADIENE IN AQUEOUS SOLUTIONS OF A CATIONIC SURFACTANT

The solubilization of organic vapors by aqueous solutions of surfactants has been studied by McBain and co-workers (1–3). Although results for a large number of cationic, anionic, and nonionic surfactants have been reported, no single agent has been investigated sufficiently to obtain the variation of the Henry's law constant for the solubility of the gas as a function of the concentration of the surfactant. We report herein the Henry's law constants for butadiene in water and in aqueous solutions of a cationic surfactant, Hyamine 1622, at 25.0°C.

The materials used were: Matheson Company's C.P. grade, 99.0% pure, 1,3-butadiene, freed from traces of air by freezing and pumping at liquid nitrogen temperature; Hyamine 1622 (Rohm and Haas Co.), 98.8% *p*-diisobutylphenoxyethoxyethyldimethyl-benzylammonium chloride monohydrate.

The apparatus used was essentially a volumetric adsorption system with a mercury manometer, which was read to the nearest 0.05 mm. by means of a cathetometer. The amount of gas solubilized was calculated from pressure measurements before and after admitting gas to the solution, the necessary corrections being made for the presence of water vapor and changes in total volume of the system. The temperature of the solution was kept constant by circulating water from a thermostat at 25°C. through the jacketed sample holder. The solution was stirred with a magnetic stirrer, to reach equilibrium sooner.

The isotherms for pure water and for three concentrations of Hyamine 1622 are given in Fig. 1. In each solution the solubility of butadiene increased linearly with the equilibrium pressure. Henry's law constants from these data are as follows:

Concentration of surfactant (wt. %):	0.00	1.00	2.00	4.00
$k \times 10^{-6}$ in mm./mole gas/mole soln.:	2.96	2.04	1.62	1.24

The Henry's law constant of butadiene in pure water compares favorably with the value of 2.72×10^6 mm./mole gas/mole soln., which can be calculated from the data reported by McBain and O'Connor (1).

The regular decrease of the Henry's law constant is found to be linear with the logarithm of the surfactant concentration, as shown in Fig. 2. Extrapolating the experimental straight line to the concentration of sur-

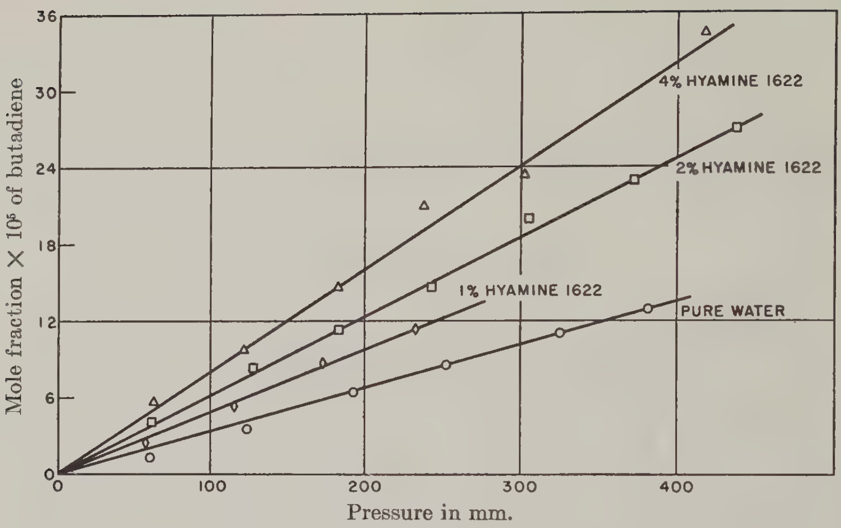

Fig. 1. Mole fraction of butadiene dissolved in pure water and in solutions of Hyamine 1622 as a function of the equilibrium partial pressure of butadiene.

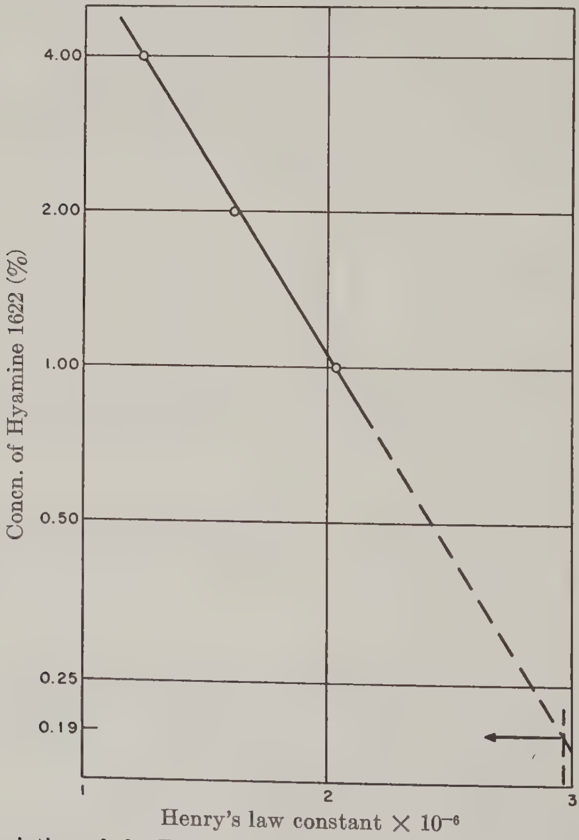

Fig. 2. Variation of the Henry's law constant for the solubility of butadiene in aqueous solutions of Hyamine 1622 with the concentration of the solution.

factant corresponding to a Henry's law constant of 2.96 × 10^6 would presumably yield a minimum concentration of surfactant below which no solubilization occurs. In terms of present-day theory, solubilization results from the presence of association micelles in solution; the existence of a minimum concentration below which solubilization does not occur is evidence of a critical micelle concentration. The value for the minimum concentration obtained from Fig. 2 is 0.19% Hyamine 1622. The critical micelle concentration of Hyamine 1622 as determined by conductivity measurements by T. H. Bramfitt in this laboratory, is 0.16%. The role of micelles in solubilization is thus unequivocally shown.

REFERENCES

1. McBain, J. W., and O'Connor, J. J., *J. Am. Chem. Soc.* **63,** 875 (1941).
2. McBain, J. W., and Soldate, A. M., *J. Am. Chem. Soc.* **64,** 1556 (1942).
3. McBain, J. W., *Advances in Colloid Sci.*, Vol. 1, p. 116 (1942).

Department of Chemistry,
Rensselaer Polytechnic Institute,
Troy, New York

Sydney Ross
John B. Hudson

Received September 16, 1957

JOURNAL OF COLLOID SCIENCE **12**, 526–527 (1957)

BOOK REVIEWS

Annals of Physics, Edited by Philip M. Morse. Academic Press Inc., New York 3, N. Y. Published monthly.

"Why another Journal?" is a natural question. We quote from the statement of purpose:

"The rapid increase in the level of activity in physics in the past decade has led to correspondingly rapid development in many fields, together with an almost explosive increase in publication. A natural consequence is that no single journal in physics can possibly satisfy the needs of all readers, which range from general interest to those of the specialist.

"The *Annals of Physics* is intended to provide a medium for original work of broad significance, in which the author will be able to give attention to clarity and intelligibility, so that his paper may be read by the widest possible audience. Opportunities for presentations of this kind are rather limited today."

No one will quarrel with these statements, and a journal under such distinguished editorship, having an editorial council of the following eminent scientists:

E. Amaldi
R. F. Bacher
H. A. Bethe
S. Chandrasekhar
E. M. McMillan
L. Nordheim
J. R. Oppenheimer
R. E. Peierls
I. I. Rabi
F. Seitz
E. P. Wigner
C. Zener

augurs well for the future.

What should interest scientists in the United States is that an independent publisher without support from any technical society can publish a monthly Journal of excellent format without imposing a charge of $25.00 per page on authors or their sponsors. It can be done!

Victor K. La Mer, New York, New York

Mechanica Aerosolej (Mechanics of Aerosols). By N. A. Fuchs. Academy of Science of the U.S.S.R., Moscow, 1955. 351 pp. Price 19 roubles.

The increasing use of aerosols in industry and medicine and the growing importance of aerosol research for solution of a number of problems in meteorology, air pollution (smog), warfare (artificial fogs, fallout particles), account for a steady increase in the rate of publications in this field, especially during the last decade. Many hundreds of articles about aerosols are scattered in a number of periodicals. Because of the special methods of investigation applied in this field and the large amount of information available, it is now possible to speak of an aerosol science, a new branch of science, which is distinctly different from colloid science, although there is a close relation between them.

To our knowledge, the book under review is the first successful attempt to systematize our knowledge about mechanical behavior of aerosol particles.

As the author states in the Preface, the term "mechanics of aerosols" is here introduced for the first time. Mechanics of aerosols, according to him, is "the study of motion of aerosol particles, of their precipitation and coagulation . . ." as well as the study of related problems "about phenomena which take place by contact between aerosol particles and particles and macroscopic bodies . . . and transfer of powders into aerosols."

In Chapter 1, the author classifies aerosols and discusses their shape, size, and size distributions and then, in accordance with this definition, in following chapters goes over to a systematic investigation of the motion of aerosols under the influence of different forces. Chapter 2 is devoted to the study of uniform rectilinear motion of aerosol particles. Stokes' law is introduced and its applicability in different size regions is discussed. The motion of spherical and nonspherical particles is investigated. The motion of aerosol particles in gravitational, electrical, and thermal field is described. In Chapter 3 nonuniform rectilinear motion of aerosol particles is treated. This includes the motion characterized by big and small Reynolds' numbers, the behavior of aerosol particles under action of sound waves, hydrodynamical interaction between particles, and electrostatic dissipation of aerosols. Chapter 4 is devoted to curvilinear motions of aerosol particles. Such topics are under discussion as gravitational and electrical precipitation of aerosols from a laminar flow, precipitation of aerosol particles in a centrifuge, principle of conifuge and cyclon, and inertial precipitation of aerosol on bodies of different form. Chapters 5 and 6 deal with Brownian motion and diffusions in aerosols under conditions of laminar flow, turbulent flow, and convection. Among topics discussed are the precipitation of aerosol particles in the respiratory tract and the filtration of aerosols through fibrous media. The subject of Chapter 7 is the coagulation of aerosols. The author discusses separately thermal and gravitational coagulation as well as coagulation of aerosols in an electric field and under influence of ultrasonic vibrations. The coagulation of aerosols in a turbulent flow and the effectiveness of collisions of aerosol particles are described in this chapter. The last chapter (Chapter 8) deals with transfer of powder-like bodies into the aerosol state.

The bibliography at the end of the book contains 581 entries. The references are taken from Russian, Anglo American (about 40%), German, and French sources.

V. Drozin, Lewisburg, Pennsylvania

"Light Scattering by Colloidal Systems. An Annotated Bibliography." By Myer M. Fishman. Published by Technical Service Laboratories, River Edge, New Jersey, January, 1957. 84 pp. Price $2.25.

This is a comprehensive guide covering all aspects of light scattering literature from recognition and inception in 1869 through 1956.

There are 850 abstracted references, and the contributions of 750 authors are indexed.

Victor K. La Mer, New York, New York

Name Reactions in Organic Chemistry

By Alexander R. Surrey

Sterling-Winthrop Research Institute, Rensselaer, New York

1954, 192 pp., illus., $5.00

In the literature of organic chemistry there is a time-honored custom of designating many reactions by the names of the chemists who discovered or developed them. These "name reactions" constitute a considerable portion of the tools available to the organic chemist. Since their discovery these reactions have been applied in organic syntheses in varying degrees, and many have been modified. New procedures, reaction conditions, solvents, and condensing agents all have contributed to their development and improvement. In addition, investigations of mechanisms have led to a better understanding of many of them. As a result, the organic chemist today has at his disposal tools that have been sharpened and polished. It seemed worth while, therefore, to assemble these reactions and make them available to the chemist in their present state. The general plan was to present a description of each reaction, its scope, applicability, and limitations, and to bring it up to date in regard to any new developments.

REVIEWS:

"This book is a 'must' for the student of synthetic organic chemistry, and is highly recommended to the inquisitive chemist in need of knowledge."

—*The Capital Chemist*

"Der Text ist leicht fasslich, lebendig und klar geschrieben, durch zahlreiche Formeln illustriert und mit Hinweisen auf Originalliteratur und zusammenfassende Artikel versehen. . . . Das Buch dürfte sich vor allem für den Unterricht bewähren; darüber hinaus kann es im Rahmen seines begrenzten Umfanges ('name reactions' aus der analytischen, theoretischen und technischen organischen Chemie wurden nicht berücksichtigt) auch als Nachschlagewerk für chemische Bibliotheken sehr empfohlen werden."

—*Chimia*

"The biographical notes give a short account of the life, background and contributions of the various chemists and the inclusion of these sketches is a particularly attractive feature of the present volume."

—*Current Science*

"The text should be helpful to the graduate student preparing for preliminary examinations in that it provides him with concise discussions of a large number of organic reactions with which he should be familiar. . . . The up-to-date references provide useful leads to the chemist wishing to keep abreast of developments involving the name reactions discussed in the text."

—*Journal of the American Chemical Society*

ACADEMIC PRESS INC., Publishers
111 Fifth Avenue, New York 3, New York

JOURNAL OF COLLOID SCIENCE **12**, 529–537 (1957)

INTERACTION OF INORGANIC MACROMOLECULAR SYSTEMS WITH SURFACE-ACTIVE AGENTS[1]

J. Fred Hazel and Harold O. Strange

Department of Chemistry, University of Pennsylvania, Philadelphia, Pennsylvania

Received June 7, 1957; revised August 21, 1957

ABSTRACT

Several inorganic macromolecular systems and ionic surface-active agents have been studied in relation to the effect of the surface-active agents on the stability of colloidal suspensions of the inorganic substances, as well as the effect of the inorganic macromolecules on the critical concentration (CMC) of the surface-active agents.

Iron (III) oxide, aluminum oxide, manganese (IV) oxide, and arsenic (III) sulfide comprised the inorganic systems. Potassium salts of a series of fatty acids, alkyl sodium sulfates, alkyl amine hydrochlorides, and alkyl pyridinium chlorides were used as the colloidal electrolytes.

The stability of the colloidal suspensions in the presence of the surface-active agents varied inversely with the chain length of the surfactant, in the cases where the surface-active ion possessed a charge opposite in sign to that of the colloidal particle. In such systems the minimum concentration required to cause complete flocculation decreased sharply with increase in chain length of the surfactant. At higher concentrations of the surfactants a restabilization of the inorganic systems was observed owing to recharging of the colloidal particles. Logarithmic plots of chain length versus flocculation values approached straight lines as the concentration of the sols decreased. When the surface-active ion had the same sign of charge as the colloid, flocculation occurred only at high concentrations and was independent of chain length. The flocculation value was the same for all members of a homologous series in the latter case.

The critical concentration of the anionic surfactants were found to be higher in iron (III) oxide sols than in water, the difference in CMC values being attributed to adsorption of the surfactant by the iron (III) oxide. In a similar manner, manganese (IV) oxide increased the critical concentration of dodecylamine hydrochloride. The critical concentrations of the surface-active ions were unaltered in the presence of colloid particles of the same sign.

---

[1] This work was supported by a grant from the Office of Naval Research. The paper is abstracted from a thesis submitted by Harold O. Strange to the faculty of the Graduate School of the University of Pennsylvania in partial fulfillment of the requirements for the degree of Doctor of Philosophy.

Presented before the Symposium on Adsorption from Solution, Division of Colloid Chemistry, at the 131st Meeting of the American Chemical Society, Miami, Florida, April, 1957.

INTRODUCTION

Low concentrations of ionic surface-active agents flocculate colloidal systems when their active ion has a charge opposite to that of the colloidal particles (1–3). In several cases recharging and restabilization of the colloidal systems has been indicated (4–6).

In the recharged form colloidal systems are stable over a much wider concentration range of electrolyte, e.g., 10^3 times as great (7), than when they have their original sign of charge. It has been suggested that the interference with coagulation caused by the presence of small amounts of detergents in water may be traceable to this course (8).

The surface-active agents employed in the present study are 1-1 electrolytes. In dilute solutions these electrolytes are known to dissociate into simple ions, but at higher concentrations they associate into polyvalent micelles. Their pronounced coagulating action at low concentration is much greater than found with most nonassociating monovalent ions and is more nearly like that of polyvalent ions or micelles.

The present report describes a detailed study of the effect of chain length in homologous series of colloidal electrolytes on the stability of suspensions of inorganic colloidal systems. A further object was to study the effect of the inorganic particles on the critical concentrations of the surface-active agents. No quantitative measurements of the effect of charged colloidal particle on the critical concentrations of association colloids have been found in the literature.

MATERIALS

The inorganic colloidal suspensions were prepared by well-known methods: iron (III) oxide by high-temperature hydrolysis of iron (III) chloride solution (9); aluminum oxide by peptization of aluminum hydroxide with dilute hydrochloric acid (10); manganese (IV) oxide by reduction of potassium permanganate solution with hydrogen peroxide (11); arsenic (III) sulfide by bubbling hydrogen sulfide gas through a solution of arsenic (III) oxide until the reaction was complete (12). The arsenic (III) sulfide sol was washed free of hydrogen sulfide by bubbling hydrogen through it. Washing was considered complete when the effusing stream of gas gave no test with moistened lead acetate paper. The other colloidal systems were

TABLE I

Inorganic Colloidal Systems

	Concentration	pH
Iron (III) oxide	6.38 g. Fe_2O_3 per liter	5.10
Aluminum oxide	1.62 g. Al_2O_3 per liter	5.70
Manganese (IV) oxide	0.61 g. MnO_2 per liter	6.10
Arsenic (III) sulfide	0.83 g. As_2S_3 per liter	

TABLE II

Ionic Surface-Active Agents

Anion active compounds	Cation active compounds
Potassium octanoate	*n*-Octyl amine hydrochloride
Potassium nonanoate	*n*-Decyl amine hydrochloride
Potassium decanoate	*n*-Dodecyl amine hydrochloride
Potassium undecanoate	*n*-Tetradecyl amine hydrochloride
Potassium dodecanoate	*n*-Hexadecyl amine hydrochloride
Potassium tridecanoate	
Potassium tetradecanoate	*n*-Octyl pyridinium chloride
Sodium decyl sulfate	*n*-Decyl pyridinium chloride
Sodium dodecyl sulfate	*n*-Dodecyl pyridinium chloride
Sodium tetradecyl sulfate	*n*-Tetradecyl pyridinium chloride
Sodium hexadecyl sulfate	*n*-Hexadecyl pyridinium chloride

dialyzed batchwise with Visking casing. Data on the purified systems are given in Table I. Systems of smaller concentrations were prepared when needed, by dilution with distilled water. The surface-active agents employed in the work are listed in Table II.

The potassium soaps of the straight-chain fatty acids were prepared by neutralization of alcoholic solutions of the acids with alcoholic potassium hydroxide (13). The salts were recrystallized from ethanol-acetone mixtures and the crystals dried at 100°C. The acids used in the preparations were obtained from Distillation Product Industries and were the purest grade available.

The sodium alkyl sulfates were prepared from the corresponding alcohols by sulfation. The alcohols were obtained from Distillation Product Industries and were used as received. Chlorosulfonic acid (14) was employed in the preparation of the normal decyl and dodecyl sulfates while concentrated sulfuric acid was employed in the preparation of the normal tetradecyl and hexadecyl sulfates (15). The corresponding sodium salts were prepared by the neutralization of the acids obtained in this way. The salts were recrystallized from an ethanol-acetone solvent, and dried at 100°C.

The alkyl amine hydrochlorides were prepared by passing anhydrous hydrogen chloride gas into ether solutions of the amines (16). Recrystallization was carried out from an acetone-ether solvent, and the crystals were dried at 75°C. under vacuum. The amines were obtained from Distillation Product Industries and Mathieson, Coleman and Bell Co., and were used as received.

The alkyl pyridinium chlorides were prepared by refluxing the alkyl chlorides with an excess of pyridine for 5 to 8 hours (17). The salts were recrystallized from acetone-ether mixtures and dried in vacuum. The alkyl chlorides were obtained from Distillation Product Industries and were used as received.

The purity of all the preparations of surface-active agents was determined by measurement of the equivalent conductivity of their solutions. Purification was considered complete when no change was observed in the equivalent conductivity after successive crystallizations.

Experimental

The effect of the surface-active agents on the stability of the inorganic colloidal suspensions was estimated by determining the minimum concentration of electrolyte required to produce flocculation at given intervals of time. Details of the procedure employed have been described previously (18). In the present case observations of the degree of flocculation were made 15 minutes, 2 hours, and 20 hours after mixing. At the end of the 20-hour period, each system was centrifuged at 540 *g* for 5 minutes and the degree of flocculation determined by observation of the optical density of the systems. The flocculation values (F.V.) given in the section on results correspond to the minimum number of millimoles of electrolyte per liter of systems, required to produce complete flocculation in 20 hours.

The critical concentrations of all surface-active agents used in the present work were determined by measuring the equivalent conductivity of their solutions and noting the break in the conductance–square root of molarity curve. The conductance measurements were made with an Industrial Instruments Co. type RC 1B conductivity bridge. The instrument employed a 1000 c.p.s. 3-volt oscillator and a Wheatstone bridge-type circuit. The results are given in Table III.

Except for the lowest member of the homologous series of potassium soaps (KC_{10}), our results with the anionic surfactants are in good agreement with those of other investigators. Conductivity data in the literature for cationic surfactants are meager and discordant. The literature results on long-chain pyridinium salts (19) appear to be less reliable than ours. Our results agree with the equation proposed by Goette (20) and Klevens (21), where A is a constant depending on the temperature and the homolo-

TABLE III

CMC Values of Surface-Active Agents and Their Logarithms

Anionic surfactant			Cationic surfactant		
Compound	CMC	Temp. (°C.)	Compound	CMC	Temp. (°C.)
KC_{10}	0.0475 M	29°	C_8NH_3Cl	0.0350 M	25°
KC_{11}	0.0375	29°	$C_{10}NH_3Cl$	0.0250	22°
KC_{12}	0.0250	29°	$C_{12}NH_3Cl$	0.0145	24°
KC_{13}	0.0138	29°	$C_{14}NH_3Cl$	0.0105	25°
KC_{14}	0.0075	30°			
$C_{10}SO_4Na$	0.0164	30°	$C_{10}pyCl$	0.0350	25°
$C_{12}SO_4Na$	0.0072	32°	$C_{12}pyCl$	0.0220	24°
$C_{14}SO_4Na$	0.0020	28°	$C_{14}pyCl$	0.0140	27°

gous series, B is a general constant, and N is the number of carbon atoms in the hydrocarbon chain.

$$\log(\mathrm{CMC}) = A + BN.$$

Results and Discussion

The flocculation values decreased sharply with increase in chain length of the ion of opposite charge to that of the colloid particle. Dilution of the inorganic colloid markedly decreased the flocculation values of the longer chain ions. This behavior is characteristic of strongly adsorbable ions (22). Data for two different concentrations of iron (III) oxide with anionic detergents are given in Fig. 1. Figure 2 contains data for two concentrations of manganese (IV) oxide with cationic detergents. It may be noted in both figures that the plots of logarithms of the flocculation values against chain length approach straight lines with the more dilute sols.

Restabilization

Concentrations of the surfactants required for restabilization of the inorganic colloids were much greater for the short-chain ions than for the

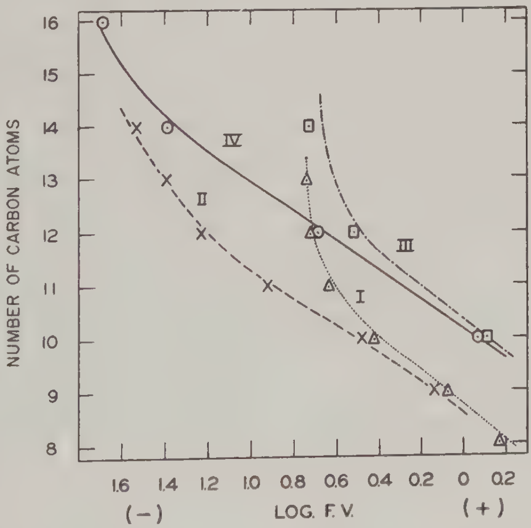

FIG. 1. Relationship of number of carbon atoms of anionic surface-active agents and the logarithm of their flocculation values with colloidal iron (III) oxide sols:

I. Fe_2O_3 (2.55 g./l.) with potassium salts of fatty acids (RCOOK).
II. Fe_2O_3 (0.065 g./l.) with RCOOK.
III. Fe_2O_3 (2.55 g./l.) with sodium alkyl sulfates ($ROSO_3Na$).
IV. Fe_2O_3 (0.065 g./l.) with $ROSO_3Na$.

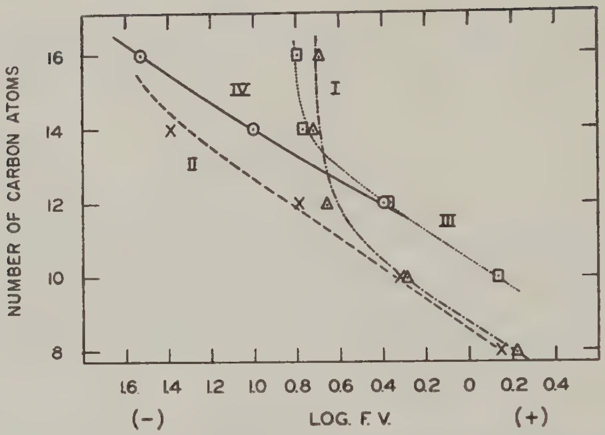

FIG. 2. Relationship of number of carbon atoms of cationic surface-active agents and the logarithms of their flocculation values with colloidal manganese (IV) oxide:

I. MnO_2 (0.25 g./l.) with alkyl amine hydrochlorides (RNH_3Cl).
II. MnO_2 (0.04 g./l.) with RNH_3Cl.
III. MnO_2 (0.25 g./l.) with alkyl pyridinium chlorides (RpyCl).
IV. MnO_2 (0.04 g./l.) with RpyCl.

ions of longer chain length. With the shorter chains, concentrations of the order of 100 times that corresponding to the flocculation values were required, whereas with the longer chain ions stability was induced at concentrations less than ten times the flocculation values.

The glass electrode was used to determine the pH of the anionic surface-active agents. Measurements were made on both the flocculated and the recharged systems in order to determine the possible effect of the hydroxyl ion, originating from the hydrolysis of the long-chain soap ions, on the results. Comparisons were made, also, with systems in which potassium hydroxide was employed as the only electrolyte. As a result of the pH studies it was concluded that flocculation and recharging in these systems was due to the long-chain anions themselves and not to the hydroxyl ions. Indeed, the sodium alkyl sulfates which do not hydrolyze showed a similar relationship to the soaps, which did undergo slight hydrolysis, with respect to chain length of the alkyl group.

Effect of Inorganic Colloids on CMC

In order to throw light on the nature of the interaction of iron oxide with anionic surface-active agents, the critical concentrations of several of the latter were determined in presence of increasing amounts of colloidal iron oxide. The procedure in this case, also, consisted of determining the break in the conductance-concentration curve of the colloidal electrolyte. Since the amount of inorganic colloid was held constant in any given deter-

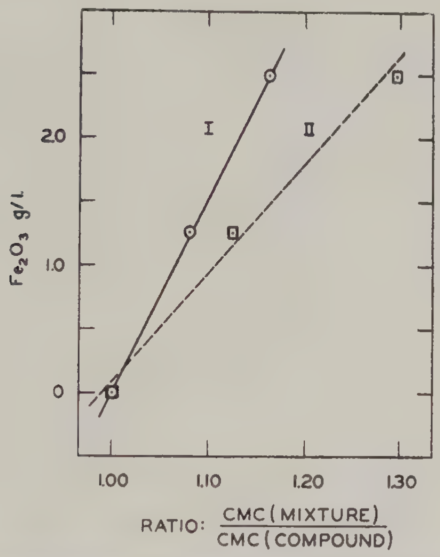

FIG. 3. Critical concentrations of anionic surface-active agents in the presence of varying amounts of colloidal iron (III) oxide:

I. Potassium dodecanoate.

II. Sodium dodecyl sulfate.

mination, it did not interfere with the conductance plot. In passing it may be noted that the conductance of the inorganic colloid was low, relatively.

The critical concentrations were increased in direct proportion to the amount of iron oxide in the system. The results with potassium dodecanoate and sodium dodecyl sulfate are given in Fig. 3. That this behavior is a general one is attested by the fact that an entirely different iron oxide preparation, Merck's "Iron Oxide Dialyzed," gave similar results with several anionic surface agents. These results are given in Table IV. In a similar manner, 1.125 g. of manganese (IV) oxide, a negative sol, increased the CMC of *n*-dodecyl amine hydrochloride, a cationic surface-active agent by 0.004 mole per liter. In all the above cases the colloids had a charge opposite to that of the surface-active ion and adsorption was expected. In one case, the CMC of a surface-active agent was determined in the presence of a colloid possessing a charge similar to that of the detergent ions: sodium lauryl sulfate in the presence of manganese (IV) oxide. The CMC was not raised by the presence of the colloid in this case.

Our data suggest, but do not prove, that colloidal particles may serve as nuclei for the formation of polyvalent micelles from oppositely charged monovalent surface-active ions. As an illustration, 2.5 g. of colloidal iron oxide raised the CMC of sodium dodecyl sulfate by 0.002 mole per liter (for the system reported in Fig. 3). It may be estimated that this amount

TABLE IV

Critical Concentrations (Molar) of Anionic Surface-Active Agents in the Presence of Varying Amounts of Merck Iron Oxide Sol

Fe_2O_3 (*g./liter*)	KC_{11}	KC_{12}	KC_{13}	$C_{10}SO_4Na$	$C_{12}SO_4Na$
0	0.0375	0.0250	0.0138	0.0164	0.0072
0.50	0.0425	0.0275	0.0164	0.0170	0.008
1.00	—	0.0300	—	—	0.009
1.50	0.0522	0.0325	0.0188	0.0202	0.0100
2.50	—	0.0350	—	—	0.0120

TABLE V

Change in CMC of Anionic Surface Active Agents in the Presence of a Constant Amount of Colloidal Iron Oxide

	Change in CMC *moles per liter*
KC_{11}	0.0147
KC_{12}	0.0075
KC_{13}	0.005
$C_{10}SO_4Na$	0.0038
$C_{12}SO_4Na$	0.003

of sodium dodecyl sulfate in the form of a condensed monolayer would occupy an area of 24×10^5 cm.^{2} (assigning an area of 20 sq. A. to each molecule). Two and one-half grams of iron oxide in the form of spheres 2×10^{-6} cm. in radius may be estimated to have a surface area of 7.5×10^5 cm.^{2} This would correspond to an adsorbed layer of detergent molecules three chain lengths in thickness. The actual particle size of the iron oxide is unknown. If the radius was 2×10^{-7} cm. instead of 10 times this value, the area of the particles would be 7.5×10^6 cm.^{2} and one-third of the surface would be covered with adsorbed ions.

As an alternative calculation the average radius of the iron oxide of density 5.2 g./cm.^{3} in the form of spheres may be expressed as 1.5 cm.^{3}/radius (cm.). From the above estimate of the area of the surfactant monolayer (24×10^5 cm.^{2}) together with the assumption that the surfactant forms a monolayer on the surface of the iron oxide particles, a value of 6.2×10^{-7} cm. is obtained for the radius of the particles.

The increases in critical concentration of the surface-active agents listed in Table IV are summarized in Table V. The values given correspond to the increase in CMC produced by 1.5 g. of iron oxide (Merck Iron Oxide Sol). If these increases are taken as a measure of the adsorption capacity of iron oxide for the ions, it follows that the adsorption capacity is smaller for the longer chain length soap ions and is larger for the soaps than for the sulfates of equal chain length. This suggests that the long-chain compounds occupy a larger space on the particle surface and that the sulfates occupy a larger surface than the soaps.

References

1. Freundlich, H., and Slottman, G., *Z. physik. Chem.* **129,** 302 (1927).
2. Freundlich, H., and Birstein, V., *Kolloidchem. Beih.* **22,** 95 (1923).
3. Nonaka, M., *J. Soc. Chem. Ind. Japan* **32,** 115 (1929).
4. Greiner, L., and Vold, R. D., *J. Phys. Colloid Chem.* **53,** 67 (1949).
5. Klinge, W., and Lange, H., *Kolloid-Z.* **127,** 19 (1952).
6. Kruyt, H. R., and Trollestra, S. A., *Kolloidchem. Beih.* **54,** 262 (1943).
7. Hazel, J. F., *J. Chem. Educ.* **26,** 22 (1949).
8. Gallagher, W. U., *J. Am. Water Works Assoc.* **42,** 22 (1950).
9. Judd, R. C., and Sorum, C. H., *J. Am. Chem. Soc.* **51,** 2598 (1930).
10. Adolf, M., and Pauli, W., *Kolloid-Z.* **29,** 281 (1921).
11. Bredig, G., and Marck, A., *Chem. Zentr.* **1911, I,** 1190.
12. Dumanski, A., *Kolloid-Z.* **9,** 262 (1911).
13. Powney, J., and Jordan, D. O., *Trans. Faraday Soc.* **34,** 363 (1938).
14. Dreger, E. E., *et al.*, *Ind. Eng. Chem.* **36,** 610 (1944).
15. Private communication from Procter and Gamble Co., Cincinnati, Ohio.
16. Fieser, L. F., and Fieser, M., "Organic Chemistry," 2nd ed., p. 682. D. C. Heath Co., Boston, 1950.
17. Knight, G. A., and Shaw, B. D., *J. Chem. Soc.* **1938**, 685.
18. Hazel, J. F., and Sorum, C. H., *J. Am. Chem. Soc.* **53,** 49 (1931).
19. Lottermoser, A., and Frotcher, H., *Kolloidchem. Beih.* **45,** 303 (1939).
20. Goette, E. K., *J. Colloid Sci.* **4,** 459 (1949).
21. Klevens, H. B., *J. Phys. Colloid Chem.* **52,** 130 (1948).
22. Hazel, J. F., *J. Phys. Chem.* **45,** 738 (1941).

JOURNAL OF COLLOID SCIENCE **12,** 538–548 (1957)

THE NATURE OF THE PARTICLE SURFACE IN HEVEA LATEX AND PASTES OF RUBBER HYDROCHLORIDE AND POLYVINYL CHLORIDE[1]

G. Schuur[2]

Rubber-Stichting, Delft, Holland

Received November 28, 1956; revised April 5, 1957

Abstract

The apparent viscosity of dispersions of rubber hydrochloride in plasticizers is considerably influenced by amines and by oxidation or methylation of the surface of the particles. Pastes of polyvinyl chloride behave similarly.

The experimental results can be explained by assuming that carboxyl groups are bound to surface polymer molecules of the rubber hydrochloride particles. The number of these carboxyl groups is increased by an oxidation of the original latex with oxygen. The mechanical stability of the latex increases simultaneously.

Indications have been found that the attraction between the particles is at least partly of a more specific character than long-range London-van der Waals' forces.

Introduction

The colloid-chemical properties of natural rubber latex are influenced by many factors, such as the pH, the concentration of surface-active agents, and the presence of ions of different kinds. Many of these factors have been studied intensively.

However, it has usually been assumed that the surface of the rubber particles consists of plain hydrocarbon. Up to now it has been impossible to investigate the properties of the surface free from adsorbed soaps and proteins, for the removal of these surface-active agents results in a coagulation of the latex. But the latex particles can be obtained in a hard and nontacky form by hydrochlorination and crystallization according to the methods of van Veersen (1) and the author (2). The various surface-active agents can then be removed by filtering, washing, and extraction with organic solvents, without the loss of the surface by coagulation of the particles.

The reactions of most organic chemical groups with hydrochloric acid are fairly well known and, though the original properties of the surface may be modified to some extent by the hydrochlorination, an investigation of the surface of rubber hydrochloride may give useful information regarding the properties of the original surface of the rubber particles.

---

[1] Communication No. 305 (1956) of the Rubber-Stichting, Delft, Holland.

[2] Present address: Koninklijke/Shell-Laboratorium, Amsterdam, Holland.

A suitable method for studying the nature of the surfaces of various rubber hydrochlorides would be to investigate the rheological properties of concentrated dispersions in organic media. Dispersions in plasticizers were selected, in the first place, because the experimental work is then not complicated by the volatility of the solvents, and secondly, because these dispersions in plasticizers are of some technical interest, since they can be used for the preparation of monofilaments from rubber hydrochloride (3).

The use of dispersions of polymers in organic media for investigating the colloid-chemical properties of dispersions in oils has the advantage that the surface of these particles can be modified by organic chemical methods. This was often done during the investigation, both with rubber hydrochloride and polyvinyl chloride. The surface was cleaned by washing and extraction with various solvents, it was modified by oxidation, methylation, and reactions with several amines, especially triethanol amine, as will be shown in the following sections.

The investigation of the rheological properties of these resins dispersed in plasticizers has shown that the surface of latex particles is not plain hydrocarbon, but that its properties and chemical composition depend on the type of the latex and on the way in which the latex has been treated and stored prior to hydrochlorination.

Experimental Methods

1. Preparation of Rubber Hydrochloride

Ammoniated latex with a dry rubber content of about 60% is stabilized with 1.05 g. Emulphor 0 per 100 g. latex. Emulphor 0 is a nonionic emulsifier, a condensation product of ethylene oxide and oleyl alcohol. The latex is mixed with half its volume concentrated (36%) hydrochloric acid. Hydrogen chloride is then passed through for about 40 hours until the maximum chlorine content is reached (approx. 32–33% Cl). The temperature is kept at or below 20°C. during all these manipulations.

All experiments described in this paper have been done with products having this maximum chlorine content.

The hydrochlorination can be followed closely by means of a rapid determination of the density of the particles (4).

The rubber hydrochloride is then crystallized by heating the latex at 75°C. for 30 minutes. The heating should be done gradually in order to avoid excessive foaming by escaping hydrogen chloride. The latex is then cooled to 60°C. and precipitated by pouring it into water at 60°C. For 100 g. ammoniated latex 2,000 ml. water were used.

The rubber hydrochloride is filtered, washed with distilled water until free from hydrochloric acid, and dried in air at 50°C.

If all manipulations are carried out properly, the latex particles preserve their individuality and a white powder is obtained with a bulkiness of approximately 2.3 ml./g. However, very bulky products may be obtained under certain conditions. For example, if the crystallization prior to coagulation is omitted, the particles will agglomerate to irregular structures during precipitation and a bulkiness up to approximately 5 ml./g. may be observed. These agglomerates cannot be redispersed afterwards and very stiff pastes are obtained which are unsuitable for our investigation (see Section 9).

2. Extraction of Rubber Hydrochloride

One hundred grams dry rubber hydrochloride and 200 ml. ethanol are milled for 24 hours in a laboratory ball mill. The rubber hydrochloride is filtered and extracted for 8 hours in a Soxhlet apparatus with ethanol. The ethanol is replaced by ether and the extraction is continued for 8 hours. The rubber hydrochloride is then dried at 50°C.

3. Oxidation of Rubber Hydrochloride

One hundred grams rubber hydrochloride are dispersed in a solution of 20 g. potassium dichromate and 20 g. concentrated sulfuric acid in 200 ml. water in a laboratory ball mill for 8 hours at room temperature, but sometimes a shorter reaction time was used. The polymer is then filtered, washed with distilled water until free from acid, and dried at 50°C. in air.

4. Methylation of Rubber Hydrochloride and Polyvinyl Chloride

Methylation of the carboxyl group (according to the formula: $R\ COOH + CH_2N_2 \rightarrow R\ COOCH_3 + N_2$) is done by adding a solution of 4 g. diazomethane in 25 g. ether to 100 g. extracted rubber hydrochloride dispersed in 200 g. ether. The mixture is kept at 10°C. for 2 hours. The polymer is then filtered, washed with ether, and dried at 50°C. in air. The methylation of P.V.C. is done in the same manner.

5. Addition of Extracted Impurities or Fatty Acids to Methylated Rubber Hydrochloride

The extracts of 100 g. rubber hydrochloride in alcohol and ether, obtained as described above, are evaporated and the residue is dissolved in 200 g. ether. This solution is added to 100 g. extracted and methylated rubber hydrochloride and mixed in a laboratory ball mill for 4 hours.

The ether is then evaporated. The same experiment was done with a solution of 1.25 g. oleic acid and 1.25 g. stearic acid in 200 g. ether. The methylated rubber hydrochloride particles are thus coated with the extracted impurities or with fatty acids.

6. Oxidation of Polyvinyl Chloride

A dispersion is made of 100 g. polyvinyl chloride (Solvic 334, I.C.I.) in a solution of 0.5 g. Emulphor 0 in 100 g. water. A solution of 100 g. KOH in 100 ml. water is added. The mixture is kept at room temperature for 2 hours. The polyvinyl chloride becomes brown in color because series of conjugated double bonds are formed. The polymer is then filtered, washed, and oxidized in the same way as rubber hydrochloride, the brown color disappearing. The oxidized polyvinyl chloride is washed with ethanol and dried at 50°C.

7. Preparation of Cyclized Rubber

One hundred grams latex with a dry rubber content of 60% is stabilized with 1.05 g. Emulphor 0. 150 g. gaseous hydrogen fluoride are added at 5°C. The mixture is kept in a polyethylene bottle for 1.5 hours. It is then poured into 1,000 ml. water at room temperature. The hydrogen fluoride is neutralized with a solution of sodium hydroxide. The temperature is kept below 25°C. in order to decrease the tendency of the particles to fuse into irregular agglomerates. The cyclized rubber is filtered, washed with distilled water, and washed with ethanol. It is dried at 50°C. *in vacuo*.

8. *The Measurements of the Rheological Properties of Pastes*

All measurements were carried out by means of a Couette-type viscosimeter, the "Drage Struktur Viskosimeter," manufactured by the "Chemisches Institut Dr. A. G. Epprecht," Zurich.

The apparatus allows the bobs to be rotated at three different speeds, and the apparent viscosities of the pastes were therefore usually measured at three different rates of shear. The measurements were done immediately after the preparation of the pastes because the apparent viscosities increase slightly with time. All measurements were done at 25°C. ± 0.2°C.

9. *The Preparation of the Dispersions of the Resins in Plasticizers*

The preparation of the pastes is the most critical part of the experiments as far as reproducibility is concerned. The pastes were made by two different methods, which will be referred to as methods I and II.

Method I consists of a premixing of the resin and the plasticizer by means of a spatula. The mixture is then passed through a small laboratory Pascal triple roll-mill. The rolls were fixed at a constant distance (0.185 mm.). The apparent viscosities of the pastes depend on the number of passes through the mill. Three passes give the best reproducible results and minimum viscosities.

Method II consists of a premixing of the resin with 60% of the plasticizer with a spatula. The paste is then passed three times through the mill. The rest of the plasticizer is then added and the paste is given a single pass through the mill. The investigations were started with pastes made according to method I, but afterwards method II appeared to give more reproducible results and lower viscosities. The amines are mixed with the pastes by means of a spatula. The reaction is fast and no further changes are observed after about 1 minute.

10. *The Reproducibility of the Various Products and the Preparation of Pastes*

To investigate the reproducibility three batches of rubber hydrochloride were made. Part of each of these batches was extracted. The pastes made from the batches of unextracted rubber hydrochloride showed a good reproducibility, but after extraction the differences between the rheological properties of the pastes were appreciably increased, presumably owing to the fact that a small proportion of the particles fused into irregular agglomerates during extraction and drying. Nevertheless, the reproducibility was sufficiently good for our purposes, as no conclusions were drawn from the absolute values of the apparent viscosities of the pastes, but only from the changes which occurred when the surface was modified, especially with triethanol amine (T.E.A.).

The plasticizers and the other products used were of a good commercial grade, but no measures were taken to purify them further because the apparent viscosities of the pastes are not influenced appreciably by small quantities of soaps, fatty acids, water, or Emulphor 0, presumably because the surface of the particles has no tendency to adsorb these substances. The apparent viscosities depend strongly on the amount and type of plasticizer. Pastes of tricresyl phosphate (T.C.P.) and dibutyl phthalate (D.B.P.) have been investigated usually. However, other plasticizers, such as dibutyl sebacate (D.B.S.), Aroclor (chlorinated diphenyl), and paraffin oil behave in a similar manner, i.e., triethanol amine increases the apparent viscosities of all these pastes.

Results and Discussion

1. Pastes of Rubber Hydrochloride

The apparent viscosity of a paste of rubber hydrochloride can be influenced appreciably by the addition of small quantities of amines. Amines which contain aromatic groups or long aliphatic chains have little influence on the apparent viscosity of a paste prepared from T.C.P. or D.B.P., but these amines may decrease the apparent viscosity of pastes from paraffin oil. On the other hand, amines which contain hydroxyl groups, such as mono-, di-, or triethanol amine, greatly increase the apparent viscosity of the pastes. In particular the stiffening caused by triethanol amine has been used as a criterion in this investigation. It will be referred to as the "T.E.A.-effect" for the sake of brevity.

The stiffening of a paste of 100 g. rubber hydrochloride in 100 g. D.B.P., prepared according to method II, is shown in Fig. 1. The stiffening increases with increasing amounts of T.E.A. until at 1.2 g. per 100 g. rubber hydrochloride the maximum is reached. Further additions of T.E.A. decrease the apparent viscosity very gradually because the volume of the continuous phase is increased. The stiffening of T.E.A. can be counteracted by the addition of acids. The decrease caused by 2.56 g. benzoic acid in a paste, which contained 1.2 g. T.E.A., is also shown in Fig. 1. Larger amounts of benzoic acid decrease the apparent viscosity still further.

The T.E.A. effect is not caused by impurities which can be removed from

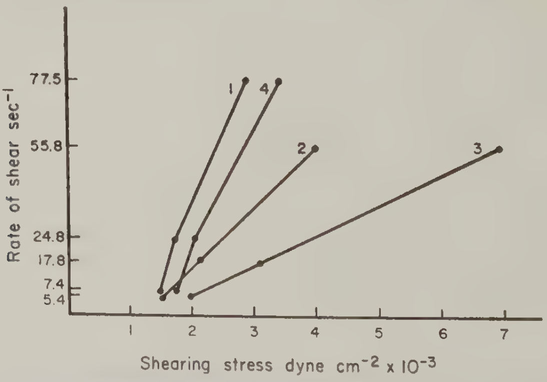

FIG. 1. Influence of triethanol amine and benzoic acid on a paste of rubber hydrochloride. *Curve 1:* 100 g. rubber hydrochloride in 100 g. D.B.P. prepared according to method II. *Curve 2:* Same as Curve 1 + 0.8 g. T.E.A. *Curve 3:* Same as Curve 1 + 1.2 g. T.E.A. *Curve 4:* Same as Curve 1 + 1.2 g. T.E.A. + 2.56 g. benzoic acid.

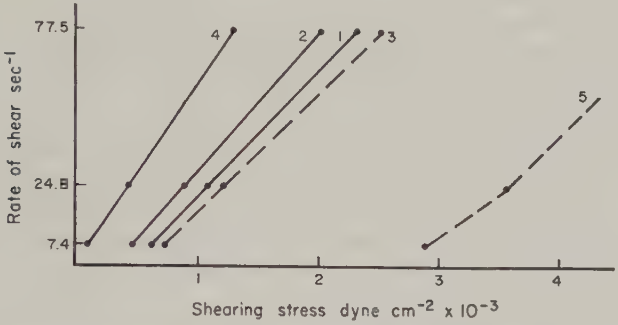

FIG. 2. Influence of T.E.A. on a paste of extracted and methylated rubber hydrochloride and on pastes of extracted, methylated, and oxidized rubber hydrochloride. *Curve 1:* 100 g. extracted and methylated rubber hydrochloride in 140 g. T.C.P. prepared according to method I both without and with 0.5 g. T.E.A. *Curve 2:* 100 g. of extracted and methylated rubber hydrochloride, oxidized for 1 hour with potassium dichromate, in 140 g. T.C.P. *Curve 3:* Same as Curve 2 + 0.2 g. T.E.A. *Curve 4:* 100 g. of extracted and methylated rubber hydrochloride, oxidized for 8 hours with potassium dichromate, in 140 g. T.C.P. *Curve 5:* Same as Curve 4 + 1 g. T.E.A.

the rubber hydrochloride by extraction. A paste of 100 g. extracted rubber hydrochloride and 140 g. T.C.P., prepared according to method I, shows already the maximum stiffening when only 0.2 g. T.E.A. is added. Pastes of normal rubber hydrochloride show the maximum stiffening usually after addition of 1 to 1.5 g. T.E.A. per 100 g. rubber hydrochloride. This difference is presumably due to the fact that fatty acids are always present in normal rubber hydrochloride. These acids, which counteract the T.E.A., are removed by extraction. It has usually been observed that the maximum stiffening is somewhat smaller for extracted rubber hydrochloride, presumably owing to the fact that some agglomeration occurs during extraction and drying.

It is very remarkable that the T.E.A. effect, which is so clearly observed in pastes of normal and extracted rubber hydrochloride, has completely vanished when pastes of methylated rubber hydrochloride are investigated. This is shown in Fig. 2, where curve 1, obtained from a paste of 100 g. methylated rubber hydrochloride in 140 g. T.C.P., prepared according to method I, remains unchanged when 0.5 g. T.E.A. is added. Large amounts of T.E.A. decrease the apparent viscosity because the volume of the continuous phase is increased.

The T.E.A. effect does not reappear when fatty acids or the extract of normal rubber hydrochloride are added to methylated rubber hydrochloride as described in the experimental section. This is additional evidence that the T.E.A. effect is not caused by extractable impurities.

However, the T.E.A. effect reappears when methylated rubber hydrochloride is oxidized with a potassium dichromate. Curves 2 and 3 in Fig. 2

show the stiffening of a paste of methylated rubber hydrochloride, which has been oxidized for 1 hour with a potassium dichromate solution as described in the experimental section. Curves 4 and 5 show the even greater T.E.A. effect after an oxidation for 8 hours. The rubber hydrochloride, which has been oxidized for 1 hour, needed only 0.2 g. T.E.A. for maximum stiffening; the rubber hydrochloride, which had been oxidized for 8 hours, needed 1 g. T.E.A. Also the T.E.A. effect of normal rubber hydrochloride can be increased by oxidation with potassium dichromate, but, if the oxidized rubber hydrochlorides are methylated, the T.E.A. effect disappears again completely.

Rubber hydrochloride is not oxidized by oxygen in the dark and at room temperature. A methylated rubber hydrochloride did not show a T.E.A. effect after storage for 7 months under these conditions.

2. Tentative Explanation of the Experiments with Rubber Hydrochloride

The experiments carried out with pastes of rubber hydrochloride can be explained qualitatively on the basis of the following assumptions:

a). Acidic groups, presumably carboxyl groups, are chemically bound to the surface polymer molecules of the rubber hydrochloride particles.

b). All other things being equal, the minimum apparent viscosity of a dispersion will be observed when the surface of the dispersed phase and the continuous phase are similar.

For instance, a dispersed phase with a polar surface will show a maximum colloid chemical stability and a minimum apparent viscosity in polar liquids, whereas in nonpolar liquids, such as paraffin oil, a maximum apparent viscosity and minimum stability will be observed. (The apparent viscosity is here defined as the shearing stress divided by the rate of shear.) A dispersed phase with a nonpolar surface, on the other hand, will show maximum stability and minimum apparent viscosity in a nonpolar continuous phase, like paraffin oil.

The influence which amines exert on the apparent viscosity of the pastes can readily be explained by the fact that they will react with the carboxyl groups of the surface. Amines with nonpolar aromatic or aliphatic groups (e.g., dibenzyl amine) will decrease the polarity of the surface and decrease therefore the apparent viscosity of dispersions in paraffin oil. Triethanol amine will increase the polarity and increase the apparent viscosity of the dispersions in plasticizers.

Methylation of the carboxyl groups makes it impossible for the amines to react with the surface under the prevailing circumstances, and consequently the amines do not change the apparent viscosity of pastes of methylated rubber hydrochloride to any extent.

The T.E.A. effect does not reappear when fatty acids or the extract of rubber hydrochloride is added to methylated rubber hydrochloride, because these substances are not adsorbed by the particles dispersed in plasticizers. But oxidation generates new carboxyl groups on the surface of methylated rubber hydrochloride and the T.E.A. effect therefore reappears.

Organic acids counteract the influence of amines because they compete with the carboxyl groups of the surface and strip the surface of its bound amines if these acids are present in sufficient amounts.

Even rubber hydrochloride, prepared from fresh latex, tapped and stored in the absence of oxygen, shows the T.E.A. effect. On the other hand, the T.E.A. effect may be increased by an oxidation of the latex by oxygen prior to hydrochlorination, as will be shown afterwards. The carboxyl groups of the surface of rubber hydrochloride may therefore originate from three sources:

a). Part of the carboxyl groups may be the end groups of the natural rubber molecule. This would be in agreement with the formation of natural rubber by a polycondensation of β-methyl-crotonic acid (5–7).

b). Another part of the carboxyl groups may be formed by oxidation of the latex during storage. The carboxyl group will evidently be the last step of the oxidation, and other oxygen-containing groups will probably also be present. These groups will make the surface of the rubber particles more hydrophilic, and they will therefore contribute to the stability of the latex.

c). The carboxyl groups of the surface may also at least partly be explained by the presence of an insoluble acidic compound in the rubber. However, the increase of the T.E.A. effect by oxidation cannot be explained on this basis.

Another conclusion which can be drawn is that not only is the latex stabilized by adsorbed fatty acids and proteins, but chemically bound carboxyl groups may also exert some influence. Moreover, part of the proteins may be chemically bound to the surface by means of the carboxyl groups. This would explain why proteins cannot be completely removed from latex by repeated washing with soap solution.

It is not possible at present to give an exact definition of the similarity which the surface of the dispersed phase and the continuous phase should possess for maximum stability. Nevertheless, the results of this investigation indicate that the properties of these dispersions are not governed only by double-layer repulsion and attraction by long-range London-van der Waals' forces (8).

Though the particles of rubber hydrochloride are too small to be clearly observed in the electrophoresis apparatus of van der Minne and Hermanie (9), some preliminary experiments indicated that the particles of oxidized rubber hydrochloride are negative, whereas the particles of methylated rubber hydrochloride appeared to be completely neutral. The negative charge may be due to an ionization of the carboxyl groups. This result is in agreement with Fig. 2, the dispersions of oxidized rubber hydrochloride showing the smallest apparent viscosity. In the presence of T.E.A. the dispersions of oxidized rubber hydrochloride show higher apparent viscosities than a paste of methylated rubber hydrochloride. As the particles of methylated rubber hydrochloride are already neutral, this effect cannot be due to a decrease of the double-layer repulsion. It is also impossible to see how small amounts of triethanol amine would increase the long-range London-van der Waals' forces considerably, and it is even more difficult to see how dibenzyl amine could decrease these forces in dispersions of rubber hydrochloride in paraffin oil. But these effects can be understood on the assumption that an increase of the polarity of the surface of the particles will increase the colloid chemical stability in polar media and decrease the stability in nonpolar media.

Therefore a more specific attraction, originating from the surface of the particles, seems to be present in these systems, but it is admitted that the experimental evidence is still slight. A systematic investigation of a range of amines and a range of plasticizers with increasing dielectric constant or increasing cohesive energy density could elucidate this point.

3. Pastes of Polyvinyl Chloride

If the explanation of the experiments with pastes of rubber hydrochloride is correct, dispersions of other polymers must show a similar behavior if carboxyl groups are present bound at the surface molecules of the particles.

Therefore a paste-grade polyvinyl chloride (Solvic 334) has been oxidized. Direct oxidation of polyvinyl chloride is very difficult, and much better results are obtained when some hydrogen chloride is removed by means of a concentrated KOH solution prior to oxidation as described in the experimental part.

A paste of normal polyvinyl chloride is not influenced by amines but after oxidation; it behaves indeed in the same way as pastes of rubber hydrochloride. Pastes of oxidized P.V.C. in T.C.P. show no yield value and the increase of the apparent viscosity, when T.E.A. is added, is small. However, a dispersion of 100 g. oxidized P.V.C. in 100 g. Aroclor 1221 has an initial yield value, and a large increase of the apparent viscosity is observed when 0.6 g. T.E.A. is added.

Benzoic acid counteracts the stiffening also in pastes of P.V.C., and no T.E.A. effect has been observed in pastes of methylated oxidized P.V.C.

The behavior of oxidized P.V.C. and that of rubber hydrochloride are indeed completely similar. To prove that this similarity is caused only by the presence of carboxyl groups at the surface of the particles and is independent of the chemical composition of the interior, finally a paste of 100 g. cyclized rubber in 120 g. T.C.P. was investigated. The T.E.A. effect was also observed in this case.

4. The Oxidation of Hevea Latex

The oxidation of latex with oxygen was investigated by McGavack and Bevilacqua (10). They found that the rate of oxidation depends on the pH of the latex. The maximum rate is observed at pH = 10.4. The oxidation is accompanied by a considerable increase of the mechanical stability of the latex.

Though the factors which control the mechanical stability are not fully understood, it seemed quite possible that the bound carboxyl groups and other oxygen-containing groups of the surface of the particles might be important. Therefore an ammoniated latex (pH = 10.4) was oxidized for 16 weeks with air at room temperature. Each day the samples were shaken with air in half-filled bottles for 15 seconds. Care was taken to lose no ammonia. The mechanical stability of the latex after 0, 1, 2, 4, 8, and 16 weeks was determined according to the A.S.T.M. Designation: 1076-54 T. The samples were also hydrochlorinated and pastes were made of 100 g. resin and 100 g. D.B.P., according to method II. So much T.E.A. was added to the pastes that the maximum stiffening was obtained (1 to 2 g. T.E.A. per 100 g. rubber hydrochloride). The mechanical stability of the latex and the apparent viscosities of the pastes as a function of the time of oxidation of the latex are seen in Fig. 3. The apparent viscosities are shown only at a rate of shear of 7.9 $sec.^{-1}$ in the absence of T.E.A. and at 5.7 $sec.^{-1}$ with T.E.A., but the viscosities at higher rates of shear showed a very similar trend. This experiment was repeated several times with differ-

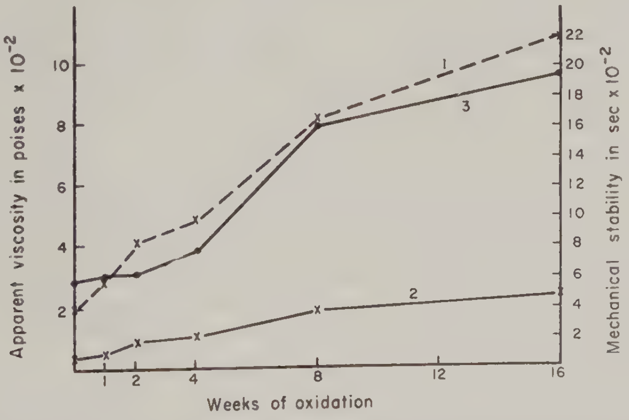

FIG. 3. The apparent viscosity of pastes of rubber hydrochloride and the mechanical stability of latex as a function of the time of oxidation. *Curve 1:* Mechanical stability. *Curve 2:* Apparent viscosity of pastes without T.E.A. at a rate of shear of 7.9 $sec.^{-1}$. *Curve 3:* Apparent viscosities after addition of the optimum amounts of T.E.A. at a rate of shear of 5.7 $sec.^{-1}$.

ent latices. Though some quantitative differences were found, the mechanical stabilities and the apparent viscosities increased always simultaneously. This indicates that bound carboxyl groups and perhaps also other oxygen-containing groups of the surface increase the mechanical stability of the latex.

The influence of the pH of the latex on the rate of oxidation was also investigated. The maximum increase of the stiffening of the pastes is observed when the oxidation is carried out at a pH of approximately 10, in agreement with the results of McGavack and Bevilacqua (10). The increase is very small when the pH of the latex is less than 7.

An attempt was made to prevent the oxidation of the surface of the rubber particles with antioxidants. More than ten antioxidants were tested, but none of these had any significant influence on the increase of the T.E.A. effect.

Titration curves were made of dispersions of 50 g. of polymer in 225 ml. of a 0.01 N sodium hydroxide solution. The titration curves indicated that P.V.C. and methylated rubber hydrochloride contained no carboxyl groups whereas an extracted rubber hydrochloride contains 0.03 % carboxyl groups, which means that about one carboxyl group would be present per 200 A^2 of the surface of the original rubber particles. However, this preliminary result should be considered with reserve, as the determination of these very small amounts is liable to errors.

ACKNOWLEDGMENTS

The author is indebted to W. Albers, Utrecht, for his kind assistance with the electrophoresis experiments. The other experiments have been carried out by P. D. Harkes and A. Klootwijk and Miss C. D. Tempelaars. The author wishes to thank the management of the Rubber-Stichting for the permission to publish this paper.

REFERENCES

1. VEERSEN, G. J. VAN, *Proc. 2nd Rubber Technol. Conf.*, London, 87 (1948).
2. SCHUUR, G., (to Rubber-Stichting) Brit. Patent 726,142; SCHUUR, G., "Some aspects of the crystallization of high polymers," Commun. No. 276 (1955) of the Rubber-Stichting, p. 71.
3. SCHUUR, G., Commun. No. 276 (1955) of the Rubber-Stichting, p. 55.
4. SCHUUR, G., AND KLOOTWŸK, A., *Anal. Chem.* **28,** 1455 (1956).
5. BONNER, J., AND ARREGUIN, B., *Arch. Biochem.* **21,** 109 (1949).
6. ARREGUIN, B., AND BONNER, J., *Arch. Biochem.* **26,** 178 (1950).
7. ARREGUIN, B., BONNER, J., AND WOOD, B. J., *Arch. Biochem. and Biophys.* **31,** 234 (1951).
8. VERWEY, E. J. W., AND OVERBEEK, J. TH. G., "Theory of the Stability of Lyophobic Colloids," Elsevier, Amsterdam, 1948.
9. MINNE, J. L. VAN DER, AND HERMANIE, P. H. J., *J. Colloid Sci.* **7,** 600 (1952).
10. MCGAVACK, J., AND BEVILACQUA, E. M., *Ind. Eng. Chem.* **43,** 475 (1951).

JOURNAL OF COLLOID SCIENCE **12**, 549–556 (1957)

THE TITRATION OF POLYMERIC ACIDS

R. Arnold

Department of Chemistry, University of Cape Town, South Africa

Received April 3, 1957

Abstract

Data in the literature for the titration of polyacrylic and polymethacrylic acids are considered. Polyacrylic acid gives straight-line graphs of pK against $\alpha^{1/3}$ provided no neutral salt is present; here pK = pH + log $1-\alpha/\alpha$ and α is the degree of ionization. For polymethacrylic acid, both in absence and presence of neutral salts, the corresponding graphs take the form of two straight lines separated by an inflection. Extrapolation of these graphs to zero degree of ionization yields estimates of pK_0, the intrinsic dissociation exponent. For both polyacids values of about 4.2 are found, which is considerably lower than previous estimates.

Consideration of the effect of substitution of carboxyl groups on simple acids show that the value of pK_0 for a polycarboxylic acid (e.g., polymethacrylic) should be about 0.5 less than the pK for the corresponding monobasic acid (isobutyric). The same considerations lead, however, to the apparently incorrect conclusion that polyacrylic acid should be weaker than polymethacrylic acid.

During the neutralization of polymeric acids there is a continuous decrease in acid strength. This is due to the electrostatic effect of the increasing charge on the polymeric anion, and must depend largely on the distance between the acid groups in the molecule. The intrinsic strength of the acid groups in the polymer must correspond to the dissociation constant K_0 of a single acid group in the uncharged molecule, i.e., to the limiting value for zero degree of ionization. Up to the present no satisfactory procedure has been found for estimating this quantity.

It has been found by Kern (1) and by Katchalsky and Spitnik (2) that the course of the neutralization of a polymeric acid may be represented by an equation of the form:

$$\mathrm{pH} = \mathrm{pG} + n \log \frac{1-\alpha}{\alpha}. \qquad [1]$$

Here α is the degree of ionization and pG and n are constants.

Subsequent to the empirical discovery of the above equation, a theoretical derivation was developed by Katchalsky and Gillis (3). In this derivation Eq. [1] is obtained as an approximation to the equation:

$$\mathrm{pH} = \mathrm{pK}_0 - \log \frac{1-\alpha}{\alpha} + 2.14 \times 10^{-5} \lambda \left(\frac{\alpha}{\lambda' s j b^2} \right)^{1/3}. \qquad [2]$$

Here pK_0 is the negative logarithm of the dissociation constant of a single acid group in the unionized polymer, s is the number of monomeric units of length b in one statistical element, j is the number of monomer units per acid group, and λ and λ' are functions of the extension of the coil. According to Katchalsky and Gillis λ and λ' change very slowly during the titration and may be assumed to be approximately constant. If this is so we may rewrite Eq. [2] in the form:

$$pH + \log \frac{1 - \alpha}{\alpha} = pK = pK_0 + \text{const. } \alpha^{1/3}. \qquad [3]$$

According to this result a graph of pK against $\alpha^{1/3}$ should yield a straight line, enabling extrapolation to $\alpha = 0$ to be carried out. From such an extrapolation the value of the intrinsic dissociation constant K_0 could be found. It should be noted that in the derivation of Eq. [2] the absence of neutral salts was assumed. However, irrespective of the validity or otherwise of the underlying theory, Eq. [3] should, if it holds, be a more useful titration equation than [1], in view of the extrapolation possibilities.

Extensive data for the titration of polyacrylic acid, both in the presence of salts such as sodium chloride and in their absence, have been reported by Samelson (4). For some of these titrations values of pK and the degree of ionization, α, have been calculated from the reported values of pH, polymer concentration, and degrees of neutralization. For the case where neutral electrolyte is absent, graphs of pK against $\alpha^{1/3}$ seem to conform

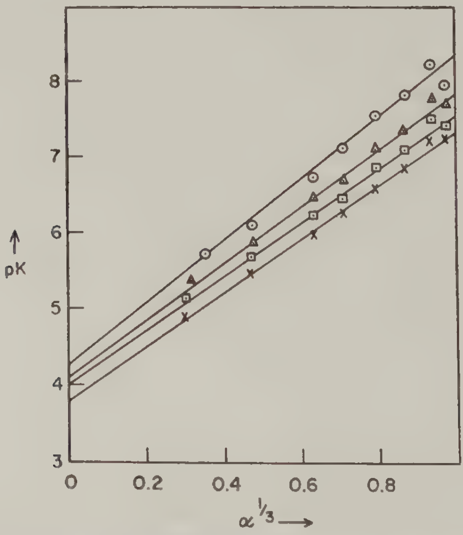

FIG. 1. Graphs of pK against $\alpha^{1/3}$ for various concentrations of polyacrylic acid in absence of neutral salt. (Data of Samelson (4).) Polymer concentrations: ⊙—0.00087 N; △—0.00436 N; ⊡—0.00871 N; ×—0.0174 N.

TABLE I

Test of the Equation $pK = pK_0 + m\ \alpha^{1/3}$; *Data of Samelson (4) for Polyacrylic Acid*

Polymer concentration (normality)	pK_0	m
0.000871	4.25	4.09
0.00436	4.13	3.75
0.00871	4.02	3.58
0.0174	3.82	3.55

moderately well to Eq. [3]. These graphs are shown in Fig. 1 for four different polymer concentrations, and the results are summarized in Table I. The straight lines were calculated by the method of least squares.

It will be seen that the values obtained for pK_0 decrease with increasing polymer concentration. Extrapolation to zero concentration gives $pK_0 = 4.28$; obviously this result can be regarded as only approximate.

Attention was first drawn to this problem by the application of Eqs. [1] and [3] to previously obtained data (5) for polymethacrylic acid, which refer to titrations in the presence of various concentrations of potassium chloride. When these titrations are plotted according to either Eq. [1] or Eq. [3], the resulting graphs clearly consist of two straight lines separated by a marked inflection. The values of α at which these inflections occur are about 0.2, the exact value increasing somewhat with increasing salt concentration. Some of the $pK - \alpha^{1/3}$ graphs are shown in Fig. 2. It will be seen that the two straight portions do not differ appreciably in slope, so that the phenomenon does not seem to suggest the existence of two sets of acid groups, each with a different acid strength.

It would seem that the intrinsic dissociation constant should be obtained by extrapolation of the first part of the $pK - \alpha^{1/3}$ curve to $\alpha = 0$. From ten titrations, using five different samples of polymethacrylic acid and carried out at 25°C. in solutions of several different concentrations of potassium chloride, the mean result obtained was:

$$pK_0 = 4.28;\ \text{standard deviation} = 0.08.$$

Calculations of pK and α have also been carried out for a number of Samelson's titrations (4) of polyacrylic acid in which sodium or potassium chloride was present. In these cases the graphs of pK against $\alpha^{1/3}$ could be interpreted as smooth curves, but appeared rather to consist of two straight portions with an inflection at $\alpha = 0.5$. (The data of Kern (1) for polyacrylic acid give a somewhat similar result.) Extrapolation of the graphs is uncertain, but would give mean values for pK_0 of 4.5 or 3.9, depending on whether the former or the latter alternative is chosen. In the presence of neutral salt of concentration greater than $0.01M$ there is no dependence on polymer concentration, as was found in the case of polymethacrylic acid (5).

In these calculations activity corrections have been applied on the basis

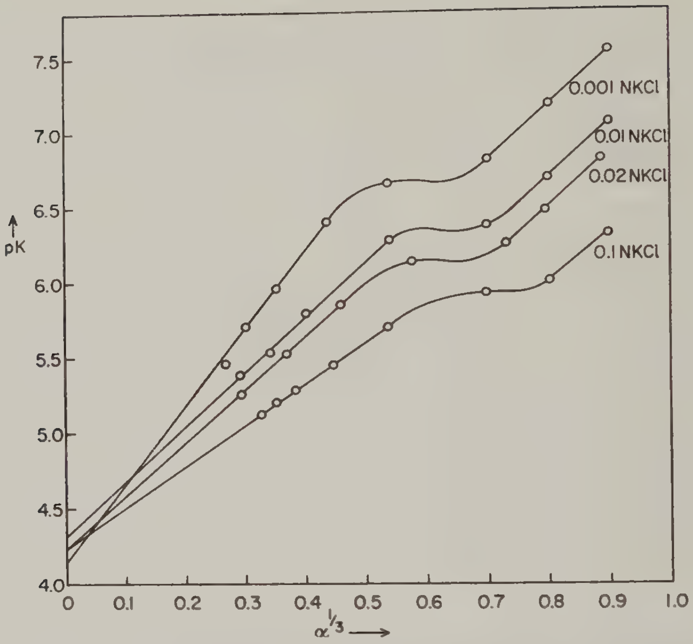

FIG. 2. Titrations of polymethacrylic acid in presence of various concentrations of KCl. (Polymer concentration 0.01 *N*, temperature 25.0°C. Molecular weight average for sample used in 0.02 *N* KCl = 52,000; other curves refer to a sample for which $\overline{M}$ = 75,000.)

of the concentration of alkali chloride in the same way as in the previous work on polymethacrylic acid (5). In the absence of salt, activity corrections have to be neglected.

These observations would lead to the conclusion that the straight-line relationship predicted by Eq. [3] holds in the absence of added electrolytes but not in their presence. This conclusion is not supported, however, by the data obtained by Oth and Doty (6) for polymethacrylic acid. In spite of the absence of neutral salts, their results yield pK $- \alpha^{1/3}$ diagrams of the same type as Fig. 2. With these graphs used in the same way their extrapolated results referring to zero concentration yield a value for pK_0 for polymethacrylic acid of 4.2. At finite concentrations lower values of pK_0 result, as in the case of polyacrylic acid.

(In comparing these different sets of measurements it might be noted that the titrations of Arnold and Overbeek (5) were carried out at finite concentrations in the absence of a salt bridge, whereas Oth and Doty (6) used a salt bridge but extrapolated their results to zero polymer concentration; Samelson's (4) results, on the other hand, refer to finite concentrations in the presence of a salt bridge.)

Discussion

With regard to the inflections observed in plots according to Eqs. [1] or [3], a similar observation has been made by Strobel and Gable (7), who report that "two straight lines intersecting at about $\alpha = \frac{1}{2}$ were obtained in the log $1 - \alpha/\alpha$ plot," for the titration of a weakly basic ion-exchange resin; their paper also includes graphs for the titration of a moderately strong anionic resin which show the beginnings of similar inflections. That inflections of this type were not observed by Katchalsky and Spitnik (2) in their titrations of polymethacrylic acid may be due to the fact that their data do not extend to low values of α.

During the neutralization of a polymeric acid (or base) the strength falls owing to the increasing charge on the polymeric ions. The inflections found for polymethacrylic acid correspond to a slowing down in the rate of decrease of acid strength; this could be caused by a sudden uncoiling of the molecules, which would increase the separation between the remaining acid groups and the charged regions of the chain. In keeping with this there is fairly close coincidence between the ranges of α over which the graphs of Fig. 2 are nonlinear and those over which the corresponding viscosity $-\alpha$ curves (5) rise most rapidly. In view, however, of the different behavior of polyacrylic acid, the phenomenon remains obscure, although the difference could in some way be connected with the greater flexibility of the polyacrylic acid molecule as compared with that of polymethacrylic acid.

A factor not taken into account in the derivation of Eq. [2] is the effect of intramolecular hydrogen bonding between unionized carboxyl groups. This would be expected to increase with decreasing ionization, causing a weakening effect on the acid. From the point of view of obtaining pK_0 by extrapolation this should have little effect, since the points on which these extrapolations are based extend down to $\alpha = 0.02$ in the case of polymethacrylic acid and to 0.03 in the case of polyacrylic acid, i.e., to the situation in which 97 %–98 % of the acid groups are already in the unionized form. There seems little reason to suppose that there would be any sudden change of behavior when the last 2 %–3 % are converted to the unionized form.

Some interesting points arise in connection with the actual values of pK_0. In polymethacrylic acid values of 4.85 (5) and 4.86 (8) have been arrived at from the difficult extrapolation of $pK - \alpha$ curves. Such values have been justified by comparison with isobutyric acid, for which $pK = 4.85$ (9). Extrapolation of $pK - \alpha^{1/3}$ graphs, on the other hand, gives a value for this acid of $pK_0 = 4.28$ (or 4.2 from the data of Oth and Doty). In view of the long extrapolation involved these values must be treated with a certain amount of caution, but they certainly point to a value of pK_0 considerably lower than previous estimates. It is of interest, therefore, to attempt to estimate the strength of these polymeric acids by comparison with simpler acids of related structure.

For propionic acid, 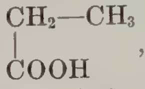 $\begin{array}{l}CH_2{-}CH_3\\ |\\ COOH\end{array}$, pK = 4.87 (9). For αα′-di-methyl-glutaric acid the first dissociation constant may be taken (10, 11) as $K_1 = 5.5 \pm 0.3 \times 10^{-5}$. Since this is a dibasic acid, the intrinsic dissociation constant of one of the acid groups will be one half this value, so that for this acid $pK_0 = \log \frac{1}{2} \times 5.5 \times 10^{-5} = 4.56 \pm 0.03$. This acid may be considered to be derived by substitution of the group: 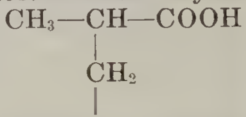 $\begin{array}{c}CH_3{-}CH{-}COOH\\ |\\ CH_2\\ |\end{array}$ in the α position in propionic acid, the substitution resulting in a lowering of the value of pK_0 by $(4.87 - 4.56) = 0.31$. Substitution of a second group of the same kind would give:

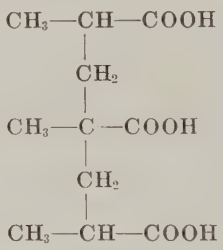

$$\begin{array}{l}CH_3{-}CH{-}COOH\\ \qquad\;\; |\\ \qquad\; CH_2\\ \qquad\;\; |\\ CH_3{-}C{-}COOH\\ \qquad\;\; |\\ \qquad\; CH_2\\ \qquad\;\; |\\ CH_3{-}CH{-}COOH\end{array}$$

which has a structure very similar to that of polymethacrylic acid. If this substitution has again the same effect on the acid strength, we obtain an estimate of $pK_0 = (4.56 - 0.31) = 4.25$ for the central carboxyl group. Substitution of further groups to give acids of higher basicity should now have little effect on the acid strength, owing to the greater distance along the chain from the carboxyl group under consideration.

The same acid may be arrived at by a different series of steps, e.g., starting with acetic acid, and using the relevant dissociation constants. (In any case, however, the "key" acid the dissociation constant of which is required is αα′ – dimethylglutaric.) The results obtained do not agree exactly, but the point is that the intrinsic strength of an acid such as polymethacrylic acid cannot be expected to be close to that of related monobasic acids (e.g., isobutyric) but must be greater, the pK value being about ½ unit lower, owing to the substitution of further carboxyl groups.

Turning to polyacrylic acid, an acid of related structure may be considered to be built up by substitution of two $—CH_2—CH_2—COOH$ groups into acetic acid, one such substitution giving glutaric acid, for which we may take $pK_0 = 4.64$ (12). The resultant lowering of the dissociation exponent from that of acetic acid (pK = 4.76 (9)) is therefore 0.12; a second substitution should then give pK_0 = 4.52 for the acid:

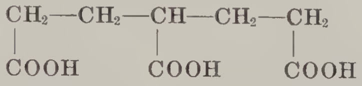

$$\begin{array}{ccccccccc} CH_2 & - & CH_2 & - & CH & - & CH_2 & - & CH_2 \\ | & & & & | & & & & | \\ COOH & & & & COOH & & & & COOH \end{array}$$

As in the previous case slightly different values would be obtained by different routes, and in particular considerably lower estimates of pK_0 would be obtained if we accepted the values of Simon, Meuche, and Heilbronner (11) for the dissociation constants of glutaric or of α-methylglutaric acid. However, consideration of comparable data shows that the strength of glutaric acid is raised by substitution of alkyl groups (as is also the case with succinic acid (13)); this is contrary to the well-known effect of alkyl groups in lowering the strength of monocarboxylic acids. Hence comparisons of this type must lead to the conclusion that polyacrylic acid is weaker than polymethacrylic acid.

The estimates of pK_0 for these two acids arrived at by extrapolation of the pH data are not sufficiently accurate to allow of a clear-cut decision as to which acid is stronger. The pH data at finite values of α, however, allow of no doubt that polyacrylic acid is the stronger of the two. The possibility therefore arises that the undissociated acids are of comparable strength (as indicated by the $pK - \alpha^{1/3}$ extrapolations), with polymethacrylic acid being perhaps somewhat stronger, but that on partial neutralization the strength of polymethacrylic acid falls more rapidly than that of polyacrylic, owing to the fact that less expansion of the molecular coil occurs. Against this possibility, however, is the fact that even when the polyacids are cross-linked, so that expansion is limited in both cases, polyacrylic acid is still the stronger of the two, and changes in the degree of cross-linking seem to have little effect on the relative strength of the two acids (14). Further data are needed to settle this point. In particular, considerable interest would attach to the actual synthesis and investigation of low molecular weight analogues of these polyacids, similar to those discussed in this paper.

The author is grateful to Prof. J. Th. G. Overbeek for his interest and for helpful discussions.

References

1. Kern, W., *Z. physik. Chem.* **A181,** 249, 1938.
2. Katchalsky, A., and Spitnik, P., *J. Polymer Sci.* **2,** 432 (1947).
3. Katchalsky, A., and Gillis, J., *Rec. trav. chim.* **68,** 879 (1949).
4. Samelson, H., Columbia Univ. thesis; Univ. Microfilms (Ann Arbor, Michigan), Publ. No. 9531 (1954).
5. Arnold, R., and Overbeek, J. Th. G., *Rec. trav. chim.* **69,** 192 (1950).

6. Oth, A., and Doty, P., *J. Phys. Chem.* **56,** 43 (1952).
7. Strobel, H. A., and Gable, R. W., *J. Am. Chem. Soc.* **76,** 5911 (1954).
8. Katchalsky, A., Shavit, N., and Eisenberg, H., *J. Polymer Sci.* **13,** 69 (1954).
9. Everett, D. H., Landsman, D. A., and Pinsent, B. R. W., *Proc. Roy. Soc. (London)* **A215**, 403 (1952).
10. Landolt, H. and Börnstein, R., *"Physikalisch-chemische Tabellen"* 5th ed., **II,** 1127. Springer, Berlin (1923).
11. Simon, W., Meuche, D., and Heilbronner, E., *Helv. Chim. Acta* **39,** 290 (1956).
12. Speakman, J. C., *J. Chem. Soc.* **1940,** 855.
13. Landolt, H. and Börnstein, R., *"Physikalisch-chemische Tabellen,"* 5th ed., **II,** 1124, 1127. Springer, Berlin (1923).
14. Fisher, S., and Kunin, R., *J. Phys. Chem.* **60,** 1030 (1956).

JOURNAL OF COLLOID SCIENCE **12**, 557-565 (1957)

THE CRITICAL MICELLE CONCENTRATION OF SODIUM DODECYL SULFATE IN ETHANOL-WATER MIXTURES

B. D. Flockhart

Department of Chemistry, University College, Upper Merrion Street, Dublin, Ireland

Received September 6, 1957

ABSTRACT

The critical micelle concentration (c.m.c.) of sodium dodecyl sulfate in water passes through a minimum as the temperature is raised. Addition of ethanol has a marked effect. In ethanol-water mixtures above 20°C. the c.m.c. increases with temperature, the temperature coefficient becoming increasingly greater as the alcohol concentration rises. Below 20°C. unambiguous c.m.c. values can be obtained only in mixtures containing up to 9% of ethanol. In the latter solvent the c.m.c. is initially temperature independent. With mixtures containing more than 9% of ethanol the Λ-$\sqrt{C}$ curve exhibits a maximum if the temperature is under 20°C.

The effects of short-chain alcohols and of temperature on the c.m.c. and the significance of the maximum in Λ are discussed in relation to theories of micellar structure.

INTRODUCTION

A common characteristic of paraffin-chain salts is the existence of a critical concentration for micelle formation (c.m.c.). In sufficiently dilute aqueous solution these salts behave as simple strong electrolytes. The appearance of micelles as the concentration increases is often so abrupt that only refined techniques indicate a smooth transition in the c.m.c. region. Despite extensive study of the phenomenon, many details of the aggregation are as yet incompletely elucidated.

The value of the c.m.c. is determined by a number of factors. It is markedly dependent on the size and shape of the paraffin chain and on the nature of the polar group. It is usually decreased by a fall in temperature and is at all times decreased by the addition of electrolytes. Organic additives often alter it appreciably.

The purpose of this investigation was to enquire into the effect of temperature on the c.m.c. of sodium dodecyl sulfate in ethanol-water mixtures. Ethanol has been found to have a marked influence on the c.m.c. of this salt, but the measurements were made at only one temperature (1). Present findings show the importance of this factor.

Critical concentrations were determined from measurements of electrical conductance. The reliability of this method has been well established (2).

Experimental

The sodium dodecyl sulfate was kindly provided by Imperial Chemical Industries (I.C.I.). Estimations based on the SO_3 liberated on acid hydrolysis gave a purity of 100%. Microanalysis and theory: C, 50.12 (49.97); H, 8.91 (8.738); S, 10.67 (11.12). Conductivity water of specific conductance around 1.5×10^{-6} mho at 25°C. was obtained by fractional condensation. Absolute alcohol was distilled through a column of approximately 25 plates in an atmosphere of nitrogen. Only the middle fraction was used.

Solvent mixtures were recorded in terms of percentage of ethanol by weight. The exact values are given in the legends and in the table. In the text these mixtures will be referred to by the nearest whole number in the percentage of alcohol.

Conductances were measured on a direct-reading Wheatstone bridge, using the modified Wagner earthing method introduced by Jones and Josephs (3). Current at 1 kc. $sec.^{-1}$ was supplied by a single frequency valve oscillator (Sullivan, London). The null point was determined with a valve amplifier (Sullivan) and telephone receiver. Bridge settings were accurate to within 0.04%. The conductance cells and the procedure were exactly similar to those described in a previous communication (4).

Measurements were made at various temperatures over the range $-9°$ to $+60°$C. Above 0°C. the temperature was controlled to within $\pm 0.05°$ or better. For measurements between $-9°$ and 0°C. an aqueous alcohol solution was used in the bath. This solution was circulated through copper spirals cooled by alcohol/solid carbon dioxide mixtures. By carefully controlling the rate of pumping the temperature was regulated to within $\pm 0.15°$.

Results

The c.m.c. values have been obtained from equivalent conductance (Λ)-$\sqrt{\text{concentration}}$ plots. Straight lines were drawn through the points lying below and immediately above the region in which a rapid change of slope was observed; the point of intersection was taken as the c.m.c. Around this concentration the points fall somewhat below the lines indicating a smooth transition. With increasing ethanol concentration, and in particular at the higher temperatures, the difference between the slopes of the lines becomes much smaller and extrapolation is less certain. The values for water and low percentage ethanol solvents are probably accurate to within ±1%, whereas for higher percentage ethanol solvents the error may be ±3%.

Figures 1 and 2 show values of the c.m.c. plotted as a function of temperature for sodium dodecyl sulfate in water and in two ethanol-water mixtures. The limited solubility of the salt prevented measurements being made at lower temperatures. A minimum in the c.m.c. versus temperature

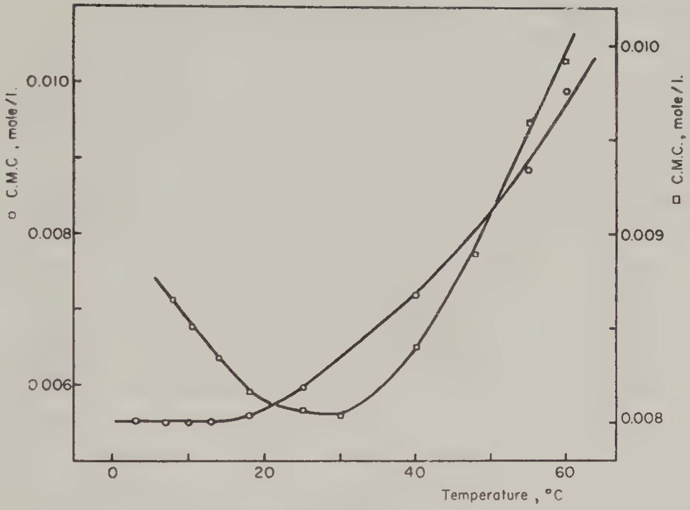

FIG. 1. Effect of temperature on the c.m.c. of sodium dodecyl sulfate in water (□) and in 9.27% ethanol (○).

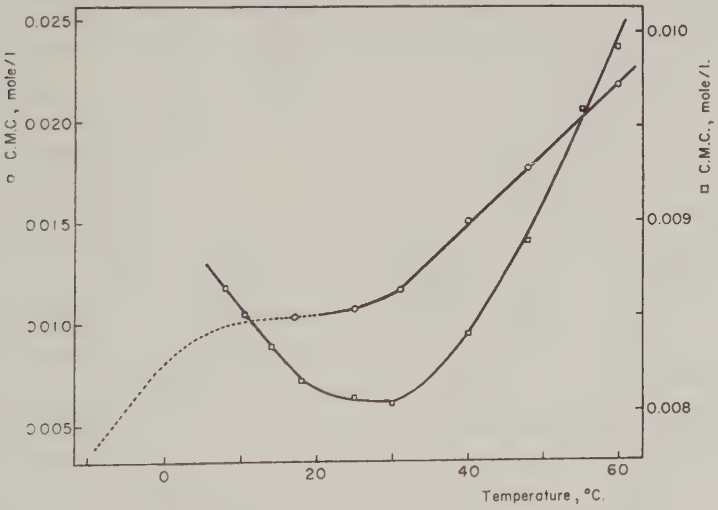

FIG. 2. Effect of temperature on the c.m.c. of sodium dodecyl sulfate in water (□), and 24.98% ethanol (○).

curve for sodium dodecyl sulfate in water was previously observed (5). No minimum occurs in a 9% ethanol solvent, but the c.m.c. remains constant over a range of almost 20°. Above 30°C. the temperature coefficient of the c.m.c. rises rapidly, as the percentage of alcohol is increased (Table I).

Precise values for the c.m.c. cannot be obtained in solvents containing more than 9% of ethanol if the temperature is much below 20°C. Under these conditions the form of the conductance function is altered; the Λ-$\sqrt{C}$ curve exhibits a maximum (Figs. 3 and 4). Using a 25% ethanol solvent measurements were carried down to −9°C. It was observed that on the high concentration side of the maximum a linear relationship existed between Λ and $\sqrt{C}$ for a considerable concentration range. The concentration at which Λ deviated by an arbitrary amount from this straight line (on the low concentration side) was noted. The general trend of these values is indicated by the broken line in Fig. 2. A similarity in shape with the curve for 9% ethanol will now be observed.

Values for the c.m.c. of sodium dodecyl sulfate in ethanol-water mixtures at 55°C. are plotted as a function of alcohol concentration in Fig. 5. The minimum at about 6% of alcohol corresponds to Ward's result of a minimum around 10% when the temperature is 20°C. (1). Because of the maximum in the Λ- $\sqrt{C}$ plot, the curve for 10°C. could not be continued.

TABLE I

Temperature Coefficient of C.M.C. of Sodium Dodecyl Sulfate

Solvent	Temp. range (°C.)	Temp. coeff. (% *per deg.*)
Water	40–60	0.9
9.27% Ethanol	30–60	1.8
24.98% Ethanol	30–60	3.0

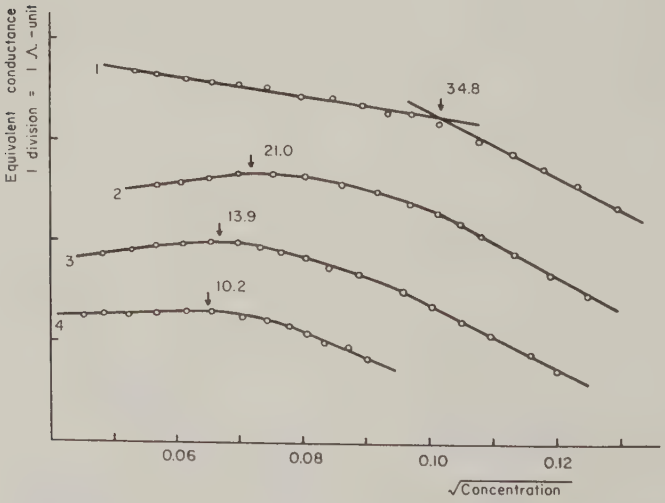

FIG. 3. Conductance curves for sodium dodecyl sulfate in 24.98% ethanol at (*1*) 25.0°C.; (*2*) 10.0°C.; (*3*) 0.2°C.; and (*4*) −6.0°C. The zeros of the ordinate axes of the curves have been adjusted to bring all in the same figure. Ordinates of the break point or maxima are as indicated.

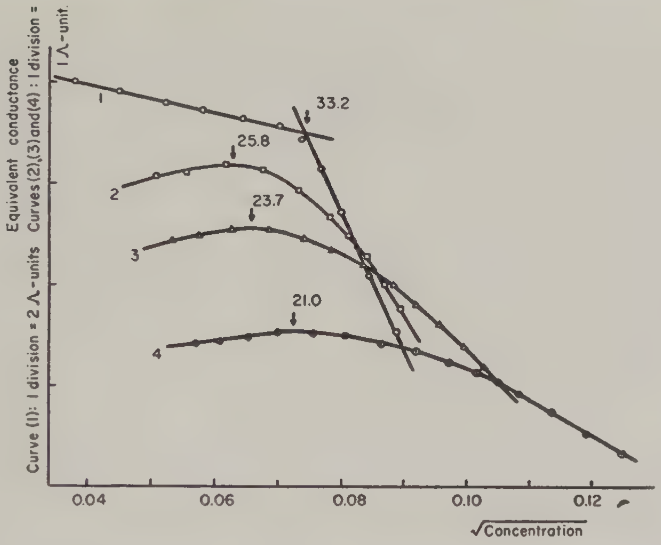

FIG. 4. Conductance curves for sodium dodecyl sulfate in ethanol-water mixtures at 10.0°C.: ethanol for curve (*1*) 9.27%, (*2*) 17.63%, (*3*) 20.78%, (*4*) 24.98%. The zeros of the ordinate axes of the curves have been adjusted to bring all in the same figure. Ordinates of the break point or maxima are as indicated.

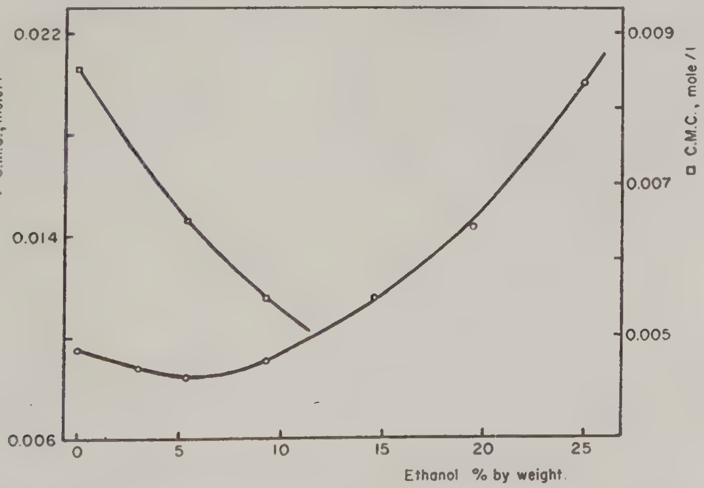

FIG. 5. Effect of ethanol on the c.m.c. of sodium dodecyl sulfate at 55.0° C. (○) and 10.0°C. (□).

DISCUSSION

Very little is known with certainty about the composition and structure of the micelles formed by the aggregation of paraffin-chain ions. In the absence of definite information it is necessary to adopt a model. For the region close to the c.m.c., Hartley's hypothesis (6) is the most convincing.

According to Hartley two energy terms are of major importance in the aggregation process. Aggregation is assumed to occur when the energy available from the destruction of the hydrocarbon-water interfaces is sufficient to overcome the electrical repulsion between the ions. Ward (1) has extended this argument to cover the addition of short-chain alcohols to these solutions. An approximate calculation indicates that for sodium dodecyl sulfate the interfacial energy is no longer the greater beyond 40% of ethanol. This is in good agreement with experimental results. Long-chain alcohols have been shown to lower the c.m.c. A possible explanation of this effect is the decreased head-group repulsion in the micelle, brought about by the introduction of alcohol molecules between the paraffin-chain ions (7).

One of the most doubtful factors in these calculations is the dielectric environment about the ionic heads in the micelle (1). This quantity cannot be even approximately calculated at the present time. The bulk value of the dielectric constant of the solvent must be used. With short-chain alcohols dielectric effects are likely to be important. Another probable source of error is the use of interfacial energy to represent the interaction energy of a single hydrocarbon chain with the surrounding solvent molecules (8). Until it is possible accurately to evaluate the energy changes involved in micelle formation, little progress can be made toward a complete analysis of the effect of alcohols on the c.m.c. Several papers dealing with various aspects of the energetics of micelle formation have been published within recent years (9–11).

C.M.C. vs. Ethanol Concentration Curves

At constant temperature small additions of ethanol lower the c.m.c. of sodium dodecyl sulfate; larger additions raise the value. Ward (1) has attributed the initial drop in the c.m.c. to adsorption of alcohol molecules on the paraffin surface of the micelle. The shift of the minimum to lower alcohol concentrations upon a rise in temperature may therefore be brought about by two contributory factors: a decrease in the amount of alcohol adsorbed on the surface of the micelle, and an increase in the solvent power of the alcohol for the hydrocarbon portion of the ion. Support for the assumption of a hydrocarbon-water interface within each micelle can be found in the work of Stigter and Mysels (12) [cf. also (10)].

C. M. C. vs. Temperature Curves

Among the smaller energy changes associated with the formation of micelles is the imposed reduction in the kinetic energy of the ions upon aggregation. The disaggregating effect of thermal agitation is evidenced by a shift of the c.m.c. to higher values with a rise in temperature [Figs. 1 and 2, and (13)]. Table I shows that the temperature coefficient of the c.m.c. increases rapidly as the alcohol content of the solvent rises. This result presumably indicates that the power of the alcohol to displace the equilibrium in the direction of single ions becomes increasingly greater as the temperature is raised.

Maximum in Λ-$\sqrt{C}$ *Curves*

The sharpness or lack of sharpness of initial micelle formation, as indicated by the break point in the Λ-$\sqrt{C}$ plot, depends greatly on *both* the ethanol concentration and the temperature. This is clearly evident from Figs. 3 and 4. A maximum appears in the Λ-$\sqrt{C}$ curves if the ethanol concentration exceeds 9% and the temperature is under 20°C. The occurrence of a maximum conductance in propanol-water mixtures of sodium dodecyl sulfate was previously reported (5). These results have obviously a significant bearing on the interpretation of the aggregation phenomena characteristic of these solutions.

Evidence has been presented which shows that even below the c.m.c. there are indications that some small micelles are formed in solution. Ekwall and co-workers (14) have obtained extensive experimental data showing that discontinuities in the behavior of paraffin-chain salts occur not only at the c.m.c. but also at concentrations that are both below and above this value. These discontinuities, however, are observed in the presence of foreign substances such as long-chain alcohols and hydrocarbons. According to these investigators the lowest concentration limit, termed the limiting association concentration, must be ascribed to association between the paraffin-chain ions and the molecules of the additive.

Whether paraffin-chain salts behave differently only in the presence of organic additives or whether *small* changes occur in the structures of the pure salt solutions below the c.m.c. is not certain. Of importance from the present point of view is the probable existence of small mixed aggregates below the c.m.c. in alcohol-water mixtures. On this assumption the maximum in the Λ-$\sqrt{C}$ curves of sodium dodecyl sulfate in ethanol-water mixtures (Figs. 3 and 4) can be tentatively explained. The small paraffin-chain ion-alcohol aggregates will possess a greater relative mobility than the single ions by virtue of Stokes's law. In such dilute solutions the secondary effects of aggregation will be small [cf. (5)].

On the assumption that the presence of premicelles is the correct explanation for the maximum effect, the equilibrium relationship between these aggregates and the simple ions must be very sensitive to temperature (Fig. 3).

Fall of C.M.C with Rise in Temperature

According to Ekwall the limiting association concentration should not be confused with the c.m.c.; they appear simultaneously in numerous colloid systems, but at different colloid concentrations (15). It may therefore be permissible to attach some significance to the values indicated by the broken line in Fig. 2. They may, in fact, be very approximate values for the c.m.c. in 25% ethanol at temperatures between −9° and +20°C. Inspection of Figs. 1 and 2 now shows that under 20°C. the c.m.c. of sodium dodecyl sulfate in water decreases as the temperature rises, in 9% ethanol it remains constant, whereas in 25% ethanol it increases.

From the temperature coefficient of the c.m.c. experimental values for the heat of micelle formation can be calculated (9). A decrease in the c.m.c. upon a rise in temperature leads to positive values. The heats of micelle formation of sodium dodecyl sulfate in water at various temperatures have already been reported (5). Corresponding heats of micelle formation may be calculated from the published work (16) on potassium laurate, lauryl sulfonic acid, and dodecylammonium chloride. At low temperature the values are positive. Recently, calorimetric measurements have been made to determine directly the heat involved in micelle formation (17, 18). For three of the salts investigated positive values were obtained.

In a very recent paper (18), Goddard, Hoeve, and Benson have shown qualitatively how small positive heat effects may be explained. According to Frank and Evans (19) water forms "frozen" patches or microscopic "icebergs" about molecules of nonpolar substances and around the nonpolar parts of molecules of polar substances. With single paraffin-chain ions in aqueous solution this quasi-solid structure formed around the hydrocarbon chain causes additional heat and entropy to be lost. Hence, aggregation of these ions at low temperature is accompanied by an increase in the energy of the system. With rise of temperature a gradual breakdown of the structure occurs. There is, therefore, an increase in the energy of the single ion state, and consequently the value for the heat of micelle formation falls and eventually becomes negative.

Present measurements would appear to support these ideas. The addition of ethanol leads to smaller values for the heat of aggregation, the value becoming zero in a 9% ethanol mixture; in higher percentage ethanol solvents it is negative. A breakdown in the quasi-solid structure as the alcohol concentration is increased seems quite likely. Dissolved ions are believed to have a big depolymerization effect on water (19). The alcohol may bring about depolymerization both by "iceberg" formation and hydrogen bonding.

REFERENCES

1. WARD, A. F. H., *Proc. Roy. Soc. (London)* **A176,** 412 (1940).
2. WILLIAMS, R. J., PHILLIPS, J. N., AND MYSELS, K. J., *Trans. Faraday Soc.* **51,** 728 (1955).
3. JONES, G., AND JOSEPHS, R. C., *J. Am. Chem. Soc.* **50,** 1049 (1928).
4. FLOCKHART, B. D., AND GRAHAM, H., *J. Colloid Sci.* **8,** 105 (1953).
5. FLOCKHART, B. D., AND UBBELOHDE, A. R., *J. Colloid Sci.* **8,** 428 (1953).
6. HARTLEY, G. S., "Aqueous Solutions of Paraffin-Chain Salts." Hermann et Cie., Paris, 1936; *Kolloid-Z.* **88,** 22 (1939).
7. HERZFELD, S. H., CORRIN, M. L., AND HARKINS, W. D., *J. Phys. & Colloid Chem.* **54,** 271 (1950).
8. CORRIN, M. L., AND HARKINS, W. D., *J. Chem. Phys.* **14,** 640 (1946).
9. STAINSBY, G., AND ALEXANDER, A. E., *Trans Faraday Soc.* **46,** 587 (1950).
10. PHILLIPS, J. N., *Trans. Faraday Soc.* **51,** 561 (1955).
11. REICH, I., *J. Phys. Chem.* **60,** 257 (1956).
12. STIGTER, D., AND MYSELS, K. J., *J. Phys. Chem.* **59,** 45 (1955).
13. POWNEY, J., AND ADDISON, C. C., *Trans. Faraday Soc.* **33,** 1243 (1937). WRIGHT, K. A., ABBOTT, A. D., SIVERTZ, V., AND TARTAR, H. V., *J. Am. Chem. Soc.* **61,** 549 (1939). RALSTON, A. W., AND HOERR, C. W., *J. Am. Chem. Soc.* **64,** 772 (1942). KLEVENS, H. B., *J. Phys. & Colloid Chem.* **52,** 130 (1948).
14. EKWALL, P., *J. Colloid Sci. Suppl.* **1,** 66 (1954); PASSINEN, K., AND EKWALL, P., *Acta Chem. Scand.* **9,** 1438, 1450 (1955); EKWALL *et al.*, *Acta Chem. Scand.* **10,** 227, 237 (1956).
15. EKWALL, P., SÖDERBERG, O., AND DANIELSSON, I., *Acta Chem. Scand.* **10,** 227 (1956).
16. BRADY, A. P., AND HUFF, H., *J. Colloid Sci.* **3,** 511 (1948). EGGENBERGER, D. N., AND HARWOOD, H. J., *J. Am. Chem. Soc.* **73,** 3353 (1951). HOYER, H. W., AND GREENFIELD, A., *J. Phys. Chem.* **61,** 818 (1957).
17. HUTCHINSON, E., MANCHESTER, K. E., AND WINSLOW, L., *J. Phys. Chem.* **58,** 1124 (1954). HUTCHINSON, E., AND WINSLOW, L., *J. Phys. Chem.* **60,** 122 (1956).
18. GODDARD, E. D., AND BENSON, G. C., *Trans. Faraday Soc.* **52,** 409 (1956). GODDARD, E. D., HOEVE, C. A. J., AND BENSON, G. C., *J. Phys. Chem.* **61,** 593 (1957).
19. FRANK, H. S., AND EVANS, M. W., *J. Chem. Phys.* **13,** 507 (1945).

JOURNAL OF COLLOID SCIENCE **12**, 566–574 (1957)

FLOCCULATION, SUBSIDENCE, AND FILTRATION OF PHOSPHATE SLIMES[1]

V. The Optimum Filtration Rate as a Function of Solid Content and Specific Area

Victor K. LaMer[2], Robert H. Smellie, Jr.,[3] and Pui-Kum Lee[4]

Received January 18, 1957; revised May 10, 1957

ABSTRACT

The optima in the concentration of various polymeric flocculating agents which produce the maxima in the filtration rates of phosphate slimes are (empirically) linear with respect to the square of the weight per cent of solids and also the square of the specific areas of the solids in the slimes.

A. INTRODUCTION

In the preceding paper (IV) of this series (1) it was demonstrated that with all the slimes and flocculating agents studied the plots of filtration rate vs. the concentration of flocculating agent show maxima in filtration rates at particular flocculating agent concentrations. The position of this maximum in filtration rate varies with the composition of the flocculating agent, the chemical composition of the solid, and the per cent by weight of the solid in the slime. Similar variations were observed with starches as flocculating agents (1). For any given slime with a particular flocculating agent the concentration of the flocculating agent corresponding to the maximum filtration rate increases with the per cent by weight of solids.

B. EXPERIMENTAL METHODS AND RESULTS

Stock slimes containing only minus 200 mesh particles were prepared from "leached zone" material by the method described in paper II of this series (2). In addition, slimes (also −200 mesh) were prepared from pure $Ca_3(PO_4)_2$ and $AlPO_4$ solids, respectively. Solid contents up to 15% were obtained by diluting the stock slimes with distilled water. The pH of the

---

[1] Supported by funds from Contract At(30-1)1189 between Columbia University and the U. S. Atomic Energy Commission. Progress Reports N.Y.O. 3289, 7402 and 7403.

[2] Department of Chemistry, Columbia University, New York, New York.

[3] Department of Chemistry, Trinity College, Hartford, Connecticut.

[4] Present address: Minnesota Mining and Manufacturing Co., St. Paul, Minnesota.

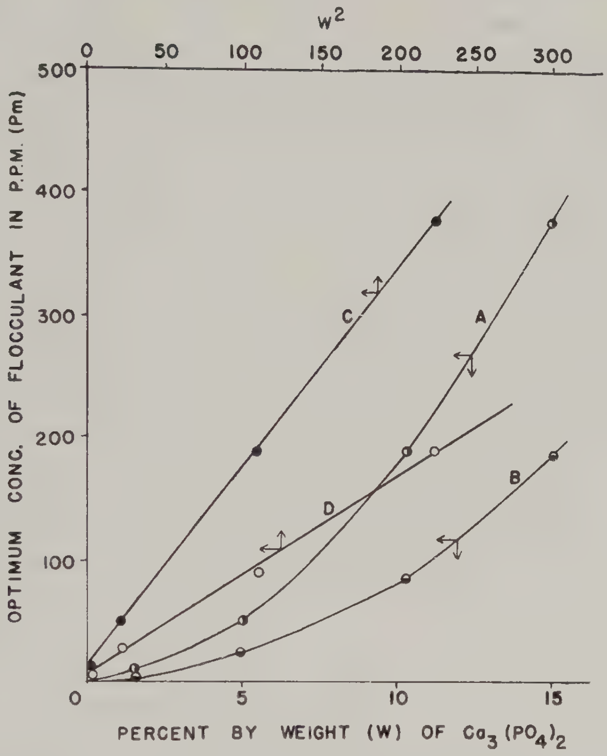

FIG. 1. The optimum in the concentration of flocculant (P_m) vs. the per cent by weight (W) of $Ca_3(PO_4)_2$ (lower abscissa) and against W^2 (upper abscissa) for $Ca_3(PO_4)_2$ slimes. *A*. P_m vs. W with Lytron 886 (product of Monsanto Chemical Company). *B*. P_m vs. W with Guartec (product of General Mills, Inc.). *C*. P_m vs. W^2 with Lytron 886. *D*. P_m vs. W^2 with Guartec.

diluted slime was then adjusted to the value for the original stock slime in each case.

The variation of the filtration rate of a particular slime with the concentration of the flocculating agent for different solid contents was determined using the vacuum filtration technique described in paper II of this series (2). The optimum concentrations of flocculant (i. e., the concentration corresponding to maximum filtration rate) were determined for different solid contents. Figure 1 shows plots of the optimum concentration of flocculating agent (P_m) vs. per cent solids (W) and P_m vs. W^2 for calcium phosphate slimes using Lytron 886 and Guartec as flocculating agents.

An examination of curves *A* and *B* of Fig. 1 suggests that the relationship between P_m and W is parabolic and, therefore, a plot of P_m vs. W^2 should be linear. The parabolic relation is confirmed by the straight lines *C* and *D* when the data are plotted as P_m vs. W^2. Subsequently, additional data obtained with other slimes and flocculating agents (not shown) were found consistently to be in agreement with the linear relationship for P_m vs. W^2. This relationship is general, and one may interpolate with confidence to obtain the optimum flocculating agent concentration for intermediate values of solid content when only a few data are available.

On the basis of other investigations in our laboratories, the linear relationship between P_m and W^2 indicated the possible existence of a more fundamental linear relationship between P_m and the square of the specific surface of the solids.

A technique for determining the specific surfaces of the solids which is especially suited to our investigations is the permeability method which was developed by Carman using a theory of Kozeny (3), in which filtration rates are related to the surface areas of the solid in the filter cakes. Further details concerning the application of this method for the determination of the specific surfaces of phosphates will be described in a later paper.

Carman has shown (4) that for a bed (filter cake) of constant and known thickness, the volume rate of flow of filtrate (Q) is related to other factors as follows:

$$Q = \frac{\Delta P g A \epsilon^3}{k \eta L S^2}$$

where Q = volume rate of flow of filtrate in cm.^{3}/sec.;
ΔP = pressure drop across the bed in g./cm.^{2};
g = acceleration of gravity (980 cm./sec.^{2});
A = cross-sectional area of the bed (cm.^{2});
ϵ = porosity of the bed (the volume of void divided by total volume of bed (AL));
$\epsilon = 1 - \frac{W}{AL\rho}$;
W = weight of solid in the bed (g.);
L = depth or thickness of bed (cm.);
ρ = bulk density of solid g./cm.^{3};
η = viscosity of fluid passing through bed;
k = constant $\cong 5$;
S = surface area of particles in unit volume of bed (cm.^{2}/cm.^{3}).

In order to measure the filtration rate through a filter cake of constant and known thickness, the *first* filtrate is passed through the cake obtained from the initial filtration in which the solid is still settling during the process. This second or *refiltration rate* is used as the Q in the Kozeny-Carman equation. The cake thicknesses were measured with a traveling microscope. The pressure gradient (ΔP) (usually about 74 cm. of Hg) was determined from a manometer connected to the suction flask in the vacuum filtration apparatus.

Comparison showed that the specific areas obtained from the Kozeny-Carman method were in satisfactory agreement with those obtained from stearic acid adsorption. It was established that the refiltration data could be used reliably as a means of determining at least the "relative" surface areas of the solids in a series of different phosphate slimes. These determinations were sufficient for the correlation with flocculation and filtration.

In order to establish whether or not the linear P_m vs. W^2 relationship corresponds to a linear P_m vs. (area)^2 relationship, samples of a single pure solid material ($Ca_3(PO_4)_2$) having different specific surfaces were obtained by fractionation of a stock sample in order to eliminate the additional uncertainty introduced by differences in the chemical composition of the surfaces.

METHOD OF FRACTIONATION

Tricalcium phosphate ($Ca_3(PO_4)_2$ N.F. precipitated), obtained from the Fisher Scientific Co., New York, New York, was subjected to fractional separation. A system of several connected containers (Fig. 2) was used for a continuous flow fractionation.

A dilute suspension having a solid content of 5% was placed in flask *A*, which was provided with a side outlet near (but not at) the bottom and a ground glass stopcock to facilitate control of the flow rate. The material remaining suspended in *A*, flowed into *B*. From the top of *B*, suspension

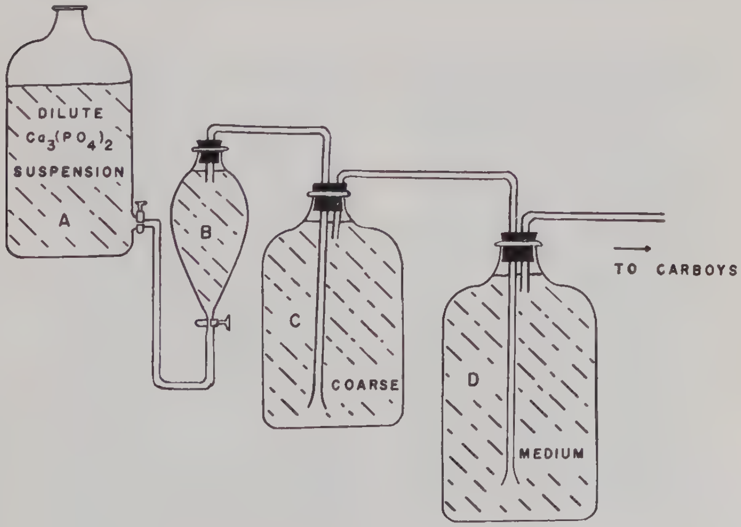

FIG. 2. Fractionation apparatus (discussed in text).

flowed into container C, through a tube with a funnel-shaped outlet, which reached almost to the bottom of C. Further separation of particle size was obtained by allowing the suspension to flow from the top of C, into a funnel shaped exit near the bottom of D. Very fine particles at the top of D flowed into 20-liter carboys where slow sedimentation took place overnight. The decantrate from the carboys, which was nearly clear, could be used for further separation.

A satisfactory fractionation of particle size is possible if a constant flow rate is maintained, and the starting suspension is sufficiently dilute (5%

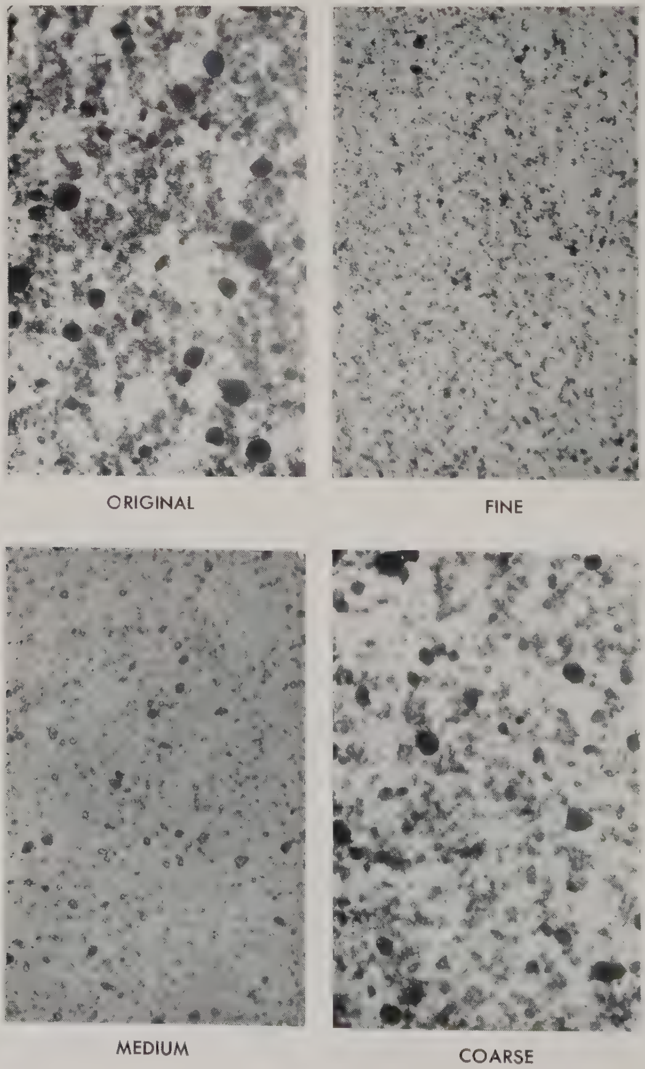

ORIGINAL FINE

MEDIUM COARSE

FIG. 3. Photomicrographs (50×) of samples of $Ca_3(PO_4)_2$ obtained by fractionation.

solids or less). When the per cent solids is too great, collective sedimentation results and fine particles are forced down by larger ones. However, excessive dilution is undesirable, since the weights of solid that can be separated from a given volume of suspension are too small.

The fractions so separated were named "coarse" (from container *C*), "medium" (from container *D*), and "fine" (from the carboys). Photomicrographs of these fractions (Fig. 3) showed that the "fine" contained particles of diameter less than 10 microns. The "medium" fraction contained particles up to 20 microns, and the "coarse" fraction contained particles of diameters up to 100 microns. Fine particles were abundant in the "medium" and "coarse" fractions; however, the average particle sizes in each fraction were sufficiently different for our purpose.

DETERMINATION OF "RELATIVE" SPECIFIC SURFACE AREAS OF THE SIZE FRACTIONS

After having obtained the $Ca_3(PO_4)_2$ in three distinct size fractions by the method just described, specific surface areas of each fraction had to be determined.

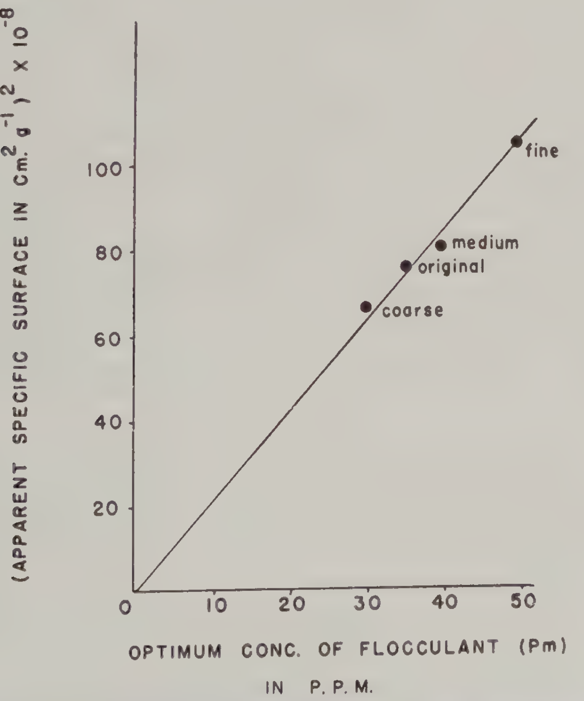

FIG. 4. The square of the apparent specific surfaces vs. the optimum concentration of Lytron 886 (flocculant) for slimes prepared from each of the various size fractions of $Ca_3(PO_4)_2$. Solid content of slimes was 5.5%.

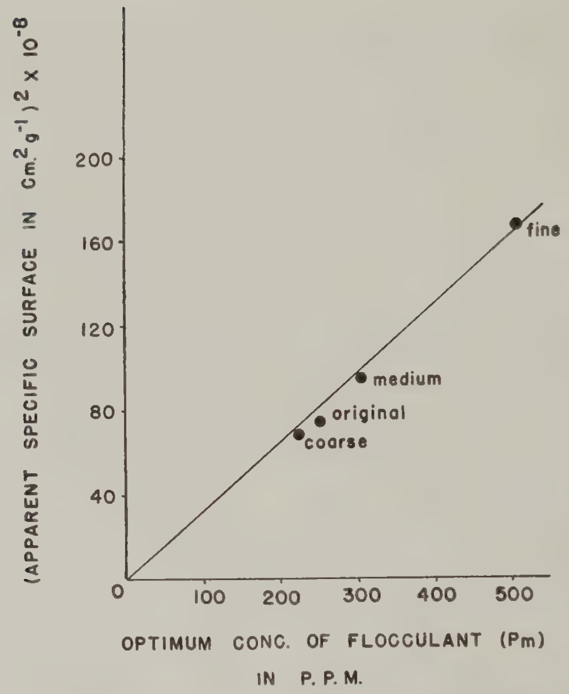

FIG. 5. The square of the apparent specific surfaces vs. the optimum concentration of PAM-M (flocculant) for slimes prepared from each of the various size fractions of $Ca_3(PO_4)_2$. Solid content of slimes was 5.5%.

PAM-M designates a polyacrylamide flocculant, prepared in the Columbia University Laboratories by P. K. Lee as follows:

Six grams of Polyacrylamide 100 (American Cyanamid Co.) and 18 ml. of 40% formaldehyde were combined with water to a volume of 300 ml. (pH = 4) and heated at 80°C. in a water bath for 30 minutes to effect cross-linking of the polyacrylamide. The liquid was then quickly chilled and ammonia (to pH = 8) was added to react with the excess formaldehyde. The solution was then adjusted to 0.5% by weight of polyacrylamide and a final pH of 5.2 with water and hydrochloric acid for use as a flocculant.

Since a very precise determination of specific surface is a complicated and unnecessary endeavor for the purposes of this investigation, the refiltration data adapted to the Kozeny-Carman permeability equation were considered sufficient.

Slimes of the different fractions of $Ca_3(PO_4)_2$ were prepared with the same per cent solids (5.5 %). Since the per cent solids in each of the $Ca_3(PO_4)_2$ slimes, so prepared, is the same, any differences in the amount of a particular polymeric flocculating agent required to produce the optimum in the refiltration rate must be due to differences in specific surface.

The expected variations in the refiltration rates of the original "blanks" of the various slimes were observed, showing that a significant fractionation of particle size and hence of specific surface had been effected, thus confirming the evidence given by the photomicrographs.

According to the discussion in connection with Fig. 1, a plot of P_m vs. S^2, i.e., (specific area of solid)^2, should be linear. Two sets of experimental data obtained with the fractionated $Ca_3(PO_4)_2$ have been plotted in this way (Figs. 4 and 5). The points correspond to a straight line passing through the origin in both cases, within the limits reasonably expected from the data obtained by the present experimental techniques.

It will be noted that the apparent specific area for the "fine" fraction in particular is significantly different in the two cases (Figs. 4 and 5). The data represented in Fig. 4 were obtained within a few days after the slimes were first prepared, whereas the data for Fig. 5 were obtained about two weeks later with the same slimes. We have frequently observed this variation in apparent surface area and hence in filtration rate with the aging of slimes. This can be attributed to the variation in the degree of aggregation produced by slow changes in the concentration and the surface adsorption of ions and modifications of the surfaces of particles due to hydrolysis. Such changes lead to a greater or lesser degree of flocculation with the corresponding variation of effective particle surface area over a relatively long period of time. This effect is usually observed more frequently with fine suspensions. The apparent surface area of the "medium" fraction changed very little during the two-week interval and the apparent areas of the "original" material and the "coarse" fraction remained the same within the errors of measurement.

Had the linear relationship between P_m and W^2 been strictly one depending upon the mass (or volume) of the particles, then, since the slimes prepared from the fractionated $Ca_3(PO_4)_2$ all had the same per cent solids, they should have exhibited the same value of P_m. This series of experiments shows that the linear P_m vs. W^2 relationship is basically a linear P_m vs. (specific area of solids)^2 function.

C. Conclusion

The specific effect of the chemical composition of the solid surface in relation to flocculation by polymeric flocculating agents may now be investigated for known relative specific surfaces, since it has been shown that the specific surface of the solids and the amount of flocculating agent necessary to produce a maximum in filtration rate are related.

At the present time data relating specific surfaces of solids to optima in flocculating agent concentration for different slimes are not sufficiently systematic and diverse to permit drawing definite conclusions concerning the specific effect of the chemical composition of the solid in the flocculation process.

Further experiments are planned in which insoluble sulfates, chlorides, and hydroxides will be used with varied specific surfaces to allow clarification of the role of chemical composition of the solid surface in flocculation by polymeric flocculating agents.

REFERENCES

1. La Mer, V. K., Smellie, R. H., Jr., and Lee, P. K., *J. Colloid Sci.* **12,** 230 (1957).
2. La Mer, V. K., and Smellie, R. H., Jr., *J. Colloid Sci.* **11,** 710 (1956).
3. Kozeny, J., *Ber. Wien. Akad.* **136a,** 271 (1927).
4. Carman, P. C., *J. Soc. Chem. Ind. (London)* **57,** 225 (1938); *ibid.* **58,** 1 (1939); *ibid.* **69,** 134 (1950).

JOURNAL OF COLLOID SCIENCE **12**, 575–580 (1957)

THE PATHS OF APPROACH AND RECESSION OF TWO SPHERES IN A SHEARING VISCOUS LIQUID

M. Mooney

The General Laboratories of the United States Rubber Company, Passaic, New Jersey

Received March 11, 1957

Recent experimental work by Manley and Mason (1), and by Bartok and Mason (2), has been concerned with the paths of near-neighbor glass spheres suspended in a viscous liquid flowing in continuous simple shear.

Without knowledge of this work I have stated without proof (3), in discussing Vand's (4) theory of the viscosity of a suspension of spheres, that the paths of approach and recession of two rigid spheres in a shearing liquid would be curvilinear and would be mirror images of each other. This theorem has been given substantial support by the experimental results reported by Bartok and Mason (2); and in correspondence on this work Dr. Mason has suggested to me that I publish the proof of the theorem. The proof follows below.

It is assumed that the two suspended spheres are perfect, rigid, too large to show appreciable Brownian movement, and subject to first-order hydrodynamic forces only. Inertial forces are thus ruled out, as well as surface forces.

First it is necessary to show that, under the assumed conditions, two spheres in passing cannot make physical contact. Consider two spheres of equal radii, a, approaching each other at relative velocity V along the line joining their centers. We then ask the question, what force, operating on each sphere, is necessary to overcome the viscous resistance of the liquid that is being forced out from between the spheres? To facilitate the mathematics, we substitute for the approaching spheres a pair of co-axial parabolic surfaces of the same curvature at their apices, where they are tangent to the spheres they replace. Each paraboloid is cut off by a right section at such a position that the section radius is equal to the radius of the spheres.

Let Q be the flux across a cylindrical surface of radius r about the axis of the system, r being less than the sphere radius. Then

$$Q = \pi r^2 V.$$

But also

$$Q = 4\pi r \int_0^h v \, dz,$$

where z is the axial distance from the central plane of the system, $2h$ is the separation of the parabolic surfaces at radial distance r, and v is the radial liquid velocity at r, z. The expression for h is

$$h = b + r^2/a,$$

where $2b$ is the apex separation of the parabolas, and a is the apex radius of curvature.

We ignore the axial components of the liquid velocity. The hydrodynamic equation is then

$$\eta \frac{\partial^2 y}{\partial z^2} = \frac{1}{r}\frac{d(rP)}{dr},$$

where η is the viscosity; and P is the pressure, taken to be zero at $r = a$. The axial hydrodynamic force on either parabola is

$$F = 2\pi \int_0^a rP\, dr.$$

Solution of the above equations gives the result

$$V = \frac{8b(a + b)^2 F}{3\pi\eta a^4}.$$

This equation is only an approximation, but it shows that V becomes proportional to b in the limit as $b \to 0$.

Now consider two spheres which at time $t = 0$ are separated by the distance $2b_0$; and let F_m be the upper limit of the external force tending to drive the two spheres together for all subsequent positions of approach. Then

$$V = -2\frac{db}{dt} < \frac{8b(a + b_0)^2 F_m}{3\pi\eta a^4} = 2kb,$$

k being defined by the above equation. Integration leads to the inequality

$$b > b_0 e^{-kt}.$$

Thus we see that b can never become zero for any finite t. But since two spheres in close proximity rotate about each other at a finite velocity of rotation, the time available for their closer approach is finite. Hence, approach to contact, or $b = 0$, is impossible if the assumptions underlying this theory are valid.

A slight variation of the above proof would establish the same conclusion for spheres of different radii. The problem of path symmetry therefore can be analyzed on the assumption that contact pressure between two spheres in apparent collision is nonexistent. Hence the only forces we have to consider are hydrodynamic forces.

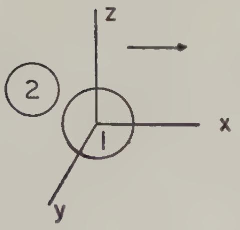

Fig. 1.
Case I. $\mu(\infty) = gz$

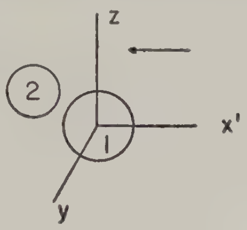

Fig. 2.
Case II. $\mu'(\infty) = -gz$

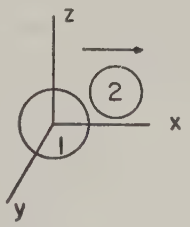

Fig. 3.
Case III. $\mu''(\infty) = gz$

Now to prove that the paths of approach and recession are mirror images of each other, we consider three different situations involving two spheres, as indicated in Figs. 1, 2, and 3; and we choose the center of Sphere 1 in each case as the origin of our reference axes. The y and z coordinates of Sphere 2 are the same in all three cases. In Case II the x-z shear is reversed in sign. In Case III the x-coordinate of Sphere 2 is reversed in sign.

If u, v, w are the velocity components, p_{i_j} the stresses, p the mean pressure, and η the viscosity, the general equations for viscous flow and the boundary conditions are as given in Eqs. [1] to [8]. The subscript i may be 1 or 2, referring to spheres No. 1 and 2, respectively. The components u_i, v_i, w_i are the velocities of the center of the sphere i, R_i its radius; l_i, m_i, n_i are the direction cosines of the radius vector from the center of sphere i to a point on its surface; l_i, l'_i, and l''_i, etc., refer to corresponding points in the three Cases I, II, and III. The integrals $\int da$ extend over the sphere surface, da being an element of area.

Field Equations

$$\begin{cases} \frac{1}{\eta}\frac{\partial p}{\partial x} + \frac{\partial^2 u}{\partial x^2} + \frac{\partial^2 u}{\partial y^2} + \frac{\partial^2 u}{\partial z^2} = 0, \\ \frac{1}{\eta}\frac{\partial p}{\partial y} + \frac{\partial^2 v}{\partial x^2} + \frac{\partial^2 v}{\partial y^2} + \frac{\partial^2 v}{\partial z^2} = 0, \\ \frac{1}{\eta}\frac{\partial p}{\partial z} + \frac{\partial^2 w}{\partial x^2} + \frac{\partial^2 w}{\partial y^2} + \frac{\partial^2 w}{\partial z^2} = 0. \end{cases} \qquad [1]$$

Boundary Conditions

At infinity:

$$\begin{cases} u = gz, \text{ Cases I and III,} \\ u = -gz, \text{ Case II,} \\ v = w = p = 0. \end{cases} \qquad [2]$$

At the sphere surfaces:

$$\begin{cases} u = u_i + (m_i\omega_{i3} + n_i\omega_{i2})R_i, \\ v = v_i + (n_i\omega_{i1} + l_i\omega_{i3})R_i, \\ w = w_i + (l_i\omega_{i2} + m_i\omega_{i1})R_i. \end{cases} \tag{3}$$

$$\int p_{ix}\,da = \int p_{iy}\,da = \int p_{iz}\,da = 0, \tag{4}$$

$$\int l_i p_{ix}\,da = \int m_i p_{iy}\,da = \int n_i p_{iz}\,da = 0. \tag{5}$$

where

$$\begin{cases} p_{ix} = l_i p_{xx} + m_i p_{xy} + n_i p_{xz}, \\ p_{iy} = l_i p_{yx} + m_i p_{yy} + n_i p_{yz}, \\ p_{iz} = l_i p_{zx} + m_i p_{zy} + n_i p_{zz}, \end{cases} \tag{6}$$

$$\begin{cases} p_{xx} = -p + 2\eta\,\dfrac{\partial u}{\partial x}, \\ p_{yy} = -p + 2\eta\,\dfrac{\partial v}{\partial y}, \\ p_{zz} = -p + 2\eta\,\dfrac{\partial w}{\partial y}, \end{cases} \tag{7}$$

$$\begin{cases} p_{yz} = p_{zy} = \eta\left(\dfrac{\partial w}{\partial y} + \dfrac{\partial v}{\partial z}\right), \\ p_{zx} = p_{xz} = \eta\left(\dfrac{\partial u}{\partial z} + \dfrac{\partial w}{\partial x}\right), \\ p_{xy} = p_{yx} = \eta\left(\dfrac{\partial v}{\partial x} + \dfrac{\partial u}{\partial y}\right). \end{cases} \tag{8}$$

Concerning the solutions of these equations, it is to be noted first that all Eqs. [1] to [8] are linear and homogeneous in the dependent variables u, v, w, p_{ij}, p, u_i, v_i, w_i, ω_{i1}, ω_{i2}, ω_{i3}, and the parameter g. Consequently, when g changes sign, this being the only difference between Cases I and II, the only change in the solution is that all dependent variables in the solution likewise change sign. Thus, $u'(x', y, z) = -u(x, y, z)$, etc., as shown in the table, Comparison of Solutions. In this table u stands for u, u_1, or u_2.

In going now from Case II to Case III, there is again a change in sign of g, and also in the sign of x for corresponding points. Case III is thus the image of Case II as mirrored in the yz plane. The solution for Case III can therefore be easily written down in terms of the solution for Case II, and consequently in terms of the solution for Case I also. The various sign changes that occur are shown in the Comparison of Solutions. It will be found that with the sign changes indicated with reference to Case I, the terms in any equation of the system [1] to [8] all change sign or all remain invariant. Hence the equations remain satisfied in either case.

It may be remarked at this point that the use of Case II in this argument is not essential. It is possible to go directly from Case I to Case III; but the interposition of Case II seems to be helpful in clarifying the problem. It is clear that Cases I and III may be taken to represent the approach and the recession of two spheres. The components of the relative velocity, $u_2 - u_1$, etc., are functions of the coordinates of Sphere 2, x_2, y_2, z_2. Furthermore, $u_2 - u_1$ is invariant in the transformation $x_2 \rightarrow -x_2$ while $v_2 - v_1$ and $w_2 - w_1$ change sign.

The velocities of the spheres with respect to their center of gravity (each sphere having unit weight) are $(u_2 - u_1)/2$, etc., and $(u_1 - u_2)/2$, etc. The velocities with respect to the center of gravity therefore have the same symmetry property as have the relative velocities, $u_2 - u_1$, etc.

From what has been proved it is now relatively easy to show that the paths of approach and recession of either sphere relative to their center of gravity are images of each other as mirrored in the yz plane which passes through the center of gravity and moves with it. Consider two spheres at the moment of passing when $x_1 = x_2 = 0$; and take this moment as zero time. Let the coordinates and velocities of sphere 2 with respect to their center of gravity be denoted by X, Y, Z and U, V, W during approach and by $\bar{X}, \bar{Y}, \bar{Z}$ and $\bar{U}, \bar{V}, \bar{W}$ during recession. Then for the path of approach, we have integral equations of the form [9]; and for the path of recession, of the form [10].

$$X(-t) = -\int_{-t}^{0} U(X, Y, Z)\, dt, \tag{9}$$

$$\bar{X}(t) = \int_{0}^{t} \bar{U}(\bar{X}, \bar{Y}, \bar{Z})\, \mathrm{dt}. \tag{10}$$

$$\begin{cases} X(-t) = -\bar{X}(t), \\ Y(-t) = \bar{Y}(t), \\ Z(-t) = \bar{Z}(t). \end{cases} \tag{11}$$

$$\begin{cases} u(X, Y, Z) = -\bar{u}(\bar{X}, \bar{Y}, \bar{Z}), \\ v(X, Y, Z) = \bar{v}(\bar{X}, \bar{Y}, \bar{Z}), \\ w(X, Y, Z) = \bar{w}(\bar{X}, \bar{Y}, \bar{Z}). \end{cases} \tag{12}$$

Assume now that within the time range $-t_1 \leqq t \leqq t_1$ we have relations [11]. It is important to note here that these equations are necessarily valid for $t = 0$.

For any symmetric paired values of X, Y, Z and $\bar{X}, \bar{Y}, \bar{Z}$ we have proved the validity of Eq. [12]. Then the integral equations [9] and [10] show that the relations of Eqs. [11] will persist for the next paired intervals of time, from t_1 to $t_1 + dt$ and from $-(t_1 + dt)$ to $-t_1$. By mathematical induction it therefore follows that Eqs. [11] are valid for all t. This constitutes the proof that the paths of approach and recession are mirror images of each other.

The proof has been given here for the paths relative to the center of gravity of the spheres; but the proof holds likewise for the path of either sphere relative to the other sphere.

Bartok and Mason report one instance in which there was disagreement with the above theory. Two spheres which approached along paths which initially were almost collinear failed to separate after rotating half a revolution about each other. Instead, they continued to rotate indefinitely as a permanent doublet. In the doublet configuration the spheres were in contact, so far as the microscope could show; and it is to be presumed that there were surface forces, ignored in the theory, which could bring and hold the spheres together, once they were brought sufficiently close by the hydrodynamic forces.

Comparison of Solutions

Case I $u(\infty) = gz$.

Case II $u'(\infty) = -gz;\ x' = x$.

$$\begin{cases} u' = -u \\ v' = -v \\ w' = -w \end{cases} \qquad \begin{cases} \omega'_{i1} = -\omega_{i1} \\ \omega'_{i2} = -\omega_{i2} \\ \omega'_{i3} = -\omega_{i3} \end{cases} \qquad \begin{cases} l_i' = l_i, \\ m_i' = m_i, \\ n_i' = n_i. \end{cases}$$

$$p' = -p.$$

Case III $u''(\infty) = gz$.

For corresponding points,

$$\begin{cases} x'' = -x' = -x, \\ \dfrac{\partial}{\partial x''} = -\dfrac{\partial}{\partial x}. \end{cases}$$

$$\begin{cases} u'' = -u' = u, \\ v'' = v' = -v, \\ w'' = w' = -w. \end{cases} \qquad \begin{cases} \omega''_{i1} = \omega'_{i1} = -\omega_{i1}, \\ \omega''_{i2} = -\omega'_{i2} = \omega_{i2}, \\ \omega''_{i3} = -\omega'_{i3} = \omega_{i3}. \end{cases} \qquad \begin{cases} l''_i = -l_i' = -l_i, \\ m''_i = m_i' = m_i, \\ n''_i = n_i' = n_i \end{cases}$$

$$p'' = p' = -p.$$

REFERENCES

1. MANLEY, R. ST. J., AND MASON, S. G., *J. Colloid Sci.* **7,** 354 (1952).
2. BARTOK, W., AND MASON, S. G., *J. Colloid Sci.* **12,** 243 (1957).
3. MOONEY, M., *J. Colloid. Sci.* **6,** 162 (1951).
4. VAND, V., *J. Phys. & Colloid Chem.* **52,** 277 (1948).

JOURNAL OF COLLOID SCIENCE **12**, 581–593 (1957)

PARTICLE SIZE AND PARTICLE SIZE DISTRIBUTION OF PIGMENTS BY SMALL-ANGLE X-RAY SCATTERING[1]

William J. Marculaitis

E. I. duPont de Nemours & Company, Inc., Newark, New Jersey

Received July 17, 1957; revised September 12, 1957

In this investigation, a standard commercial X-ray diffraction unit is readily adapted to give small-angle X-ray scattering measurements and the technique is applied to pigment systems. The X-ray scattering curves for the dry pigments correlate with the average particle sizes calculated from specific surface measurements by nitrogen adsorption (BET method) and electron micrographs.

Introduction

Small-angle X-ray scattering is a useful tool for determining certain physical structure properties of materials which contain discontinuities in electronic density. It has been found especially useful for determining the average particle size and the particle size distribution of materials such as proteins, high polymers, catalysts, carbons, and colloidal dispersions. Guinier *et al.* (1) has recently made a comprehensive review of the subject and included a complete bibliography.

This investigation involves the simple adaptation of a standard, commercial, X-ray diffraction unit to give small-angle scattering measurements; the measurement of X-ray scattering for pigment systems; and the interpretation of the scattering curves in terms of an average particle size and particle size distribution.

Discussion of Theory

A measure of the scattering of X-rays at small angles by a colloidal system is, in effect, a measure of the distribution of electronic density. By making certain assumptions, this distribution can be interpreted in terms of a radius of gyration for a monodispersed system or a distribution of radii of gyration for a polydispersed system. The radius of gyration is defined as the root mean square of the distances of all the electrons in the particle to its center of electronic gravity and represents an average particle size. For simplicity, reference will be made in this report to an average particle size (radius) instead of radius of gyration.

---

[1] The material in this report was presented at the meeting of the American Chemical Society, Colloid Division, in Miami Beach, Florida, on April 8, 1957.

X-ray scattering measurements are theoretically applicable to a wide range of particle sizes but are limited experimentally to an "effective particle size range." Large particles (larger than 1000 A. radius) limit the scattering to inaccessibly small angles, and very small particles (smaller than $R = 50$ A.) spread out the scattering to large angles but the intensities are weak and difficult to observe.

The scattering equation for N_P particles of uniform size is:

$$I_\theta = N_P I_e N_e^2 f^2(k, R) \tag{1}$$

where I_θ is the intensity of scattered radiation at angle θ, N_P is the number of particles, I_e is the Thomson scattering factor for a single electron, N_e is the number of electrons in the particle, and $f(k, R)$ is the structure factor.

In a monodispersed system, assuming spherical particles

$$f^2(k, R) = \left(\frac{3}{(kR)^3}\left[\sin(kR) - (kR)\cos(kR)\right]\right)^2$$

and using Guinier's approximation (1),

$$f^2(k, R) = e\,\frac{-k^2R^2}{3},$$

where $k = \dfrac{2\pi\theta}{\lambda}$.

θ = scattering angle.
λ = wavelength of incident radiation.

Substituting and taking the logarithms of both sides, Eq. [1] reduces to:

$$\ln I\theta = \ln K - \frac{4\pi^2\theta^2R^2}{3\lambda^2}, \tag{2}$$

where K = constant. In the formulae, the small-angle approximation $\sin\theta = \theta$ has been made. From the slope of a "log I_θ vs. θ^2" plot, the particle size can be calculated. Experimentally, dilute systems are preferred since Eq. [1] assumes that multiple scattering, refraction, and interference are negligible.

For polydispersed systems, various methods (2, 3, 7) have been proposed for interpreting experimental scattering curves in terms of a particle size distribution. In this investigation the position and curvature of the "log I_θ versus θ^2" plot is used as a qualitative measure of the particle size distribution and the method of Jellinek *et al.* (3) is used to obtain an average particle size.

EXPERIMENTAL ARRANGEMENT

The geometrical arrangement of the North American Phillips Company X-Ray High Angle Diffractometer, adapted to the measurement of X-ray scattering at small angles, is illustrated in Fig. 1.

Source—Copper target tube (*A*).

Excitation Potential—10 kv./7 ma.

Monochromatic X-Rays—A nickel filter (*B*) was employed to monochromatize the copper radiation to CuKα. A crystal monochromator was considered but could not be fit into the general arrangement without making serious and difficult changes. The background radiation was reduced by the use of a low excitation potential (10 kg./7 ma.).

Definition of X-Ray Beam—The slit system (*D*, *E*, *G*, *H*) defined the X-ray beam in such a manner that the cross section, divergence, and parasitic scattering were at a minimum. Slits *D*, *E*, *G*, and *H* have widths of 0.006, 0.006, 0.004, and 0.019 inch, respectively.

Attenuation of the X-Ray Beam—The Geiger counter employed in this investigation could not measure intensities in excess of 1500 counts per second because of counter saturation. Therefore, it was occasionally necessary to attenuate the incident beam by the use of additional nickel filters (*C*).

Sample—The sample was mounted in an X-ray diffraction sample holder (Standard North American Phillips Company powder holder) and placed normal to the incident beam at position *F*. The thickness of the sample holder (1.3 mm.) regulated the specimen thickness. In most cases a dry powdered sample was used.

Radiation Detector—The radiation was detected by a Geiger-Mueller Counter (*I*) and automatically recorded by a North American Phillips counting rate computer.

SMALL-ANGLE X-RAY SCATTERING FOR LATEX

To test the scattering equipment on a material of known particle size, a Dow Polystyrene Latex suspension containing spherical particles (440

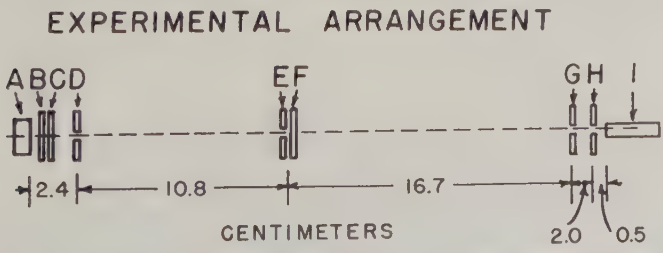

FIG. 1. Schematic diagram showing the geometrical arrangement of North American Phillips Company X-Ray Diffraction Apparatus, adapted to the measurement of X-ray scattering at small angles.

A. radius) was subjected to scattering measurements. The result of plotting the logarithm of the intensity with respect to the square of the scattering angle is shown in Fig. 2. The solid line is the plot of the experimental data and the dashed line illustrates the deviation of the experimental data from linearity. The portion of the scattering curve near zero angle (below $\theta^2 = 0.001$ degrees^2) was obtained by extrapolation. The data were determined at 0.01 degree increments.

According to the scattering equation for a monodispersed system, the "log I vs scattering angle squared" plot should result in a straight line the slope of which will determine the particle size. The deviation of the experimental data from linearity is recognized as the invalidity of Guinier's ap-

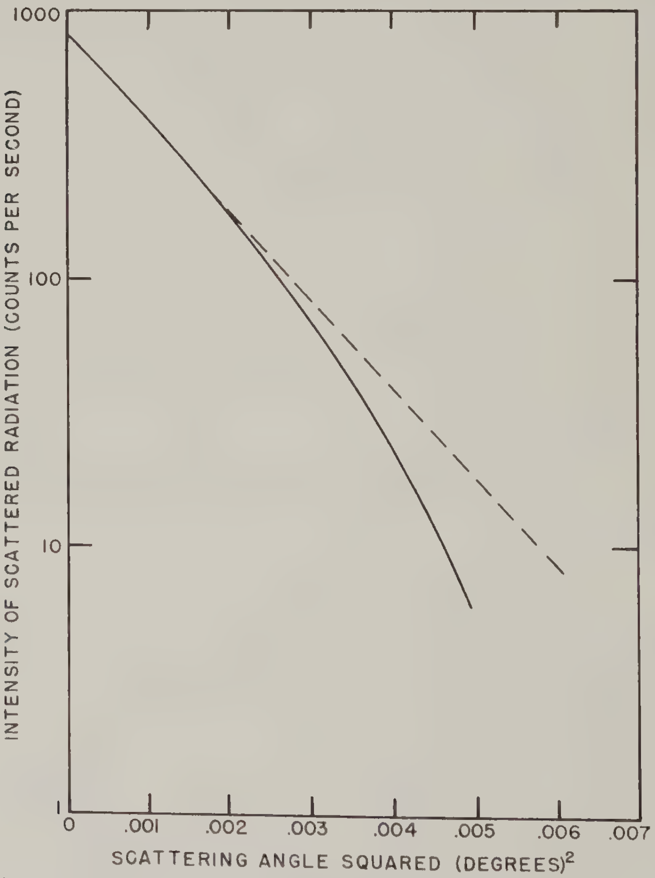

FIG. 2. Result of measuring the X-ray scattering for a sample of latex. The scale of ordinates gives the logarithm of the scattered intensity and the scale of abscissas, the square of the scattering angle. The dashed line illustrates the deviation of the experimental data from linearity.

proximation at large angles. For a particle of given form and radius of gyration, there is a limiting value of the scattering angle, beyond which Guinier's approximation is no longer valid. If the exact form of the structure factor is used instead of Guinier's approximation, the scattering equation is

$$\log I_\theta = -\alpha\theta^2R^2 + \beta\theta^4 + \ldots . + \text{constant},$$

where α and β are constants. For such a form, the slope of the curve would be proportional to the particle size only when $\theta = 0$. Therefore, the slope at the origin is used in calculating the average particle size.

The radius of gyration calculated from the slope of the curve at the origin

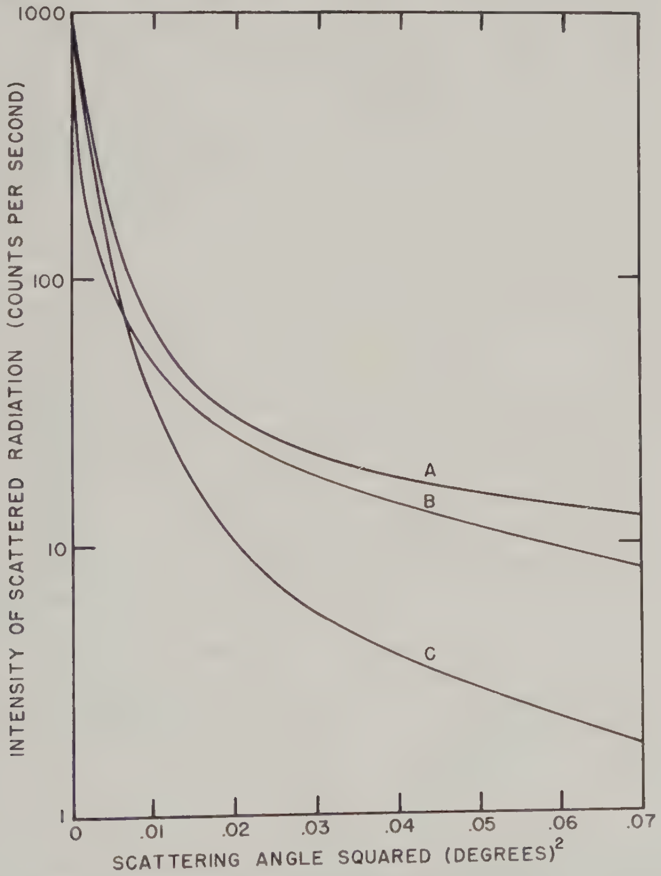

FIG. 3. Results of measuring the X-ray scattering for Copper Phthalocyanine I (Curve *A*), Copper Phthalocyanine II (Curve *B*), and Toluidine Red (Curve *C*). The scale of ordinates gives the logarithm of the scattered intensity and the scale of abscissas, the square of the scattering angle.

in Fig. 2 is 680 A. This can be compared with the reported value of 440 A. The larger value was expected, since no correction was made for parasitic scattering and the latex was dispersed in a liquid medium.

Further standardization and practical application tests were made on pigment samples which differed in particle size distributions. Average particle sizes of these samples were shown by electron micrographs and calculated from specific surface data (BET method).

SMALL-ANGLE X-RAY SCATTERING FOR PIGMENTARY SAMPLES OF COPPER PHTHALOCYANINE AND TOLUIDINE RED

Scattering measurements were made on pigmentary Copper Phthalocyanine I (Sample A), Copper Phthalocyanine II (Sample B), and Toluidine Red, Color Index No. 69 (Sample C). The average particle sizes (radii) calculated from specific surface measurements by nitrogen adsorption (BET method) are 230 A., 300 A., and 2500 A. for Samples A, B, and C, respectively. The scattering curves for these samples are shown in Fig. 3.

In this and subsequent experiments, the data were determined at 0.01 degree increments, the portion of the scattering curve near zero degrees (below $\theta^2 = 0.001$ degrees^2) was obtained by extrapolation, and the curves were normalized to 1000 counts per second at zero scattering angle. Deviation of the scattering data, obtained at 0.01 degree intervals, from the scattering curves shown in the figures was small (maximum observed deviation was 4%).

It is apparent that Sample A contains a distribution of smaller particles than Sample B, and Sample C contains a distribution of much larger particles than Samples A and B (larger slopes indicate larger particles).

In this and subsequent experiments measurements were made on dry samples. It is important to realize that the powder samples contain nonuniform particles which are closely packed. The "closeness of packing" or interparticle interference complicates the data and prevents a complete description of the distribution of particle forms and sizes from the scattering curve.

SMALL-ANGLE X-RAY SCATTERING FOR COPPER PHTHALOCYANINE SAMPLES SUBJECTED TO DIFFERENT PERIODS OF GRINDING

The following samples of Copper Phthalocyanine (CPC) were examined:
Sample A—CPC unmilled.
Sample B—CPC salt milled (5) for 4 hours.
Sample C—CPC salt milled for 12 hours.
Sample D—CPC salt milled for 16 hours.
Sample E—CPC salt milled for 20 hours.
Sample F—CPC salt milled for 24 hours.

Figure 4 shows the scattering curves for Samples A to F. Curves *A* to *F* represent Samples A to F, respectively. From this figure it is evident that

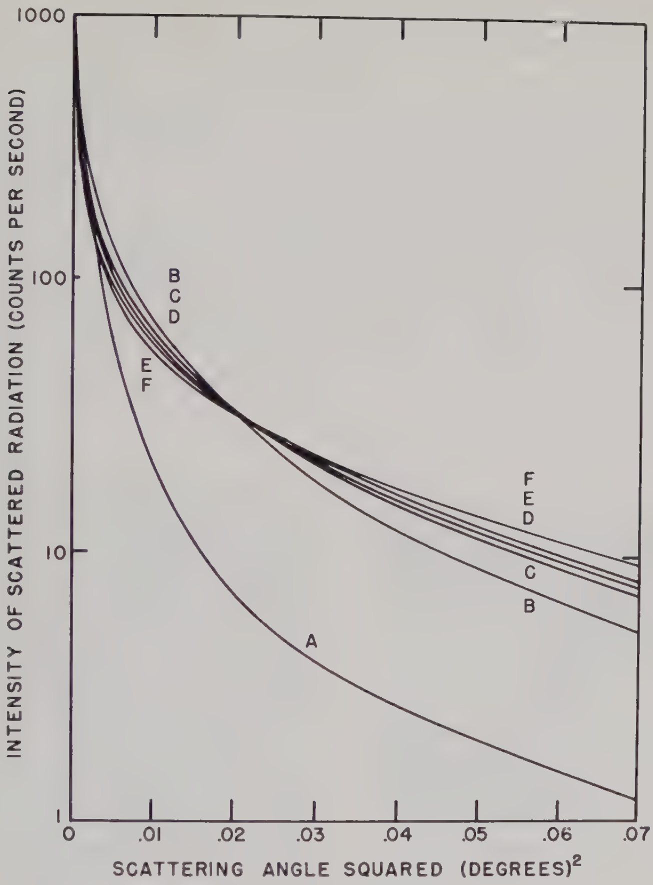

FIG. 4. Results of measuring the X-ray scattering for a Copper Phthalocyanine unmilled sample (Curve *A*), 4 hour salt milled sample (Curve *B*), 12 hour salt milled sample (Curve *C*), 16 hour salt milled sample (Curve *D*), 20 hour salt milled sample (Curve *E*), and 24 hour salt milled sample (Curve F).

The scale of ordinates gives the logarithm of the scattered intensity and the scale of abscissas gives the square of the scattering angle.

the unmilled material (Curve *A*) has a much larger average particle size than the other samples (a lower scattering curve and larger slopes). Curves *B* to *F* indicate a smaller "average" particle size for the samples which were milled for longer periods of time.

Average particle sizes of Samples A to F were calculated from the scattering curves by the method of Jellinek, Solomon, and Fankuchen (3) and are summarized in Table I. The correlation of the average particle size calculated from the scattering curves to that from specific surface measurements is poor for the unmilled sample and the 4 hour grind. In these samples large particles are present which cannot be accounted for in the scattering curves. Since the samples were examined in the dry compact form, the values determined from the scattering curves should be considered only qualitatively.

Figure 5 shows the electron micrographs of Samples A, B, C, and D. The

TABLE I

The Average Particle Size of Copper Phthalocyanine Samples Subjected to Different Periods of Salt Milling (5)

Sample	Period of milling	Average particle size (radius)	
		From specific surface measurements (*Angstroms*)	From small-angle X-ray scattering measurements (*Angstroms*)
A	Unmilled	3775	386
B	4 hours	525	213
D	16 hours	315	187
F	24 hours	287	160

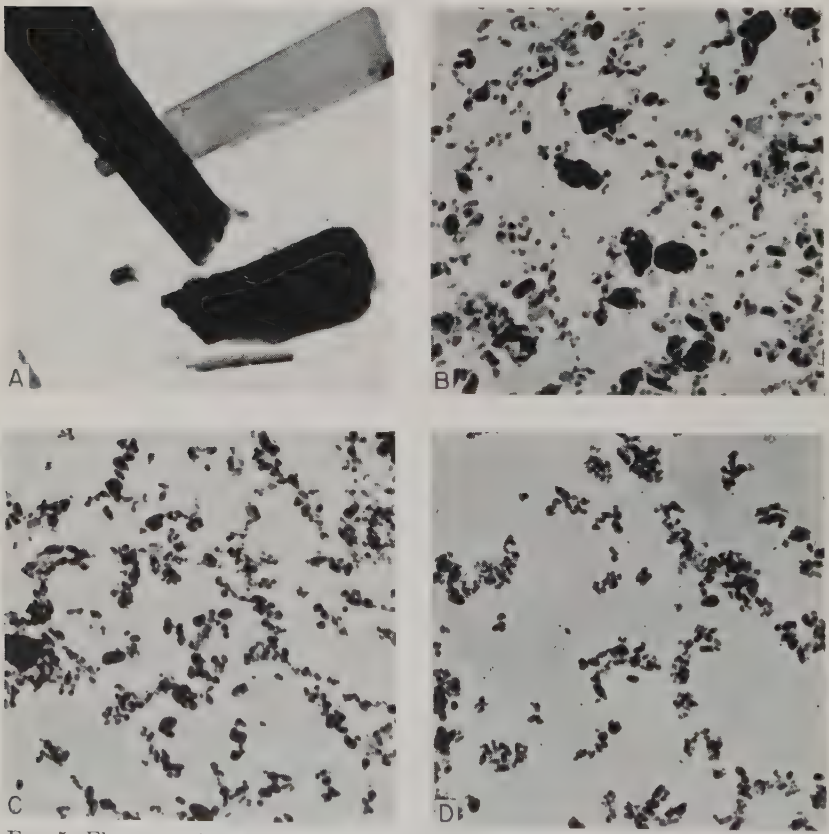

FIG. 5. Electron micrographs of Copper Phthalocyanine samples subjected to different periods of grinding. Picture *A* is the unmilled sample, Picture *B* is the 4 hour salt milled sample, Picture *C* is the 16 hour salt milled sample, and Picture *D* is the 24 hour salt milled sample.

decrease in particle size with increased milling is shown by the micrographs. Most of the crystallites in the unmilled sample (Fig. 5*A*) have a platelike habit. Since two of the dimensions of the plate (length and width) are outside the range of applicability of X-ray scattering, Curve *A* in Fig. 4 probably represents the smallest dimension (thickness) of the crystallite and not the average particle size.

SMALL-ANGLE X-RAY SCATTERING FOR COPPER PHTHALOCYANINE (CPC) SAMPLES SUBJECTED TO DIFFERENT METHODS OF PARTICLE SIZE REDUCTION

The following samples of Copper Phthalocyanine (CPC) were examined:
Sample A—"Commercial" CPC.

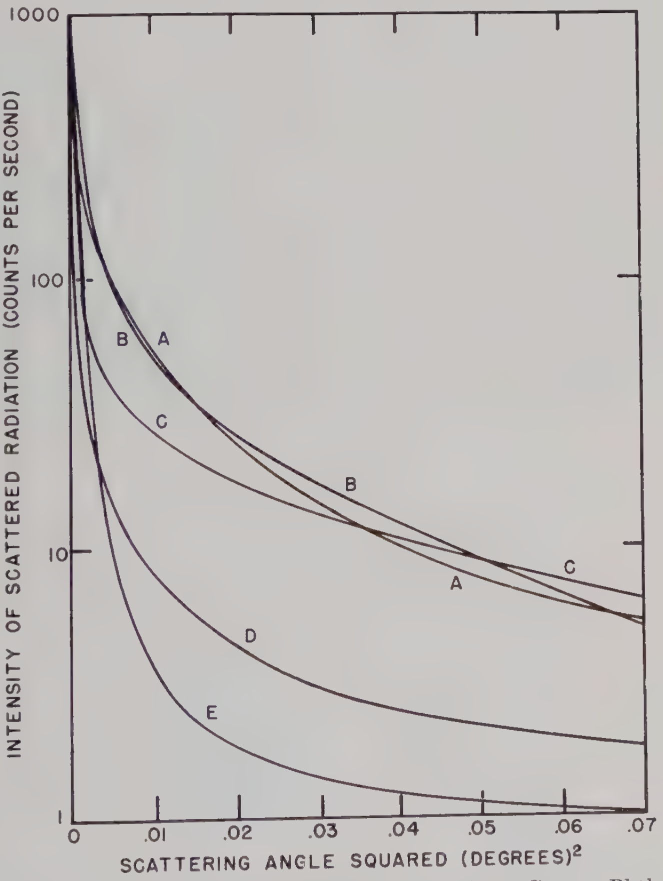

FIG. 6. Results of measuring the X-ray scattering for a Copper Phthalocyanine "Commercial" sample (Curve *A*), salt milled sample (Curve *B*), solvent milled sample (Curve *C*), acid pasted sample (Curve *D*), and dry milled sample (Curve *E*).

The scale of ordinates gives the logarithm of the scattered intensity, and the scale of abscissas gives the square of the scattering angle.

Sample B—CPC ball milled with salt (5).
Sample C—CPC ball milled with solvent (4).
Sample D—CPC acid pasted (6).
Sample E—CPC ball milled (dry).

The scattering curves for these samples are shown in Fig. 6. Curves *A*, *B*, *C*, *D*, and *E* correspond to Samples A, B, C, D, and E, respectively. It is apparent from the scattering curves that the average particle sizes of Samples A and B are approximately the same. The extended small slope portion of Curve *C* indicates a smaller average particle size for Sample C than for A and B. Curves *D* and *E* indicate larger average particle sizes for Samples D and E.

Average particle sizes of Samples A to E were calculated from the scattering curves by the method of Jellinek *et al.* (3) and are summarized with the values determined from specific surface measurements in Table II. Electron micrographs of Samples A to E are shown in Fig. 7. The electron micrograph of Sample C (Fig. 7*C*) indicates the presence of smaller particles than in Sample A (Fig. 7*A*) and a more uniform distribution than Sample B (Fig. 7*B*). The ultimate particles of Sample B appear to be smaller than those of Sample C, but larger aggregates are also present in Sample B which account for the larger average particle size calculated from specific surface measurements and X-ray scattering.

According to Table II, Sample A has approximately the same size as Sample B by X-ray scattering but a much larger average particle size by specific surface measurements. From the electron micrographs of Samples A and B, smaller ultimate particles and larger aggregates can be seen in Sample B. The larger average particle size calculated for Sample A from specific surface measurements may be due to the presence of the surface coating on agglomerates of Sample A which may have made the particles impenetrable to nitrogen (low surface area). X-ray scattering measured the electronic discontinuities within the loosely bound coated agglomerates.

The large aggregates in Samples D and E shown in the electron micro-

TABLE II

The Average Particle Size of Copper Phthalocyanine Samples Subjected to Different Methods of Treatment

Sample	Method of treatment	Average particle size (radius)	
		From specific surface measurements (*Angstroms*)	From small-angle X-ray scattering measurements (*Angstroms*)
A	"Commercial" sample	590	191
B	Salt milled	357	198
C	Solvent milled	306	144
D	Acid pasted	5,450	474
E	Dry milled	20,400	613

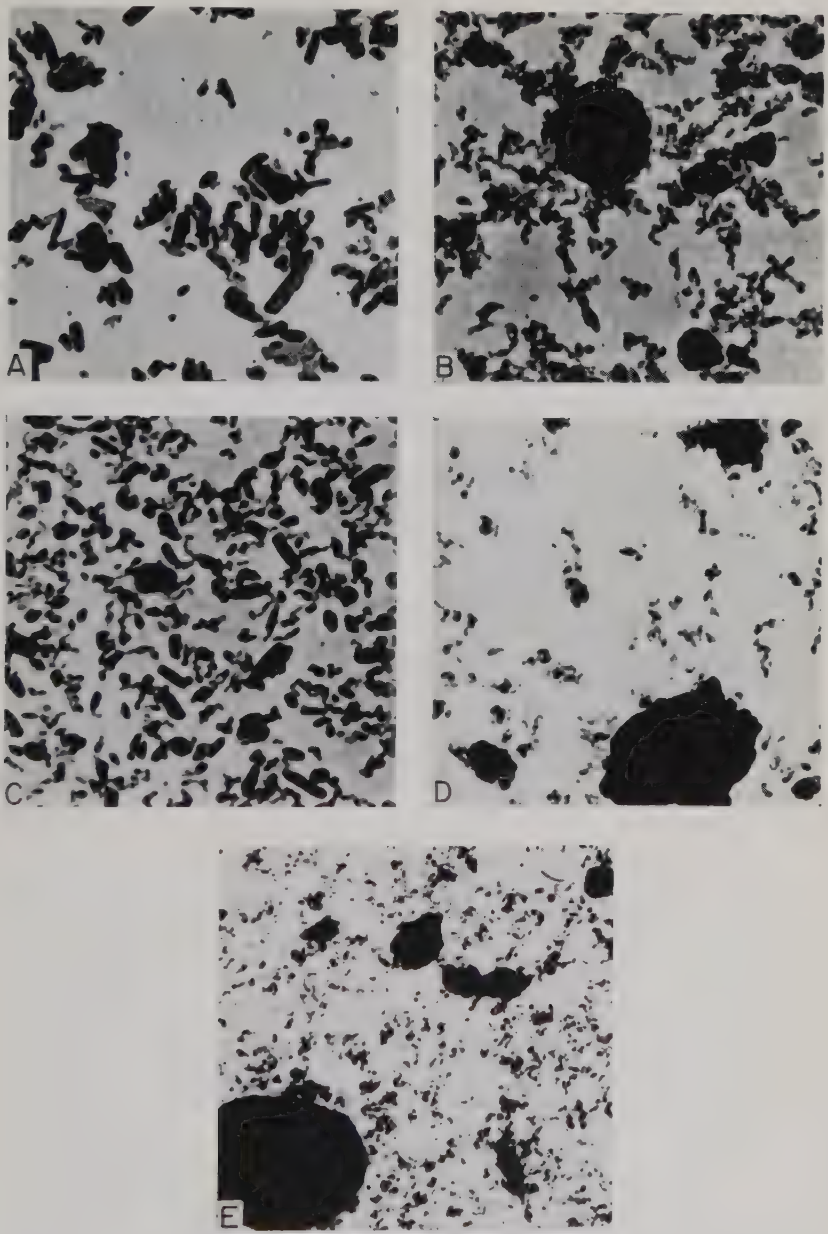

FIG. 7. Electron micrographs of Copper Phthalocyanine samples subjected to different methods of particle size reduction. Picture *A* is the "commercial" sample, Picture *B* is the salt milled sample, Picture *C* is the solvent milled sample, Picture *D*, the acid pasted sample, and Picture *E*, the dry milled sample.

graphs D and E in Fig. 7 are responsible for the large average particle sizes calculated from specific surface measurements and small angle X-ray scattering. However, since the dimensions of some of the aggregates are outside the range of applicability of X-ray scattering, they will contribute to the average particle size calculated from specific surface measurements but not to the scattering curves.

Small-Angle X-Ray Scattering for Inks

The following Copper Phthalocyanine (CPC) samples were examined:

Sample A—CPC 24 hour salt mill grind dispersed in lithographic varnish (1:1 ratio).

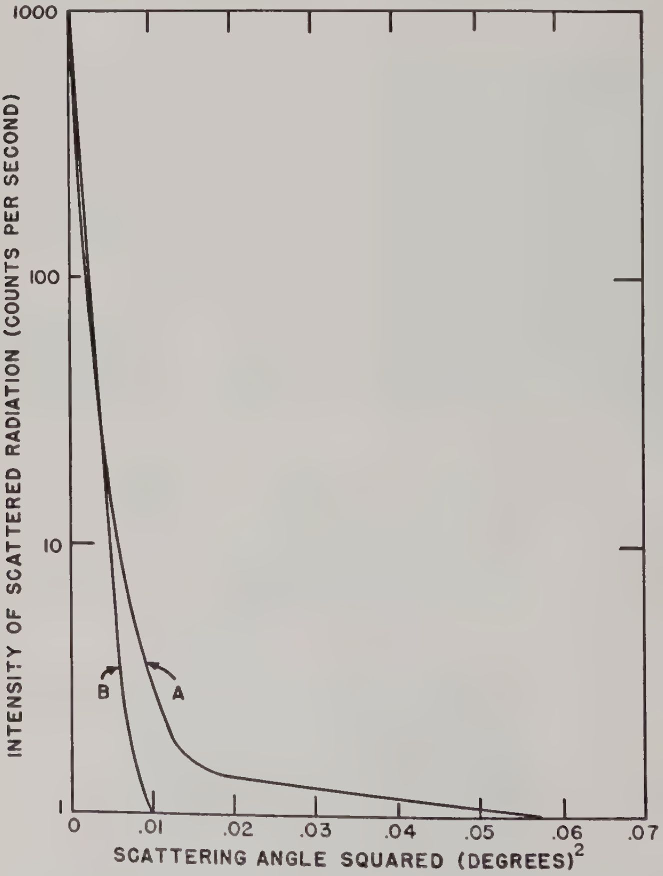

FIG. 8. Results of measuring the X-ray scattering for a Copper Phthalocyanine 24 hour grind (Curve A) and crude (Curve B) dispersed in lithographic varnish.

The scale of ordinates gives the logarithm of the scattered intensity and the scale of abscissas, the square of the scattering angle.

Sample B—CPC unmilled sample dispersed in lithographic varnish (1:1 ratio).

The scattering curves of Samples A and B are shown in Fig. 8. Curves *A* and *B* correspond to Samples A and B. The scattering curves of the CPC material in the dry form were reported in a previous section.

The overall smaller slope of Curve *A* indicates the presence of smaller particles in Sample A as compared to Sample B but the scattering by both ink systems is small. The difference in electron density between pigment and varnish dryer is smaller than that between pigment and air. In general, the scattered intensity depends on the square of the difference of the electron density between the particle and surrounding medium. Therefore, X-ray scattering can be applied to pigment dispersions but necessitates the use of a dispersing medium with an electronic density as different as possible from that of the pigment particle.

Conclusions

1. A standard X-Ray Diffractometer can be adapted to give small angle X-ray scattering measurements.

2. Useful particle size and particle size distribution information can be estimated from the scattering data.

Acknowledgments

The author gratefully acknowledges the assistance and helpful suggestions of B. H. Perkins, A. R. Hanke, and C. W. Manger. The author also wishes to express his appreciation to A. Micelli for his assistance in carrying out the experiments.

References

1. Guinier, A., Fournet, G., Walker, C., and Yudowitch, K. L., "Small-Angle Scattering of X-rays." Wiley, New York, 1955.
2. Hosemann, R., *Ergeb. exakt. Naturw.* **24,** 142 (1951).
3. Jellinek, M. H., Solomon, E., and Fankuchen, I., *Ind. Eng. Chem.* **18,** 172 (1946).
4. Lane, F. W., and Stratton, A. J. (to E. I. duPont de Nemours & Co., Inc.), U. S. Patent 2,556,727 (June 12, 1951).
5. Lang, J. W., and Detrick, S. R. (to E. I. duPont de Nemours & Co., Inc.), U. S. Patent 2,402,167 (June 18, 1946).
6. Lubs, H. A., "The Chemistry of Synthetic Dyes and Pigments." Reinhold, New York, 1955.
7. Shull, C. G., and Roess, L. C., *J. Appl. Phys.* **18,** 295 (1947).

JOURNAL OF COLLOID SCIENCE **12,** 594–605 (1957)

LIGHT SCATTERING BY IDEAL COLLOIDAL ELECTROLYTES[1]

L. H. Princen and Karol J. Mysels

Department of Chemistry, University of Southern California, Los Angeles, California

Received October 8, 1956; revised August 1, 1957

I. Introduction

The measurement of light scattering is a well-established tool in the determination of particle weights of uncharged colloids. For particles small compared to the wavelength of light, this involves essentially the extrapolation of values of concentration divided by turbidity, c/τ, to infinite dilution where ideal behavior prevails. The intercept thus obtained is inversely proportional to the molecular weight. A proportionality constant H takes into account geometric and refractive index factors.

In case of colloidal electrolytes, particularly those of the association type, and especially in the presence of simple salts, the situation is somewhat more complex because of interaction of the various charged species. An exact discussion of this situation has been recently given by Prins and Hermans (P-H) (1) and by one of us (2). Both treatments assume ideality and a constancy of the concentration of simple ions above the critical micelle concentration (c_0). The latter assumption is further analyzed by Mysels and seems to introduce only a minor correction. Unfortunately, the two treatments use very different nomenclatures, making an intercomparison difficult; P-H are not entirely clear about the nature of their extrapolation which is different from that of Mysels; and the latter's results involve several misprints and a sign error. Furthermore, the results of such calculations are most useful when they give the structural quantities, weight and charge, in terms of the experimentally determined ones such as turbidity and refractive indices. This is not given explicitly by P-H. Recent developments (3) show that the micelle-forming ions tend to dimerize below c_0, making the system even more complicated. Finally the discussion of association colloidal electrolytes given in these two papers can be adopted with minor modifications to simple, nonassociation, colloidal electrolytes.

It may therefore be worth while to review some steps of the reasoning involved in the extrapolations, to give results in both notations and in experimental terms, to apply them to nonassociation colloids, and to show the effect of dimerization.

---

[1] Part of this paper was presented at the Symposium on Light Scattering in honor of V. K. La Mer, 1956 Kendall Award recipient—129th meeting of the American Chemical Society, Dallas, April, 1956.

II. The Different Extrapolations

The turbidity of a simple association colloidal electrolyte changes with concentration as indicated schematically in Fig. 1. At low concentration the turbidity is very low, being due only to the monomeric ions. At high concentration it is due mainly to the micelles and increases less than linearly because of their mutual electric interactions. If the assumption is made that the concentration of monomeric ions increases linearly up to c_0 and then remains constant, which seems a reasonable assumption (2, 4, 5), this makes the change of slope at c_0 abrupt as shown by the solid line (instead of the smooth transition indicated by the dotted line) and presumably decreases somewhat the turbidity at higher concentrations. The latter effect being small and of less interest in the present discussion is not shown in the figure.

With this assumption about the composition of the solution and with the further assumption that its behavior is ideal (at least in terms of an effective charge p) and that micelles are of constant single size and charge, it is possible to calculate rigorously the turbidity of the solution at any concen-

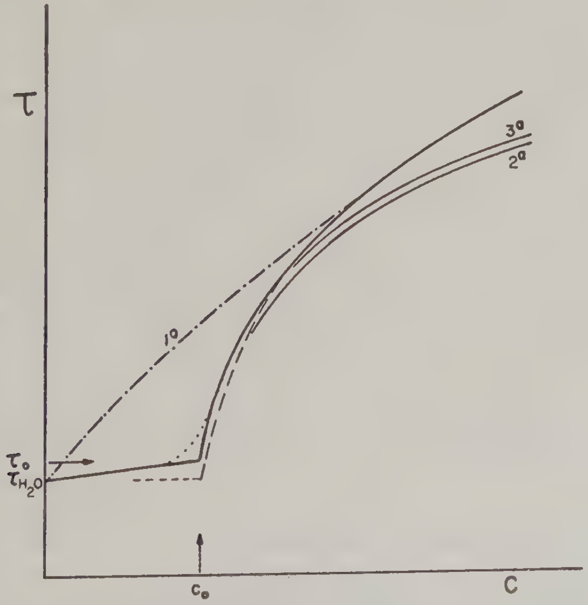

Fig. 1. Schematic presentation of the turbidity of solutions of association colloids: Dotted line—probable reality; solid line—approximation of Eq. 1; the dashed and numbered lines correspond to lines of Fig. 2.

tration. This is given directly from P-H equations [1] and [10] as

$$\tau' = \frac{ZV\nu_1^2}{kT} \cdot \frac{N_1^2 + 2N_1N_3(1 - f + f^2) + f^2N_3^2 + \{\Phi + m^2pN_m\}N_m}{2N_1 + 2N_3 + (p^2 + p)N_m} \qquad [1]$$

in which

$$\Phi = N_1(p^2 + p + 2m^2 - 2mp) + N_3(f^2p^2 + f^2p + 2m^2 - 2fmp)$$

τ' = turbidity due to solute.
Z = proportionality constant = $32\pi^3kT\nu^2/3\lambda^4$.
V = volume.
ν_1 = refractive increment of monomer = $\left(\frac{\partial \nu}{\partial N_1}\right)_{p,T}$.
k = Boltzmann constant.
T = absolute temperature.
N_1 = number of monomer molecules.
N_3 = number of salt molecules.
N_m = number of micelles.
p = charge.
m = aggregation number.
f = relative refractive increment of salt and monomer = $\left(\frac{\partial \nu}{\partial N_3} \middle/ \frac{\partial \nu}{\partial N_1}\right)_{p,T}$.

The turbidity thus calculated for the idealized system is shown schematically by the solid line of Fig. 1. We shall now consider how different methods of extrapolation use such values to obtain structural data.

If the customary plot of Hc/τ is drawn from these calculated values the shape shown by line 1 of Fig. 2 is obtained. Here c is the total concentration of solute and τ the turbidity due to this solute, i.e., excess turbidity of the solution above that of the solvent. This curve reaches the vertical axis at a value corresponding to the solute present at zero concentration, i.e., the monomer, which is of little interest. If its lower portion is extrapolated along a straight line, 1^a (Fig. 2), as has been done occasionally with experimental data (6, 7), the result does not seem to be subject to any simple interpretation. Physically, it amounts to assuming that as the concentration of the simple ions decreases the effect is the same as when it is the concentration of micelles that decreases. In other words this extrapolation crosses c_0 without taking into account the radical changes which occur there in the solution. The dashed line, 1^a, of Fig. 1 shows this extrapolation in terms of turbidity.

Debye (8), several years ago, pointed out that by extrapolating to c_0, one can account for intermicellar interactions. If $H(c - c_0)/\tau$ from the calculated data is plotted vs. $c - c_0$, one obtains a curve such as indicated by 2 in Fig. 2. This curve tends to zero as c_0 is approached because the turbidity due to solute remains finite at c_0 while $(c - c_0)$ tends to zero. However, this

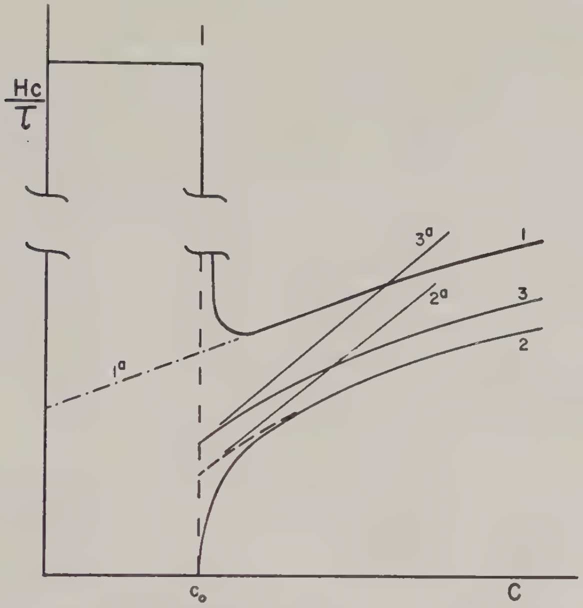

FIG. 2. Schematic presentation of Hc/τ plots and extrapolations of the solid line of Fig. 1: (1) $Hc/(\tau - \tau_{H_2O})$; (2) $H(c - c_0)/(\tau - \tau_{H_2O})$; (3) $H(c - c_0)/(\tau - \tau_0.)$

turbidity due to the monomer is very small so that the downturn occurs quite close to c_0. P-H treat this by making two approximations essentially as follows. First the terms causing the rapid downturn are neglected, which corresponds to the drawing of the dashed extension of line 2 (P-H equation [13]). Then the higher terms in $c - c_0$ are in turn omitted, which corresponds to drawing the straight line 2^a, tangent to the dashed extension at the c_0 (P-H equation [18]). The slope and intercept (at c_0) of this tangent are thus expressed in terms of the structure of the micelles.

When applied to experimental results, this rigorous interpretation encounters a minor obstacle, namely, that the straight line 2^a is not tangent to the curve 2 representing these data, but only to the dotted extension which cannot be readily drawn. This discrepancy is considerably exaggerated in our schematic figures and is near the limit of current light-scattering techniques, but should become more important as these techniques improve. It stems from the fact that the limits of validity of the two approximations made by P-H overlap somewhat.

Debye noted already that the turbidity due to solute at c_0 can be more than strictly negligible so that the turbidity due to the micelles may be considered as that above the turbidity at c_0, i.e., $\tau - \tau_{c_0}$. If now $H(c - c_0)/(\tau - \tau_{c_0})$ is calculated, the line marked 3 in Fig. 2 is obtained. This remains finite as c_0 is approached and thus requires no extrapolation. If the higher terms in $(c - c_0)$ are now neglected, one obtains the equation of the tangent at the intercept indicated by 3^a. Its intercept and slope differ only slightly from those of H-P's line 2^a. We shall calculate the properties of this tangent, which was the one used by Mysels, in the next section. In principle its advantage is that it is tangent to the actual calculated values and not to an extrapolation. This is probably an illusory advantage because the real concentration of micelles may depart from the calculated one precisely in this region, as shown by the dotted line of Fig. 1. It is also in this region that the assumptions of constant size and charge are least likely to hold true. It does, however, provide a more direct insight into the nature of any deviations from linearity on the Hc/τ plot and directs attention to the problem of the proper base turbidity (τ_0). The experimental determination of τ_0 can be quite troublesome for solutions of detergents as has been discussed by Williams, Phillips, and Mysels (9).

III. General Theory

The basic equation [1] obtained by P-H is already given above. For the turbidity at c_0 ($N_m = 0$) it gives

$$\tau'_{N_m=0} = \frac{ZV\nu_1^2}{kT}\,\frac{N_1^2 + 2N_1N_3(1 - f + f^2) + f^2N_3^2}{2N_1 + 2N_3}. \qquad [2]$$

We use this as the base turbidity and note that $\tau' - \tau'_{N_m=0}$ is necessarily equal to $\tau - \tau_0$ where τ is total turbidity and τ_0 is the total turbidity at c_0. This gives (instead of P-H equation [13]):

$$\frac{ZV\nu_m^2N_m}{(\tau - \tau_0)kT} = \frac{(N_1 + N_3)\{2N_1 + 2N_3 + p(p + 1)N_m\}}{2N_1^2d_1 + 4N_1N_3d_2 + 2N_3^2d_3 + (N_1 + N_3)pN_m}. \qquad [3]$$

Series expansion in powers of concentration then gives

$$\frac{H(c - c_0)}{\tau - \tau_0} = \frac{q}{M_m}\left[1 + (c - c_0)\,\frac{p^2 + p - pq}{2M_m(n_1 + n_3)} + 0(c - c_0)^2\cdots\right], \qquad [4]$$

where M_m = micellar weight.

$$q = \frac{(n_1 + n_3)^2}{n_1^2d_1 + 2n_1n_3d_2 + n_3^2d_3}. \qquad [5]$$

n_1 = conc. of monomer at c_0 in moles/ml.

n_3 = conc. of salt in moles/ml.

$$d_1 = 1 - \alpha + \frac{\alpha^2}{4} + \frac{\alpha}{4m}. \qquad [6]$$

$$d_2 = 1 - \frac{\alpha}{2} - f\frac{\alpha}{2} + f\frac{\alpha^2}{4} + f\frac{\alpha}{4m}. \qquad [7]$$

$$d_3 = 1 - f\alpha + f^2\frac{\alpha^2}{4} + f^2\frac{\alpha}{4m}. \qquad [8]$$

$\alpha = p/m$

Equation [4] is similar to P-H equation [18], but our q is different from their g.[2]

In the absence of simple salt ($n_3 = 0$) Eq. [4] is reduced to:

$$\frac{H(c - c_0)}{\tau - \tau_0} = \frac{1}{M_m d_1}\left[1 + (c - c_0)\frac{p^2 + p - p/d_1}{2c_0 m}\right], \tag{9}$$

which is equivalent to P-H equation [21] with d_1 differing slightly from their b_1.[3]

On the other hand, when c_0 becomes very small in the presence of a high concentration of salt, expression [4] becomes:

$$\frac{Hc}{\tau - \tau_0} = \frac{1}{M_m d_3}\left[1 + c\,\frac{p^2 + p - p/d_3}{2n_3 M_m}\right]. \tag{10}$$

Here, again, d_3 differs slightly from the b_3 used by P-H.

The expressions which give directly the charge, p, and the aggregation number, m, as a function of experimentally obtainable intercept A and initial slope B of the Hc/τ line are, for the general case:

$$p = \frac{2(n_1 + n_3)\sqrt{2(n_1 + n_3)B} + 2(n_1 + n_3)(n_1 + fn_3)BM_1}{2(n_1 + n_3)A - (n_1 + fn_3)A^2M_1}; \tag{11}$$

---

[2] The difference in the two treatments is formally shown as follows. Equation [1] is of the form:

$$\tau' = \frac{W + (Q + RN_m)N_m}{T + UN_m}.$$

P-H neglect the term W and obtain as the final result:

$$\tau_{P\text{-}H} = \frac{(Q + RN_m)N_m}{T + UN_m},$$

whereas our treatment is as follows:

$$\tau - \tau_0 = \frac{W + (Q + RN_m)N_m}{T + UN_m} - \lim_{N_m=0}\frac{W + (Q + RN_m)N_m}{T + UN_m} = \frac{\left(Q + RN_m - \frac{WU}{T}\right)N_m}{T + UN_m}.$$

So the difference lies in the term $\frac{WU}{T}$.

[3] d_1 is equivalent to the factor in brackets of Mysels' Eq. [10] and in correct form this factor should read in his notation:

$$\left[\left(1 - \frac{p}{2n}\right)^2 + \frac{p}{4n^2}\right].$$

where n is the degree of association.

Mysels' Eq. [11] has a sign error and here the factor in brackets should be:

$$\left[1 - \frac{p}{2n} - \frac{1}{2n}\right].$$

$$m = \frac{1}{AM_1} + \frac{E^2M_1 \cdot 2(n_1+n_3)B + 4E\sqrt{2(n_1+n_3)B} - E^2M_1A\sqrt{2(n_1+n_3)B}}{4A - 2EA^2M_1}, \qquad [12]$$

where M_1 is the molecular weight of the monomer and $E = (n_1 + fn_3)/(n_1 + n_3)$. Translated into Mysels' notation they become:

$$p = p'\left[\frac{2n' + p'E}{2n' - E}\right]; \qquad [13]$$

$$n = n' + \frac{E^2p'^2 - E^2p' + 4En'p'}{4n' - 2E}, \qquad [14]$$

in which n' is the "uncorrected" aggregation number $1/AM_1$ and p' is the "uncorrected" charge $= \sqrt{2(n_1 + n_3)B}/A$. These are the corrected forms of his Eqs. [16] and [17]. In the absence of added salt [11] and [12] become

$$p = \frac{2\sqrt{2c_0BM_1} + 2c_0BM_1}{2AM_1 - A^2M_1^2}; \qquad [15]$$

$$m = \frac{1}{AM_1} + \frac{2c_0BM_1 + 4\sqrt{2c_0BM_1} - AM_1\sqrt{2c_0BM_1}}{4AM_1 - 2A^2M_1^2}. \qquad [16]$$

In the presence of large amounts of salt they give:

$$p = \frac{2\sqrt{2n_3B} + 2fn_3BM_1}{2A - fA^2M_1}; \qquad [17]$$

$$m = \frac{1}{AM_1} + \frac{f^2M_1 \cdot 2n_3B + 4f\sqrt{2n_3B} - f^2AM_1\sqrt{2n_3B}}{4A - 2fA^2M_1}. \qquad [18]$$

From Eqs. [13] and [14] one can derive the very useful expression:

$$2(n - n') = E(p + p'), \qquad [19]$$

which is indicated in Eq. [17] of Mysels.

IV. DIMERIZATION

Kraus (10) has interpreted his conductivity results on some long-chain quaternary ammonium salts as indicating the existence of only dimers or only trimers at all concentrations below c_0. More recently Mukerjee (3) has shown by conductivity and transference measurements that in sodium lauryl-sulfate there is a reversible equilibrium between monomeric and dimeric lauryl-sulfate (LS^-) ions:

$$2LS^- \rightleftarrows LS_2^{=}$$

which leads to about 50% dimerization at c_0 for this salt. This brings up the question of the effect of dimerization on light scattering and on its interpretation. We have therefore used the procedure of Section II to develop the corresponding equations for the simple case of complete dimerization of the micelle-forming ion and in the absence of salt. The total turbidity due to solute is now given by the equivalent of Eq. [1]

$$\tau' = \frac{ZV\nu_1^2}{kT} \cdot \frac{8N_2^2 + \{6m^2 - 8mp + 4(p^2 + p)\}N_2N_m + m^2pN_m^2}{6N_2 + (p^2 + p)N_m}, \qquad [20]$$

in which N_2 = number of dimers, and the tangent at the cmc is given in analogy to Eq. [9] by

$$\frac{H(c - c_0)}{\tau - \tau_0} = \frac{1}{M_m\, z_2}\left[1 + \frac{p^2 + p - p/z_2}{3c_0\, m}(c - c_0) + \cdots\right], \qquad [21]$$

in which

$$z_2 = 1 - \frac{4}{3}\alpha + \frac{4}{9}\alpha^2 + \frac{4}{9}\frac{\alpha}{m}. \qquad [22]$$

Figure 3 shows graphically the effect of dimerization in case of micelles having a degree of association $m = 60$ and a charge $p = 10$. It may be noted that the slope and the curvature of the Hc/τ plot are much less pronounced in case of complete dimerization while the intercept is shifted to higher values. The expressions for the structural quantities in terms of experimental intercept A and slope B of the tangent to the $H(c - c_0)/(\tau - \tau_0)$ line become, in analogy to [15] and [16],

$$p = \frac{6c_0BM_1 + 3\sqrt{3c_0BM_1}}{3AM_1 - 2A^2M_1^2}; \qquad [23]$$

$$m = \frac{1}{AM_1} + \frac{12c_0BM_1 + 12\sqrt{3c_0BM_1} - 4AM_1\sqrt{3c_0BM_1}}{9AM_1 - 6A^2M_1^2}. \qquad [24]$$

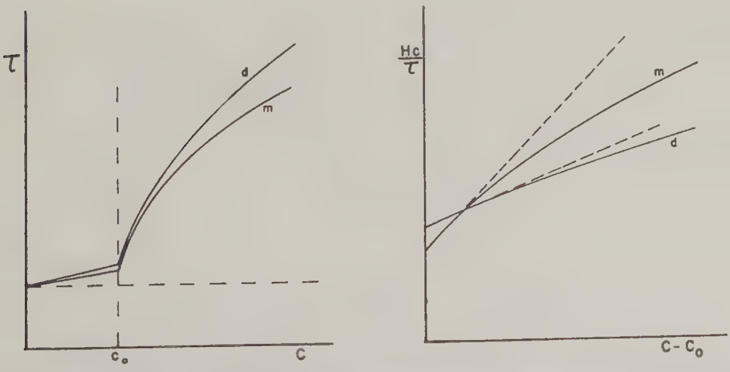

FIG. 3. Comparison of calculated turbidities and Hc/τ lines for a given micellar size and charge assuming that below c_0 only monomer (m) or only dimer (d) is formed.

If the values shown in Fig. 3 for the dimer are interpreted as if only monomer were present one obtains $m = 54.6$ and $p = 7.5$. Thus interpretation of light-scattering data without taking complete dimerization into account where it exists can produce an error of the order of 10% in the degree of association and of 25% in the effective charge.

V. Nonassociation Colloidal Electrolytes

With a simple (nonassociation) colloidal electrolyte, its particles behave like micelles but the monomeric ions are absent. Hence, Eq. [4] becomes in the presence of salt:

$$\frac{Hc}{\tau - \tau_0} = \frac{1}{Me_3}\left[1 + c\,\frac{p^2 + p - p/e_3}{2Mn_3} + \cdots\right], \qquad [25]$$

in which

$$e_3 = 1 - lp + l^2\frac{p^2}{4} + l^2\frac{p}{4}. \qquad [26]$$

In order to express the structural quantities in terms of the experimental ones, the relative refractive increment has to be expressed in terms of the gravimetric concentration of colloid rather than in terms of the unknown molar concentration. This leads to a substitution of l by l'. These are both defined by

$$l' = \frac{\partial\nu}{\partial n_3}\bigg/\frac{\partial\nu}{\partial c_m} = \left[\frac{\partial\nu}{\partial n_3}\bigg/\frac{\partial\nu}{\partial n_m}\right]M = lM. \qquad [27]$$

Using this quantity l' and the slope and intercept of the $Hc/(\tau - \tau_0)$ line one finds for the charge:

$$p = \frac{2\sqrt{2n_3B} + 2l'n_3B}{2A - l'A^2}. \qquad [28]$$

The expression for the molecular weight becomes:

$$M = \frac{1}{A} + \frac{2l'^2n_3B + 4l'\sqrt{2n_3B} - l'^2A\sqrt{2n_3B}}{4A - 2l'A^2}. \qquad [29]$$

Written in Mysels' notation they become:

$$p = p'\left[\frac{2 + l'Ap'}{2 - l'A}\right]; \qquad [30]$$

$$M = M' + \frac{l'^2Ap'^2 - l'^2Ap' + 4l'p'}{4 - 2l'A}. \qquad [31]$$

where M' is the "uncorrected" molecular weight $1/A$. From Eqs. [30] and [31] one can again obtain the useful expression:

$$2(M - M') = l'(p + p'). \qquad [32]$$

VI. CONCLUSION

Equations [17] and [18] and also [28] and [29] can become useless because in the presence of swamping electrolyte the slope, B, of the $Hc/(\tau - \tau_0)$ line tends to zero. This slope is given, according to Eq. [10], by:

$$B = \frac{p^2d_3 + pd_3 - p}{2n_3M_m{}^2d_3{}^2}. \qquad [33]$$

Hence, B tends to zero if the charge p becomes zero, but it also tends to zero at constant p when the salt concentration, n_3, increases. Under these latter conditions the product n_3B remains finite but, because of the smallness of B, cannot be determined experimentally and, therefore, p (Eq. [17]) and the last term of Eq. [18] cannot be evaluated. In Mysels' notation p', the uncorrected charge, cannot be determined by the experiment, and therefore Eq. [13] cannot be used nor the correction term of Eq. [14] calculated.

Thus, a negligible slope of the $Hc/(\tau - \tau_0)$ line in high salt concentration does not show, as has been suggested (6, 11), that the charge is zero, nor

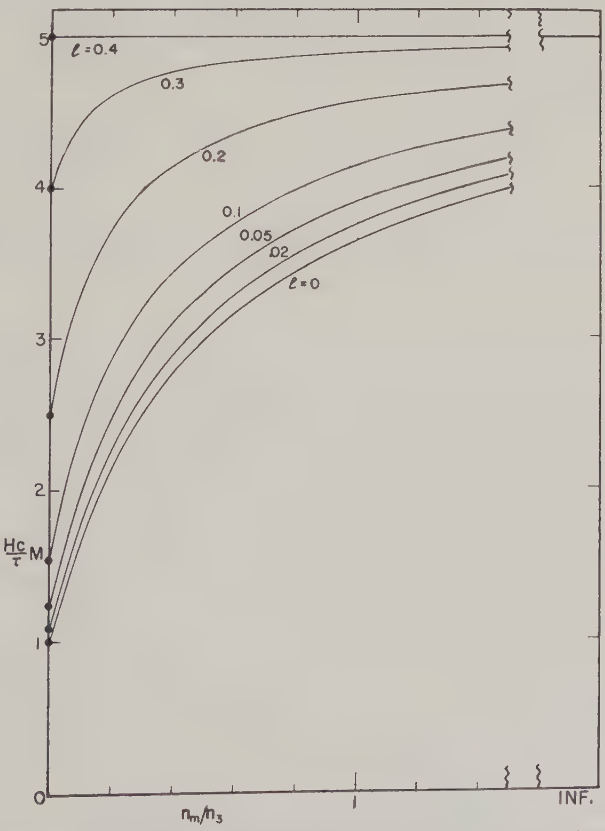

FIG. 4. The effect of the refractivity of simple salt upon the calculated light scattered by a charged colloid, assuming an effective charge $p = 4$ [$l = (\partial\nu/\partial n_3)/(\partial\nu/\partial n_m)$].

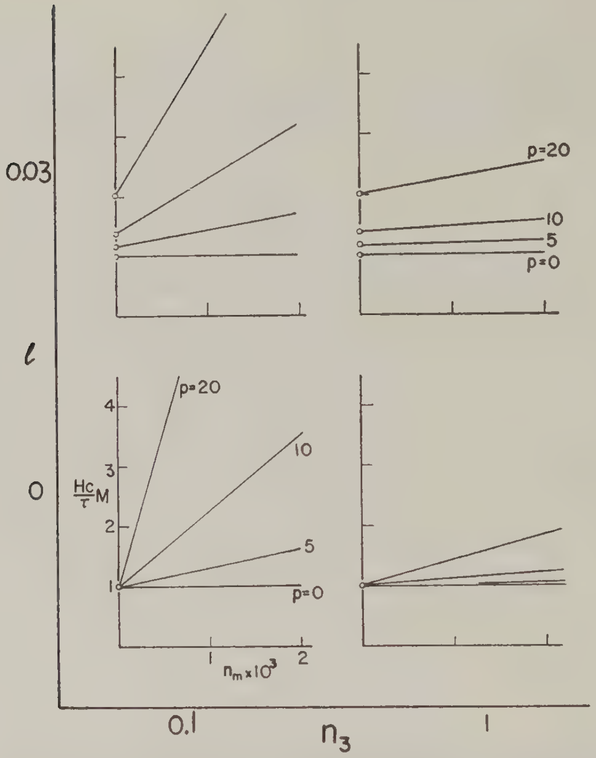

FIG. 5. Schematic illustration of the effect of charge p of the colloid and of the refractivity l of the simple salt upon the slope and intercept of the Hc/τ lines in the absence and presence of swamping electrolyte.

does the intercept at infinite dilution of a charged colloid give the real molecular weight. This last point is in striking contrast with other phenomena, such as osmotic pressure or diffusion, where, under ideal condition, charge effects are eliminated by such treatment. This is due to the fact that the turbidity of a solution depends not only on the ease of fluctuation in concentration, which behaves like osmotic pressure, but also on the optical efficiency of this fluctuation, which is dependent on the presence of salt (2).

These results are summarized schematically in Figs. 4 and 5, which show the calculated $Hc/(\tau - \tau_0)$ lines for a number of systems. In Fig. 4 the charge p is assumed constant at 4 and the effect of the relative refractive increment l of the salt is shown to shift the intercept and the slope. The higher values of l are not likely to be encountered in practice. Figure 5 shows the effect of increasing the concentration of salt, x, and of its relative refractive increment, l, upon the intercept and initial slope of the $Hc/\tau - \tau_0$ lines for a number of assumed charges p. If the refractive increment of the salt is negligible, the intercept is unaffected by the charge. However, if this increment is significant, the effect on the intercept is not erased by a swamping concentration, even though the slope may be thus drastically reduced.

ACKNOWLEDGMENTS

This work was supported by the Office of Naval Research through project NR 356-254 1111 for which it forms the 9th Technical Report. Reproduction in part or in whole for purposes of the United States Government is permitted. We are also indebted to Prof. J. J. Hermans for very enlightening correspondence.

REFERENCES

1. PRINS, W., AND HERMANS, J. J. *Koninkl. Ned. Akad. Wetenschap. Proc.* **B59,** 162 (1956).
2. MYSELS, K. J., *J. Colloid Sci.* **10,** 507 (1955).
3. MUKERJEE, P., Ph.D. Dissertation, University of Southern California (1957). Meeting of the American Chemical Society, Miami, April, 1957.
4. MYSELS, K. J., AND DULIN, C. I., *J. Colloid. Sci.* **10,** 461 (1955).
5. KOLTHOFF, I. M., AND JOHNSON, W. F., *J. Phys. & Colloid. Chem.* **52,** 22 (1948).
6. HUTCHINSON, E., *J. Colloid Sci.* **9,** 192 (1954).
7. MANKOWICH, A. M., *J. Phys. Chem.* **58,** 1027 (1954).
8. DEBYE, P., *J. Phys. & Colloid. Chem.* **53,** 1 (1949).
9. WILLIAMS, R. J., PHILLIPS, J. N., AND MYSELS, K. J., *Trans. Faraday Soc.* **51,** 728 (1955).
10. KRAUS, C. A., *et al.*, *J. Am. Chem. Soc.* **73,** 1129 (1951); *ibid.* **72,** 3676 (1950); *ibid.* **73,** 2170 (1951).
11. PRINS, W., Thesis, Leiden, The Netherlands, 1955.

JOURNAL OF COLLOID SCIENCE **12,** 606–607 (1957)

BOOK REVIEW

Chemical Surface Compounds and Their Role in Adsorption Phenomena. Proceedings of a Conference on adsorption commemorating the 2nd centenary of the Moscow State University (1755–1955). Moscow University Press, Moscow, 1957. 368 pages. Price Rub. 14.30.

There was a time when adsorption seemed to be a very simple and a very specific phenomenon. Solid surfaces, perfectly smooth and absolutely uniform, were surrounded by a field of force, not unlike that of gravitation, and gas or solute molecules (or ions) were attracted to these surfaces as a heavy body falls toward the center of the earth. For systems of this kind it was reasonable to assume that the uptake was governed by Gibbs' adsorption theorem, that the adsorbed particles formed a surface film, and so on.

Now, not much is left of this picture of adsorption. First it was shown that ions usually are not adsorbed but rather exchanged; what 50 years ago was enthusiastically measured as adsorption of ions (including dyes) proved to be a regular chemical exchange reaction differing from the reactions in a solution only by the insolubility of one of the initial and one of the final components. Then it was realized also that uncharged molecules very often react either with the bulk of the adsorbent, or with some impurities in it, or with its lattice defects. The book under review deals with these reactions, and its very title is a challenge to the old adsorption theory.

It is possible, of course, formally to describe, say, a dilute aqueous hydrochloric acid as water containing "active sites" which preferentially adsorb alkali with evolution of heat; it is possible to invent ingenious models of these sites; but the classical chemical approach appears to be more fruitful, and it is as a rule used in the book.

The book is divided into four sections. In the first, 10 papers deal with gas adsorption on active carbon and metals. Among other topics, oxygen and hydrogen compounds of carbon present in its surface either as a separate phase or as single molecules are discussed; for instance, the fact that oxygen "adsorbed" by carbon is more difficult to remove electrochemically the longer it has been adsorbed, is attributed to slow diffusion of the oxygen or the oxygen-containing compound into the bulk of the "adsorbent"; the reviewer places "adsorbed" and "adsorbent" in quotation marks to show that the actual effect is different from the nonchemical surface phenomenon previously understood by the term adsorption.

The second section includes 14 papers and treats silica gels and silicates as adsorbents. In this group, water and hydroxyls in the surface usually determine the course of adsorption.

The properties of the adsorbent-adsorbate system are considered in the third section in 12 papers. The dielectric constant, the luminescence and the infrared absorption of the layers modified by adsorption are particularly well studied. Even in the instance of adsorption of *n*-pentane on barium sulfate molecular complexes in the surface are considered possible.

The fourth section is devoted mainly to catalysis, and the reviewer did not read it.

The book, in addition to its considerable scientific value, throws some light on an important problem of the organization of research. In the English-speaking countries many people believe that scientific research in Russia is planned. They attribute to this planning the present state of science there, which, according to the political preference of the commentators, is either a success or a failure. In reality, planning does not exist or, if it exists, is disregarded. In the concluding speech of the conference, its chairman (Professor A. V. Kiselev) appealed to the participants to introduce some voluntary planning: "It is not right to erect identical huge apparatus requiring fine specialization in every laboratory"; different laboratories should cope with different problems and be in close touch with each other. This advice would not be amiss in the United States either.

J. J. Bikerman, Cambridge, Massachusetts

AUTHOR INDEX

A

Arnold, R., 549

B

Bartok, W., 243
Basu, Sadhan, 19
Bauer, S. H., 460
Bennett, M. C., 434
Berge, John W., 400
Bloksma, A. H., 40, 135
Bondi, A., 510
Brown, A. B., 283
Brown, Wayne S., 195
Burcik, Emil J., 10

C

Cadle, R. D., 356
Chaudhury, Phanibhusan Roy, 19
Child, William C., Jr., 53, 327 389
Cutler, Ivan B., 195

D

Deeley, C. W., 363
de Luca, Guido, 108
Diamond, H., 510
Dixon, J. K., 452
Dunning, H. N., 68

E

Eigen, Manfred, 181
Epstein, M. B., 345
Eley, D. D., 419

F

Ferry, John D., 53, 327, 389, 400
Ferington, T. E., 325
Flockhart, B. D., 557
Ford, Roger A., 271
Frank, H. P., 480
Fujita, Hiroshi, 204

G

Gallily, Isaiah, 161
Goring, D. A. I., 412

H

Hazel, J. Fred, 529
Heller, Wilfried, 25, 173, 294
Hedge, D. G., 417, 419
Hudson, John B., 523
Huque, M. M., 412

J

Johansen, Robert T., 68
Joslyn, M. A., 108

K

Kaufman, Samuel, 465
Kitahara, Ayao, 342
Kline, D. E., 363
Koefoed, Jørgen, 131
Kuroda, Haruo, 496

L

La Mer, Victor K., 230, 566
Landel, Robert F., 53, 308, 400
Lee, Pui-Kum, 230, 566
Luchak, George, 144

M

McAllister, Archie, 80
Marculaitis, William J., 581
Maron, Samuel H., 99
Mason, S. G., 243
Melanson, B., 412
Milburn, Richard H., 378
Mooney, M., 575
Mukerjee, Pasupati, 267
Mysels, Karol J., 594

N

Nandi, U. S., 321
Newman, Robert C., 10
Ninomiya, Kazuhiko, 204

P

Princen, L. H., 594
Pugh, Thomas L., 173, 294

R

Ross, John, 345
Ross Sydney, 523

S

Sauer, J. A., 363
Schadt, C. F., 356
Schuur, G., 538
Schwarz, Gerhard, 181
Senez, M., 412
Singleterry, C. R., 465
Sisko, Arthur W., 99
Smellie, Robert H., Jr., 230, 566
Smith, F. M., 283
Sparks, J. W., 283
Stamberger, Paul, 433
Steiner, R. F. 80
Stern, Donald M., 53
Strange, Harold O., 529
Street, Norman, 1

T

Tabibian, Richard M., 25
Takeuchi, T., 263
Tobolsky, A. V., 325

V

Valko, Emery I., 241

W

Williams, E. F., 452
Williams, Malcolm L., 53
Wilson, A., 345
Woodberry, N. T., 452
Woodward, A. E., 363

Y

Yamaguchi, S., 263

Z

Zand, Robert, 53

SUBJECT INDEX

A

Adsorption, of sodium lauryl sulfate and lauryl alcohol, Wilson *et al.*, 345

Aerosols, distribution of coagulating aerosols, Luchak, 144; filtration, Gallily, 161; thermal forces on aerosol particles, Schadt and Cadle, 356

Asphalt, viscoelastic properties, Brown *et al.*, 283

B

Butadiene, Henry's law constants, Ross and Hudson, 525

C

Carbon black, x-ray scattering, Kuroda, 496; deflocculation, Bondi and Diamond, 510

Catalysis, promotors in contact catalysts, Yamaguchi and Takeuchi, 263

Cellulose tributyrate, viscosities, Landel *et al.*, 400

Clay pastes, sodium and iodide ions in clay pastes, Bloksma, 40

Colloidal electrolytes, light scattering, Princen and Mysels, 594

Colloidal particles, refractive index, Heller and Pugh, 294

Colloidal suspensions, and surface activity, Hazel and Strange, 529

D

Dodecyl sulfate, critical micelle concentration, Flockhart, 557

Donnan, F. G., in memoriam, Stamberger, 433

E

Electroviscous effect, in colloidal systems, Mukerjee, 267

Erratum, 344

Extrusion, of soft solids through a tube, Brown and Cutler, 195

F

Fatty acids, micelle formation of fatty acids salts, Kitahara, 342

Film, concentration gradients in thin films, Bauer, 460

Flow, Ree-Eyring generalized flow theory, Maron and Sisko, 99

I

Insulin, fluorescent conjugates, Steiner and McAlister, 80

K

Kaolinite suspension, and polyanion, Street, 1

L

Latex (see also *Rubber*), density of polystyrene and polyvinyltoluene latex particles, Pugh and Heller, 173

Lecithin, equation of state for monolayers, Hedge, 417

Light scattering, of colloidal spheres, Heller and Tabibian, 25; calibration, Goring *et al.*, 412

Lipid-protein, interactions, Eley and Hedge, 419

M

Methyl methacrylate, polymerization, Nandi, 321; Ferington and Tobolsky, 325

Micelle formation, by sulfonates in benzene, Kaufman and Singleterry, 465; of azo dyes, Frank, 480

N

Nylon, free radical reactions in nylon, Ford, 271; dynamic mechanical behavior, Woodward *et al.*, 363

P

Particle motions, in sheared suspensions, Bartok and Mason, 243

Particle size, and x-ray scattering, MARCULAITIS, 581
Pauli, Wolfgang, Sr., in memoriam, VALKO, 241
Pectinic acids, aluminum pectinates, JOSLYN AND DE LUCA, 108
Permeability, of porous media (alundum), JOHANSEN AND DUNNING, 68
Phosphate slimes, flocculation and filtration, LA MER *et al.*, 230, 566
Polyelectrolytes, field effect of polyelectrolytes in solution, EIGEN AND SCHWARZ, 181
Polyethyl methacrylate, dynamic mechanical properties, FERRY *et al.*, 53
Polymethacrylic acids, titration, ARNOLD, 549
Polymethyl acrylate, mechano-chemical behavior, BASU AND CHAUDHURY, 19
Poly-*n*-butyl methacrylate, properties, CHILD AND FERRY, 327
Poly-*n*-hexyl methacrylate, CHILD AND FERRY, 389
Polyurethane elastomer, in rubber-to-glass transition zone, LANDEL, 308
Polyvinyl acetate films, stress-relaxation, NINOMIYA AND FUJITA, 204

R

Rubber (see also *Latex*), viscosity of dispersions, SCHUUR, 538

S

Soap, surface plasticity of sodium soap solutions, BURCIK AND NEWMAN, 10
Sugar juice, adsorbed protein, BENNETT, 434
Sulfosuccinates, purification, WILLIAMS *et al.*, 452
Suspension effect, Overbeek's treatment, BLOKSMA, 135

T

Thermodynamics, and Brønstad's principles, KOEFOED, 131

V

Viscosity, two spheres in a shearing viscous liquid, MOONEY, 575

W

Water clouds, theory of evaporation, MILBURN, 378

INDEX OF BOOK REVIEWS

Annals of Physics, (Journal) MORSE, P. M. (ed.) (LA MER, V. K.), 523
Chemical Surface Compounds and Their Role in Adsorption Phenomena (BIKERMAN, J. J.), 606
CREMER, H. W., AND DAVIES, T. (eds.), Chemical Engineering Practice. Vol. 1: General; Vol. 2: Solid State (FRIEDLANDER, S. K.), 431
FISHMAN, M. M. Light Scattering by Colloidal Systems. An Annotated Bibliography (LA MER, V. K.), 524
FUCHS, N. A., Mechanica Aerosolej (Mechanics of Aerosols), (DROZIN, V.), 523
MARTIN, R. W., The Chemistry of Phenolic Resins (BENDER, H. L.), 430
NEWMAN, M. S. (ed.), Steric effects in Organic Chemistry (RAMIREZ, F.), 430

JOURNAL OF COLLOID SCIENCE

Editor-in-Chief

Victor K. La Mer, Columbia University, New York

Advisory Board

C. O. Beckmann
K. F. Bonhoeffer (deceased)
J. A. Christiansen
P. J. W. Debye
John T. Edsall
I. Fankuchen
John D. Ferry
Wilfried Heller
John G. Kirkwood
E. C. Lingafelter
L. G. Longsworth
S. G. Mason
J. Th. G. Overbeek
R. Ruyssen
William Seifriz
Leo Shedlovsky
Theodore Shedlovsky
Robert Simha
R. H. Smellie
Jacinto Steinhardt
The Svedberg
Hugh S. Taylor
Arne Tiselius
Robert D. Vold
Bernard Vonnegut
Ralph W. G. Wyckoff
Bruno H. Zimm

VOLUME 12

1957

ACADEMIC PRESS INC.—PUBLISHERS
NEW YORK, N. Y.

Copyright© 1957, by Academic Press Inc.
Made in United States of America

Contents of Volume 12

Number 1, February, 1957

Norman Street. Effect of a Polyanion on the Rheology of a Kaolinite Suspension 1
Emil J. Burcik and Robert C. Newman. The Surface Plasticity of Homologous Series of Sodium Soap Solutions 10
Sadhan Basu and Phanibhusan Roy Chaudhury. Studies on Mechanochemical Systems. Part I 19
Wilfried Heller and Richard M. Tabibian. Experimental Investigations on the Light Scattering of Colloidal Spheres. II. Sources of Error in Turbidity Measurements 25
A. H. Bloksma. The Diffusion of Sodium and Iodide Ions and of Urea in Clay Pastes 40
John D. Ferry, William C. Child, Jr., Robert Zand, Donald M. Stern, Malcolm L. Williams and Robert F. Landel. Dynamic Mechanical Properties of Polyethyl Methacrylate 53
Robert T. Johansen and H. N. Dunning. Homogeneous Fluid Flow Through Consolidated Porous Media 68
R. F. Steiner and Archie McAllister. Studies upon Fluorescent Insulin Conjugates 80
Samuel H. Maron and Arthur W. Sisko. Application of Ree-Eyring Generalized Flow Theory to Suspensions of Spherical Particles. II. Flow in Low Shear Region 99
M. A. Joslyn and Guido de Luca. The Formation and Properties of Aluminum Pectinates 108

LETTER TO THE EDITOR

Jørgen Koefoed. Irreversible Thermodynamics by the Principles of J. N. Brønsted and its Application to Elastic Solutions 131

Number 2, April 1957

A. H. Bloksma. An Experimental Test of Overbeek's Treatment of the Suspension Effect 135
George Luchak. The Theory of the Electric Charge Distribution of Monodispersed Lightly Charged Aerosols of Spherical Particles Coagulating in a Bipolar Ionized Atmosphere 144
Isaiah Gallily. On the Filtration of Aerosols by Filter Models of Various Porosities 161

Thomas L. Pugh and Wilfried Heller. Density of Polystyrene and Polyvinyltoluene Latex Particles 173
Manfred Eigen and Gerhard Schwarz. Orientation Field Effect of Polyelectrolytes in Solution 181
Wayne S. Brown and Ivan B. Cutler. Extrusion of Soft Solids Through a Tube 195
Kazuhiko Ninomiya and Hiroshi Fujita. Stress-Relaxation Behavior of Polyvinyl Acetate Films 204
Victor K. La Mer, Robert H. Smellie, Jr., and Pui-Kum Lee. Flocculation, Subsidence, and Filtration of Phosphate Slimes. IV. Flocculation by Gums, and Polyelectrolytes and their Influence on Filtration Rate 230

Number 3, June 1957

Emery I. Valko. In Memoriam. Wolfgang Pauli, Sr. 241
W. Bartok and S. G. Mason. Particle Motions in Sheared Suspensions. V. Rigid Rods and Collision Doublets of Spheres 243
S. Yamaguchi and T. Takeuchi. Observation of Promotors Found in Contact Catalysts 263
Pasupati Mukerjee. The Electroviscous Effect in Colloidal Systems 267
Roger A. Ford. Photochemical Processes in Solids: The Kinetics of Free Radical Reactions in Nylon 271
A. B. Brown, J. W. Sparks, and F. M. Smith. Viscoelastic Properties of a High-Consistency Asphalt 283
Wilfried Heller and Thomas L. Pugh. Experimental Investigations on the Effect of Light Scattering upon the Refractive Index of Colloidal Particles 294
Robert F. Landel. Mechanical Properties of a Polyurethane Elastomer in the Rubber-to-Glass Transition Zone 308
U. S. Nandi. Rate Constants in the Polymerization of Methyl Methacrylate 321
T. E. Ferington and A. V. Tobolsky. Rate Constants in the Polymerization of Methyl Methacrylate 325
William C. Child, Jr., and John D. Ferry. Dynamic Mechanical Properties of Poly-*n*-Butyl Methacrylate 327

LETTER TO THE EDITOR

Ayao Kitahara. On Micelle Formation of Dodecylammonium Salts of Fatty Acids in Non-Polar Solvents 342
Erratum 344

Number 4, August 1957

A. Wilson, M. B. Epstein, and John Ross. The Adsorption of Sodium Lauryl Sulfate and Lauryl Alcohol at the Air-Liquid Interface 345
C. F. Schadt and R. D. Cadle. Thermal Forces on Aerosol Particles in a Thermal Precipitator 356

A. E. Woodward, J. A. Sauer, C. W. Deeley, and D. E. Kline. The Dynamic Mechanical Behavior of Some Nylons........... 363
Richard H. Milburn. Theory of Evaporating Water Clouds...... 378
William C. Child, Jr., and John D. Ferry. Dynamic Mechanical Properties of Poly-*n*-Hexyl Methacrylate..................... 389
Robert F. Landel, John W. Berge, and John D. Ferry. Viscosities of Concentrated Polymer Solutions. IV. Cellulose Tributyrate.... 400
D. A. I. Goring, M. Senez, B. Melanson, and M. M. Huque. Light-Scattering Calibration with Ludox..................... 412
D. G. Hedge. An Equation of State for Lecithin Monolayers........ 417
D. D. Eley and D. G. Hedge. The Energetics of Lipid-Protein Interactions.. 419

BOOK REVIEWS

Fausto Ramirez. Steric Effects in Organic Chemistry.............. 430
Howard L. Bender. The Chemistry of Phenolic Resins............ 430
S. K. Friedlander. Chemical Engineering Practice, Volume I...... 431

Number 5, October 1957

Paul Stamberger. In Memorium: Frederic G. Donnan............ 433
M. C. Bennett. Behavior of Adsorbed Protein in Cane Sugar Juice.. 434
E. F. Williams, N. T. Woodberry, and J. K. Dixon. Purification and Surface Tension Properties of Alkyl Sodium Sulfosuccinates.. 452
S. H. Bauer. On the Measurement of Concentration Gradients in Thin Films.. 460
Samuel Kaufman and C. R. Singleterry. Effect of the Cation on Micelle Formation by Sulfonates in Benzene................. 465
H. P. Frank. The Formation of Micelles of Some Azo Dyes...... 480
Haruo Kuroda. X-Ray Small-Angle Scattering of Carbon Blacks.... 496
A. Bondi and H. Diamond. Deflocculation in Hydrocarbon Oils.... 510

LETTER TO THE EDITOR

Sydney Ross and John B. Hudson. Henry's Law Constants of Butadiene in Aqueous Solutions of a Cationic Surfactant...... 523

BOOK REVIEWS

Victor K. LaMer. Journal Review: *Annals of Physics*........... 526
V. Drozin. Mechanica Aerosolej (Mechanics of Aerosols).......... 526
Victor K. La Mer. Light Scattering by Colloidal Systems. An Annotated Bibliography....................................... 527

Number 6, December 1957

J. Fred Hazel and Harold O. Strange. Interaction of Inorganic Macromolecular Systems with Surface-Active Agents.......... 529
G. Schuur. The Nature of the Particle Surface in Hevea Latex and Pastes of Rubber Hydrochloride and Polyvinyl Chloride...... 538
R. Arnold. The Titration of Polymeric Acids.................. 549

B. D. FLOCKHART. The Critical Micelle Concentration of Sodium Dodecyl Sulfate in Ethanol-Water Mixtures 557
VICTOR K. LAMER, ROBERT H. SMELLIE, JR., AND PUI-KUM LEE. Flocculation, Subsidence, and Filtration of Phosphate Slimes. V. The Optimum Filtration Rate as a Function of Solid Content and Specific Area 566
M. MOONEY. The Paths of Approach and Recession of Two Spheres in a Shearing Viscous Liquid 575
WILLIAM J. MARCULAITIS. Particle Size and Particle Size Distribution of Pigments by Small-Angle X-Ray Scattering 581
L. H. PRINCEN AND KAROL J. MYSELS. Light Scattering by Ideal Colloidal Electrolytes 594

BOOK REVIEW

J. J. BIKERMAN. Chemical Surface Compounds and Their Role in Adsorption Phenomena 606

Author Index 609
Subject Index 611
Index of Book Reviews 612